

Whole-body MRI Screening

Ralf Puls
Norbert Hosten
Editors

 Springer

Whole-body MRI Screening

Ralf Puls • Norbert Hosten
Editors

Whole-body MRI Screening

 Springer

Editors

Ralf Puls
Institute of Diagnostic and Interventional
Radiology and Neuroradiology
HELIOS Klinikum Erfurt
Erfurt
Germany

Norbert Hosten
Diagnostic Radiology and Neuroradiology
Universitätsklinikum Greifswald
Greifswald
Germany

Translation from the German language edition:
Ganzkörper-MRT-Screening: Befunde und Zufallsbefunde by Ralf Puls and Norbert Hosten
© ABW Wissenschaftsverlag GmbH Berlin 2010. All Rights Reserved.

ISBN 978-3-642-55200-7 ISBN 978-3-642-55201-4 (eBook)
DOI 10.1007/978-3-642-55201-4
Springer Heidelberg New York Dordrecht London

Library of Congress Control Number: 2014944552

© Springer-Verlag Berlin Heidelberg 2014

This work is subject to copyright. All rights are reserved by the Publisher, whether the whole or part of the material is concerned, specifically the rights of translation, reprinting, reuse of illustrations, recitation, broadcasting, reproduction on microfilms or in any other physical way, and transmission or information storage and retrieval, electronic adaptation, computer software, or by similar or dissimilar methodology now known or hereafter developed. Exempted from this legal reservation are brief excerpts in connection with reviews or scholarly analysis or material supplied specifically for the purpose of being entered and executed on a computer system, for exclusive use by the purchaser of the work. Duplication of this publication or parts thereof is permitted only under the provisions of the Copyright Law of the Publisher's location, in its current version, and permission for use must always be obtained from Springer. Permissions for use may be obtained through RightsLink at the Copyright Clearance Center. Violations are liable to prosecution under the respective Copyright Law.

The use of general descriptive names, registered names, trademarks, service marks, etc. in this publication does not imply, even in the absence of a specific statement, that such names are exempt from the relevant protective laws and regulations and therefore free for general use.

While the advice and information in this book are believed to be true and accurate at the date of publication, neither the authors nor the editors nor the publisher can accept any legal responsibility for any errors or omissions that may be made. The publisher makes no warranty, express or implied, with respect to the material contained herein.

Printed on acid-free paper

Springer is part of Springer Science+Business Media (www.springer.com)

Preface and Acknowledgment

Magnetic resonance imaging offers exquisite soft tissue contrast and not only provides morphologic information but also enables evaluation of function and metabolism. It is unique among cross-sectional imaging modalities in that all of this can be had without radiation exposure or the need to administer an iodine-based contrast agent.

With the advent of dedicated whole-body MRI scanners, we are now able to image the human body from head to toe with excellent spatial resolution and the usual sensitivity and specificity of conventional MRI systems. A comprehensive screening examination by MRI relies crucially on fast image acquisition, and using several very recent developments, including multichannel techniques, new surface coil systems, and automatic table movement, this is now possible.

Initial screening studies have focused on cardiovascular conditions (MR angiography and cardiac MRI) and cancer. They have been conducted in healthy populations and in high-risk groups such as patients with diabetes mellitus or a familial disposition.

Since 2008, Greifswald University Hospital has performed whole-body MRI examinations in a sample of subjects from the general population recruited for the Study of Health in Pomerania (SHIP), a German population-based observational study. The screening MRI examination performed in the setting of this study includes a comprehensive protocol for the evaluation of all body regions, a functional cardiac examination, and contrast-enhanced MRI modules for whole-body MR angiography, breast imaging, and delayed enhancement imaging of the left ventricle. The aim of the SHIP is to investigate the general state of health of the German population in the north eastern region of Pomerania using whole-body MRI. An important aspect of this study is to correlate whole-body MRI findings with the results of clinical and laboratory examinations and with the results of a genome-wide analysis, which are also part of the SHIP.

Not surprisingly, the daily analysis of whole-body MRI datasets uncovers many incidental findings. The SHIP investigators set up an interdisciplinary advisory board of physicians from all specialties for deciding how to manage incidental findings in a way that considers not only the most recent clinical insights but also ethical aspects with a view to protecting subjects' welfare and safeguarding research integrity. Our experience suggests that about 30 % of all study subjects have abnormal findings that must be reported to their physicians.

The wealth of experience amassed by this advisory board was the inspiration for compiling and publishing a book on incidental findings in whole-body MRI. The radiologists involved in the project wrote chapters on each organ system, presenting a structured compilation of the most common findings, their morphologic appearances in whole-body MRI, and guidance for their clinical management. A note of caution here is that a tailored individual workup and differential diagnostic assessment of incidental findings is not possible in subjects examined as part of epidemiologic, screening, or staging studies.

We hope that our book and the experience we have to share is useful to other diagnosticians and that our guidance may help them in deciding how to handle the most common incidental findings encountered in whole-body MRI.

We would like to thank all authors, without whose expertise and contributions this book could not have been compiled. Our thanks are also due to Julia Kühn and Bianca Ladwig, both coordinators of the Greifswald SHIP-MRI study. The authors would like to thank Bettina Herwig for translating the German text.

All contributors hope that the English edition of this monograph will be received as favorably as the German edition.

Erfurt, Germany
Greifswald, Germany

Ralf Puls
Norbert Hosten

Contents

1 The Ethics of Incidental Findings in Population-Based MRI Research.	1
Martin Hoffmann and Reinold Schmücker	
2 MR Imaging in Population-Based Research	21
Henry Völzke	
3 Technical Prerequisites for Whole-Body MRI Screening.	29
Harald H. Quick	
4 Contrast Agent Administration and Imaging Protocols for Whole-Body MRI.	45
Achim Seeger, Stephan Miller, and Heinz-Peter Schlemmer	
5 The Head and Neck	57
Sönke Langner	
6 The Chest	115
Christian Rosenberg	
7 The Heart	133
Saskia Ungerer	
8 The Abdomen	169
Jens-Peter Kühn and Christoph Lühken	
9 The Vascular System	213
Michael Kirsch and Marcel Mohr	
10 The Musculoskeletal System and Spine	225
Katrin Hegenscheid and Martin Petrik	
11 The Breast.	277
Saskia Ungerer	
12 The Urogenital System.	311
Birger Mensel and Ralf Puls	
Index	365

Contributors

Katrin Hegenscheid Institute of Diagnostic Radiology and Neuroradiology, University Medicine Greifswald, Greifswald, Germany

Martin Hoffmann Department of Philosophy, Universität of Hamburg, Hamburg, Germany

Norbert Hosten Diagnostic Radiology and Neuroradiology, Universitätsklinikum Greifswald, Greifswald, Germany

Michael Kirsch Institute of Diagnostic Radiology and Neuroradiology, University Medicine Greifswald, Greifswald, Germany

Jens-Peter Kühn Institute of Diagnostic Radiology and Neuroradiology, University Medicine Greifswald, Greifswald, Germany

Sönke Langner Institute of Diagnostic Radiology and Neuroradiology, University Medicine Greifswald, Greifswald, Germany

Christoph Lühken Institute of Diagnostic Radiology and Neuroradiology, University Medicine Greifswald, Greifswald, Germany

Birger Mensel Institute of Diagnostic Radiology and Neuroradiology, University Medicine Greifswald, Greifswald, Germany

Stephan Miller Department of Diagnostic and Interventional Radiology, Eberhard-Karls-University Tuebingen, Tuebingen, Germany

Marcel Mohr Institute of Diagnostic Radiology and Neuroradiology, University Medicine Greifswald, Greifswald, Germany

Martin Petrik Institute of Diagnostic Radiology and Neuroradiology, University Medicine Greifswald, Greifswald, Germany

Ralf Puls Institute of Diagnostic and Interventional Radiology and Neuroradiology, HELIOS Klinikum Erfurt, Erfurt, Germany

Harald H. Quick Erwin L. Hahn Institute for MR Imaging, University of Duisburg-Erlangen, Essen, Germany

Christian Rosenberg Institute of Diagnostic Radiology and Neuroradiology,
University Medicine Greifswald, Greifswald, Germany

Heinz-Peter Schlemmer Department of Radiology, Deutsches
Krebsforschungszentrum, Heidelberg, Germany

Reinold Schmücker Department of Philosophy,
Westfälische Wilhelms-Universität Münster, Münster, Germany

Achim Seeger Department of Diagnostic and Interventional Radiology,
Eberhard-Karls-University Tuebingen, Tuebingen, Germany

Saskia Ungerer Institute of Diagnostic Radiology and Neuroradiology,
University Medicine Greifswald, Greifswald, Germany

Henry Völzke Institute for Community Medicine, Study of Health in Pomerania
(SHIP)/Clinical-Epidemiological Research, University Medicine Greifswald,
Greifswald, Germany

Abbreviations

2D	Two-dimensional
3D	Three-dimensional
ADC	Apparent diffusion coefficient
BLADE	Motion correction with radial blades (Siemens)
BMI	Body mass index
BW	Body weight
CAD	Computer-aided diagnosis
CISS	Constructive interference in steady state
CM	Contrast medium
CNR	Contrast-to-noise ratio
CNS	Central nervous system
CSF	Cerebrospinal fluid
CT	Computed tomography
CUP	Cancer of unknown primary
DSA	Digital subtraction angiography
DWI	Diffusion-weighted imaging
EPI	Echo-planar imaging
ERC	Endoscopic retrograde cholangiography
ERCP	Endoscopic retrograde cholangiopancreatography
F	Female
FA	Flip angle
FISP	Fast imaging with steady-state precession
FLAIR	Fluid-attenuated inversion recovery
FLASH	Fast low-angle shot
FOV	Field of view
FS	Fat saturation
FSE	Fast spin echo
Gd-DTPA	Gadopentetate dimeglumine
GRE	Gradient-recalled echo
HASTE	Half-Fourier acquisition single-shot turbo spin echo
IR	Inversion recovery
IV	Intravenous
M	Male

MIP	Maximum intensity projection
MPR	Multiplanar reconstruction
MPRAGE	Magnetization-prepared rapid acquisition gradient echo
MRA	Magnetic resonance angiography
MRCP	Magnetic resonance cholangiopancreatography
MRI	Magnetic resonance imaging
PACS	Picture archiving and communication system
PD	Proton-density weighted
PET	Positron emission tomography
PSIR	Phase-sensitive inversion recovery
RARE	Rapid acquisition with relaxation enhancement
RF	Radiofrequency
ROI	Region of interest
SAR	Specific absorption rate
SE	Spin echo
SHIP	Study of Health in Pomerania
SNR	Signal-to-noise ratio
SPAIR	Spectral attenuated inversion recovery
SPECT	Single-photon emission computed tomography
SSFP	Steady-state free precession
STIR	Short-tau inversion recovery
SWI	Susceptibility-weighted imaging
T1w	T1-weighted
T2w	T2-weighted
TE	Echo time
TI	Inversion time
TIRM	Turbo inversion recovery magnitude
TOF-MRA	Time-of-flight magnetic resonance angiography
TR	Repetition time
TSE	Turbo spin echo
VIBE	Volume-interpolated breath-hold examination
VIBE Dixon	Volume-interpolated breath-hold examination for chemical-shift imaging (Siemens)

The Ethics of Incidental Findings in Population-Based MRI Research

1

Martin Hoffmann and Reinold Schmücker

1.1 Introduction

The occurrence of incidental findings in epidemiologic studies is a well-recognized problem in medical research methodology. Radiologists and epidemiologists have discussed incidental findings in terms of empirical frequency and methodological implications for some time, and there has been an upsurge of interest in this topic over the last few years. In large measure, this growing interest has been fueled by an increase in incidental findings, which is attributable to the fact that state-of-the-art imaging modalities have become established research tools and are now widely used in population-based studies. It is estimated that 1–8 % of human subjects participating in research involving magnetic resonance imaging (MRI) of the brain have clinically relevant findings (Katzman et al. 1999; Alphas et al. 2006; Vernooij et al. 2007; Gupta and Belay 2008). Still, the brain appears to be among the organs that generate relatively few incidental findings. Recent data suggest that incidental findings are much more common when other organs are examined. Brudermanns (2008), for instance, reported a rate of 41 % in cardiac multidetector computed tomography (CT) studies. Valid estimates on the frequency of incidental findings in whole-body MRI studies are still lacking, probably because, up to now, this complex imaging modality has very rarely been used on a large scale for research purposes. The Study of *Health in Pomerania* (SHIP) is one of the first population-based studies using whole-body MRI in a large sample of normal volunteers.

M. Hoffmann (✉)
Department of Philosophy, Universität of Hamburg,
Von-Melle-Park 6, Hamburg 20146, Germany
e-mail: martin.hoffmann@uni-hamburg.de

R. Schmücker
Department of Philosophy, Westfälische Wilhelms-Universität Münster,
Domplatz 6, Münster 48143, Germany
e-mail: schmuecker@uni-muenster.de

With more incidental findings being encountered in imaging research, it has become apparent that dealing with them not only affects research methodology but also raises fundamental ethical issues. A survey of the literature reveals that researchers first began discussing the ethics of incidental findings in greater depth around 2005, highlighting the need for a systematic ethical analysis that would offer investigators guidance in handling incidental findings detected with modern imaging technology in the context of epidemiologic research. The SHIP investigators set up an *Advisory Board* to address the problem of incidental findings, to decide which findings to disclose and, where necessary, to make decisions on an individual basis (for more details, see Chap. 2).

In this chapter, we take a broader perspective, going beyond the specific problems of incidental findings encountered in the SHIP, and seek instead to identify the core of the ethical problems posed by incidental findings in general. We have chosen to do so because there is currently no general consensus on what constitutes the core of the ethical problems and how these problems are related to each other. An accurate description of the core problem is indispensable for arriving at a solution that is sound in both theory and practice.

Following a brief discussion of the meaning of “incidental findings” (Sect. 1.2), we will work out the core of the ethical dilemma, based on what medical research ethics discussions have focused on so far. We will then go on to outline some of the ethical issues arising indirectly from incidental findings (Sect. 1.3). We present our reasoning and explain why we believe it is crucial to identify the central ethical dilemma before we can suggest possible solutions and provide ethically adequate guidance in dealing with incidental findings. To conclude, we present a preliminary sketch of a possible solution to the central ethical dilemma underlying the problems researchers face in dealing with incidental findings (Sect. 1.4) and outline areas for further investigation.

1.2 What Are Incidental Findings?

While there is no generally accepted definition of what constitutes an incidental finding, in the literature it is usually characterized by three features. These features, which are largely undisputed, are included in the widely quoted definition proposed by Wolf et al. that an incidental finding is “a finding concerning an individual research participant that has potential health or reproductive importance and is discovered in the course of conducting research but is beyond the aims of the study” (Wolf et al. 2008, p 219). Restricting the occurrence of incidental findings to research subjects may at first glance appear too narrow. After all, there is also a risk of discovering incidental findings of potential relevance to an individual’s health in activities other than research (e.g., the acquisition of MR images for an anatomic atlas or in other examinations of healthy subjects). However, this restriction makes sense for our line of argument and also in conjunction with the third feature, namely, that an incidental finding is a finding that is beyond the aims of the study. Alternatively, some authors use the term “unexpected” to characterize incidental

findings (Illes et al. 2006, p 783; Heinemann et al. 2007, p A1982). This characterization is misleading, though, since investigators are now generally aware of the significant potential for incidental findings when performing research using MRI. Characterizing these findings as unexpected only makes sense with regard to the individual subject but not when the study population as a whole is concerned. Quite the contrary appears to be true today: incidental findings are anticipated by researchers (Rangel 2010, p 124). Therefore, unexpectedness is not what distinguishes incidental findings from other findings. What is crucial, instead, is that incidental findings are not what the researcher is looking for, i.e., they are *unintended*. As will become clear as we proceed, the fact that incidental findings are not intended is central to the ethical issues they give rise to.

The crucial point regarding the second feature is that incidental findings are characterized as being of *potential* rather than actual health or reproductive importance. By definition, then, incidental findings also include findings that may be so marginal as to have no clinical significance. Moreover, they include false-positive findings, i.e., abnormalities that are found to be harmless upon further diagnostic evaluation (Woodward and Toms 2009).

Some authors characterize incidental findings as being detected in *normal* volunteers (Hoggard et al. 2009), but restricting the definition to normal volunteers is inadequate for two reasons. First, an incidental finding can relate to a hitherto undiagnosed condition in a person with a known disease (e.g., when a cancer patient taking part in a clinical study is diagnosed with multiple sclerosis). Second, a central feature of an incidental finding is precisely that a volunteer *considered to be healthy* at the time of enrollment in a study turns out to be (potentially) ill. Strictly speaking then we should say: *incidental findings concern a disease of which the subject was unaware at the time of the study*. In light of this more precise characterization of incidental findings, we refer to the persons in whom incidental findings can be detected as subjects or volunteers rather than patients.

1.3 Ethical Problems Posed by Incidental Findings in Epidemiologic Population-based Research

Although research ethics has become an established domain of medical ethics and medical law over the last two decades, there are relatively few publications on the ethics of incidental findings in epidemiologic studies. Caughlin and Beauchamp's *Ethics and Epidemiology* from 1996 does not deal with this topic. The first publications addressing the ethical issues arising from incidental findings appeared at the beginning of this century (Illes et al. 2002, 2004). A wider debate of incidental findings ensued after the 2005 meeting on *Detection and Disclosure of Incidental Findings in Neuroimaging Research* in Bethesda (MD), which was organized by Stanford University and the National Institutes of Health (NIH). A brief summary of the results of this meeting was published in *Science* (Illes et al. 2006), triggering an intensified interest in the management of incidental findings by the research community.

A set of seminal articles appeared in the summer 2008 issue of the *Journal of Law, Medicine & Ethics* (36:216–383). These articles were the result of a 2-year project on *Managing Incidental Findings in Human Subjects Research*, funded by the NIH and the National Human Genome Research Institute (NHGRI). The project involved 21 scientists (Principal Investigator: Susan M. Wolf) and dealt with the ethical, legal, clinical, and scientific issues arising in the management of incidental findings. Although this set of articles represents a breakthrough in the debate, the authors treat the ethics of incidental findings as only one of several aspects.

In German-speaking countries, treatment of these ethical issues is limited to a few publications (Hentschel and Klix 2006; Heinemann et al. 2007, 2009b; Schleim et al. 2007; Fuchs et al. 2010, p 183–184; Langanke and Erdmann 2011; Schmücker 2013) and discussions in *Deutsches Ärzteblatt* (2007, 46:A3184–88) and *Clinical Neuroradiology* (Hentschel and von Kummer 2009; Heinemann et al. 2009a). A comprehensive legal framework governing the management of incidental findings is still lacking in both Germany and the USA (*Code of Federal Regulations* (United States Department of Health and Human Services 2005)) (see the overview of current recommendations given by Booth et al. 2010). Lately, however, researchers have been lamenting this situation and calling for guidelines to be developed (Brown and Hasso 2008; van der Lugt 2009). In Germany, the process of developing a guideline sparked a controversy (Hentschel and von Kummer 2009; Heinemann et al. 2009a). “Incidental findings” is not listed as an index term in current textbooks of bioethics (Gert et al. 2006; Beauchamp and Childress 2013) or reference works on applied and biomedical ethics (Frey and Wellman 2003).

Although many of the above-quoted authors discuss the legal, ethical, and practical issues surrounding the detection of incidental findings in great depth, we feel that they have not addressed the true core of the ethical problem.

We proceed by briefly summarizing the central concerns of research ethics (Sect. 1.3.1) and discussing them in relation to incidental findings. While these concerns may easily be interpreted to imply that incidental findings do not pose specific medical ethical problems, we will argue that scientists dealing with incidental findings are indeed confronted with a serious ethical conflict (Sect. 1.3.2).

1.3.1 Central Ethical Concerns in Human Subjects Research

Currently, the focus of medical research ethics is on three main topics: (a) clinical research in patients, (b) research involving vulnerable subjects (e.g., children, cognitively impaired persons, prisoners), and (c) the conduct of pharmaceutical trials in developing countries (see, e.g., Maio 2002). The reason that these are the central ethical concerns of medical research ethics is apparent from the serious conflicts, in terms of individual and social ethics, that these research practices generate:

- (a) *Clinical research* is typically conducted in patients, i.e., diseased persons who seek or require medical treatment. Thus, in the framework of a clinical study, both the doctor and the patient assume dual roles. The former is both physician and researcher, and the latter is both patient and research subject. As a

patient, an individual has a right to the best medical care available, while as a study subject he or she may not receive the best treatment possible – when the study protocol assigns him or her to a control group treated with placebo, for example. Whether – and, if so, to what extent – it is ethically justifiable to deny subjects/patients therapeutic options that might be more effective than what they receive in the clinical trial is still under debate (Freedman 1987; Miller and Brody 2003, 2007; Veatch 2007; Hoffmann and Schöne-Seifert 2009).

- (b) *Research involving vulnerable populations* gives rise to an ethical conflict because vulnerable subjects are unable or limited in their ability to give informed consent (Fischer 2008). Nevertheless, such research is necessary, for example, to ensure that children receive the best possible treatment. The organism of a child is different in its physiologic and metabolic processes, and adult medications and dosages must be adjusted to be effective. Not doing research in children simply because they cannot give informed consent would render them therapeutic orphans, who would rely for treatment on drugs whose efficacy, safety, and dosage have only been proven in adults. The ethical problems are especially acute when children enrolled in pharmacologic trials do not themselves benefit from the research (Merkel 2003; Fleischman and Collogan 2008), but even research performed in the child's best interest raises a number of ethical concerns (Hoffmann and Schöne-Seifert 2010).
- (c) *Pharmacologic research in developing countries* is attractive to profit-oriented companies, which sponsor most of these trials: it saves costs, and the laws governing human subjects research are usually less strict. However, these research practices violate the principle of justice in two respects. First, destitute persons in developing countries may be more willing to participate in research for little pay because of their threatening economic situation. Second, the results of research conducted in developing countries will mostly benefit patients in countries with better healthcare systems and not the research subjects contributing to these results by their participation (Macklin 2004).

At first glance, none of these ethical problems appears to arise in research subjects recruited for participation in epidemiologic or population-based studies.

Problem (a): Epidemiologic or population-based studies are not performed in patients but in individuals from the general population. Consequently, researchers do not owe their research subjects the same duty of personal care as in a physician-patient relationship.

Problem (b): Epidemiologic studies usually do not recruit subjects who are unable to give informed consent. Hence, epidemiologic study populations are not vulnerable. On the contrary, we can assume that participants in epidemiologic research have in fact been especially well informed, during the consent process, about all aspects of the study they are participating in. This does not imply that there are no incidental findings in pediatric research. On the contrary, it has been recognized that specific ethical problems arise when incidental findings are discovered in children (Wilfond and Carpenter 2008; Hens et al. 2011). These specific issues do not concern us here.

Problem (c): Unlike research in developing countries, epidemiologic studies do not violate the principle of fair selection of subjects. There is neither a financial incentive to attract persons in desperate economic circumstances,¹ nor are the research participants excluded from ever being able to benefit from the research results in the future.

1.3.2 The Core of the Ethical Dilemma Posed by Incidental Findings

What has been said so far may suggest that there are no specific ethical and legal issues arising in association with epidemiologic research. At first sight, the central ethical problem with incidental findings appears to be a mere conflict between an ethical imperative and a methodological standard, where it seems obvious that the ethical imperative should carry greater weight. On closer scrutiny, however, this problem turns out to be a true ethical dilemma, i.e., a situation that requires a choice between two ethical principles which cannot both simultaneously be adhered to. While a similar ethical conflict can challenge clinical investigators, the choices available to the researcher for overcoming the conflict are different in clinical and epidemiologic studies. In the following, we elaborate on this ethical conflict and consider an example. In our opinion, the conflict is so grave that, unless an acceptable solution is found, it may threaten the legitimacy of population-based research.

If we wish to come to terms with the methodological implications that lead to what we consider to be the core of the ethical dilemma posed by incidental findings, we must first recall how the design of population-based studies differs from that of clinical trials. Two aspects are important here. First, an epidemiologic study investigates a set of individuals recruited from the general population and not a set of *patients*, who are recruited for a clinical study with a specific diagnosis or an indication for a specific treatment. This is methodologically important because the primary goal of epidemiologic research is to obtain quantitative data on the natural history of diseases in the general population. The results are valid only if the sample investigated is truly representative of the general population in terms of those aspects that are relevant to the goal of the study. Second, we are here dealing with *noninterventional* studies. While a clinical study is usually conducted to investigate the safety and effectiveness of a medical intervention, population-based epidemiologic research is observational: the aim is to evaluate the health status of the research subject without performing any study-specific interventions.

How then does the ethical dilemma arise? Let us consider an example. A whole-body MRI examination performed in the setting of an epidemiologic study reveals a kidney tumor that is still treatable if immediate measures are taken. It is undisputed that a finding of such import for the subject's quality of life and life

¹The participants of the SHIP receive no payment. The diagnostic procedures performed in the study are the only incentive for participation. The absence of payment gives this incentive extra weight – especially in light of study subjects' expectations (Kesseling 2009).

expectancy must be disclosed. The investigator's moral obligation to act in the interest of the research subject in such a situation is not simply a matter of medical ethics. Even if study participation does not establish a physician-patient relationship between the investigator and the research subject, a *direct duty of care and assistance* arises when an incidental abnormality is so serious as to constitute an exigency (see Schleim et al. 2007, p 1044). This is the case when an incidentally detected abnormality is life-threatening.² In such a situation, there is a general (limited) moral obligation to provide assistance, which is independent of a physician's professional duties. According to German law, anyone who recognizes such a situation of exigency must provide assistance according to his or her ability. In a medical context, it is even more difficult to deny such an obligation because study subjects have often agreed to participate in the study precisely because they expect to receive the medical care necessary to deal with a critical finding revealed by the study-related examinations.³

While in the best interest of study subjects, the communication of incidental findings compromises the validity of the study. Each disclosure of an incidental finding alters the study sample such that the disease courses observed in the sample will *systematically* deviate from the natural evolution of disease in the general population. This conflicts with the primary aim of epidemiologic research, which is to observe how diseases evolve without interference from study-related interventions. Valid epidemiologic data can be derived from a study sample only if the subjects investigated are representative of the general population with regard to the aspects under investigation throughout the study. Once an incidental finding has been communicated to a study subject, it is no longer justified to assume that the sample is representative (Hoffmann 2013). The disclosure provides study subjects with information on their health that is not available to the general population, of which they are supposed to be representative. With this knowledge, they can seek treatment at an earlier time than would have been possible had they not participated in the study. Thus, medical interventions are different in the study population and in the general population, and disease evolution in the study population *systematically* deviates from that in the normal population. This is how disclosure of incidental findings results in a biased sample, compromising the validity of the study and generating knowledge that cannot be generalized to the normal population. Sample theory states that a systematic bias in a sample, as it may result from the disclosure of

²This is a widely accepted, fundamental norm. In most countries, citizens have a legal obligation to provide assistance in emergencies, and this obligation is independent of the physician-patient relationship. In Germany, for instance, failure to provide first aid to a person in need is punishable under Section 323c of the Criminal Code (Strafgesetzbuch, StGB) and applies to those who fail to provide assistance in case of an accident, general danger, or emergency.

³There is now ample empirical evidence for what is known as the "therapeutic misconception" – the tendency of patient volunteers to believe that, despite explanation, research protocols are designed to benefit them directly rather than to investigate and compare different treatments (Appelbaum et al. 1987, 2004). Moreover, obtaining scientifically sound information on their own health appears to be an important incentive for healthy individuals to participate in a medical study (Kirschen et al. 2006). These findings have also been confirmed in SHIP participants (see Chap. 2).

incidental findings, escapes the statistical methods used to estimate sampling errors. This means that such a systematic bias cannot be controlled by increasing the sample size (Schäffer 1996).

The so-called *Literary Digest* disaster in the USA is the classic example of a biased sample. The journal conducted a telephone survey among its readers in the 1936 presidential campaign between Alfred M. Landon und Franklin D. Roosevelt. As the *Literary Digest* was a fairly nonpolitical journal, it was assumed that the readership would not have a systematically biased preference for either of the candidates. The poll predicted a landslide victory for the Republican candidate, Landon, when in fact Roosevelt was reelected by a large margin. What was the reason for this wildly incorrect estimate of the vote despite the huge sample size of 2.3 million persons? It turned out later (Squire 1988) that conducting the survey by telephone had been the crucial error. In 1936, the people who had telephones were mostly people with high incomes, who also tended to vote Republican. Therefore, the choice of method led to a systematic selection bias. This poll also nicely illustrates the central issue that concerns us here: when a systematic sampling error occurs while a study is under way, this cannot simply be remedied by increasing the sample size. The *Literary Digest* survey evaluated the voting behavior of telephone owners and not that of all voters. Analogously, when incidental findings are disclosed to participants of an epidemiologic study, the study population differs from the population at large in that study subjects can undergo further diagnostic procedures and seek treatment for a disease they would not have been aware of in the normal course of events. Therefore, the disclosure of incidental findings compromises the empirical validity of the study and limits the generalizability of its results.

This still appears to be a mere conflict between an ethical duty and a methodological research standard: the ethical duty to provide medical care to an individual on the one hand and the researcher's responsibility for safeguarding good research practice by ensuring an unbiased study population on the other. The genuineness of the ethical dilemma becomes clear, however, when we consider the following point. In contrast to some fields of basic research, in epidemiologic research the adherence to methodological standards is not simply a matter of good methodology. After all, the results of these studies are intended to help improve medical care for *future patient generations*. Thus, there can be no ethical justification for performing epidemiologic research if it is clear from the start that it will not serve this goal. If the aim of advancing medical care is compromised by flawed methodology, which undermines the generalizability of the results generated by population-based research as outlined above, then these studies betray their purported *raison d'être* and guiding principle. Hence, with regard to epidemiologic research, the conflict is a genuine ethical conflict, namely, a conflict between the well-being of individual research participants currently living with a disease and the well-being of future patient generations, who might potentially benefit from the research results.

Here it might be argued that this position is only tenable if one postulates the existence of a general ethical obligation to do medical research. Are we indeed ethically obliged to keep expanding our medical knowledge in order to provide increasingly better medical care to an increasingly larger number of people? An argument

supporting the existence of such a duty is that we, as patients today, benefit from the research done by earlier generations. This position is further supported by the fact that we accept such duties of solidarity in other social contexts (Merkel 2003). Nevertheless, it is not generally agreed that there is a social duty to conduct medical research. It should be noted, however, that an adherence to methodological standards is ethically significant not only when we assume an ethical duty to conduct medical research but also when we assume at all that there are ethical norms that should guide us in terms of our approach to medical research (Hübner 2003). The central ethical dilemma of incidental findings, as we have identified it, also arises if we do not postulate an ethical obligation to advance and improve medical knowledge. Even if we accept that it may be legitimate to request that all medical research in humans be stopped (e.g., to protect human subjects), those who opt for doing medical research in human subjects still have a moral duty to strictly adhere to the principles of Good Scientific Practice. Medical research not only requires large funds and extensive resources but also exposes human subjects to certain risks. This can only be justified by adherence to the highest methodological standards. Moreover, poor research methodology will compromise the external validity of research data. If an epidemiologic study does not generate generalizable knowledge, then it is no longer useful for advancing medical care and undermines the very rationale for conducting such studies. Poorly validated results might even expose future patients to unpredictable risks. This is how the communication of incidental findings to the participants of a population-based study can harm future patients. Therefore, the disclosure of incidental findings is just as ethically questionable as their nondisclosure, although nondisclosure may mean that a research subject is denied the care necessary to treat a serious condition.

In light of these considerations, the question to be answered regarding the disclosure of incidental findings is how we should balance the well-being of a research subject against that of future patient generations. In other words, are we justified in denying research subjects a chance to receive adequate treatment for the sake of study validity? The central ethical dilemma with incidental findings arises from the fact that an epidemiologic study generates not only the desired research results but also unintended additional information in the form of incidental findings. *Disclosure of such incidental findings may be highly relevant to the health of an affected research subject. At the same time, however, it also leads to a biased sample as the treatment a study subject may receive after disclosure of an incidental finding is unique to the study situation. This means, of course, that the results obtained in that sample no longer represent generalizable knowledge.*

What has just been said reveals the analogy that exists between epidemiologic research and clinical studies in terms of the central ethical dilemma of incidental findings. In a clinical study, the research subjects are patients, who expect to receive treatment as part of the study protocol, while research subjects in an epidemiologic study are usually recruited from the general population to participate in a purely diagnostic (noninterventional) study. What both kinds of studies have in common is that the management of incidental findings requires that investigators strike a balance between the well-being of individual research subjects and the improvement of

medical care for future patients. What is different is the sacrifices that are expected from the subjects as part of the research protocol: when a novel treatment is withheld from a patient in a clinical trial because the randomization procedure assigns him or her to the control group receiving standard treatment, the question is whether a researcher is ethically justified in actively and deliberately submitting a group of study subjects to a presumably less optimal treatment in the name of advancing medical knowledge to benefit future patients (Freedman 1987). Conversely, in purely diagnostic, population-based research, the question that arises is whether the researcher can withhold information from research subjects that is relevant to their health for the benefit of future patient generations. *Ethically*, the question also arises when, in the consent procedure, a research subject explicitly states that he or she wishes not to be informed about incidental findings. While such an explicit wish exempts the researcher from a legal duty to inform the subject, this does not mean that obtaining such consent is ethically innocuous (Schmücker 2007, 2013). Hence, an improved consent process does not eliminate the central ethical problem posed by incidental findings.

The situation is different when research subjects explicitly make use of their *right not to know* by consenting to participate in the study on condition that no findings should be disclosed to them. In such cases, a conflict may arise between the duty to intervene in an acute life-threatening situation and a moral duty to respect a subject's wish not to be informed about study results under any circumstances (Heinemann et al. 2007, p A1986). Such a conflict between duty of care and respect for an individual's autonomy can be avoided by not enrolling persons who make use of their right not to know. This is the normative recommendation also given by Schleim et al. (2007, p 1043). However, as Heinrichs (2011, p 61–62) points out, this recommendation does not solve the conflict of moral norms but merely circumvents it: a subject who waives his or her right not to know in the consent process may later decide to make use of this right, precisely at a time when a serious incidental finding has been detected but not yet disclosed. Moreover, using the right not to know as an exclusion criterion may lead to a systematic bias in the sample, aggravating the core problem we are dealing with. Empirically, this problem appears to be negligible as the majority of subjects expect to obtain reliable additional information on their health, which is their main motivation for participating in a non-interventional epidemiologic study (Kirschen et al. 2006). For this reason, virtually no subject makes use of his or her right not to know. This has also been overwhelmingly confirmed in the course of the SHIP, in which only two of the first 3,000 subjects who underwent whole-body MRI declared that they did not wish to be informed about any MR findings (see Chap. 2). Hence, study enrollment would only minimally suffer from excluding those who exercise their right not to know, neither preventing epidemiologic studies from being performed nor compromising their validity.

Available evidence unanimously indicates that participants' wishes to learn more about their health is their chief motivation for participating in purely diagnostic, empirical studies. This points to another difference between clinical and epidemiologic research, the ethical significance of which has not yet been fully appreciated.

For patients, the main incentive to participate in a clinical trial is to have access to novel treatment options otherwise not available to them. It seems obvious that no patients would be motivated to join a clinical trial if it were clear beforehand that the therapeutic options provided by the study protocol were inferior to standard treatment.

No hope of immediate therapeutic benefits can be entertained by volunteers who join a noninterventional epidemiologic study. The only direct benefit they may hope for is a free medical checkup. This would imply that study subjects can legitimately expect to be informed about the findings, especially if an abnormality is revealed that requires immediate management. However, if it were generally known that such an expectation is not justified, potential study participants would know that there is no immediate personal benefit to be derived from taking part in an epidemiologic study. This would likely have devastating effects on the recruitment of volunteers. Evidence from the above-quoted publications unanimously suggests that obtaining reliable additional information on one's own health is the chief motivation for participating in epidemiologic research. Hence, a general policy of not disclosing incidental findings, including serious ones, would make it very difficult for epidemiologists to find enough volunteers for their studies. The recruitment of volunteers for epidemiologic studies relies on potential candidates entertaining a legitimate hope of at least learning about a possibly life-threatening condition of which they are not aware. The alternative would be to offer a financial incentive for study participation. In some sense, we can therefore interpret the disclosure of serious incidental findings to affected subjects as the empirical condition enabling epidemiologic research to be performed in the first place: *as long as it is an unrefuted fact that the vast majority of volunteers expect a health-related benefit from taking part in a noninterventional medical study and as long as this is their chief incentive for participation, population-based epidemiologic research will only be possible as long as this expectation is adequately accommodated in the research design.*

This has important implications for the ethical problems of incidental findings. The problems posed by epidemiologic research cannot simply be regarded as a special case of the ethical concerns in clinical studies. Instead, the disclosure of serious incidental findings to research subjects is an empirical precondition for the possibility of conducting population-based research at all. Without it, an important incentive for study participation would fall away. Nondisclosure means that investigators accept possible harm to research subjects as a necessary evil. Furthermore, a general policy of nondisclosure would potentially eliminate an important incentive for study participation and might render epidemiologic research difficult or impossible in the long run.

In light of these considerations, we must also not forget that the disclosure of incidental findings compromises the validity of an epidemiologic study and may harm future patients. Epidemiologic research flawed in this way may have difficulties attracting the necessary funding. For large-scale studies, the costs are considerable, and such expenditure is only justified when a study yields valid and relevant results.

It should be clear by now why we regard the above problem as the core of the ethical dilemma of incidental findings: both the disclosure and the nondisclosure of incidental findings appear to violate fundamental and well-founded ethical and normative principles and to undermine the empirical feasibility of population-based epidemiologic research. Researchers seeking to avoid harm to individual research subjects and providing care based on the diagnostic information obtained thereby risk harm to future patients and also compromise the validity of their research. Such research becomes useless and will not (and should not) be funded in the long run (apart from individual cases). Conversely, a researcher safeguarding the validity of research in order to prevent harm to future patients is accepting harm to individual research subjects and, according to German law, is even at risk of punishment for nonassistance to a person in danger. Such a practice, if it were to become the general standard, would undermine the chief motivation for study participation and result in a lack of volunteers for such studies in the future.

This is a conflict that touches on the very foundations of population-based epidemiologic research – in terms of both its ethical legitimation and its practical feasibility. An ethically responsible researcher cannot escape this deep ethical conflict simply by artificially restricting his or her field of vision and positing, for instance, that a researcher-physician has no duty of care to study subjects because participation in a study does not constitute a physician-patient relationship (e.g., Heinemann et al. 2009a, p 243 and Sect. 1.4.2 below). What we believe instead to be ethically necessary is to carefully consider each case on an individual basis, weighing the well-being of the individual subject against the advancement of medical knowledge to the benefit of future patients. Such a case-by-case approach relies on several prerequisites not available at present.

1.4 Two Possible Solutions

The central ethical dilemma, as outlined in the preceding section, is a serious one but not one that leaves the researcher without an ethically acceptable course of action. The problem arising from incidental findings in population-based epidemiologic research requires that we make a well-founded decision between two moral imperatives, the obligation to care for a research subject in whom an incidental finding has been detected and the obligation to aid future patients, who might benefit from medical advancement but might also be placed at risk if research findings are flawed. Essentially, there are several options for weighing these alternative courses of action. The number of future patients who could benefit from robust research data is far greater than the number of research subjects with incidental findings, but when it comes to making a decision on the matter, this consideration does not carry us very far. The idea that the rights of individual research subjects can be overridden by a benefit to a greater number of future patients comes into conflict with existing moral and legal norms and also widely held moral beliefs. Two fairly obvious courses of action are presented below and examined critically.

1.4.1 Financial Incentives for Study Participation

One way to mitigate the ethical conflict might be to pay money to research subjects as an incentive to irrevocably waive their right to be informed about study findings. This would be a strong enough incentive for participation, similar to an expected health benefit, to ensure recruitment of enough volunteers for epidemiologic studies. Ruling out the communication of incidental findings in this way is morally justified in that an explicit agreement is entered into between the researcher and the research subject, who might potentially be harmed by such a practice. In Western industrialized countries, the payment for participating in a study and irrevocably signing away one's right to potentially life-saving information and care would have to be considerable. Otherwise the agreement could be seen as putting one party (the research subject) at such a disadvantage as to be considered contrary to public policy and therefore unenforceable.

The latter aspect is overlooked, or at least not mentioned, by those proponents of the nondisclosure of incidental findings who argue that there are fundamental differences between the physician-patient relationship and the researcher-subject relationship. According to this position, a subject participating in research cannot expect the same standard of medical care that doctors owe their patients. To prevent study subjects from falling victim to the therapeutic misconception, proponents of this position argue, the investigator must adequately clarify the difference between research and standard clinical care as part of the consent process and make sure that the subject has truly understood the difference when giving consent (Miller and Brody 2003; Veatch 2007; Heinemann et al. 2009a, p 243). We, however, do not believe that the difference between participation in medical research and standard patient care alone can justify a policy of not disclosing incidental findings (for a detailed discussion of the concepts of therapeutic misconception and diagnostic misconception, see Schmücker 2013, p 960–963). This is because the ethical conflict posed by incidental findings is not simply a pseudoproblem resulting from a misinterpretation of the relationship between medical researchers and research subjects as a physician-patient relationship. In the research context, the dilemma arises from a general moral obligation to provide assistance, a principle deeply rooted in individual and social ethics as well as in the legal systems of most states based on the rule of law (see footnote 2 above). A researcher who is able to provide assistance by virtue of his or her medical training and may reasonably be expected to do so can only be released from this duty if the research subject explicitly waives his or her entitlement to the assistance the researcher can provide. This means that the subject must be fully aware that he or she is waiving a right to be informed about all medical conditions – even life-threatening ones – and may also be signing away a chance at receiving state-of-the-art medical treatment. This safeguard is necessary to ensure that, in a situation of extreme helplessness, a research subject, qua study participation alone, should not be worse off than someone not participating in research. A comparable situation outside a research context might arise, for example, when a physician detects a serious incidental finding during a medical examination of a candidate applying for permanent employment.

In this context, no physician would deny disclosure of such a finding although such an examination does not constitute a physician-patient relationship in the usual sense either.

The option of paying research subjects in exchange for their waiving all rights to information and assistance would make population-based research much more expensive. This does not represent an insurmountable obstacle. Rather, the very fact that large-scale epidemiologic studies using state-of-the-art imaging technology are already very expensive may justify the extra expenditure, as it would eliminate the selection bias resulting from the disclosure of incidental findings. Financial incentives are already widely used to recruit subjects for clinical trials that do not directly benefit them, and there appears to be no reason why volunteers in population-based research, from which they do not derive any personal benefits either, should be at a disadvantage compared with the participants of clinical trials. The question of what constitutes adequate payment for research participants is the subject of ongoing debate (Phillips 2011).

On the other hand, if researchers offer cash payments in exchange for study participants agreeing to waive their rights to be informed and provided with medical assistance, they run the risk of attracting individuals in poor economic circumstances. This also produces selection bias (albeit a different kind of selection bias) and subverts the reason for paying subjects in the first place – to ensure a representative sample. Moreover, payment of research subjects – in conjunction with the need to recruit large study populations – may lead to the exploitation of individuals in poor financial circumstances. Research ethicists are discussing these concerns in light of the tendency to conduct more clinical research in developing countries (Resnik 2003).

Even if we assume that the concerns regarding cash payments to research subjects are negligible, the amount of public funding required would have to be high enough to morally justify the waiver of the right to be informed and provided with assistance. Such expenditure would only be justified in cases where study validity cannot be ensured by a less expensive alternative that is equally acceptable or preferable in ethical terms. We therefore offer the following approach for serious consideration as a promising alternative and as a means of coming to terms with the ethical problems of incidental findings.

1.4.2 Decision-Making Based on a Classification of Incidental Findings

A second approach to the ethical problems posed by incidental findings emerges when one realizes that it is not necessary to make a categorical decision, i.e., to disclose either all incidental findings or none. There may be incidental findings that should be communicated to subjects and others that need not or should not be revealed. To be ethically sound, decisions regarding the disclosure of incidental findings cannot be made ad hoc but should be based on a set of rational criteria. While radiologic knowledge is required to identify these criteria, they must be

justifiable publicly and meet with broad acceptance. For each finding or type of finding, it is necessary to consider how the risk-benefit potentials for current study subjects and potential future patient generations stand in relation to one another. To this end, it is necessary for researchers to compile an inventory of adequately differentiated findings (see Puls et al. 2010). Below we outline some aspects which we consider important for decision-making and worthy of being taken into account in setting up such an inventory.

- (a) Of central importance is the differentiation between life-threatening conditions and abnormalities that are not life-threatening. An ethical decision about disclosure will have to take into account how serious an abnormality will be for the research subject. A clear-cut decision in favor of disclosure will usually be made when a life-threatening condition is detected. This follows from the duty to provide assistance to a person in danger, from which the researcher can be exempted only by a valid contract with the research subject as outlined above. In the case of MRI studies, scientists must identify imaging features that allow reliable diagnosis of life-threatening abnormalities and distinguish them from features that do not.
- (b) The management of incidental findings must also take into account that the disclosure of a (potentially serious) disease may pose social and economic burdens. Knowledge of a serious disease may have implications for the subject's insurability and employability or suitability for certain jobs. Indirect effects on a subject's life may include restricted ability to achieve professional self-fulfillment, a loss of income, or more limited access to social security insurance. A responsible approach to the management of incidental findings cannot ignore these kinds of potential disadvantages.
- (c) The incidental detection of a serious condition in a research subject can also affect others. Hence, a researcher may have moral and legal responsibilities toward third parties. An incidental finding suggesting that a subject is no longer fit to drive (e.g., an abnormality associated with epileptic seizures) is one such example. Lesions triggering seizures, or epileptogenic foci, can easily be detected by MRI brain scans, and findings of this kind or the detection of a brain tumor may mean a risk to others if the subject is a pilot, crane operator, train driver, or truck driver, for example. In such cases, the decision to disclose the finding affects not only the subject but others who may be put at risk by his or her condition as well. This also poses the question of whether such situations may even put the researcher under an obligation to report the finding to a third party, e.g., an authority, in order to protect other members of society from a potential threat.
- (d) Incidental findings can also have direct implications for family members, e.g., when a genetically transferable condition, such as breast cancer in a young woman, is diagnosed. In such a case, a research subject's offspring is affected by the incidental finding because of the risks of inheriting the disease. The affected children have never consented to participation in the study, and the investigator has no influence on what the study subject communicates to family members.

All of these concerns must be considered in making an ethical decision about which incidental findings should be disclosed and which ones should not. These aspects must be adequately taken into account in establishing a general classification of findings that can be used to decide individual cases and to provide detailed guidance on how to handle the major types of incidental findings. In preparing such a criteria-based inventory, those involved can adequately take the risk-benefit potentials for the affected research subjects and for future patient generations into account. We therefore consider this approach to be superior for dealing with the ethical dilemma posed by the discovery of incidental findings in epidemiologic research. However, the inventory required for this approach to function remains to be established. Moreover, such an inventory must be easy to handle in practice and should provide medical researchers with guidance on how to deal with incidental findings in human subjects research in an ethical manner. Before we can compile such an inventory, we need to determine how this case-by-case approach to the disclosure of incidental findings can accommodate the conflicting interests of individual research subjects on the one hand and future patient generations on the other.

Conclusion

The ethical problems arising from incidental findings in epidemiologic studies do not constitute a narrow or marginal domain of bioethics. Rather, incidental findings are a source of information which – once made available – may have considerable implications for research subjects and their relatives but also for uninvolved third parties. Nevertheless, generally accepted guidelines for dealing with these ethical issues are still lacking for nearly all aspects of this field of application. One reason for this deplorable state of affairs appears to be that the central ethical dilemma underlying these issues has not been rigorously defined.

What we have identified to be the core of the problem is a conflict between a duty of care toward the individual research subject and the need to ensure research validity (especially external validity) by applying the highest methodological standards. Although it appears *prima facie* to be a collision of an ethical norm with a methodological standard, on closer examination, this conflict turns out to be a genuine ethical dilemma. There is, after all, a moral duty to assure a rigorous methodology when engaging in human subjects research. This moral duty does not derive from a moral obligation to perform medical research. Rather, it is sufficient to assume that there are moral principles that should guide an investigator engaging in human subjects research: studies aimed at generating knowledge that can help improve the care of future patients must be conducted with adherence to the most rigorous methodological standards in order to preclude degradation of results, which may be potentially harmful to future patients.

The challenge of the decision, arising from the conflict between the researcher's general moral duty to provide assistance and his or her simultaneous responsibility to guarantee the quality of medical research, directly concerns the researcher's personal responsibility in the ethical-normative sense. This moral dilemma exists regardless of whether the study subjects are the researcher's patients or not. The issues involved in dealing with incidental findings boil down

to the following question: Should the researcher disclose incidental findings, if this is in the interest of the research subject, or is this duty overruled by his or her responsibility to safeguard the external validity of the study results by not disclosing such findings? We have argued that, from an empirical descriptive perspective and regardless of how an individual investigator may decide, this conflict can lead to a situation where it may become impossible or at least difficult to conduct population-based research at all.

Two possible courses of action are available for overcoming the central ethical problem of incidental findings while still avoiding the risk of rendering population-based research altogether impossible. The first approach is to offer cash payments to research volunteers in compensation for them explicitly waiving their right to be informed or to receive assistance should something medically relevant, even life-threatening, be found. This approach has two drawbacks. Offering payment as an incentive for study participation may lead to a selection bias in that it may attract a large proportion of economically destitute research volunteers. Moreover, researchers would run the risk of exploiting the economic need of potential research subjects.

We therefore consider it ethically more acceptable to differentiate between incidental findings that should be disclosed and those that should not. To this end, further research is needed. As a first step, a set of criteria, derived from known incidental findings, should be compiled. As a second step, it would be desirable to develop a general classification of incidental findings that allows researchers to arrive at well-founded decisions regarding disclosure in individual cases. A variety of aspects have to be taken into account in developing such a classification.

References

- Alphs HH, Schwartz BS, Stewart WF et al (2006) Findings on brain MRI from research studies of occupational exposure to known neurotoxicants. *Am J Roentgenol* 187:1043–1047
- Appelbaum PS, Roth LH, Lidz CW, Benson P, Winslade W (1987) False hopes and best data: consent to research and the therapeutic misconception. *Hastings Cent Rep* 17:20–24
- Appelbaum PS, Lidz CW, Grisso T (2004) Therapeutic misconception in clinical research: frequency and risk factors. *IRB* 26:1–8; Correction and clarification: *IRB: Ethics and Human Research* 26:18
- Beauchamp TL, Childress JF (2013) *Principles of biomedical ethics*, 7th edn. Oxford University Press, New York/Oxford
- Booth TC, Jackson A, Wardlaw JM, Taylor SA, Waldman AD (2010) Incidental findings found in “healthy” volunteers during imaging performed for research: current legal and ethical implications. *Br J Radiol* 83:456–465
- Brown DA, Hasso AN (2008) Toward a uniform policy for handling incidental findings in neuroimaging research. *AJNR Am J Neuroradiol* 29:1425–1427
- Brudermanns B (2008) Kardiale MDCT. Hohe Prävalenz von Zufallsbefunden. *Fortschr Röntgenstr* 180:951
- Caughlin SS, Beauchamp TL (1996) *Ethics and epidemiology*. Oxford University Press, New York/Oxford
- Fischer G (2008) Clinical research in vulnerable populations. The legal framework. In: Thiele F, Fegert JM, Stock G (eds) *Clinical research in minors and the mentally ill*. Europäische Akademie, Bad Neuenahr-Ahrweiler, pp 63–75

- Fleischman AR, Collogan LK (2008) Research with children. In: Emanuel EJ, Grady C, Crouch RA, Lie RK, Miller FG, Wendler D (eds) *The Oxford textbook of clinical research ethics*. Oxford University Press, Oxford/New York, pp 446–460
- Freedman B (1987) Equipoise and the ethics of clinical research. *N Engl J Med* 317:141–145
- Frey RG, Wellman CH (2003) *A companion to applied ethics*. Blackwell, Malden/Oxford
- Fuchs M, Heinemann T, Heinrichs B, Hübner D, Kipper J, Rottländer K, Runkel T, Spranger TM, Vermeulen V, Völker-Albert M (2010) *Forschungsethik. Eine Einführung*. J.B. Metzler, Stuttgart/Weimar
- Gert B, Culver CM, Clouser KD (2006) *Bioethics: a systematic approach*, 2nd edn. Oxford University Press, New York/Oxford
- Gupta SN, Belay B (2008) Intracranial incidental findings on brain MR images in a pediatric neurology practice: a retrospective study. *J Neurol Sci* 264:34–37
- Heinemann T, Hoppe C, Listl S, Spickhoff A, Elger CE (2007) Zufallsbefunde bei bildgebenden Verfahren in der Hirnforschung: Ethische Überlegungen und Lösungsvorschläge. *Dtsch Ärztebl* 104:A-1982/B-1748/C-1684
- Heinemann T, Hoppe C, Weber B, Elger C (2009a) Ethically appropriate handling of incidental findings in human neuroimaging research. *Clin Neuroradiol* 19:242–243
- Heinemann T, Hoppe C, Weber B, Spickhoff A, Listl F, Kipper J, Rottländer K, Schmetz M, Gogolok S, Lehmacher K (2009b) Ethisch angemessener Umgang mit Zufallsbefunden bei bildgebenden Verfahren in der Hirnforschung – Leitlinienvorschlag (19 June 2009). http://www.psychologie.hu-berlin.de/institut/intra/ethik/Leitlinie%20Zufallsfunde/at_download/file. Accessed 15 July 2013
- Heinrichs B (2011) A new challenge for research ethics: incidental findings in neuroimaging. *Bioethical Inq* 8:59–65
- Hens K, Nys H, Cassiman JJ, Dierickx K (2011) The return of individual research findings in paediatric genetic research. *J Med Ethics* 37:179–183
- Hentschel F, Klix WE (2006) Management inzidenter Befunde in der bildgebenden Diagnostik und Forschung. *Fortschr Neurol Psychiatr* 74:651–655
- Hentschel F, von Kummer R (2009) Response of the German Society of Neuroradiology to the guideline “Ethically appropriate reaction to incidental imaging findings in brain research”, suggested by Thomas Heinemann, Institut für Wissenschaft und Ethik, and Christian Hoppe, Klinik für Epileptologie, Universität Bonn, Germany, on January 9, 2009. *Clin Neuroradiol* 19:108–110
- Hoffmann M (2013) Two basic ethical problems of incidental findings in population-based, non-intervening magnetic resonance imaging (MRI) research. *J Eval Clin Pract* 19:427–432
- Hoffmann M, Schöne-Seifert B (2009) Equipoise – ein Kriterium für die ethische Zulässigkeit klinischer Studien? In: Boos J, Merkel R, Raspe H, Schöne-Seifert B (eds) *Nutzen und Schaden aus klinischer Forschung am Menschen. Abwägung, Equipoise und normative Grundlagen*. Deutscher Ärzte Verlag, Cologne, pp 53–79
- Hoffmann M, Schöne-Seifert B (2010) Potenziell eigennützige Forschung an Kindern: Kriterien ethischer Zulässigkeit. In: Marckmann G, Niethammer D (eds) *Ethische Aspekte der pädiatrischen Forschung*. Deutscher Ärzte Verlag, Cologne, pp 19–35
- Hoggard N, Darwent G, Capener D, Wilkinson ID, Griffiths PD (2009) The high incidence and bioethics of findings on magnetic resonance brain imaging of normal volunteers for neuroscience research. *J Med Ethics* 35:194–199
- Hübner D (2003) Gibt es eine Pflicht zur medizinischen Forschung? *Allgemeine Z Philosophie* 28:21–50
- Illes J, Desmond JE, Huang L et al (2002) Ethical and practical considerations in managing incidental findings in functional magnetic resonance imaging. *Brain Cogn* 50:358–365
- Illes J, Rosen CA, Huang L et al (2004) Ethical consideration of incidental findings on adult brain MRI in research. *Neurology* 62:888–890
- Illes J, Kirschen MP, Edwards E et al (2006) Incidental findings in brain imaging research. *Science* 311:783–784

- Katzman GL, Dagher AP, Patronas NJ (1999) Incidental findings on brain magnetic resonance imaging from 1000 asymptomatic volunteers. *JAMA* 282:36–39
- Kesselring D (2009) Gesundheitscheck zum Nulltarif. *Ostsee-Zeitung* 17 Aug 2009, 3
- Kirschen MP, Jaworska A, Illes J (2006) Subjects' expectations in neuroimaging research. *J Magn Reson Imaging* 23:205–209
- Langanke M, Erdmann P (2011) Die MRT als wissenschaftliche Studienuntersuchung und das Problem der Mitteilung von Zufallsbefunden. Probandenethische Herausforderungen. In: Theißen H, Langanke M (eds) *Tragfähige Rede von Gott. Festgabe für Heinrich Assel zum 50. Geburtstag am 9. Februar 2011*. Verlag Dr. Kovac, Hamburg, pp 197–240
- Macklin R (2004) *Double standards in medical research in developing countries*. Cambridge University Press, Cambridge/New York
- Maio G (2002) *Ethik der Forschung am Menschen*. Frommann-Holzboog, Stuttgart-Bad Cannstatt
- Merkel R (2003) Nichttherapeutische klinische Studien an Einwilligungsunfähigen: Rechtsethisch legitim oder verboten? In: Bernat E, Kröll W (eds) *Recht und Ethik der Arzneimittelforschung*. Manz, Vienna, pp 171–206
- Miller FG, Brody H (2003) A critique of clinical equipoise. *Therapeutic misconception in the ethics of clinical trials*. *Hastings Cent Rep* 33:19–28
- Miller FG, Brody H (2007) Clinical equipoise and the incoherence of research ethics. *J Med Philos* 32:151–165
- Phillips TB (2011) A living wage for research subjects. *J Law Med Ethics* 39:243–253
- Puls R, Hamm B, Hosten N (2010) MRT ohne Radiologen – ethische Aspekte bei bevölkerungs-basierten Studien mit MR-Untersuchungen. *Fortschr Röntgenstr* 182:469–471
- Rangel EK (2010) The management of incidental findings in neuro-imaging research: framework and recommendations. *J Law Med Ethics* 38:117–126
- Resnik DB (2003) Exploitation in biomedical research. *Theor Med* 24:233–259
- Schäffer K (1996) Planung von Stichprobenerhebungen. In: Erdfelder E, Mausfeld R, Meiser T, Rudinger G (eds) *Handbuch Quantitative Methoden*. Psychologie Verlags Union, Weinheim, pp 23–35
- Schleim S, Spranger T, Urbach H, Walter H (2007) Zufallsfunde in der bildgebenden Hirnforschung. Empirische, rechtliche und ethische Aspekte. *Nervenheilkunde* 26:1041–1045
- Schmücker R (2007) Illegal, aber legitim? In: Schüttauf K, Bruder Müller G (eds) *Globalisierung – Probleme einer neuen Weltordnung*. Königshausen & Neumann, Würzburg, pp 75–93
- Schmücker R (2013) Zufallsbefunde – was gebietet die Menschenwürde? In: Joerden JC, Hilgendorf E, Thiele F (eds) *Menschenwürde und Medizin. Ein interdisziplinäres Handbuch*. Duncker & Humblot, Berlin, pp 949–981
- Squire P (1988) Why the 1936 Literary Digest poll failed. *Public Opin Q* 52:125–133
- United States Department of Health and Human Services (DHHS), 45 Code of Federal Regulations (CFR) § 46, revised 23 June 2005. <http://www.hhs.gov/ohrp/documents/OHRPRegulations.pdf>. Accessed 17 Oct 2011
- Van der Lugt A (2009) Incidental findings on brain magnetic resonance imaging. *BMJ* 339:522–523
- Veatch RM (2007) The irrelevance of equipoise. *J Med Philos* 32:167–183
- Vernooij MW, Ikram MA, Tanghe HL et al (2007) Incidental findings on brain MRI in the general population. *N Engl J Med* 357:1821–1828
- Wilfond BS, Carpenter KJ (2008) Incidental findings in pediatric research. *J Law Med Ethics* 36:332–340
- Wolf SM, Lawrenz FP, Nelson CA, Kahn JP et al (2008) Managing incidental findings in human subjects research: analysis and recommendation. *J Law Med Ethics* 36:219–248
- Woodward CI, Toms AP (2009) Incidental findings in “normal” volunteers. *Clin Radiol* 64:951–953

Henry Völzke

2.1 Introduction

Epidemiologic research is aimed at estimating the prevalence and incidence of risk factors and diseases and at identifying the complex associations that exist among them. A central approach used by epidemiologists is to observe the evolution of both risk factors and diseases over time.

In a classic cohort study, investigators compile baseline data on risk factors pertinent to the questions they seek to answer and relate them to the later occurrence of diseases and to mortality. A case in point is the Framingham Heart Study, which began in 1948 and provided the data that led to the identification of an association between serum lipid levels and the risk of developing coronary heart disease later in life (Kannel et al. 1964).

With the technical advances made over the last decades, imaging modalities have gained an increasingly important role in clinical routine and in epidemiologic research. In epidemiologic studies, imaging examinations are performed to diagnose clinical diseases and identify subclinical conditions. The methods used include photography, ultrasound examinations, and MR and CT imaging.

2.1.1 Diagnosis of Clinical Disease

Health-related data obtained by interview or questionnaire often have limited validity. Both acute and chronic conditions may be asymptomatic, or signs and symptoms are overlooked because they are mild or because an individual's perception is reduced or distorted. In such cases, imaging modalities provide objective and independent evidence of prior or existing diseases. For instance, MR imaging will detect

H. Völzke
Institute for Community Medicine, Study of Health in Pomerania (SHIP)/
Clinical-Epidemiological Research, University Medicine Greifswald,
Walther-Rathenau-Straße 48, Greifswald 17487, Germany
e-mail: voelzke@uni-greifswald.de

brain lesions persisting after a stroke or a myocardial scar secondary to a silent myocardial infarction.

2.1.2 Detection of Subclinical Abnormalities

Subclinical changes on MR images are not diseases but may point to beginning or ongoing disease processes that would otherwise go unnoticed. In the development of diseases, such subclinical changes are intermediate between risk factors and outcome, which is why they are often considered to have a high predictive value for the development of clinical disease and are therefore of interest as surrogate parameters.

Imaging can detect morphologic and functional subclinical changes. Morphologic changes are apparent on individual images, while dysfunction requires a series of images, obtained in some cases after provocation. Examples of relevant subclinical alterations include an increase in carotid wall thickness (Chambless et al. 2004) and reduced flow-mediated vasodilation (Shimbo et al. 2007). These can be detected by ultrasound and are considered to be indicators of an increased risk of atherosclerosis. Carotid wall thickness is measured with the subject at rest and is a morphologic finding, while the degree of loss of flow-mediated vasodilation is a functional finding and is estimated during a brief high-flow state in the brachial artery following temporary ischemia.

2.2 Imaging in the Study of Health in Pomerania

The *Study of Health in Pomerania* (SHIP) is a population-based study conducted in the northeast of Germany (Völzke et al. 2011). Its goal is to estimate the prevalence and incidence of risk factors and clinical diseases in the general population of the German Federal State of Mecklenburg-Vorpommern, elucidating the complex relationships among risk factors, subclinical findings, and clinical diseases. A distinctive feature of SHIP is that it does not focus on a specific organ or organ system but instead aims at characterizing health and disease in a very comprehensive way.

SHIP investigators have been using imaging modalities for detecting subclinical abnormalities since 1997 when the study began. In the baseline examination (SHIP-0), ultrasound was used to measure carotid wall thickness and to detect atherosclerotic plaque; to determine thyroid size and to identify thyroid nodules; to evaluate cardiac valve function, left ventricular mass, and pump function; and to diagnose fatty liver and gallstones. Additional imaging modalities were introduced for 5-year follow-up examinations (SHIP-1). These included measurement of flow-mediated vasodilation as well as photography and sonographic examinations to identify varicose veins below the knee.

The spectrum of imaging modalities was expanded even further for the most recent investigations – the 11-year follow-up study of the first SHIP cohort (SHIP-2) and the baseline examinations of a second, independent SHIP cohort (SHIP-Trend).

The additional procedures include photography to document and quantify changes in the ocular fundus and ultrasound to estimate bone stiffness and to identify morphologic changes in the kidneys and pancreas.

MR imaging is staff-intensive and expensive, which is why it is rarely used as an imaging tool in population-based research. All current studies making use of this imaging modality do so for dedicated examinations of individual organs or body regions. Examples include MR brain scans in the Rotterdam Study (Vernooij et al. 2007), cardiac MR imaging in the Multi-Ethnic Study of Atherosclerosis (Nasir et al. 2007), and MR spectroscopy for quantifying hepatic fat content in the Dallas Heart Study (Romeo et al. 2008). SHIP-2 and SHIP-Trend are the first population-based studies using whole-body MR imaging on a large scale (Hegenscheid et al. 2009). The use of whole-body MR imaging in epidemiology has considerable scientific potential but also presents great challenges in terms of quality assurance and application of ethical standards.

2.3 Scientific Potential of Whole-Body MR Imaging Examinations in Population-Based Research

The large-scale use of whole-body MR imaging in a population-based cross-sectional study provides a wealth of data for answering a multitude of scientific questions of high clinical relevance. These include the establishment of reference values for MR examinations, prevalence estimates, and association studies.

Radiologists performing clinical MR examinations currently have to rely on reference values that, in most cases, have been defined in small, unrepresentative samples. For most organ systems, data from population-based MR imaging studies are lacking. Hence, available reference values are probably prone to considerable selection bias. SHIP-Trend data will allow generation of MR reference values for the volumetric examination of different organs (e.g., kidney, liver, spleen, visceral fat, prostate, and male gonads) and organ parts (e.g., brain structures and right ventricle), for the width of arteries (e.g., aorta and pulmonary arteries), and for functional parameters (e.g., parameters of right and left ventricular function, pulse wave velocity, and aortic stiffness).

The SHIP-Trend examinations, which are representative of the general population, are expected to provide very accurate estimates of the prevalence of different subclinical conditions and clinical diseases. One goal is to estimate the MR-based prevalence of suspicious lesions in the brain, female breast, liver, kidneys, uterus, ovaries, and prostate. In addition, there is also great scientific and practical interest in obtaining data on the prevalence of nontumorous conditions detected by MR imaging. These include cerebral microangiopathy (white matter lesions), intracranial aneurysms and arteriovenous malformations, left ventricular hypertrophy, systolic and diastolic dysfunction of the left ventricle, silent myocardial infarction, fatty liver, polycystic ovaries, uterine fibroids, disc herniation, and cartilage disease.

Whole-body MR imaging findings provide a variety of options for conducting association studies. In conjunction with the genome-wide data available for the SHIP subjects (Vasan et al. 2009), the findings can be used to identify variants associated with organ shapes and sizes or subclinical abnormalities. Analyzing MR imaging findings in conjunction with data from interviews and questionnaires, we can identify possible relationships between physical complaints and imaging findings such as between subjective back pain and the MR appearance of the spine or between mental disorders and structural cerebral abnormalities. Cardiopulmonary data derived from spiroergometry or the diagnostic evaluation of sleep apnea can be correlated with cardiac MR parameters.

Systematic follow-up MR examinations will considerably increase the scientific value of the data, allowing determination of the incidence and progression of subclinical changes as well as evaluation of the prognostic significance of subclinical MR imaging abnormalities for the development of morbidities and mortality. Finally, longitudinal MR imaging data on the evolution of risk factors, subclinical abnormalities, and clinical diseases will also help us identify causal relationships.

2.4 Quality Assurance for Whole-Body MR Imaging in Population-Based Research

Epidemiologic research is conducted in large populations. This means that, as a rule, several investigators perform the examinations to collect the data within a reasonable period of time. To ensure internal validity of the study data, measures must be implemented to minimize variability among the investigators involved. This point is of particular concern when investigating subjects scheduled to undergo serial examinations over a long time in longitudinal cohort studies. Here, quality assurance measures are crucial to ensure that similar methodology be used for baseline and follow-up examinations.

Ensuring high external validity of data is another important function of quality assurance. Here, internationally accepted, standardized methods must be used to ensure that the data can be compared with the results of other studies, e.g., when defining reference values or estimating regional prevalence disparities.

This is why the degree of standardization is often much higher in epidemiologic research compared with examinations performed under routine clinical conditions (Hoffmann et al. 2005). Epidemiologic researchers ideally use standardized and validated protocols that have proven useful in earlier clinical or epidemiologic studies. For all examinations, standard operating procedures are available and must be read by all investigators. Investigators need to be certified before they perform examinations on research subjects. To be certified for reading whole-body MR imaging datasets in SHIP, radiologists must correctly interpret a set of 100 images, showing good agreement with the gold standard (defined as a kappa coefficient of at least $\kappa=0.9$). For continuous data, such as volume measurements, the statistical analysis is performed using Bland-Altman plots. The mean bias for intra- and interobserver variability must not exceed 5 %, and two standard deviations of the

bias must not exceed 25 %. The skills of technicians performing MR examinations of study subjects are verified by physician investigators before and during the phases of data acquisition. MR device performance in terms of resolution and geometric distortion is monitored by daily phantom measurements. Software updates are not allowed during the study period unless absolutely necessary for proper functioning. An external scientific advisory board monitors data quality during the acquisition phase.

In SHIP, MR images are viewed and analyzed in three steps. First, a physician investigator scans the images during the examination and, on the basis of a list of 15 items, looks for signs of an acute condition (ischemic infarction, hemorrhage, or abscess). In the second step, clinical scientific reading is carried out independently by two certified physicians. The scientific reading is performed in a standardized manner using a list of 200 findings and is completed within 2 weeks of the examination. All discrepancies are resolved by a certified senior physician. The third and final step is a scientific analysis of the datasets and mainly involves quantitative measurements of signal intensity differences, identification of anatomic variants, and volume measurements of structures of interest. Most of these measurements are performed using computer-assisted algorithms, either available software tools, algorithms modified for the purpose of SHIP, or homemade software.

2.5 Ethical Issues in Population-Based Research Using Whole-Body MR Imaging

Disclosure of MR findings is a central concern in the debate over ethical issues in human subjects research. The moral dilemma confronting the researcher is illustrated by the two extreme positions taken in this debate: on the one hand, it is argued that the researcher-subject relationship is different from the physician-patient relationship (Heinemann et al. 2007). While physicians have a duty of care, requiring them to inform their patients, researchers are only bound to the rules of Good Scientific Practice and are thus not required to communicate incidental findings to subjects. The opposing view holds that the high-quality interpretation of MR images requires the expertise of a physician and that physicians – because of their professional code of ethics – are obliged to communicate relevant findings to their research subjects. This is the case, for instance, when imaging reveals signs of early disease that might be prevented from progressing if adequate diagnostic and therapeutic measures are initiated (von Kummer 2007). In the final analysis, this position would mean that research subjects, as autonomous persons, are entitled to be informed about all findings.

Neither of these two extreme views is reasonable in the context of an epidemiologic study conducted to gain insights that are expected to be valid for the general population while at the same time elucidating the natural evolution of subclinical disorders for correlation with the later manifestation of clinical disease.

A policy of consistent nondisclosure would have the advantage of enabling investigators to observe the natural progression of abnormalities without possible

effects of treatment. On the other hand, only a few participants of a population-based study would be willing to undergo an MR examination under these conditions, severely compromising the representativeness of the results for the population under investigation.

However, disclosing all findings would not truly resolve all ethical issues confronting physician investigators. Since whole-body MR imaging has not yet been validated for screening, the results disclosed to subjects would include many false-positive findings. In addition, if true-positive findings are disclosed although their clinical relevance for the affected person is questionable or there is no evidence-based strategy for diagnostic and therapeutic management, physician investigators are merely passing on their medical responsibility to their study subjects. What must also be considered is that it is well established that an individual may develop symptoms after having been informed about a diagnosis or that the disclosure of an incidental finding may lead to unnecessary diagnostic and therapeutic measures – which may be invasive and come with risks of complications. The problem is even further exacerbated by the fact that, in population-based research, investigators are not aware of signs and symptoms or other clinical data that might help them in evaluating the relevance of an abnormality detected by MR imaging. To adequately deal with these issues in the setting of a study investigating the evolution of MR findings, researchers must carefully weigh the pros and cons in each case before communicating any MR findings.

2.5.1 Ethical Considerations in Handling Whole-Body MR Imaging in SHIP

SHIP is the first population-based study using whole-body MR imaging. Before beginning the actual examinations, investigators discussed in depth the ethical concerns posed by incidental MR findings. The main concern in establishing a feasible procedure for dealing with the findings of whole-body MR imaging in SHIP was to adequately reconcile the aim of ensuring research integrity with the aim of protecting the interests of research subjects. No claim is being made that the solution proposed in the setting of this study should be applied to other study settings.

In the consent procedure, SHIP participants can declare that they do not wish to be informed about any MR findings. However, our initial experience suggests that this seems to be a minor concern in a population-based study: only two of the first 3,000 SHIP subjects undergoing MR imaging made use of their right not to know. Moreover, all subjects are informed that this right can be overruled when the examination reveals a condition that might endanger others (e.g., risk of fainting in drivers).

The possible disadvantages of being informed about unexpected MR findings are explained in detail to subjects during the consent process. This question is addressed both in the written information on the study the subjects receive and during the in-person explanation of the study. The possible problems of disclosing MR imaging findings are illustrated using incidental detection of herniated discs as an example. Based on this example, the investigator explains that there is still no definitive

evidence that mild forms of a slipped disc contribute to back pain, but that being informed about such an MR finding can actually trigger or exacerbate symptoms or lead to unnecessary medical procedures with possible side effects. Despite these concerns, subjects are informed that, if they do have symptoms, the MR images acquired in the study can be made available to their treating physician for clinical review.

All abnormal MR findings in SHIP are presented to an Advisory Board of radiologists, clinicians, and epidemiologists, who discuss the cases, weighing the interests of the research against the interests of the subjects, and jointly decide whether or not to disclose the findings. Each case settled by the board in this way establishes a precedent for handling similar cases in the future. Despite the high threshold for disclosing incidental MR findings, about one in four subjects in SHIP are confronted with MR findings that require follow-up measures.

How this disclosure policy affects subjects' quality of life and their willingness to undergo follow-up examinations in the setting of SHIP is currently being investigated in a telephone survey. We hypothesize that, while disclosure of an unexpected MR finding will cause temporary distress, the subsequent diagnostic workup will have little or no impact on subjects' willingness to continue participating in SHIP follow-up examinations. This hypothesis is supported by initial results of a pilot study. Ongoing research is also investigating how disclosure of findings and possible interventions may alter the natural evolution of subclinical abnormalities.

References

- Chambless LE, Heiss G, Shaha E, Earp MJ, Toole J (2004) Prediction of ischemic stroke risk in the Atherosclerosis Risk in Communities Study. *Am J Epidemiol* 160:259–269
- Hegenscheid K, Kuhn JP, Volzke H, Biffar R, Hosten N, Puls R (2009) Whole-body magnetic resonance imaging of healthy volunteers: pilot study results from the population-based SHIP study. *Rofo* 181:748–759
- Heinemann T, Hoppe C, Listl S, Spickhoff A, Elger CE (2007) Zufallsbefunde bei bildgebenden Verfahren in der Hirnforschung: Ethische Überlegungen und Lösungsvorschläge. *Dtsch Arztebl* 104:A-1982/B-1748/C-1684
- Hoffmann W, Latza U, Terschuren C (2005) Guidelines and recommendations for ensuring Good Epidemiological Practice (GEP) – revised version after evaluation. *Gesundheitswesen* 67:217–225
- Kannel WB, Dawber TR, Friedman GD, Glennon WE, McNamara PM (1964) Risk factors in coronary heart disease. An evaluation of several serum lipids as predictors of coronary heart disease; the Framingham Study. *Ann Intern Med* 61:888–899
- Nasir K, Tsai M, Rosen BD, Fernandes V, Bluemke DA, Folsom AR, Lima JA (2007) Elevated homocysteine is associated with reduced regional left ventricular function: the Multi-Ethnic Study of Atherosclerosis. *Circulation* 115:180–187
- Romeo S, Kozlitina J, Xing C, Pertsemlidis A, Cox D, Pennacchio LA, Boerwinkle E et al (2008) Genetic variation in PNPLA3 confers susceptibility to nonalcoholic fatty liver disease. *Nat Genet* 40:1461–1465
- Shimbo D, Grahame-Clarke C, Miyake Y, Rodriguez C, Sciacca R, Di Tullio M, Boden-Albala B et al (2007) The association between endothelial dysfunction and cardiovascular outcomes in a population-based multi-ethnic cohort. *Atherosclerosis* 192:197–203

- Vasan RS, Glazer NL, Felix JF, Lieb W, Wild PS, Felix SB, Watzinger N et al (2009) Genetic variants associated with cardiac structure and function: a meta-analysis and replication of genome-wide association data. *JAMA* 302:168–178
- Vernooij MW, Ikram MA, Tanghe HL, Vincent AJ, Hofman A, Krestin GP, Niessen WJ et al (2007) Incidental findings on brain MRI in the general population. *N Engl J Med* 357:1821–1828
- Völzke H, Alte D, Schmidt CO, Radke D, Lohr R, Friedrich N, Aumann N et al (2011) Cohort profile: the study of health in Pomerania. *Int J Epidemiol* 40:294–307
- von Kummer R (2007) Zufallsbefunde bei bildgebenden Verfahren in der Hirnforschung. Ethische Überlegungen und Lösungsvorschläge: Ignoranz als ethisches Prinzip in der Medizin? *Dtsch Arztebl* 104:A-3186/B-2803/C-2705

Harald H. Quick

3.1 Introduction

Magnetic resonance imaging (MRI) examinations have traditionally been confined to regions of the body that are covered by the field of view of the MR imager, typically less than 50 cm in the long axis. This coverage permits imaging of an individual organ or a single body region. There are clinical situations, however, in which imaging of a larger part of the body is desirable – diagnostic evaluation of the spine or MR angiography (MRA) of the arteries of the pelvis and legs, for example. The demands are even greater when it comes to whole-body MRI screening. Screening examinations may require evaluation of the entire vascular system (whole-body MRA) or of the entire body volume (whole-body MRI). Before imaging of the entire body was possible, strategies for extending the effective imaging range first had to be devised. This was accomplished by developing multistation techniques, which involve the serial acquisition of individual body regions. The individual datasets overlap slightly and are combined to generate a composite whole-body image. Further technical advances have since enabled the acquisition of seamless three-dimensional (3D) whole-body MRI datasets using continuous table movement techniques.

H.H. Quick
Erwin L. Hahn Institute for MR Imaging,
University of Duisburg-Erlangen,
Arendahls Wiese 199,
Essen, 45141, Germany
e-mail: harald.quick@uni-due.de

The aim of whole-body MRI screening is to rapidly and efficiently image the patient from head to toe for a comprehensive diagnostic evaluation of the entire body or large parts of it with different image contrasts in the shortest possible time. At the same time, whole-body protocols should yield images with good spatial resolution and a minimum of artifacts. This chapter provides an overview of the hardware and software requirements for performing whole-body MRI and presents the most recent technical developments.

3.2 Components of an MRI System

The effective imaging region (field of view (FOV)) of an MRI system depends crucially on three hardware components and their performance parameters: (1) the main magnet providing a uniform magnetic field over the whole imaging volume, (2) the gradient system providing linearity over the imaging volume, and (3) the radiofrequency (RF) system providing RF signal homogeneity and signal sensitivity over the imaging volume. Whole-body MRI places exacting demands on these three major hardware components of the MR imager.

3.2.1 The Main Magnet

In general, whole-body MRI requires that the magnet for generating the main field have high enough field strength to be able to provide enough basic magnetization – which is the prerequisite for achieving a high signal-to-noise ratio (SNR) and good image quality. While whole-body MRI can be performed at 1.0 T, it is better to have at least 1.5 T. Standard clinical MR imagers operating at these field strengths are increasingly being replaced by 3.0-T systems. The main magnetic field should be uniform over the target volume to minimize image distortion and maximize signal homogeneity. The uniform target volume must be large enough to consistently acquire artifact-free and nondistorted images of the entire body. A cylindrical configuration of the main magnet is conducive to all of these requirements and is currently the most frequently used magnet shape in medical MR systems (Figs. 3.1 and 3.2).

3.2.2 The Gradient System

Whole-body MRI also requires a high-performance gradient system, meaning that it should combine a fast slew rate (given in mT/m/ms) with a high gradient amplitude (given in mT/m). These features enable short repetition and echo times (TR and TE), which are needed for fast image acquisition and hence coverage of a large volume in a short period of time. This is an important prerequisite for whole-body MRI to achieve diagnostic image quality within clinically acceptable acquisition



Fig. 3.1 A modern cylindrical 1.5-T whole-body MR imager (Magnetom Aera, Siemens Healthcare Sector, Erlangen, Germany)

times. A short TR is also important to achieve maximum T1 contrast, ensuring high conspicuity of contrast-enhancing vessels against saturated static tissue in MRA. High gradient linearity over a large area is necessary to minimize image distortion, especially at the periphery of the FOV. Again, these requirements are best met if the gradient coils are cylindrical as well (Figs. 3.1 and 3.2).

3.2.3 The Radiofrequency System

The radiofrequency (RF) system should be capable of providing uniform excitation of a large imaging volume. Excitation of the entire target volume with a largely constant flip angle (FA) is crucial for the resulting image contrast. This is accomplished by using the scanner's built-in whole-body RF coils, which are large cylindrical volume coils (Figs. 3.1 and 3.2).

Uniformity across a large volume is also required for signal readout. Here, however, signal sensitivity is somewhat more important than uniformity because it determines inherent image contrast, while nonuniformity merely degrades brightness distribution in the image. Although the large built-in whole-body RF coil

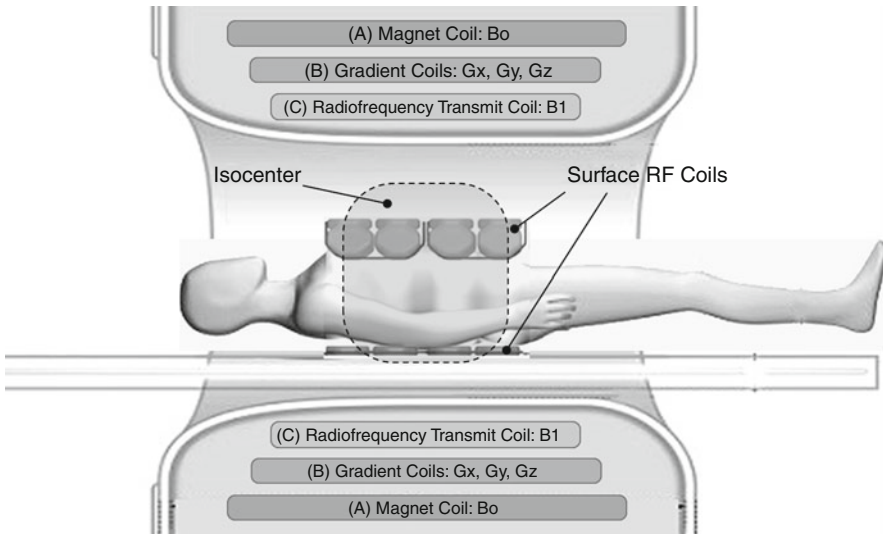


Fig. 3.2 Longitudinal diagram of a cylindrical MR imager. The housing typically contains three types of coil systems (from the outside to the inside): (A) the magnet coil producing the scanner's homogeneous static main magnetic field (B_0) for alignment of magnetic spins; (B) a set of gradient coils to generate spatially varying gradient fields (G_x, G_y, G_z) in all three spatial dimensions for spatial encoding of the MR signal; and (C) the radiofrequency (RF) transmit coil, which generates an RF field (B_1) for inducing the aligned spins inside the patient's body to precess at Larmor frequency. The three electromagnetic coil systems (B_0, G_{xyz}, B_1) are designed to generate an optimal imaging volume in the isocenter, or center of the magnet, where the B_0 and B_1 fields are very uniform and the gradient fields, G_{xyz} , are largely linear. The RF signal response of the excited spins inside the patient is collected by one or several local RF surface coils positioned above and/or below the target anatomy. To obtain good MR images, the target anatomy must be in the isocenter of the magnet. In whole-body MRI, this can be accomplished by using a moving table: the table with the patient is advanced through the bore of the magnet to successively move different body regions into the isocenter

ensures homogeneity across a large volume, signal readout is limited by a moderate SNR. To overcome this limitation, a variety of approaches using RF surface coils have been employed (Fig. 3.2). Surface coils are placed directly on or over the target anatomy and selectively receive signal from nearby tissue. This spatially selective sensitivity improves signal detection from the body part of interest and also confines the contribution of image noise to this small region. In this way, surface coils can improve SNR, which translates into better image quality and spatial resolution. At the same time, however, the small sensitivity range is a major drawback of surface coils. To image a large volume, many coil elements arranged in a phased array are necessary. Phased-array coils combine the high SNR of a local coil with extended coverage. Utilizing the full potential of this technology requires a large number of RF receivers, to which the coil elements are connected either individually or in small groups. This is also a basic prerequisite for the use of parallel imaging techniques.

3.3 From Local to Global Imaging: Toward Stepwise Extension of the Imaging Field

3.3.1 Moving Table Platforms: *SKIP*, *AngioSURF*, and Others

The traditional imaging field of 400–500 mm is clearly too small for a comprehensive angiographic evaluation of the vascular system or for a comprehensive search for metastases. One option for extending the effective FOV is to perform imaging in a series of discrete steps, moving the scanner table between acquisitions so as to shift the position of the patient relative to the imaging field (Ho et al. 1998, 1999; Wang et al. 1998; Meaney et al. 1998; Ruehm et al. 2000a, 2000b, 2001; Leiner et al. 2000, 2004; Goyen et al. 2001; Busch et al. 2001; Huber et al. 2003). This technique, known as multistation imaging, allows step-by-step scanning of different body regions in the magnet's isocenter, which is defined and limited by field homogeneity, gradient linearity, and RF signal excitation and readout. While the individual stations must meet the same requirements as in conventional MRI, the multistation technique extends the overall scope of the examination by enabling successive imaging of different parts of the patient's body.

Multistation imaging requires a table moving relative to the isocenter of the magnet. The maximum table range directly determines the imaging range or how much of the patient's body can be successively moved through the scanner's effective FOV. The automatic patient tables of older scanners have a maximum range of less than 150 cm, which is sufficient for peripheral MRA of the pelvis and legs. For head-to-toe imaging, however, it is necessary to reposition the patient at least once between acquisitions: positioning the patient head-first for the first part of the examination and feet-first for the second part, or vice versa.

True whole-body MRI, the next step in the development, is no longer hampered by table range limitations and avoids the need for repositioning the patient during a full-body examination. Its technical implementation was made possible by important contributions from several independent study groups working in this field. The table range limitations were overcome by the advent of manually moved table platforms such as *SKIP* (Stepping Kinematic Imaging Platform, Magnetic Moments, Bloomfield, MI, USA) (Shetty et al. 2002) and *AngioSURF* (Angiographic System for Unlimited Rolling Field-of-views, MR-Innovation GmbH, Essen, Germany) (Ruehm et al. 2000a, b; Goyen et al. 2002; Winterer et al. 2003). These new platforms mark the beginning of true whole-body MRI, extending the range of motion to approx. 200 cm and enabling serial whole-body imaging in five or six stations. The problem of ensuring adequate signal readout over this extended imaging range was elegantly solved by using a stationary pair of RF coils in the isocenter of the magnet (Fig. 3.3). One coil of this pair is integrated in the patient table, contributing signal from the posterior body regions. The second coil, mounted on a coil glider, is height-adjustable and is held in position in the isocenter of the magnet by two flexible arms. This allows the coil to adjust to the body contour as the patient is being moved through the bore of the magnet for optimal signal readout from anterior body regions. The patient is positioned on an MR-compatible rolling table platform, allowing rapid

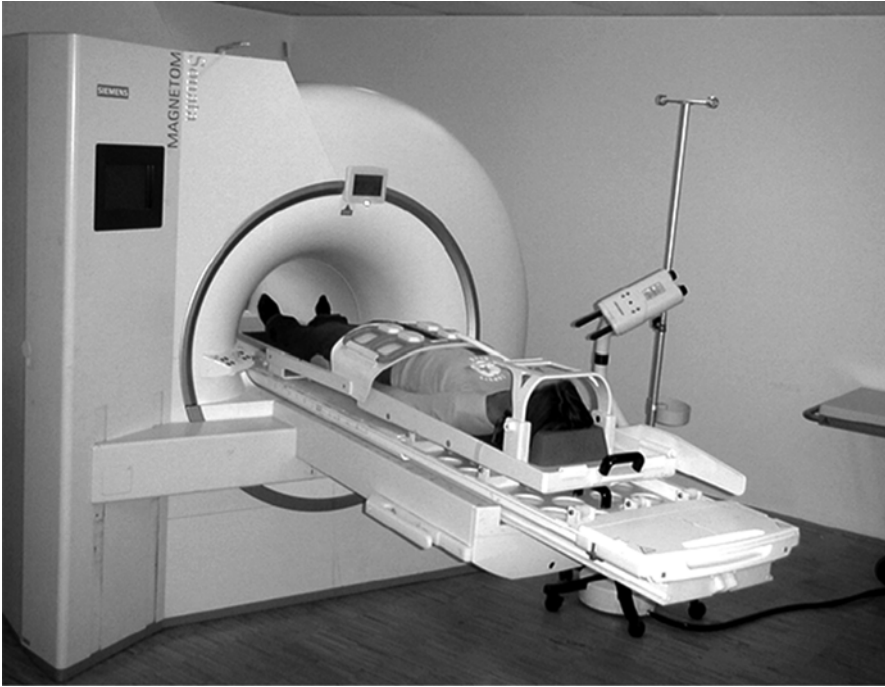


Fig. 3.3 *AngioSURF* table platform (MR-Innovation GmbH, Essen, Germany) mounted on top of the original patient table of a Siemens Sonata MR scanner. A patient is positioned feet first. The picture shows the table and coil positions for imaging the third of five stations; for better illustration, the table is shown moved out of the bore; during image acquisition, the height-adjustable coil glider is in the isocenter of the magnet. For a whole-body MRI examination from head to toe, five adjacent 3D datasets are sequentially acquired by moving the table platform manually between two stations, bringing the patient into the desired position for each acquisition. The table platform advances the patient between a stationary RF receive coil positioned posteriorly and a second receive coil positioned anteriorly. The latter is mounted on the coil glider, allowing it to adjust to the patient's habitus. In this way, the distance between the patient and the readout coil is always very small, ensuring optimal SNR and image quality. A safety bar protects the patient's face. Using the *AngioSURF* platform, a whole-body MRI examination can be performed quickly and with high image quality

and stepwise advancement of the patient through the main magnet and between the two stationary surface coils (Fig. 3.3). With this RF surface coil setup, an adequate SNR is achieved without the need for completely covering the patient's body with surface coils. This technique has been widely used in clinical whole-body MRA (Shetty et al. 2002; Ruehm et al. 2000a, b; Goyen et al. 2002; Winterer et al. 2003; Quick et al. 2004; Herborn et al. 2004), in whole-body metastasis screening in oncologic patients (Lauenstein et al. 2002a, b; Lauenstein et al. 2004; Ghanem et al. 2004), and in MRI-based screening examinations (Ruehm et al. 2004; Goehde et al. 2005). The phased-array surface coil technology used is also suitable for performing parallel imaging to improve spatial resolution (Quick et al. 2004).

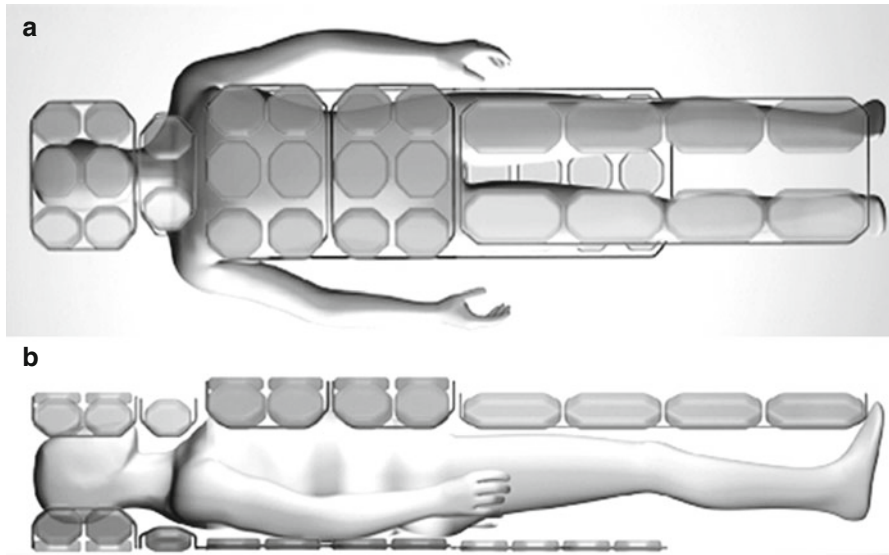


Fig. 3.4 Diagrams of the Tim™ (Total imaging matrix) RF technology (Siemens Healthcare Sector, Erlangen, Germany): top view (a) and lateral view (b). The patient's entire body can be covered with a large number of dedicated RF surface coils. The RF matrix shown in this example allows up to 76 coil elements to be connected to up to 32 independent RF receivers in different modes. Complete coverage of the patient's body with individual RF surface coils in conjunction with motorized table movement over a range of approx. 185 cm enables whole-body image acquisition with good SNR. This technology can also be used for parallel imaging

3.3.2 RF Coils from Head to Toe and Multistation Techniques

Newer generations of MRI scanners increasingly come equipped for whole-body imaging: an automatically moving table with a range of approx. 200 cm, comprehensive solutions for covering the patient's body with a set of dedicated phased-array RF surface coils, and a large number of independent RF receiver channels to process the signals from these coils. With this equipment, it is possible to evenly cover the patient with highly sensitive RF surface coils from head to toe for optimal signal readout from all body regions. All vendors provide their most recent machines with a variety of phased-array RF surface coils for versatile applications in different body regions. Siemens (Healthcare Sector, Erlangen, Germany), for instance, offers an RF system called Tim (Total imaging matrix), which includes up to 76 coil elements and up to 32 readout channels for a table range of 185 cm (Fig. 3.4). Tim includes a variety of dedicated RF coils, which are optimized for individual body regions and integrated into a whole-body RF system. The individual coil elements can be flexibly combined with a large number of RF receivers, allowing excellent exploitation of the potential SNR. Full body coverage with RF readout coils and a table range of approx. 200 cm are the basic hardware requirements for multistation

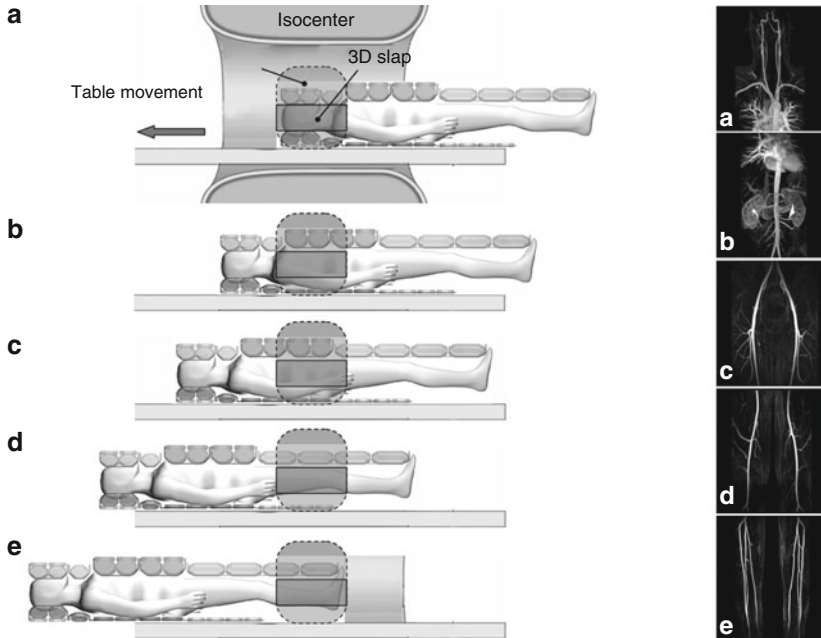


Fig. 3.5 Multistation whole-body MRA. Longitudinal diagram of an MR imager. Following placement of RF surface coils on the patient's body, the head/neck region is positioned in the isocenter of the magnet (a). The coronal 3D slab is positioned within the isocenter. In the course of the examination, the patient is moved through the isocenter in a stepwise fashion, from head to toe. (b–e) Multistation contrast-enhanced MRA is performed by synchronizing acquisition with the administration of the contrast medium bolus in such a way as to time the acquisition of each station with the presence of the contrast medium, chasing the bolus from the aorta to the pelvic and leg arteries and to the feet. In this way, the multistation technique enables imaging of vessels that are too long for assessment with a single conventional FOV (A–E on the right show MR angiograms acquired at each of the five stations). Multistation imaging using a moving table is the technical prerequisite for performing whole-body MRI and MRA

imaging, that is, automatic movement of the table for discontinuous image acquisition at a discrete number of stations (Fig. 3.5).

3.3.3 Software Requirements

In addition to the hardware developments outlined above, multistation imaging techniques would not have been possible without new software for a variety of new tasks: (1) rapid switching of RF coil elements between stations for selective signal readout by the coils at each given station; (2) acquisition of prescans (before the actual examination) to separately optimize and store parameters for each station related to tuning, shimming, specific absorption rate (SAR), and flip angle;

determining these parameters before a whole-body scan is especially important in applications where the imaging window is small and timing is critical (e.g., contrast-enhanced MRA); and (3) capability for separately positioning and angling the image slab for each station and flexibly selecting spatial resolution (matrix, slice thickness). This flexibility is desirable to optimize parameters for the body part being imaged at each station and to make adjustments for differences in individual anatomy. With the new demands arising for the processing of whole-body MRI datasets, image postprocessing has also been taken from local to global. Manufacturers are increasingly offering postprocessing packages (e.g., composer tools) for virtually combining the images from the individual stations to create composite images for easier viewing and interpretation.

3.4 MRI on the Move: Continuous Table Advancement

Multistation techniques have inherent disadvantages: the time necessary for moving the table between successive acquisitions, typically 2–3 s, is not available for imaging. Additional time is lost due to redundant data acquisition, as there is generally some overlap between adjacent stations. Extra time is also needed for restoring basic magnetization. In terms of image quality, the lower signal sensitivity at the edges of individual FOVs can cause inhomogeneities in the composite images, while the geometric distortions resulting from gradient nonlinearities at the edges can cause artifacts at the interfaces of adjacent stations (Fig. 3.6). Many of these limitations impair interpretation, especially at the seams of composite images. These limitations could be overcome with a seamless whole-body 3D dataset of consistent quality that would be processed as a whole during display and interpretation.

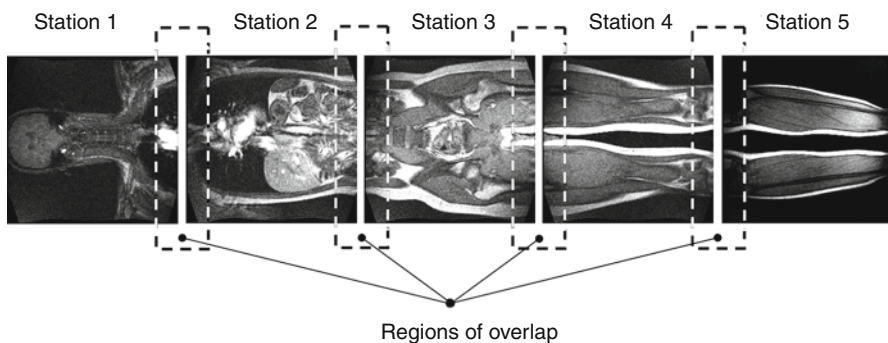


Fig. 3.6 The four or five individual datasets acquired using the multistation moving table technique are postprocessed to generate a composite whole-body image. The diagram illustrates an inherent drawback of this technique: the individual images overlap a few centimeters, meaning that there is redundancy in that approx. 10 % of the image data are acquired twice. Moreover, data acquisition needs to be interrupted to move the patient table to the next station (approx. 2 s). These two limitations reduce imaging efficiency. Finally, gradient nonlinearities at the edges of the individual FOVs can cause discontinuity artifacts at the interfaces of adjacent stations

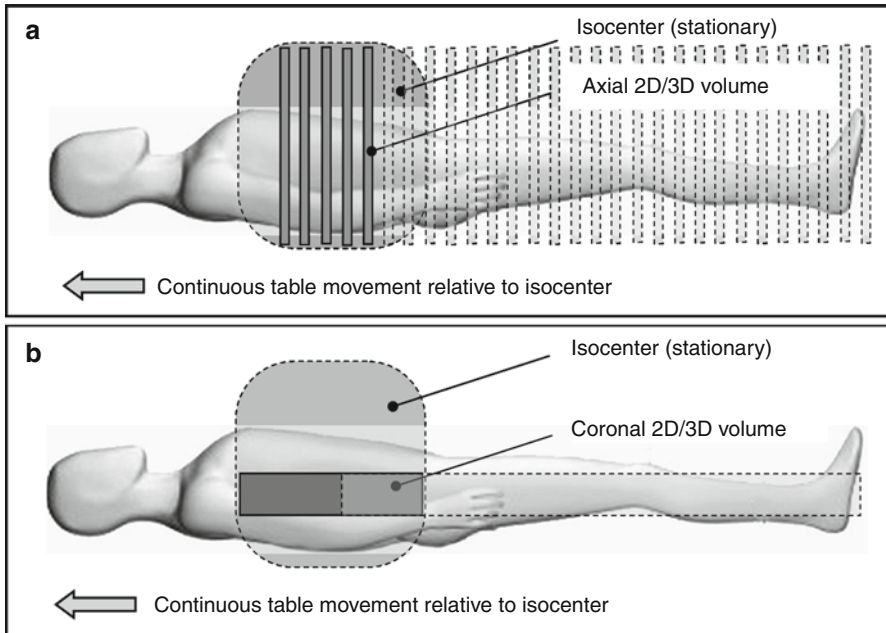


Fig. 3.7 Further development of the multistation technique aims at enabling continuous table movement *during* acquisition of imaging data. The table with the patient on top moves continuously through the isocenter of the magnet while images are being acquired. In this way, seamless 3D datasets of the whole body or large parts of it can be generated. Continuous acquisition can be done in the axial (a) or coronal plane (b). Axial imaging (a) is predominantly used for nonangiographic applications, e.g., in searching for soft tissue metastases. With the simplest version, a rapidly acquired stack of 2D slices is used to reconstruct a 3D whole-body volume. The technique of axial imaging with continuous table movement resembles data acquisition with computed tomography (CT). Imaging in the coronal plane (b) is preferred for MRA as it allows the thickness of the 3D volume (3D slab) to be confined to the anteroposterior extent of the vascular system

Various techniques using a continuously moving table have been proposed and investigated as alternatives to multistation imaging (Fig. 3.7). The simplest approach to imaging during continuous table movement involves the acquisition of fast two-dimensional (2D) axial sequences in the isocenter of the magnet, which are subsequently combined (Johnson et al. 1997; Barkhausen et al. 2001) (Fig. 3.7a). Artifacts are tolerable with this technique as long as table movement is less than the acquired section thickness.

Fast 2D acquisition of axial sections during continuous table movement has some disadvantages. Spatial resolution is limited, and the rather large slice thickness restricts coronal and sagittal reconstruction of the axial source dataset. When this technique was first introduced, only GRE and EPI sequences could be used. Conventional multistation imaging, on the other hand, can be performed with high resolution and the whole range of MR contrasts, but it suffers from the limitations outlined above, most notably time inefficiency and susceptibility to artifacts at the seams. Hence, it would be desirable to have a whole-body MRI technique that combines the advantages of both approaches.

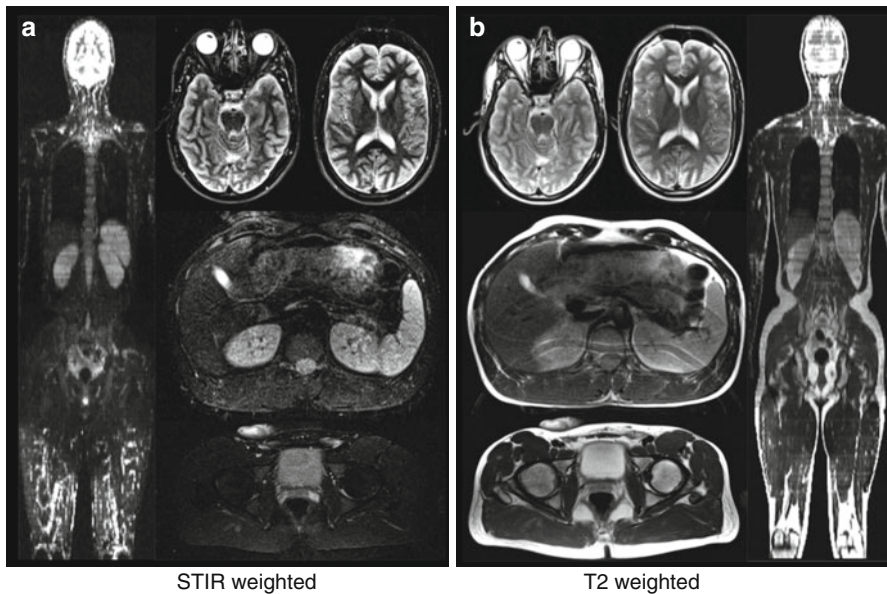


Fig. 3.8 Whole-body MRI using continuous table movement. Images were acquired in the axial plane. Two image contrasts were acquired during table movement: STIR weighting (**a**) and T2 weighting (**b**). Taken together, the axial stacks form a whole-body dataset, which allows coronal reformation (leftmost and rightmost parts) (Courtesy of Dr. Gregor Sommer, Dr. Hans-Peter Fautz, Dr. Ute Ludwig, and Prof. Jürgen Hennig, University of Freiburg, Germany)

This is what the most recent developments in whole-body MRI promise. They enable either phase encoding or frequency encoding (Kruger et al. 2002, 2005; Zhu and Dumoulin 2003; Fain et al. 2004; Madhuranthakam et al. 2004) along the axis of the moving table, making it possible to acquire 2D or 3D datasets. Imaging *during* continuous table movement places heavy demands on data acquisition, hardware, and image reconstruction: inhomogeneities of the main magnetic field and gradient non-linearities can lead to blurring in the periphery of the FOV, which in this case is a function of time as the table is moving through the magnet during data acquisition (Polzin et al. 2004). While multistation imaging involves an extra step before the actual examination for adjusting imaging parameters, moving table approaches rely on the ability to automatically adjust these parameters and selectively activate the RF surface coil elements that are in the FOV at any given time while the table is moving. This includes RF transmit output, transmit and receive frequency, RF transmit power, RF receive amplification, and shimming of the magnet as well as other parameters for ensuring optimal and homogeneous image quality and patient safety. Otherwise, the flip angle, for instance, may be different in the pelvis and in the chest, causing unpredictable variations in image contrast. Although the problem of adjusting these parameters on the fly, so to speak, has not yet been fully solved, initial studies of whole-body MRI with a continuously moving table have shown promising results in volunteers (Zenge et al. 2005, 2006) and patients (Zenge et al. 2006; Vogt et al. 2007) (Figs. 3.8 and 3.9). When used in conjunction with surface coils connected to separate RF

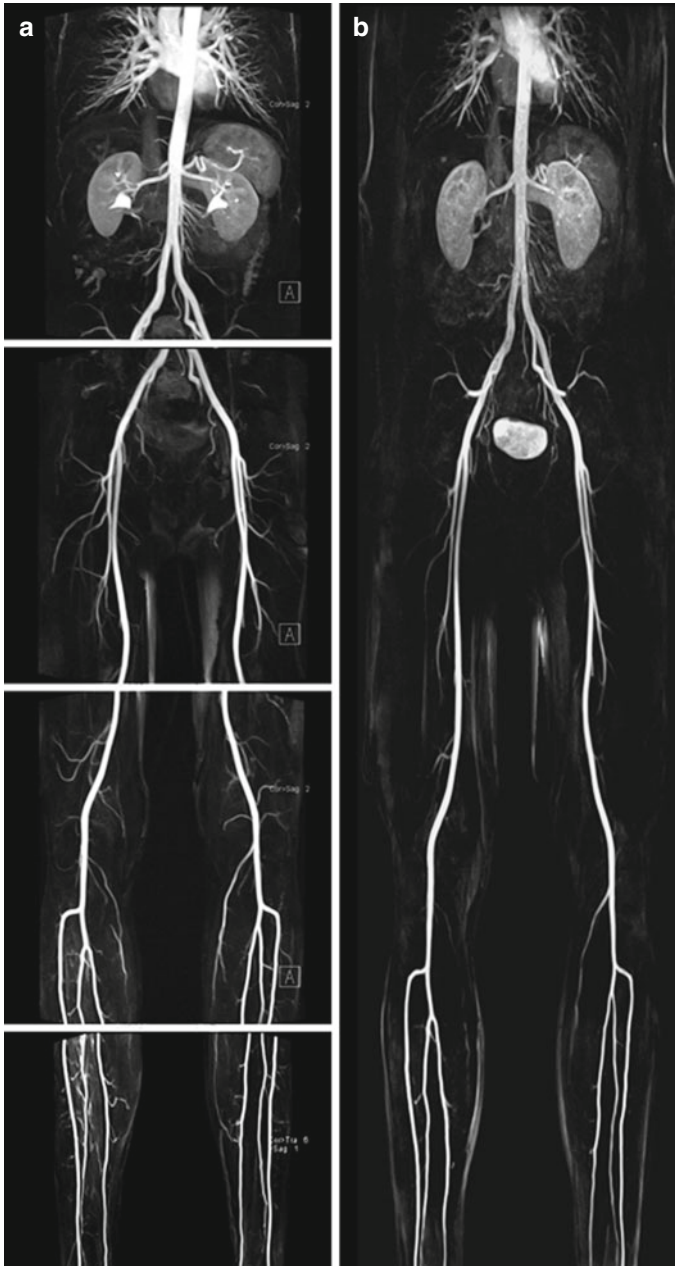


Fig. 3.9 Contrast-enhanced peripheral MRA using the multistation technique (a) in comparison to the continuously moving table technique (b) with continuous data acquisition while the table is moving. The conventional multistation technique involves separate acquisitions with several, slightly overlapping FOVs (a) (see Figs. 3.5 and 3.6), while the moving table technique yields one large seamless image (FOV). Both techniques can potentially be used for whole-body MRA. Images in this example were acquired in the coronal plane (see Fig. 3.7b)

receivers, the continuously moving table approach can also be used for parallel imaging (Zenge et al. 2006; Keupp et al. 2005). In this way, it is possible to exploit the potential for faster image acquisition to increase anatomic coverage per unit time, to acquire images with higher resolution, or both.

In recent years, several study groups have developed and technically implemented different strategies for continuous data acquisition (Börnert and Aldefeld 2008; Schaefer et al. 2010). Two approaches have been pursued: (1) image acquisition in the axial plane (Fig. 3.7a) for soft tissue evaluation throughout the body using different contrast weightings (Fig. 3.8) (Fautz and Kannengiesser 2006; Ludwig et al. 2006; Sommer et al. 2006, 2008; Fautz et al. 2007; Zenge et al. 2009; Brauck et al. 2008; Han et al. 2011; Baumann et al. 2010) and (2) coronal imaging (Fig. 3.7b) for MRA of individual vascular territories (Fig. 3.9) or of the whole body (Kruger et al. 2002, 2005; Madhuranthakam et al. 2004; Zenge et al. 2006; Vogt et al. 2007; Rasmus et al. 2008). In addition, work is being done to improve imaging during continuous table movement. Recently, new techniques for reducing respiratory artifacts (Honal et al. 2010) and algorithms for automatic table positioning (Koken et al. 2009) have been proposed.

Conclusion

The advent of whole-body MRI has brought many changes involving MRI hardware and software as well as image acquisition and reconstruction. It has also meant changes within the entire field of image postprocessing and display as well as in the interpretation and archiving of MRI datasets, which have become larger and more complex. The larger amounts of data make the use of PACS for storage indispensable. They have also spurred the development of new software tools for computer-aided diagnosis (CAD), which help the radiologist in coping with the larger number of images to look at. The technique of continuous table movement during imaging has led to a paradigm shift – one that has repercussions for all aspects of MRI and that will allow this imaging modality to tap new indications and attractive applications in the field of whole-body imaging.

References

- Barkhausen J, Quick HH, Lauenstein T, Goyen M, Ruehm SG, Laub G, Debatin JF, Ladd ME (2001) Whole-body MR imaging in 30 seconds with real-time true FISP and a continuously rolling table platform: feasibility study. *Radiology* 220:252–256
- Baumann T, Ludwig U, Pache G, Fautz HP, Kotter E, Langer M, Schaefer O (2010) Continuously moving table MRI with sliding multislice for rectal cancer staging: image quality and lesion detection. *Eur J Radiol* 73:579–587, Epub 2009 Jan 28
- Börnert P, Aldefeld B (2008) Principles of whole-body continuously-moving-table MRI. *J Magn Reson Imaging* 28:1–12, Review
- Brauck K, Zenge MO, Vogt FM, Quick HH, Stock F, Trarbach T, Ladd ME, Barkhausen J (2008) Feasibility of whole-body MR with T2- and T1 weighted real-time steady-state free precession sequences during continuous table movement to depict metastases. *Radiology* 246:910–916, Epub 2008 Jan 9

- Busch HP, Hoffmann HG, Rock J, Schneider C (2001) MR angiography of pelvic and leg vessels with automatic table movement technique ("MobiTrak"): clinical experience with 450 studies. *Rofo* 173:405–409
- Dietrich O, Hajnal JV (1999) Extending the coverage of true volume scans by continuous movement of the subject. In: ISMRM, 7th Scientific Meeting and Exhibition, Philadelphia, p 1653
- Fain SB, Browning FJ, Polzin JA, Du J, Zhou Y, Block WF, Grist TM, Mistretta CA (2004) Floating table isotropic projection (FLIPR) acquisition: a time-resolved 3D method for extended field-of-view MRI during continuous table motion. *Magn Reson Med* 52:1093–1102
- Fautz HP, Kannengiesser SA (2006) Sliding multislice (SMS): a new technique for minimum FOV usage in axial continuously moving-table acquisitions. *Magn Reson Med* 55:363–370
- Fautz HP, Honal M, Saueressig U, Schäfer O, Kannengiesser SA (2007) Artifact reduction in moving-table acquisitions using parallel imaging and multiple averages. *Magn Reson Med* 57:226–232
- Ghanem N, Kelly T, Althoefer C, Winterer J, Schafer O, Bley TA, Moser E, Langer M (2004) Whole-body MRI in comparison to skeletal scintigraphy for detection of skeletal metastases in patients with solid tumors [Article in German]. *Radiologe* 44:864–873
- Goehde SC, Hunold P, Vogt FM, Ajaj W, Goyen M, Herborn CU, Forsting M, Debatin JF, Ruehm SG (2005) Full-body cardiovascular and tumor MRI for early detection of disease: feasibility and initial experience in 298 subjects. *AJR Am J Roentgenol* 184:598–611
- Goyen M, Ruehm SG, Barkhausen J, Kroger K, Ladd ME, Truemmler KH, Bosk S, Requardt M, Reykowski A, Debatin JF (2001) Improved multi-station peripheral MR angiography with a dedicated vascular coil. *J Magn Reson Imaging* 13:475–480
- Goyen M, Quick HH, Debatin JF, Ladd ME, Barkhausen J, Herborn CU, Bosk S, Kuehl H, Schleputz M, Ruehm SG (2002) Whole-body three-dimensional MR angiography with a rolling table platform: initial clinical experience. *Radiology* 224:270–277
- Han Y, Weigel M, Huff S, Ludwig U (2011) Whole-body diffusion-weighted imaging with a continuously moving table acquisition method: preliminary results. *Magn Reson Med* 65:1557–1563. doi:10.1002/mrm.22833. Epub 2011 Mar 22
- Herborn CU, Goyen M, Quick HH, Bosk S, Massing S, Kroegeer K, Stoesser D, Ruehm SG, Debatin JF (2004) Whole-body 3D MR angiography of patients with peripheral arterial occlusive disease. *AJR Am J Roentgenol* 182:1427–1434
- Ho KY, Leiner T, de Haan MW, Kessels AG, Kitslaar PJ, van Engelshoven JM (1998) Peripheral vascular tree stenoses: evaluation with moving-bed infusion-tracking MR angiography. *Radiology* 206:683–692
- Ho KY, Leiner T, de Haan MW, van Engelshoven JM (1999) Peripheral MR angiography. *Eur Radiol* 9:1765–1774
- Honal M, Leupold J, Huff S, Baumann T, Ludwig U (2010) Compensation of breathing motion artifacts for MRI with continuously moving table. *Magn Reson Med* 63:701–712
- Huber A, Scheidler J, Wintersperger B, Baur A, Schmidt M, Requardt M, Holzknrecht N, Helmberger T, Billing A, Reiser M (2003) Moving-table MR angiography of the peripheral runoff vessels: comparison of body coil and dedicated phased array coil systems. *AJR Am J Roentgenol* 180:1365–1373
- Johnson KMR, Leavitt GD, Kayser HWM (1997) Total-body MR imaging in as little as 18 seconds. *Radiology* 202:262–267
- Keupp J, Aldefeld B, Bornert P (2005) Continuously moving table SENSE imaging. *Magn Reson Med* 53:217–220
- Koken P, Dries SP, Keupp J, Bystrov D, Pekar V, Börner P (2009) Towards automatic patient positioning and scan planning using continuously moving table MR imaging. *Magn Reson Med* 62:1067–1072
- Kruger DG, Riederer SJ, Grimm RC, Rossman PJ (2002) Continuously moving table data acquisition method for long FOV contrast-enhanced MRA and whole-body MRI. *Magn Reson Med* 47:224–231

- Kruger DG, Riederer SJ, Polzin JA, Madhuranthakam AJ, Hu HH, Glockner JF (2005) Dual-velocity continuously moving table acquisition for contrast-enhanced peripheral magnetic resonance angiography. *Magn Reson Med* 53:110–117
- Lauenstein TC, Goehde SC, Herborn CU, Treder W, Ruehm SG, Debatin JF, Barkhausen J (2002a) Three-dimensional volumetric interpolated breath-hold MR imaging for whole-body tumor staging in less than 15 minutes: a feasibility study. *AJR Am J Roentgenol* 179:445–449
- Lauenstein TC, Freudenberg LS, Goehde SC, Ruehm SG, Goyen M, Bosk S, Debatin JF, Barkhausen J (2002b) Whole-body MRI using a rolling table platform for the detection of bone metastases. *Eur Radiol* 12:2091–2099
- Lauenstein TC, Goehde SC, Herborn CU, Goyen M, Oberhoff C, Debatin JF, Ruehm SG, Barkhausen J (2004) Whole-body MR imaging: evaluation of patients for metastases. *Radiology* 233:139–148
- Leiner T, Ho KY, Nelemans PJ, de Haan MW, van Engelshoven JM (2000) Three-dimensional contrast-enhanced moving-bed infusion-tracking (MoBI-track) peripheral MR angiography with flexible choice of imaging parameters for each field of view. *J Magn Reson Imaging* 11:368–377
- Leiner T, Nijenhuis RJ, Maki JH, Lemaire E, Hoogeveen R, van Engelshoven JM (2004) Use of a three-station phased array coil to improve peripheral contrast-enhanced magnetic resonance angiography. *J Magn Reson Imaging* 20:417–425
- Ludwig U, Sommer G, Zaitsev M, Ghanem N, Hennig J, Fautz HP (2006) 2D axial moving table acquisitions with dynamic slice adaptation. *Magn Reson Med* 55:423–430
- Madhuranthakam AJ, Kruger DG, Riederer SJ, Glockner JF, Hu HH (2004) Time-resolved 3D contrast-enhanced MRA of an extended FOV using continuous table motion. *Magn Reson Med* 51:568–576
- Meaney JF, Ridgway JP, Chakraverty S, Robertson I, Kessel D, Radjenovic A, Kouwenhoven M, Kassner A, Smith MA (1998) Stepping-table gadolinium-enhanced digital subtraction MR angiography of the aorta and lower extremity arteries: preliminary experience. *Radiology* 211:59–67
- Polzin JA, Kruger DG, Gurr DH, Brittain JH, Riederer SJ (2004) Correction for gradient nonlinearity in continuously moving table MR imaging. *Magn Reson Med* 52:181–187
- Quick HH, Vogt FM, Maderwald S, Herborn CU, Bosk S, Gohde S, Debatin JF, Ladd ME (2004) High spatial resolution whole-body MR angiography featuring parallel imaging: initial experience. *Rofo* 176:163–169
- Rasmus M, Bremerich J, Egelhof T, Huegli RW, Bongartz G, Bilecen D (2008) Total-body contrast-enhanced MRA on a short, wide-bore 1.5-T system: intra-individual comparison of Gd-BOPTA and Gd-DOTA. *Eur Radiol* 18:2265–2273, Epub 2008 Apr 23
- Ruehm SG, Goyen M, Quick HH, Schlepütz M, Schlepütz H, Bosk S, Barkhausen J, Ladd ME, Debatin JF (2000a) Whole-body MRA on a rolling table platform (AngioSURF). *Rofo* 172:670–674
- Ruehm SG, Hany TF, Pfammatter T, Schneider E, Ladd M, Debatin JF (2000b) Pelvic and lower extremity arterial imaging: diagnostic performance of three-dimensional contrast-enhanced MR angiography. *AJR Am J Roentgenol* 174:1127–1135
- Ruehm SG, Goyen M, Barkhausen J, Kroger K, Bosk S, Ladd ME, Debatin JF (2001) Rapid magnetic resonance angiography for detection of atherosclerosis. *Lancet* 357:1086–1089
- Ruehm SG, Goehde SC, Goyen M (2004) Whole body MR angiography screening. *Int J Cardiovasc Imaging* 20:587–591
- Schaefer AO, Langer M, Baumann T (2010) Continuously moving table MRI in oncology. *Rofo* 182:954–964, Epub 2010 Oct 4. Review
- Shetty AN, Bis KG, Duerinckx AJ, Narra VR (2002) Lower extremity MR angiography: universal retrofitting of high-field-strength systems with stepping kinematic imaging platforms initial experience. *Radiology* 222:284–291
- Sommer G, Fautz HP, Ludwig U, Hennig J (2006) Multicontrast sequences with continuous table motion: a novel acquisition technique for extended field of view imaging. *Magn Reson Med* 55:918–922

- Sommer G, Schaefer AO, Baumann T, Ludwig UA, Fautz HP (2008) Sliding multislice MRI for abdominal staging of patients with pelvic malignancies: a pilot study. *J Magn Reson Imaging* 27:666–672
- Vogt FM, Zenge MO, Ladd ME, Herborn CU, Brauck K, Luboldt W, Barkhausen J, Quick HH (2007) Peripheral vascular disease: comparison of continuous MR angiography and conventional MR angiograph--ilot study. *Radiology* 243:229–238, Epub 2007 Feb 28
- Wang Y, Lee HM, Khilnani NM, Jagust MB, Winchester PA, Bush HL, Sos TA, Sostman HD (1998) Bolus-chase MR digital subtraction angiography in the lower extremity. *Radiology* 207:263–269
- Winterer JT, Strecker R, Lohrmann C, Schaefer O, Ghanem N, Bley T, Kotter E, Lehnhardt S, Hennig J (2003) Background suppression using magnetization preparation for contrast-enhanced 3D MR angiography of the pelvic and lower leg arteries. *Rofo* 175:28–31
- Zenge MO, Ladd ME, Vogt FM, Brauck K, Barkhausen J, Quick HH (2005) Whole-body magnetic resonance imaging featuring moving table continuous data acquisition with high-precision position feedback. *Magn Reson Med* 54:707–711
- Zenge MO, Vogt FM, Brauck K, Jökel M, Barkhausen J, Kannengiesser S, Ladd ME, Quick HH (2006) High-resolution continuously acquired peripheral MR angiography featuring partial parallel imaging GRAPPA. *Magn Reson Med* 56:859–865
- Zenge MO, Ladd ME, Quick HH (2009) Novel reconstruction method for three dimensional axial continuously moving table whole-body magnetic resonance imaging featuring autocalibrated parallel imaging GRAPPA. *Magn Reson Med* 61:867–873
- Zhu Y, Dumoulin CL (2003) Extended field-of-view imaging with table translation and frequency sweeping. *Magn Reson Med* 49:1106–1112

Contrast Agent Administration and Imaging Protocols for Whole-Body MRI

4

Achim Seeger, Stephan Miller,
and Heinz-Peter Schlemmer

For a meaningful application of whole-body MRI in the clinical setting, it is necessary to have flexible imaging protocols. The use of protocols that can be modified to address an individual patient's clinical situation enables us to image the entire body with the highest quality and in the shortest time possible.

In devising such protocols for whole-body MRI, we can draw on earlier experience by trying to incorporate imaging strategies that have proven effective in examining individual body regions or organ systems. This experience also helps us in optimizing the use of contrast medium in the setting of whole-body MRI.

When whole-body MRI is used for cancer staging, for instance, the imaging strategy depends on the patient's primary tumor. In patients with rectal cancer, a dynamic contrast-enhanced series of the liver should be included, while, for patients with lung cancer, the protocol should include a multiphasic MR angiogram instead. To meet these requirements, a good whole-body MRI protocol is not a rigid series of pulse sequences but should instead provide for a flexible combination of different sequences to tailor the examination to best answer the diagnostic needs of a patient.

These are the guiding principles of the imaging strategy that is favored by the authors and that will be presented in this chapter. There are other approaches, and the choice depends on many factors, including the technology available for performing whole-body MRI.

A. Seeger (✉) • S. Miller
Department of Diagnostic and Interventional Radiology,
Eberhard-Karls-University Tuebingen, Hoppe-Seyler-Str. 3,
Tuebingen 72076, Germany
e-mail: achim.seeger@med.uni-tuebingen.de; stephan.miller@med.uni-tuebingen.de

H.-P. Schlemmer
Department of Radiology, Deutsches Krebsforschungszentrum,
Im Neuenheimer Feld 280, Heidelberg 69120, Germany

4.1 MRI Contrast Agents

An MRI contrast agent improves image contrast by altering relaxation times, especially when combined with a T1-weighted pulse sequence. After IV administration, the contrast agent distributes in the interstitial space and produces nonspecific enhancement on first-pass images. Extracellular gadolinium chelates are eliminated by glomerular filtration, resulting in rapid renal clearance of these contrast agents. Although generally well tolerated, MRI contrast agents should never be used uncritically. Special caution is required in patients with impaired renal function, in whom the administration of gadolinium-based MR contrast agents has been linked to nephrogenic systemic fibrosis (NSF) (Kuo et al. 2007). Gd-based contrast agents for MRI may be ionic or nonionic. Structurally, a distinction is made between linear and macrocyclic complexes.

4.1.1 Commonly Used MRI Contrast Agents

1. *Macrocyclic complexes*: greater chemical stability reduces likelihood of release of gadolinium ions
 - Gadoterate meglumine (Dotarem™, Guerbet, France)
 - Gadobutrol (Gadavist™, Bayer HealthCare Pharmaceuticals): high Gd concentration (1 mmol/mL)
 - Gadoteridol (ProHance™, Bracco, Italy)
2. *Linear ionic complexes*:
 - Gd-DTPA (gadopentetate dimeglumine): Magnevist™ (Bayer HealthCare Pharmaceuticals) and generic agents (e.g., Magnegita™, Insight Agents). First approved MRI contrast agent, market introduction in 1988
 - Gd-BOPTA (gadobenate dimeglumine): MultiHance™ (Bracco, Italy), an extracellular contrast agent with some hepatobiliary clearance (2–4 %)
3. *Linear nonionic complexes*:
 - Gadodiamide (Omniscan™, GE Healthcare)
 - Gadoversetamide (OptiMARK™, Tyco Healthcare)

While whole-body MRI can be performed using liver-specific contrast agents (see Sect. 4.3), these agents are usually reserved for specific diagnostic tasks or may be helpful for workup of suspicious findings demonstrated by whole-body MRI. An example of a hepatocyte-specific agent is Gd-EOB-DTPA (Primovist™ in Europe and Eovist™ in the USA, Bayer HealthCare Pharmaceuticals). Other MR contrast agents for specific diagnostic purposes are preparations of iron oxide particles, which are selectively taken up by the mononuclear phagocytic system, and intravascular or blood pool contrast agents, which can be used for MR angiography. A reader interested in these MR contrast agents should check current information to find out which agents are available in their country.

Table 4.1 Contrast agent administration

Timing	Diagnostic task	Suggested procedure	Injection rate	Dose	Typical sequences
Timing not critical	Standard contrast-enhanced imaging	Internal standards to ensure comparability with single-step examinations	Not critical	0.1–0.2 mmol/kg BW	T1w (fs) post CM
Accurate timing essential	MRA	Test bolus for determining individual circulation time	1–3 mL/s by automatic injector	Test bolus of 1–2 mL Scan at 0.1–0.2 mmol/kg BW	MRA T1w FLASH 3D
Timing important	Tissue perfusion	Standardized delay	1–4 mL/s by automatic injector	0.1–0.2 mmol/kg BW	T1w FLASH 3D VIBE
Delay important (specific tissues)	Late imaging	Internal standards to ensure comparability with single-step examinations	Not critical	Depends on CM used	Liver: T1w post CM (delay ≥20 min) Heart: late enhancement (delay 10–15 min) Brain: T1w post CM (delay >5 min)

BW body weight, *CM* contrast medium, *T1w* T1-weighted, *fs* fat saturation, *MRA* magnetic resonance angiography, *FLASH* fast low-angle shot, *VIBE* volume-interpolated breath-hold examination

4.1.2 Mode of Contrast Agent Administration

It is recommended that the contrast agent be administered at a standardized injection rate using an automatic injector. Timing is particularly critical for dynamic imaging studies and first-pass MR angiography (Table 4.1).

4.1.3 Spasmolytic Medication

The diagnostic quality of MRI of the gastrointestinal tract can be improved by administration of a spasmolytic agent such as butylscopolamine bromide (Buscopan™, Boehringer Ingelheim GmbH, Germany; single adult dose of 20–40 mg, or 1–2 ampoules). Buscopan is contraindicated in subjects with allergies, mechanical obstruction of the gastrointestinal tract, megacolon, prostate hypertrophy with urinary retention, narrow angle glaucoma, tachycardia, and myasthenia gravis. Subjects should be advised not to drive due to possible transient disturbance of accommodation. Alternatively, glucagon can be given as a spasmolytic agent.

4.2 Pulse Sequence Protocols

There are so many potential protocol variations that anything but the most general of recommendations is impossible. In the following, we offer some general guidance, along with some examples of proven protocols.

It is important to plan multistation imaging with enough overlap between adjacent stations (up to 6 cm, depending on the pulse sequence used). This ensures adequate diagnostic evaluation even if wraparound artifacts occur at the seams of adjacent images.

Major whole-body MRI protocol variants, which focus on cardiovascular, oncologic, and musculoskeletal imaging, are discussed in more detail below. In individual cases, these variants can be combined.

4.2.1 Cardiovascular Protocol

Because atherosclerosis is a systemic disease, existing MRI protocols permit assessment of the entire vascular system and at the same time include options for imaging the most important target organs affected by atherosclerotic conditions – the brain, the heart, and the kidneys. Early detection of stenosis (e.g., of the renal or carotid arteries) may have crucial clinical implications. Robust clinical protocols for a comprehensive routine evaluation of the coronary arteries are not yet available. In individual cases, however, imaging approaches that are still under investigation can be used.

In whole-body MRA, adequate timing is important to capture the first pass of the contrast medium bolus and to sample central k-space data during bolus passage. Since the optimal moment for image acquisition after contrast medium administration is influenced by many different factors (e.g., cardiac output, injection rate, saline chaser), it is recommended that individual circulation time after administration of a test bolus be estimated (1–2 mL of contrast medium administered at a defined flow rate of 1–3 mL/s).

MRA lends itself to combination with pulse sequences aimed at identifying post-ischemic changes in the brain and heart (Kramer et al. 2005; Fenchel et al. 2005). For the brain, we recommend a TOF MRA sequence, a precontrast FLAIR sequence, and postcontrast T1-weighted imaging. Postinfarction myocardial scars are best identified by hyperenhancement on delayed enhancement images acquired 10–15 min after administration of Gd-based contrast medium for MRA. If deemed useful for the diagnostic question to be answered, the interval between MRA and delayed enhancement imaging may be used for acquiring functional sequences (2D cine TrueFISP) for a full cardiovascular evaluation.

Table 4.2 presents an example of an established protocol for whole-body cardiovascular imaging using two contrast medium injections (Seeger et al. 2008).

Several alternative protocols have been proposed. These variants include protocols with single-dose contrast medium administration followed by rapid imaging of the neck/chest/abdomen/pelvis (Fenchel et al. 2009), use of a rolling table

Table 4.2 Cardiovascular protocol/whole-body MR angiography: suggested protocol for imaging with two contrast medium injections

Body region/task	Sequence type	Estimated duration
Brain	FLAIR	2:40 min
Intracranial vessels	TOF-MRA	4:00 min
Determination of circulation time	Test bolus	1:00 min
Vessels: abdomen/pelvis, thigh, calf ^a (pre-CM)	FLASH 3D	0:50 min
<i>First contrast bolus</i>		
Vessels: abdomen/pelvis, thigh, calf ^a (arterial)	FLASH 3D (start scan based on circulation time of test bolus)	0:50 min
Cardiac function	Cine TrueFISP	6×0:15 min
Brain	T1w post CM	4:00 min
Myocardial viability	IR T1w TurboFLASH (late enhancement)	6×0:15 min
Vessels: thorax/neck, calf ^a (pre-CM)	FLASH 3D	0:17 min
<i>Second contrast bolus</i>		
Vessels: thorax/neck, calf ^a (arterial)	FLASH 3D (start scan based on circulation time of test bolus)	0:17 min

CM contrast medium, *FLAIR* fluid-attenuated inversion recovery, *TOF-MRA* time-of-flight magnetic resonance angiography, *FLASH* fast low-angle shot, *FISP* fast imaging with steady-state precession, *IR* inversion recovery, *T1w* T1-weighted

^aAlternative variants: calf can be acquired either after first contrast bolus (abdomen/pelvis, thigh) or after second bolus (thorax/neck)

platform (AngioSURFTM, see Chap. 3 (Ruehm et al. 2000)) or a continuously moving table (TIM-CTTM, Siemens (Kramer et al. 2008)), and combinations of different techniques (Koziel et al. 2011). Recently, the application of high-resolution time-resolved four-dimensional MRA sequences with a triple injection protocol has been proposed (Kinner et al. 2013) and has shown good diagnostic quality without venous overlay.

4.2.2 Oncologic Protocol

The imaging strategy, including selection of pulse sequences and contrast medium administration, is largely determined by the patient's primary tumor (Goyen and Schlemmer 2007). When imaging involves a body region for which an established dynamic MRI protocol exists, contrast medium administration is timed for optimized imaging of that region. Examples include dynamic liver MRI and late hepatocyte-phase imaging following administration of a hepatocellular contrast agent.

When whole-body MRI is performed for cancer screening, the protocol is planned according to the individual risk profile. Table 4.3 provides an overview of commonly used pulse sequences, introducing the abbreviations that will be used in the following. Table 4.4 presents examples of oncologic protocols for imaging patients with different primary malignancies. The tables have been modified from Schaefer and Schlemmer (2006).

Table 4.3 Commonly used pulse sequences for whole-body MRI grouped by body region

Body region	Sequence ID	Sequence	Contrast medium	Plane	Breathing mode	Estimated acquisition time (min:s)	Spatial resolution (mm ³)
Whole body	WB1	T2w STIR TSE	Unenhanced	Coronal	Free	15:00	1.8×1.3×5.0
	WB2	T1w TSE	Unenhanced	Coronal	Free	10:00	1.7×1.3×5.0
	WB3	T1w TSE fs	Post CM	Coronal	Free	12:00	2.0×1.5×5.0
	WB4	FLASH 3D	Dynamic CM series	Coronal	Free	4× (0:15–0:22)	1.4×1.4×1.4
Brain	B1	FLAIR	Unenhanced	Axial	Free	2:40	1.2×0.9×4.0
	B2	T1w SE	Unenhanced	Axial	Free	3:50	0.9×0.9×4.0
	B3	T1w SE	Post CM	Axial	Free	3:50	0.9×0.9×4.0
	B4	T1w SE	Post CM	Coronal	Free	4:20	0.9×0.9×4.0
	B5	TOF 3D	Unenhanced	Axial	Free	4:00	0.8×0.8×0.8
Neck	N1	T2w TSE	Unenhanced	Coronal	Free	2:30	1.2×0.9×5.0
	N2	T1w FLASH 2D	Unenhanced	Axial	Free	0:50	1.1×0.8×5.0
	N3	T1w FLASH 2D fs	Post CM	Axial	Free	1:20	1.1×0.8×5.0
Thorax	T1	T2w STIR TSE	Unenhanced	Axial	Breath hold	0:46	1.8×1.2×6.0
	T2	PD VIBE 3D	Unenhanced	Axial	Breath hold	2× 0:18	2.0×2.0×2.0
	T3	T1w VIBE 3D	Post CM	Axial	Breath hold	2× 0:18	2.0×2.0×2.0
	T4	Dynamic T1w VIBE	Dynamic CM series	Coronal	Breath hold	4× 0:22	2.6×1.6×2.0
Ribs	R1	FLASH 2D	Unenhanced	Axial	Breath hold	1:00	2.1×1.5×6.0
	R2	FLASH 2D, fs	Post CM	Axial	Breath hold	1:30	2.1×1.5×6.0
Cardio	C1	Cine TrueFISP 2D	Unenhanced	Double oblique	Breath hold	6× 0:15	1.8×1.6×6.0
	C2	IR FLASH 2D	Post CM	Double oblique	Breath hold	10× 0:15	1.8×1.4×6.0
	C3	T2w whole heart	Unenhanced	Axial	Pace	5:00	1.1×1.1×1.1
Abdomen	A1	T2w TSE fs	Unenhanced	Axial	Pace	2:00	1.6×1.2×6.0
	A2	T1w FLASH 2D fs	Unenhanced	Axial	Breath hold	1:00	2.1×1.5×6.0
	A3	T1w FLASH 2D fs	Post CM	Axial	Breath hold	1:00	2.1×1.5×6.0
	A4	Dynamic T1w VIBE 3D	Dynamic CM series	Axial	Breath hold	3× 0:18	1.9×1.3×2.0
	A5	MRC T1w VIBE 3D	Post CM	Coronal	Breath hold	4× 0:23	2.0×2.0×1.8

Pelvis	P1	T2w STIR TSE	Unenhanced	Axial	Free	4:30	1.5×1.2×4.0
	P2	T1w FLASH 2D fs	Unenhanced	Axial	Free	1:00	2.1×1.5×4.0
	P3	T1w FLASH 2D fs	Post CM	Axial	Free	1:00	2.1×1.5×4.0
	P4	T2w TSE	Unenhanced	Axial	Free	4:00	1.3×0.6×4.0
Spine	S1	T2w STIR TSE	Unenhanced	Sagittal	Free	5:00	1.5×1.0×3.0
	S2	T1w TSE	Unenhanced	Sagittal	Free	3:20	1.4×1.0×3.0
	S3	T1w TSE fs	Post CM	Sagittal	Free	3:30	1.7×1.3×3.0

T1w T1-weighted, *T2w* T2-weighted, *PD* proton density-weighted, *fs* fat-saturated, *CM* contrast medium, *IR* inversion recovery, *STIR* short-tau inversion recovery, *SE* spin echo, *TSE* turbo spin echo, *FISP* fast imaging with steady-state precession, *FLAIR* fluid-attenuated inversion recovery, *FLASH* fast low-angle shot, *VIBE* volume-interpolated breath-hold examination, *MRC* magnetic resonance colonoscopy

Table 4.4 Suggested oncologic protocols for different indications. Adjustments may have to be made to tailor an examination to suit individual needs

Indication	Whole body	Brain	Neck	Thorax	Abdomen	Pelvis	Spine
Search for bone metastases	WB1–2			T1, R1–2			S1–2
Search for visceral metastases		B1–4	N1–3	T1–3	A1–3/4 ^d	P1–3	
Lung cancer staging ^a	WB1	B1–4		T1–4	A1–3		
Prostate cancer ^b	WB1–2 (3)			R1–2		P4	S1–2
Breast cancer ^c	WB1	B1–4		T1–3, R1	A1–4		
Colorectal cancer	WB1	B1–4		T1–3, R1	A1–3, (A5)	P1–3	
Ovarian, cervical, and endometrial cancer	WB1			T1–3	A1–4	P1–3	
Multiple myeloma	WB1–3			R1–2			S1–2, (S3)
Neuroendocrine tumors	WB1			T1–3	A1–4	P1–3	
Cancer screening	WB1	B1–4	N1–3	T1–3	A1–3, (A5 ^e)	P1–3	

^aCT or FDG-PET/CT is the gold standard for assessment of the primary cancer

^bEndorectal coil may be used for prostate imaging

^cBreast imaging with dedicated breast coil

^dA4 if hypervascularized metastases can be expected (e.g., breast cancer, renal cell cancer)

^eOptional, depending on expected diagnostic benefit (in terms of sensitivity/specificity) compared with other modalities

4.2.2.1 Organ Metastasis

Whole-body MRI allows the combination of state-of-the-art pulse sequences optimized for individual organs including the brain and liver. For some cancers, whole-body MRI has been shown to be superior to other imaging modalities such as CT or PET/CT (Schmidt et al. 2007a, b). A dynamic series is helpful (Table 4.4: *sequence A4*) if, based on the underlying malignancy, hypervascularized metastases can be expected.

Suggested protocol: *B1–4, N1–3, T1–3, A1–3/4, P1–3*

4.2.2.2 Bone Metastasis

Many cancers spread to bone. More than 80 % of bone metastases are from cancers of the breast, prostate, lung, thyroid gland, and kidney. The standard pulse sequence, coronal STIR, is supplemented by a non-fat-saturated T1-weighted sequence for improved detection of osteoblastic lesions. Breath-hold T1-weighted and T2-weighted sequences are used to search for rib metastases. In patients with hematologic malignancy (e.g., multiple myeloma), MRI can be used to evaluate the extent of disease and the response to treatment (Delorme and Baur-Melnyk 2009; Schmidt et al. 2007a, b).

Suggested protocol: *WB1–2 (3), T1, R1–2, S1–3*

4.2.2.3 Lymph Node Metastasis

As with all imaging modalities, whole-body MRI is limited in identifying metastatic lymph nodes due to a lack of specificity of morphologic features, especially

when lymph nodes are small. Enlarged lymph nodes are best detected with TIRM and T2-weighted TSE sequences. The morphology of suspicious lymph nodes can be evaluated further by acquiring high-resolution fat-saturated T1-weighted images of that region following administration of contrast medium.

4.2.2.4 Colorectal Cancer

A virtual colonoscopy based on MRI (A5, VIBE sequences) can be integrated into a whole-body MRI protocol. Endoscopy, however, continues to be the gold standard for detecting tumors within the intestinal lumen. MRI is most useful for the staging and detection of enlarged locoregional lymph nodes and organ metastases (in the liver, bones, and – with some limitations – the lungs).

Suggested protocol: *WB1, B1–4, T1–3, R1, A1–3 (A5), P1–3*

4.2.2.5 Lung Cancer

Imaging of the lung is the domain of CT and FDG-PET/CT. However, 3D GRE sequences allow detection of nodules >4 mm with enhancement kinetics contributing to the differentiation between benign and malignant lesions (Kono et al. 2007). The assessment of other organ systems by whole-body MRI can provide useful staging information (Puls et al. 2010).

Suggested protocol: *WB1, B1–4, T1–4, A1–3*

4.2.2.6 Breast Cancer

Practical considerations preclude the integration of an MR mammogram into a whole-body MRI protocol, as this would require the use of a dedicated breast coil to achieve high resolution. However, whole-body MRI may contribute to the detection of liver and bone metastases, for which sagittal images of the spine (*SI–2*) can also be helpful.

Suggested protocol: *WB1, B1–4, T1–3, R1, A1–4, SI–2*

4.2.2.7 Prostate Cancer

MRI using a combined endorectal and body phased-array coil plays an important role in local prostate cancer staging, having high sensitivity for evaluating cancer growth beyond the prostate. The use of an endorectal coil for improved spatial resolution is time consuming, making it very difficult to integrate this technique into a whole-body MRI protocol.

Multiplanar T2-weighted imaging of the pelvis allows assessment of the local extent of prostate cancer; bone metastases can be detected on STIR or T1-weighted images. The sensitivity for identifying metastatic lymph nodes is limited.

Suggested protocol: *WB1–2 (3), R1–2, P4, SI–2*

4.2.2.8 Other Cancers

In principle, whole-body MRI can be used for the staging of any cancer. Renal cell carcinoma, for instance, is well amenable to (both local and systemic) evaluation by MRI. PET/CT, however, continues to be the modality of choice in patients with cancer of unknown primary (CUP).

4.2.3 Musculoskeletal Protocol

Whole-body MRI is especially useful for evaluating the extent of systemic diseases (inflammatory, rheumatologic, idiopathic, traumatic, and neoplastic) and for monitoring the response to treatment. A combination with high-resolution imaging of individual joints (e.g., hands or feet in patient with rheumatoid disease) is not possible; this would require the use of dedicated surface coils.

It takes 14 min to perform a coronal whole-body STIR survey with high spatial resolution (*WB1*), which allows assessment of anatomy and rapid detection of abnormal signal intensities of muscles and bones. This survey is followed by targeted series according to the clinical question(s) and the STIR findings, e.g., T1-weighted sequences if osteoblastic metastases have been detected (*WB2–3*).

Sagittal oblique sections are especially useful for imaging the spine (*S1–3*).

In trauma patients, CT is still the preferred imaging modality because it is faster and more widely available. Whole-body MRI, however, may have a role in identifying injuries that are not seen on radiographs, and it may be used when battered child injuries are suspected (Schaefer and Kramer 2011).

As with regional MRI examinations, contrast medium administration is indicated in evaluating inflammatory disorders (e.g., synovitis).

4.2.4 Whole-Body Fat Measurement

Increased deposition of fat alters the ratio of muscle and bone to body fat. Visceral and subcutaneous fat as well as regional fat deposits can be visualized by MRI using T1-weighted TSE and GRE sequences. Whole-body MRI has been used to follow up adipose tissue compartments during a lifestyle intervention program (Machann et al. 2010).

4.2.5 Combination of All Protocols

MRI has a central role as a screening modality or for early detection of disease, enabling identification of both vascular abnormalities (carotid stenosis, intracerebral aneurysm, renal artery stenosis, myocardial infarction, etc.) and inflammatory or neoplastic disease before symptoms occur (Table 4.5). False-positive findings pose a problem, however, which is why it is important to discuss this in detail with individuals undergoing MRI screening.

4.3 Whole-Body MRI with Liver-Specific Contrast Agents

Gd-EOB-DTPA (Eovist™) and Gd-BOPTA (MultiHance™, Bracco) combine the imaging properties of conventional extracellular contrast agents (such as Magnevist™ or Gadavist™) and hepatocyte-specific contrast agents. They can be

Table 4.5 Suggested nononcologic protocols for different indications. Adjustments may have to be made to tailor an examination to suit individual needs

Protocol		Whole body	Brain	Neck	Thorax	Abdomen	Pelvis	Spine
Cardiovascular	Myocardial infarction, PAOD, AAA ^a	WB4	B1–3, B4		C1–2, (C3 ^b)	(A3 ^a)		
Inflammatory diseases	Fever of unknown origin (FUO)	WB1	B1–4	N1,3	T1–3	A1–3	P3	
	Myositis	WB1						
	Rheumatoid arthritis	WB1,						
	Ankylosing spondylitis	WB3						S1–2
Musculoskeletal	Battered child syndrome	WB1						S1
	Search for fractures ^c	WB1–2			R1–2			S1

PAOD peripheral artery occlusive disease, AAA abdominal aortic aneurysm

^aA3 for AAA

^bC3 may be used when evaluating patients with suspected coronary anomaly or proximal stenosis

^cCT is faster and more widely available in emergencies

injected intra-arterially for whole-body MRI, while their uptake by intact hepatocytes in the delayed phase provides additional information for improved detection and characterization of liver lesions.

Since these two contrast agents have no effect on T2 signal and since the liver-specific phase occurs with a delay of 20 min (EovistTM) or 40–120 min (MultiHanceTM), the interval between the dynamic liver series and hepatocyte-phase imaging can be used for acquiring TIRM and T2-weighted sequences (Ringe et al. 2010).

References

- Delorme S, Baur-Melnyk A (2009) Imaging in multiple myeloma. *Eur J Radiol* 70:401–408
- Fenchel M, Requardt M, Tomaschko K, Kramer U, Stauder NI, Naegele T et al (2005) Whole-body MR angiography using a novel 32-receiving-channel MR system with surface coil technology: first clinical experience. *J Magn Reson Imaging* 21:596–603
- Fenchel M, Doering J, Seeger A, Kramer U, Rittig K, Klumpp B et al (2009) Ultrafast whole-body MR angiography with two-dimensional parallel imaging at 3.0 T: feasibility study. *Radiology* 250:254–263
- Goyen M, Schlemmer HP (2007) Whole body MRI—diagnostic strategy of the future? *Radiologe* 47:904–914
- Kinner S, Quick HH, Maderwald S, Hunold P, Barkhausen J, Vogt FM (2013) Triple-TWIST MRA: high spatial and temporal resolution MR angiography of the entire peripheral vascular system using a time-resolved 4D MRA technique. *Eur Radiol* 23:298–306

- Kono R, Fujimoto K, Terasaki H, Muller NL, Kato S, Sadohara J et al (2007) Dynamic MRI of solitary pulmonary nodules: comparison of enhancement patterns of malignant and benign small peripheral lung lesions. *AJR Am J Roentgenol* 188:26–36
- Koziel K, Attenberger UI, Lederle K, Haneder S, Schoenberg SO, Michaely HJ (2011) Peripheral MRA with continuous table movement: imaging speed and robustness compared to a conventional stepping table technique. *Eur J Radiol* 80:537–542
- Kramer H, Schoenberg SO, Nikolaou K, Huber A, Struwe A, Winnik E et al (2005) Cardiovascular screening with parallel imaging techniques and a whole-body MR imager. *Radiology* 236:300–310
- Kramer H, Zenge M, Schmitt P, Glaser C, Reiser MF, Herrmann KA (2008) Peripheral magnetic resonance angiography (MRA) with continuous table movement at 3.0 T: initial experience compared with step-by-step MRA. *Invest Radiol* 43:627–634
- Kuo PH, Kanal E, Abu-Alfa AK, Cowper SE (2007) Gadolinium-based MR contrast agents and nephrogenic systemic fibrosis. *Radiology* 242:647–649
- Machann J, Thamer C, Stefan N, Schweszer NF, Kantartzis K, Haring HU et al (2010) Follow-up whole-body assessment of adipose tissue compartments during a lifestyle intervention in a large cohort at increased risk for type 2 diabetes. *Radiology* 257:353–363
- Puls R, Kuhn JP, Ewert R, Hosten N (2010) Whole-body magnetic resonance imaging for staging of lung cancer. *Front Radiat Ther Oncol* 42:46–54
- Ringe KI, Husarik DB, Sirlin CB, Merkle EM (2010) Gadoxetate disodium-enhanced MRI of the liver: part 1, protocol optimization and lesion appearance in the noncirrhotic liver. *AJR Am J Roentgenol* 195:13–28
- Ruehm SG, Goyen M, Quick HH, Schleputz M, Schleputz H, Bosk S et al (2000) Whole-body MRA on a rolling table platform (AngioSURF). *Rofo* 172:670–674
- Schaefer JF, Kramer U (2011) Whole-body MRI in children and juveniles. *Rofo* 183:24–36
- Schaefer JF, Schlemmer HP (2006) Total-body MR-imaging in oncology. *Eur Radiol* 16:2000–2015
- Schmidt GP, Kramer H, Reiser MF, Glaser C (2007a) Whole-body magnetic resonance imaging and positron emission tomography-computed tomography in oncology. *Top Magn Reson Imaging* 18:193–202
- Schmidt GP, Reiser MF, Baur-Melnyk A (2007b) Whole-body imaging of the musculoskeletal system: the value of MR imaging. *Skeletal Radiol* 36:1109–1119
- Seeger A, Kramer U, Fenchel M, Grimm F, Bretschneider C, Doring J et al (2008) Comparison between a linear versus a macrocyclic contrast agent for whole body MR angiography in a clinical routine setting. *J Cardiovasc Magn Reson* 10:63

Sönke Langner

5.1 The Head

5.1.1 Introduction

Magnetic resonance imaging is a well-established diagnostic tool for imaging the brain (Roberts and Mikulis 2007). Apart from providing excellent discrimination between gray and white matter, it is unique among imaging modalities in that the technique of diffusion-weighted imaging allows in vivo evaluation of normal water diffusion (Schaefer 2001, 2005).

While in the past dedicated head coils were only available on specialized MRI systems, today's state-of-the-art imagers with whole-body coil systems include optimized head coils for neuroradiologic evaluation as part of a whole-body or screening examination. The basic brain protocol should always include T1-weighted and T2-weighted imaging in different planes (Roberts and Mikulis 2007). T1-weighted sequences acquired in at least two planes perpendicular to each other are useful for a detailed evaluation of the topography of brain structures. Alternatively, to shorten acquisition time, high-resolution T1-weighted 3D datasets can be acquired with MPRAGE or FLASH sequences, for example. Midline structures are best evaluated on sagittal T2-weighted images acquired with thin-slice thickness and small interslice gaps. An axial T2-weighted sequence covering the entire brain is important for reliable detection of pathology. The FLAIR technique is very sensitive for the detection of white matter lesions, and it can be used for 2D imaging or for 3D imaging with subsequent multiplanar

S. Langner
Institute of Diagnostic Radiology and Neuroradiology,
University Medicine Greifswald, Ferdinand-Sauerbruch-Straße,
17487 Greifswald, Germany
e-mail: soenke.langner@uni-greifswald.de

reformation. FLAIR sequences are therefore of special interest for screening MRI examinations, which are typically performed without administration of contrast medium. Calcifications or hemosiderin deposits are reliably detected by MRI using susceptibility-weighted imaging (SWI) or a conventional T2*-weighted sequence (Haacke et al. 2009). Diffusion-weighted imaging (DWI) is highly sensitive and specific for the early detection of diffusion abnormalities in conditions such as ischemic stroke or inflammatory diseases. Time-of-flight magnetic resonance angiography (TOF-MRA) is another useful screening technique, providing angiographic information without contrast medium administration. TOF-MRA allows reliable evaluation of the anatomy of the circle of Willis and identification of abnormalities.

Lesions of the central nervous system (CNS) are common incidental findings on screening MRI. Characterizing these lesions and deciding which of them need workup is a challenging task. This chapter provides an overview of the most common incidental CNS findings, discussing the strengths and limitations of whole-body MRI and making recommendations for further diagnostic management.

5.1.2 Anomalies and Tumor-Like Lesions

5.1.2.1 Arachnoid Cysts

Arachnoid cysts are benign developmental collections of cerebrospinal fluid (CSF) within the arachnoid membrane (Pradilla and Jallo 2007). About 60 % of arachnoid cysts are located in the posterior cranial fossa, with the cerebellopontine angle, the suprasellar region, and the atypical locations accounting for 10 % each (Table 5.1). MRI depicts them as extra-axial oval to round lesions with sharp

Table 5.1 Arachnoid cysts

Frequency	Prevalence of approx. 0.5 %
Age predilection	Any age
Sex predilection	F:M ratio of 3–5:1
Location	60 % middle cranial fossa 10 % cerebellopontine angle 10 % suprasellar 10 % other
Type of lesion	Benign
Signs and symptoms	Asymptomatic Very large cysts may rarely cause headache, vertigo, sensorineural hearing loss, facial hemispasm
Differential diagnosis	Epidermoid Chronic subdural hematoma Subdural hygroma Nonneoplastic intra-axial cysts

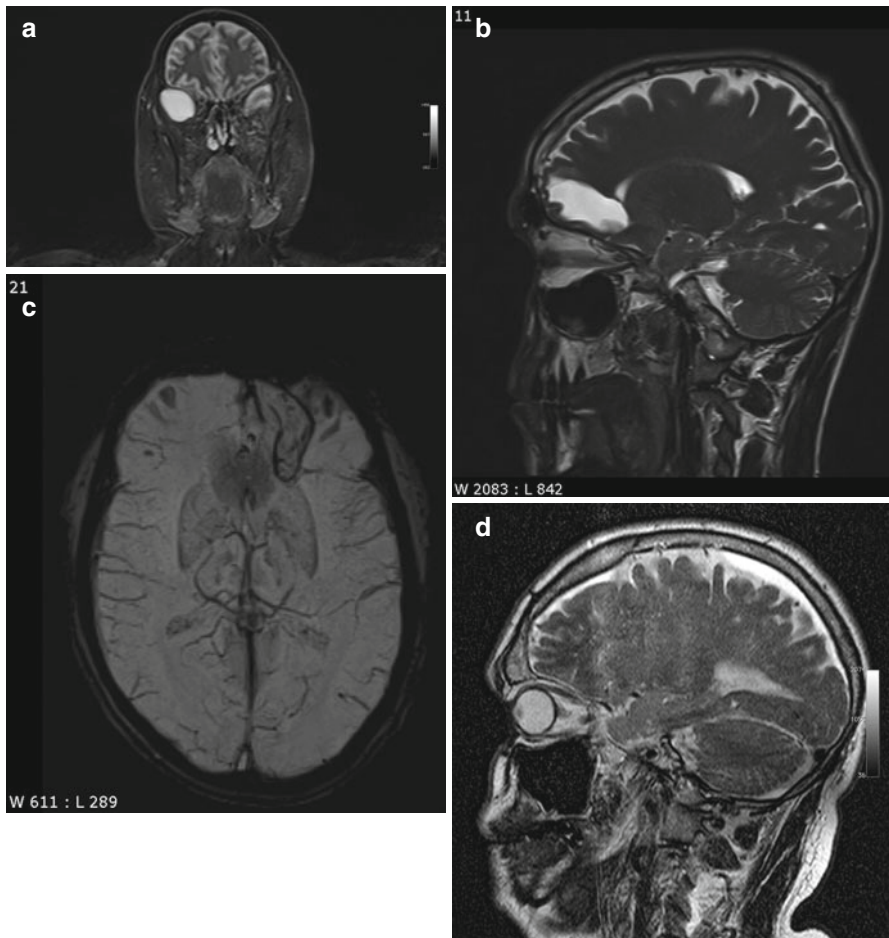


Fig. 5.1 Incidental screening findings in several subjects. (a) A 42-year-old male subject with a cystic mass in the middle cranial fossa on the right side. Coronal T2w TIRM image shows no reactive changes in surrounding brain. The lesion is isointense to fluid with all weightings, consistent with an arachnoid cyst. (b, c) A 33-year-old male subject with an intra-axial cyst in the left frontobasal region on sagittal T2w TSE image (b). Susceptibility-weighted image (c) demonstrates hemosiderin deposition, consistent with a defect after contusion. (d) A 51-year-old male subject with a convex extra-axial parietal mass of high signal intensity on sagittal T2w TSE image

borders that range in size from a few millimeters to several centimeters. The cysts are isointense to CSF on T1-weighted and T2-weighted images with complete loss of signal on FLAIR images (Fig. 5.1). DWI shows unrestricted diffusion (Bergui et al. 2001).

Clinical Management

Most arachnoid cysts are asymptomatic, and there is no need for follow-up as long as the MRI diagnosis is not in doubt. If an arachnoid cyst is very large and the mass effect causes complications, fenestration may be indicated (Cincu et al. 2007). The most important differential diagnosis is epidermoid cyst, which has high signal intensity on FLAIR images and DWI. SWI is useful for differentiation of an arachnoid cyst from a posttraumatic brain lesion, the latter typically being surrounded by hemosiderin. A subdural hygroma or hematoma is usually not isointense to CSF on all sequences and covers the brain surface in a cap-like manner. If these MRI techniques do not produce a diagnosis, it should be determined whether the subject has a history of head trauma.

5.1.2.2 Colloid Cysts

Colloid cysts are congenital intraventricular tumors and contain mucin. They arise from the rostral roof of the third ventricle close to the interventricular foramen (Grunwald et al. 2007), varying in size from a few millimeters to 3 cm (Table 5.2). Because they contain cholesterol, colloid cysts typically have high signal intensity on T1-weighted images (Fig. 5.2a) and tend to be isointense to brain on T2-weighted images (Fig. 5.2b). There is no signal drop on FLAIR images (Wilms et al. 1990). Due to their vicinity to the interventricular foramen, colloid cysts can cause chronic intermittent obstruction of CSF flow. Although they are congenital, most colloid cysts do not become apparent until age 30–50, when they typically present with intermittent headache. The differential diagnosis includes infection and CSF flow artifact (Prasad et al. 2008). In most cases, flow artifact can be ruled out by looking at images acquired with different weighting and in a different plane.

Table 5.2 Colloid cysts

Frequency	0.5–1 % of all primary brain tumors 15–20 % of all intraventricular masses
Age predilection	Individuals aged 40; rarely in children
Sex predilection	F=M
Location	Rostral roof of the third ventricle close to the interventricular foramen Very rarely in other sites (lateral ventricles, 4th ventricle, extraventricular)
Type of lesion	Benign
Signs and symptoms	Asymptomatic Risk of obstruction of interventricular foramen with acute obstruction of CSF flow (life-threatening)
Differential diagnosis	Neurocysticercosis Flow artifact Tumor (subependymoma, craniopharyngeoma)

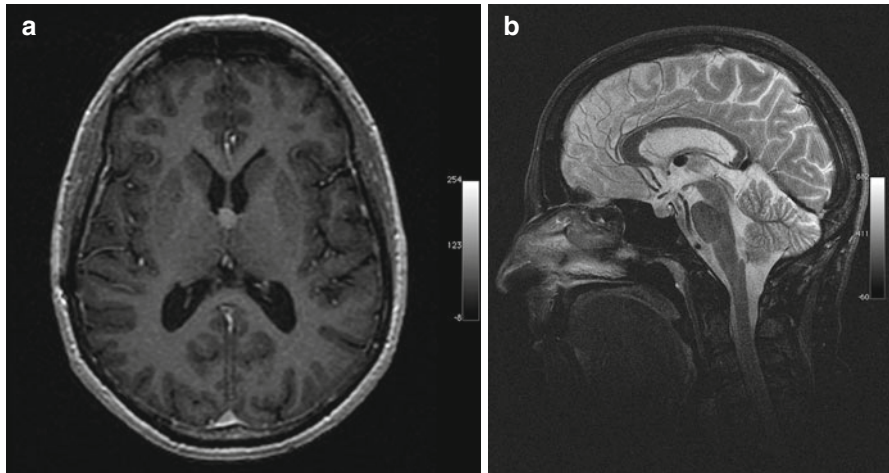


Fig. 5.2 Incidental screening finding and preoperative imaging in a 38-year-old female subject. (a) Axial T1w MPR image depicts a smoothly margined lesion of high signal intensity at the roof of the third ventricle, suggesting a colloid cyst. (b) Preoperative sagittal T2w IR-TSE image shows a homogeneous lesion of low signal intensity

Clinical Management

The risk of acute CSF obstruction should prompt timely workup of a colloid cyst by a neurosurgeon (Tirakotai et al. 2004). A suspected colloid cyst with an atypical shape should always be assessed further by contrast-enhanced MRI to rule out an inflammatory process or malignancy.

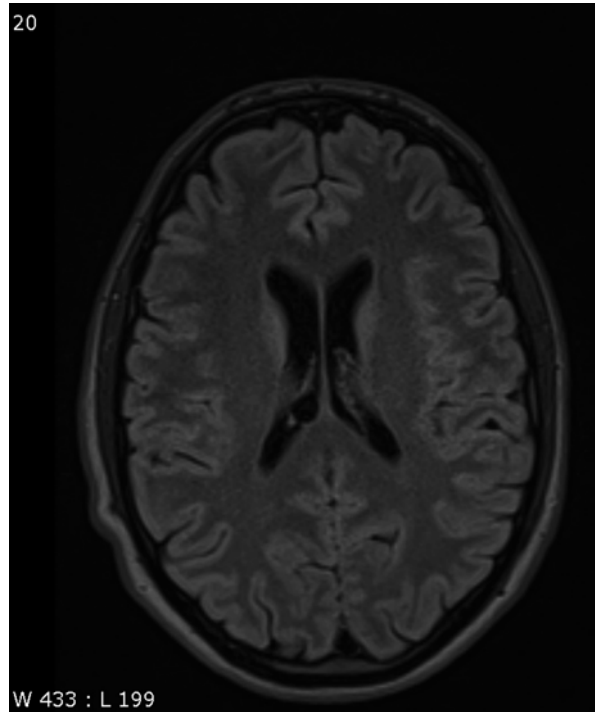
Table 5.3 Choroid plexus cysts

Frequency	Prevalence increases with age
Age predilection	Any age
Sex predilection	M=F
Location	Trigone bilaterally
Type of lesion	Benign
Signs and symptoms	Asymptomatic
Differential diagnosis	Inflammatory processes Ependymal cyst Malignancy

5.1.2.3 Choroid Plexus Cysts

A choroid plexus cyst is a nonneoplastic, noninflammatory cyst of the choroid plexus (Naeni et al. 2009). In adults, it is the most common choroid plexus lesion. The adult form, also known as xanthogranuloma, is typically degenerative in nature. Most choroid plexus cysts are bilateral and located in the trigone. The majority are small, measuring 2–8 mm. Cysts greater than 2 cm are very rare. Multiple cysts are

Fig. 5.3 Incidental screening finding in a 43-year-old female subject. Axial T2w FLAIR image shows a smoothly demarcated mass isointense to CSF in the choroid plexus on the right side. The appearance is consistent with a choroid plexus cyst



common (Kariyattil and Panikar 2008) (Table 5.3). The MRI signal intensity relative to CSF is isointense to slightly hyperintense on T1-weighted images, hyperintense on T2-weighted images, and isointense on FLAIR images (Fig. 5.3). Peripheral calcification is common and can be detected on susceptibility-weighted images. DWI demonstrates restricted diffusion in approx. 60 % of choroid plexus cysts (Bonneville et al. 2007).

Clinical Management

If there is no doubt about the diagnosis of a choroid plexus cyst, no additional diagnostic measures are needed. If it is not possible to clearly localize the cyst to the choroid plexus, the topographic relationship should be assessed further using a high-resolution T2-weighted sequence (e.g., CISS, constructive interference in steady state). A contrast-enhanced MRI examination should be performed to rule out an inflammatory process or malignant tumor.

5.1.2.4 Intra-axial Cystic Lesions

Neuroepithelial or neuroglial cysts are benign developmental cysts lined with epithelium. These cysts are more often supratentorial than infratentorial in location, and they are most commonly found in the frontal lobe and close to the lateral

Table 5.4 Intra-axial cystic lesions

Frequency	Prevalence increases with age
Age predilection	Any age
Sex predilection	M=F
Location	Supra- and infratentorially, predominantly in the frontal lobe and in close relationship to a lateral ventricle
Type of lesion	Benign
Signs and symptoms	Typically asymptomatic; large cysts may cause symptoms
Differential diagnosis	Inflammatory processes Ependymal cyst Malignancy

ventricle. They vary considerably in size, from a few millimeters to several centimeters, and typically cause no symptoms (Table 5.4). Neuroepithelial cysts are isointense to CSF on T1-weighted and T2-weighted images. On FLAIR images, there is no abnormal high signal intensity of surrounding brain (Bergui et al. 2001; Poptani et al. 1995).

Neuroepithelial cysts must not be confused with enlarged perivascular spaces, also known as Virchow-Robin spaces, which are interstitial, fluid-filled perivascular channels lined by pia mater (Fig. 5.4a, b). These spaces surround penetrating arteries as they enter the brain and are not contiguous with the subarachnoid space. Common locations are the basal ganglia, midbrain, deep white matter, subinsular cortex, and external capsule. Virchow-Robin spaces are usually <5 mm in diameter but may become very large, causing local mass effect. They are also isointense to CSF with all pulse sequences. In approx. 25 % of cases, however, the surrounding brain has increased signal intensity on FLAIR images (Fig. 5.4c) (Kwee and Kwee 2007).

Clinical Management

If the vessel surrounded by an enlarged perivascular space is not identified as a flow void on T2-weighted images, the MRI appearance may not allow differentiation between a Virchow-Robin space and a neuroepithelial cyst. This distinction, however, has no clinical relevance. Enlarged perivascular spaces will be seen nearly anywhere in the brain, especially when MRI is performed at higher field strength. They are also found in 30 % of children undergoing cerebral MRI. No follow-up is needed (“leave me alone lesions”). In contrast, a subject with a cystic lesion that has an atypical configuration and differs in signal intensity from CSF should undergo contrast-enhanced MRI to rule out an infectious lesion or a malignant tumor. In older subjects, especially those with risk factors, the differential diagnosis should always include a lacunar infarct.

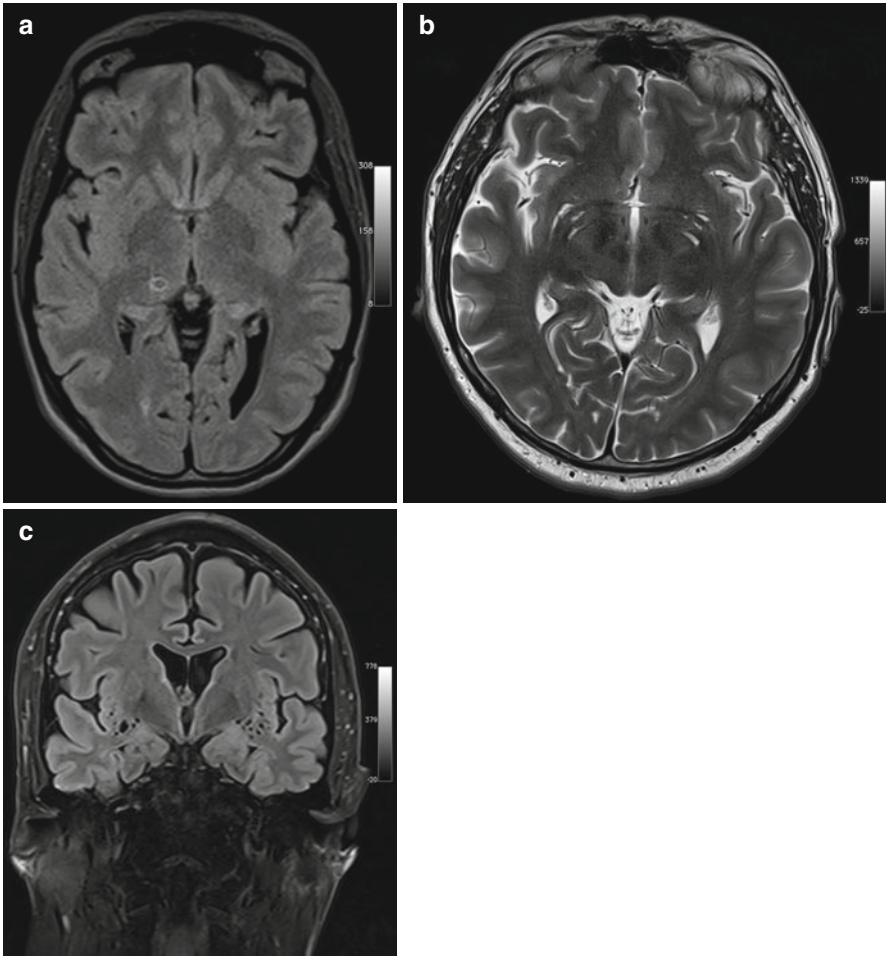


Fig. 5.4 Incidental screening findings and workup in two subjects. **(a)** A 42-year-old male subject with a smoothly marginated lesion isointense to CSF in the thalamus on the right and slightly increased signal intensity of surrounding brain on axial T2w FLAIR image. This appearance suggests an enlarged perivascular space. **(b, c)** In a second case, a 23-year-old man, enlarged perivascular spaces are demonstrated by MRI workup performed at 3 T. There is enlargement of the perivascular spaces in the basal ganglia on axial T2w TSE image **(b)** and in the insular region bilaterally on coronal T2w FLAIR image **(c)**

5.1.2.5 Septum Pellucidum Variants

The septum pellucidum consists of two leaves forming a partition between the two lateral ventricles. Failure of the fetal septum pellucidum to obliterate can give rise to persistent CSF-filled spaces in this area. Three types are distinguished: the cavum septi pellucidi, which is located between the two anterior horns; the cavum vergae (Fig. 5.5a), which extends over the entire length of the septum; and the cavum veli interpositi (Fig. 5.5b), which is situated posteriorly and does not extend rostrally

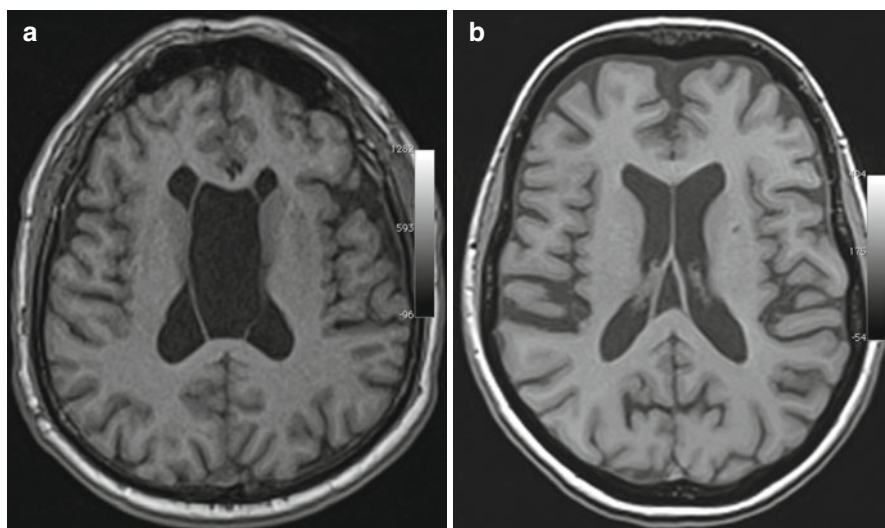


Fig. 5.5 Incidental screening findings in two subjects. (a) In a 41-year-old female subject, axial T1w MPR image demonstrates a hollow space isointense to CSF between the leaves of the septum pellucidum, consistent with a cavum vergae. (b) In a 59-year-old female subject, axial T1w MPR image demonstrates a cavum veli interpositi

Table 5.5 Septum pellucidum variants

Frequency	Cavum septi pellucidum, up to 20 % in adults Cavum vergae, <1 % in adults Cavum veli interpositi, <1 %
Age predilection	Any age
Sex predilection	F=M
Location	Interventricular septum
Type of lesion	Benign
Signs and symptoms	Asymptomatic
Differential diagnosis	Epidermoid cyst

beyond the level of the interventricular foramen (Table 5.5) (Gangemi et al. 1997). The fluid-filled spaces are isointense to surrounding brain on T1-weighted and T2-weighted images, and DWI shows no diffusion restriction. If there is no signal drop on FLAIR images, the differential diagnosis should include epidermoid cyst (Donati et al. 2003).

Clinical Management

Septum pellucidum variants are of no clinical significance, and no further diagnostic workup is required (Born et al. 2004).

5.1.2.6 Lipoma

Lipomas are very rare in the brain. They are congenital tumors containing normal fat. Intracranial lipomas are neither hamartomas nor true neoplasms (Radner et al. 2002). Intracranial lipomas commonly occur in the corpus callosum with more than 50 % in the posterior portion. Other sites include the quadrigeminal plate (Fig. 5.6), superior vermis, tuber cinereum, and hypophyseal stalk (Table 5.6) (Yildiz et al. 2006; Yilmazlar et al. 2005). Lipomas have high signal intensity on T1-weighted images and low signal intensity on T2-weighted SE images. With the T2-weighted TSE sequences now generally used for brain imaging, lipomas also have high T2 signal intensity.

Fig. 5.6 Incidental screening finding in a 37-year-old male subject. Axial T1w MPR image shows a high-signal-intensity mass adjacent to the aqueduct, consistent with lipoma

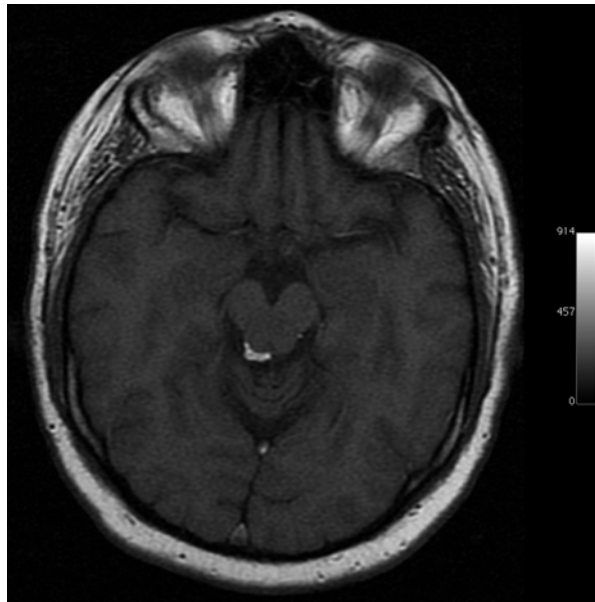


Table 5.6 Lipoma

Frequency	<0.5 % of all intracranial masses
Age predilection	Any age
Sex predilection	F=M
Location	80 % supratentorial: 50 % interhemispheric fissure, 15 % suprasellar, 15 % pineal region 20 % infratentorial: most commonly cerebellopontine angle
Type of lesion	Benign
Signs and symptoms	Asymptomatic
Differential diagnosis	Dural dysplasia Dermoid Teratoma Subacute hemorrhage

Clinical Management

Most lipomas in the brain are asymptomatic and detected incidentally. When a lipoma is detected in an epileptic subject, attention must be paid to the presence of concomitant anomalies. If a confident diagnosis of lipoma cannot be made, MRI with fat suppression or even a cranial CT scan should follow.

5.1.3 Brain Tumors**5.1.3.1 Introduction**

Brain tumors can be classified according to different criteria. They are generally divided into primary brain tumors (approx. 60 % of cases) and secondary or metastatic brain tumors (approx. 40 % of cases) (Radner et al. 2002; Rousseau et al. 2008).

Among primary brain tumors, an important distinction in terms of surgical management is made between intra-axial tumors, which arise in glial or neuronal cells, and extra-axial tumors, which compress the brain from the outside (Bonnevillie et al. 2007).

Primary brain tumors differ from tumors elsewhere in the body in that, even if they are histologically benign, they may have “malignant” potential due to their location and possible mass effect.

Most intracranial tumors can be detected without contrast medium administration. With few exceptions, contrast-enhanced MRI is only performed to obtain additional information for tumor characterization such as presence and extent of blood-brain barrier (BBB) disruption or degree of tumor vascularization (Niedermayer et al. 1998).

5.1.3.2 Intra-axial Tumors**5.1.3.2.1 Primary Brain Tumors**

With an incidence of 8 per 100,000 population per year, primary brain tumors account for 1.4 % of all malignancies, and the risk increases with age (Table 5.7) (Chamberlain and Kormanik 1998). The WHO classification of brain tumors is the most widely utilized classification scheme (Radner et al. 2002; Rousseau et al. 2008). Last revised in 2007, it classifies primary brain tumors according to their tissue of origin and additionally distinguishes four histologic grades based on biological activity (WHO I-IV). The majority of primary brain tumors are of glial origin. Astrocytomas are the most common gliomas, constituting approx. 60 % of cases. Approx. 65–75 % of astrocytomas are accounted for by higher-grade anaplastic astrocytoma (WHO III) and glioblastoma multiforme (WHO IV).

Clinical symptoms depend on tumor location and size. Brain tumors often present with a focal neurologic deficit or symptoms related to increased intracranial pressure. A seizure may be the initial symptom of a cortical tumor such as low-grade astrocytoma.

Table 5.7 Primary brain tumors

Frequency	8/100,000 population/year
Age predilection	Low-grade tumors: children and young adults aged 20–40 Higher-grade tumors: typically after age 50, rarely before age 30
Sex predilection	M=F
Location	Depends on histology
Type of lesion	Depends on histology and location
Signs and symptoms	Vary with tumor site: focal neurologic deficits or even stroke, obstruction of CSF flow, seizures in case of cortical tumors
Differential diagnosis	Atypical infarction Postcontusional gliosis Lymphoma Metastasis Inflammatory processes (abscess, tuberculosis)

Low-grade brain tumors typically have uniform low T1 signal intensity (Fig. 5.7a) and appear bright on T2-weighted or FLAIR images (Pope et al. 2005). As there is usually no diffusion restriction, DWI can help in differentiating a brain tumor from atypical infarction. A small cortical tumor may be difficult to distinguish from post-traumatic gliosis, but the absence of signal voids on susceptibility-weighted images may be helpful in making the distinction. With increasing malignancy, a brain tumor becomes more inhomogeneous on both T1-weighted and T2-weighted images (Fig. 5.7b), and diffusion restriction also occurs (Seo et al. 2008).

Clinical Management

A subject with a suspected primary brain tumor requires prompt supplementary imaging with contrast-enhanced sequences for a comprehensive MRI evaluation (Fig. 5.7c). Along with information on tumor site and extent of perifocal edema, enhancement features contribute to determining the histologic grade. Timely neurosurgical consultation is also important. While higher-grade primary brain tumors must be differentiated from lymphoma and metastasis, this is usually not possible with conventional pulse sequences. However, whole-body MRI can help in identifying a possible primary tumor or, when lymphoma is suspected, in confirming or ruling out systemic disease (Fig. 5.7d).

Fig. 5.7 Incidental screening findings and workup in two subjects. **(a)** A 39-year-old male subject with a solid mass in the periventricular white matter of the right trigone. Axial T1w MPR image demonstrates a lesion of homogeneously low signal intensity with only minimal perifocal edema. The histologic diagnosis was WHO grade III astrocytoma. **(b–d)** In a second subject, a 52-year-old woman, a sagittal T2w TSE screening image reveals an inhomogeneous mass in the splenium **(b)**. At workup, the mass shows peripheral contrast enhancement on axial T1w FLASH image acquired at 3 T **(c)**. In this case, the histologic diagnosis was B-cell lymphoma. The whole-body screening MRI, coronal T2w TIRM image **(d)**, reveals no other lesion, confirming primary CNS lymphoma

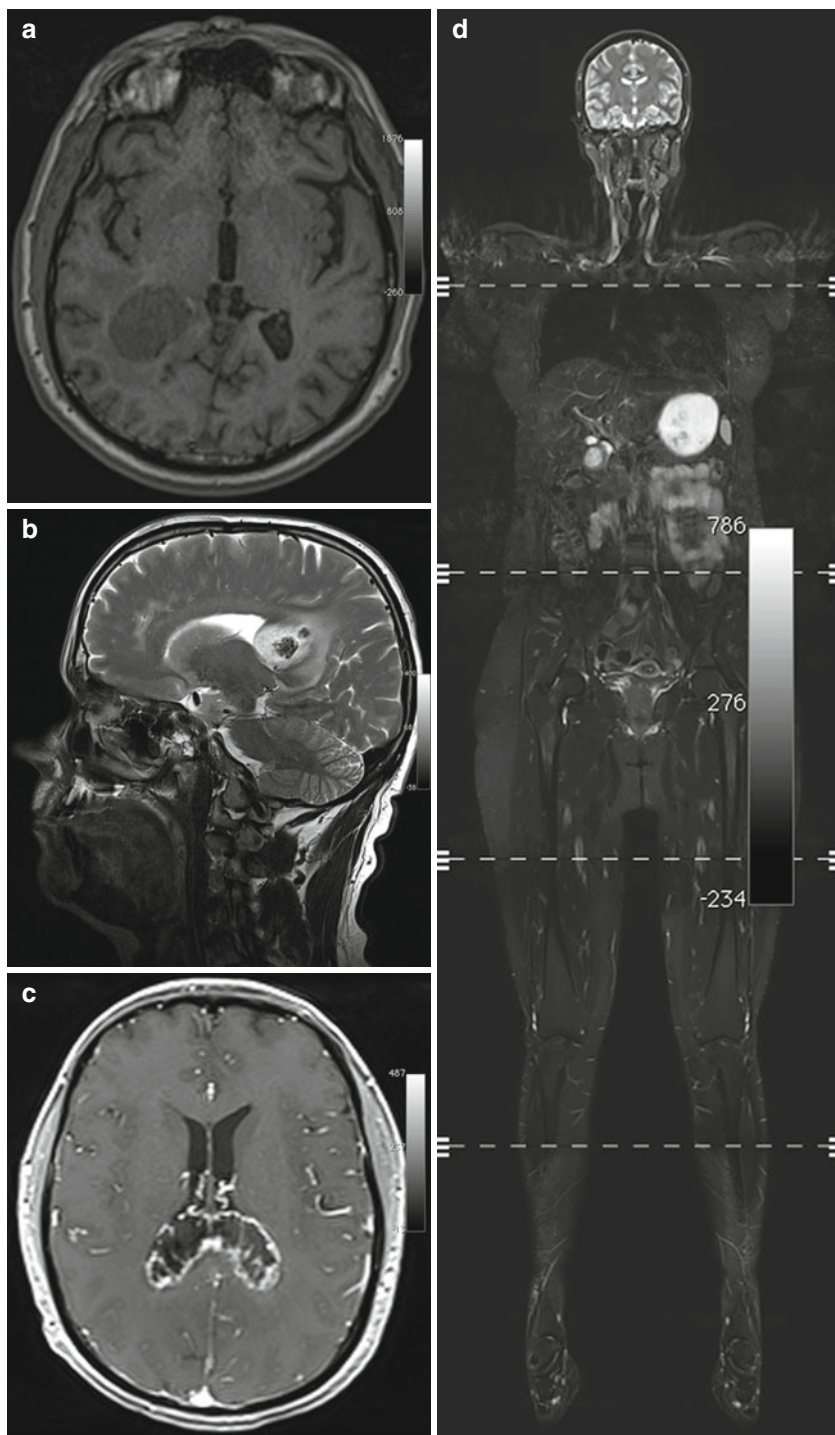


Table 5.8 Pineal cysts

Frequency	Detected in up to 10 % of all head MRI examinations Most common in women aged 20–30
Age predilection	Puberty to age 40
Sex predilection	F:M ratio of 3:1
Location	Pineal compartment
Type of lesion	Benign
Signs and symptoms	Rare; tumors compressing the tegmentum and aqueduct may cause Parinaud syndrome or obstruct CSF flow
Differential diagnosis	Arachnoid cyst Cavum veli interpositi Meningioma Pineocytoma (very rare)

5.1.3.3 Extra-axial Tumors

5.1.3.3.1 Pineal Cysts

Cystic lesions of the pineal region are among the most common incidental findings on cranial MRI, occurring in approx. 10 % of all examinations (Table 5.8) (Costa et al. 2008; Pu et al. 2007). Pineal cystic lesions measuring at least 5 mm should be classified as cysts (Sato and Kubota 2009). Pineal cysts typically have the same signal intensity as CSF on both T1-weighted and T2-weighted images (Fig. 5.8a). Depending on the protein content, the cyst fluid may have high signal intensity on FLAIR images. A benign pineal cyst can be septated and contain calcifications. Even contrast enhancement has been described.

Most pineal cysts are asymptomatic. Occasionally, a large cyst compressing the quadrigeminal plate (Fig. 5.8b, c) may cause Parinaud syndrome or headache due to obstruction of CSF flow.

The most important differential diagnoses are infratentorial arachnoid cyst and cavum veli interpositi. If solid components predominate, the differential diagnosis also includes meningioma originating in the tentorium, falx, or velum interpositum. Primary pineal tumors are extremely rare (<1 % of intracranial tumors).

Clinical Management

As pineal cysts are very common, follow-up should be purely clinical (Tirakotai et al. 2004). A contrast-enhanced MRI scan is recommended for pineal cysts first diagnosed in adults over 40, for cysts with an irregular and thickened wall (≥ 2 mm), and for cysts with solid components.

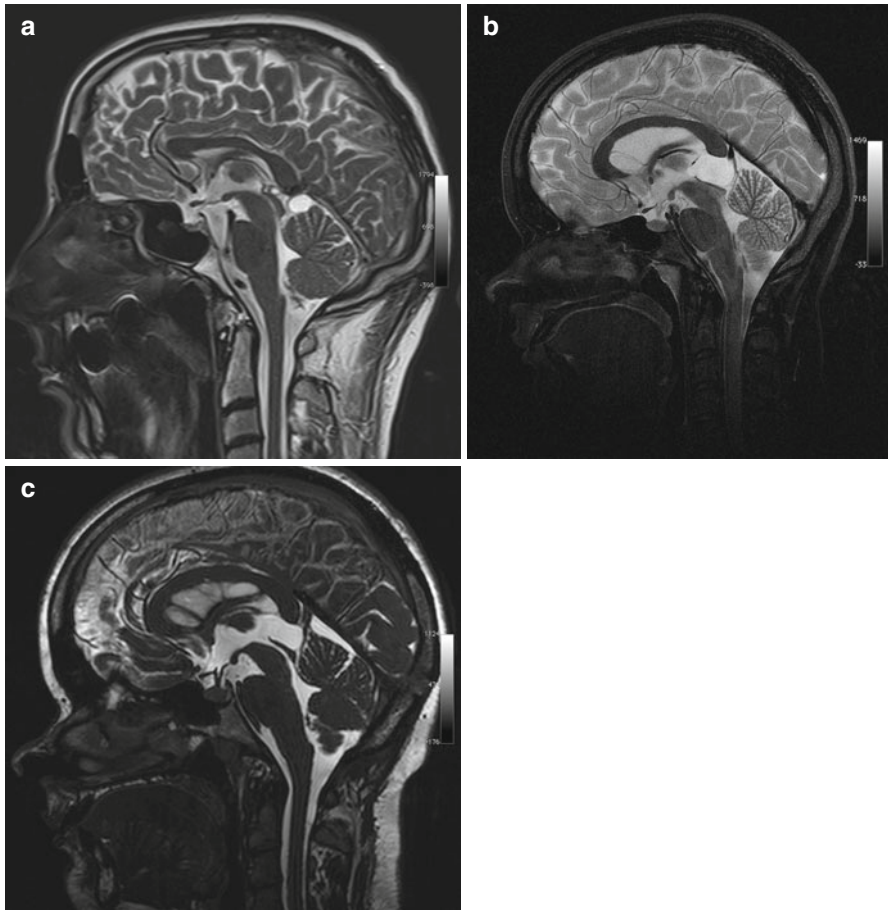


Fig. 5.8 Incidental screening findings in two subjects and postoperative follow-up. (a) A 36-year-old male subject with a cystic lesion of the pineal region. The cyst has a thin wall and causes no mass effect on the tegmentum, consistent with a pineal cyst. The sagittal T2w TSE image also reveals an infratentorial arachnoid cyst. (b, c) In a second subject, a 24-year-old woman, sagittal T2w TSE screening image shows a cyst of the pineal region with mass effect (b). She had a history of double vision and progressive headache. The sagittal T2w CISS image shows the situation after neurosurgical cyst fenestration (c)

5.1.3.4 Sellar Lesions

5.1.3.4.1 Pituitary Adenoma

The anatomy of the sella turcica is complex. With the cavernous sinus adjacent to it, the cranial nerves running through it, and the internal carotid artery lying in close proximity, this rather small region includes many important anatomic structures as

Table 5.9 Pituitary adenoma

Frequency	10–15 % of all intracranial neoplasms
Age predilection	30–60 years
Sex predilection	F:M ratio of 2:1
Location	Intrasellar, parasellar, suprasellar
Type of lesion	Benign
Signs and symptoms	Functioning adenomas: effects vary with the hormone produced Local mass effect on optic chiasm and cavernous sinus with cranial nerve paresis (III, IV, VI)
Differential diagnosis	Craniopharyngioma Meningioma Internal carotid artery aneurysm with (partial) thrombosis Pars intermedia cyst, Rathke cleft cyst Epidermoid/dermoid cysts

well as a variety of tissues, giving rise to a wide spectrum of congenital and acquired lesions. In general, sellar MRI should be performed by acquiring thin-slice T2- and T1-weighted sequences (≤ 3 mm slice thickness) before and after contrast medium administration. These sequences are usually not included in a whole-body screening protocol, often making it difficult to differentiate sellar lesions on screening datasets.

Pituitary adenoma is the most common intrasellar mass, constituting approx. 10–15 % of all intracranial tumors (Table 5.9) (Rousseau et al. 2008; Glezer et al. 2008). The pituitary gland consists of two major divisions, the adeno-hypophysis (anterior lobe) and the neurohypophysis (posterior lobe). Adenomas arise in the anterior lobe. The normal pituitary gland is isointense relative to brain on both T1-weighted and T2-weighted images. On sagittal images, the normal size of the pituitary gland is ≤ 10 mm in women (Donovan and Nesbit 1996; Cox and Elster 1991) and ≤ 8 mm in men. An increased diameter is normal in pregnant and breast-feeding women. In about half of individuals below 35 years of age, the cranial portion of the pituitary gland has a convex shape (Donovan and Nesbit 1996).

Pituitary adenomas are classified by size and hormonal activity. By definition, a microadenoma is less than 10 mm in diameter, while a macroadenoma is 10 mm or larger (Fig. 5.9a). Based on hormonal activity, a distinction is made between functioning and nonfunctioning tumors (30 % of pituitary adenomas). Most nonfunctioning adenomas are macroadenomas. They typically come to clinical attention due to local mass effect causing bitemporal hemianopia by compressing the optic chiasm or causing paresis of cranial nerves III, IV, and VI by invading the cavernous sinus. Conversely, microadenomas present with symptoms related to excess hormone production.

Pituitary adenomas characteristically have a solid appearance but may also have cystic components or be completely cystic (Fig. 5.9b). The differential diagnosis includes craniopharyngioma, especially when the cyst fluid has high T1 and T2 signal intensity and when the largest portion of the tumor is suprasellar in location (Karavitaki et al. 2008). Other differential diagnostic considerations for intrasellar

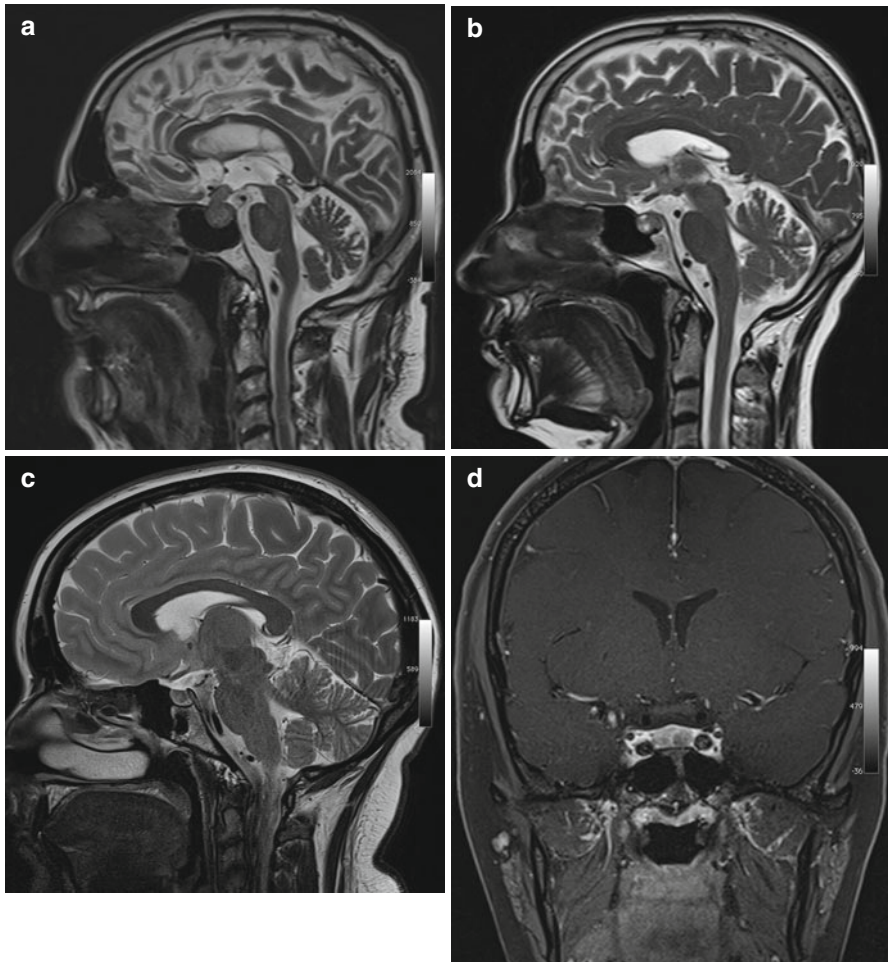


Fig. 5.9 Incidental screening findings and workup in three subjects. **(a)** A 52-year-old male subject with a sellar mass on sagittal T2w TSE image. The mass is isointense to white matter and compresses the optic chiasm by suprasellar expansion. The appearance is consistent with a macroadenoma, which was histologically proven. **(b)** In a second subject, a 49-year-old woman, sagittal T2w TSE image demonstrates a sellar mass with cystic and solid components. Laboratory testing revealed markedly elevated growth hormone (GH), consistent with an adenoma. **(c, d)** In a third subject, a 24-year-old woman, sagittal T2w TSE image shows borderline enlargement of the sella and pituitary gland **(c)**. She reported a history of amenorrhea. Laboratory testing revealed elevated prolactin. Diagnostic workup with 3-T MRI demonstrates a perfusion deficit of the sella, as shown on coronal T1w SE image with fat saturation after contrast medium administration **(d)**. The findings are consistent with a microprolactinoma

cystic lesions include Rathke cleft cysts, pars intermedia cysts, epidermoids, and dermoid cysts (Glezer et al. 2008; Noh et al. 2007; Naylor et al. 1995), all of which have high T1 signal intensity and low T2 signal intensity.

Clinical Management

All sellar masses should be followed up using contrast-enhanced MRI. When a microadenoma is suspected, a dynamic contrast-enhanced series should be acquired. Alternatively, an MRI examination at half the usual contrast medium dose should be performed, as otherwise a small lesion may be obscured by rapidly enhancing normal pituitary tissue (Fig. 5.9c, d). The radiologist must be aware that seemingly normal changes, especially in the adenohipophysis, may mask a tumor. When an abnormality is suspected, the subject's history may provide further clues.

A pituitary lesion with suprasellar or parasellar extension and compression or infiltration of surrounding structures requires timely primary neurosurgical workup; in other cases, the first diagnostic step is medical/endocrinologic workup.

5.1.3.4.2 Meningioma

Meningiomas are the second most common primary brain tumors after gliomas. With an incidence of approx. 6/100,000 population, meningiomas account for 13–26 % of primary brain tumors (Rousseau et al. 2008). They are most common between the ages of 40 and 70, and they are more common in women than in men (ratio of 3:2 to 2:1) (Table 5.10).

Meningiomas arise from arachnoid cap cells, and, because they attach to the dura, they have a characteristic spherical shape. A less common diffuse type, called en plaque meningioma, grows in a flattened fashion along dural structures. The most frequent sites of occurrence of meningiomas are along the parasagittal convexities, along the falx, and along the sphenoid ridges in the hemispheres, at the skull base – particularly along the olfactory grooves and within the sella or in the parasellar region – and in the posterior cranial fossa (Fig. 5.10). Less commonly, meningiomas extend along the optic nerve or occur in intraventricular location. Up to 15 histologic subtypes are distinguished. Most meningiomas are WHO grade I

Table 5.10 Meningioma

Frequency	13–26 %
Age predilection	50–70 years
Sex predilection	F:M ratio of 3:2 to 2:1
Location	Parasagittal, falx, sphenoid ridges, skull base, posterior cranial fossa, intraventricular, optic nerve
Type of lesion	Benign
Signs and symptoms	Most meningiomas are asymptomatic Focal neurologic deficits may occur, depending on site and extent of meningioma
Differential diagnosis	Metastasis Extramedullary hematopoiesis

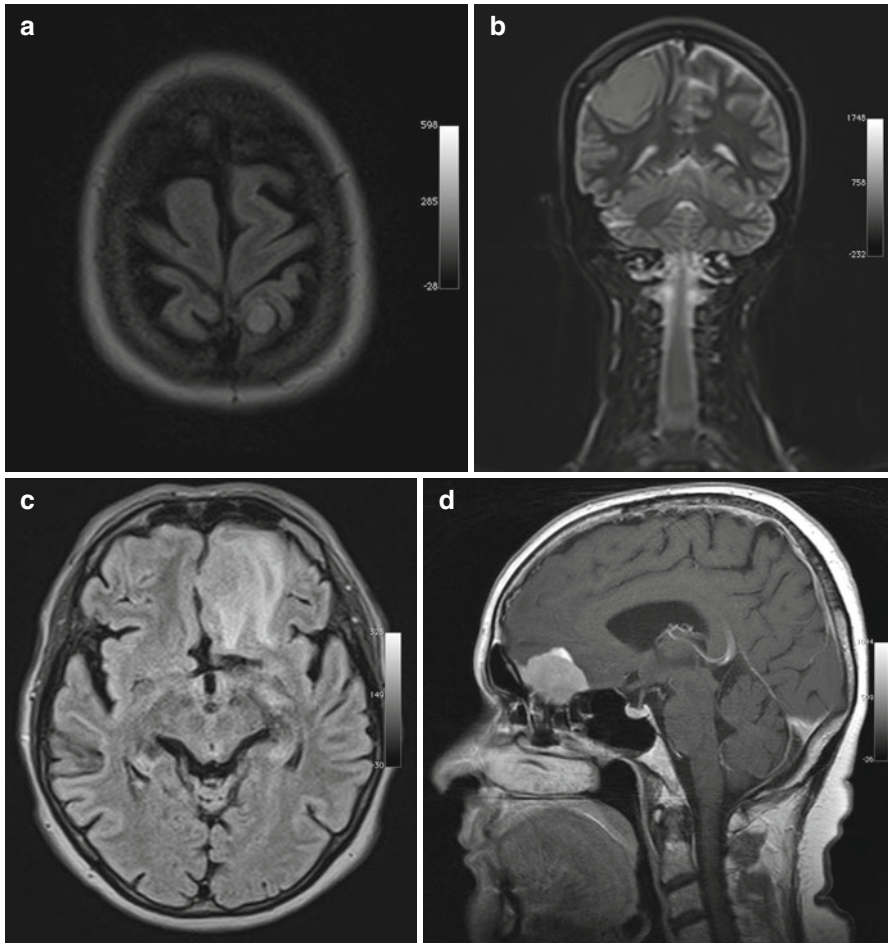


Fig. 5.10 Incidental screening findings in three subjects. **(a)** A 46-year-old female subject with a small left parietal parasagittal convexity meningeoma. The lesion is isointense to white matter on axial T2w FLAIR image. There is no perifocal edema. **(b)** A 32-year-old female subject with a mass measuring approx. 8 cm. On coronal T2w TIRM image, the mass is isointense to white matter and protrudes convexly from the dura mater toward the brain. There are no reactive changes in surrounding brain. Histologically proven convexity meningeoma. **(c, d)** A 64-year-old female subject with a left frontobasal mass that is contiguous with the dura mater. The tumor is nearly isointense to white matter but is surrounded by extensive perifocal edema on axial T2w FLAIR image **(c)**. Workup of this subject at 1.5 T reveals homogeneous enhancement on sagittal T1w SE image acquired after contrast medium administration **(d)**. The MRI appearance is consistent with an olfactory groove meningeoma. The diagnosis was confirmed by histologic examination

tumors, and morphologic imaging features usually enable no further differentiation (Niedermayer et al. 1998; Nagar et al. 2008).

Meningiomas have nearly the same signal intensity as the brain on both T1-weighted and T2-weighted images (Grunwald et al. 2007) with approx. 20–25 %

containing calcifications in the tumor matrix. Calcifications may be seen as hyperintensities on plain T1-weighted images but are best detected as signal voids on susceptibility-weighted images. Rapid growth may be associated with development of perifocal edema. Slowly growing meningiomas can become very large without any major effect on surrounding brain. Slight enlargement of CSF spaces around a meningioma is common and can serve as an indicator that a mass is extra-axial in location (Grunwald et al. 2007; Bonneville et al. 2007).

Clinical Management

Surgery is indicated if a meningioma invades the orbit or impinges on the optic nerve, if the subject is young, if extensive perifocal edema is present, or if the tumor causes neurologic symptoms. In unclear cases, a contrast-enhanced MRI study is helpful, showing strong uniform enhancement if a meningioma is present. Meningiomas with uniform calcification (susceptibility-weighted images) can be left alone as they are not likely to grow further. Noncalcified meningiomas should be followed up on a long-term basis using contrast-enhanced MRI. If a meningioma is close to the large venous channels, their patency should be established by TOF-MRA.

5.1.3.5 The CSF System

5.1.3.5.1 Pseudotumor Cerebri

The Monro-Kellie doctrine states that the cranial cavity is a closed rigid box (Brazis 2008) and that if any of the three CNS components (brain, CSF, blood) increases in volume, intracranial pressure (ICP) will increase as well, unless there is compensatory reduction in the volume of another component. Pseudotumor cerebri, or idiopathic intracranial hypertension, is characterized by increased ICP in the absence of an intracranial mass lesion and is most commonly seen in obese young women. The incidence is approx. 1/100,000 population/year, increasing to approx. 20/100,000/year in women between ages 20 and 40 whose body mass index (BMI) is more than 20 % above the ideal weight (Ball and Clarke 2006). Typical clinical symptoms are headache in 90–95 % of cases and visual impairment in approx. 65–70 % (Brazis 2008). Visual impairment commonly takes the form of optical sensations that can be elicited by a change in posture or Valsalva maneuver. Headache related to pseudotumor cerebri may be transient or permanent and of varying intensity and must be differentiated from tension headache and migraine. Another symptom is pulsatile tinnitus; if the latter is present, the differential diagnosis includes dural arteriovenous (AV) fistula (Table 5.11).

An increase in ICP causes widening of the external CSF spaces along both optic nerves (Rohr et al. 2008). Widened CSF spaces are well detected on coronal T2-weighted fat-saturated images or axial FLAIR images (Fig. 5.11b, c). Concomitant papilledema can be identified as protrusion of the optic disc and flattening of the posterior sclera on axial T2-weighted images. Finally, there will be

Table 5.11 Pseudotumor cerebri

Frequency	1–20/100,000 population/year
Age predilection	20–40 years
Sex predilection	F:M ratio of 8:1
Location	–
Type of lesion	–
Signs and symptoms	Headache, visual impairment, pulsatile tinnitus, nausea, vomiting, fatigue
Differential diagnosis	Secondary ICP increase Dural AV fistula

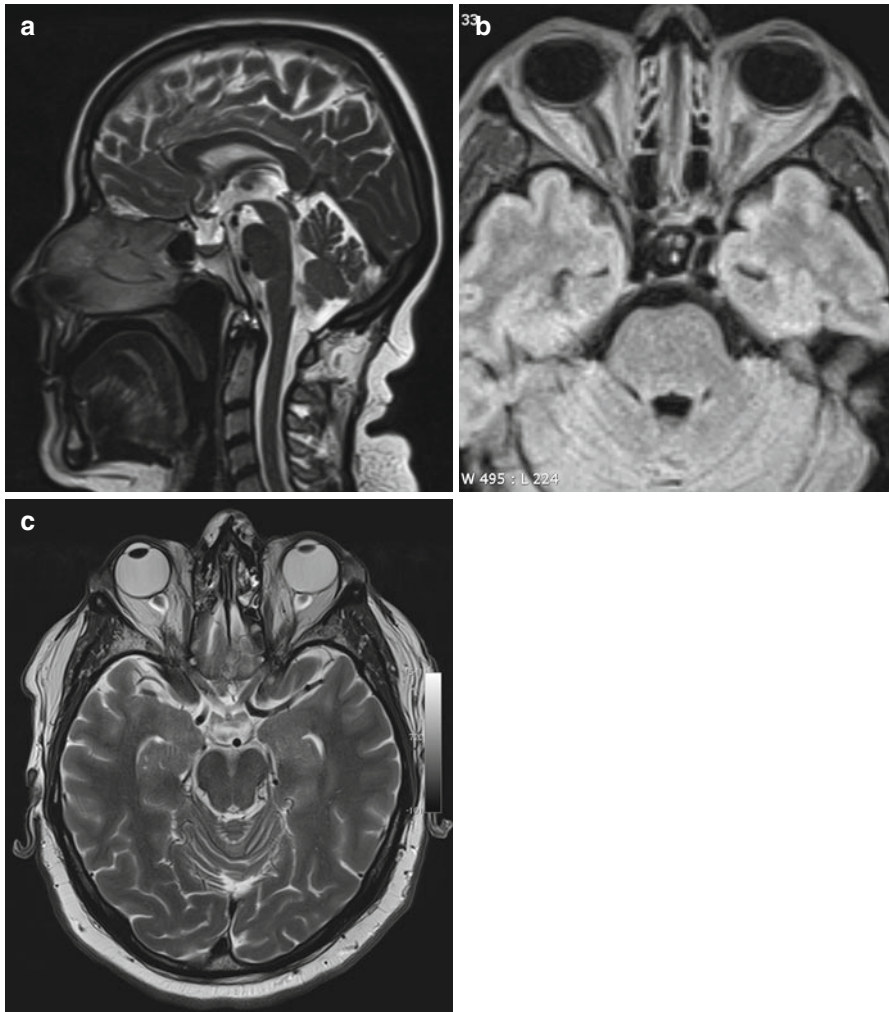


Fig. 5.11 Incidental screening finding and workup at 3 T in a 32-year-old female subject with a BMI of 32 kg/m². MRI demonstrates an empty sella with only a thin strip of tissue left at the base of the sella on sagittal T2w TSE image (a). Axial T2w image shows dilated CSF spaces along both optic nerves (b). Workup, axial T2w TSE image (c), in this subject demonstrates bilateral optic disc protrusion with flattening of the posterior sclera as signs of papillary edema

enlargement of the suprasellar cistern with protrusion into the sella and compression of the pituitary gland, giving rise to the typical empty sella appearance on sagittal images (Fig. 5.11a).

Clinical Management

Pseudotumor cerebri is an often overlooked cause of headache, especially in young obese women. If this condition is suspected on the basis of MRI findings, a subject should undergo MR venography, which will typically reveal unilateral or bilateral stenosis of the transverse sinus. In addition, an examination by an ophthalmologist is indicated to confirm or rule out papilledema. Lumbar puncture demonstrating elevated CSF pressure is diagnostic, which is why all subjects with suspected pseudotumor cerebri should see a neurologist.

5.1.3.5.2 Normal Pressure Hydrocephalus

Hydrocephalus occurs when there is an imbalance between the production and resorption of CSF, which, according to the Monro-Kellie doctrine, results in widening of the cerebral ventricles. The most sensitive imaging sign is dilation of the temporal horns with the posterior horns, which are normally pointed, becoming rounded (Greitz 2004).

Normal pressure hydrocephalus (NPH) is a form of communicating hydrocephalus (Kitagaki et al. 1998) with a prevalence of approx. 0.4 % after age 65. NPH is characterized clinically by the classic triad of dementia, unsteady gait, and urinary incontinence, which may vary in severity (Table 5.12) (Bateman 2008).

MRI demonstrates the typical morphology of communicating hydrocephalus, which is characterized by symmetrical enlargement of the ventricles. The fourth ventricle may be spared and retain its narrow shape (Fig. 5.12a, b). A conspicuous finding is a discrepancy between the width of the internal and external CSF spaces, with the external spaces being narrow, especially in the high frontoparietal region

Table 5.12 Normal pressure hydrocephalus

Frequency	0.4 % prevalence in individuals aged 65 or older
Age predilection	–
Sex predilection	F:M ratio of 8:1
Location	–
Type of lesion	–
Signs and symptoms	Classic triad of dementia, unsteady gait, and urinary incontinence
Differential diagnosis	Dementia of other etiology Hydrocephalus ex vacuo Obstructive hydrocephalus

(Fig. 5.12c). T2-weighted and FLAIR images will show cap-shaped areas of high signal intensities in the periventricular brain. Another typical finding in NPH is a conspicuous CSF flow void through the aqueduct on sagittal T2-weighted images (Fig. 5.12d) (Scollato et al. 2009).

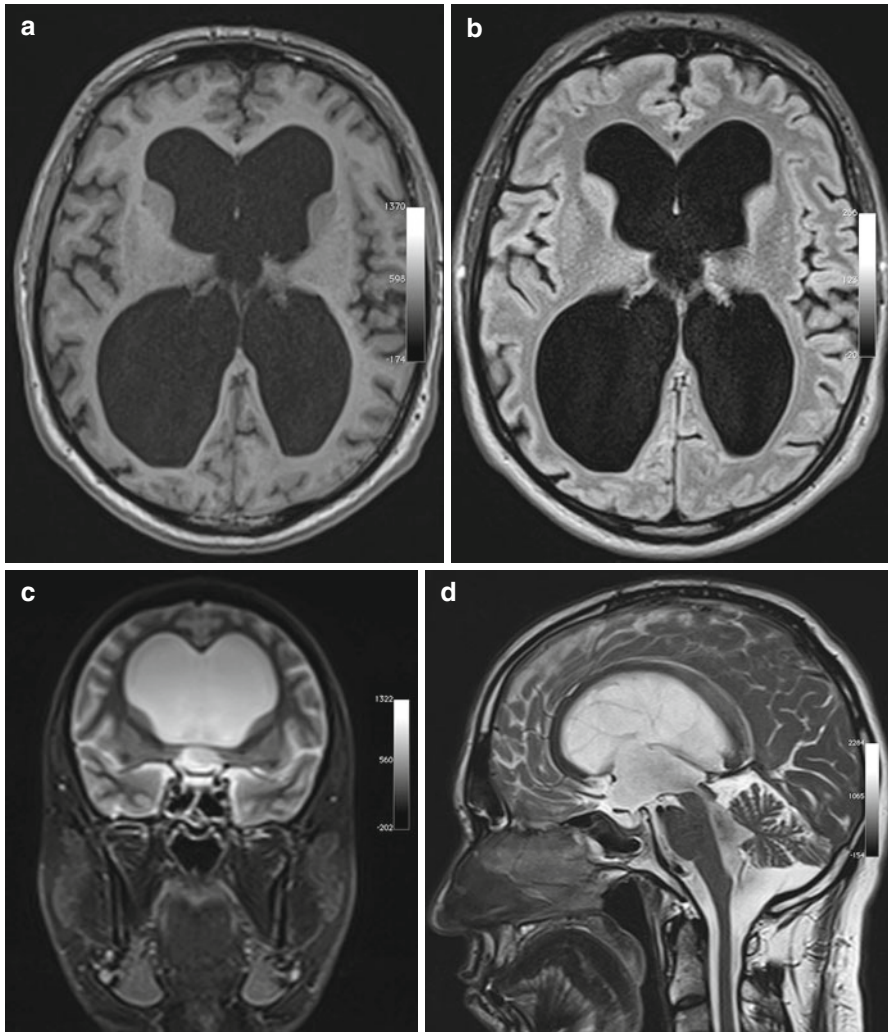


Fig. 5.12 Incidental screening findings in a 74-year-old male subject with a history of loss of cognitive function and small-stepped gait having persisted for some time. In conjunction with the clinical presentation, the morphologic changes seen on MRI give rise to the suspicion of NPH. Axial T1w MPR image reveals symmetrically dilated internal CSF spaces (a) without any significant periventricular signal changes on axial T2w FLAIR image (b). Coronal T2w TIRM image shows very narrow external CSF spaces supratentorially (c). Sagittal T2w TSE image shows strong flow signal over the aqueduct (d)

Clinical Management

When dilated ventricles have been identified, the foremost task of imaging is to rule out acute excessive accumulation of CSF and obstructive hydrocephalus secondary to a block of CSF outflow. Therefore, as a rule, demonstration of enlarged supratentorial ventricles should be followed up by a dedicated MRI examination with acquisition of high-resolution sagittal T2-weighted images (e.g., CISS) and phase-encoded flow measurement over the aqueduct to rule out outflow obstruction. A subject with suspected acute CSF obstruction should see a neurosurgeon immediately. The diagnosis of NPH cannot be made on the basis of MRI findings alone but must take the clinical context into account. NPH often responds well to treatment, which is why neurologic/neurosurgical workup is indicated.

5.1.4 Vascular Conditions

5.1.4.1 Cerebral Ischemia

In industrialized countries, cerebral ischemia is the most common cause of permanent disability in adults. The incidence of ischemic stroke is 150–300/100,000 population/year. Following a first stroke, there is an approx. 10–15 % risk of suffering a second stroke. Approx. 15 % of patients die within 3 months of an ischemic cerebrovascular event, either because of the initial or recurrent stroke or because of secondary complications (Coutts et al. 2008; Boulanger et al. 2007).

The traditional classification of ischemic strokes is based on the duration of symptoms, distinguishing transient ischemic attack (TIA), with symptoms resolving within 24 h and no morphologic changes at imaging; prolonged reversible ischemic neurologic deficit (PRIND); and complete stroke. This is a purely clinical classification with no relevance for radiologic image interpretation. Nevertheless, even clinicians support initiatives aiming at establishing a new terminology. With state-of-the-art imaging techniques, ischemic lesions can also be detected in 30 % of patients with TIA (Sylaja et al. 2008; Coutts et al. 2005).

An alternative classification scheme, based on underlying causes, distinguishes four major subtypes of ischemic strokes: large-artery atherosclerosis, small-vessel occlusion, stroke of other determined etiology, and stroke of undetermined etiology (approx. 30 % of cases). Rare causes include vasculitis and vessel injury or dissection (see Chap. 9), abuse of medications or drugs, and clotting disorders.

Large-artery disease is the underlying cause in territorial infarcts and border-zone infarcts. The latter are due to hemodynamically reduced perfusion of distal vascular territories in individuals with a proximal stenosis in a cerebral artery or the circle of Willis and poor or absent collateralization (see Chap. 9). The stenosis is typically due to atherosclerosis, while territorial infarcts are commonly caused by a thromboembolic event, which in 30 % of cases has a cardiac origin. Risk factors for large-artery atherosclerosis are arterial hypertension, diabetes mellitus,

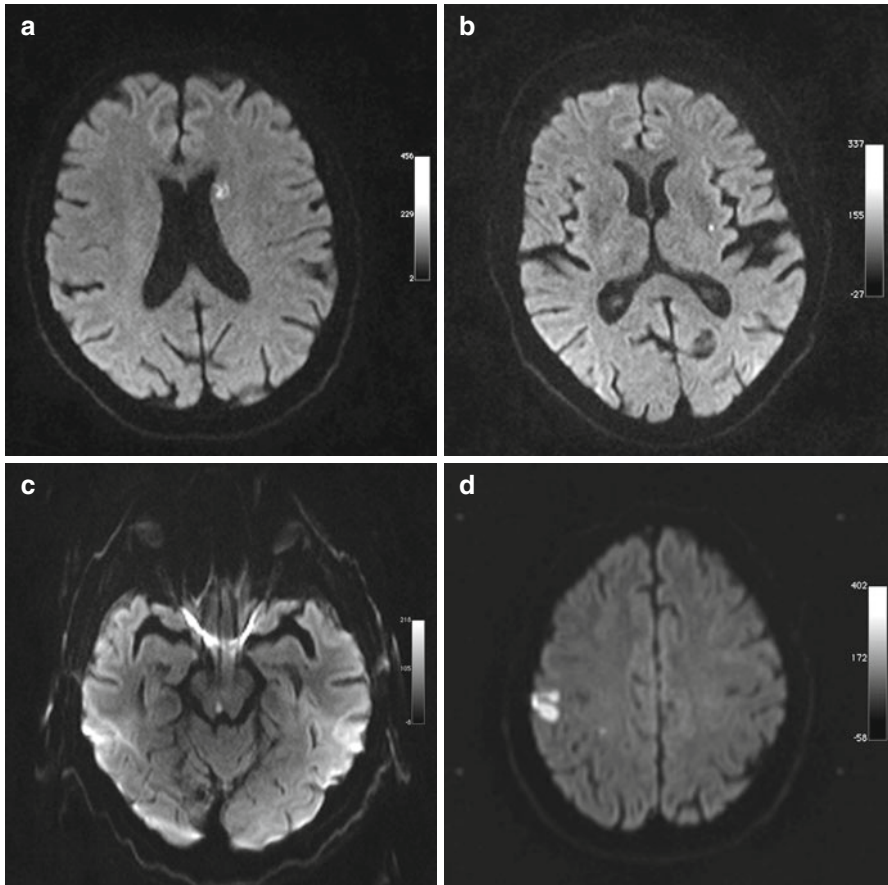


Fig. 5.13 Incidental screening findings in several subjects (DWI at $b=1,000$ s/mm²). (a) A 72-year-old male subject with abnormal perfusion in the left frontal periventricular white matter. (b) 69-year-old male subject with punctiform lacunar ischemia of the left external capsule. (c) A 53-year-old female subject with fresh lacunar ischemia in the right periaqueductal region. (d) A 78-year-old male subject with small cortical middle cerebral artery infarction on the right and small subcortical lacunar lesion in the mid-portion of the middle cerebral artery territory

sex (men > women), oral contraceptive use, and migraine (Coutts et al. 2008; Sciolla and Melis 2008).

Small-vessel disease arises on the basis of lipohyalinosis and primarily affects small perforating cerebral arteries. The hallmark feature of lipohyalinosis is luminal narrowing, causing ischemic lacunar lesions in adjacent deep gray and white matter. Confluence of these lesions is known as subcortical atherosclerotic encephalopathy (SAE) and is typically associated with dementia (see Sect. 5.1.4.3.2 below).

Diffusion-weighted imaging (DWI) is the most sensitive technique for detecting ischemic lesions (Schaefer 2001; Schaefer et al. 2000). To avoid artifacts resulting from very bright lesions on T2 weighting, apparent diffusion coefficient (ADC) maps should be computed from the DWI datasets (Fig. 5.13). Changes in diffusion

characteristics are seen within a few minutes of the onset of ischemia, while conventional T1-weighted and T2-weighted images will not show any changes until approx. 2–4 h after the event. Ischemic lesions have low T1 signal intensity and high intensity on T2-weighted and FLAIR images. In older lesions, susceptibility-sensitive imaging techniques (SWI, T2*) often demonstrate areas of low signal intensity, which correspond to hemorrhagic transformation of infarcted brain tissue (Nandigam et al. 2009; Barnes and Haacke 2009).

Clinical Management

In subjects with clinical symptoms, demonstration of diffusion abnormalities by MRI requires immediate neurologic diagnostic and therapeutic management.

Subjects with a TIA and diffusion abnormalities have a markedly increased 90-day stroke risk. This is why all diffusion abnormalities require prompt workup, especially since a subject may not be aware of having had a TIA.

5.1.4.2 Cavernoma

Cavernomas are clusters of grossly dilated blood vessels without intervening brain parenchyma. The dilated vessels resemble sinusoidal cavities. They are lined with a single layer of endothelium. No other layers of the mature vessel wall are present. Cavernomas have an incidence of approx. 0.4–0.9 % and account for approx. 8–15 % of all intracranial vascular malformations. Most cases are sporadic and solitary. Others occur after radiotherapy for brain tumors, particularly when performed in childhood. Familial cases also exist. Ninety percent of individuals with the familial form have multiple cavernomas (Table 5.13) (Forsting 2005).

Approximately 30 % of cavernomas are associated with a so-called developmental venous anomaly (DVA), a developmental variant of venous drainage of medullary veins. These veins are arranged in a radial pattern and drain into a single central vein (spoke-wheel pattern or caput medusae sign). The collecting vein in turn drains into a dural sinus or into a deep epidural vein. A concomitant DVA is especially common in brainstem cavernoma (Wanke et al. 2007).

Table 5.13 Cavernoma

Frequency	0.4–0.9 %; 8–15 % of all intracranial vascular malformations
Age predilection	–
Sex predilection	M=F
Location	Ubiquitous
Type of lesion	–
Signs and symptoms	Depend on location. Risk of clinically symptomatic bleeding of 0.7 %/lesion/year; higher risk for brainstem cavernoma (approx. 4–5 %/lesion/year)
Differential diagnosis	Hypertensive microbleeds Amyloid angiopathy

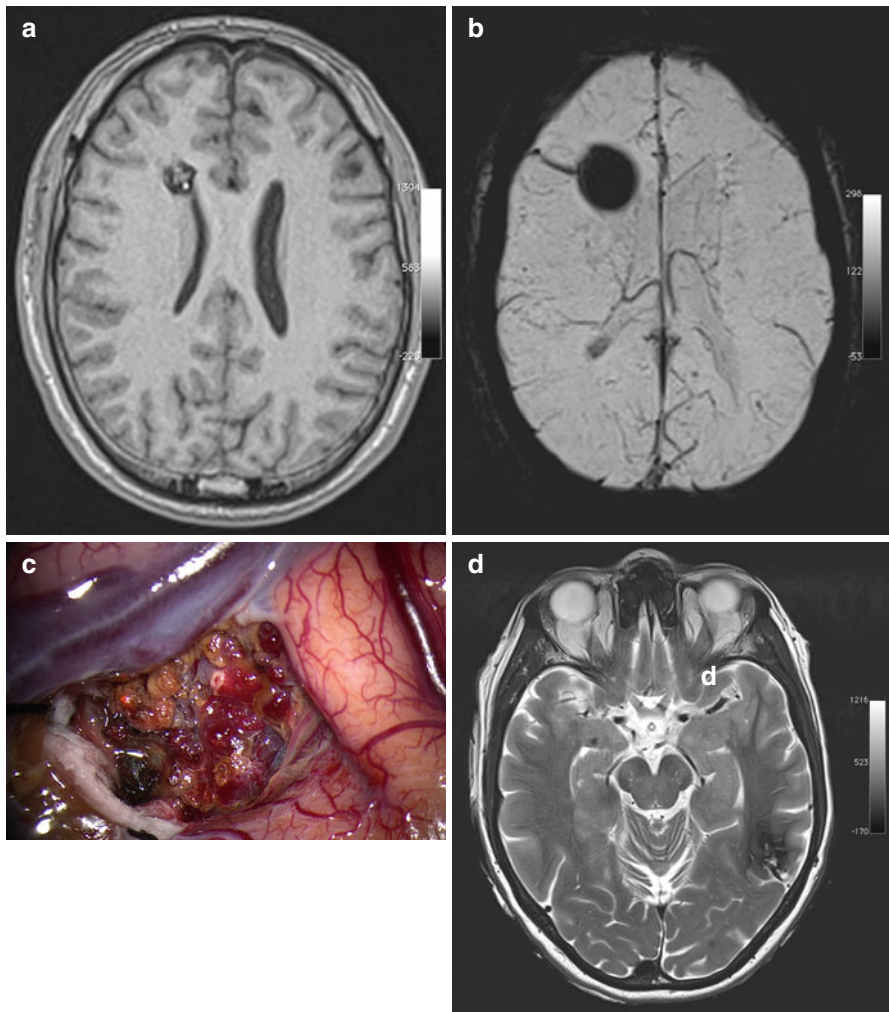


Fig. 5.14 Incidental screening findings and workup in two subjects. (a–c) A 40-year-old male subject with inhomogeneous mass in the periventricular white matter of the right anterior horn. Compared with the axial T1w MPR image (a), the lesion appears markedly larger (blooming phenomenon) on minimum intensity projection reconstruction of axial SWI (b), which also allows excellent delineation of the associated DVA. The intraoperative site (c) in this subject nicely illustrates the popcorn appearance of the cavernoma (Courtesy of Prof. Dr. H.W. Schroeder, Dept. of Neurosurgery, Greifswald, Germany). (d) Preoperative workup at 3 T in a female subject with a left occipital cavernoma. The axial T2w TSE image nicely depicts the hemosiderin rim around the lesion, which may be an epileptogenic focus

Cavernomas have a conspicuous configuration that resembles popcorn or mulberries. They are characterized by an inhomogeneous appearance on both T1-weighted and T2-weighted images (Fig. 5.14a), which is attributable to the presence of blood breakdown products of different ages and different blood flow

velocities within the compartments. T2-weighted images frequently show a markedly hypointense margin, which corresponds to hemosiderin deposits (Forsting 2005). On T1-weighted pulse sequences, the center of a cavernoma often has higher signal intensity than the surrounding parenchyma, but it may also have slightly lower intensity. A cavernoma of uniform high T1 signal intensity also has high signal intensity on TOF-MRA and may be confused with an aneurysm. On susceptibility-sensitive images (SWI, T2*), a cavernoma produces a signal void, making the lesion appear larger than it is on T2-weighted images (blooming phenomenon) (Fig. 5.14b) (Haacke et al. 2009; Mittal et al. 2009).

Clinical Management

There is a risk of clinically symptomatic bleeding from a cavernoma of approx. 0.7 %/lesion/year. Subjects with no clinical evidence of an earlier bleeding episode should be followed up clinically. Exceptions are subjects with brainstem cavernomas, who have a higher risk of hemorrhage (approx. 4–5 %/lesion/year). Symptomatic bleeding from brainstem cavernoma usually has disastrous consequences, and these subjects should undergo regular follow-up. A subject with morphologic MRI evidence of subclinical bleeding should see a neurosurgeon for further management (Fig. 5.14c, d).

Other indications for neurosurgical consultation include cavernoma in young patients, cavernoma in noneloquent areas, and cavernoma-associated epilepsy not responding to drug treatment.

An incidentally detected cavernoma should always be communicated to the subject since subclinical bleeding can also lead to hemosiderin deposition, which may represent an epileptogenic focus.

5.1.4.3 Microbleeds

Cerebral microbleeds can be identified as small foci of decreased signal intensity on susceptibility-weighted images. In many cases, no changes are apparent on T1-weighted or T2-weighted SE or TSE images (Barnes and Haacke 2009). Histopathologically, cerebral microbleeds are hemosiderin deposits from extravasated red blood cells. Cerebral microbleeds are common (Vernooij et al. 2008) and increase with age (Nandigam et al. 2009). There are two conditions, presented below, in which cerebral microbleeds can be found.

5.1.4.3.1 Cerebral Amyloid Angiopathy

Cerebral amyloid angiopathy (CAA) refers to a very heterogeneous group of vascular diseases that become more common with age. The prevalence of CAA ranges from 8 % in individuals aged 75–84 to approx. 12 % in those over 84. CAA is more common in Alzheimer patients (Table 5.14) (Haacke et al. 2009).

Amyloid is an eosinophilic, non-water-soluble extracellular protein. In CAA, β -amyloid is deposited in the media and adventitia of arterioles and small arteries in the cortex and leptomeninges. The resulting changes in the vessel wall are associated

Table 5.14 Cerebral amyloid angiopathy

Frequency	Rare before age 50 50 % in individuals aged 90 or older
Age predilection	Older individuals
Sex predilection	No sex predilection
Location	Corticomedullary junction of the cerebral hemispheres; cortical
Type of lesion	–
Signs and symptoms	Usually asymptomatic Increased risk of atypical lobar bleeding and lacunar ischemia Associated with different types of dementia
Differential diagnosis	Hypertensive microbleeds Multiple cavernomas

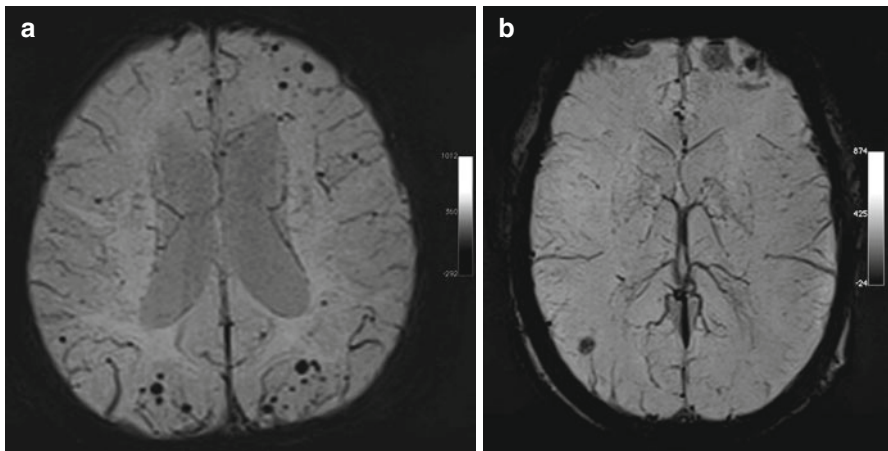


Fig. 5.15 Incidental screening findings in two subjects (SWI). (a) A 64-year-old female subject with multiple superficial, punctiform foci of signal loss on minimum intensity projection reconstruction of axial SWI. The appearance is consistent with amyloid angiopathy. (b) A 45-year-old male subject with a transverse oval signal void in the right parietal region on minimum intensity reconstruction of axial SWI. The appearance suggests a cavernoma

with an increased risk of lacunar ischemia and multiple punctiform microbleeds or even lobar hemorrhage. The definitive diagnosis of CAA still requires histologic confirmation from biopsy. Histopathologic demonstration of vascular amyloid is also required by the Boston diagnostic criteria (Knudsen et al. 2001).

MRI is the diagnostic modality of choice for corroborating suspected CAA. Susceptibility-weighted sequences are well suited for detecting microbleeds, which are typically located superficially and at the corticomedullary junction (Fig. 5.15). Concomitant cortical involvement is common. In contrast, microbleeds in hypertensive encephalopathy more frequently also involve deeper structures (Knudsen et al. 2001). SWI has been shown to detect up to 25 % more microbleeds than conventional T2*-weighted sequences (Haacke et al. 2009).

Clinical Management

Cerebral amyloid angiopathy is associated with an increased risk of lobar bleeding and lacunar stroke. CAA is more common in dementia of the Alzheimer type; however, evidence regarding its potential predictive value is inconclusive. Patients with CAA have a higher risk of bleeding complications when they undergo thrombolytic treatment. Definitive data on the bleeding risk associated with oral anticoagulation treatment are still lacking. Subjects should always be informed about an incidental finding of CAA, although there are no therapeutic consequences for the time being.

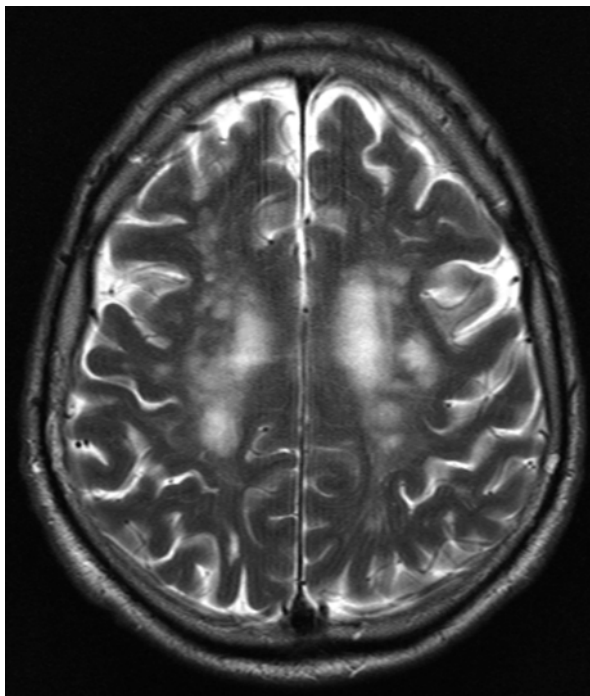
5.1.4.3.2 Hypertensive Encephalopathy

Hypertensive encephalopathy describes changes in the brains of individuals with a long history of untreated or inadequately treated hypertension (Table 5.15). It is characterized by chronically reduced parenchymal perfusion due to irreversible structural damage to the walls of small arterioles. Subsequently, there may be multiple lacunar microinfarcts, which predominantly occur in the lentiform nucleus, pons, thalamus, internal capsule, and head of caudate nucleus (Pantoni and Garcia 1997). In addition, chronic hypoperfusion causes demyelination of the periventricular and deep white matter, seen as hyperintensity on T2-weighted or FLAIR images (Fig. 5.16). The resulting fragility of the vessel wall gives rise to microbleeds. Hypertensive encephalopathy differs from amyloid angiopathy in that the microbleeds predominantly occur in deeper structures, mainly the basal ganglia. Hemosiderin deposits can be identified using susceptibility-weighted sequences (Nandigam et al. 2009; Haacke et al. 2007). Clinically, patients experience a stepwise or gradual loss of memory and dementia type changes. The full-blown clinical condition with the requisite morphologic MRI changes is referred to as subcortical atherosclerotic encephalopathy (Binswanger disease).

Table 5.15 Hypertensive encephalopathy

Frequency	–
Age predilection	Increases with age
Sex predilection	M > F
Location	–
Type of lesion	–
Signs and symptoms	Stepwise or gradual loss of memory Symptoms of dementia and cognitive impairment dementia Symptoms of stroke
Differential diagnosis	Amyloid angiopathy Nonvascular types of dementia CADASIL Vasculitis

Fig. 5.16 Workup of an oropharyngeal lesion at 1.5 T in a 53-year-old male subject. Axial T2w TSE image shows abnormal high signal intensities in both hemispheres, consistent with hypertensive encephalopathy. The subject had a history of untreated hypertension



Clinical Management

Multiple small foci of high signal intensity in the basal ganglia, thalamus, brainstem, and periventricular cerebral parenchyma on SWI should alert the examiner to the possibility of hypertensive encephalopathy. Because the damage is irreversible, timely intervention is important to stop disease progression. This is why an MRI suspicion of chronic hypertensive encephalopathy should prompt timely medical workup.

5.1.4.4 White Matter Lesions

Leukoaraiosis is a purely descriptive term for patchy or diffuse, confluent white matter lesions (Fig. 5.17a, b). These lesions result from vascular changes affecting the small arterioles and causing ischemic leukoencephalopathy and multiple lacunar microinfarcts. By definition, the microinfarcts are subcortical in location but completely spare subcortical U fibers, which constitute a 3–4 mm zone of immediately subcortical white matter.

White matter lesions are part of the normal aging process of the brain with an exponential increase in incidence and lesion size after age 50 (Table 5.16) (Pantoni and Garcia 1997). Imaging evaluation of leukoaraiosis is best performed using a T2-weighted FLAIR sequence, which will reveal tiny bright white matter foci. The foci are isointense to CSF on T1-weighted and T2-weighted images.

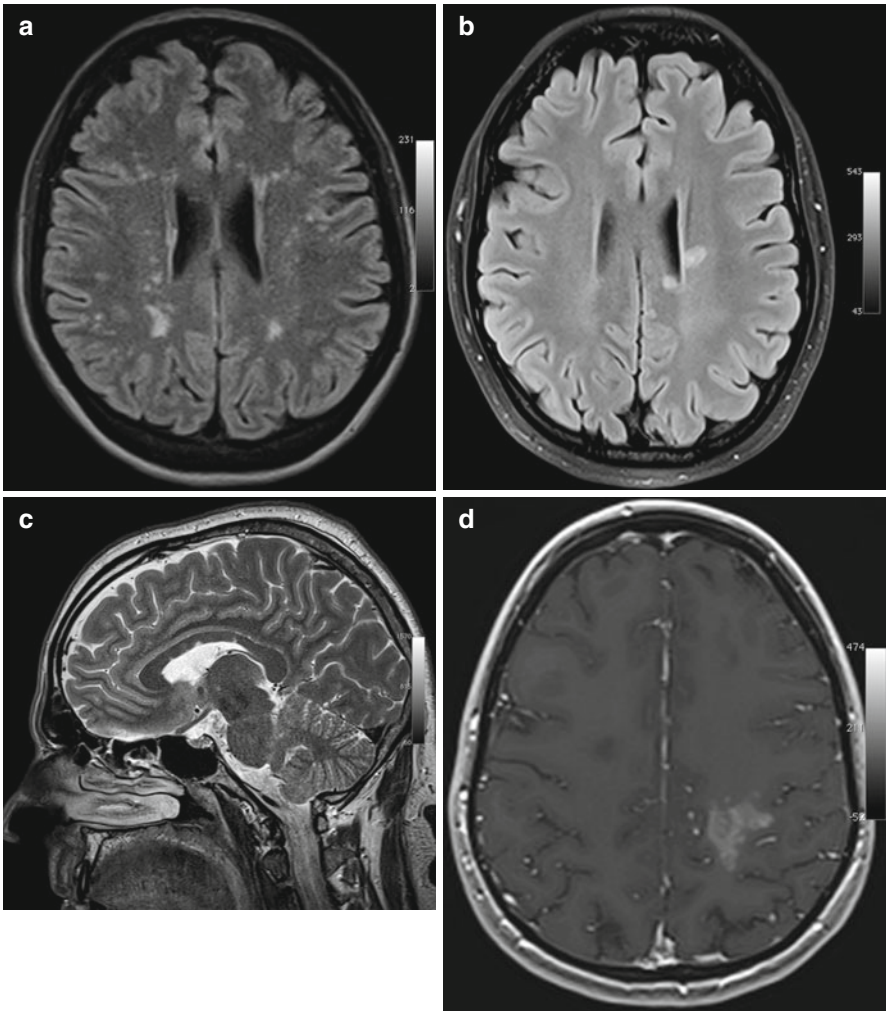


Fig. 5.17 Incidental screening findings (SWI) and workup in several subjects. **(a)** A 83-year-old female subject with multiple – both patchy and confluent – hyperintensities in the periventricular and deep white matter on axial T2w FLAIR image, consistent with microvascular leukoencephalopathy. **(b)** Workup of a 27-year-old male subject at 3 T. Axial T2w FLAIR image shows hyperintensities in abnormal location in the left periventricular region. CSF and serology studies yielded the diagnosis of neuroborreliosis. **(c, d)** Workup at 3 T of a 29-year-old female subject with multiple high-signal-intensity areas on FLAIR sequence. MRI shows finger-shaped lesions of the corpus callosum on sagittal T2w TSE image **(c)** and an enhancing focal lesion in the postcentral gyrus on contrast-enhanced axial T1w FLASH image **(d)**. In conjunction with the CSF result, these MRI findings are consistent with multiple sclerosis

Table 5.16 White matter lesions

Frequency	–
Age predilection	Exponential increase after age 50
Sex predilection	M=F
Location	Subcortical, periventricular, thalamus, brainstem
Type of lesion	–
Signs and symptoms	Stepwise or gradual loss of memory Symptoms of dementia Symptoms of acute stroke
Differential diagnosis	Acute or chronic demyelinating conditions Infectious processes Storage diseases

Clinical Management

MRI findings alone cannot establish a diagnosis of microvascular leukoencephalopathy. Especially in younger individuals, the differential diagnosis includes acute or chronic demyelinating conditions. However, small-vessel disease virtually never involves the corpus callosum, which can be well evaluated on sagittal T2-weighted images (Fig. 5.17c, d). When MRI demonstrates lesions of the corpus callosum, further neurologic workup is warranted.

5.2 The Neck**5.2.1 Introduction**

There are only a few body regions that are of similar anatomic complexity as the neck. The neck contains a wide variety of tissues and organ systems in close vicinity to each other. Many different classification systems have been proposed to facilitate systematic evaluation and reporting of imaging findings in the neck. An established system distinguishes the nasopharynx, the oropharynx, the hypopharynx, and the larynx (Greene et al. 2002); however, it is limited by the fact that these regions are not readily identified on axial MR images. These regions are further subdivided into compartments by the layers of the deep cervical fascia. Therefore, the model derived from the work of Harnsberger et al. has emerged as the most practical approach for reporting radiologic findings in the clinical setting (Harnsberger 1995).

The superior soft tissue contrast of MRI compared with CT makes it the method of choice for detection and characterization of abnormalities in this anatomically complex region. Another advantage of MRI is that it is not susceptible to artifacts caused by fixed dentures, which is especially important when imaging the oral cavity and oropharynx (King et al. 2004).

A neck MRI scan should typically include non-contrast-enhanced T1-weighted pulse sequences in all three planes, an axial T2-weighted sequence, and a

contrast-enhanced T1-weighted sequence with fat suppression (Weber et al. 2003). Dedicated coil systems may be needed, depending on the clinical indication and suspected site of pathology (Lee and Fernandes 2008).

In the screening situation, there is often not enough time to use a sequence protocol optimized for evaluating the soft tissues of the neck. Another limitation is that screening MRI is typically performed without contrast medium, making it difficult to detect small lesions in this region (Yamamoto et al. 2001). However, state-of-the-art MRI scanners with multichannel imaging capability and coil systems enabling flexible combination of coil elements allow high-resolution imaging of the neck including the region near the skull base and the cervicothoracic junction.

With the whole-body screening protocol used here, the neck is imaged using an axial T1-weighted TSE sequence extending from the body of the tongue to the level of the aortic arch. In addition, coronal T2-weighted TIRM images, acquired as part of the whole-body protocol, and a sagittal T2-weighted TSE sequence of the head protocol are available. The latter allows evaluation of parasagittal structures. Finally, the soft tissues of the neck can be evaluated on a sagittal T2-weighted TSE sequence of the spine, which extends from the skull base to the thoracoabdominal junction.

5.2.2 Paranasal Sinuses

5.2.2.1 Sinusitis

Inflammatory conditions of the nasal cavity and paranasal sinuses are very common, and their prevalence has increased in recent years. This development has been attributed to increasing air pollution and resistance to antibiotics (Willett et al. 1994; Anand 2004). Sinusitis can be caused by bacterial, fungal, or viral infection or allergy (Winstead 2003). Up to 90 % of patients with upper respiratory tract infection have concomitant viral or bacterial sinusitis (Winstead 2003). Sinusitis is classified by duration as acute, subacute, or chronic. Acute sinusitis is less than 1 month in duration. Chronic sinusitis is defined as symptoms persisting longer than 3 months. Persistence of symptoms for 1–3 months defines subacute sinusitis (Table 5.17) (Winstead 2003).

Table 5.17 Sinusitis

Prevalence	High
Age predilection	Occurs at any age
Sex predilection	No sex predilection
Location	Acute: ethmoidal > maxillary > other paranasal sinuses Chronic: ethmoidal > maxillary > frontal > sphenoidal sinuses
Type of lesion	Benign Note: Rarely, intracranial/orbital complications may occur
Signs and symptoms	Headache, secretions
Differential diagnosis	Posttraumatic air-fluid level Poststenotic retention Polyposis Wegener granulomatosis Sinonasal non-Hodgkin lymphoma

Fig. 5.18 Workup in a 63-year-old male subject with complete obstruction of the left maxillary sinus. The secretion had low T2 signal intensity. Coronal reconstruction of CT scan shows multiple calcifications. Aspergillus sinusitis was suspected and confirmed by microbiologic testing



Common imaging findings in acute sinusitis include mucosal thickening and air-fluid levels. The mucosa and secretions have high T2 signal intensity. On T1-weighted images, the mucosa is isointense to connective tissue. Secretions are initially isointense to fluid and become brighter with increasing protein content (Zinreich 2004).

Acute sinusitis predominantly affects the ethmoid cells and maxillary sinus. Chronic sinusitis is most common in the ethmoid cells, followed by, in decreasing order, the maxillary, frontal, and sphenoidal sinus. Mucosal thickening is seen in both acute and chronic sinusitis. Chronic sinusitis is distinguished by sclerosis and thickening of the sinus wall, while the sinus volume may appear normal or reduced. T2-weighted images are well suited for identifying these changes. Other underlying causes that can impair sinus ventilation must be ruled out, especially in chronic sinusitis (Dammann 2007). The two most common malignancies to be considered in the differential diagnosis are squamous cell carcinoma and lymphoma. In individuals with evidence of bone destruction, especially if the septum is involved, and in those with predominant involvement of the nasal cavity, the differential diagnosis also includes Wegener granulomatosis. Very low T2 signal intensity of secretions may suggest fungal infection (Fig. 5.18) (Dammann 2007).

Clinical Management

Nasal mucosal abnormalities are frequent incidental findings. Mucosal thickness is subject to circadian variation and is considered abnormal when it exceeds 3 mm. An air-fluid level suggests acute sinusitis. A subject with chronic sinusitis and suspected complications or possible underlying malignancy should undergo contrast-enhanced MRI (Figs. 5.19 and 5.20) and thin-slice CT of the paranasal sinuses and see an ENT specialist.

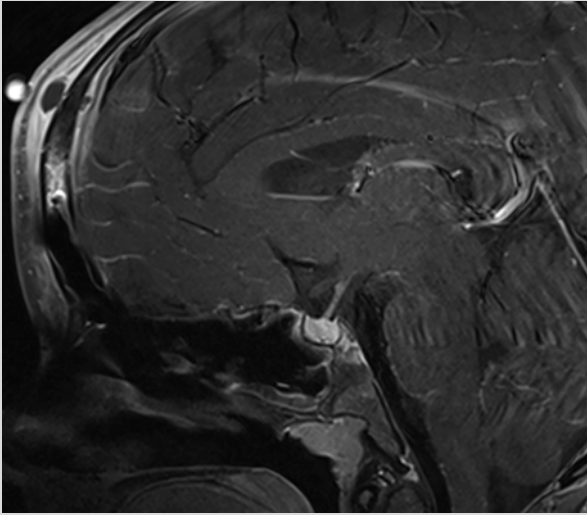


Fig. 5.19 Workup at 3 T in a 22-year-old female subject with a 4-week history of persistent headache following a common cold. Contrast-enhanced fat-saturated sagittal T1w image demonstrates osteomyelitis of the frontal bone with concomitant epidural abscess as an intracranial complication and a small soft tissue abscess. Note the capsule placed to indicate the site of maximum pain

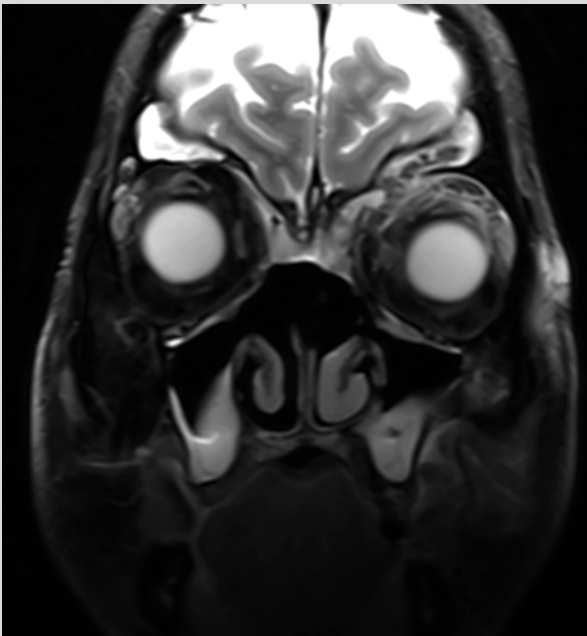
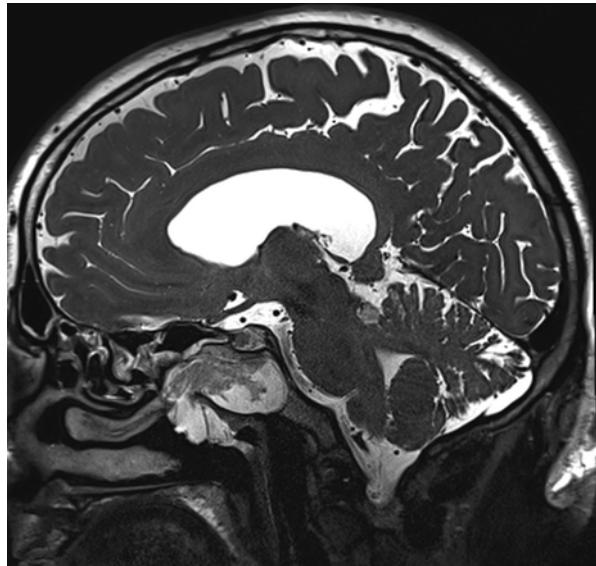


Fig. 5.20 Workup at 3 T in a 60-year-old male subject. Fat-saturated coronal T2w image demonstrates extensive pansinusitis despite surgical revision of the paranasal sinuses. There is also concomitant inflammatory involvement of the left orbit

Table 5.18 Sinonasal polyposis

Prevalence	1–2 % of the normal population
Age predilection	Occurs at any age
Sex predilection	No sex predilection
Location	Paranasal sinuses (especially lateral wall of anterior portions) and nasal cavity
Type of lesion	Benign Note: Bone deformity may occur in very rare cases
Signs and symptoms	Headache, secretion
Differential diagnosis	Retention cyst Allergic fungal sinusitis Wegener granulomatosis

Fig. 5.21 Workup at 3 T of a mass posterior to the quadrigeminal lamina (lipoma) in a 47-year-old male subject. Sagittal T2w CISS image shows extensive polyposis of the sphenoidal sinus with inhomogeneous signal intensity. Histology yielded the diagnosis of a sinonasal polyp without signs of atypia



5.2.2.2 Sinonasal Polyposis

Sinonasal polyposis refers to a benign inflammatory condition of the nasal and paranasal sinus mucosa and is characterized by polyp-like protrusions. These changes typically involve the lateral wall of the nasal cavity, close to the ostiomeatal complex, and the ethmoid cells. Polyposis is more common in anterior than posterior parts of the nose (Table 5.18) (Larsen and Tos 2004). Most patients with polyposis have concomitant chronic sinusitis. Subjects with bronchial asthma, ciliary dysfunction (primary ciliary dyskinesia, cystic fibrosis), and aspirin intolerance are more prone to sinonasal polyposis (Pawankar 2003).

The MRI appearance depends on the composition of nasal secretions. In early polyposis, secretions have a high water content, resulting in homogeneous low T1 and high T2 signal intensity (Fig. 5.21). Over time, retained secretions thicken, and their appearance on both T1-weighted and T2-weighted images becomes more inhomogeneous.

Clinical Management

Simple cases of sinonasal polyposis require no further diagnostic testing or treatment. In some instances, a polyp cannot be differentiated from a retention cyst, especially when the lesion is located in the maxillary sinus. If there is concern about Wegener granulomatosis due to bone destruction, particularly of the septum, an ENT consultation is indicated. Further diagnostic workup is also indicated in unilateral maxillary sinus involvement and unilateral disease in general. Here, the differential diagnosis includes antrochoanal polyp and inverted papilloma (Fig. 5.22).

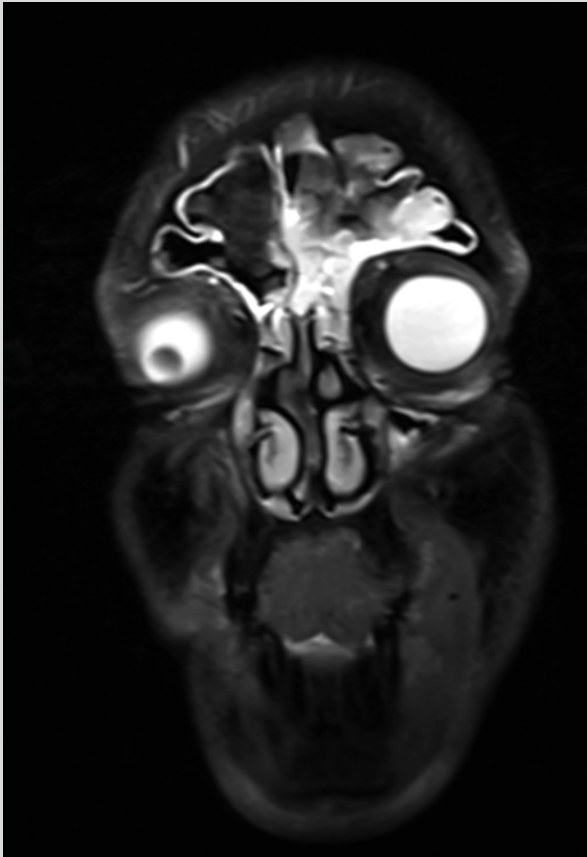


Fig. 5.22 Workup at 3 T of white matter lesions in a 58-year-old male subject. Fat-saturated coronal T2w TSE image shows polyp of the frontal sinus extending into the nasal cavity and ethmoid cells (histologically proven)

5.2.2.3 Paranasal Sinus Mucocele

A mucocele is an epithelium-lined, mucus-containing cystic lesion completely filling the affected sinus. It arises secondary to chronic retention of secretions, causing

Fig. 5.23 Incidental asymptomatic mucocele of the right maxillary sinus in a 19-year-old female subject. Axial T1w image shows continuous extension of the mucocele into the maxilla

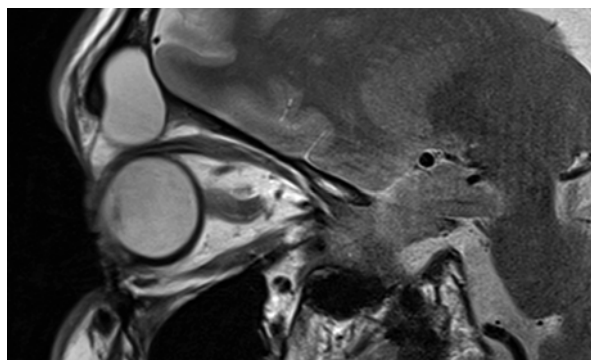


Table 5.19 Paranasal sinus mucocele

Prevalence	–
Age predilection	Occurs at any age
Sex predilection	No sex predilection
Location	Frontal > ethmoidal > maxillary > sphenoidal sinuses
Type of lesion	Benign Note: bone deformity may occur in very rare cases
Signs and symptoms	Headache, secretion
Differential diagnosis	Retention cyst Allergic fungal sinusitis Wegener granulomatosis

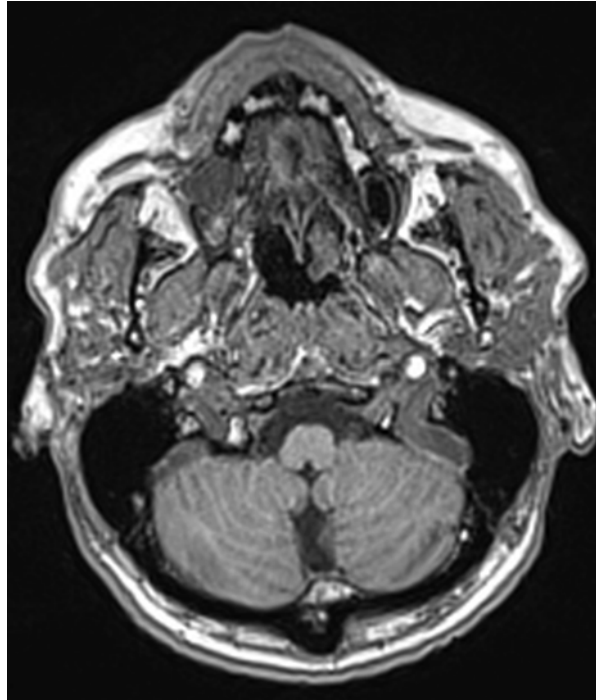
pressure buildup with bone atrophy and ultimate expansion of the sinus (Lloyd et al. 2000). Most mucoceles are found in the frontal sinus (60–65 %) (Fig. 5.23), followed by the ethmoidal sinus (25 %), the maxillary sinus (5–10 %), and the sphenoidal sinus (2–5 %) (Table 5.19) (Kosling et al. 2004). The underlying chronic obstruction may be due to acute or chronic inflammation, trauma, or postoperative changes. A neoplastic process must be considered in the differential diagnosis.

The MRI appearance of paranasal sinus mucoceles depends on water content. High water content results in uniform low signal intensity on T1-weighted images (Fig. 5.24) and high signal intensity on T2-weighted images (Van Tassel et al. 1989).

Clinical Management

Subjects with complete obstruction of a sinus cavity and bony destruction should see an ENT specialist. If there is suspicion of concomitant orbital and/or intracranial involvement or complications, a contrast-enhanced MRI examination should be performed. A circumscribed nodule of soft tissue intensity within a mucocele may suggest malignancy and should also prompt an ENT consultation and contrast-enhanced MRI examination (Lloyd et al. 2000).

Fig. 5.24 Workup at 3 T in a 23-year-old male subject. Sagittal T2w TSE image shows a high-signal-intensity mass in the left lateral frontal sinus. The mass has destroyed the bony lamella toward the orbit and impinges on the superior rectus muscle and bulb. No signs of inflammatory involvement of the orbit are apparent



5.2.3 Neck Lymph Node Enlargement

Owing to the complex anatomy of the neck, a number of different approaches have been proposed to group the lymph nodes in this region. The most widely used classification schemes are the ones of the *American Joint Committee on Cancer and the American Academy of Otolaryngology – Head and Neck Surgery* (Robbins 1998; Fleming et al. 1997). In 2000, Som et al. proposed an imaging-based system of reference lines that allows reliable anatomic localization of the lymph nodes in the neck and has since gained increasing popularity in clinical routine (Som et al. 2000; Habermann et al. 2004).

Swollen lymph nodes in the neck may be caused by a number of conditions, ranging from inflammation (Fig. 5.25) and infection to metastatic spread from local or systemic malignancy (Van den Brekel et al. 1996).

Inflammatory nodal enlargement is usually reactive. Neck lymph nodes larger than 2 cm may suggest sarcoidosis. Tuberculosis or HIV lymphadenopathy should be considered when central liquefaction is detected. Central liquefaction is also common in nodal metastasis from primary head and neck malignancy (Fig. 5.26). Liquefied lymph nodes must not be confused with cysts (Van den Brekel et al. 1996; Ishikawa and Anzai 2002).

Reactive inflammatory enlargement of the lateral retropharyngeal lymph nodes is common in young patients. These lymph nodes are located in the suprahyoid soft

Fig. 5.25 Workup at 3 T in a 23-year-old female subject. Coronal T1w TSE image shows multiple oval lymph nodes of variable size on both sides. No major changes are apparent compared with the screening findings 3 months earlier. Laboratory tests were normal. Histology confirmed inflammatory reactive changes

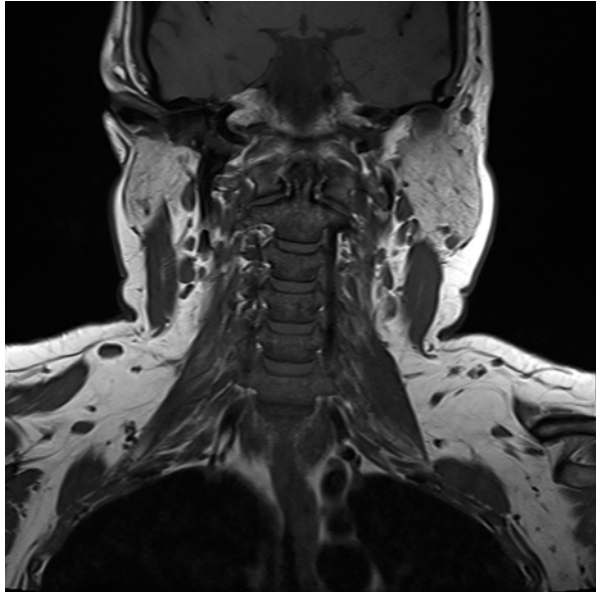


Fig. 5.26 Workup at 3 T in a 58-year-old male subject. Coronal fat-saturated T2w TSE image demonstrates mild enlargement of a lymph node in the inferior portion of the lower group of the internal jugular chain. Histology demonstrated metastasis from signet ring cell cancer of the stomach

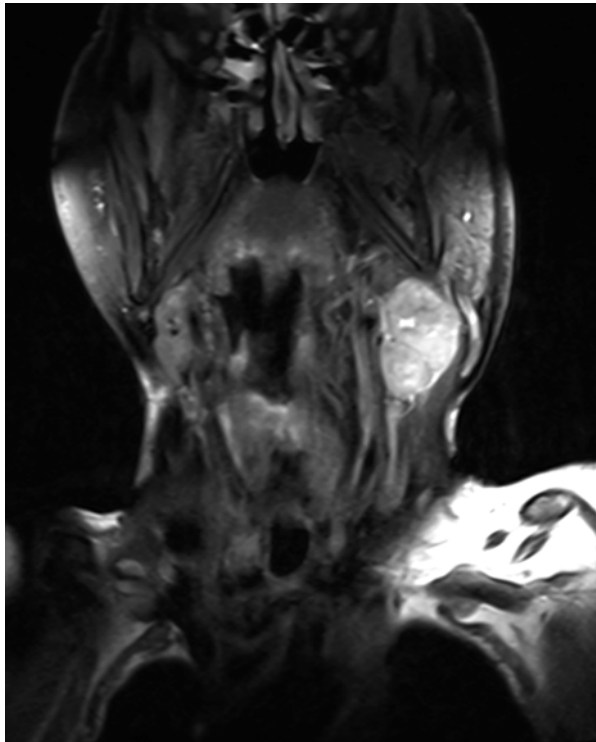


Fig. 5.27 Workup at 3 T in a 51-year-old male subject. Coronal fat-saturated T2w TSE image shows bilateral lymphoma masses along the carotid sheath at the level of the internal carotid artery. There was no morphologic MRI evidence of a tumor of the head or neck. Histologically proven lymphoma

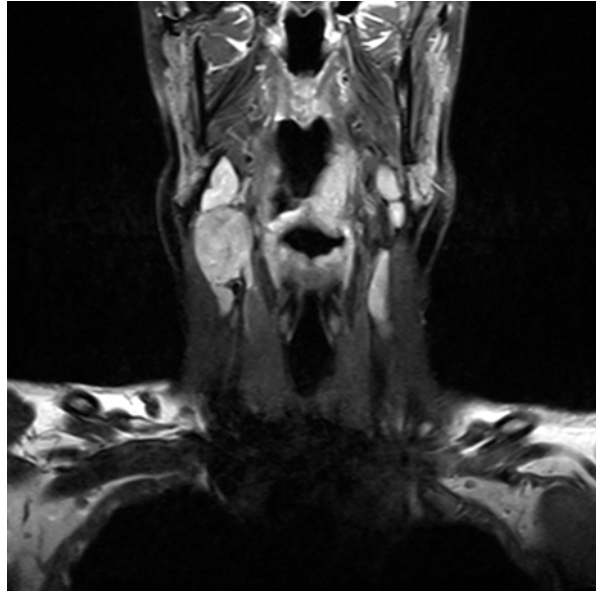
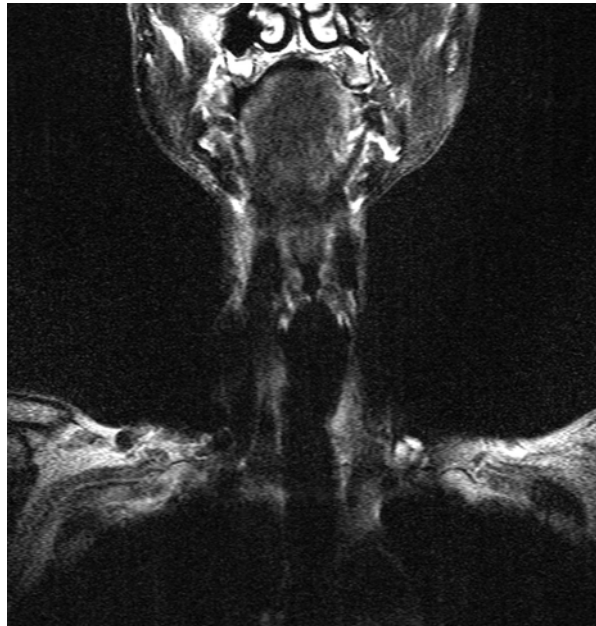


Fig. 5.28 Workup in a 71-year-old male subject. Coronal fat-saturated T2w TSE image shows two lymph nodes with central necrosis along the carotid sheath on the left. Whole-body MRI failed to reveal a primary tumor. Panendoscopy demonstrated a superficial nasopharyngeal carcinoma. Neck dissection was performed with histology confirming lymph node metastasis



tissues lateral to the prevertebral muscles and medial to the internal carotid artery (Fig. 5.27).

Enlargement of a single lymph node along the lower internal jugular vein (Virchow lymph node) may be due to metastasis from a thoracic, abdominal, or pelvic primary (Fig. 5.28) as this lymph node receives the thoracic duct.

Clinical Management

Lymph node enlargement in the neck may be reactive, infectious, or metastatic. Fat-suppressed T2-weighted pulse sequences are especially helpful for detecting nodal abnormalities in the neck (Ishikawa and Anzai 2002). If whole-body MRI does not reveal a likely cause, the subject should have a blood count and possibly an endoscopy. If the cause still remains unclear, then lymph node resection or biopsy should be considered.

5.2.4 Salivary Glands

5.2.4.1 Introduction

The salivary glands consist of two main groups: the three large paired major glands – parotid, submandibular, and sublingual – and a second group of minor glands. The minor glands include approx. 600–1,000 separate clusters of glandular tissue underneath the mucosa. Most of these clusters are distributed in the oral cavity and the remainder in the pharynx, larynx, paranasal sinuses, and trachea (Som and Brandwein 1996).

The parotid gland is the largest of the paired salivary glands. It lies in the subcutaneous fat over the mandibular ramus and masseter muscle. The parotid gland is surrounded by a well-defined fibrous capsule. Because the capsule develops after the formation of glandular tissue, the parotid may contain lymph nodes (Salama and Ord 2008). While there is no intraglandular anatomic division, the parotid is clinically divided into a superficial part and a deep part by emerging branches of the facial nerve (Som and Brandwein 1996).

The submandibular gland is located in the space bounded by the angle of the mandible. Like the parotid, it consists of a superficial part and a deep part. The deep part has a fingerlike extension into the sublingual space. The submandibular gland is closely related to the sublingual gland, the smallest of the paired salivary glands. The sublingual gland is located in the submucosa of the floor of the mouth and overlies the mylohyoid muscle (Som and Brandwein 1996).

The parotid gland is slightly hypointense to subcutaneous fat and hyperintense to muscle tissue on T1-weighted and T2-weighted images. The submandibular gland has lower T1 and T2 signal intensity compared with the parotid gland. The sublingual gland has slightly lower T2 signal intensity than the submandibular gland. The higher signal intensity of the parotid gland has been attributed to its relatively large fatty content (Mandelblatt et al. 1987).

5.2.4.2 Pleomorphic Adenoma

Pleomorphic adenomas, the most common salivary gland tumors, are benign mixed tumors composed of epithelial, myoepithelial, and stromal elements (Fig. 5.29). They can occur in any of the salivary glands but are most common in the parotid gland (80%), where they arise in the deep or superficial part. Those arising in the deep parotid gland may become quite large before causing symptoms (Table 5.20) (Salama and Ord 2008; Gnepp 2001).

When small, pleomorphic adenomas have homogeneous low signal intensity on T1-weighted images. They become more heterogeneous as they grow. If hemorrhage is

Fig. 5.29 Screening finding in a 56-year-old male subject with painless swelling in the right parotid compartment. Coronal fat-saturated T2w TSE image reveals a solid mass with a multicystic component in the superficial portion of the right parotid gland. Histologically proven pleomorphic adenoma

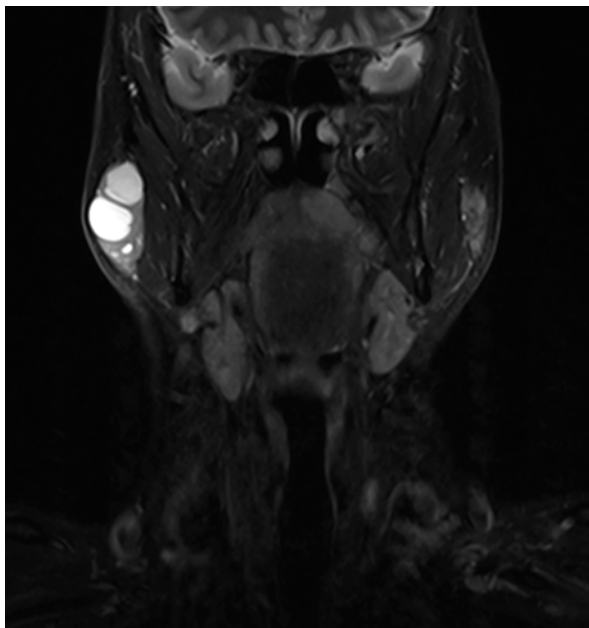


Table 5.20 Pleomorphic adenoma

Prevalence	80 % of all pleomorphic adenomas occur in the parotid gland
Age predilection	Between 30 and 60 years, most commonly after age 40
Sex predilection	M:F ratio of 2:1
Location	Deep or superficial part of parotid gland
Type of lesion	Benign
Signs and symptoms	Painless swelling
Differential diagnosis	Warthin tumor Primary parotid cancer Non-Hodgkin lymphoma Lymph node metastasis

present, bright foci may be seen within the lesion. On T2-weighted images, pleomorphic adenomas have high signal intensity with small lesions appearing homogeneous and larger ones appearing inhomogeneous (Salama and Ord 2008; Ikeda et al. 1996).

Clinical Management

A large mass originating in the deep part of the parotid gland is most likely a pleomorphic adenoma. All subjects diagnosed with a salivary gland mass should undergo an MRI examination of the neck, including contrast-enhanced pulse sequences, and see an ENT specialist. Low signal intensity on T2-weighted images makes a malignant tumor more likely (Figs. 5.30 and 5.31).

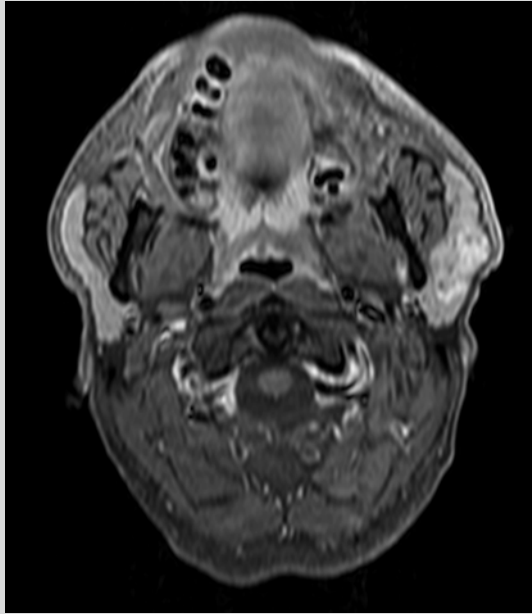


Fig. 5.30 Workup of an asymmetry of the parotid glands in a 49-year-old male subject. Contrast-enhanced axial T1w TSE image with fat saturation demonstrates a tumor of the left parotid gland with mild contrast enhancement. The tumor consists of cystic and solid portions. Histologically proven well-differentiated adenocarcinoma

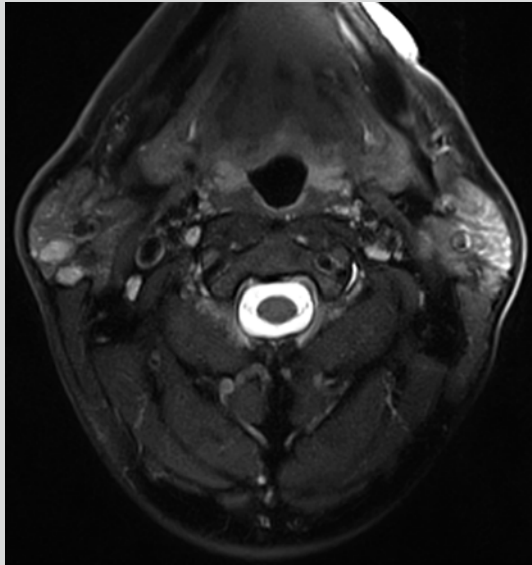


Fig. 5.31 Workup of a right occipital subcutaneous mass (not shown) in a 73-year-old female subject. Fat-saturated axial T2w TSE image shows the lesion in the lower pole of the right parotid gland, which has progressed compared with the screening MRI findings. Histologically proven metastasis from occipital malignant melanoma

5.2.5 Thyroid

5.2.5.1 Thyroid Nodules

Nodules of the thyroid gland are common. The reported prevalence strongly depends on the diagnostic methods used and the age and composition of the patient population studied. The incidence of both symptomatic and asymptomatic thyroid nodules increases with age and is higher in women and in individuals with iodine deficiency (Table 5.21) (Dean and Gharib 2008). An increased risk has also been reported for individuals with a history of neck irradiation (Gharib et al. 2008). Early population-based studies report asymptomatic thyroid nodules in 3–7 % of cases (Vander et al. 1968). In autopsy studies, the prevalence is 50–70 % (Dean and Gharib 2008).

Histomorphometrically, a distinction is made between adenomas and colloid nodules (adenomatous hyperplasia). The latter are characterized by an incomplete fibrous capsule (Dean and Gharib 2008). Palpable and incidentally discovered nonpalpable thyroid nodules of similar size have the same risk of malignancy (approx. 10 %) (Cooper et al. 2009). The risk of malignancy is increased in individuals with a history of radiation exposure of the head and neck or whole-body radiotherapy and in subjects with a family history of thyroid cancer. Other risk factors include rapid growth, presence of a firm, immobile nodule, and concomitant swelling of neck lymph nodes. Malignancy should also be suspected if a new thyroid nodule occurs before age 30 or after age 60 or if a thyroid lesion is incidentally discovered in men (Gharib et al. 2008; Cooper et al. 2009).

Thyroid nodules are usually isointense or hypointense to muscle tissue on T1-weighted images (Fig. 5.32). Intranodal foci of increased signal intensity indicate calcification or hemorrhage. On T2-weighted images, thyroid nodules typically have high signal intensity (Gotway and Higgins 2000).

Clinical Management

Reliable noninvasive differentiation between benign and malignant thyroid nodules is not possible. Therefore, each nodular regressive lesion of the thyroid must be worked up, including a history, physical examination, thyroid function tests, and ultrasound. Depending on the findings, additional tests, such as scintigraphy or fine needle biopsy, may be warranted.

Table 5.21 Thyroid nodules

Prevalence	3–70 %
Age predilection	Occurs at any age
Sex predilection	M:F ratio of 1:4
Location	Within the thyroid
Type of lesion	10 % risk of malignancy
Signs and symptoms	Typically asymptomatic; rarely local mass effect
Differential diagnosis	Thyroid cyst Goiter Parathyroid adenoma Differentiated thyroid carcinoma

Fig. 5.32 Incidental screening finding in a 78-year-old male subject. Axial T1w TSE image shows multiple nodular masses of muscle signal intensity in the right thyroid lobe. Histologically proven adenoma

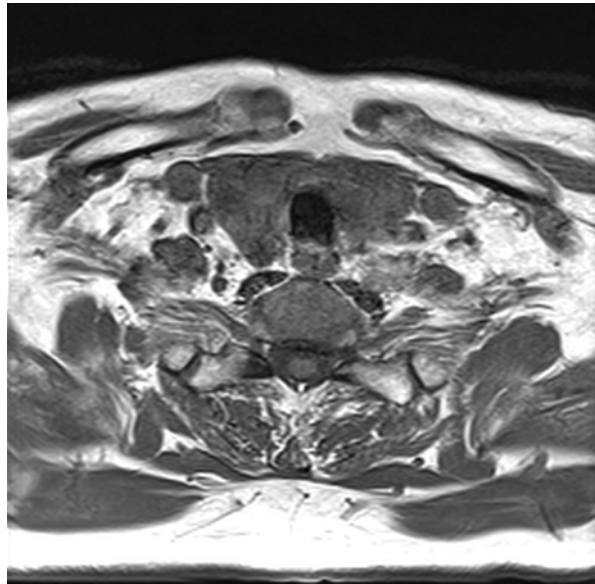


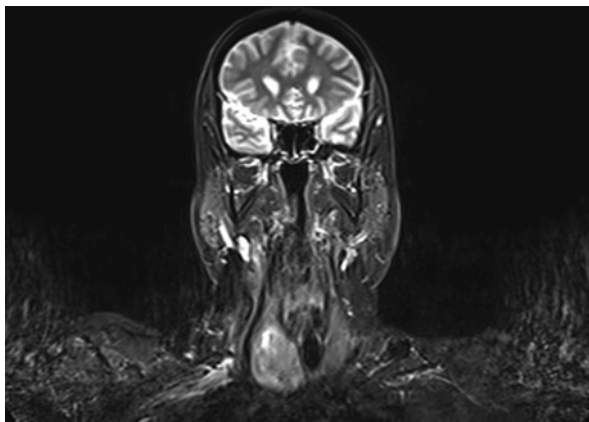
Table 5.22 Goiter

Prevalence	Sporadic versus endemic
Age predilection	Sporadic goiter occurs at any age Endemic goiter increases in size after onset in childhood
Sex predilection	M:F ratio of 1:2–4
Location	–
Type of lesion	10 % risk of malignancy
Signs and symptoms	Typically asymptomatic Rarely local mass effect
Differential diagnosis	Colloid cyst Thyroid adenoma Differentiated thyroid carcinoma Undifferentiated thyroid carcinoma Non-Hodgkin lymphoma

5.2.5.2 Goiter

A goiter develops secondary to chronic TSH stimulation and is characterized by diffuse, multinodular enlargement of the thyroid gland. It is the most common underlying cause of asymmetric thyroid enlargement. Goiter is endemic in iodine-deficient regions and sporadic elsewhere. Endemic goiter due to lack of dietary iodine is found in approx. 13 % of the world population. The risk of developing goiter is 5–20 % in mild iodine deficiency and increases to over 30 % in severe deficiency. Individuals with goiter have an approximately 5 % risk of developing anaplastic thyroid carcinoma (Table 5.22).

Fig. 5.33 Incidental screening finding in a 61-year-old female subject with a right-sided goiter. Coronal T2w image shows areas of cystic degeneration. Workup with ultrasound and nuclear medicine revealed no signs of malignancy



An advantage of whole-body MRI is that, in case of suspicious thyroid findings, images are available for detecting and evaluating abnormal lymph nodes in the neck and chest. Unlike thyroid nodules, a goiter may contain areas of regressive cystic change (Fig. 5.33).

In areas of regression, fibrosis and calcification lead to low T1 and T2 signal intensity. Degenerative hemorrhage causes high T1 and T2 signal intensity.

Clinical Management

An incidentally detected nonpalpable, asymptomatic goiter requires no treatment. Suspicious nodules should be further characterized using endocrino-

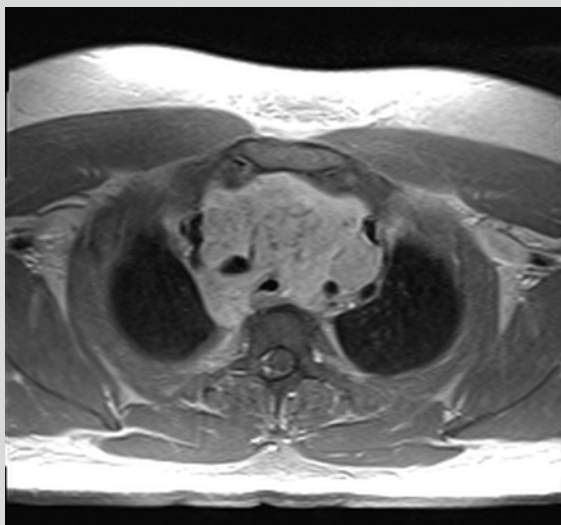


Fig. 5.34 Workup in a 21-year-old male subject who reported having been treated for a sonographically proven goiter for about 6 months. Screening MRI revealed a large mass with cystic regression in the anterior mediastinum. Contrast-enhanced axial T1w TSE image confirms an upper mediastinal mass with uniform contrast enhancement and vessel encasement. The histologic diagnosis was highly malignant lymphoma

logic, sonographic, and nuclear medicine procedures. Workup is also indicated in subjects with concomitant cervical lymphadenopathy (Fig. 5.34). If there is mass effect on the trachea, a surgeon should be consulted.

Fig. 5.35 Workup at 3 T of white matter lesions in a 35-year-old male subject. Sagittal T2w TSE image additionally reveals a smoothly marginated midline lesion at the posterior roof of the nasopharynx. This image illustrates the characteristic appearance of a Tornwaldt cyst



5.2.6 Pharynx and Larynx

5.2.6.1 Introduction

A widely used approach to neck anatomy divides the neck into the suprahyoid and infrahyoid regions. These two regions are separated by the hyoid bone and are further subdivided into fascially defined spaces. Some of these spaces communicate with each other. The suprahyoid neck encompasses the nasopharynx and oropharynx. It is bordered anteriorly by the orbits, paranasal sinuses, nasal cavity, and oral cavity. The infrahyoid neck includes the hypopharynx and larynx.

The fascially defined spaces contain a large variety of tissues, from which both benign and malignant tumors may arise (Smoker and Harnsberger 1991).

The parapharyngeal space is crucial in the diagnosis of neck abnormalities. It extends from the pharyngeal mucosa medially and the parotid gland laterally. Anteriorly, it is bordered by the masticator space and posteriorly by the carotid sheath and by the perivertebral space. The styloid process divides the parapharyngeal space into the prestyloid and poststyloid compartments. The parapharyngeal space largely contains fat, and the direction of fat displacement can help in identifying the anatomic origin of a neck mass and narrowing the differential diagnosis (Harnsberger and Osborn 1991).

5.2.6.2 Cystic Lesions

Tornwaldt cysts are benign developmental cysts of the nasopharynx. They are smoothly marginated and located in the midline (Table 5.23) (Fig. 5.35). Most

Fig. 5.36 Workup at 3 T of an asymmetry of the nasopharynx in a 55-year-old male subject. The image confirms mild asymmetry of the roof and left lateral wall close to the torus tubarius and a slightly hyperintense lesion. Histology yielded the diagnosis of a retention cyst



Table 5.23 Tornwaldt cyst

Prevalence	–
Age predilection	No age predilection
Sex predilection	–
Location	Midline, nasopharyngeal roof
Type of lesion	Benign
Signs and symptoms	Typically asymptomatic
Differential diagnosis	Lymphoid tissue hyperplasia Retention cyst Pleomorphic adenoma of minor salivary glands Nasopharyngeal cancer

Tornwaldt cysts are less than 2 cm in size. Typically, they are covered by mucosa rostrally and bounded by prevertebral muscles posteriorly. Tornwaldt cysts appear bright on T2-weighted images (Fig. 5.35). On T1-weighted images, their signal intensity is still high but varies with protein content (Ikushima et al. 1999). Major differential diagnosis are retentions cysts which are slightly hypointen to CSF on T2-weighted images (Fig. 5.36).

Clinical Management

A typical Tornwaldt cyst is asymptomatic and can be left alone.

Table 5.24 Malignant tumors

Prevalence	Depends on location
Age predilection	Usually after age 50
Sex predilection	M:F ratio of 2.5:1 for nasopharynx M:F ratio of 10:1 for oropharynx M > F for hypopharynx and larynx
Location	–
Type of lesion	Malignant
Signs and symptoms	Nasopharynx: patients typically first present with lymph node metastasis Oropharynx: nonhealing ulcer of the oral cavity Larynx/hypopharynx: hoarseness; lymph node metastasis presenting as neck mass
Differential diagnosis	Depends on location Lymphatic tissue hyperplasia Pleomorphic adenoma of salivary glands Malignancy of minor salivary glands Lymphoma Inflammatory processes

5.2.6.3 Solid Lesions

Benign and malignant solid tumors may arise from any of the soft tissues in the neck. Therefore, some compartments can harbor a variety of different tumors (Table 5.24). In most cases, morphologic MRI features alone do not allow reliable differentiation between benign and malignant neck masses with the notable exception of lipomas. Lipomas have unique imaging features, which will usually allow a definitive diagnosis to be made. They appear as bright lesions on T1-weighted and T2-weighted images with characteristic loss of signal intensity on fat-suppressed sequences. Thirty percent of unilateral masses in the soft tissues of the neck are malignant (Koivunen et al. 2002). Most malignant tumors in the neck are of epithelial origin. Smoking and excessive alcohol consumption are important risk factors (Gross et al. 2004).

Although rare compared with cancers in other neck compartments, nasopharyngeal carcinomas are clinically important due to the high rate of lymph node metastasis at the time of diagnosis (Shah 1990). Most oropharyngeal malignancies arise in the tongue or in the region of the tongue base (Fig. 5.37). Up to 75 % of patients present with metastatic lymph nodes (often bilateral). Lymphomas are also common in this region, originating in the lymphoid tissue of the tongue base and pharyngeal lymphatic ring (Fig. 5.38) (Shah 1990). Laryngeal malignancies may be supraglottic, glottic, or subglottic with glottic tumors being the most common and having the best prognosis. Metastatic spread to neck lymph nodes is most common in supraglottic cancer (Shah 1990).

Regardless of their site of origin, solid tumors of the neck are typically hypointense or isointense to muscle on T1-weighted images and hyperintense on T2-weighted images (Yamamoto et al. 2001; Lau et al. 2004). They tend to enhance strongly after contrast medium administration (Fig. 5.39). Edema-sensitive T2-weighted sequences are especially useful for evaluating tongue tumors, which will appear bright compared with surrounding tongue tissue (Lau et al. 2004).

Fig. 5.37 A 68-year-old female subject with a several-week history of difficulty swallowing. There is a small increase in volume at the base of the tongue. The hyperintense mass is slightly asymmetric on coronal T2w TIRM image. Histologically proven tonsillitis at the tongue base

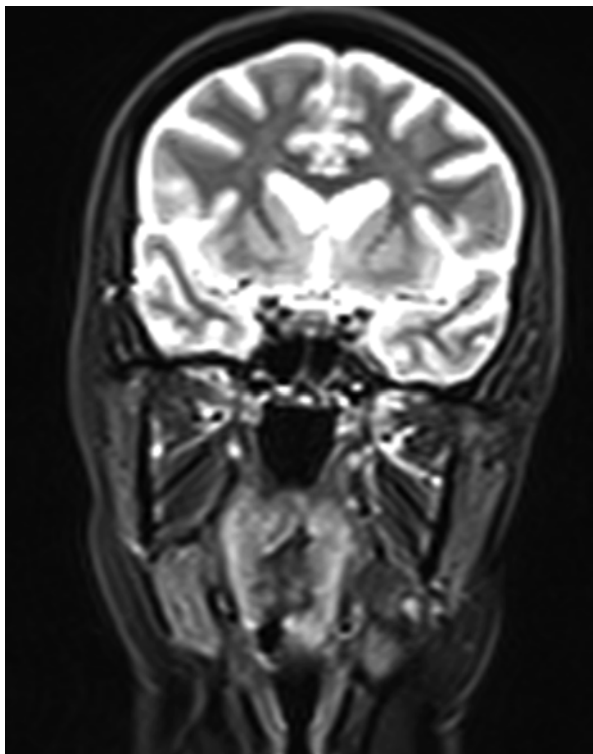


Fig. 5.38 A 71-year-old male subject. Painless asymmetry of the oropharynx in the area of the Waldeyer tonsillar ring on the left. The mass is isointense to muscle on axial T1w TSE image. Histologically proven tonsillar lymphoma

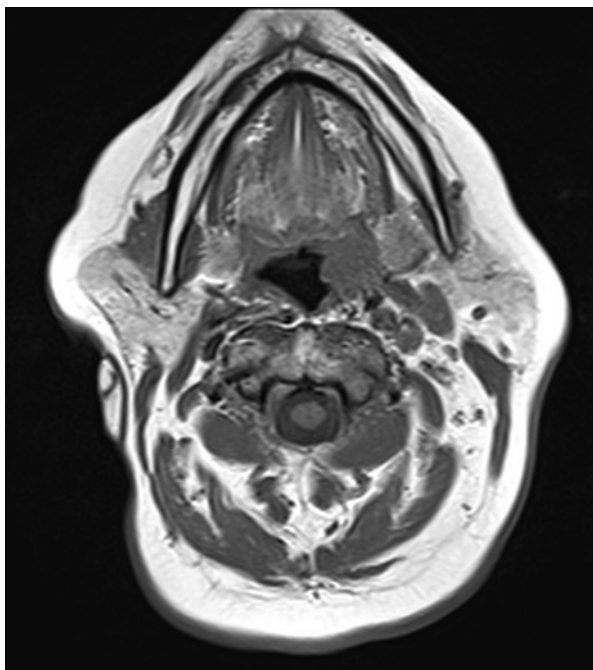
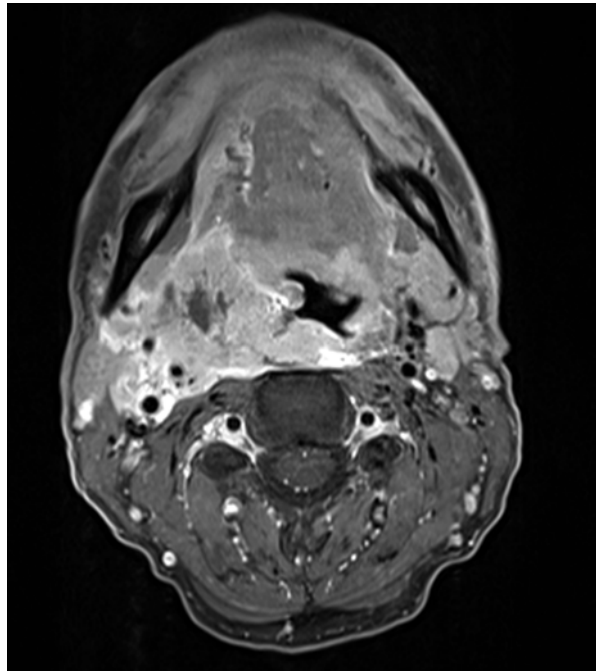


Fig. 5.39 Workup of an asymmetry in the soft tissues of the neck at 3.0 T in a 57-year-old male subject reporting hoarseness and mild difficulty swallowing. Axial T1w TSE image with fat saturation shows a large, inhomogeneous mass with marked contrast enhancement in the right tonsillar compartment. The mass invades the base of the tongue and the parapharyngeal and prevertebral spaces. Lymph node metastases along the right carotid sheath with vascular infiltration. Histologically and clinically proven tonsillar cancer



Clinical Management

A symmetrical asymptomatic mass in the soft tissues of the neck must be considered malignant until proven otherwise. Therefore, an incidental neck mass should be worked up by a dedicated MRI examination of the neck, including contrast-enhanced images, and a timely ENT consultation.

References

- Anand VK (2004) Epidemiology and economic impact of rhinosinusitis. *Ann Otol Rhinol Laryngol Suppl* 193:3–5
- Ball AK, Clarke CE (2006) Idiopathic intracranial hypertension. *Lancet Neurol* 5:433–442
- Barnes SR, Haacke EM (2009) Susceptibility-weighted imaging: clinical angiographic applications. *Magn Reson Imaging Clin N Am* 17:47–61
- Bateman GA (2008) The pathophysiology of idiopathic normal pressure hydrocephalus: cerebral ischemia or altered venous hemodynamics? *AJNR Am J Neuroradiol* 29:198–203
- Bergui M, Zhong J, Bradac GB, Sales S (2001) Diffusion-weighted images of intracranial cyst-like lesions. *Neuroradiology* 43:824–829
- Bonneville F, Savatovsky J, Chiras J (2007) Imaging of cerebellopontine angle lesions: an update. Part 2: intra-axial lesions, skull base lesions that may invade the CPA region, and non-enhancing extra-axial lesions. *Eur Radiol* 17:2908–2920

- Born CM, Meisenzahl EM, Frodl T, Pfluger T, Reiser M, Möller HJ, Leinsinger GL (2004) The septum pellucidum and its variants. An MRI study. *Eur Arch Psychiatry Clin Neurosci* 254:295–302
- Boulanger JM, Coutts SB, Eliasziw M, Subramaniam S, Scott J, Demchuk AM (2007) Diffusion-weighted imaging-negative patients with transient ischemic attack are at risk of recurrent transient events. *Stroke* 38:2367–2369
- Brazis PW (2008) Clinical review: the surgical treatment of idiopathic pseudotumour cerebri (idiopathic intracranial hypertension). *Cephalalgia* 28:1361–1373
- Chamberlain MC, Kormanik PA (1998) Practical guidelines for the treatment of malignant gliomas. *West J Med* 168:114–120
- Cincu R, Agrawal A, Eiras J (2007) Intracranial arachnoid cysts: current concepts and treatment alternatives. *Clin Neurol Neurosurg* 109:837–843
- Cooper DS, Doherty GM, Haugen BR et al (2009) Revised American Thyroid Association management guidelines for patients with thyroid nodules and differentiated thyroid cancer. *Thyroid* 19:1167–1214
- Costa F, Fornari M, Valla P, Servello D (2008) Symptomatic pineal cyst: case report and review of the literature. *Minim Invasive Neurosurg* 51:231–233
- Coutts SB, Hill MD, Simon JE, Sohn CH, Scott JN, Demchuk AM, VISION Study Group (2005) Silent ischemia in minor stroke and TIA patients identified on MR imaging. *Neurology* 65:513–517
- Coutts SB, Hill MD, Campos CR, Choi YB, Subramaniam S, Kosior JC, Demchuk AM, VISION Study Group (2008) Recurrent events in transient ischemic attack and minor stroke: what events are happening and to which patients? *Stroke* 39:2461–2466
- Cox TD, Elster AD (1991) Normal pituitary gland: changes in shape, size, and signal intensity during the 1st year of life at MR imaging. *Radiology* 179:721–724
- Dammann F (2007) Imaging of paranasal sinuses today. *Radiologe* 47(576):578–583
- Dean DS, Gharib H (2008) Epidemiology of thyroid nodules. *Best Pract Res Clin Endocrinol Metab* 22:901–911
- Donati P, Sardo L, Sanzo M (2003) Giant cyst of the cavum septi pellucidi, cavum Vergae and veli interpositi. *Minim Invasive Neurosurg* 46:177–181
- Donovan JL, Nesbit GM (1996) Distinction of masses involving the sella and suprasellar space: specificity of imaging features. *AJR Am J Roentgenol* 167:597–603
- Fleming I, Cooper J, Henson D (1997) American Joint Committee on Cancer staging manual. Lippincott Raven, Philadelphia
- Forsting M (2005) Cavernomas: a dangerous disease? *Clin Neuroradiol* 15:14–19
- Gangemi M, Donati P, Maiuri F, Sigona L (1997) Cyst of the velum interpositum treated by endoscopic fenestration. *Surg Neurol* 47:134–136; discussion 136–137
- Gharib H, Papini E, Paschke R (2008) Thyroid nodules: a review of current guidelines, practices, and prospects. *Eur J Endocrinol* 159:493–505
- Glezer A, Paraiba DB, Bronstein MD (2008) Rare sellar lesions. *Endocrinol Metab Clin North Am* 37:195–211
- Gnepp D (2001) Diagnostic surgical pathology of the head and neck. W.B. Saunders, Philadelphia
- Gotway MB, Higgins CB (2000) MR imaging of the thyroid and parathyroid glands. *Magn Reson Imaging Clin N Am* 8:163–182
- Greene FL, Page DL, Fleming ID et al (2002) AJCC cancer staging handbook. Springer, New York
- Greitz D (2004) Radiological assessment of hydrocephalus: new theories and implications for therapy. *Neurosurg Rev* 27:145–165; discussion 166–167
- Gross ND, Ellingson TW, Wax MK, Cohen JI, Andersen PE (2004) Impact of retropharyngeal lymph node metastasis in head and neck squamous cell carcinoma. *Arch Otolaryngol Head Neck Surg* 130:169–173
- Grunwald I, Dillmann K, Roth C, Backens M, Reith W (2007) Supratentorial tumors. *Radiologe* 47:471–485
- Haacke EM, DelProposto ZS, Chaturvedi S, Sehgal V, Tenzer M, Neelavalli J, Kido D (2007) Imaging cerebral amyloid angiopathy with susceptibility-weighted imaging. *AJNR Am J Neuroradiol* 28:316–317

- Haacke EM, Mittal S, Wu Z, Neelavalli J, Cheng YC (2009) Susceptibility-weighted imaging: technical aspects and clinical applications, part 1. *AJNR Am J Neuroradiol* 30:19–30
- Habermann CR, Weiss F, Metternich FU et al (2004) Imaging-based anatomy of the neck – multi-slice CT and MRI. *Rofo* 176:668–678
- Harnsberger HR (1995) Introduction to the suprahyoid neck. In: *Handbook of head and neck imaging*. Mosby, St Louis
- Harnsberger HR, Osborn AG (1991) Differential diagnosis of head and neck lesions based on their space of origin. 1. The suprahyoid part of the neck. *AJR Am J Roentgenol* 157:147–154
- Ikeda K, Katoh T, Ha-Kawa SK et al (1996) The usefulness of MR in establishing the diagnosis of parotid pleomorphic adenoma. *AJNR Am J Neuroradiol* 17:555–559
- Ikushima I, Korogi Y, Makita O et al (1999) MR imaging of Tornwaldt's cysts. *AJR Am J Roentgenol* 172:1663–1665
- Ishikawa M, Anzai Y (2002) MR imaging of lymph nodes in the head and neck. *Magn Reson Imaging Clin N Am* 10:527–542
- Karavitaki N, Scheithauer BW, Watt J, Ansorge O, Moschopoulos M, Llaguno AV, Wass JA (2008) Collision lesions of the sella: co-existence of craniopharyngioma with gonadotroph adenoma and of Rathke's cleft cyst with corticotroph adenoma. *Pituitary* 11:317–323
- Kariyattil R, Panikar D (2008) Choroid plexus cyst of the third ventricle presenting as acute triventriculomegaly. *Childs Nerv Syst* 24:875–877
- King AD, Tse GM, Ahuja AT et al (2004) Necrosis in metastatic neck nodes: diagnostic accuracy of CT, MR imaging, and US. *Radiology* 230:720–726
- Kitagaki H, Mori E, Ishii K, Yamaji S, Hirono N, Imamura T (1998) CSF spaces in idiopathic normal pressure hydrocephalus: morphology and volumetry. *AJNR Am J Neuroradiol* 19:1277–1284
- Knudsen KA, Rosand J, Karluk D, Greenberg SM (2001) Clinical diagnosis of cerebral amyloid angiopathy: validation of the Boston criteria. *Neurology* 56:537–539
- Koivunen P, Laranne J, Virtaniemi J et al (2002) Cervical metastasis of unknown origin: a series of 72 patients. *Acta Otolaryngol* 122:569–574
- Kosling S, Hintner M, Brandt S, Schulz T, Bloching M (2004) Mucocoeles of the sphenoid sinus. *Eur J Radiol* 51:1–5
- Kwee RM, Kwee TC (2007) Virchow-Robin spaces at MR imaging. *Radiographics* 27:1071–1086
- Larsen PL, Tos M (2004) Origin of nasal polyps: an endoscopic autopsy study. *Laryngoscope* 114:710–719
- Lau KY, Kan WK, Sze WM et al (2004) Magnetic resonance for T-staging of nasopharyngeal carcinoma – the most informative pair of sequences. *Jpn J Clin Oncol* 34:171–175
- Lee J, Fernandes R (2008) Neck masses: evaluation and diagnostic approach. *Oral Maxillofac Surg Clin North Am* 20:321–337
- Lloyd G, Lund VJ, Savy L, Howard D (2000) Optimum imaging for mucocoeles. *J Laryngol Otol* 114:233–236
- Mandelblatt SM, Braun IF, Davis PC et al (1987) Parotid masses: MR imaging. *Radiology* 163:411–414
- Mikulis DJ, Roberts TP (2007) Neuro MR: protocols. *J Magn Reson Imaging* 26:838–847
- Mittal S, Wu Z, Neelavalli J, Haacke EM (2009) Susceptibility-weighted imaging: technical aspects and clinical applications, part 2. *AJNR Am J Neuroradiol* 30:232–252
- Naeini RM, Yoo JH, Hunter JV (2009) Spectrum of choroid plexus lesions in children. *AJR Am J Roentgenol* 192:32–40
- Nagar VA, Ye JR, Ng WH, Chan YH, Hui F, Lee CK, Lim CC (2008) Diffusion-weighted MR imaging: diagnosing atypical or malignant meningiomas and detecting tumor dedifferentiation. *AJNR Am J Neuroradiol* 29:1147–1152
- Nandigam RN, Viswanathan A, Delgado P et al (2009) MR imaging detection of cerebral microbleeds: effect of susceptibility-weighted imaging, section thickness, and field strength. *AJNR Am J Neuroradiol* 30:338–343
- Naylor MF, Scheithauer BW, Forbes GS, Tomlison FH, Young WF (1995) Rathke cleft cyst: CT, MR, and pathology of 23 cases. *J Comput Assist Tomogr* 19:853–859

- Niedermayer I, Kolles H, Feiden W (1998) Classification and grading of gliomas and meningiomas. *Radiologe* 38:888–897
- Noh SJ, Ahn JY, Lee KS, Kim SH (2007) Pituitary adenoma and concomitant Rathke's cleft cyst. *Acta Neurochir (Vienna)* 149:1223–1228
- Pantoni L, Garcia JH (1997) Pathogenesis of leukoaraiosis: a review. *Stroke* 28:652–659
- Pawankar R (2003) Nasal polyposis: an update: editorial review. *Curr Opin Allergy Clin Immunol* 3:1–6
- Pope WB, Sayre J, Perlina A, Villablanca JP, Mischel PS, Cloughesy TF (2005) MR imaging correlates of survival in patients with high-grade gliomas. *AJNR Am J Neuroradiol* 26:2466–2474
- Poptani H, Gupta RK, Jain VK, Roy R, Pandey R (1995) Cystic intracranial mass lesions: possible role of in vivo MR spectroscopy in its differential diagnosis. *Magn Reson Imaging* 13:1019–1029
- Pradilla G, Jallo G (2007) Arachnoid cysts: case series and review of the literature. *Neurosurg Focus* 22:E7
- Prasad A, Gupta RK, Pradhan S, Tripathi M, Pandey CM, Prasad KN (2008) What triggers seizures in neurocysticercosis? A MRI-based study in pig farming community from a district of North India. *Parasitol Int* 57:166–171
- Pu Y, Mahankali S, Hou J, Li J, Lancaster JL, Gao J-H, Appelbaum DE, Fox PT (2007) High prevalence of pineal cysts in healthy adults demonstrated by high-resolution, noncontrast brain MR imaging. *AJNR Am J Neuroradiol* 28:1706–1709
- Radner H, Blümcke I, Reifenberger G, Wiestler OD (2002) The new WHO classification of tumors of the nervous system 2000. *Pathology and genetics. Pathologe* 23:260–283
- Robbins KT (1998) Classification of neck dissection: current concepts and future considerations. *Otolaryngol Clin North Am* 31:639–655
- Roberts TP, Mikulis D (2007) *Neuro MR: principles*. *J Magn Reson Imaging* 26:823–837
- Rohr A, Riedel C, Reimann G, Alfke K, Hedderich J, Jansen O (2008) Pseudotumor cerebri: quantitative in-vivo measurements of markers of intracranial hypertension. *Rofo* 180:884–890
- Rousseau A, Mokhtari K, Duyckaerts C (2008) The 2007 WHO classification of tumors of the central nervous system – what has changed? *Curr Opin Neurol* 21:720–727
- Salama AR, Ord RA (2008) Clinical implications of the neck in salivary gland disease. *Oral Maxillofac Surg Clin North Am* 20:445–458
- Sato K, Kubota T (2009) Pathology of pineal parenchymal tumors. *Prog Neurol Surg* 23:12–25
- Schaefer PW (2001) Applications of DWI in clinical neurology. *J Neurol Sci* 186(Suppl 1):S25–S35
- Schaefer PW, Grant PE, Gonzalez RG (2000) Diffusion-weighted MR imaging of the brain. *Radiology* 200:331–345
- Schaefer PW, Copen WA, Lev MH, Gonzalez RG (2005) Diffusion-weighted imaging in acute stroke. *Neuroimaging Clin N Am* 15:503–530, ix–x
- Sciolla R, Melis F (2008) Rapid identification of high-risk transient ischemic attacks: prospective validation of the ABCD score. *Stroke* 39:297–302
- Scollato A, Gallina P, Gautam B, Pellicanò G, Cavallini C, Tenenbaum R, Di Lorenzo N (2009) Changes in aqueductal CSF stroke volume in shunted patients with idiopathic normal-pressure hydrocephalus. *AJNR Am J Neuroradiol* 30:1580–1586
- Seo HS, Chang K-H, Na DG, Kwon BJ, Lee DH (2008) High b-value diffusion ($b = 3000$ s/mm²) MR imaging in cerebral gliomas at 3T: visual and quantitative comparisons with $b = 1000$ s/mm². *AJNR Am J Neuroradiol* 29:458–463
- Shah JP (1990) Patterns of cervical lymph node metastasis from squamous carcinomas of the upper aerodigestive tract. *Am J Surg* 160:405–409
- Smoker WR, Harnsberger HR (1991) Differential diagnosis of head and neck lesions based on their space of origin. 2. The infrahyoid portion of the neck. *AJR Am J Roentgenol* 157:155–159
- Som PM, Brandwein M (1996) Salivary glands. In: Som PM, Curtin HD (eds) *Head and neck imaging*. Mosby, St. Louis
- Som PM, Curtin HD, Mancuso AA (2000) Imaging-based nodal classification for evaluation of neck metastatic adenopathy. *AJR Am J Roentgenol* 174:837–844
- Sylaja PN, Coutts SB, Krol A, Hill MD, Demchuk AM (2008) When to expect negative diffusion-weighted images in stroke and transient ischemic attack. *Stroke* 39:1898–1900

- Tirakotai W, Schulte DM, Bauer BL, Bertalanffy H, Hellwig D (2004) Neuroendoscopic surgery of intracranial cysts in adults. *Childs Nerv Syst* 20:842–851
- Van den Brekel MW, Castelijns JA, Snow GB (1996) Imaging of cervical lymphadenopathy. *Neuroimaging Clin N Am* 6:417–434
- Van Tassel P, Lee YY, Jing BS, De Pena CA (1989) Mucoceles of the paranasal sinuses: MR imaging with CT correlation. *AJR Am J Roentgenol* 153:407–412
- Vander JB, Gaston EA, Dawber TR (1968) The significance of nontoxic thyroid nodules. Final report of a 15-year study of the incidence of thyroid malignancy. *Ann Intern Med* 69:537–540
- Vernooij MW, Ikram MA, Wielopolski PA, Irestin GP, Breteler MM, van der Lugt A (2008) Prevalence and risk factors of cerebral microbleeds: the Rotterdam Scan Study. *Neurology* 70:1208–1214
- Wanke I, Panagiotopoulos V, Forsting M (2007) Bleeding risk of intracranial vascular malformations. *Rofo* 179:365–372
- Weber AL, al-Arayedh S, Rashid A (2003) Nasopharynx: clinical, pathologic, and radiologic assessment. *Neuroimaging Clin N Am* 13:465–483
- Willett LR, Carson JL, Williams JW Jr (1994) Current diagnosis and management of sinusitis. *J Gen Intern Med* 9:38–45
- Wilms G, Marchal G, Van Hecke P, Plets C, Lammens M, Goffin J, Baert AL (1990) Colloid cysts of the third ventricle: MR findings. *J Comput Assist Tomogr* 14:527–531
- Winstead W (2003) Rhinosinusitis. *Prim Care* 30:137–154
- Yamamoto S, Takano H, Motoori K et al (2001) Detection of nasopharyngeal carcinoma: fast short time inversion recovery images compared with fat suppression, contrast enhanced T 1 weighted spin echo images. *Br J Radiol* 74:805–810
- Yildiz H, Hakyemez B, Koroglu M, Yesildaq A, Baykal B (2006) Intracranial lipomas: importance of localization. *Neuroradiology* 48:1–7
- Yilmazlar S, Kocaeli H, Aksoy K (2005) Quadrigeminal cistern lipoma. *J Clin Neurosci* 12:596–599
- Zinreich SJ (2004) Imaging for staging of rhinosinusitis. *Ann Otol Rhinol Laryngol Suppl* 193:19–23

Christian Rosenberg

6.1 Focal Pulmonary Lesions

6.1.1 Introduction

The solitary pulmonary nodule is by far the most common abnormality detected by whole-body screening MRI. Published data suggest that up to 69 % of asymptomatic smokers without a history of cancer have noncalcified pulmonary nodules on screening CT scans (Swensen et al. 2003).

Therefore, the differentiation between benign and malignant nodules is the greatest challenge facing the radiologist in interpreting chest images acquired as part of a whole-body MRI screening protocol. Less important chest abnormalities to be evaluated by the radiologist in this context include lymphadenopathy, lesions of the pulmonary parenchyma, and pleural processes. Binding guidelines are available for the efficient interpretation of chest screening images and management of abnormal findings.

Pulmonary nodules have many different etiologies, both benign and malignant, including tumor, infection, and inflammation as well as vascular and congenital disorders. The majority of pulmonary nodules are benign. The most common malignancies are pulmonary metastasis and primary lung cancer (Table 6.1).

Lung cancer is the third most common malignancy in both men and women in Germany, with 32,500 newly diagnosed cases in men and 14,600 in women each year. Lung cancer constitutes 14 % of malignant tumors in men and 7 % in women but accounts for a much higher proportion of all cancer deaths, 26 and 12 %, respectively. The proportionately higher death rates are attributable to the fact that lung cancer patients tend to have advanced disease at presentation and generally have a

C. Rosenberg

Institute of Diagnostic Radiology and Neuroradiology, University Medicine Greifswald,
Ferdinand-Sauerbruch-Straße, Greifswald 17487, Germany

e-mail: christian.rosenberg@uni-greifswald.de

Table 6.1 Etiology of pulmonary nodules (defined as relatively round lesions up to 3 cm in diameter)

Most common malignant lesions	Primary lung cancer (adenocarcinoma, bronchoalveolar carcinoma, squamous cell carcinoma, small-cell lung cancer) Primary pulmonary lymphoma Primary pulmonary carcinoid Pulmonary metastasis
Benign	Hamartoma, fibroma, chondroma, leiomyoma, lipoma
Infectious or inflammatory	Granuloma Opportunistic infection Rounded pneumonia Abscess Focal organizing pneumonia Scar fibrosis Necrobiotic nodule in rheumatoid arthritis Wegener granulomatosis
Vascular	Pulmonary artery embolism Pulmonary varices Pulmonary arteriovenous malformation Pulmonary infarct Hematoma
Other	Intrapulmonary lymph node Rounded atelectasis Bronchogenic cyst Mucoid impaction

poor prognosis (overall 5-year survival rate of 15 %). The mean age at diagnosis is 69 years in both men and women (Robert-Koch-Institut und die Gesellschaft der Epidemiologischen Krebsregister in Deutschland e.V. 2010).

A large autopsy study conducted in the USA identified pulmonary metastases in 20–54 % of all patients dying with a malignant neoplasm (Crow et al. 1981). This is much higher than the incidence of metastatic lung involvement at the time patients are first diagnosed with cancer. For obvious reasons, statistical data on the incidence of pulmonary metastases in the healthy population are hard to come by. The incidence reflects the prevalence of underlying primary tumors spreading to the lungs. Therefore, most pulmonary metastases are from colorectal cancer. A diagnosis of carcinoma of unknown primary (CUP) without identification of the primary tumor is very rare in the setting of whole-body MRI screening.

6.1.2 Pulmonary Nodules

A pulmonary nodule is defined as a more or less round lesion with a maximum diameter of 3 cm that is completely surrounded by normal lung (Figs. 6.1, 6.2, and 6.3) (Ost et al. 2003). Focal pulmonary lesions larger than 3 cm in size are generally considered indeterminate lung masses (Tan et al. 2003) and are much

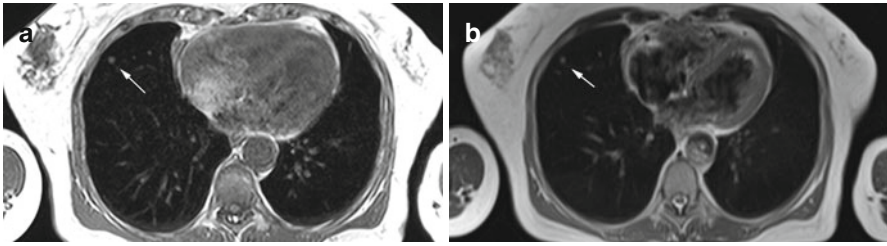


Fig. 6.1 Solitary pulmonary nodule (6 mm) in the right middle lobe in a 69-year-old female subject on T1w image (a) and on T2w HASTE image (b)

Fig. 6.2 Solitary pulmonary nodule (12 mm) in a 72-year-old male subject. The nodule is located near the pericardium and contiguous with the pleura

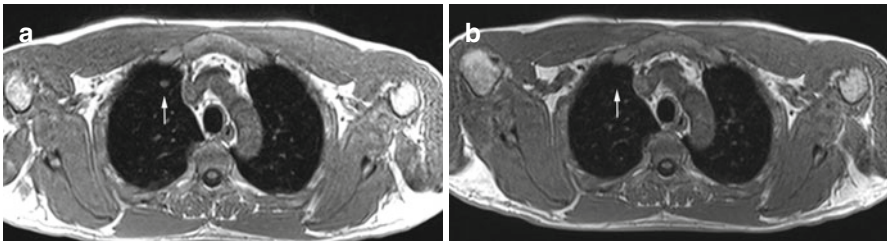
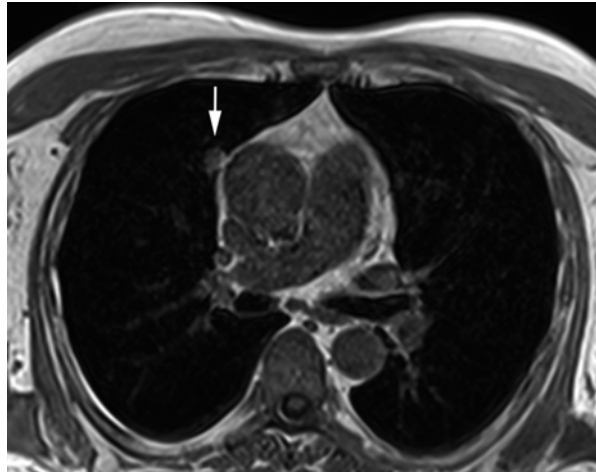


Fig. 6.3 Incidental solitary pulmonary nodule with follow-up MRI in a 49-year-old male subject. T1w screening image shows a 9-mm nodule in the right upper lobe (a). No lesion is detectable on follow-up MRI performed 3 months later (b)

more likely to be malignant than smaller nodules (Winer-Muram 2006). Data obtained in larger CT screening populations suggest that, with a size threshold of 1–2 mm for the detection of pulmonary nodules, less than 5 % of all detected nodules with a diameter of up to 1 cm are malignant (Kim et al. 2002; Biederer et al. 2008). Based on the literature, it appears realistic to assume a threshold size of

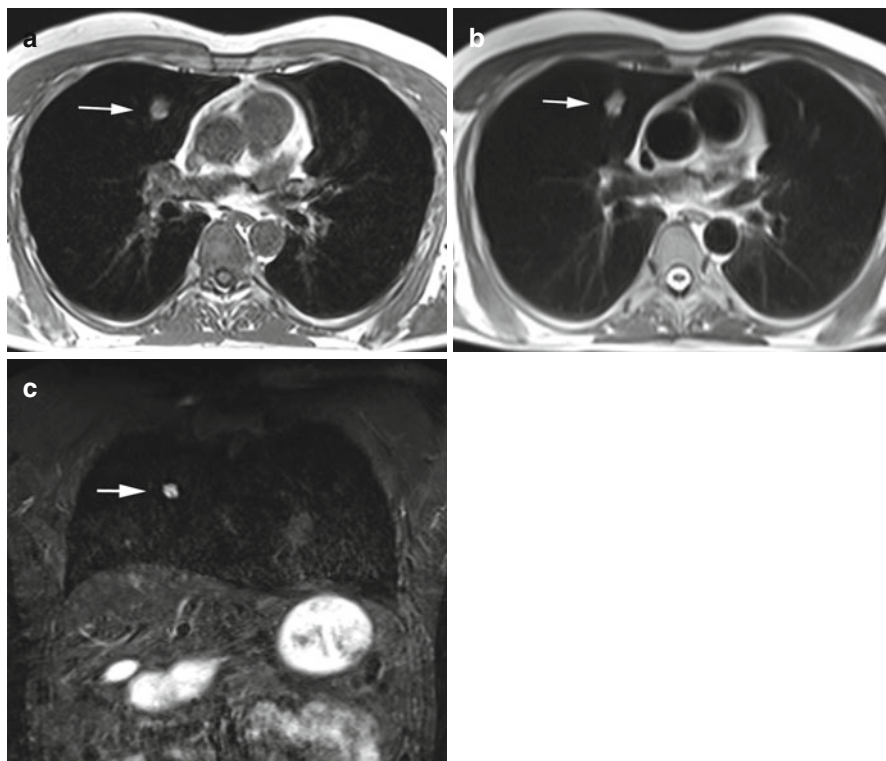


Fig. 6.4 Primary lung cancer in a 56-year-old male subject. Images demonstrate a solitary pulmonary nodule (20×14 mm) in the right middle lobe (a–c). Invasive diagnostic workup with CT-guided core biopsy yielded the diagnosis of primary lung cancer without nodal or parenchymal metastasis

3–4 mm for lung nodule detection with MRI performed at 1.5 T (The National Lung Screening Trial Research Team 2011). The sensitivities reported for MRI are greater than 80 % for pulmonary nodules measuring 5–10 mm and nearly 100 % for nodules larger than 10 mm (Girvin and Ko 2008; Feuerstein et al. 1992; Kersjes et al. 1997).

6.1.2.1 The Solitary Pulmonary Nodule

Most solitary pulmonary nodules are benign. Eighty percent of all benign nodules are granulomatous inflammatory processes and lymph nodes (Kradin et al. 1985), 10 % are hamartomas, and 10 % other rare entities (Beigelman-Aubry et al. 2007). Nevertheless, some are early lung cancers or metastases (Fig. 6.4). In subjects with no history of malignancy, the only generally accepted criteria for ruling out a malignant nodule are age under 30 at the time of diagnosis and the presence of intranodular fat (hamartoma, lipoid pneumonia) (Diederich and Das 2006). With CT, certain calcification patterns suggest benign pulmonary nodules. With MRI, however, calcification is difficult to detect, and the interpreting radiologist therefore cannot make

Table 6.2 Recommended management strategy for the solitary pulmonary nodule detected by MRI screening in a healthy study population (Diederich and Das 2006)

Nodule size (mm)	Recommended follow-up
<5	No follow-up needed (<1 % malignant)
5–10	Interval screening using non-contrast-enhanced CT
>10	Contrast-enhanced CT, PET, and/or image-guided biopsy

use of benign calcification patterns to rule out malignancy. The ability of MRI to demonstrate intranodular fat varies with the pulse sequence used and the size of the nodule. Since typically only non-contrast-enhanced chest images are obtained, contrast enhancement is another criterion not available for differentiating between benign and malignant nodules in the screening situation. Hence, demographic factors (age, pack years) are crucial in interpreting screening findings, while morphologic imaging features (well-defined versus ill-defined, smooth versus irregular contour) and localization within the lung (apical versus basal or peripheral versus central) can be considered but will not reliably rule out malignancy in many cases. This is because most pulmonary nodules seen on screening MRI are small, and the reliability of morphologic features decreases with lesion size.

Clinical Management

CT continues to be the method of choice for the workup of indeterminate pulmonary nodules. Solitary pulmonary nodules larger than 10 mm in diameter require further diagnostic evaluation by contrast-enhanced CT, PET, and/or biopsy. Lesions up to 10 mm in size should be followed up by unenhanced CT scans, ideally using computer-assisted volumetric analysis. Solitary pulmonary nodules smaller than 5 mm can be left alone, except in the setting of screening programs for high-risk groups. Less than 1 % of these very small nodules are malignant (Table 6.2) (Diederich and Das 2006; Henschke and Yankelevitz 2008; MacMahon et al. 2005).

6.1.2.2 Multiple Pulmonary Nodules

If multiple pulmonary nodules are detected, the rule of thumb is that each lesion must be evaluated individually (Fig. 6.5). The presence of multiple nodules makes a granulomatous or metastatic etiology more likely (Laurent and Remy 2002).

Clinical Management

As with solitary pulmonary nodules larger than 10 mm, multiple nodules require diagnostic workup with contrast-enhanced CT, PET, and/or biopsy (if expected to be diagnostic) (Beigelman-Aubry et al. 2007; Henschke and Yankelevitz 2008).

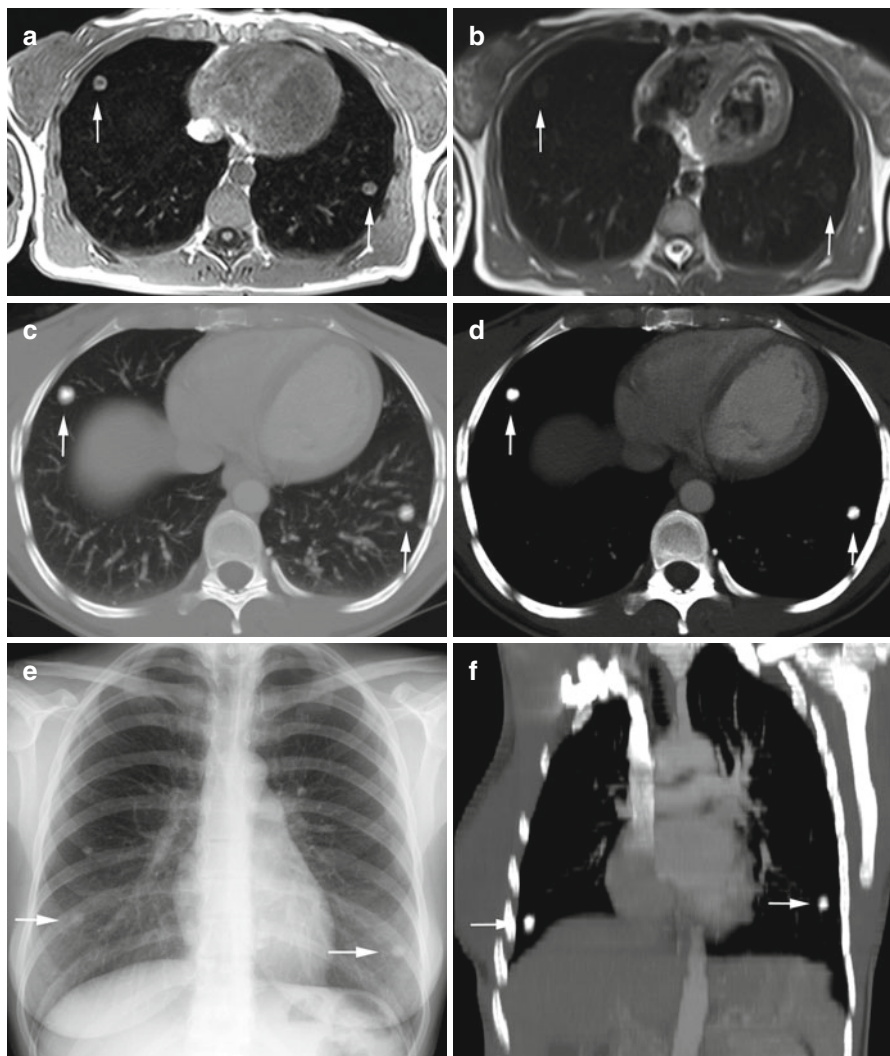


Fig. 6.5 Incidental multiple pulmonary nodules with diagnostic workup in a 37-year-old female subject. T1w image shows a 13-mm lesion in the right middle lobe and a 12-mm lesion in the left lower lobe (a); the lesions have high-signal-intensity rims with less intense centers. The lesions are difficult to see on T2w HASTE image (b). Workup with CT (c, d, f) and conventional radiography (e) demonstrates homogeneously calcified nodules. Diagnostic resection (VATS) confirmed post-tuberculous granulomas

6.1.3 Focal Pulmonary Masses >3 cm

Even larger pulmonary masses may not exhibit morphologic features that allow them to be reliably classified as benign or malignant; however, there are several features that are helpful in arriving at a characterization. Unfortunately, some

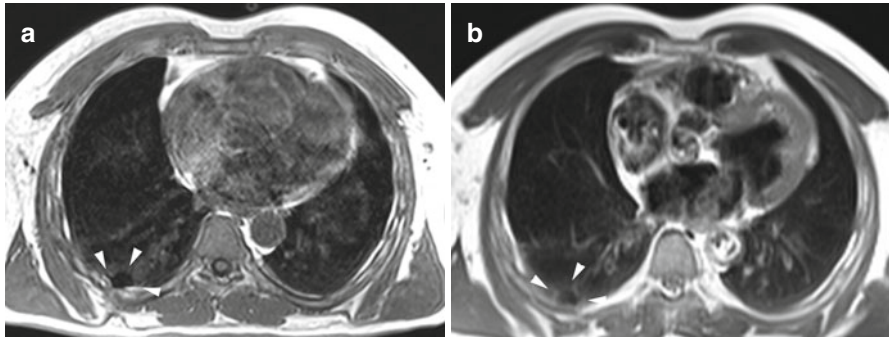


Fig. 6.6 Pleural calcinosis in a 68-year-old male subject. Post-inflammatory focal calcification of the posterior pleura can be identified by absence of signal on T1w image (a) and T2w image (b)

criteria that can be assessed on CT scans, attenuation values, for example, are not available to the radiologist interpreting MR images. Solid and nonsolid lesions cannot be distinguished with certainty. Patterns of calcification that indicate benign pulmonary lesions on CT scans are only rarely seen on MR images (Fig. 6.6). The fluid sensitivity of T2-weighted pulse sequences may, however, allow differentiation between cystic lesions and solid nodules. Some lesions have a characteristic imaging appearance. These include arteriovenous malformations, aspergillomas in preexisting cavities, rounded atelectasis, bronchoceles, and circumscribed mucus retention (Beigelman-Aubry et al. 2007). While a smooth, well-defined contour is suggestive of benignity (Ost and Fein 2000), 21 % of malignant pulmonary nodules, especially metastases, have well-defined margins (Erasmus et al. 2000). An ill-defined, irregular, or spiculated contour is typically associated with malignant growth, but it may also be seen in focal organizing pneumonia (FOP), some forms of vasculitis (e.g., Wegener and lymphomatoid granulomatosis), and other granulomatous diseases (tuberculosis) (Kohno et al. 1993; Zwirowich et al. 1991). Cavitation is more frequently seen in malignant lesions but is also typical of pulmonary abscess and other granulomatous inflammatory processes (Woodring and Fried 1983). Intralesional fat is diagnostic of a benign nodule. Most fat-containing masses are hamartomas; less common are fatty granuloma, lipoma, and lipomatoid pneumonia. Hamartomas, however, tend to be smaller than 25 mm (Siegelman et al. 1986).

Clinical Management

Masses larger than 3 cm in diameter are much more likely to be malignant compared with smaller pulmonary nodules. Each of these masses requires diagnostic workup using contrast-enhanced CT, PET, and/or biopsy. When lung cancer is suspected, the radiologist must also report all imaging information relevant for TNM staging.

6.2 Lymphadenopathy

6.2.1 Introduction

Older studies report an incidence of lymphadenopathy of less than 1 % per year in family practices (Allhiser et al. 1981; Fijten and Blijham 1988). Twenty-five percent of patients have generalized lymphadenopathy, and 50 % have isolated cervical lymphadenopathy (Allhiser et al. 1981; Abba et al. 2002). According to a study from the Netherlands, in 1.1 % of cases, lymph node enlargement is due to an underlying malignant disease (Fijten and Blijham 1988).

The estimated incidence of primary malignant lymphoma is 2–3/100,000 population/year for Hodgkin lymphoma and 15/100,000 population for non-Hodgkin lymphoma (Robert-Koch-Institut und die Gesellschaft der Epidemiologischen Krebsregister in Deutschland e.V. 2010). While some investigators have suggested a second peak of incidence of Hodgkin lymphoma after the 5th decade, this is still debated. For non-Hodgkin lymphoma, the risk is assumed to increase with age, peaking in the 7th to 8th decade. Both benign and malignant lymphadenopathy can have many different underlying causes (Kawaguchi 2001). Standard reference works regularly list more than 50 causes of lymph node enlargement, including infectious, immunologic, neoplastic, and metabolic conditions. Key aspects that aid in the evaluation and identification of the underlying cause are lymph node size, distribution, and duration of lymphadenopathy. Information on the development of enlarged lymph nodes over time is not available in the standard screening situation. In advanced lymphadenopathy, morphologic changes such as rounding of the normally ovoid shape, an irregular contour, and effacement of nodal architecture may point to a malignant cause. There is no generally accepted size threshold for identifying abnormally enlarged lymph nodes. In adults, palpable lymph nodes of up to 1 cm are considered normal. A diameter of more than 1.5 cm markedly increases the likelihood of a nonreactive, malignant process (Pangalis et al. 1993). Whether lymphadenopathy is localized or generalized also helps narrow the differential diagnosis. The site of localized lymphadenopathy can also provide clues (with varying degrees of specificity) on the underlying pathology.

6.2.2 Hilar and Mediastinal Lymphadenopathy

Bilateral hilar lymphadenopathy is typical of sarcoidosis (Fig. 6.7) but is also found in other chronic granulomatous diseases of the lung, in malignant lymphoma, and in metastatic lung cancer. Unilateral mediastinal lymphadenopathy is due to localized pulmonary disease of benign or malignant etiology. Rare causes of hilar lymphadenopathy include histoplasmosis, coccidioidomycosis, tularemia, psittacosis, and whooping cough. Calcification indicates tuberculosis, sarcoidosis, histoplasmosis, or silicosis.

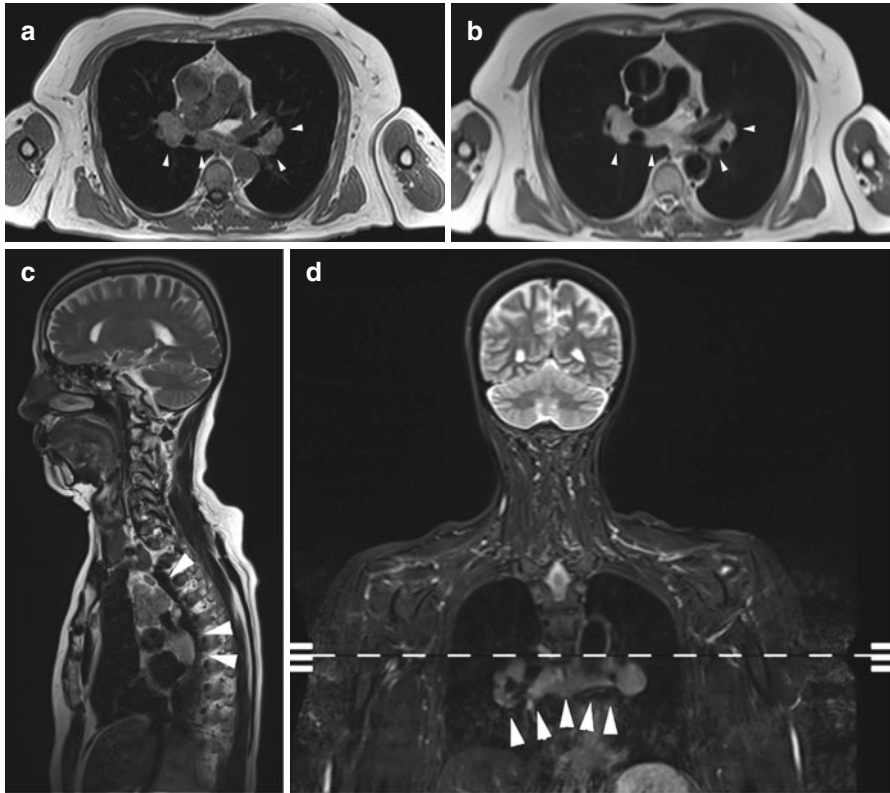


Fig. 6.7 Sarcoidosis in a 79-year-old female subject with a history of sarcoidosis without pulmonary involvement. Bilateral hilar and mediastinal lymphadenopathy with extensive conglomerate masses on axial T1w image (a), axial T2w HASTE image (b), sagittal T2w image (c), and coronal TIRM image (d)

Clinical Management

If hilar and/or mediastinal lymphadenopathy is diagnosed in subjects with concomitant localized pulmonary disease (see Sects. 6.1 and 6.3), the two entities are evaluated and managed together. If (unilateral or bilateral) lymphadenopathy alone is detected and at least one lymph node has a short-axis diameter of 1.5 cm or greater, the subject should undergo contrast-enhanced CT no earlier than 6 weeks after the MRI examination. CT follow-up is not necessary if the subject's history and/or laboratory results are highly indicative of a nonmalignant cause.

6.2.3 Supraclavicular Lymphadenopathy

Isolated supraclavicular lymphadenopathy should raise strong suspicion of metastatic involvement (Fijten and Blijham 1988; Ellison et al. 1999; Steel et al. 1995). Some authors advocate diagnostic workup for all supraclavicular lymph nodes larger than 5 mm. Metastatic involvement of the right and left supraclavicular lymph nodes is seen in mediastinal, pulmonary, esophageal, and breast cancer. Moreover, gastric and pancreatic cancers may spread through the thoracic duct to a left supraclavicular node (signal node or Virchow node). In rare instances, enlarged supraclavicular lymph nodes are caused by chronic fungal infection or mycobacteriosis (Jung and Trumper 2008).

Clinical Management

Detection of localized supraclavicular lymphadenopathy by whole-body MRI should prompt further evaluation with contrast-enhanced chest CT and/or biopsy if there is at least one lymph node with a short-axis diameter of 1 cm or greater (Fijten and Blijham 1988; Pangalis et al. 1993; Ferrer 1998). If the standard MRI protocol does not allow adequate evaluation of the breasts, women should be referred for mammography to rule out breast cancer. This is only indicated for male subjects if there are clinical signs to suggest breast cancer.

6.2.4 Axillary Lymphadenopathy

Draining the arms, the axillary lymph nodes may become enlarged in response to a variety of bacterial infections including staphylococcal and streptococcal infections as well as tularemia or cat scratch disease and other zoonoses (Fig. 6.8).

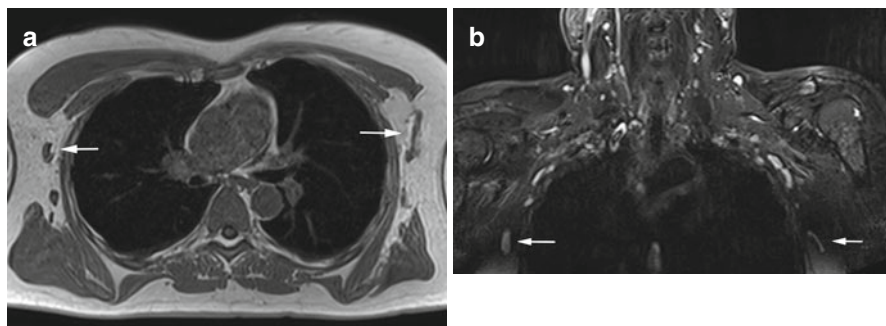


Fig. 6.8 Reactive lymphadenopathy. Bilaterally enlarged axillary lymph nodes (with maximum long-axis diameter of 4.5 cm and maximum short-axis diameter of 0.9 cm) with normal morphologic appearance and preserved fatty hilum on axial T1w image (a) and coronal TIRM image (b)

Longer persistence of enlarged axillary lymph nodes may point to toxoplasmosis, mononucleosis, or tuberculosis. Axillary lymph nodes are a common site for metastasis from primary lymphoma and in-transit metastasis from breast cancer and melanoma.

Clinical Management

If screening MRI identifies isolated unilateral or bilateral axillary lymphadenopathy but no local pathology to explain the enlargement and if there are no diagnostic clues in the history or laboratory results, follow-up imaging is warranted no earlier than 6 weeks after the MRI examination (same as for mediastinal and hilar lymphadenopathy). An ultrasound examination is usually sufficient. If no underlying cause is identified and lymphadenopathy does not resolve, biopsy should be considered. At this stage, as with indeterminate supraclavicular lymphadenopathy, adequate imaging evaluation for ruling out breast cancer is required in all women and in men if clinical signs are present.

6.2.5 Generalized Lymphadenopathy

The risk that generalized lymphadenopathy is due to a systemic hematologic condition increases with age. Infectious causes of generalized lymphadenopathy include infectious mononucleosis caused by Epstein-Barr virus; active Cytomegalovirus infection; HIV infection, acute measles and rubella, or responses to vaccination for these diseases; typical and atypical mycobacteriosis; secondary syphilis; and yersiniosis, brucellosis, histoplasmosis, and toxoplasmosis. Important autoimmune diseases associated with generalized lymphadenopathy include chronic polyarthritis, especially Still disease, and systemic lupus erythematosus. Rare causes are serum disease, drug reactions, and extraintestinal Crohn disease. Generalized lymphadenopathy with concomitant splenomegaly (less than 10 % of cases) is most commonly seen in mononucleosis, Hodgkin and non-Hodgkin lymphoma as well as chronic and acute leukemia.

Clinical Management

All cases of generalized lymphadenopathy require diagnostic workup. A careful history and laboratory tests (including, as a minimum, a differential blood count, liver enzymes, and LDH) often provide important diagnostic clues. Evaluation must rule out extranodal lymphoma, especially in the spleen, intestine, and central nervous system. In subjects with nondiagnostic initial studies, a tissue diagnosis must be obtained, typically by open excision biopsy or alternatively by imaging-guided core biopsy.

6.3 Pneumonia, Effusion, and Atelectasis

Unlike focal pulmonary lesions, the MRI findings described here involve larger anatomic structures and include diffuse parenchymal changes. Acute and chronic atelectasis is detected by both T1-weighted VIBE and T2-weighted HASTE sequences. These two pulse sequences are comparable to CT in terms of sensitivity and allow affected areas to be localized to anatomic sites (Fig. 6.9). They also enable good visualization of diffuse loose infiltrates or, for instance, of peribronchial infiltrates (Fig. 6.10).

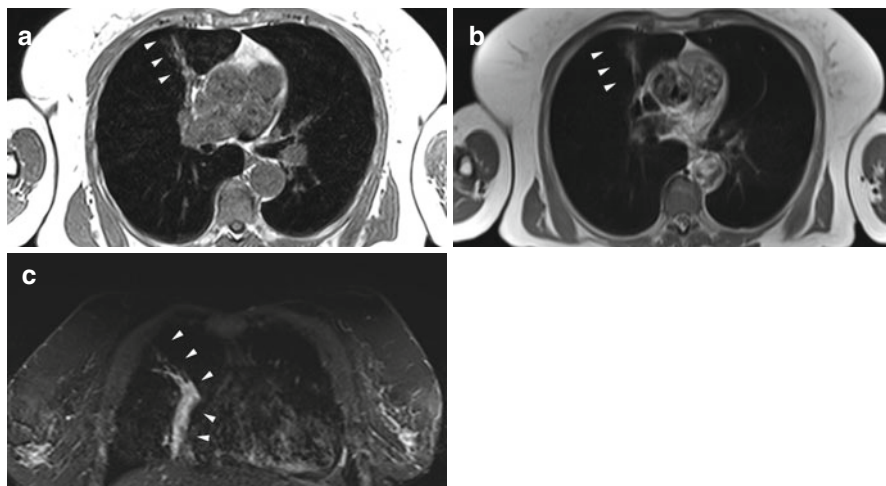


Fig. 6.9 Atelectasis. 69-year-old female subject with partial atelectasis of middle lobe on axial (a, b) and coronal (c) images

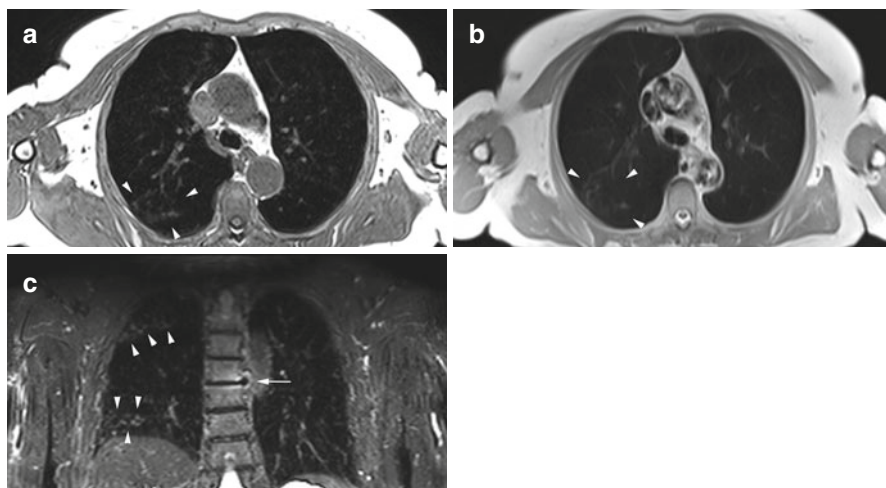


Fig. 6.10 Inflammatory infiltrate. Same subject as in Fig. 6.9. Axial (a, b) and coronal (c) images show circumscribed alveolar infiltrate in the periphery of the right lower lobe. Also seen is reactive inflammation (arrow in c) secondary to osteochondrosis of the mid-thoracic spine

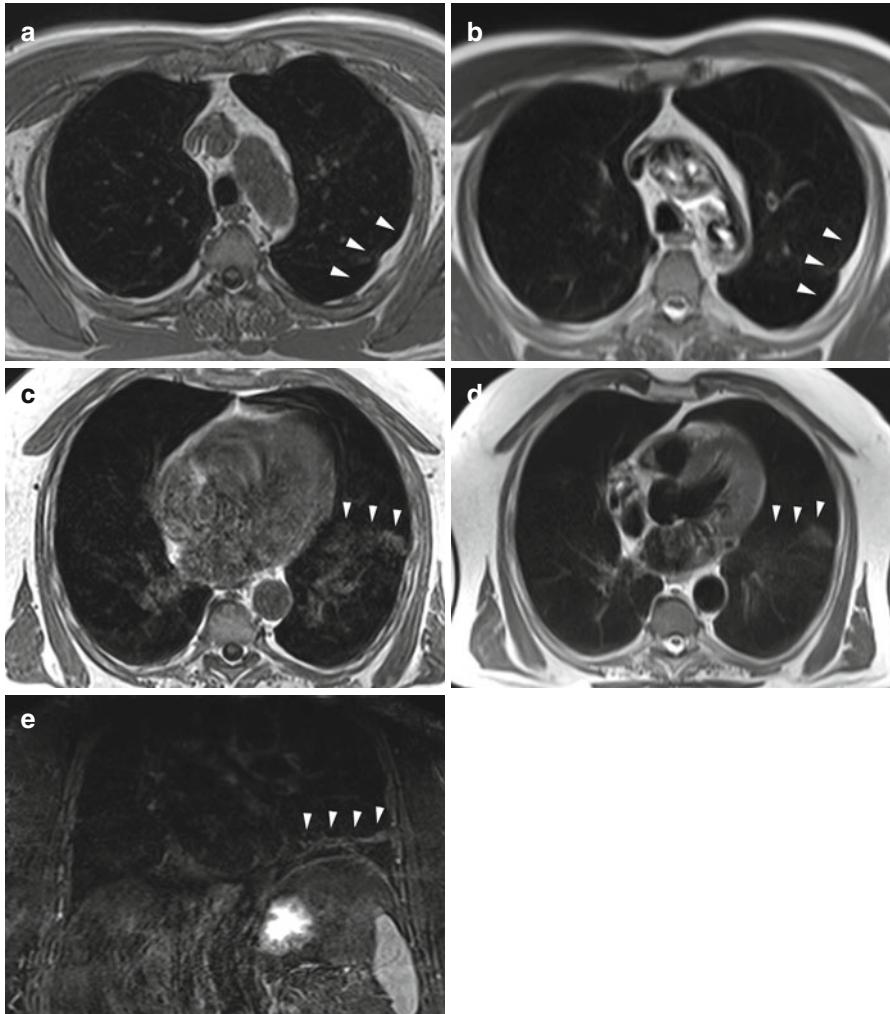


Fig. 6.11 Pleural effusion. Sickle-shaped fluid collection of high T2 signal intensity near the chest wall (a, b) and interlobar fluid collection (c–e). The interlobar fluid collection is also seen on the coronal TIRM image (e)

Infiltrates that contain reactive fluid and pleural fluid collections can be detected with high sensitivity using the T2-weighted HASTE sequence or the coronal TIRM sequence, which is also part of the protocol (Fig. 6.11). Hence, these sequences make it possible to differentiate between infiltrates and fibrous parenchymal processes (Fig. 6.12). Pulmonary embolism is a special form of parenchymal abnormality. A fresh thromboembolus is seen on T1-weighted images as an elongated structure of high signal intensity and is isointense to muscle on HASTE images (Fig. 6.13). Emphysema-related changes, when they manifest as circumscribed bullae at least, can also be detected by MRI (Fig. 6.14).

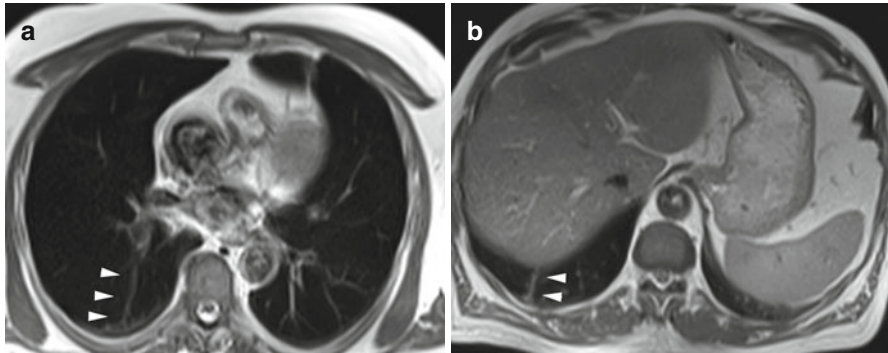


Fig. 6.12 Pleural fibrosis in two subjects. Fibrous strands contiguous with the pleura in the right basal lung seen as stripes of high signal intensity on T2w image (a) and T1w image (b)

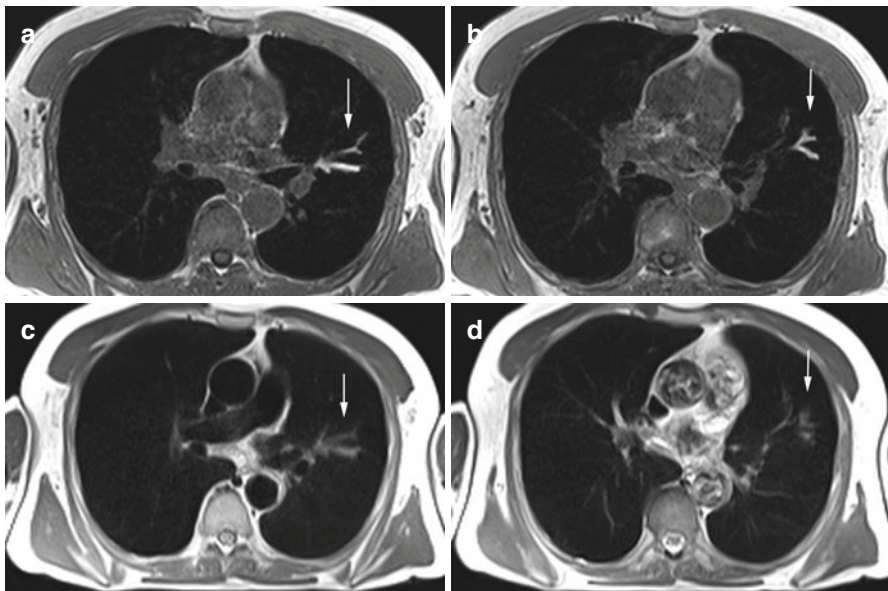


Fig. 6.13 Pulmonary artery embolism. Incidental finding of segmental pulmonary artery embolism in the left upper lobe in a 64-year-old male subject. T1w VIBE images show thrombotic material of very high signal intensity (a, b). On T2w HASTE images, the thrombotic material appears blurred due to reactive perivascular fluid collection (c, d)

Clinical Management

The management of impaired pulmonary ventilation and infiltration primarily depends on the subject's clinical symptoms. Consequently, most cases need not be evaluated further. However, it is important to rule out an underlying pulmonary or hilar mass. Diagnostic workup is required if MRI demonstrates unilateral pleural effusion, unless there is strong evidence of a reactive or circulatory pathogenesis.

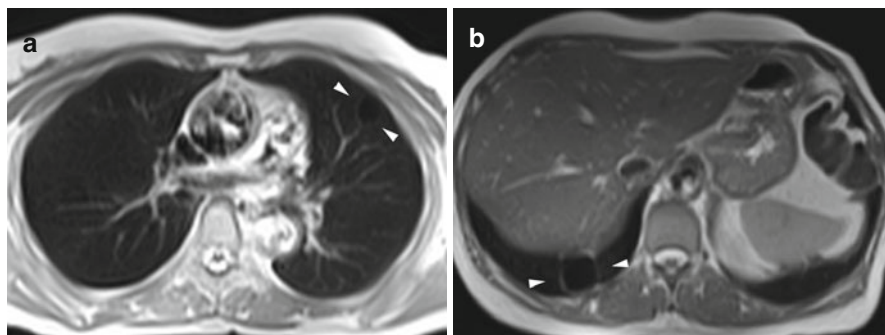


Fig. 6.14 Bullous emphysema. Two subjects with isolated subpleural bullae in different sites: 18-mm bulla on T2w HASTE image in a 55-year-old woman (a) and 28-mm bulla on T1w VIBE image in a 63-year-old woman (b)

Table 6.3 Common and rare lesions of each of the three mediastinal compartments

Compartment	Common	Rare
Anterior	Thymoma, teratoma, lymphoma, goiter, pericardial cyst, bone tumor	Bronchogenic cyst, echinococcosis, parathyroid tumor, paraganglioma
Middle	Bronchogenic cyst, goiter, hiatus hernia, achalasia, lymphoma	Pancreatic pseudocyst, parathyroid tumor, neurinoma
Posterior	Neurofibroma, schwannoma, ganglioneuroblastoma, abscess, bone tumor, hiatus hernia	Teratoma, bronchogenic cyst, Bochdalek hernia, lymphoma, pancreatic pseudocyst, paraganglioma, echinococcosis

6.4 Mediastinal Masses

The majority of mediastinal masses are inflammatory or neoplastic in nature. Clinical symptoms and tumor site within the mediastinum are the most important clues to the diagnosis (Table 6.3). The conspicuity of a mass and its topographic relationship to mediastinal anatomy may suggest the underlying cause – a diaphragmatic hernia, for instance (Fig. 6.15). Inflammatory mediastinal conditions are not uncommonly due to a process descending from the neck.

Lesions that are typically isointense to fluid on T2-weighted images include pericardial cysts, bronchogenic cysts, and cystic thymomas. Calcification may be seen in aneurysm, goiter, teratoma, lymph nodes, and ganglioneuroblastoma.

Clinical Management

A subject in whom MRI detects a mediastinal mass should always be referred for diagnostic workup. Depending on the subject's age, history, and, if available, prior imaging findings, a tissue diagnosis must be obtained using imaging-guided core biopsy or possibly mediastinoscopy.



Fig. 6.15 Thoracic stomach in an 81-year-old female subject. Paraesophageal hernia and upside-down stomach with mass effect in the lower mediastinum, predominantly on the right, on axial T1w image (a), fat-suppressed images (b, c), and sagittal T2w image (d)

References

- Abba AA, Bamgboye AE, Afzal M, Rahmatullah RA (2002) Lymphadenopathy in adults: a clinicopathological analysis. *Saudi Med J* 23:282–286
- Allhiser JN, McKnight TA, Shank JC (1981) Lymphadenopathy in a family practice. *J Fam Pract* 12:27–32
- Beigelman-Aubry C, Hill C, Grenier PA (2007) Management of an incidentally discovered pulmonary nodule. *Eur Radiol* 17:449–466
- Biederer J, Hintze C, Fabel M (2008) MRI of pulmonary nodules: technique and diagnostic value. *Cancer Imaging* 8:125–130
- Crow J, Slavin G, Kreef L (1981) Pulmonary metastasis: a pathologic and radiologic study. *Cancer* 47:2595–2602
- Diederich S, Das M (2006) Solitary pulmonary nodule: detection and management. *Cancer Imaging* 6:42–46

- Ellison E, LaPuerta P, Martin SE (1999) Supraclavicular masses: results of a series of 309 cases biopsied by fine needle aspiration. *Head Neck* 21:239–246
- Erasmus JJ, Connolly JE, McAdams HP, Roggli VL (2000) Solitary pulmonary nodules: part I. Morphologic evaluation for differentiation of benign and malignant lesions. *Radiographics* 20:43–58
- Ferrer R (1998) Lymphadenopathy: differential diagnosis and evaluation. *Am Fam Physician* 15:1313–1320
- Feuerstein IM, Jicha DL, Pass HI, Chow CK, Chang R, Ling A, Hill SC, Dwyer AJ, Travis WD, Horowitz ME et al (1992) Pulmonary metastases: MR imaging with surgical correlation – a prospective study. *Radiology* 182:123–129
- Fijten GH, Blijham GH (1988) Unexplained lymphadenopathy in family practice: an evaluation of the probability of malignant causes and the effectiveness of physicians' workup. *J Fam Pract* 27:373–376
- Girvin F, Ko JP (2008) Pulmonary nodules: detection, assessment, and CAD. *Am J Roentgenol* 191:1057–1069
- Henschke CI, Yankelevitz DF (2008) CT screening for lung cancer: update 2007. *Oncologist* 13:65–78
- Jung W, Trumper L (2008) Differential diagnosis and diagnostic strategies of lymphadenopathy. *Internist* 49:305–318
- Kawaguchi T (2001) Pathological features of lymph node metastasis: 2) from morphological aspects. *Nippon Geka Gakkai Zasshi* 102:440–444
- Kersjes W, Mayer E, Buchenroth M, Schunk K, Fouda N, Cagil H (1997) Diagnosis of pulmonary metastases with turbo-SE MR imaging. *Eur Radiol* 7:1190–1194
- Kim YH, Lee KS, Primack SL, Kim H, Kwon OJ, Kim TS, Kim EA, Kim J, Shim YM (2002) Small pulmonary nodules on CT accompanying surgically resectable lung cancer: likelihood of malignancy. *J Thorac Imaging* 17:40–46
- Kohno N, Ikezoe J, Johkoh T, Takeuchi N, Tomiyama N, Kido S, Kondoh H, Arisawa J, Kozuka T (1993) Focal organizing pneumonia: CT appearance. *Radiology* 189:119–123
- Kradin RL, Spirn PW, Mark EJ (1985) Intrapulmonary lymph nodes: clinical, radiologic, and pathologic features. *Chest* 87:662–667
- Laurent F, Remy J (2002) Management strategy of pulmonary nodules. *J Radiol* 83:1815–1821
- MacMahon H, Austin JH, Gamsu G, Herold CJ, Jett JR, Naidich DP, Patz EF Jr, Swensen SJ (2005) Guidelines for management of small pulmonary nodules detected on CT scans: a statement from the Fleischner Society. *Radiology* 237:395–400
- Ost D, Fein A (2000) Evaluation and management of the solitary pulmonary nodule. *Am J Respir Crit Care Med* 162:782–787
- Ost D, Fein AM, Feinsilver SH (2003) Clinical practice: the solitary pulmonary nodule. *N Engl J Med* 348:2535–2542
- Pangalis GA, Vassilakopoulos TP, Boussiotis VA, Fessas P (1993) Clinical approach to lymphadenopathy. *Semin Oncol* 20:570–582
- Robert-Koch-Institut und die Gesellschaft der Epidemiologischen Krebsregister in Deutschland e.V (2010) Krebs in Deutschland 2005/2006. Häufigkeiten und Trends. Berlin
- Siegelman SS, Khouri NF, Scott WW Jr, Leo FP, Hamper UM, Fishman EK, Zerhouni EA (1986) Pulmonary hamartoma: CT findings. *Radiology* 160:313–317
- Steel BL, Schwartz MR, Ramzy I (1995) Fine needle aspiration biopsy in the diagnosis of lymphadenopathy in 1,103 patients: role, limitations and analysis of diagnostic pitfalls. *Acta Cytol* 39:76–81
- Swensen SJ, Jett JR, Hartman TE, Midthun DE, Sloan JA, Sykes AM, Aughenbaugh GL, Clemens MA (2003) Lung cancer screening with CT: Mayo Clinic experience. *Radiology* 226:756–761
- Tan BB, Flaherty KR, Kazerooni EA, Iannettoni MD (2003) The solitary pulmonary nodule. *Chest* 123(1 Suppl):89S–96S
- The National Lung Screening Trial Research Team (2011) Reduced lung-cancer mortality with low-dose computed tomographic screening. *N Engl J Med* 365:395–409

-
- Winer-Muram HT (2006) The solitary pulmonary nodule. *Radiology* 239:34–49
- Woodring JH, Fried AM (1983) Significance of wall thickness in solitary cavities of the lung: a follow-up study. *AJR Am J Roentgenol* 140:473–474
- Zwirewich CV, Vedal S, Miller RR, Muller NL (1991) Solitary pulmonary nodule: high-resolution CT and radiologic-pathologic correlation. *Radiology* 179:469–476

Saskia Ungerer

7.1 Introduction to Techniques and Applications

Magnetic resonance imaging of the heart has become a central noninvasive tool for the evaluation of patients with cardiovascular disease.

MRI provides excellent soft tissue contrast and tissue characterization, and advances made over the last decade have improved the evaluation of both cardiac morphology and function (ACCF/ACR/AHA/NASCI/SCMR 2010). A variety of MRI protocols are available for analysis of cardiac function, including wall motion at rest and stress, identification of inflammation and ischemia, viability imaging, and evaluation of valve function, making MRI a versatile imaging modality for a wide range of diagnostic tasks in patients with cardiac disease (ACCF/ACR/AHA/NASCI/SCMR 2010).

Currently, the most important indications for cardiac MRI are (Jiji and Kramer 2011):

- Assessment of left ventricular function and myocardial viability in ischemic heart disease
- Imaging of patients with suspected infiltrative cardiomyopathies, hypertrophic (obstructive) cardiomyopathies, or arrhythmogenic right ventricular cardiomyopathy
- Patients with ischemic heart disease or cardiac failure in whom echocardiography does not allow adequate evaluation of cardiac structures or function
- Imaging of myocardial viability prior to revascularization
- Evaluation of pericardial tissue or constrictive pericarditis
- Assessment of myocardial mass and evaluation for thrombus
- Analysis of nearby vessels prior to ablation therapy

S. Ungerer
Institute of Diagnostic Radiology and Neuroradiology,
University Medicine Greifswald, Ferdinand-Sauerbruch-Straße,
Greifswald 17487, Germany
e-mail: sungerer@uni-greifswald.de

All cardiac MRI examinations are performed during breath-hold and require careful timing using a reliable triggering technique (electrocardiogram or, when a good ECG signal cannot be obtained, peripheral pulse monitoring).

7.1.1 Cardiac Function Imaging

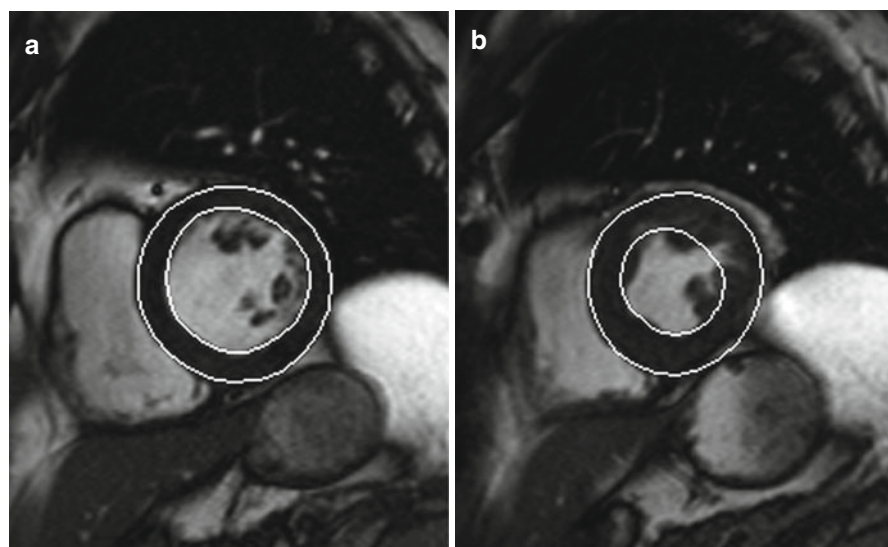
Four-dimensional cine MR imaging is highly accurate and reproducible. Hence, it has become the method of choice (gold standard) for assessing left ventricular function and identifying cardiac wall motion abnormalities (Palumbo et al. 2010). Images are acquired over several cardiac cycles, which eliminates motion artifacts and ensures adequate resolution per cardiac phase.

MRI is an excellent modality for the assessment of cardiac function, allowing determination of standard functional parameters such as left ventricular ejection fraction (LVEF), left ventricular end-diastolic volume (LVEDV), left ventricular end-systolic volume (LVESV), and left ventricular mass (LVM) (Walsh and Hundley 2007).

Cardiac function can be determined using long-axis or short-axis views:

1. Long-axis views: Cardiac function in the long axis is assessed using the area-length method (ALM), which provides a very accurate measure of cardiac dimensions in individuals with normal-sized hearts and normal contractile function. When using this method, it is important to exclude the papillary muscles, or else left ventricular mass may be overestimated and left ventricular volume underestimated.
2. Short-axis views: This method is more accurate but also more time-consuming, and the postprocessing software required for it is provided by most manufacturers as part of the standard package. Functional parameters are calculated using the slice summation method (SSM). In a stack of contiguous short-axis slices covering the complete ventricle from apex to base (valvular plane), the end-systolic, end-diastolic, and epicardial areas are outlined in each slice. The outlined areas are converted to volumes and summed to produce estimates of end-diastolic and end-systolic volumes and myocardial mass. In contrast to the first method, here it is important to include the papillary muscles, as they account for approx. 8–10 % of the left ventricular mass, and the SSM allows their size and location to be determined accurately (Nassenstein et al. 2009) (Fig. 7.1).

Fig. 7.1 Assessment of the left ventricle using the slice summation method (SSM). Short-axis views in end diastole (**a**) and end systole (**b**). (**c**) Parameters determined in assessing left ventricular function are *EF* ejection fraction, *EDV* end-diastolic volume, *ESV* end-systolic volume, *SV* stroke volume, *CO* cardiac output, and myocardial mass (at end diastole and average); measures of ventricular ejection and filling rates: peak ejection rate, time to peak ejection rate, peak filling rate, and time from end systole to peak filling rate



Pat. ID: 00008... Untersuch. Datum: 22.07.2008
 Pat.Größe: 178.00 cm. Pat.Gewicht: 79.30 kg. Herzrate: 66 Schläge/min

c				
Linker Ventrikel - Absolut				
Herzfunktion			Normaler Bereich (M) (MRI)	Einheiten
Auswurffraktion	EF	62.5	56.00 ... 78.00	%
ED-Volumen	EDV	174.7	77.00 ... 195.00	ml
ES-Volumen	ESV	65.5	19.00 ... 72.00	ml
Schlagvolumen	SV	109.1	51.00 ... 133.00	ml
Herzminutenvolumen	CO	7.20	2.82 ... 8.82	l/min
Myokardmasse (in ED)		130.7	118.00 ... 238.00	g
Myokardmasse (Mittelwert)		151.6 ± 15.0	118.00 ... 238.00	g
Füll- und Auswurfdaten				
Max. Auswurfrate		412.6	n.a.	ml/sec
Max. Auswurfzeit		153.7	n.a.	msec
Max. Füllrate		353.8	n.a.	ml/sec
Max. Füllzeit nach ES		133.2	n.a.	msec

Prüfen Sie die Konturen. Diese können von den anatom. Strukturen abweichen.

Cine sequences also permit visual assessment of ventricular contraction, detection of global or locoregional wall motion abnormalities, and evaluation of valve function (Figs. 7.2 and 7.3).

Quantitative estimation of stenosis severity and valve incompetence requires the use of a flow-sensitive imaging technique. Flow across the valve is typically assessed by acquisition perpendicular to the valvular plane and is known as through-plane acquisition.

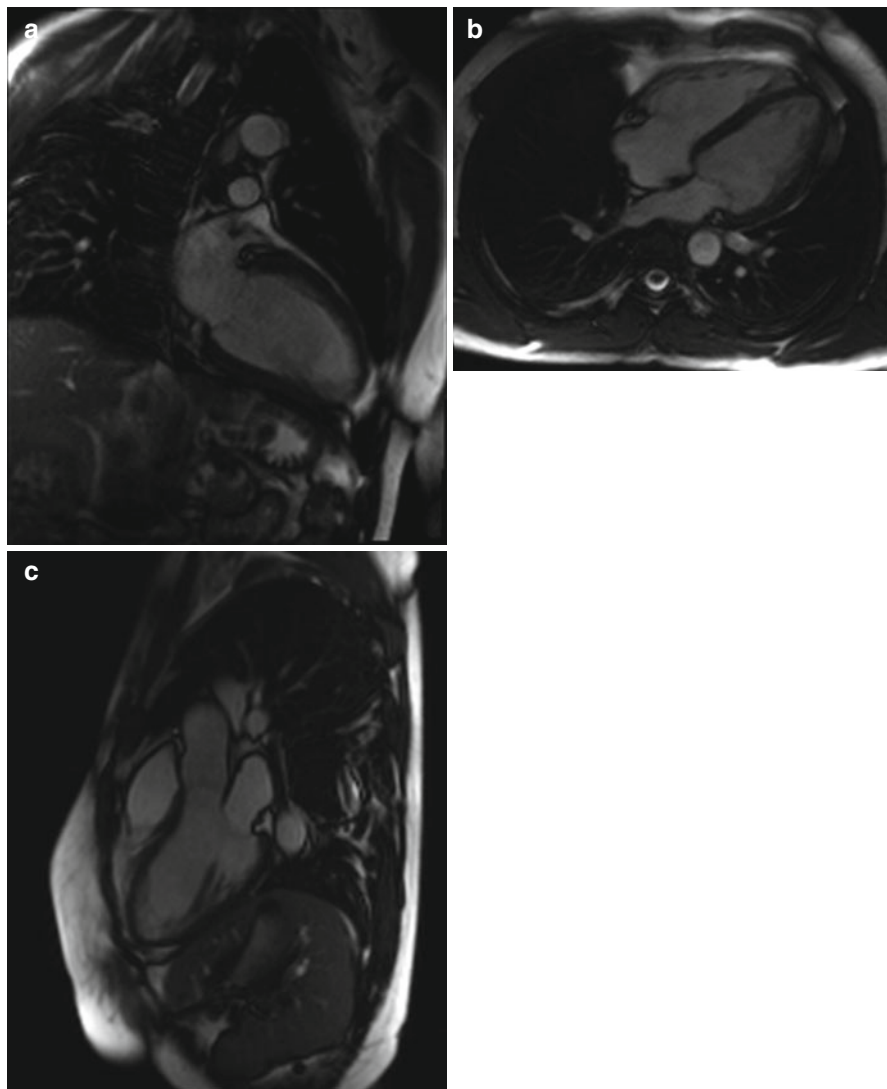


Fig. 7.2 Cine images from a healthy subject. (a) Two-chamber view, (b) four-chamber view, and (c) three-chamber view

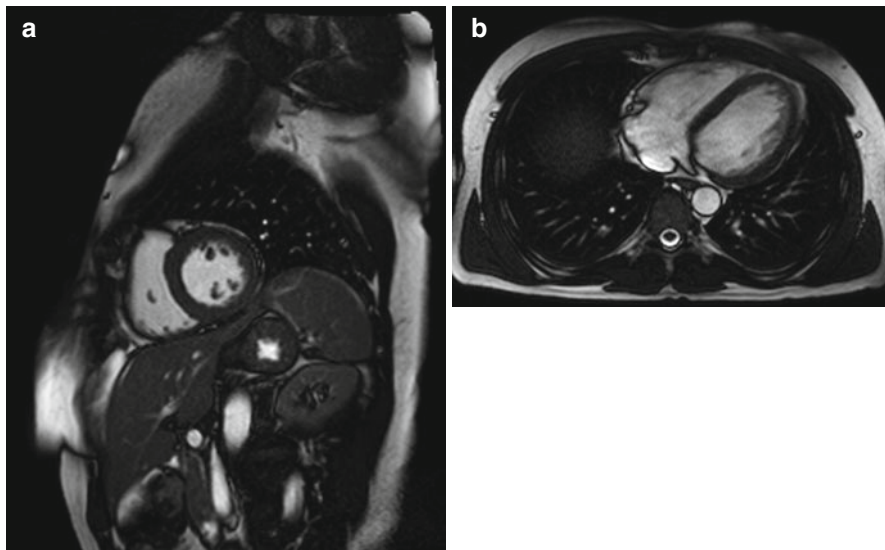


Fig. 7.3 Cine images from a healthy subject. (a) Short-axis view (midventricle) and (b) true axial view (midventricle)

7.1.2 Edema Imaging

A clinical cardiac MRI protocol used in patients with suspected myocarditis or cardiomyopathy should always include a fat-saturated T2-weighted sequence (Carbone and Friedrich 2012). Because it suppresses signal from fat and flowing blood, this pulse sequence is highly sensitive for detecting fluids in tissues. It has approx. 80 % sensitivity in identifying myocardial edema and is also well suited for detecting concomitant pericardial effusion. Myocardial edema imaging using newer pulse sequences with much improved image quality provides useful additional diagnostic and prognostic information, allowing identification of acute or recent myocardial ischemic injury in patients with acute chest pain, distinguish acute from chronic myocardial infarction and contributing to the determination of myocardium at risk (Eitel and Friedrich 2011). Despite these advances, cardiac MRI is only a supplementary tool and not the first-line imaging modality in patients undergoing imaging for evaluation of myocarditis or cardiomyopathy.

Inflammation damages the cell membrane, resulting in a larger distribution volume of contrast medium in injured myocardium. This is one of the mechanisms underlying late enhancement in cardiac imaging.

However, the presence of late enhancement alone does not allow discrimination between inflammatory processes and scar tissue. Areas of late enhancement resulting from retention of contrast medium are seen in a variety of disorders associated with myocardial injury and edema, necrosis, or fibrosis (Manrique et al. 2009). Some additional features such as distribution and location of delayed enhancement may help the radiologist in narrowing the differential diagnosis among ischemic and nonischemic disorders. For instance, when contrast medium accumulates in the epicardium, a

myocardial scar of ischemic origin is unlikely because such a scar is typically seen in a subendocardial location. Furthermore, delayed enhancement occurring in coronary artery territories can contribute to the differentiation between scar and edema. In unclear cases, acquisition of the delayed enhancement sequence can be repeated after 15–20 min. At this point in time, a scar still has high signal intensity due to delayed washout of contrast medium from injured myocardium, while edema has low signal intensity (Abdel-Aty and Schulz-Menger 2007; Aletras et al. 2008).

7.1.3 Ischemia Imaging

Imaging of ischemic myocardial injury is an important component of a cardiac MRI protocol and is done by assessing late enhancement, typically 12–15 min after administration of a Gd-DPTA-based contrast agent (e.g., gadobutrol as in the SHIP). Differential enhancement of infarcted myocardium is primarily due to diffusion and delayed clearance of contrast medium from the zone of infarction. In addition, myocardial injury shortens longitudinal relaxation (T_1). Compared with other imaging methods, contrast-enhanced cardiac MRI is more sensitive in detecting even small subendocardial infarcts. Furthermore, the extent of delayed enhancement on MRI closely correlates with the size of myocardial injury determined by established methods (Kim et al. 1999; Saraste et al. 2008). In contrast, PET and SPECT usually detect large transmural infarcts or nearly transmural defects but may miss smaller, subendocardial infarcts (Wagner et al. 2003).

Cardiac MRI may also detect complications of acute myocardial infarction such as the development of left ventricular pseudoaneurysm (Jiji and Kramer 2011).

Single-shot sequences are widely used for delayed enhancement imaging, offering the advantage that all data can be acquired in a single cardiac cycle. This comes at the cost of a loss of image sharpness.

After administration of gadolinium-based contrast medium, infarcted myocardium exhibits delayed enhancement and can be identified using an inversion recovery (IR) sequence, which greatly improves contrast between viable myocardium and infarction. When magnitude reconstruction is used, IR delayed enhancement imaging is highly sensitive to the inversion time (TI) selected (Kellman et al. 2002). The optimal TI to null signal from viable myocardium (i.e., to render it dark) for an individual can be determined by obtaining a TI scout series with progressively larger TIs (TI surfing). Typical TIs are between 200 and 300 ms, depending on the amount of contrast medium administered (usually 0.1–0.2 mmol/kg body weight), time of image acquisition after contrast administration, and individual contrast medium clearance (Stork et al. 2007). An optimal TI enhances the contrast between dark viable myocardium and bright infarcted tissue. When delayed enhancement studies are performed with a phase-sensitive inversion recovery (PSIR) sequence, it is possible to use a nominal value of TI, which eliminates the need for TI surfing and achieves a consistent contrast over a wide range of TIs without artifacts due to incorrect polarity (Kellman et al. 2002).

Phase-sensitive reconstruction is used to remove the background phase while preserving the sign of the desired magnetization during IR. The phase-sensitive reconstruction method reduces the variation in apparent infarct size observed in magnitude images as TI is changed. Phase-sensitive detection also has the

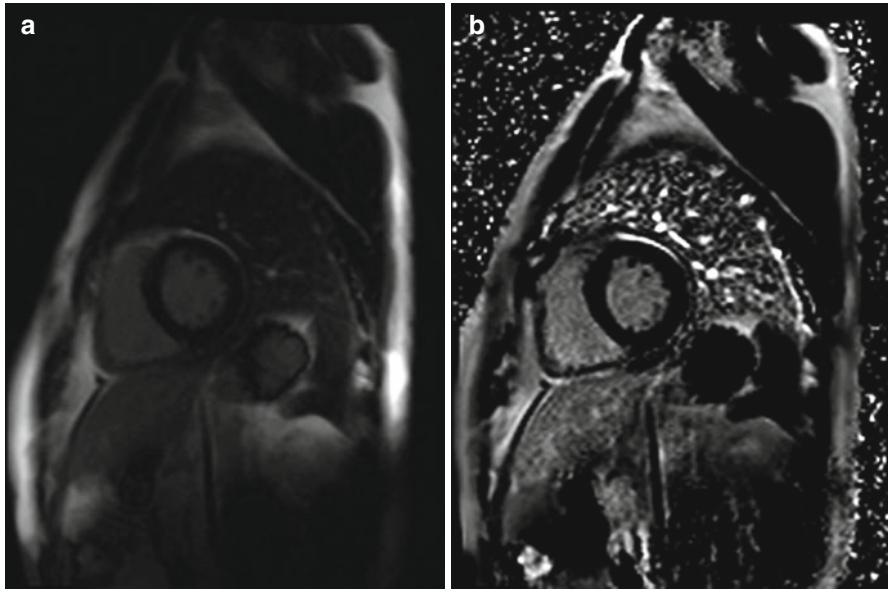


Fig. 7.4 Single-shot inversion recovery sequences (short axis) for delayed enhancement imaging in a healthy subject. (a) magnitude reconstruction (b) phase-sensitive reconstruction

advantage of decreasing the sensitivity to changes in tissue T1 with increasing delay from contrast medium injection (Kellman et al. 2002) (Fig. 7.4).

There are certain pitfalls one must be aware of when interpreting delayed enhancement images. Mural thrombi do not take up contrast medium and will appear dark, just like normal myocardium. Regions of microvascular obstruction after acute myocardial infarction also have low signal intensity (Jiji and Kramer 2011). Hence, it is not possible to reliably differentiate thrombus, microvascular obstruction, and viable myocardium, precluding accurate estimation of infarct size (Karamitsos et al. 2009).

7.1.4 Viability Imaging

The use of specialized pulse sequences allows myocardial perfusion imaging by assessing contrast medium inflow and clearance from the myocardium. Myocardial perfusion can be assessed at rest and stress. Pharmacologic stress is induced by administration of adenosine or dobutamine. Areas of reduced myocardial perfusion show delayed contrast medium uptake, i.e., after administration of contrast medium, they remain dark longer than well-perfused myocardium (Karamitsos et al. 2011).

Myocardial perfusion MRI allows noninvasive assessment of myocardial viability and differentiation of infarcted areas from dysfunctional but viable myocardium (Saraste et al. 2008; Wellnhofer et al. 2004). In conjunction with cine MRI and delayed enhancement imaging, cardiac perfusion MRI enables reliable detection of coronary stenosis >70 % (De Mello et al. 2012).

7.1.5 Imaging in Rare Diseases of the Heart

Cardiac MRI also has an important role in diagnosing less common diseases of the heart such as arrhythmogenic right ventricular cardiomyopathy, cardiac sarcoidosis, myocardial involvement in amyloidosis, and tumors of the heart. Moreover, it can contribute to the detection of pericardial or endocardial disease (ACCF/ACR/AHA/NASCI/SCMR 2010).

7.1.6 Cardiac Imaging in Whole-Body MRI

Due to time constraints, a cardiac MRI examination performed as part of a whole-body MRI protocol cannot include all components of a comprehensive cardiac MRI study. The cardiac MRI protocol used in the SHIP included cine sequences for functional assessment in four-chamber, three-chamber, and two-chamber views as well as short-axis views for left ventricular function assessment. Strict axial cine sequences were acquired for evaluation of right ventricular function. A fat-saturated T2-weighted pulse sequence was deliberately not included although edema may persist for some time after a myocardial event. Delayed enhancement imaging was performed using an inversion recovery single shot sequence with magnitude reconstruction, highly sensitive to the inversion time (TI) selected and a phase-sensitive inversion recovery (PSIR) single shot sequence acquired 15 min after administration of 0.15 mmol/kg body weight of gadobutrol. The PSIR sequence used in the SHIP MRI protocol creates two image data records. First dataset contains images with magnitude reconstruction, in the second dataset phase-sensitive reconstruction images are generated.

The following sections give an overview of the most common incidental findings detected by cardiac MRI performed as part of a whole-body screening examination.

7.2 Diseases of Myocardium

Areas of delayed myocardial enhancement are the most common incidental findings in the heart at screening MRI. Note, however, that delayed enhancement is a mere descriptive term and provides no clues to possible underlying causes, which are multifarious (Kim et al. 2006). Classic causes include acute and chronic myocardial infarction, cardiomyopathy, and acute or chronic myocarditis (Stork et al. 2007). In a cardiac MRI protocol, late enhancement sequences enable accurate and noninvasive quantification of the extent of myocardial infarction (gold standard). The transmural extent of delayed enhancement may be used to predict functional outcome in ischemic heart disease (Saraste et al. 2008).

7.2.1 Ischemic Heart Disease

Ischemic heart disease (IHD) or myocardial ischemia is characterized by reduced blood supply to the heart muscle and is usually due to atherosclerosis of the coronary arteries (ACCF/ACR/AHA/NASCI/SCMR 2010) (Table 7.1).

Table 7.1 Ischemic heart disease

Frequency	Common, prevalence of up to 20 %, increases with age M:F ratio of 4:1
Causes	Endothelial damage by atherogenic risk factors, e.g., hypercholesterinemia, hyperlipoproteinemia, smoking, diabetes mellitus, arterial hypertension, obesity, and familial predisposition Subsequent development of atheromatous plaque with narrowing of arterial lumen (critical when lumen loss is 70 % or greater) Resulting mismatch between myocardial oxygen supply and demand
Clinical presentation	Angina pectoris, exercise-induced dyspnea, cardiac insufficiency, cardiac dysrhythmia, myocardial infarction in coronary artery occlusion

Flow-limiting coronary stenosis causes coronary insufficiency, or a mismatch between oxygen supply and demand. The resulting myocardial ischemia has different clinical presentations:

- Angina pectoris (stable/unstable; Canadian Cardiovascular Society (CCS) classification system)
- Acute coronary syndrome (ACS)/myocardial infarction
- Ischemic cardiomyopathy with cardiac insufficiency
- Cardiac arrhythmia/sudden cardiac death

In patients first presenting with IHD, angina pectoris (55 %) is most common, followed by myocardial infarction (25 %) and sudden cardiac death (20 %).

IHD remains a leading cause of mortality and morbidity.

Cardiac MRI is highly accurate and has robust prognostic value in the evaluation of patients with both acute and chronic IHD (Heydari and Kwong 2014).

MRI Features

- Lines of myocardial calcification or subendocardial fatty metaplasia.
- Myocardial thinning with akinesia, hypokinesia, and dyskinesia.
 - Akinesia is common in areas of transmural infarction and manifests as absence of systolic thickening and contraction in affected wall segments.
 - Hypokinesia is reduced systolic thickening and contraction of myocardium.
 - Dyskinesia is paradoxical motion, often involving predominantly the septal segments of the left ventricle (septal dyskinesia).
- Myocardial aneurysm or pseudoaneurysm can develop.
- Subendocardial to transmural delayed enhancement, usually without an increase in T2 signal intensity, which can be localized to the area supplied by a particular coronary artery (Stork et al. 2007). In acute infarction, concomitant edema of affected wall segments may be detectable on fat-saturated T2-weighted images (Karamitsos et al. 2011).

The severity of wall motion abnormality varies with the transmural extent of infarction. Wall motion disturbance and myocardial thinning are usually more marked when MRI shows full-thickness late enhancement compared with subendocardial enhancement (Fig. 7.5).

Myocardial infarction involving the papillary muscles can impair mitral valve closure. Short-axis views are well suited to localize infarcted myocardial segments to specific coronary artery territories.

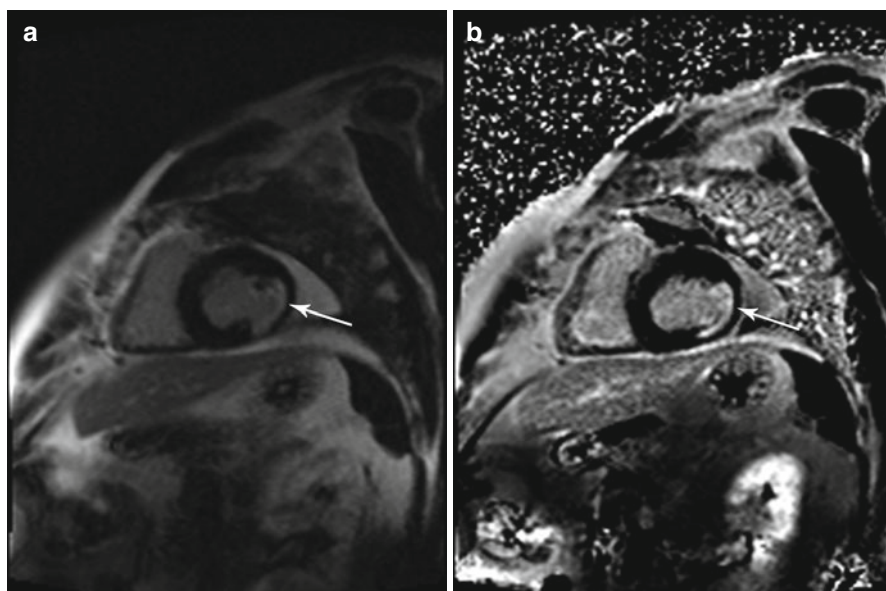


Fig. 7.5 Incidental findings in a 57-year-old subject. Typical subendocardial delayed enhancement in the lateral walls of the left ventricle (*arrow*). Late enhancement imaging with single shot inversion recovery sequences (short axis) (a) phase sensitive reconstruction (b) magnitude reconstruction

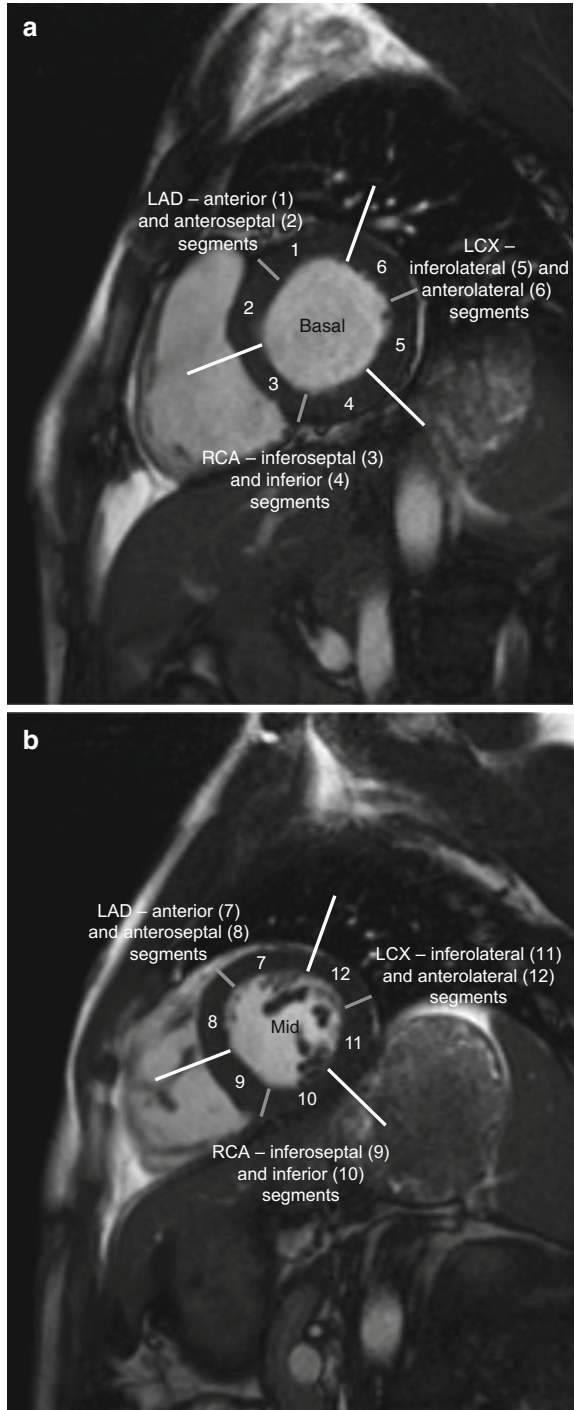
Among coronary dominance patterns, so-called balanced circulation is the most common type (80 %). In balanced circulation, the left coronary artery supplies the anterior wall of the left ventricle and most of the interventricular septum. The right coronary artery supplies the right ventricle and the posterior wall segments. The left coronary artery divides into the left anterior descending artery (LAD), or anterior interventricular branch, and the circumflex branch (LCX) (Cerqueira et al. 2002) (Fig. 7.6).

Differential Diagnosis

- *Delayed enhancement of other cause* (Stork et al. 2007)
- *Acute myocardial infarction* (edema on fat-saturated T2-weighted sequences, myocardial thickening, fatty metaplasia, calcification, or aneurysm detectable) (Perazzolo et al. 2011)
- *Acute myocarditis* (see below; edema on fat-saturated T2-weighted sequences)
- *Nonischemic cardiomyopathy* (see below; nonischemic myocardial fibrosis or scar has a variety of delayed enhancement patterns but is never subendocardial, making it easy to differentiate from ischemic infarction) (Stork et al. 2007)

In most patients, a variety of further cardiac and myocardial changes can be observed secondary to a myocardial infarction. Ventricular function may be impaired by left ventricular remodeling. Left ventricular dilatation is common and can evolve into full-blown dilated cardiomyopathy (De Smet et al. 2012). Initially the Frank-Starling mechanism maintains a constant left ventricular ejection fraction by responding to an increase in volume with an increase in wall tension. At some point,

Fig. 7.6 Myocardial segmentation and assignment of the 17 myocardial segments to coronary artery territories. Short-axis views at basal level (a), at midventricular level (b), and at apical level (c) and apical long-axis view (d) (LAD left anterior descending artery, LCX left circumflex branch, RCA right coronary artery) (According to Cerqueira et al. (2002))



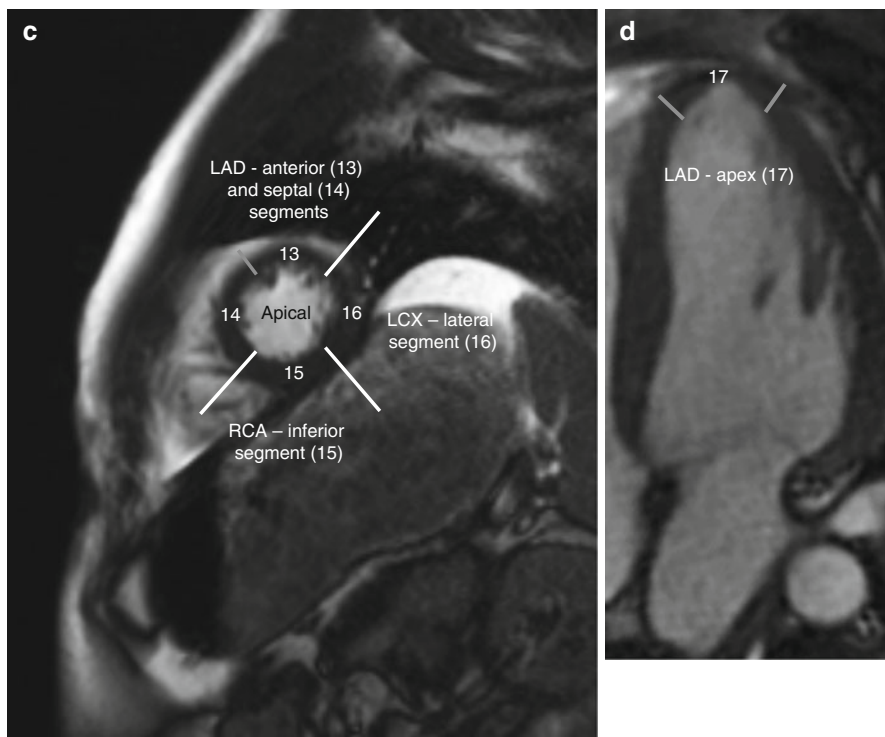


Fig. 7.6 (continued)

however, the bulge becomes so large that a marked drop in LVEF results. Mitral regurgitation due to remodeling of the chordal fibers of the papillary muscles is another common sequela.

Finally, pseudoaneurysm may develop, typically involving the posterior and lateral walls, less commonly the anterior wall.

Clinical Management

A previous small subendocardial or transmural myocardial infarction with well-preserved pump function requires no further clinical diagnostic evaluation. A larger subendocardial scar is critical even when pump function is preserved. It should be disclosed if a subject has another significant pathologic finding elsewhere in the body that may require surgery. The same holds true for transmural late enhancement with wall motion abnormalities. Markedly impaired pump function due to myocardial scar formation, which may be associated with concomitant pericardial or pleural effusion, should always be revealed to the subject. In this case, electrocardiography, ergometry, and echocardiography are recommended as supplementary diagnostic tests. Depending on the findings, cardiac catheterization may be the next step.

7.2.2 Cardiomyopathies

According to a consensus of the WHO and the International Society and Federation of Cardiology Task Force (1995), cardiomyopathies are diseases of the myocardium associated with cardiac dysfunction. Five main types are distinguished: dilated cardiomyopathy (DCM), hypertrophic cardiomyopathy (HCM and HOCM), restrictive cardiomyopathy (RCM), arrhythmogenic right ventricular cardiomyopathy (ARVC), and unclassified cardiomyopathies, such as noncompaction cardiomyopathy and Takotsubo cardiomyopathy. They are primarily not based on valvular, pericardial, or cardiovascular disorders (ACCF/ACR/AHA/NASCI/SCMR 2010) (Tables 7.2 and 7.8).

Diseases of the heart muscle associated with cardiac or systemic disorders are referred to as specific cardiomyopathies in the WHO classification. They comprise ischemic, valvular, hypertensive, inflammatory, and metabolic cardiomyopathies, general system diseases, muscular dystrophies, neuromuscular disorders, sensitivity and toxic reactions, and peripartum cardiomyopathy. Dilated cardiomyopathy is the most common (Richardson et al. 1996) (Tables 7.2 and 7.3).

New scientific insights led to a revision of the definition and classification of cardiomyopathies in 2006. According to this revised definition, the cardiomyopathies are a heterogeneous group of diseases of the myocardium associated with mechanical and/or electrical dysfunction that usually exhibit inappropriate ventricular hypertrophy or dilatation and are due to a variety of causes that frequently are genetic. Cardiomyopathies either are confined to the heart or are part of generalized systemic disorders, often leading to cardiovascular death or progressive heart failure-related disability (Maron et al. 2006).

The revised classification distinguishes two major groups based on predominant organ involvement: primary cardiomyopathies, in which the clinically relevant disease processes solely or predominantly involve the myocardium, and secondary

Table 7.2 WHO classification of cardiomyopathies

Type	Abbreviation	Characteristics
Dilated cardiomyopathy	DCM	Systolic dysfunction with reduced ejection fraction
Hypertrophic cardiomyopathy, subtype: hypertrophic obstructive cardiomyopathy	HCM, subtype: HOCM	Thickening of ventricular walls prevents adequate left ventricular expansion during diastole, impairing diastolic compliance
Restrictive cardiomyopathy	RCM	Increased wall stiffness due to endocardial fibrosis, impairing diastolic compliance
Arrhythmogenic right ventricular cardiomyopathy	ARVC	Right ventricular diastolic and systolic dysfunction and concomitant ventricular tachycardia as well as localized aneurysms of the right ventricle
Unclassified cardiomyopathies	UCCM	For example, noncompaction cardiomyopathy, Takotsubo cardiomyopathy

Modified according to Richardson et al. (1996)

Table 7.3 Dilated cardiomyopathy

Frequency	6/100,000 population/year
Causes	Idiopathic
	Genetic (familial)
	Primary and secondary causes
	Postinfectious (viral, bacterial, fungal, parasitic), toxic (alcohol, medications), autoimmune (vasculitis, systemic lupus erythematosus), endocrine (thyroid dysfunction, pheochromocytoma), neuromuscular and metabolic, infiltrative (amyloidosis), inflammatory (sarcoidosis) End stage of long-standing arterial hypertension, ischemia based on coronary artery disease, and progressive valvular dysfunction
Clinical presentation	Progressive left ventricular failure with exercise-induced dyspnea; global insufficiency and ventricular arrhythmia in advanced disease

cardiomyopathies, which show pathologic myocardial involvement as part of a large number and variety of generalized systemic (multiorgan) disorders.

Primary cardiomyopathies are further subdivided by etiology: genetic (hypertrophic cardiomyopathy, hypertrophic obstructive cardiomyopathy, arrhythmogenic right ventricular cardiomyopathy, and noncompaction cardiomyopathy), mixed (dilated cardiomyopathy and restrictive cardiomyopathy), and acquired (inflammatory cardiomyopathy based on myocarditis, Takotsubo cardiomyopathy). Secondary cardiomyopathies appear in the context of various diseases: infiltrative (amyloidosis), inflammatory (sarcoidosis), storage (hemochromatosis), endomyocardial (endomyocardial fibrosis, hypereosinophilic syndrome (Löffler's endocarditis)), endocrine (diabetes mellitus, hyperthyroidism, pheochromocytoma), and neuromuscular diseases; nutritional deficiencies; autoimmune disorders (vasculitis, systemic lupus erythematosus); and exposure to toxic substances (cancer therapy) or drugs (Maron et al. 2006).

Dilated cardiomyopathies, which may be genetic or acquired, are the most common type. Causes of acquired dilated cardiomyopathy include a history of myocarditis or alcohol abuse. In addition, dilated cardiomyopathy may develop as the terminal stage of a variety of preexisting cardiac diseases, such as coronary heart disease or arterial hypertension (Richardson et al. 1996) (Tables 7.2 and 7.3).

Cardiac MRI has an important role in the diagnostic and clinical management of patients with cardiomyopathies, allowing evaluation of myocardial morphology and function in a single examination and hence also enabling identification of less common underlying causes (De Smet et al. 2012). The five main types of cardiomyopathy distinguished in the WHO classification are presented in more detail in the following sections.

7.2.2.1 Dilated Cardiomyopathy

Dilated cardiomyopathy (DCM) is characterized by left ventricular dilation and systolic dysfunction with a left ventricular ejection fraction of less than 40 % with or without concomitant right ventricular involvement (ACCF/ACR/AHA/NASCI/SCMR 2010) (Fig. 7.7).

The severity of left ventricular dysfunction determines the patient's prognosis.

DCM is probably the result of myocardial damage due to a variety of primary and secondary underlying causes: infectious agents; viral or chronic myocarditis; other bacterial, fungal, and parasitic infections; toxic myocardial damage (alcohol, cocaine); chemotherapy (primarily doxorubicin); metabolic defects (e.g., hyperphosphatemia, hypocalcemia, uremia); myocardial involvement in other tissue disorders (vasculitis, e.g., Churg-Strauss syndrome, systemic lupus erythematosus); endocrine disorders (thyroid dysfunction, pheochromocytoma, Cushing disease); infiltrative or inflammatory diseases such as amyloidosis or sarcoidosis; and neuromuscular diseases. In rare cases, DCM is associated with pregnancy (peripartum cardiomyopathy). DCM is also the end stage of other myocardial conditions, such as long-standing arterial hypertension, ischemia based on coronary artery disease, or progressive valvular dysfunction. Approx. 20–35 % of DCM cases are assumed to be familial. In many cases, no etiology is apparent (idiopathic DCM) (Table 7.3) (De Smet et al. 2012; Maron et al. 2006).

DCM is characterized by progressive heart failure and a decline in left ventricular contractile function, ventricular and supraventricular arrhythmias, conduction system abnormalities, thromboembolism, and sudden or heart failure-related death (Maron et al. 2006). Patients with symptomatic DCM have a mortality rate of 11–13 %.

Cardiac MRI provides very accurate estimates of left and right ventricular volumes, atrial dimensions, myocardial mass, and left ventricular ejection fraction, and it also offers a quick and reliable means of detecting areas of fibrotic transformation (Schalla et al. 2010). The prognosis of idiopathic DCM depends on the severity of left ventricular dysfunction, with delayed enhancement being an additional prognostic factor. Areas of delayed enhancement indicate more extensive fibrotic transformation of myocardium, which is usually associated with lower LVEF and an increase in end-diastolic volume (Lehrke et al. 2011).

However, the estimates should be verified by echocardiography to confirm an initial MRI-based diagnosis of DCM.

MRI Features

- Enlargement of the left ventricle without an increase in mass; globally reduced systolic inward motion and wall thickening as well as markedly reduced LVEF (De Smet et al. 2012).
- Markedly reduced pump function and enlarged volume lead to circular movement of blood with an increased risk of thrombus formation.
- Ventricular dilation additionally causes regurgitation through the mitral valve and possibly through the tricuspid valve as well.
- This can result in enlargement of both atria.
- Depending on the severity of DCM, end-diastolic and end-systolic volumes (EDV and ESV) may be increased.
- In idiopathic DCM, first-pass perfusion usually appears normal.
- Concomitant enlargement of the right ventricle indicates advanced DCM.
- Thirty to forty percent of patients with idiopathic cardiomyopathy show midwall enhancement from the base to the midventricle (De Smet et al. 2012) (Fig. 7.8);

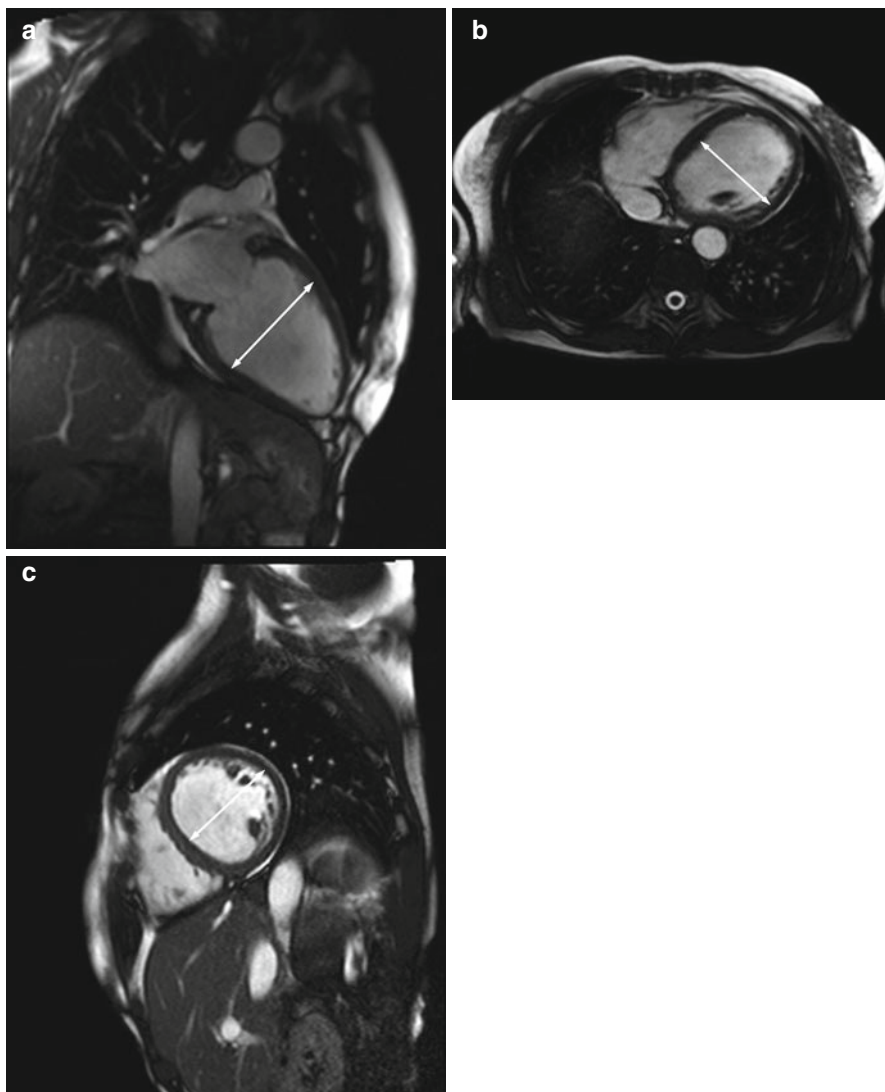


Fig. 7.7 DCM in a 66-year-old subject with reduced pump function (approx. 45 % EF) and global hypokinesia in all wall segments. Left ventricular enlargement (*arrow* indicates left ventricular diameter). **(a)** Two-chamber cine view, **(b)** true axial cine view, and **(c)** short-axis cine view

the typical pattern of late enhancement is in the form of longitudinal striae not corresponding to a coronary artery territory (Schalla et al. 2010; Stork et al. 2007).

- As DCM can also develop secondary to ischemic heart disease, marked subendocardial or transmural delayed enhancement may be seen in conjunction with left ventricular enlargement (McCrohon et al. 2003).
- An occasional patient may show no delayed enhancement at all (Jiji and Kramer 2011).

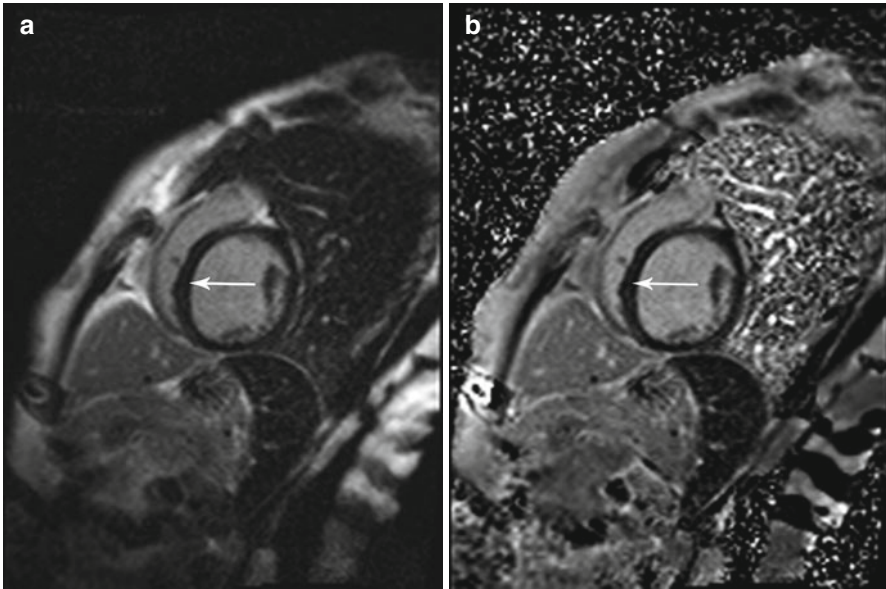


Fig. 7.8 Phase-sensitive inversion recovery (PSIR) single shot sequence for delayed enhancement imaging in the same subject as in Fig. 7.7. Typical midwall enhancement predominantly involving the septum (*arrow*). (a) Magnitude reconstruction and (b) phase-sensitive reconstruction

Differential Diagnosis

- *Restrictive cardiomyopathy* (see below; typically, isolated enlargement of both atria with normal ventricular size and diastolic dysfunction) (Mookadam et al. 2011)
- *Hypertrophic or hypertrophic obstructive cardiomyopathy* (see below; no dilatation but left ventricular wall thickening, predominantly of the basal inter-ventricular septum) (De Smet et al. 2012)
- *Valvular diseases* (predominantly chronic reflux through the aortic or mitral valve, resulting in increased volume load and reduced systolic function) (Bonow et al. 2008)

Clinical Management

When dilated cardiomyopathy (DCM) with markedly reduced pump function is suspected, the subject should be informed and undergo further diagnostic workup. The ventricular size measured by MRI should be confirmed by echocardiography as a second imaging modality and vice versa. In addition, most patients subsequently require myocardial biopsy.

7.2.2.2 Hypertrophic and Hypertrophic Obstructive Cardiomyopathy

Hypertrophic cardiomyopathy (HCM) and its obstructive form, hypertrophic obstructive cardiomyopathy (HOCM), are inherited heart diseases that run in families. They are characterized by left ventricular hypertrophy, predominantly of the anteroseptal wall segments near the base (70 % of cases) (Table 7.4). In the obstructive form, hypertrophy causes obstruction of the left ventricular outflow tract (Fig. 7.9). Atypical patterns of hypertrophy with involvement of midventricular and/or apical segments have been described as well (De Smet et al. 2012).

Electrocardiogram (ECG) data obtained in large cohorts indicate that sudden deaths in HCM are attributable to rapid ventricular tachycardia or ventricular fibrillation (Hoey et al. 2014).

MRI Features

- Asymmetric or symmetric thickening of left ventricular wall segments; septal involvement is very common.
- Reduced LV diastolic compliance (prolonged diastolic relaxation), in most cases caused by increased intracellular calcium.
- In HOCM, there is additional end-systolic narrowing of the left ventricular outflow tract (LVOT) due to asymmetric septal hypertrophy and a suction effect of the turbulent jet at the insufficient mitral valve during systole (Bernoulli effect) with systolic anterior motion (SAM) of the anterior mitral leaflet (Guarise et al. 2011).
- Diffuse or focal delayed enhancement in areas of myocardial fibrosis; can occur anywhere in the left ventricle and is not confined to the distribution of a single coronary artery, most commonly involves septal and anteroseptal segments (De Smet et al. 2012; Stork et al. 2007).
- The extent of delayed enhancement correlates with the risk of sudden cardiac death (Rickers et al. 2005; Rochitte et al. 2006).

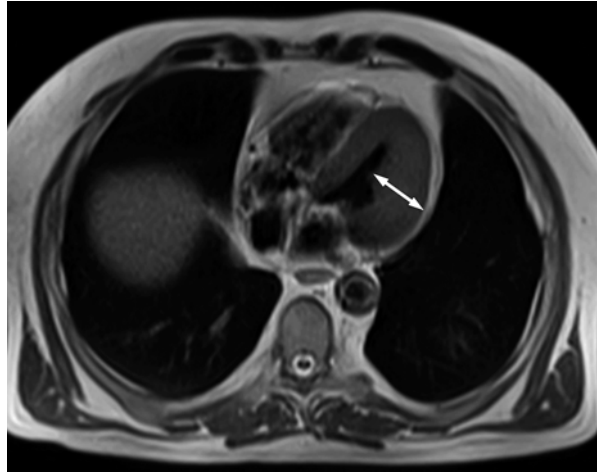
Differential Diagnosis

- *Aortic stenosis* (thickening, calcification, or fusion of aortic valve leaflets, typically resulting in concentric rather than focal LV hypertrophy) (Proctor et al. 2011)
- *Restrictive cardiomyopathy* (see below; disease of unknown etiology or terminal stage of a variety of diseases, e.g., amyloidosis, sarcoidosis, hemochromatosis, damage caused by chemotherapy or radiotherapy, endocardial thickening with

Table 7.4 Hypertrophic and hypertrophic obstructive cardiomyopathy

Frequency	Up to 0.2 % of the population; ratio of HCM to HOCM of approx. 3:1
Cause	Usually hereditary
Clinical presentation	Uncharacteristic, often asymptomatic (incidental finding); some patients present with dyspnea, angina pectoris, and higher-grade ventricular arrhythmia or even ventricular tachycardia; most common cause of sudden cardiac death in competitive athletes If the critical heart weight of 500 g is exceeded, the resulting reduction in perfusion reduction can trigger small infarctions

Fig. 7.9 Severe, more concentric, hypertrophy of the left ventricular wall on a T2-weighted HASTE image obtained in a 58-year-old subject (*arrow* indicates thickness of LV free wall)



deposits, thrombus formation and risk of embolism, and development of diastolic dysfunction) (Penugonda 2010)

- *Systemic arterial hypertension* (pressure overload typically results in concentric LV hypertrophy)

Clinical Management

If MRI detects focal or concentric LV hypertrophy, the finding should be communicated to the subject along with a recommendation to undergo further cardiac diagnostic evaluation including auscultation (HOCM is characterized by a late-onset systolic ejection murmur with a crescendo-decrescendo configuration, best heard at the apex and accentuated by physical activity or Valsalva maneuver, and the presence of a fourth heart sound), an electrocardiogram (to detect signs of LV hypertrophy), and an echocardiographic examination. In addition, a blood test should be performed. If these examinations provide no diagnosis, a left heart catheter examination should follow.

7.2.2.3 Restrictive Cardiomyopathy

Restrictive cardiomyopathy (RCM) is characterized by severe diastolic dysfunction due to endocardial thickening in the presence of normal ventricular systolic function (Mookadam et al. 2011). Typically, both atria are markedly dilated with backup of blood into the inferior vena cava and hepatic veins (Table 7.5). Sporadic and familial forms have been described (Maron et al. 2006).

One of the clinical challenges in patients with suspected RCM is its differentiation from pericardial constriction, which shares a similar clinical presentation but is treatable with pericardectomy. Cardiac MRI is helpful because it allows anatomic evaluation of pericardial thickening, assessment of the hemodynamic effects of constriction, and detection of abnormality of the underlying myocardium (Quarta et al. 2011).

Table 7.5 Restrictive cardiomyopathy

Frequency	Rare
Causes	Endocardial thickening with thrombus formation on the endocardium Chronic RCM with progressive endocardial fibrosis and diastolic ventricular dysfunction as well as development of therapy-refractory cardiac insufficiency with inflow congestion at the entrance to the right heart
Clinical presentation	Signs of cardiac failure including dyspnea, fatigue, edema, and pleural effusion; atrial and/or ventricular arrhythmia

MRI Features

- Small LV with normal wall thickness and normal LVEF
- Enlargement of both atria
- Abnormal diastolic filling
- Abnormal, typically patchy, delayed enhancement in secondary forms with myocardial involvement or inflammation (Stork et al. 2007)
- Normal pericardium (<3 mm) without adhesions, no abnormal contrast enhancement (Rochitte et al. 2006)

Differential Diagnosis

- *Constrictive pericarditis* (see below; pericardial thickening >4 mm with pericardial delayed enhancement seen in pericardial inflammation or fibrosis, which is not a feature of RCM. Constrictive pericarditis is also characterized by conspicuous ventricular filling obstruction during diastole; however, obstruction occurs secondary to pericardial inflammation and can be eliminated by surgical excision of pericardium (Francone et al. 2006; Hancock 2001)
- *Secondary cardiomyopathies with myocardial restriction* (myocardial involvement in systemic diseases such as amyloidosis, hemochromatosis, or sarcoidosis; after radiotherapy or chemotherapy; also characterized by patchy delayed enhancement (ACCF/ACR/AHA/NASCI/SCMR 2010))

Clinical Management

Subjects with suspected RCM should be referred to a cardiologist for further diagnostic evaluation including echocardiography, electrocardiography, CT, and possibly endomyocardial biopsy. The combined results of all of these modalities are usually necessary to establish the diagnosis of RCM.

7.2.2.4 Arrhythmogenic Right Ventricular Cardiomyopathy

Arrhythmogenic right ventricular cardiomyopathy (ARVC) is characterized by fibrofatty replacement of myocardium on myocardial biopsy and localized aneurysms of the right ventricle. The pathogenesis is unknown, but it is assumed that myocyte loss is the result of generalized apoptosis.

In addition to structural changes, patients with ARVC also have functional impairment of the right ventricle due to dilatation, increased trabeculation, and

Table 7.6 Arrhythmogenic right ventricular cardiomyopathy

Frequency	1/5,000 population/year before age 30
Causes	Unknown, gene mutations have been identified (autosomal dominant inheritance)
Clinical presentation	Right heart failure, arrhythmia, syncope, ventricular tachycardia, and even sudden cardiac death

regional wall motion abnormalities (dyskinesia) (Table 7.6). Moreover, the ECG demonstrates conduction abnormalities. ARVC is often demonstrated by autopsy or biopsy in patients with familial cardiomyopathy. In severe ARVC, the left ventricle may be affected as well (De Smet et al. 2012; Murphy et al. 2010).

MRI Features

- Regional RV wall motion abnormalities.
- RV dilatation for which no other cause – such as shunt defects, pulmonary hypertension, or tricuspid insufficiency – can be found.
- Microaneurysms in the RV (Ferrari et al. 2005).
- Increased RV trabeculation (“stack of dishes” sign) with thinning of the wall.
- On T1-weighted images (dark blood spin echo sequence), fatty dysplasia has high signal intensity (subepicardial, predominantly involving the lateral wall and the right ventricular outflow tract (RVOT) anteriorly) (Jain et al. 2008; Tandri et al. 2005).
- Delayed enhancement of RV areas of fibrofatty degeneration; the most common sites of involvement are the subtricuspid area, the RV apex, and the RVOT (triangle of dysplasia) (Ferrari et al. 2005; Stork et al. 2007).

Differential Diagnosis

- *Uhl disease* (anomaly of the right ventricle, characterized by near or complete absence of RV myocardium)
- *Valve defects* (RV dilatation caused by valve defects, e.g., tricuspid insufficiency, ASD, VSD)
- *Idiopathic right ventricular tachycardia* (absence of fibrofatty transformation of RV myocardium)

Clinical Management

Arrhythmogenic right ventricular cardiomyopathy (ARVC) is rare.

When ARVC is suspected, the subject must be informed so that further diagnostic tests can be done.

Although not consistently present on an electrocardiogram, a characteristic epsilon wave (a terminal notch in the QRS complex) in leads V1–V3 is a sure diagnostic sign of the disease. Fibrofatty deposits in the right ventricular wall, which are often demonstrated by MRI, can be confirmed by myocardial biopsy.

7.2.2.5 Unclassified Cardiomyopathies

7.2.2.5.1 Takotsubo Cardiomyopathy

Takotsubo cardiomyopathy, also known as stress-induced cardiomyopathy or broken heart syndrome, is characterized by sudden onset of transient akinesia or dyskinesia of the LV apex without significant coronary stenosis (>50 %). The left ventricular ejection fraction is reduced (Eitel et al. 2011).

Takotsubo cardiomyopathy is triggered by intense emotional stress or a traumatizing event. Findings include acute chest pain, reversible electrocardiogram changes, and elevated cardiac enzymes (Table 7.7).

MRI Features

- Akinesia or dyskinesia due to LV apical ballooning (Eitel et al. 2011).
- Delayed enhancement imaging usually reveals no signs of myocardial damage.
- Fat-saturated T2-weighted images may occasionally show myocardial edema (high signal intensity) (Celik et al. 2009; Eitel et al. 2011).

Differential Diagnosis

- *Acute myocardial infarction* (While patients also present with chest pain and dyspnea, cardiac MRI typically detects significant atherosclerotic plaques in the coronary arteries and demonstrates perfusion deficits, often with concomitant myocardial edema in affected areas (fat-saturated T2-weighted pulse sequence) (Abdel-Aty and Schulz-Menger 2007). Another characteristic of myocardial infarction is subendocardial or transmural delayed contrast enhancement in a vascular distribution.) (Perazzolo et al. 2011)

Table 7.7 Unclassified cardiomyopathies

Frequency	Altogether rare
Cause	Heterogeneous group of diseases of different etiologies Stress-induced, increased blood catecholamines (Takotsubo cardiomyopathy) Failure of myocardial development during embryogenesis due to gene mutation (noncompaction cardiomyopathy)
Clinical presentation	Takotsubo cardiomyopathy Symptoms resemble those of myocardial infarction, in particular angina pectoris and dyspnea Noncompaction cardiomyopathy Affected individuals remain asymptomatic for a long time, first diagnosed in adults; signs of cardiac insufficiency, tachyarrhythmia, sudden cardiac death, thromboembolism

- *Acute myocarditis* (see below; delayed enhancement tends to be subepicardial or to appear as diffuse enhancement of the entire myocardial wall not corresponding to a coronary artery territory. Fat-saturated T2-weighted images will show high-signal-intensity edema in 80 % of cases.) (Stensaeth et al. 2012)
- *Coronary vasospasms*

7.2.2.5.2 Noncompaction Cardiomyopathy

Noncompaction cardiomyopathy (NCCM) is an anomaly resulting from arrested myocardial development during embryogenesis. The failure of the initial meshwork of interwoven myocardial fibers to compact results in a myocardial wall with a thickened appearance due to the presence of prominent trabeculations and deep intertrabecular recesses, known as spongy myocardium. Noncompaction predominantly affects the apex (Yousef et al. 2009) (see Table 7.7 and Fig. 7.10). The left ventricular ejection fraction may be reduced. There is a risk of thrombus formation within the intertrabecular recesses, and arrhythmia may occur (De Smet et al. 2012).

MRI Features

- Prominent trabeculation with deep intertrabecular recesses of the LV mainly involving the apical and midventricular inferior and lateral segments.
- The abnormal trabeculations make the wall appear thickened, but due to the deep intertrabecular recesses, the wall is actually thinner than normal; contractility is preserved in most patients.
- An occasional patient has a dilated LV and reduced LVEF.
- Subendocardial perfusion defects or delayed enhancement may be observed in some patients (Petersen et al. 2005).

Differential Diagnosis

- *HCM or HOCM* (see above; primarily when there is apical involvement)
- *DCM* (see above; primarily when there is LV dilation and reduced pump function)
- *Secondary cardiomyopathy* (cardiomyopathy caused by a known medical condition, e.g., amyloidosis or sarcoidosis, or occurring secondary to radiotherapy or chemotherapy) (Penugonda 2010)

Clinical Management

Noncompaction cardiomyopathy is altogether rare and should be communicated especially if LV function is impaired.

Table 7.8 MRI features of the different cardiomyopathies

Parameter	DCM	HCM/HOCM	RCM	ARVC	NCCM
Atrial size	Typically both LA and RA are enlarged	Typically both LA and RA are enlarged	Typically both LA and RA are enlarged	LA of normal size, RA occasionally enlarged	LA and RA of normal size
Ventricular size	Enlargement of both LV and RV or of LV alone	LV and RV of normal size, rarely reduced in size	LV and RV of normal size	RV enlarged, LV usually of normal size	LV and RV typically of normal size, LV enlarged in rare cases
LV mass	LV normal or slightly hypertrophied; LV and RV mass normal or increased	Generalized hypertrophy of LV; septal hypertrophy, primarily apical, in 25 % of cases	LV and RV of normal size	RV wall involved at apex and inflow/outflow tract Wall thinning giving rise to microaneurysms Prominent trabeculation (stack of dishes) and fat deposition in RV wall	LV wall normal or thickened at apex and/or midventricle
LVEF	LVEF reduced	LVEF usually normal; may be increased in HOCM due to obstruction	LVEF normal	LVEF normal RVEF reduced	LVEF normal or reduced
Delayed enhancement	Atypical delayed enhancement (in 10–40 % of cases): intramural, subepicardial	Diffuse or confluent delayed enhancement; often patchy enhancement of septum in HOCM	Absent	Diffuse patchy delayed enhancement of RV (often difficult to evaluate)	Absent

Modified according to Hombach (2006)

LA left atrium, RA right atrium, LV left ventricle, LVEF left ventricular ejection fraction, RVEF right ventricular ejection fraction

Table 7.9 Acute and chronic myocarditis

Frequency	Cardiac involvement in approx. 1 % of patients with cardiotropic viral infection, approx. 4–5 % in Coxsackievirus infection
Causes	Infectious Viruses (50 % of cases), especially enteroviruses, e.g., Coxsackie B1-B5 viruses, but also influenza or herpes viruses Bacteria, especially staphylococci, enterococci Fungi, especially in immunocompromised individuals Protozoa, e.g., toxoplasmosis Parasites, e.g., trichina, echinococci
	Noninfectious Rheumatoid arthritis, connective tissue diseases, vasculitis, mediastinal radiotherapy, hypersensitivity myocarditis caused by certain medications
Clinical presentation	Highly variable, from asymptomatic or mild forms (common) to fulminant fatal disease (rare) Infectious myocarditis presents with fatigue, feeling of weakness, fever, tachycardia, arrhythmia (especially premature beats), and signs of cardiac insufficiency

7.2.3 Acute and Chronic Myocarditis

Myocarditis is an acute or chronic recurrent inflammatory process of the myocardium, which may show focal or diffuse involvement (Table 7.9). It can result in necrosis and myocyte loss.

Chronic myocarditis can progress to dilated cardiomyopathy (De Smet et al. 2012; Ling et al. 1999).

Because of the nonspecificity of its symptoms, signs, and test findings, myocarditis is often diagnosed by exclusion of other cardiac diseases (Friedrich and Marcotte 2013).

When performed as part of a whole-body imaging protocol, the examination is less comprehensive than a dedicated MRI study of the heart. The whole-body protocol used in the SHIP does not include a fat-saturated T2-weighted pulse sequence for edema imaging, precluding the detection of chronic or acute myocarditis. Cine sequences typically reveal systolic dysfunction in the presence of generalized hypokinesia; less commonly they reveal diastolic dysfunction. However, this findings are not specific for myocarditis and may also be seen in DCM and other cardiac diseases.

Most patients with myocarditis have concomitant relative mitral insufficiency due to mitral ring dilatation. Isolated pericardial effusion may also point to an inflammatory condition of the myocardium (Ong et al. 2011).

MRI Features

- On fat-saturated T2-weighted images, inflamed myocardium has high signal intensity (edema); areas of inflamed myocardium cannot be identified without acquisition of fat-saturated T2-weighted images; on the other hand, even these sequences will detect edema in only 80 % of cases (Mahrholdt et al. 2006).

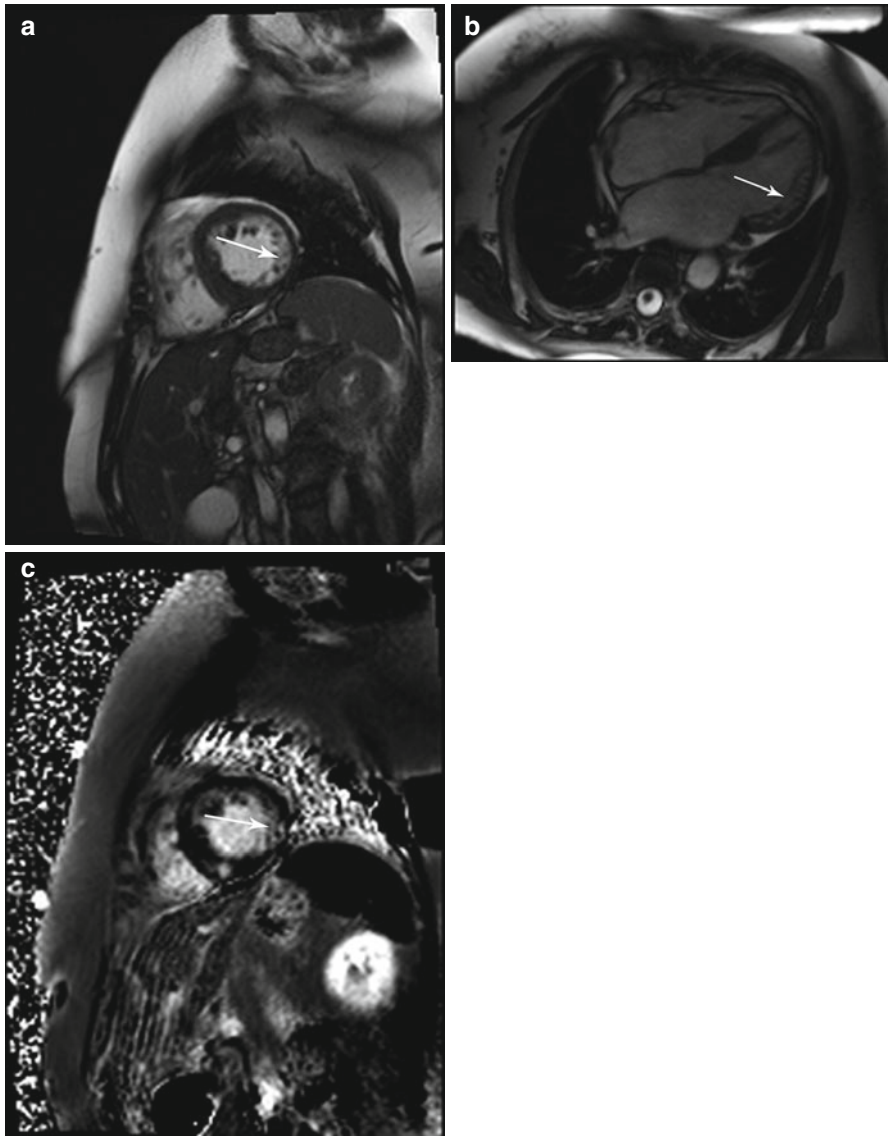


Fig. 7.10 Noncompaction cardiomyopathy in a 58-year-old subject. **(a)** Short-axis cine view. Prominent trabeculation of anterior and lateral wall segments of the left ventricle (*arrow*). **(b)** Four-chamber cine view. Spongy myocardium with deep intratrabecular spaces is apparent (*arrow*). **(c)** Phase-sensitive inversion recovery (PSIR) image showing atypical patchy delayed enhancement (*arrow*)

- T1-weighted imaging after contrast medium administration enables calculation of an enhancement ratio of inflamed myocardium to skeletal muscle; an enhancement ratio >4.0 is highly indicative of acute myocarditis (the normal ratio is <2.5) (Friedrich et al. 1998; Stensaeth et al. 2012).
- On delayed enhancement images, acute myocarditis typically shows subepicardial enhancement in the inferolateral wall, predominantly in the midventricular portion (Goitein et al. 2009). However, some patients may show diffuse delayed enhancement that includes subendocardial segments and some may show no delayed enhancement at all (De Smet et al. 2012; Gahide et al. 2010).
- Nevertheless, it is usually possible to differentiate myocarditis from myocardial infarction, which is characterized by subendocardial delayed enhancement confined to a vascular territory (Stensaeth et al. 2012; Stork et al. 2007).

Differential Diagnosis

- *Ischemic cardiomyopathy* (subendocardial delayed enhancement in the distribution of a coronary artery)
- *Nonischemic dilated cardiomyopathy* (typical midwall enhancement primarily involving the septum)
- *Other forms of cardiomyopathy* (nonspecific patchy delayed enhancement)

Clinical Management

Pericardial effusion is not an uncommon finding in whole-body screening. It should be communicated to the subject if the width of the effusion is 1 cm or more or if the perfusion is hemodynamically relevant.

Echocardiography allows rapid and sensitive confirmation of pericardial effusion (when 50 mL or more is present).

7.3 Diseases of Pericardium

Cardiac MRI is well suited for evaluating conditions affecting the pericardium such as inflammatory processes or thickening, lesions such as cysts, calcification, and pericardial masses or malignant tumors. Because of its three-dimensional capabilities, MRI enables complete evaluation of the heart and surrounding anatomy (Bogaert and Francone 2013).

Fat-saturated T2-weighted pulse sequences reliably identify inflammatory processes of the myocardium and pericardium. In most cases, pericardial effusion is already visible on cine images. Cardiac MRI using a combination of different T1-weighted and T2-weighted pulse sequences even enables identification of the type of fluid present (transudate, exudate, hemorrhagic effusion) (Abbara and Miller 2005).

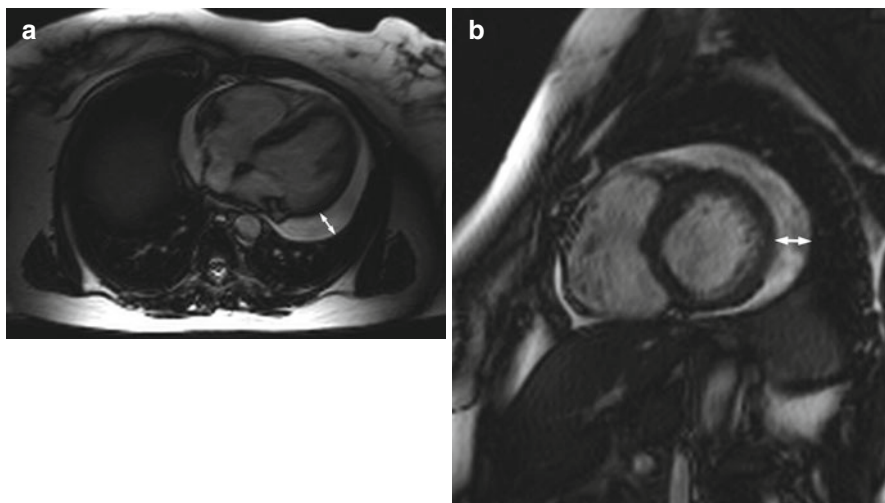


Fig. 7.11 Pericardial effusion in a 48-year-old subject. (a) Strict axial cine image (b) short-axis cine image (arrow indicates width of pericardial effusion near the base)

7.3.1 Pericardial Effusion

Pericardial effusion is an abnormal fluid collection in the pericardial space (Fig. 7.11). Excess fluid collects in the pericardial space for a variety of reasons including inflammatory and infectious processes, cardiac congestion, and tumors (Ong et al. 2011).

MRI Features

- Transudate has low T1 signal intensity and high T2 signal intensity.
- Exudate, due to its high protein content, has moderate to high signal intensity on T1-weighted images and low signal intensity on T2-weighted images.
- Hemorrhagic effusion has high T1 signal intensity, especially when fresh blood is present, while it is iso- to hyperintense with T2 weighting.
- LV and RV function is usually normal as long as the fluid collection has no hemodynamic effects.
- Large pericardial fluid collections impair diastolic filling (Hombach 2006).

Differential Diagnosis

- *Myocarditis* (see above; edema confined to affected wall segments, high signal intensity on fat-saturated T2-weighted sequences; subepicardial or patchy non-specific pattern of delayed enhancement) (Stensaeth et al. 2012)
- *Acute myocardial infarction* (typical pain pattern, edema on fat-saturated T2-weighted images, subendocardial delayed enhancement) (Perazzolo et al. 2011)
- *Cardiac disease of other etiology* (e.g., rheumatic disease, usually asymptomatic)
- *Pericarditis* (see below; typically with pericardial edema, high signal intensity on fat-saturated T2-weighted images, pericardial thickness usually >4 mm, pericardial delayed enhancement) (Goyle and Walling 2002)

Table 7.10 Pericarditis

Frequency	Cardiac involvement in approx. 1 % of patients with cardiotropic viral infection, approx. 4–5 % in Coxsackievirus infection
Causes	Infectious Viruses are the most common infectious agents; the pathogen spectrum is the same as in myocarditis
	Immunologic Systemic lupus erythematosus and rheumatic fever, postmyocardial infarction syndrome/Dressler syndrome (febrile pericarditis/pleuritis 1–6 weeks after myocardial infarction or cardiac surgery), uremia, tumors, radiotherapy
Clinical presentation	Typically, sharp chest pain, often located behind the sternum, which intensifies with deep inspiration/coughing or when lying down Pericardial friction rub on auscultation Electrocardiogram in acute pericarditis: concave upward ST segment elevation originating from S wave; transition to a negative T wave with disease progression. Absence of loss of R wave allows differentiation from myocardial infarction!

7.3.2 Pericarditis

Pericarditis has infectious and noninfectious causes. Infectious pericarditis is caused by a variety of viral and bacterial agents. Noninfectious pericarditis can develop after surgery or after myocardial infarction (Table 7.10). Pericarditis presents with fever, coughing, and other general symptoms of inflammation. Most patients report retrosternal chest pain (Abbara and Miller 2005).

MRI Features

- Pericardial thickening ≥ 4 mm (normal 1–3 mm).
- Cine sequences reveal no wall motion abnormalities; most patients have normal LV and RV function.
- Fat-saturated T2-weighted sequences depict high-signal-intensity pericardium; a reliable diagnosis of pericarditis or inflammatory pericardial involvement cannot be made without use of a fat-saturated T2-weighted sequence (Friedrich et al. 1998; Mahrholdt et al. 2006).
- Global delayed enhancement of the pericardium (Goyle and Walling 2002).

Differential Diagnosis

- *Cardiac disease of other etiology* (e.g., rheumatic disease, usually asymptomatic)
- *Acute myocardial infarction* (typical pain pattern, edema on fat-saturated T2-weighted images, subendocardial delayed enhancement) (Perazzolo et al. 2011)
- *Myocarditis* (see above; edema confined to affected wall segments; high signal intensity on fat-saturated T2-weighted sequences; subepicardial or patchy non-specific pattern of delayed enhancement) (Stensaeth et al. 2012)

Table 7.11 Constrictive pericarditis

Frequency	Idiopathic (33 %); secondary to pericarditis or infection (19 %); mechanical, e.g., after trauma or cardiac surgery (18 %); after radiotherapy (13 %, e.g., for breast cancer, Hodgkin disease); metabolic (uremia); in association with rheumatic diseases
Causes	Abnormal pericardial thickening with fibrosis and calcification secondary to one of the conditions listed above, most severe after tuberculosis
Clinical presentation	Symptoms secondary to right ventricular inflow obstruction (right heart failure, dyspnea, hepatomegaly with ascites, edema, congestive proteinemia) Low-cardiac-output syndrome with physical weakness and dyspnea on exertion

Clinical Management

A subject with a suspected myocardial or pericardial condition should see a cardiologist for further examinations including an electrocardiogram (possibly long-term) and echocardiography. Laboratory testing is required and should cover cardiac enzymes (CK/CK-MB and troponin) and inflammatory parameters (BSR, blood count, CRP). The initial laboratory work should be followed by special bacteriologic/virologic tests (fecal enteroviruses, anti-body titer, etc.).

7.3.3 Constrictive Pericarditis

Constrictive pericarditis results from fibrotic thickening of the pericardium secondary to pericarditis, cardiac surgery, trauma, radiotherapy, or chemotherapy (Table 7.11).

Fibrosis and calcification of the pericardium can lead to the development of a rigid shell around the heart. The shell impairs expansion of the heart, resulting in inadequate filling of the ventricles during diastole. This is seen as inflow obstruction. Patients with longer-standing constrictive pericarditis develop myocardial atrophy (Ling et al. 1999).

If the heart size is normal but clinical signs of right-sided heart failure are present, this should alert the physician to the possibility of constrictive pericarditis. Surgical pericardiectomy is potentially curative in constrictive pericarditis (Mookadam et al. 2011).

MRI Features

- Pericardial thickening ≥ 4 mm.
- Intrapericardial calcification will be seen as areas of very low signal intensity.
- Restricted diastolic filling with secondary dilatation of the right atrium and congestion of blood at the entrance to the right heart.
- Clinical signs of right heart failure (Francone et al. 2006)
- Pericardial delayed enhancement seen in pericardial inflammation or fibrosis.

Differential Diagnosis

- *Restrictive cardiomyopathy* (typically no pericardial thickening, no delayed enhancement) (Hancock 2001; Cheng et al. 2011)
- *Right heart failure of other etiology*

Clinical Management

Hemodynamically significant valve defects should be communicated.

7.4 Diseases of Endocardium

The endocardium lines the cardiac chambers and covers the cardiac valves (Bonow et al. 2008). Infectious endocarditis remains a diagnostic and therapeutic challenge. Patient outcome depends on a rapid diagnosis and accurate risk stratification (Bruun et al. 2014).

7.4.1 Valvular Disease

Most acquired abnormalities of the cardiac valves occur secondary to endocarditis, typically appearing several years later. Acquired valvular disease predominantly affects the left heart (mitral/aortic valves) because it is subject to greater mechanical stress and pressure, causing the valves to become incompetent. The severity of valve incompetence varies with the presence of prior cardiac damage, virulence of the pathogen involved, and the patient's immune status (Bonow et al. 2008; Morris et al. 2010) (see Table 7.12 and Fig. 7.12).

Other causes of valvular disease are myocardial ischemia and cardiomyopathies.

Ischemic damage of the myocardium and papillary muscles can compromise the valves. In dilated cardiomyopathy, incomplete closure of leaflets may result when the left ventricle is markedly dilated.

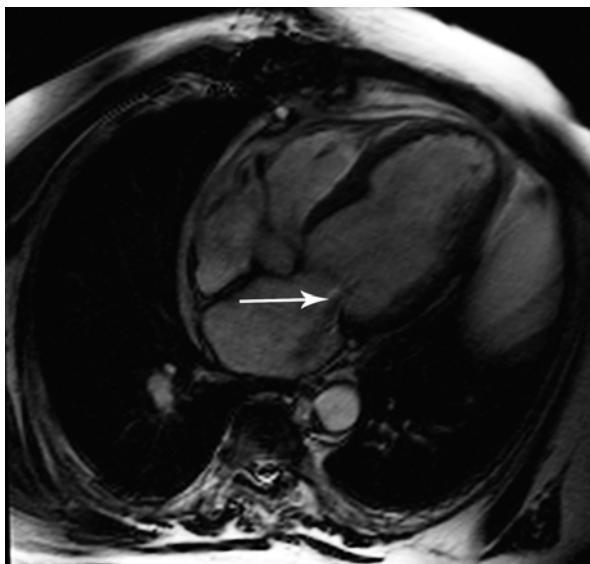
Cine imaging allows visual evaluation of the jet across the valve, but this is not a definitive diagnostic test and can only suggest the possibility of valve incompetence. With the whole-body MRI protocol used here, it is not possible to grade the severity of stenosis or valve incompetence. Grading requires measurement of flow velocities across the valve. However, with adjustments to the protocol, MRI can provide quantitative and reproducible information on valvular stenosis and insufficiency. In addition, MRI allows detection of dilatation or narrowing of the major arteries such as the aortic root or ascending aorta (D'Arcy and Myerson 2010).

With its poorer temporal resolution compared with Doppler echocardiography, MRI underestimates the peak gradient. In determining the mean pressure gradient, however, there is good agreement between the two modalities. Overall, MRI only enables incomplete valvular assessment and is markedly inferior to echocardiography.

Table 7.12 Diseases of endocardium

Frequency	Infectious causes are most common: 5–10/100,000 population/year
Causes	Infectious <ul style="list-style-type: none"> (a) Acute (bacterial infection) (b) Subacute (endocarditis lenta) (c) Viral or mycotic
	Noninfectious <ul style="list-style-type: none"> (a) Rheumatic endocarditis = complication of acute fever, in which a rheumatic immune reaction to streptococci produces an autoimmune attack against elements of the endocardium (antigen-antibody reaction) (b) Nonbacterial thrombotic endocarditis = vegetations on mitral and aortic valves occurring in the terminal stages of severe chronic diseases (e.g., cancer) (c) Libman-Sacks endocarditis = associated with systemic lupus erythematosus; presence of fibrin vegetations on cardiac valves and thickening of chordae tendineae; often with concomitant pericarditis or pleuritis (aggregation of immune complexes) (d) Eosinophilic endocarditis (Löffler syndrome) = accumulation of eosinophils in the lung and other organs (e.g., heart, brain, gastrointestinal tract) due to an allergic drug reaction or in response to parasitic or fungal infection; often also idiopathic
	Endocardial fibrosis
Clinical presentation	Acute onset: may present with sepsis (fever and chills); rapid progression to acute cardiac failure due to valve dysfunction
	Subacute onset: weight loss, fatigue, subfebrile temperatures, night sweat

Fig. 7.12 Marked regurgitation through the mitral valve (*arrow*) in a 63-year-old subject (four-chamber cine view)



With MRI, the mitral, aortic, and tricuspid valves are depicted. The most common valvular abnormality encountered in the setting of whole-body MRI is a jet across the mitral valve. In most instances, the jet has no hemodynamic relevance (Bonow et al. 2008).

References

- Abbara S, Miller SW (2005) Pericardial and myocardial disease. In: Miller SW (ed) *Cardiac imaging. The requisites*, 2nd edn. Mosby, Philadelphia, pp 270–272
- Abdel-Aty H, Schulz-Menger J (2007) Cardiovascular magnetic resonance T2-weighted imaging of myocardial edema in acute myocardial infarction. *Recent Pat Cardiovasc Drug Discov* 2:63–68
- Aletras AH, Kellman P, Derbyshire JA, Arai AE (2008) ACUT2E TSE-SSFP: a hybrid method for T2-weighted imaging of edema in the heart. *Magn Reson Med* 59:229–235
- American College of Cardiology Foundation Task Force on Expert Consensus Documents, Hundley WG, Bluemke DA, Finn JP, Flamm SD, Fogel MA, Friedrich MG, Ho VB, Jerosch-Herold M, Kramer CM, Manning WJ, Patel M, Pohost GM, Stillman AE, White RD, Woodard PK (2010) ACCF/ACR/AHA/NASCI/SCMR 2010 expert consensus document on cardiovascular magnetic resonance: a report of the American College of Cardiology Foundation Task Force on Expert Consensus Documents. *J Am Coll Cardiol* 55:2614–2662
- Bogaert J, Francone M (2013) Pericardial disease: value of CT and MR imaging. *Radiology* 267:340–356
- Bonow RO, Carabello BA, Chatterjee K, American College of Cardiology/American Heart Association Task Force on Practice Guidelines et al (2008) 2008 focused update incorporated into the ACC/AHA 2006 guidelines for the management of patients with valvular heart disease: a report of the American College of Cardiology/American Heart Association Task Force on Practice Guidelines (Writing Committee to revise the 1998 guidelines for the management of patients with valvular heart disease). Endorsed by the Society of Cardiovascular Anesthesiologists, Society for Cardiovascular Angiography and Interventions, and Society of Thoracic Surgeons. *J Am Coll Cardiol* 52:e1–e142
- Bruun NE, Habib G, Thuny F et al (2014) Cardiac imaging in infectious endocarditis. *Eur Heart J* 35:624–632
- Carbone I, Friedrich MG (2012) Myocardial edema imaging by cardiovascular magnetic resonance: current status and future potential. *Curr Cardiol Rep* 14:1–6
- Celik T, Iyisoy A, Yuksel C (2009) Stress-induced (Takotsubo) cardiomyopathy: a transient disorder. *Int J Cardiol* 131:265–266
- Cerqueira MD, Weissman NJ, Dilsizian V, American Heart Association Writing Group on Myocardial Segmentation and Registration for Cardiac Imaging et al (2002) Standardized myocardial segmentation and nomenclature for tomographic imaging of the heart. A statement for healthcare professionals from the Cardiac Imaging Committee of the Council on Clinical Cardiology of the American Heart Association. *Int J Cardiovasc Imaging* 18:539–542
- Cheng H, Zhao S, Jiang S et al (2011) The relative atrial volume ratio and late gadolinium enhancement provide additive information to differentiate constrictive pericarditis from restrictive cardiomyopathy. *J Cardiovasc Magn Reson* 13:15
- D'Arcy J, Myerson SG (2010) Investigations in valvular heart disease. *Clin Med* 10:172–176
- De Mello RA, Nacif MS, dos Santos AA, Cury RC, Rochitte CE, Marchiori E (2012) Diagnostic performance of combined cardiac MRI for detection of coronary artery disease. *Eur J Radiol* 81:1782–1789
- De Smet K, Verdries D, Tanaka K, De Mey J, De Maeseener M (2012) MRI in the assessment of non ischemic myocardial diseases. *Eur J Radiol* 81:1546–1548
- Eitel I, Friedrich MG (2011) T2-weighted cardiovascular magnetic resonance in acute cardiac disease. *J Cardiovasc Magn Reson* 13:13
- Eitel I, von Knobelsdorff-Brenkenhoff F, Bernhardt P et al (2011) Clinical characteristics and cardiovascular magnetic resonance findings in stress (takotsubo) cardiomyopathy. *JAMA* 306:277–286
- Ferrari VA, Scott CH, Basso C (2005) Arrhythmogenic right ventricular dysplasia/cardiomyopathy. *Curr Cardiol Rep* 7:70–75
- Francone M, Dymarkowski S, Kalantzi M, Rademakers FE, Bogaert J (2006) Assessment of ventricular coupling with real-time cine MRI and its value to differentiate constrictive pericarditis from restrictive cardiomyopathy. *Eur Radiol* 16:944–951

- Friedrich MG, Marcotte F (2013) Cardiac magnetic resonance assessment of myocarditis. *Circ Cardiovasc Imaging* 6:833–839
- Friedrich MG, Strohm O, Schulz-Menger J, Marciniak H, Luft FC, Dietz R (1998) Contrast media-enhanced magnetic resonance imaging visualizes myocardial changes in the course of viral myocarditis. *Circulation* 97:1802–1809
- Gahide G, Bertrand D, Roubille F et al (2010) MR delayed enhancement imaging findings in suspected acute myocarditis. *Eur Radiol* 20:65–72
- Goitein O, Matetzky S, Beinart R et al (2009) Acute myocarditis: noninvasive evaluation with cardiac MRI and transthoracic echocardiography. *AJR Am J Roentgenol* 192:254–258
- Goyle KK, Walling AD (2002) Diagnosing pericarditis. *Am Fam Physician* 66:1695–1702
- Guarise A, Faccioli N, Foti G, Da Pozzo S, Meneghetti P, Morana G (2011) Role of echocardiography and cardiac MRI in depicting morphological and functional imaging findings useful for diagnosing hypertrophic cardiomyopathy. *Radiol Med* 116:197–210
- Hancock EW (2001) Differential diagnosis of restrictive cardiomyopathy and constrictive pericarditis. *Heart* 86:343–349
- Heydari B, Kwong RY (2014) Cardiac magnetic resonance imaging for ischemic heart disease: update on diagnosis and prognosis. *Top Magn Reson Imaging* 23:21–31
- Hoey ET, Teoh JK, Das I, Ganeshan A, Simpson H, Watkin RW (2014) The emerging role of cardiovascular MRI for risk stratification in hypertrophic cardiomyopathy. *Clin Radiol* 69:221–230
- Hombach V (2006) *Kardiovaskuläre Magnetresonanztomographie. Kursbuch und Repetitorium*. Schattauer, Stuttgart
- Jain A, Tandri H, Calkins H, Bluemke DA (2008) Role of cardiovascular magnetic resonance imaging in arrhythmogenic right ventricular dysplasia. *J Cardiovasc Magn Reson* 10:32
- Jiji RS, Kramer CM (2011) Cardiovascular magnetic resonance: applications in daily practice. *Cardiol Rev* 19:246–254. doi:10.1097/CRD.0b013e31821f4d6a
- Karamitsos TD, Francis JM, Myerson S, Selvanayagam JB, Neubauer S (2009) The role of cardiovascular magnetic resonance imaging in heart failure. *J Am Coll Cardiol* 54:1407–1424
- Karamitsos TD, Dall'Armellina E, Choudhury RP, Neubauer S (2011) Ischemic heart disease: comprehensive evaluation by cardiovascular magnetic resonance. *Am Heart J* 162:16–30
- Kellman P, Arai AE, McVeigh ER et al (2002) Phase-sensitive inversion recovery for detecting myocardial infarction using gadolinium-delayed hyperenhancement. *Magn Reson Med* 47:372–383
- Kim RJ, Fieno DS, Parrish TB et al (1999) Relationship of MRI delayed contrast enhancement to irreversible injury, infarct age, and contractile function. *Circulation* 100:1992–2002
- Kim DH, Choi SI, Chang H-J, Choi DJ, Lim C, Park JH (2006) Delayed hyperenhancement by contrast-enhanced magnetic resonance imaging: clinical application for various cardiac diseases. *J Comput Assist Tomogr* 30:226–232
- Lehrke S, Lossnitzer D, Schöb M et al (2011) Use of cardiovascular magnetic resonance for risk stratification in chronic heart failure: prognostic value of late gadolinium enhancement in patients with non-ischaemic dilated cardiomyopathy. *Heart* 97:727–732
- Ling LH, Oh JK, Schaff HV et al (1999) Constrictive pericarditis in the modern era: evolving clinical spectrum and impact on outcome after pericardiectomy. *Circulation* 100:1380–1386
- Mahrholdt H, Wagner A, Deluigi CC et al (2006) Presentation, patterns of myocardial damage, and clinical course of viral myocarditis. *Circulation* 114:1581–1590
- Manrique A, Gerbaud E, Derumeaux G et al (2009) Cardiac magnetic resonance demonstrates myocardial oedema in remote tissue early after reperfused myocardial infarction. *Arch Cardiovasc Dis* 102:633–639
- Maron BJ, Towbin JA, Thiene G et al (2006) *Contemporary definitions and classification of the cardiomyopathies: an American Heart Association Scientific Statement from the Council on Clinical Cardiology, Heart Failure and Transplantation Committee; Quality of Care and Outcomes Research and Functional Genomics and Translational Biology Interdisciplinary Working Groups; and Council on Epidemiology and Prevention*. *Circulation* 113:1807–1816
- McCrohon JA, Moon JCC, Prasad SK et al (2003) Differentiation of heart failure related to dilated cardiomyopathy and coronary artery disease using gadolinium-enhanced cardiovascular magnetic resonance. *Circulation* 108:54–59

- Mookadam F, Jiamsripong P, Raslan SF, Panse PM, Tajik AJ (2011) Constrictive pericarditis and restrictive cardiomyopathy in the modern era. *Future Cardiol* 7:471–483
- Morris MF, Maleszewski JJ, Suri RM et al (2010) CT and MR imaging of the mitral valve: radiologic-pathologic correlation. *Radiographics* 30:1603–1620
- Murphy DT, Shine SC, Cradock A, Galvin JM, Keelan ET, Murray JG (2010) Cardiac MRI in arrhythmogenic right ventricular cardiomyopathy. *AJR Am J Roentgenol* 194:W299–W306
- Nassenstein K, de Greiff A, Hunold P (2009) MR evaluation of left ventricular volumes and function: threshold-based 3D segmentation versus short-axis planimetry. *Invest Radiol* 44:635–640
- Ong P, Athansiadis A, Hill S et al (2011) Usefulness of pericardial effusion as new diagnostic criterion for noninvasive detection of myocarditis. *Am J Cardiol* 108:445–452
- Palumbo A, Maffei E, Martini C (2010) Functional parameters of the left ventricle: comparison of cardiac MRI and cardiac CT in a large population. *Radiol Med* 115:702–713
- Penugonda N (2010) Cardiac MRI in infiltrative disorders: a concise review. *Curr Cardiol Rev* 6:134–136
- Perazzolo Marra M, Lima JAC, Iliceto S (2011) MRI in acute myocardial infarction. *Eur Heart J* 32:284–293
- Petersen SE, Selvanayagam JB, Wiesmann F et al (2005) Left ventricular non-compaction: insights from cardiovascular magnetic resonance imaging. *J Am Coll Cardiol* 46:101–105
- Proctor RD, Shambrook JS, McParland P, Peebles CR, Brown IW, Harden SP (2011) Imaging hypertrophic heart diseases with cardiovascular MR. *Clin Radiol* 66:176–186
- Quarta G, Sado DM, Moon JC (2011) Cardiomyopathies: focus on cardiovascular magnetic resonance. *Br J Radiol* 84:S296–S305
- Richardson P, McKenna W, Bristow M et al (1996) Report of the 1995 World Health Organization/International Society and Federation of Cardiology Task Force on the Definition and Classification of cardiomyopathies. *Circulation* 93:841–842
- Rickers C, Wilke NM, Jerosch-Herold M et al (2005) Utility of cardiac magnetic resonance imaging in the diagnosis of hypertrophic cardiomyopathy. *Circulation* 112:855–861
- Rochitte CE, Tassi EM, Shiozaki AA (2006) The emerging role of MRI in the diagnosis and management of cardiomyopathies. *Curr Cardiol Rep* 8:44–52
- Saraste A, Nekolla S, Schwaiger M (2008) Contrast-enhanced magnetic resonance imaging in the assessment of myocardial infarction and viability. *J Nucl Cardiol* 15:105–117
- Schalla S, Bekkers SC, Dennert R (2010) Replacement and reactive myocardial fibrosis in idiopathic dilated cardiomyopathy: comparison of magnetic resonance imaging with right ventricular biopsy. *Eur J Heart Fail* 12:227–231
- Sensaeth KH, Hoffmann P, Fossum E, Mangschau A, Sandvik L, Klow NE (2012) Cardiac magnetic resonance visualizes acute and chronic myocardial injuries in myocarditis. *Int J Cardiovasc Imaging* 28:327–335. doi:[10.1007/s10554-011-9812-7](https://doi.org/10.1007/s10554-011-9812-7)
- Stork A, Müllerleile K, Bansmann PM et al (2007) Patterns of delayed-enhancement in MRI of ischemic and non-ischemic cardiomyopathies. *Rofo* 179:21–30. doi:[10.1055/s-2006-927204](https://doi.org/10.1055/s-2006-927204)
- Tandri H, Saranathan M, Rodriguez ER et al (2005) Noninvasive detection of myocardial fibrosis in arrhythmogenic right ventricular cardiomyopathy using delayed-enhancement magnetic resonance imaging. *J Am Coll Cardiol* 45:98–103. doi:[10.1016/j.jacc.2004.09.053](https://doi.org/10.1016/j.jacc.2004.09.053)
- Wagner A, Mahrholdt H, Holly TA et al (2003) Contrast-enhanced MRI and routine single photon emission computed tomography (SPECT) perfusion imaging for detection of subendocardial myocardial infarcts: an imaging study. *Lancet* 361:374–379
- Walsh TF, Hundley WG (2007) Assessment of ventricular function with cardiovascular magnetic resonance. *Cardiol Clin* 25:15–33
- Wellnhofer E, Olariu A, Klein C et al (2004) Magnetic resonance low-dose dobutamine test is superior to SCAR quantification for the prediction of functional recovery. *Circulation* 109:2172–2174
- Yousef ZR, Foley PWX, Khadjooi K (2009) Left ventricular non-compaction: clinical features and cardiovascular magnetic resonance imaging. *BMC Cardiovasc Disord* 9:37

Jens-Peter Kühn and Christoph Lühken

8.1 The Liver

8.1.1 Focal Liver Lesions in Whole-Body Screening MRI

Focal liver lesions are present in more than 5 % of the population and are often detected incidentally when an imaging study is performed for another reason. In 40 % of cases, it is not possible to categorize such incidental lesions adequately by imaging (Strobel and Bernatik 2006). Liver lesions are especially challenging for the radiologist interpreting whole-body screening MRI studies, which typically only include non-contrast-enhanced pulse sequences. With unenhanced MR images, only a crude characterization of focal liver lesions is possible.

In the screening situation, we can roughly distinguish three categories of focal liver lesions: benign cysts and cyst-like lesions, benign solid masses, and solid malignancies (Table 8.1). Lesions with a cystic appearance such as dysontogenetic cysts, echinococcal cysts, and cavernous hemangiomas can be diagnosed with confidence on the basis of an unenhanced MRI examination (including conventional T1- and T2-weighted sequences), and treatment recommendations can be made accordingly. This is not the case for solid liver lesions such as focal nodular hyperplasia, hepatocellular adenoma, metastasis, hepatocellular carcinoma, or cholangiocellular carcinoma. In most instances, a contrast-enhanced study is necessary to characterize solid liver lesions and estimate their total extent.

J.-P. Kühn (✉) • C. Lühken
Institute of Diagnostic Radiology and Neuroradiology, University Medicine Greifswald,
Ferdinand-Sauerbruch-Straße, 17487 Greifswald, Germany
e-mail: kuehn@uni-greifswald.de; luehken@uni-greifswald.de

Table 8.1 Focal liver lesions in the general population

Type of lesion	Morphology	Entity	Prevalence	Age predilection	Sex predilection
Benign	Cystic	Liver cysts	2.5–18 %	<40 years	Women
		Liver hemangioma	7 %	<50 years	Women
	Solid	Focal nodular hyperplasia (FNH)	2–8 %	20–50 years	Women
		Hepatocellular adenoma	>5 %	30–40 years	Women
Malignant	Solid	Metastasis	Approx. 50 % in cancer patients	<40 years	Depends on the primary tumor
		Hepatocellular carcinoma (HCC)	Rare	<40 years	Men
		Cholangiocellular carcinoma (CCC)	Rare	<40 years	–

Table 8.2 Short standardized protocol for non-contrast-enhanced liver imaging in the setting of whole-body MRI screening

	TR (ms)	TE (ms)	Flip angle	Slice thickness (mm)	Matrix	Acquisition time (min)
T1w FLASH 2D FS	251	4.13	70	6	129×256	1:17
T2w TSE BLADE FS	2,720	116	150	6	129×256	1:16
VIBE Dixon	17.48	2.4/4.8	10	5	126×224	0:19
DWI ^a	1,700	72		6	115×192	2:55

^aLiver DWI with *b* values (diffusion gradients) of 0, 400, and 1,000

TR repetition time, *TE* echo time, *T1w* T1-weighted, *T2w* T2-weighted, *FS* fat saturation, *FLASH* fast low-angle shot, *BLADE* motion correction with radial blades (Siemens), *VIBE Dixon* volume-interpolated breath-hold examination for chemical shift imaging (Siemens), *DWI* diffusion-weighted imaging

8.1.2 Pulse Sequence Protocols and Characterization of Focal Liver Lesions

An example of a standard protocol for non-contrast-enhanced imaging of the liver as part of a whole-body MRI examination is presented in Table 8.2.

Most benign and malignant hepatic lesions have lower T1 and higher T2 signal intensity compared with healthy liver tissue. The T2 signal intensity relative to splenic tissue allows characterization of most focal liver lesions as benign or malignant. For example, isointensity to normal spleen on T2-weighted images is always suspicious for malignancy. High T2 signal intensity relative to the spleen and sharp demarcation from surrounding parenchyma indicate a cyst or hemangioma. Liver masses with lower signal intensity on T2-weighted images than normal spleen include focal nodular hyperplasia (FNH), hepatocellular adenoma, and hepatocellular carcinoma (HCC). Non-contrast-enhanced images, especially T2-weighted turbo

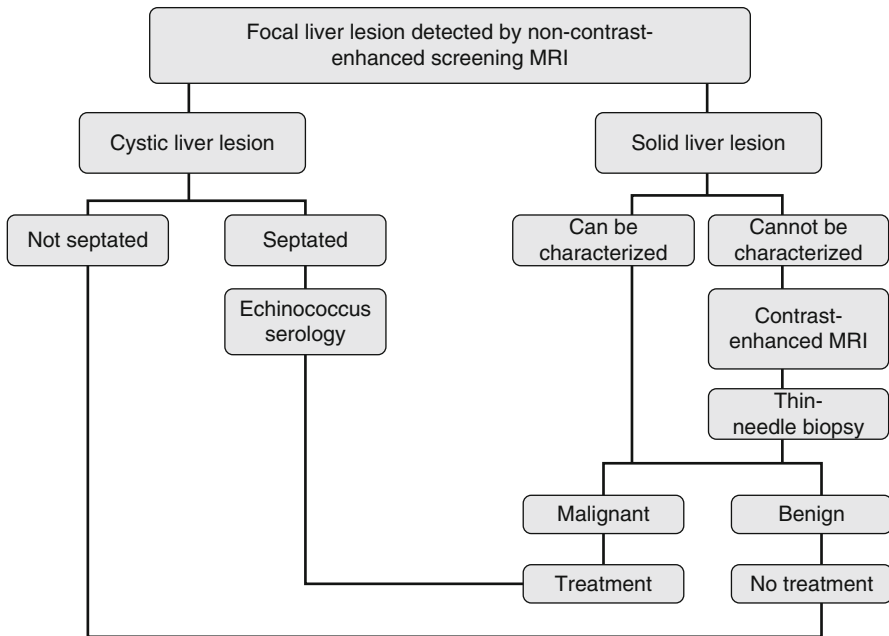


Fig. 8.1 Diagnostic and therapeutic management of focal liver lesions detected by non-contrast-enhanced screening MRI

spin echo (TSE) images, provide the most important information for detecting and characterizing focal liver lesions. In the screening situation, it is therefore most important to ensure high-quality T2-weighted TSE imaging. Respiratory-triggered diffusion-weighted imaging (DWI) of the liver is a new MRI technique that improves detection of focal lesions and provides supplementary information for their characterization (Holzapfel et al. 2008). In contrast, T1-weighted pulse sequences provide anatomic orientation, while offering little additional information for lesion characterization (except for focal hepatic steatosis).

The flow chart presented in Fig. 8.1 summarizes the strategy we propose for the differentiation and management of focal liver lesions detected by non-contrast-enhanced screening MRI.

8.1.3 MRI Morphology of Cystic Liver Lesions

Typical cystic lesions are sharply delineated and have high signal intensity compared to surrounding liver and spleen on T2-weighted images. Examples are congenital cysts of the liver, hemangiomas, and inflammatory lesions such as echinococcal cysts and abscess. Cystic liver lesions are benign and are treated as such. Standard non-contrast-enhanced T1- and T2-weighted datasets do not allow reliable

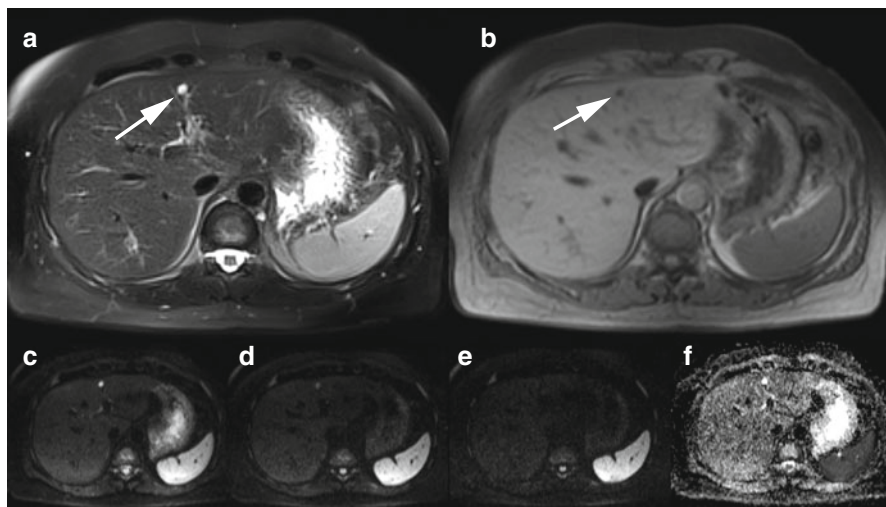


Fig. 8.2 A 37-year-old male subject with incidental simple liver cyst in segment IV (*arrow*). (a) Fat-saturated T2w TSE image (a) and fat-saturated 2D T1w FLASH image (b) show sharply demarcated, cystic lesion in segment IV. Liver cysts and hemangiomas cannot be differentiated without injection of contrast medium. (c–f) On diffusion-weighted images, acquired with different b values (diffusion gradients), the liver lesion has high signal intensity at $b=0$ (c), moderately high signal intensity at $b=400$ (d), and the same signal intensity as hepatic parenchyma at $b=800$ (e). (f) Liver cysts have a mean ADC value of $(3.14 \pm 0.31) \times 10^{-3} \text{ mm}^2/\text{s}$ (Sun et al. 2005)

differentiation between hepatic cysts and hemangiomas since both have long T2 relaxation times (>130 ms). Hemangiomas generally have a sharp but irregular outline and tend to develop central fibrosis, which appears bright on T1-weighted images. DWI with calculation of apparent diffusion coefficients (ADC) may provide supplementary information for differentiating between these two entities (Sun et al. 2005).

8.1.3.1 Hepatic Cysts

Liver cysts are fluid-filled spaces that are found within the parenchyma or bulge from the liver capsule (Sun et al. 2005). A simple liver cyst (or bile duct cyst) is a benign congenital fluid-containing lesion with an epithelium-lined wall. Liver cysts may be single or multiple (Fig. 8.2). The presence of multiple cysts may suggest autosomal dominant polycystic liver disease. Simple cysts are the most common benign liver lesions. In autopsy series, a prevalence of over 18 % with a preference for women has been found (Carrim and Murchison 2003). Hepatic cysts become increasingly common after age 40 (Caremani et al. 1993). Depending on the imaging modality used, liver cysts are incidentally detected in 2.5–18 % of examinations (Gaines and Sampson 1989; Carrim and Murchison 2003). Virtually all liver cysts are asymptomatic. An occasional large cyst with mass effect may present with dragging pain in the upper abdomen. Rare complications such as intracystic hemorrhage

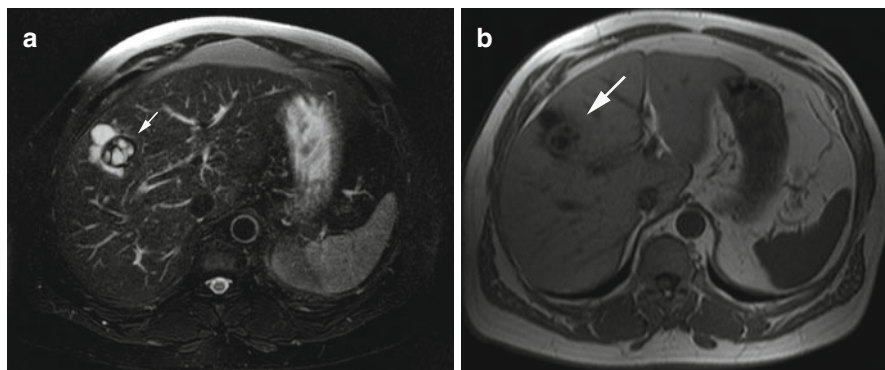


Fig. 8.3 A 50-year-old Mediterranean man with an echinococcal cyst of the liver suggested by MRI appearance (*arrow*) and confirmed by serology. Fat-saturated T2w TSE image (**a**) and 2D T1w FLASH image (**b**) show a septated cystic mass with sharp margins in segment VIII

or rupture with peritoneal seeding cause severe abdominal pain of sudden onset. If MRI shows internal septation or an irregular contour, a hydatid cyst (echinococcus cyst) must be ruled out by laboratory testing (Fig. 8.3).

Clinical Management

Small, asymptomatic liver cysts that are not caused by parasites can be left alone. For nonparasitic liver cysts that become symptomatic, elective surgery should be contemplated. All parasitic cysts must be excised (echinococcus serology) (Rückert et al.).

Complications such as hemorrhage, rupture, or penetration into adjacent structures are not usually encountered in the screening situation but would require emergency surgery.

8.1.3.2 Liver Hemangioma

A hemangioma is a benign proliferation of blood vessels that may occur in any vascularized tissue in the body. Among the parenchymal organs of the upper abdomen, the liver is the most common site of hemangiomas. A typical liver hemangioma is a small, blood-filled tumor less than 3 cm in size (Fig. 8.4). Cavernous hemangiomas have a prevalence of 7 % and are the second most common benign hepatic tumors (Semelka and Sofka 1997; Takagi 1985; Nufer et al. 1999). Postmenopausal women are affected 5–6 times more frequently than men (Cherqui et al. 1995). There is an association with FNH. About 25 % of all hemangiomas are incidentally detected in patients whose liver is being evaluated for the presence of metastasis. Hemangiomas have no risk of malignant transformation, although 30 % are initially categorized as indeterminate or suspicious. The vast majority of cavernous hemangiomas (95 %)

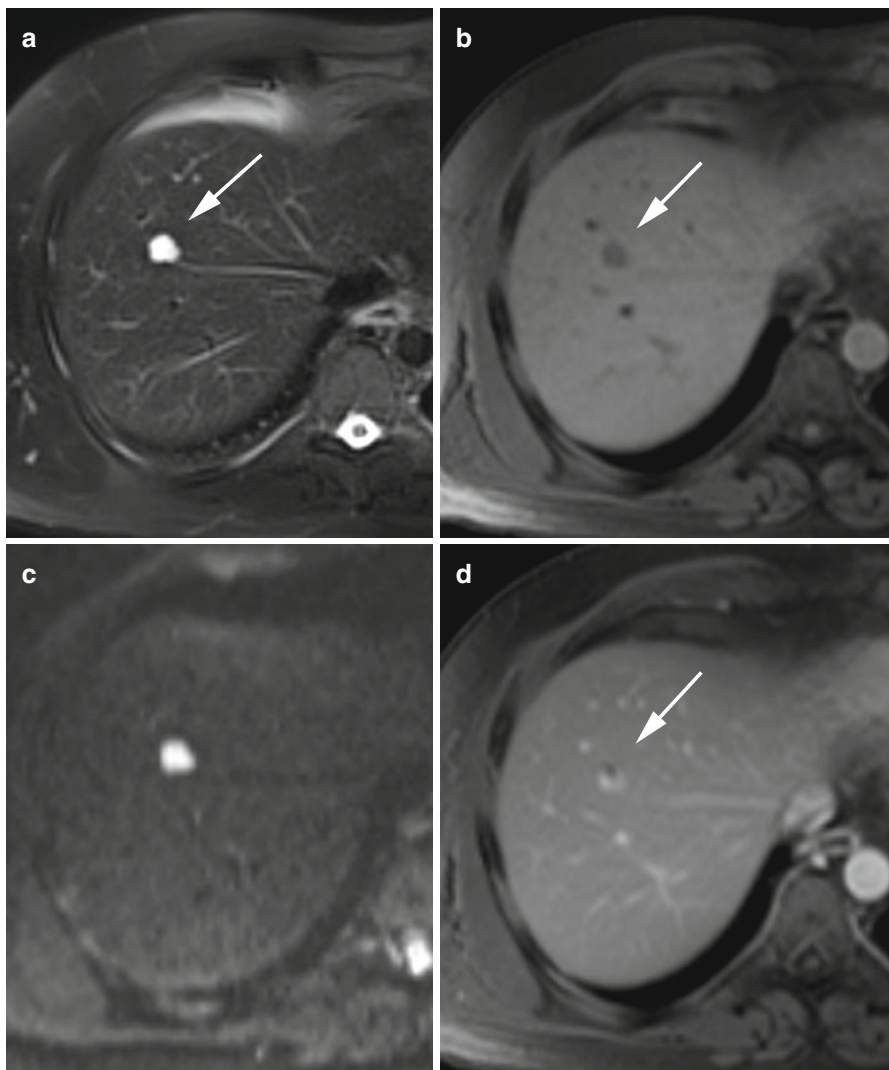


Fig. 8.4 A 45-year-old male subject with an incidentally detected liver hemangioma (*arrow*). (a) Fat-saturated T2w TSE image shows a sharply demarcated mass, measuring 2.2 cm, in segment VIII. (b) On 2D T1w Flash image, the lesion has low signal intensity relative to surrounding liver. (c) On DWI, the lesion retains its high signal intensity even at high b values; the image shown was acquired with $b=800$. Liver hemangiomas have a mean ADC value of $(1.86 \pm 0.36) \times 10^{-3} \text{ mm}^2/\text{s}$ (Sun et al. 2005). (d) For lesion differentiation, an extracellular MR contrast agent was administered. On the postcontrast images, the lesion showed centripetal fill-in, consistent with hemangioma

are asymptomatic, while 40 % of giant liver hemangiomas (>4 cm) cause symptoms (Fig. 8.5). Symptoms are nonspecific, including upper abdominal pain, early satiety, nausea, and vomiting (Trastek et al. 1983). An occasional large hemangioma may rupture (5 % risk), which, in 70 % of cases, is fatal.

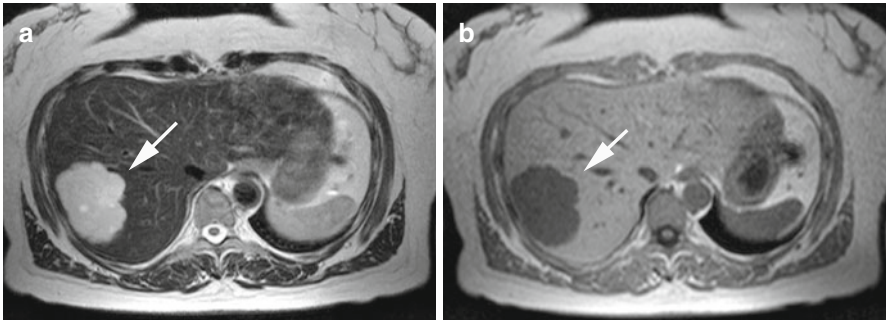


Fig. 8.5 A 42-year-old female subject with incidentally detected giant hemangioma with central fibrosis (*arrow*). (a) T2w TSE image reveals a sharply marginated, very bright lesion in segment VII. The lesion measures 8.2 cm and is located near the capsule. The appearance is heterogeneous. (b) On T1 weighted image, the lesion is hypointense to surrounding liver

Clinical Management

Asymptomatic cavernous liver hemangioma requires no treatment. In symptomatic patients, elective surgical excision and interventional angiographic embolization may be contemplated. There is an increased surgical risk when a hemangioma is very large (>10 cm) or in a troublesome area (Nufer et al. 1999). Large symptomatic hemangiomas that continue to grow have a 5 % risk of rupture. Prognosis is good after resection.

8.1.3.3 Abscess

Patients with liver abscess (circumscribed collection of purulent exudates) will have sepsis with severe symptoms such as fever, upper abdominal pain, nausea, and vomiting. They will not be participating in MRI screening.

8.1.4 MRI Morphology of Solid Liver Lesions

Non-contrast-enhanced screening MR images provide only limited information for the characterization of solid liver lesions. Benign solid liver lesions include FNH and hepatocellular adenoma. No less common are malignant liver lesions such as metastasis, hepatocellular carcinoma, and cholangiocellular carcinoma. Several criteria have been proposed to differentiate between benign and malignant liver lesions on the basis of unenhanced MR imaging (Table 8.3) (Grebe et al. 1994). All solid liver lesions that are not cystic on unenhanced images require further evaluation (ultrasound, contrast-enhanced ultrasound, biphasic computed tomography, contrast-enhanced MRI).

Table 8.3 Criteria for assessing the malignancy of focal liver lesions on non-contrast-enhanced MRI

	Sensitivity	Specificity
<i>T1 weighting</i>		
Hypointense to liver	0.90	0.023
Hypointense to spleen	0.40	0.60
Hyperintense to muscle	0.43	0.67
Heterogeneous	0.50	0.52
Lesion demarcation: irregular, blurred	0.37	0.86
<i>T2 weighting</i>		
Hyperintense to liver	0.93	0.02
Hypo- or isointense to spleen	0.73	0.90
Hyper- or isointense to muscle	1.00	0.02
Heterogeneous	0.87	0.50
Lesion demarcation: irregular, blurred	0.43	0.90

Modified from Grebe et al. (1994)

8.1.5 MRI Morphology of Benign Solid Liver Lesions

8.1.5.1 Focal Nodular Hyperplasia

Focal nodular hyperplasia (FNH) is a benign proliferation of hepatocytes and matrix components and is characterized by the presence of abnormal vascular or biliary structures. The pathogenesis of FNH is a matter of debate. An association with the use of hormones, especially oral contraceptives, has been postulated (Eisenberg and Margulis 1991). Autopsy studies have revealed a prevalence of 2–8 % for this tumor (Buetow et al. 1996). FNH is the third most common benign liver tumor and is seen predominantly in women of reproductive age, with a female-to-male ratio of 8:1 (Stocker and Ishak 1981; Dröge et al. 1996). Individuals with FNH often have other liver tumors such as hemangiomas or hepatocellular adenomas. Asymptomatic FNH is almost exclusively discovered as an incidental finding at autopsy, elective surgery, or imaging performed for other reasons (Figs. 8.6 and 8.7). Symptomatic FNH is very rare, presenting with right upper quadrant abdominal pain. The risk of rupture is less than 1 % (Dröge et al. 1996).

8.1.5.2 Hepatocellular Adenoma

Adenoma of the liver is rare and difficult to detect with unenhanced MRI because it is nearly isointense to liver parenchyma on both T1- and T2-weighted images

Clinical Management

In the absence of a central scar, no definite FNH diagnosis can be made, and a contrast-enhanced scan should be considered to rule out other solid liver tumors. If, however, there are no doubts about the diagnosis, no treatment is required as there is no risk of malignant transformation, and the risk of rupture is less than 1 %. Elective surgical resection is an option for symptomatic FNH (Rückert et al.). The prognosis is good.

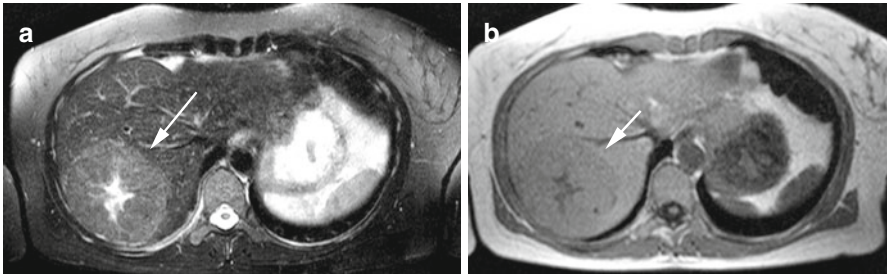


Fig. 8.6 A 36-year-old female subject with incidentally detected focal nodular hyperplasia (*arrow*). (a) Fat-saturated T2w TSE image reveals a slightly hyperintense lesion with central scar in segment VII. The characteristic spoke wheel pattern confirms the diagnosis of FNH. (b) T1w FLASH image reveals the anatomic relationship of the focal liver lesion

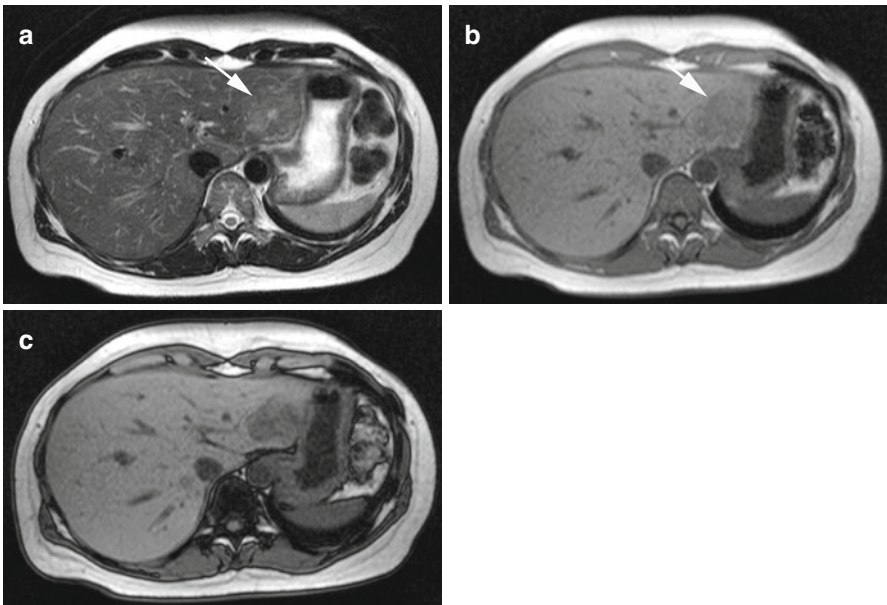


Fig. 8.7 A 48-year-old female subject with incidentally detected focal nodular hyperplasia (*arrow*). (a) Fat-saturated T2w TSE images reveals a slightly hyperintense lesion with central scar in segment III. (b) 2D T1w FLASH images shows the anatomic relationship of the focal liver lesion. (c) Out-of-phase chemical shift image shows loss of signal intensity in the lesion, confirming the presence of fat. Fat is present in up to 50 % of FNHs

(Fig. 8.8). Hepatic adenomas are nearly exclusively found in women with a long history of oral contraceptive use (>5 years) and in patients with diabetes mellitus. They are most common in young women of reproductive age with a peak between the third and fourth decades. In men, hepatocellular adenoma has been associated with the use of anabolic steroids.

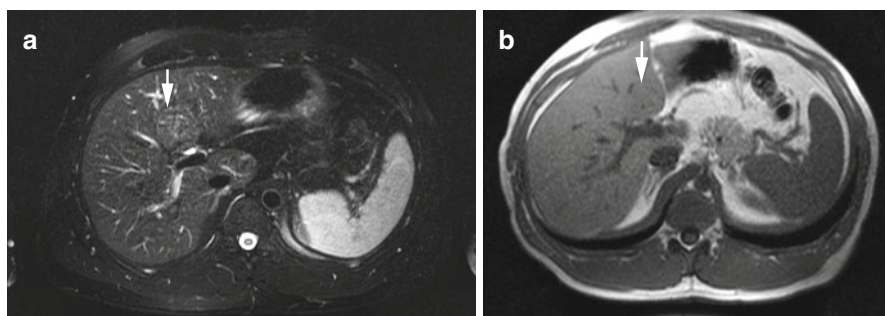


Fig. 8.8 An 18-year-old female subject with incidentally detected hepatocellular adenoma (arrow). (a) Fat-saturated T2w TSE image and (b) 2D T1w FLASH image show nearly isointense mass in central segment IV. The mass is 4.3 cm in size and appears to displace surrounding structures; adjacent bile ducts are dilated

The occurrence of multiple adenomas ($n > 10$) is known as adenomatosis and is frequently seen in patients with type I/type III glycogen storage disease. Symptoms depend on the size of adenoma. Approx. 40 % of patients report upper abdominal discomfort. Rupture with hemoperitoneum has been observed in 20 % of cases. Spontaneous rupture is more common during the menstrual period, pregnancy, and after delivery. There is a risk of malignant transformation to hepatocellular carcinoma that increases with lesion size: 5 % for adenomas < 10 cm and 10 % for adenomas > 10 cm.

Clinical Management

Because they are isointense to surrounding parenchyma on T1- and T2-weighted images, hepatocellular adenomas are easily overlooked by non-contrast-enhanced MRI. Close follow-up is recommended for adenomas < 5 cm. Oral contraceptives or other hormones should be discontinued. Larger adenomas (> 5 cm) should be resected due to the risk of malignant transformation and rupture (Chuang et al. 2002; de Wilt et al. 1998). The risk of rupture is higher during pregnancy. Some authors advocate elective surgical resection of all hepatocellular adenomas, regardless of size or symptoms (Rückert et al.). The prognosis is good after radical surgical resection.

8.1.6 MRI Morphology of Malignant Solid Liver Lesions

8.1.6.1 Liver Metastasis

Metastatic disease is by far the most common hepatic malignancy, being 20 times more frequent than primary liver malignancy. Up to 50 % of cancer patients are found to have liver metastases at autopsy. Metastatic spread to the liver occurs through the systemic or portal venous circulation. Liver metastases are most common

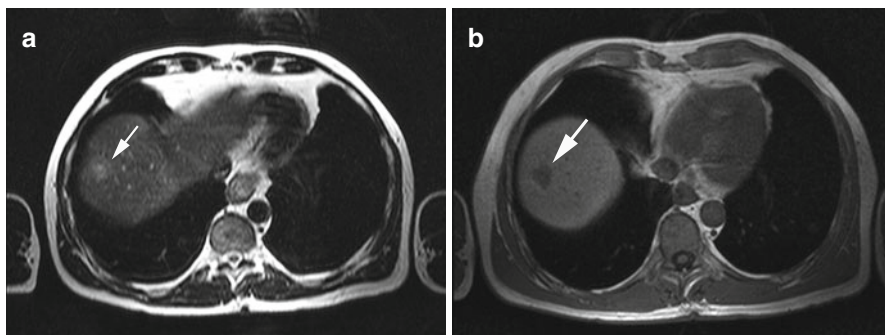


Fig. 8.9 A 68-year-old male subject with incidentally detected subdiaphragmatic focal liver lesion in segments VII/VIII (*arrow*). Subsequent diagnostic workup revealed colorectal cancer with metastatic spread to the liver that had not been diagnosed before. **(a)** T2w TSE image shows a high-signal-intensity mass with target sign. **(b)** On the corresponding 2D T1w FLASH images, the lesion has low signal intensity

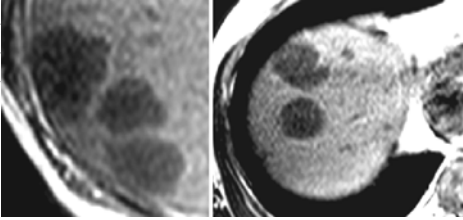
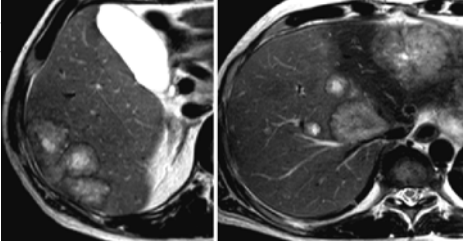
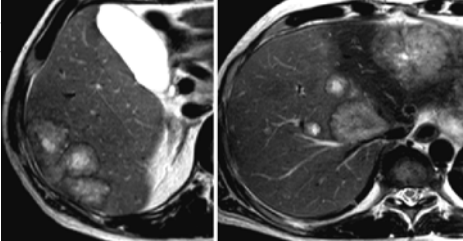
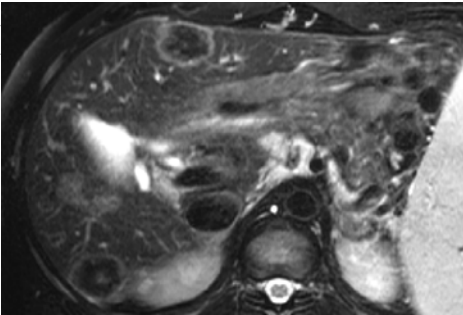
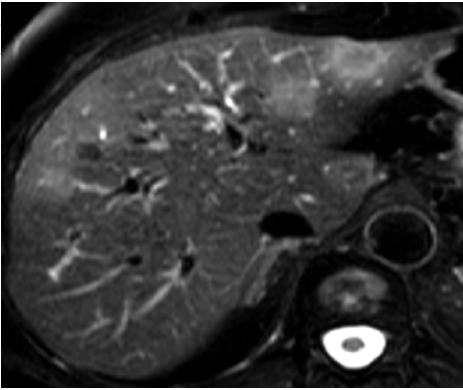
in patients with primary cancer of the colon or rectum (42 %), stomach (23 %), pancreas (21 %), breasts (14 %), and lungs (13 %). In terms of imaging morphology and histology, liver metastases mimic the primary tumor. Patients with single or multiple hepatic metastases may have concomitant lymph node involvement and metastatic spread to other organs.

Non-contrast-enhanced MR imaging usually shows multifocal lesions with unspecific low T1 signal intensity and mild hyperintensity (isointensity to spleen) on T2 weighting (Fig. 8.9). Hepatic metastases typically have markedly shorter T2 relaxation times than cysts or hemangiomas. An occasional metastasis has an appearance suggesting a cyst-like lesion. Generally, there are several imaging signs that suggest metastasis on unenhanced MR images (Table 8.4) (Wittenberg et al. 1988). These are very important to look for in the screening situation. With T1-weighted images, it is usually impossible to differentiate metastases from other focal liver lesions.

Clinical Management

Most liver metastases cannot be reliably diagnosed using unenhanced MRI alone. If solid liver lesions are detected, the next step involves noninvasive additional imaging modalities for further evaluation (contrast-enhanced CT/MRI). If there is a high suspicion of malignancy, thin-needle biopsy is indicated. Treatment of liver metastases depends on the primary tumor and the total tumor burden. When there is diffuse metastatic involvement of the liver, systemic chemotherapy is often the first-line treatment option. Surgical resection is only indicated in 5 % of cases and is restricted to patients with one or a few hepatic metastases. Interventional ablation and embolization are alternative options. Patients with metastatic liver disease have a poor overall prognosis, but the disease course may vary depending on the primary tumor.

Table 8.4 Imaging signs of liver metastases on non-contrast-enhanced MRI

T1 weighting	<i>Doughnut sign</i>	
	27 % of all metastases 6 % of benign lesions	
T2 weighting	<i>Target sign</i>	
	26 % of all metastases	
	<i>Target sign</i>	
	High-signal-intensity center surrounded by a slightly less hyperintense rim, indicating partial necrosis	
	<i>Halo sign</i>	
	13 % of all metastases	
	Bright rim around the lesion, indicating perifocal edema	
	<i>Heterogeneous</i>	
	45 % of all metastases	
	Blurred lesion contour and signal intensity isointense to spleen	

8.1.6.2 Hepatocellular Carcinoma

Hepatocellular carcinoma (HCC) is the most common primary malignant neoplasm of the liver, and dysplastic nodules are assumed to be precancerous lesions of HCC. HCC accounts for 5.6 % of all tumors worldwide, with incidence rates of 7.1/100,000

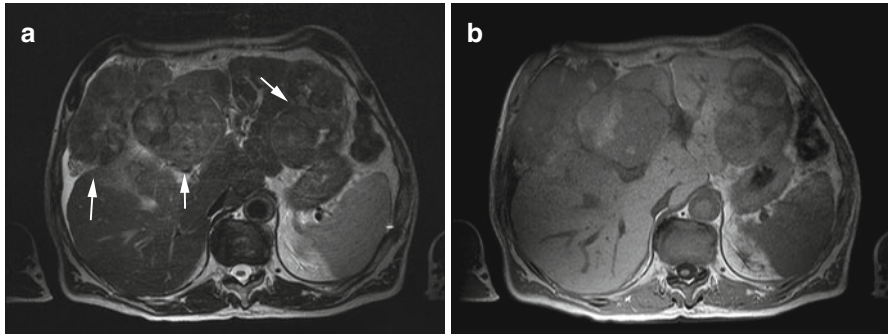


Fig. 8.10 A 72-year-old male subject with incidentally detected large hepatocellular carcinoma (arrows). (a) Axial T2w TSE image with shows heterogeneous tumor nodules with extrahepatic extension in segment IV and in the left hepatic lobe. (b) 2D T1w images shows multifocal malignancy with central hyperintensity

population/year in men and 2.7/100,000/year in women (Velázquez et al. 2003). HCC is the fifth most common malignancy in men and the eighth most common malignancy in women, causing 250,000–1,000,000 deaths worldwide each year. Risk factors for HCC are cirrhosis, viral hepatitis, fatty liver disease, hemochromatosis, and aflatoxin exposure. Patients usually have advanced inoperable HCC by the time the first symptoms appear. Symptoms include malaise, fever, abdominal pain, weight loss, and, rarely, symptoms of jaundice (Ros et al. 1990). Liver function tests are typically elevated, reflecting parenchymal damage. More than half of patients have an elevated α -fetoprotein (AFP) level. HCC releases proteins and can cause paraneoplastic syndrome (erythrocytosis, hypercalcemia, hyperglycemia, hirsutism) (Kew 1998).

Clinical Management

A large invasive HCC is straightforward to diagnose; the differential diagnosis includes only cholangiocellular carcinoma and large metastasis (Figs. 8.10 and 8.11). A smaller HCC may be confused with regenerative nodules in a cirrhotic liver or with other focal lesions. A contrast-enhanced scan may be needed if the diagnosis is unclear. Metastasis is extremely rare in a cirrhotic liver, and this should be borne in mind when considering differential diagnoses. Curative treatment is usually not possible because most patients have multifocal HCC, a large tumor bulk, or extensive cirrhosis at the time of diagnosis. A variety of interventional embolization procedures are available for palliative treatment. Total mortality is >90 %. Mean survival after diagnosis is 6 months with a 5-year survival rate of 30 %.

8.1.6.3 Cholangiocellular Carcinoma

Cholangiocellular carcinoma (CCC) is a malignant tumor arising from the small (peripheral CCC – 6 %; Fig. 8.12) or large bile ducts (hilar CCC – 67 %; Fig. 8.13) inside the liver or from the extrahepatic bile ducts (27 %) (Blum 1995). Unlike HCC, CCC usually occurs in the noncirrhotic liver. Peripheral CCC is much less common than HCC, constituting approx. 10–20 % of primary malignant liver tumors. The incidence is 0.8/100,000 population/year (Shaib and El-Serag 2004). A variety of risk factors have been identified, including carcinogen exposure (nitrosamines, aflatoxins, anabolic steroids), congenital anomalies of the bile ducts, and other predisposing conditions (primary sclerosing cholangitis, ulcerative colitis, α -antitrypsin deficiency, chronic hepatitis C, alcoholic and nonalcoholic hepatitis).

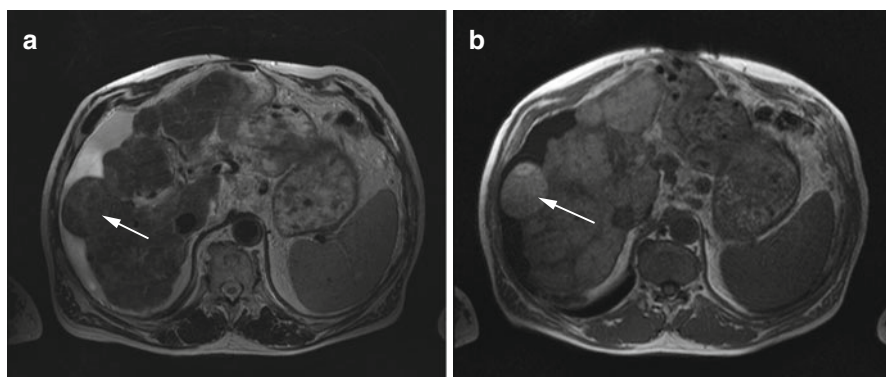


Fig. 8.11 A 54-year-old cachectic man without symptoms at the time of whole-body MRI screening. (a) Axial T2w TSE image demonstrates diffuse septation of liver parenchyma, hypertrophy of the caudate lobe, a nodular liver contour, and perihepatic ascites (indicating decompensated cirrhosis). (b) T1w FLASH images shows high-signal-intensity nodule with extrahepatic extension in segment VII/VIII. The diagnosis of HCC (*arrow*) was confirmed later

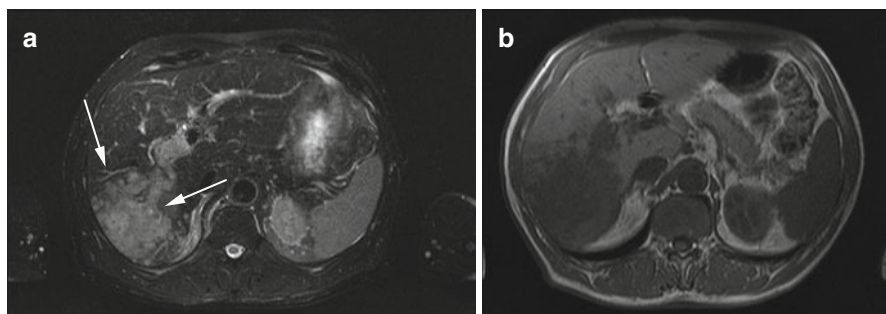


Fig. 8.12 A 67-year-old asymptomatic male subject with incidentally detected mass (*arrows*) in the right hepatic lobe. Subsequent invasive diagnostic workup demonstrated cholangiocellular carcinoma. (a) Fat-saturated T2w TSE image demonstrates high-signal-intensity mass in the right hepatic lobe with segmental portal vein invasion. (b) On 2D T1 weighted FLASH image, the lesion has lower signal intensity than surrounding liver

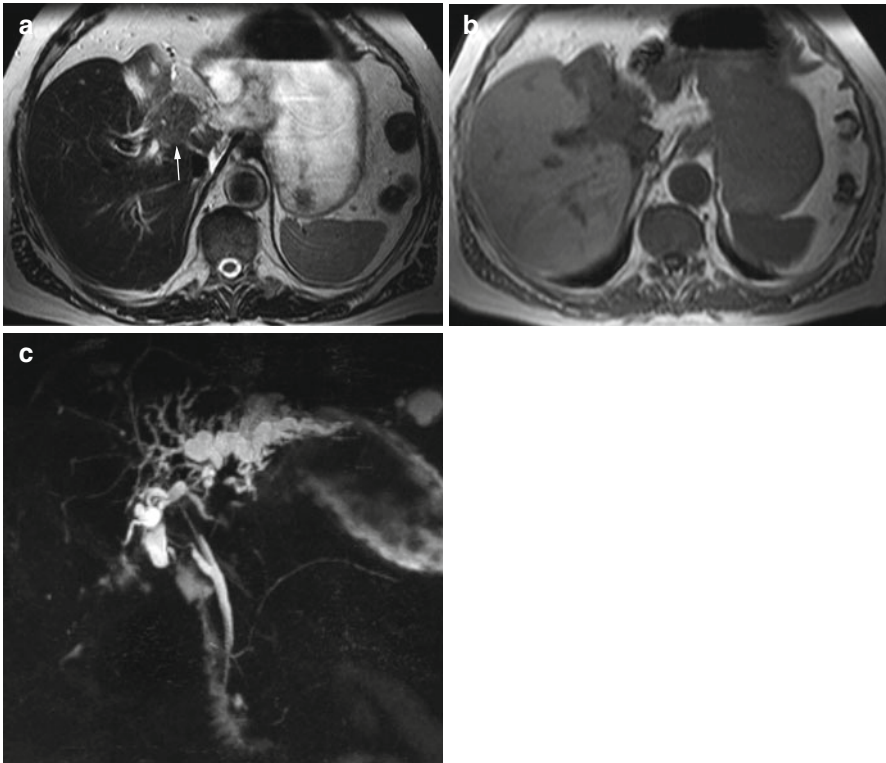


Fig. 8.13 A 73-year-old male subject without symptoms at the time of incidental detection of a central mass with segmental congestion of the bile ducts in the left hepatic lobe and consecutive atrophy of the left lobe (*arrow*). (a, b) T2w TSE and T1w FLASH images show central mass. (c) MRCP image suggests central cholangiocellular carcinoma (Klatskin tumor)

Clinical Management

Elective surgery is the only treatment for CCC patients that offers a chance of cure.

8.1.7 Structural Abnormalities of the Liver

8.1.7.1 Cirrhosis

Cirrhosis is a chronic diffuse condition of the liver characterized by necrosis and loss of the lobular architecture (Fig. 8.14). Normal hepatocytes are replaced by fibrous connective tissue and regenerative hepatic nodules. Cirrhosis is twice as common in men as in women and presents in middle-aged to elderly adults. The incidence of cirrhosis is 250/100,000 population/year. Cirrhosis is commonly

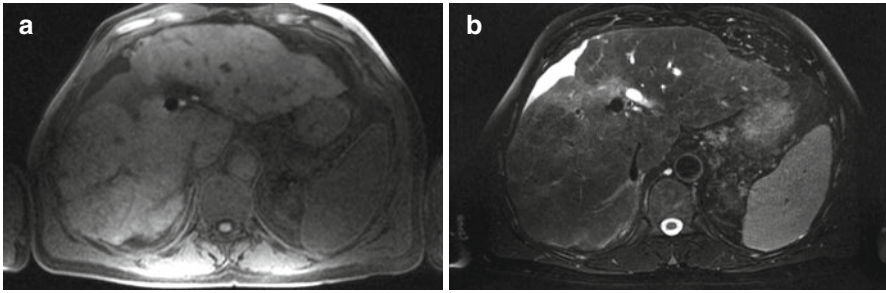


Fig. 8.14 A 75-year-old male subject with diagnosis of cirrhosis based on MR morphology. (a) T1w and (b) T2w images show typical signs of cirrhosis including enlarged left lateral and caudate lobes, irregular surface, and irregular intrahepatic septa

Table 8.5 Morphologic imaging findings in cirrhosis

Liver surface nodularity
Enlargement of the caudate and left lobes
Atrophy of the right lobe
Septations and fibrotic strands within the liver
Diffuse hepatic nodules (regenerative nodules)
Macronodular/micronodular cirrhosis
Dilated portal vein
Splenomegaly
Portocaval collateral circulation
Ascites (advanced cirrhosis)

caused by chronic intake of alcohol or medications or develops secondary to viral hepatitis. Rare etiologies include hepatic iron overload, bile duct diseases (primary biliary cirrhosis, primary sclerosing cholangitis), and autoimmune diseases. Clinical symptoms are nonspecific and occur late in the course of disease. They include fatigue, loss of weight, jaundice, and an increase in body circumference due to ascites in advanced cirrhosis. The morphologic imaging features of cirrhosis are summarized in Table 8.5.

Clinical Management

Cirrhosis is an irreversible damage to liver parenchyma without a chance of cure. Management focuses on stopping exposure to the damaging substance or treating the underlying cause. Most subjects know that they have cirrhosis.

Regenerative nodules can mimic malignant lesions. HCC is associated with cirrhosis in over 80 % of patients. A suspicious lesion detected in a cirrhotic liver should be evaluated by a dynamic contrast-enhanced series.

8.1.7.2 Hepatic Steatosis

Fatty infiltration of the liver is a common incidental finding; it can be caused by diabetes mellitus, obesity, and abuse of alcohol or other chemical substances. Individuals in whom fatty liver progresses to cirrhosis have an increased risk of HCC or may develop fatal liver failure (unless a transplant is available). The reported prevalence ranges between 10–24 % for alcoholic hepatosteatois and 3–58 % for nonalcoholic fatty liver disease (NAFLD) (Angulo 2002; Kojima et al. 2003). This wide variation is mainly attributable to socioeconomic factors (Kojima et al. 2003).

Clinical Management

Incidentally detected fatty liver can usually be left untreated (Fig. 8.15). Nutritional counseling aimed at stopping intake of the damaging substance (alcohol, other chemical substances) and better treatment of underlying disease (diabetes mellitus) are desirable. Focal steatosis and focal sparing can suggest a malignant liver lesion. If malignancy can be reliably ruled out, no further diagnostic tests are required.

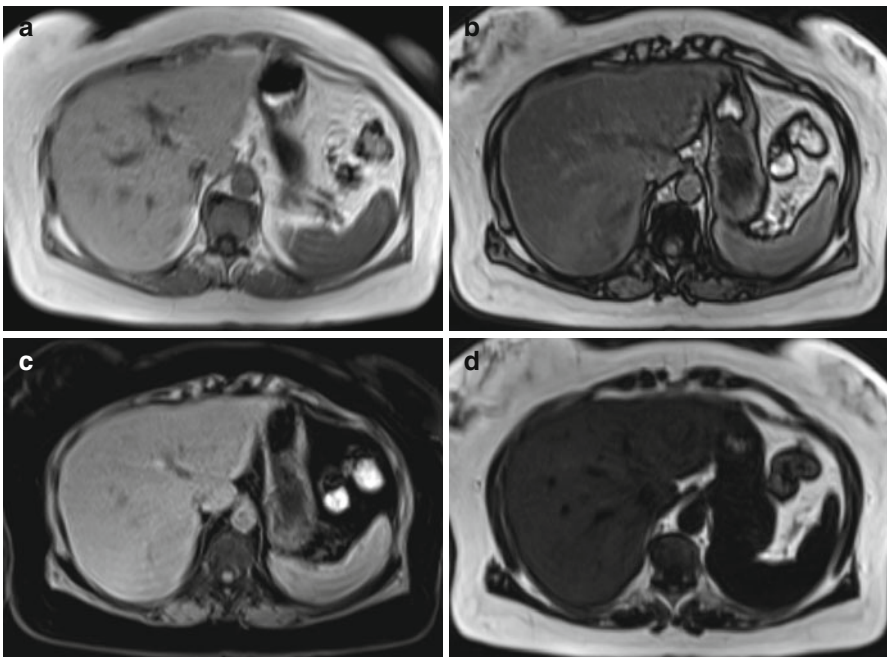


Fig. 8.15 A 56-year-old obese female subject. Chemical shift-encoded MRI allows determination of liver fat. (a, b) Signal intensity drop on out-of-phase images demonstrates diffuse fatty infiltration of the liver. Supplementary fat-saturated (c) and water-saturated (d) images confirm the diagnosis of hepatic steatosis

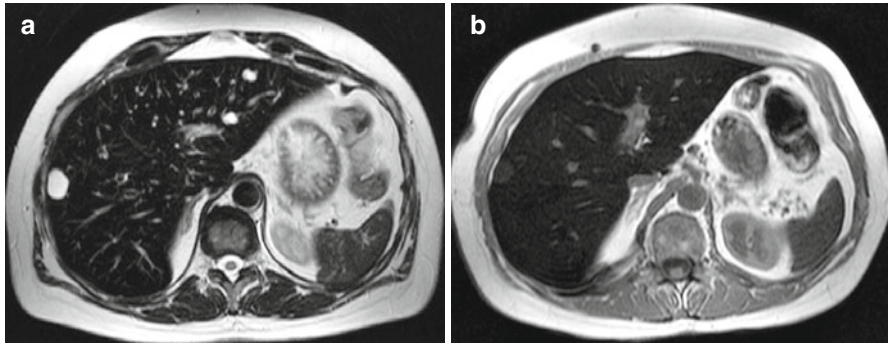


Fig. 8.16 A 45-year-old female subject with incidentally detected iron overload in the liver and spleen. She reports having received repeated blood transfusions for recurrent hemolytic anemia. (a, b) T2w TSE and T1w FLASH images indicate iron overload as a homogeneous signal drop of liver and spleen parenchyma. In addition, there are a total of three cystic masses (liver cysts; differential diagnosis: hemangiomas) in the left hepatic lobe and segment VIII

8.1.7.3 Hepatic Iron Overload

Abnormal iron deposition in the body occurs in primary (genetic) hemochromatosis or as an acquired condition. Acquired iron overload is due to increased intake and accumulation of iron secondary to a known cause such as multiple transfusions (Robson et al. 2000). Iron shortens T2 and T2* relaxation times, resulting in a loss of signal on T1-weighted and T2-weighted MR images (Fig. 8.16). New MRI approaches permit noninvasive quantification of liver iron by measurement of either T2 shortening or T2* decay (FERRISCAN; Gandon et al. 2004). Primary hemochromatosis only affects the liver, while secondary overload is characterized by iron accumulation in the liver, pancreas, spleen, heart, and brain.

Clinical Management

Subjects with suspected iron overload should undergo laboratory tests (transferrin, serum ferritin) to clarify diagnosis. Secondary forms of the disorder can be treated by discontinuing increased intake; an additional measure is to deplete or reduce iron stores.

8.2 The Bile Ducts

While an MRI scan of the liver also includes the bile ducts, the standard liver protocol is not optimized for biliary imaging and therefore only allows for a general assessment. A dedicated MRI examination of the biliary system is

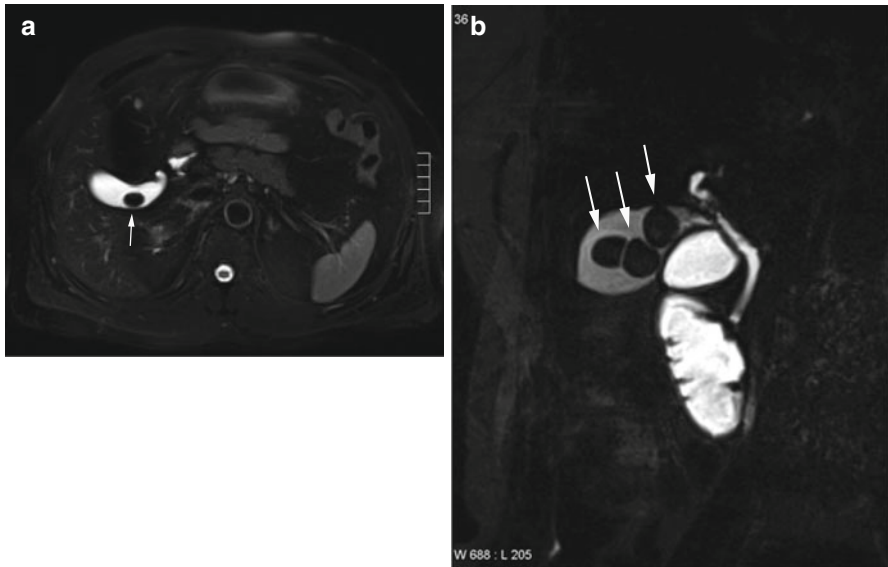


Fig. 8.17 A 62-year-old female subject without symptoms at the time of whole-body MRI screening. Several calculi (*arrows*) are seen within the gallbladder. (a) Axial fat-saturated T2w TSE image depicts bright bile. (b) MRCP can be helpful for detecting calculi near the infundibulum

performed using magnetic resonance cholangiopancreatography (MRCP). MRCP techniques are based on heavily T2-weighted sequences. MRCP can be performed using a projection technique (RARE – rapid acquisition with relaxation enhancement) or multislice imaging, either with a 2-dimensional fast spin echo (FSE) sequence acquired during breath-hold (2–15 s) or with a 3-dimensional FSE sequence (with respiratory trigger or navigator; 3–6 min) (Kim et al. 2005; Soto et al. 2000).

8.2.1 Cholecystolithiasis

Gallstones are common, occurring in 10–15 % of the European population (Aubé et al. 2005) (Fig. 8.17). Risk factors include obesity, diabetes mellitus, bile acid malabsorption in chronic inflammatory bowel disease, multiple pregnancies, age over 40, and genetic factors. Gallstones become symptomatic over time in 15–20 % of affected individuals. Symptoms include bloating after meals, intolerance of fatty foods, and biliary colic. Symptomatic cholecystolithiasis can be complicated by pancreatitis, gallbladder empyema, and gallbladder cancer. The rate of gallbladder carcinoma has been reported to increase to 11 % in women over 60 (Assisi et al. 1998).

Clinical Management

Gallstones are asymptomatic or may cause acute or chronic symptoms. Subjects with asymptomatic disease should be informed so that, if they become symptomatic, prompt treatment can be initiated. Medical litholysis with ursodeoxycholic acid can be contemplated as an additional therapeutic option. Acute symptomatic gallstones are not encountered in the context of screening. Patients with chronic symptomatic gallstones can be operated on after other causes of their symptoms have been ruled out (Escourrou et al. 1984; Tanaka et al. 1987).

8.2.2 Choledocholithiasis

Choledocholithiasis is the presence of at least one gallstone in the common bile duct. Mechanical obstruction of the biliary tree with dilation of intra- and extrahepatic bile ducts is common. Stones frequently arise in the gallbladder (cholecystolithiasis) and migrate into the ducts or form directly within a bile duct. Complications include cholestatic jaundice, cholangitis, and biliary pancreatitis.

Clinical Management

An endoscopic retrograde cholangiography (ERC) with stone extraction is indicated in symptomatic and asymptomatic patients (Neubrand et al. 2000). Postprocedural pancreatitis is observed in 4–40 % of patients, depending on their risk factors (Lieb and Draganov 2007). Therefore, invasive diagnostic/therapeutic ERC is reserved for cases with definitive demonstration of a stone by MRCP.

8.2.3 Cholecystitis

In 90–95 % of cases, inflammation of the gallbladder occurs secondary to cholecystolithiasis or choledocholithiasis (calculous cholecystitis). Acute or subacute symptomatic cholecystitis is unlikely to be encountered in the screening situation while chronic cholecystitis may (Fig. 8.18). Chronic cholecystitis evolves from acute inflammation and is often asymptomatic. Symptomatic patients report pain in the right upper quadrant below the costal arch with radiation into the right shoulder. Complications include acute-on-chronic cholecystitis, concomitant pancreatitis, and gallbladder carcinoma (Levy et al. 2001).

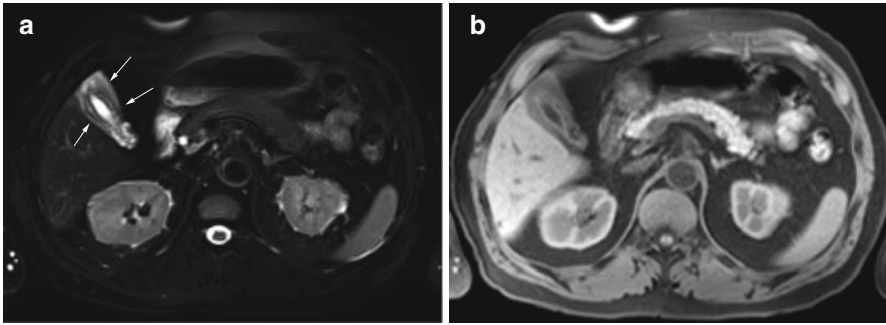


Fig. 8.18 A 54-year-old male subject. When questioned after the whole-body screening examination, he reported a history of recurrent upper abdominal discomfort. Both fat-saturated T2w TSE image (a) and 2D T1w FLASH image (b) depict subacute inflammatory changes and three-layered appearance of the gallbladder wall (*arrows* in a)

Clinical Management

Chronic cholecystitis always requires diagnostic workup or resection of the gallbladder. It cannot be distinguished with certainty from early gallbladder carcinoma (Yun 2003). Porcelain gallbladder is a complication of chronic cholecystitis and has a 60 % risk of malignant transformation.

8.2.4 Other Causes of Dilated Bile Ducts

Dilation of intra- and extrahepatic bile ducts can be caused by mechanical obstruction in choledocholithiasis, inflammatory and postinflammatory strictures, and compression/obstruction by tumor. The extrahepatic bile ducts can dilate after cholecystectomy because they take over the reservoir function of the gallbladder (Fig. 8.19). Postinflammatory strictures and tumors are rare. Flow artifacts and incomplete visualization of the biliary system can mimic stricture or tumor.

Clinical Manifestation

Bile duct dilation in subjects with a history of cholecystectomy and no evidence of another underlying cause requires no medical attention. If a gallstone is identified as the underlying cause, management is the same as for choledocholithiasis (see Sect. 8.2.2). A tumor or suspicious lesion requires diagnostic workup.

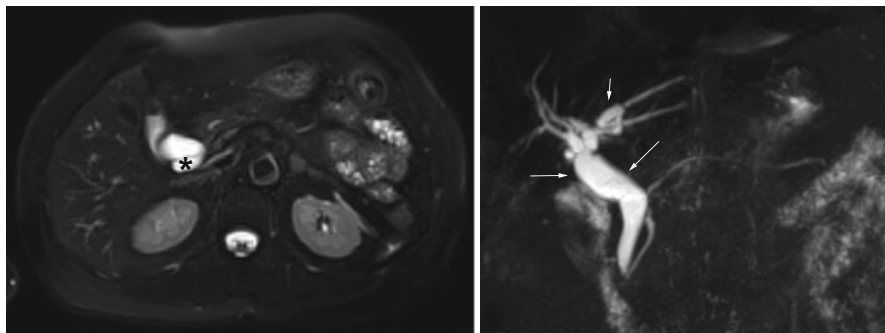
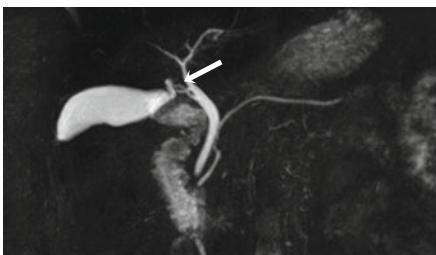


Fig. 8.19 A 73-year-old female subject with history of cholecystectomy; no symptoms at the time of whole-body screening MRI. (a) Fat-saturated T2w TSE image reveals dilation of common bile duct and of cystic duct stump (*asterisk*) after cholecystectomy. (b) MRCP image shows no evidence of intraductal concretions in the common bile duct (*arrow*)

Fig. 8.20 Asymptomatic subject. MIP image from MRCP sequence depicts pancreatic duct and spiral fold of cystic duct (*arrow*)



8.3 The Pancreas

A whole-body MRI protocol includes several non-contrast-enhanced pulse sequences that already allow a fairly comprehensive diagnostic evaluation for pancreatic disease. In case of pancreatic disease, the morphologic information provided by standard pulse sequences is supplemented by evaluation of the biliary tree on MRCP and assessment of possible vascular involvement on the whole-body MR angiogram. MR imaging not only detects endocrine tumors but also improves the identification of smaller lesions, especially cystic alterations, and lipodystrophy (Fig. 8.20).

The symptoms of acute inflammation of the pancreas are so severe that this condition will not be seen in the screening situation. Screening MRI may reveal changes resulting from chronic inflammation and an occasional tumor. Other than pancreas divisum (incomplete fusion) and annular pancreas (forming a ring around the duodenum) (Fig. 8.21), anatomic variants have no clinical relevance (Morgan et al. 1999).

The features of chronic pancreatitis are summarized in Table 8.6. Recurrent inflammation causes progressive pancreatic damage with subsequent loss of

Fig. 8.21 A 42-year-old male subject without complaints. Incidental demonstration of pancreas divisum by secretin-enhanced MRCP (with magnified detail)

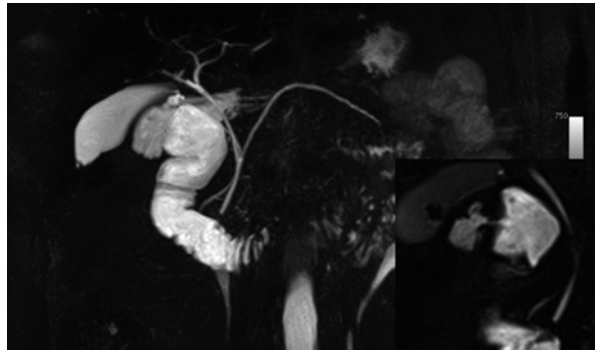


Table 8.6 Chronic pancreatitis

Definition	Irreversible inflammatory damage of the pancreas resulting in decreased enzyme and hormone release
Etiology	75 % of cases worldwide are related to alcohol
Imaging findings	Parenchymal atrophy, ductal dilation, calcifications, fascial thickening, low-signal-intensity parenchyma with focal nodularity, pseudocysts, splenic vein thrombosis, splenomegaly
Clinical presentation	Epigastric pain, which may spread in a girdle-like fashion; weight loss; cholestasis
Prognosis	Poor, often recurrent
Differential diagnosis	Pancreatic cancer, IPMN

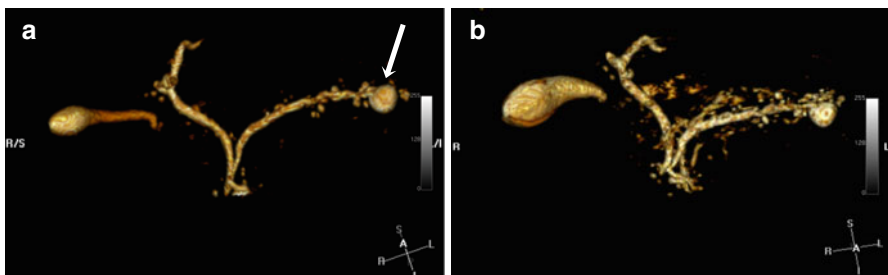


Fig. 8.22 A 42-year-old asymptomatic male subject with moderately severe chronic pancreatitis. (a) Dilated pancreatic duct with irregular side branches and a pseudocyst (<1 cm) in the tail of pancreas (arrow). (b) Reduced secretin-stimulated pancreatic secretion

exocrine function. This parenchymal changes may be difficult to see on MR images. Morphologic abnormalities of the pancreatic ductal system, however, are highly suggestive of chronic pancreatitis. Depending on the stage, changes range from a mildly dilated duct with an enlarged pancreas to the presence of large pseudocysts, intraductal filling defects, and loss of response to secretin stimulation (Figs. 8.22 and 8.23) (Cappelliez et al. 2000).

Fig. 8.23 Chronic pancreatitis with dilated pancreatic duct (*arrow*) and parenchymal atrophy

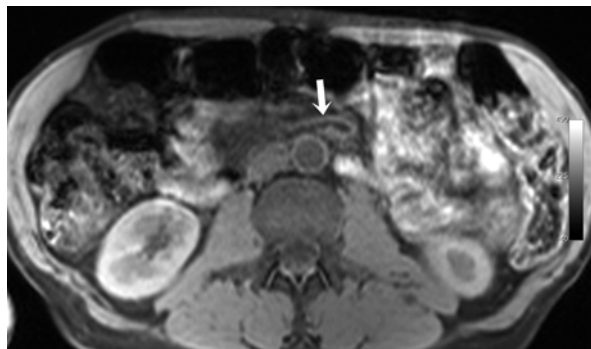


Table 8.7 Pancreatic pseudocysts

Incidence	5–16 % in acute pancreatitis 20–40 % in chronic pancreatitis Up to 75 % in alcohol-induced pancreatitis
Age and sex predilection	Young adults, M > F
Imaging findings	Low T1 signal intensity, high (or intermediate) T2 signal intensity; circumscribed fluid collections with firm fibrous capsule
Clinical presentation	Drinking history, abdominal pain, palpable mass, discomfort varies with cyst size
Complications	Infection, perforation with peritonitis, bile duct obstruction with cholestasis
Prognosis	Spontaneous resolution in 20–40 % of cases; 90 % of patients can be treated with percutaneous/transgastric drainage
Differential diagnosis	Congenital cysts, serous or mucinous cystadenoma, IPMN

8.3.1 Pancreatic Pseudocysts

Up to 50 % of patients with alcohol-induced pancreatitis have pancreatic calcifications, and pseudocysts are observed in approx. 25 % of cases of chronic pancreatitis. Pseudocysts typically arise from necrotic spaces and are primarily seen in alcoholic pancreatitis (Table 8.7). Most pseudocysts do not communicate with the ductal system, allowing excellent detection with an MRCP sequence. Other pancreatic cysts are retention cysts (often communicating with the duct) and congenital cysts. Serous and mucinous cystadenoma and intraductal papillary mucinous neoplasm (IPMN) make up less than 5 % of pancreatic cystic lesions.

8.3.2 Solid Masses

Chronic pancreatitis is at times difficult to differentiate from neoplasm, especially when advanced postinflammatory fibrosis with ductal irregularities is present.

Table 8.8 Pancreatic cancer

Incidence	Adenocarcinoma accounts for 90 % of pancreatic cancers
Age and sex predilection	50–70 years; M:F ratio of 2:1
Imaging findings	Low T1 signal intensity, irregular mass of variable size, little to no contrast enhancement, ductal obstruction, double-duct sign
Location	60 % head, 20 % body, 15 % diffuse, 5 % tail
Clinical presentation	Often asymptomatic, weight loss, pain, jaundice
Prognosis	Poor because of early invasive growth and metastatic spread
Differential diagnosis	Chronic pancreatitis, islet cell tumor, metastasis, lymphoma

A solid mass detected on MRI suggests a malignant tumor. Up to 90 % of pancreatic malignancies are adenocarcinomas of ductal origin, with up to 70 % occurring in the pancreatic head. Mucinous cystic tumors constitute 2 % of pancreatic malignancies. Over two thirds of patients have advanced inoperable pancreatic cancer at the time of diagnosis with a 5-year survival rate of less than 5 % (Schneider et al. 2005). This means that the cancer has already spread to the lymph nodes and often to the retroperitoneum and liver as well. Imaging findings suggesting a tumor include abrupt dilation of the pancreatic duct without concomitant atrophy, demonstration of a circumscribed mass that tends to be of lower signal intensity and does not enhance after contrast medium administration, and the double-duct sign (simultaneous dilation of the common bile and pancreatic ducts). In addition to nonfunctioning tumors, hormonally active neuroendocrine tumors (islet cell tumors) may be found in the pancreas as well, meaning that the diagnostic workup must include hormone testing (Table 8.8).

The wide variety of benign and malignant cystic abnormalities of the pancreas is diagnostically challenging. Therefore, in arriving at a diagnostic classification of a pancreatic tumor, a radiologist must take a comprehensive approach, carefully weighing all relevant factors, which include the subject's sex as well as underlying conditions (alcoholic chronic pancreatitis) (Fernandez-del Castillo et al. 2003; Warsaw et al. 1990).

Clinical Management

An enlarged pancreas demonstrated by screening MRI is most often postinflammatory in nature.

The need for further gastroenterologic evaluation depends on other pancreatic and peripancreatic findings (lymph node status, vascular involvement, ductal congestion no interruption needed).

Adequate staging is necessary to estimate the patient's prognosis, which means that histologic evaluation is urgently recommended if a focal solid pancreatic mass is detected in conjunction with ductal irregularities (double-duct sign) (Balthazar 2002; Lankisch et al. 2001).

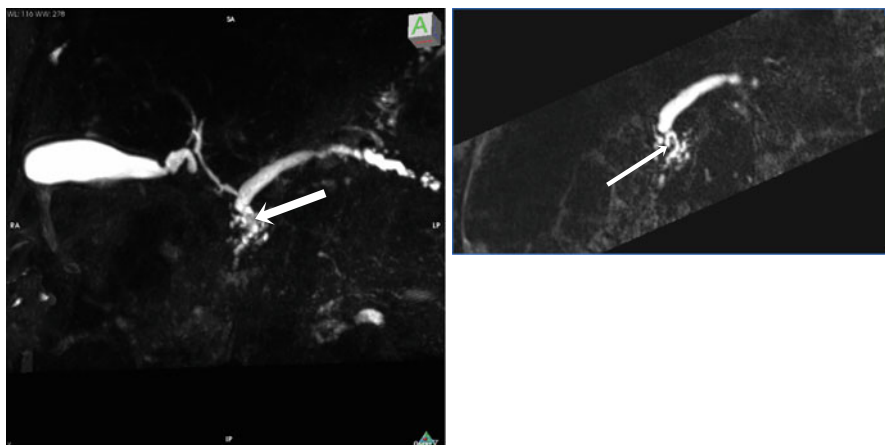


Fig. 8.24 (a) MRCP image demonstrating a calculus (*arrow*) in the pancreatic duct. (b) Magnified detail (MPR)

As already outlined in Sect. 8.2.2 (Cholelithiasis), an MRI diagnosis of concretions (Fig. 8.24) should only prompt an endoscopic retrograde cholangiopancreatography (ERCP) if pertinent clinical symptoms are present or if this invasive procedure is desired by the subject. ERCP can be combined with papillotomy and stone extraction.

A cystic lesion is usually a pseudocyst, which should be followed up sonographically after 3–6 months. Subjects with a cystic lesion larger than 5 cm (risk of rupture) should see a gastroenterologist. The differential diagnosis includes several rare conditions such as serous or mucinous cystadenoma and intraductal papillary mucinous neoplasm (IPMN) (Fernandez-del Castillo et al. 2003; Warshaw et al. 1990; Aghdassi et al. 2006).

8.4 The Spleen

The spleen, the largest lymphatic organ in the human body, has low signal intensity on T1-weighted images and high signal intensity on T2-weighted images compared with the liver (Fig. 8.25).

The spleen is not only involved in the regulation of portal circulation but also plays a role in humoral and cellular immune defense and in hematopoiesis. This functional versatility explains not only the considerable size variation of the normal spleen but also the fact that splenomegaly can have many underlying causes (de Porto et al. 2010). Primary disease of the spleen is uncommon.

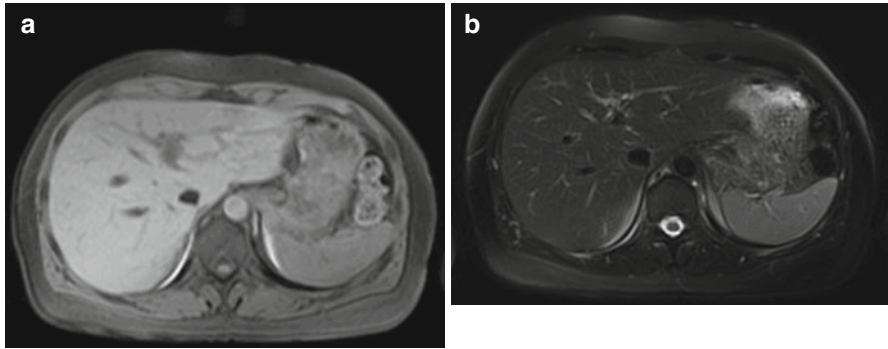
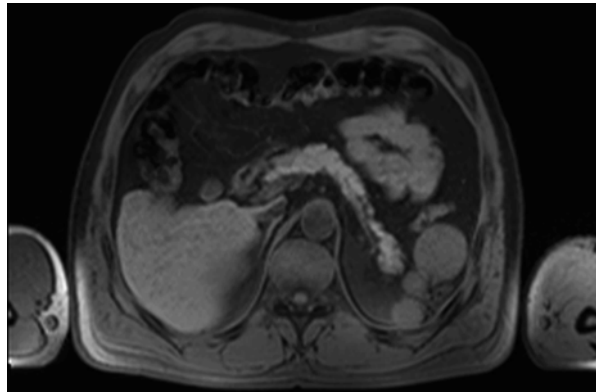


Fig. 8.25 Normal-sized spleen with slightly lower signal intensity relative to liver parenchyma on T1w image (a) and slightly higher signal intensity on T2w image (b)

Fig. 8.26 A 46-year-old female subject with polysplenia, a normal variant detected by screening MRI



8.4.1 Embryonic Development

During fetal life, the spleen has a lobulated contour with deep grooves separating the individual segments. The segments ultimately fuse, and the surface of the spleen becomes smooth. This embryonic development explains the size variability of the spleen and also the possible presence of an accessory spleen. Accessory spleens are a common normal variant and have been found in up to 30 % of individuals, often near the hilum (Sica and Reed 2000).

Complete failure of fusion gives rise to polysplenia (Fig. 8.26). Asplenia may also be seen and is rarely associated with other anomalies (Ivemark syndrome).

Fig. 8.27 A 53-year-old male subject with enlarged spleen revealed on coronal image. The subject's history suggests portal hypertension as the underlying cause



8.4.2 Parenchymal Changes

The normal spleen measures 3–5 cm × 6–8 cm × 10–12 cm. Splenomegaly is diagnosed when the spleen is greater than 14 cm in longitudinal diameter or when its volume exceeds 500 cm³ (Fig. 8.27). In Europe and North America, an enlarged spleen is most commonly found in individuals with portal hypertension. Non-contrast-enhanced pulse sequences do not allow adequate evaluation of the spleen. However, unenhanced images can detect diseases such as liver disease, bone marrow infiltration, varicosis, or vascular thrombosis that cause secondary adenopathy and splenomegaly. Other conditions that can cause parenchymal changes in the spleen are anemia and infections. Splenomegaly secondary to systemic conditions such as hematopoietic disorders is more common than enlargement due to primary splenic disease.

Occasional calcifications seen in the splenic parenchyma (low T1 and T2 signal intensity) may be due to so-called Gamna-Gandy bodies (siderotic nodules), which are small, firm yellow-brown foci occurring chiefly in the spleen (less commonly in the liver and ovaries) and consisting of iron-calcium incrustations of organized blood (Rabushka et al. 1994; Robertson et al. 2001).

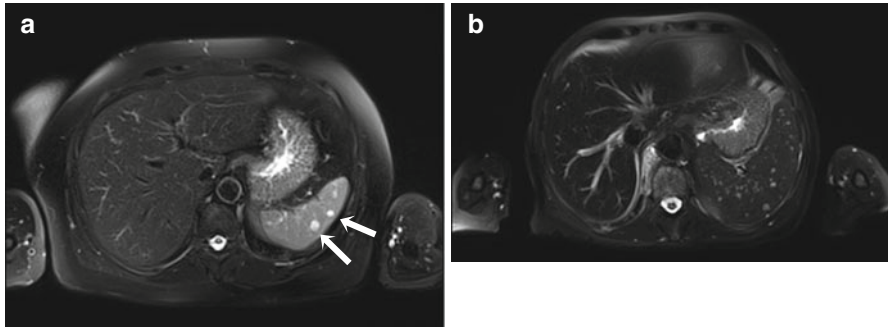
Calcifications in the region of the spleen and splenic hilum are primarily attributable to calcified vessels or a small thrombotic splenic artery aneurysm.

8.4.3 Splenic Cysts

Cysts of the spleen are uncommon, having been found in approx. 0.076 % of autopsies (Robbins et al. 1978). They are asymptomatic and are usually detected incidentally. Splenic cysts include congenital cysts and intrasplenic pseudocysts as well as posttraumatic and degenerative cysts (Table 8.9). Some cysts are sequelae of splenic infarction (Fig. 8.28) (Labruzzo et al. 2002).

Table 8.9 Splenic cysts

Incidence	8/10,000 population
Imaging findings	Sharply demarcated lesion, isointense to fluid, may have capsule
Etiology	Congenital, posttraumatic, postinflammatory, lipoid necrosis
Differential diagnosis	Inflammatory or vascular abnormalities, pseudocysts, neoplasm
Type of lesion	Benign >> malignant
To do	Check history for infection and trauma

**Fig. 8.28** Splenic cysts. (a) Small cysts within the renal parenchyma (*arrows*). (b) Polycystic spleen with secondary splenomegaly**Table 8.10** Solid splenic lesions

Incidence	Very rare
Imaging findings	Often poorly demarcated; tend to have low T1 signal intensity and high T2 signal intensity; contrast-enhanced imaging required for differentiation
Differential diagnosis	Cyst, hemangioma, infection, sarcoidosis
Type of lesion	Benign > malignant
To do	Check history for previous infection and likelihood of malignancy; biopsy may be necessary, depending on clinical presentation

8.4.4 Solid Splenic Lesions

Splenic malignancy may be similar in signal intensity to normal parenchyma on unenhanced T1- and T2-weighted images and typically causes enlargement of the spleen. A dedicated MRI examination may be indicated (Table 8.10). Lymphoma is the most common malignancy of the spleen and includes primary splenic lymphoma and secondary involvement of the spleen in disseminated disease. Cysts are the most common benign tumors (Rabushka et al. 1994; Robertson et al. 2001).

Metastatic spread to the spleen is very rare, occurring in only 7 % of patients with metastatic cancer (breast, lungs, colon, ovaries, and melanoma) (Ito et al. 1997).

Clinical Management

An accessory spleen (splenule) is nonfused splenic tissue in the posterior mesogastrium; it is not a pathology.

Uncomplicated cysts, single or multiple, with typical signal characteristics do not require further investigation or follow-up.

Complicated cysts (e.g., septated or hemorrhagic) should be followed up at 3–6 months or, when echinococcosis is suspected, serologic testing should be ordered.

The list of differential diagnoses for splenomegaly is long, and a supplementary ultrasound examination should be contemplated. If deemed necessary, a dedicated imaging examination after contrast medium administration and hematologic workup should be performed. The underlying causes include portal hypertension, inflammation, and tumors (malignant lymphoma being the most common splenic malignancy).

8.5 The Adrenal Glands

8.5.1 Introduction

Adrenal tumors are often detected incidentally by radiologists. They have been reported to occur in 9 % of the population (Dunnick et al. 1996; Glazer et al. 1982). The most common adrenal masses are benign adenomas and metastases (Table 8.11). Rare adrenal tumors include adrenocortical carcinoma, lymphoma, and pheochromocytoma. On unenhanced MRI, these rare tumors cannot be distinguished from adrenal metastases.

Chemical shift imaging is very useful for characterizing adrenal masses. This technique exploits the fact that, except for a rare lipid-rich metastasis, only benign

Table 8.11 Adrenal lesions in the general population

Entity	Type of lesion	Prevalence	Age predilection	Sex predilection
Adrenal adenoma	Benign	1.5–5.7 %	40–60 years	Women
Adrenal cyst	(incidentaloma)		40–60 years	Women
Pheochromocytoma	10 % are malignant	0.13 %	40–60 years	Women
Adrenal metastasis	Malignant	50–75 % in cancer patients, depending on primary tumor	>50 years	–
Adrenal cancer			Two age peaks: childhood, <50 years	Women

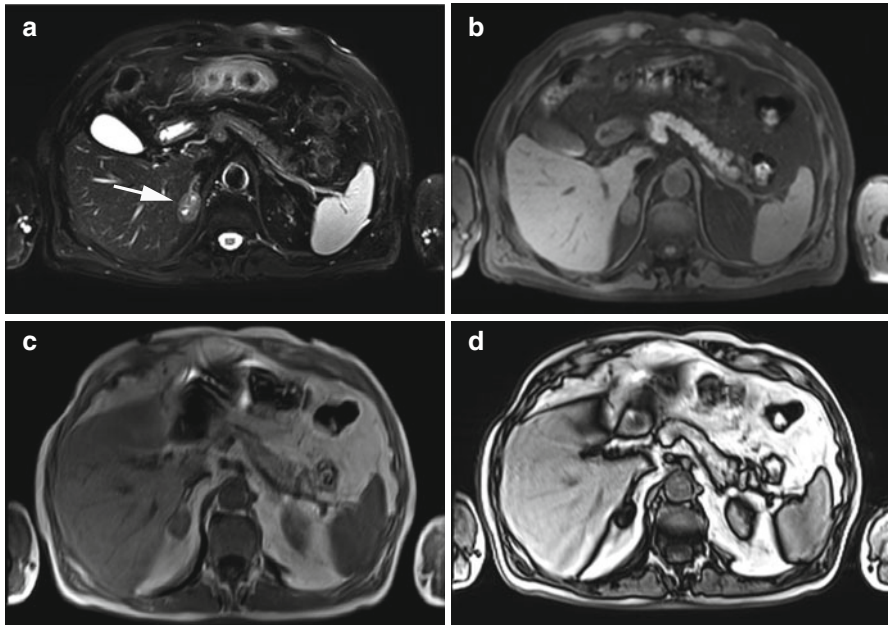


Fig. 8.29 A 65-year-old male subject without symptoms at the time of whole-body screening MRI. (a) Fat-saturated T2w TSE image shows a heterogeneous mass with a liquid center measuring $3.3 \times 2.1 \times 2.5$ cm (arrow). (b) On fat-saturated T1w FLASH image, the mass is isointense to muscle. (c, d) Chemical shift imaging allows characterization of the mass. The characteristic decrease in signal intensity on the out-of-phase image (d) indicates a fatty tumor. The appearance is typical of an adenoma

adrenal tumors contain fat (adenoma, hyperplasia, myelolipoma). Fatty lesions such as adrenal adenomas are identified by their loss of signal intensity on opposed-phase images relative to inphased images. Chemical shift imaging has 90–95 % sensitivity and up to 100 % specificity for differentiating between benign and malignant adrenal tumors (Kreft et al. 1995).

8.5.2 Benign Adrenal Tumors

Benign adrenal tumors include adrenal adenomas and adrenal cysts.

8.5.2.1 Adrenal Adenoma

Adrenal adenoma is the most common benign adrenal tumor with a reported frequency of 2–10 % at autopsy. MRI shows a well-demarcated fatty mass of homogeneous appearance. Adrenal adenomas have a size of 1–8 cm and may be hyperfunctioning or nonhyperfunctioning (Figs. 8.29 and 8.30).

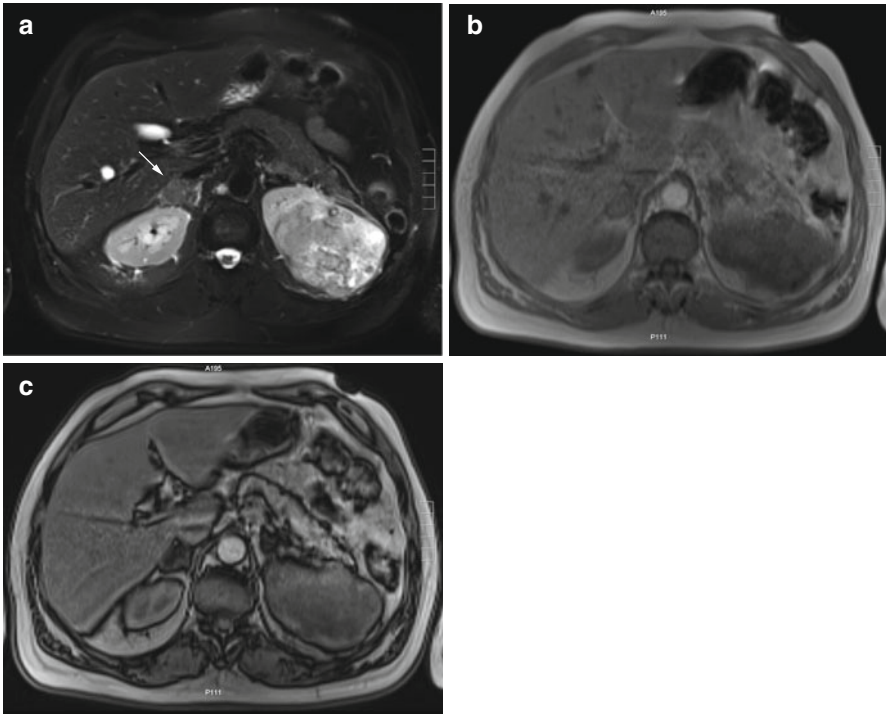


Fig. 8.30 A 63-year-old male subject without symptoms at the time of whole-body screening MRI. (a) Fat-saturated T2w TSE image depicts a heterogeneous mass with central necrosis in the left kidney. The appearance is suspicious for renal cell carcinoma. In addition, a homogeneous mass isointense to muscle is demonstrated in the right adrenal gland (*arrow*). Chemical shift imaging allows discrimination between metastasis and adenoma. The adrenal mass has a signal intensity of 251 (AU) on the inphase image (b) and of 36.3 (AU) on the out-of-phase image (c), ruling out metastasis

Clinical Management

Subjects with an adrenal adenoma larger than 1 cm should undergo hormone testing to rule out hyperfunctioning disease. Most adrenal adenomas smaller than 4 cm are benign but should be followed up (6/12 months). Masses larger than 6 cm require surgery (NIH State-of-the-Science Statement 2002).

8.5.2.2 Adrenal Cysts

Adrenal cysts are very rare. They are asymptomatic and often detected incidentally (Fig. 8.31). A frequency of 0.064–0.18 % has been reported in two autopsy series (Wahl 1951; Hodges and Ellis 1958). They are 2–3 times more common in women aged 40–60 than in men. The widespread use of imaging has led to an increased detection of large adrenal cysts. Adrenal cysts larger than 5 cm have a 7 % risk of malignancy.

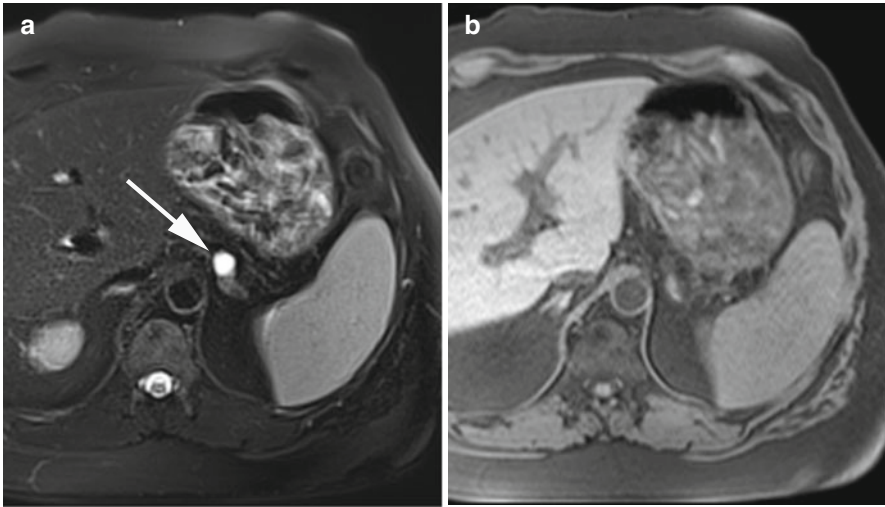


Fig. 8.31 A 45-year-old asymptomatic male subject with incidentally detected cyst of the adrenal gland. (a) Fat-saturated T2w TSE image depicts a smoothly margined lesion measuring 1.1 cm (*arrow*). (b) Fat-saturated 2D T1w FLASH image confirms that the lesion is of adrenal origin

Clinical Management

When MRI detects an adrenal cyst over 5 cm in diameter, laboratory testing is indicated to rule out pheochromocytoma or functioning adrenal carcinoma. Adrenalectomy is indicated when an adrenal cyst causes clinical symptoms, is hyperfunctioning, shows signs of malignancy, or increases in size over time (Banas et al. 2003).

8.5.3 Suspicious Adrenal Tumors

At autopsy, 27 % of all patients with advanced cancer have adrenal metastases (Moulton 1988). The most common primary tumors with metastatic spread to the adrenal glands include lung cancer, breast cancer, melanoma, medullary thyroid cancer, and pancreatic cancer. Primary adrenal cancer and malignant pheochromocytoma (10 %) are rare. These entities cannot be reliably differentiated using MRI (Fig. 8.32).

Clinical Management

Whole-body MR datasets should be evaluated for evidence of a primary tumor. Further diagnostic investigations are warranted for any adrenal mass that cannot be confidently diagnosed as an adenoma on the basis of the MRI appearance.

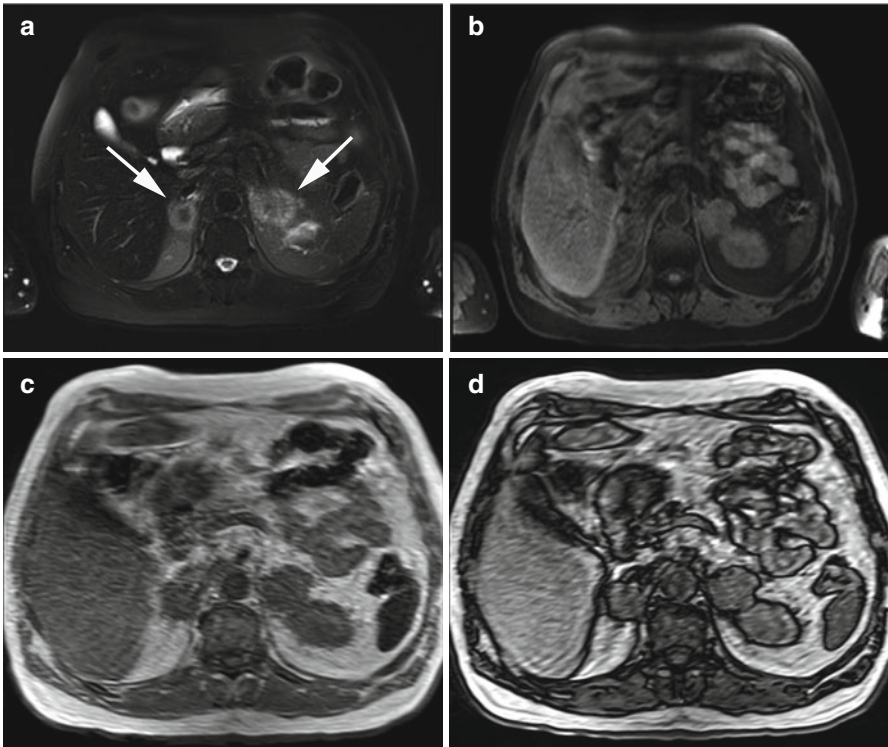


Fig. 8.32 A 68-year-old male subject with incidentally detected lung cancer. (a) Fat-saturated T2w TSE image demonstrates bilateral adrenal masses with lower signal intensity in the center (*arrows*). (b) On fat-saturated T1w FLASH image, the adrenal masses are isointense to muscle. Based on these findings, the masses may be malignant or benign. The masses have the same signal intensity on inphase (c) and out-of-phase (d) images, corroborating the suspicion of bilateral adrenal metastasis

8.6 The Gastrointestinal Tract

8.6.1 Introduction

Whole-body MRI is still limited in evaluating the gastrointestinal (GI) tract, typically because image quality is degraded by inadequate bowel distention and by peristaltic motion (Fig. 8.33). When no contrast medium or spasmolytic agent is used, the detection of GI pathology relies on morphologic information.

8.6.2 Hernias

The tissues normally containing the abdominal organs have several natural openings or weaknesses through which parts of the GI tract can protrude. Herniation of

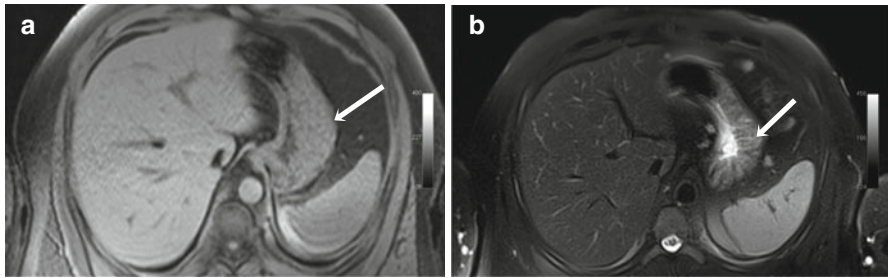


Fig. 8.33 Normal peristaltic contraction makes the gastric wall appear thickened (*arrow*) on fat-saturated T1w image (a). Individual gastric crypts can be appreciated on fat-saturated T2w image (b)

Table 8.12 Hernias

Incidence	M > F; increases with age
Imaging findings	Protrusion of portions of the stomach or intestine through an opening, e.g., through the esophageal hiatus or into the inguinal canal
Etiology	Widening of normal openings in the abdominal wall, loss of elasticity of ligaments, increase in intra-abdominal pressure
Complications	Incarceration, recurrent inflammation (e.g., GERD)
Type of lesion	Benign

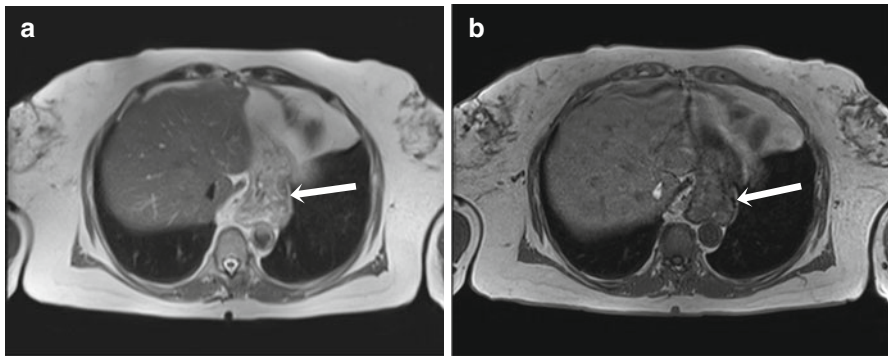


Fig. 8.34 A 68-year-old male subject with axial hernia. A part of the stomach (*arrow*) protrudes into the chest cavity, seen on (a) T2w HASTE image and (b) fat-saturated VIBE image

abdominal contents can occur through such a natural opening or through a congenital or acquired defect (Table 8.12). Most hernias are initially asymptomatic and may be detected incidentally during whole-body imaging. In the upper GI tract, diaphragmatic hernias can occur. Of these, more than 95 % are sliding or axial hernias (Fig. 8.34). Herniation of part or all of the stomach into the chest cavity through the esophageal hiatus is known as thoracic stomach (Fig. 8.35). Inguinal hernias are the most common hernias in the remainder of the GI tract, constituting 75–80 % of cases (5:1 ratio of indirect to direct hernias). Less common types are umbilical and incisional hernias.

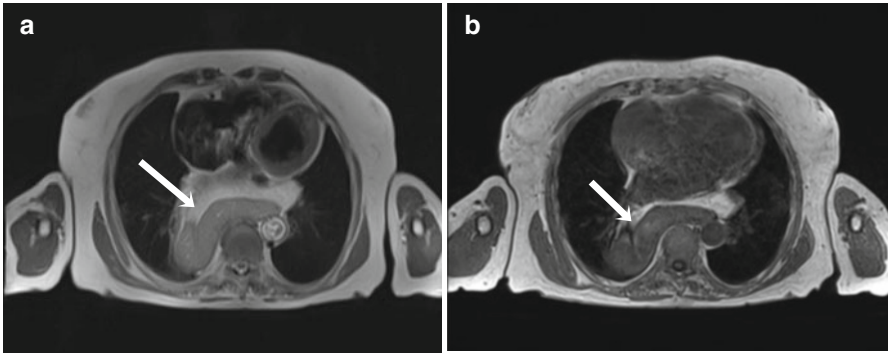


Fig. 8.35 Thoracic stomach (*arrow*) not causing clinical discomfort. There is a large opening in the diaphragm without signs of incarceration. (a) T2-weighted HASTE image; (b) fat-saturated axial VIBE image

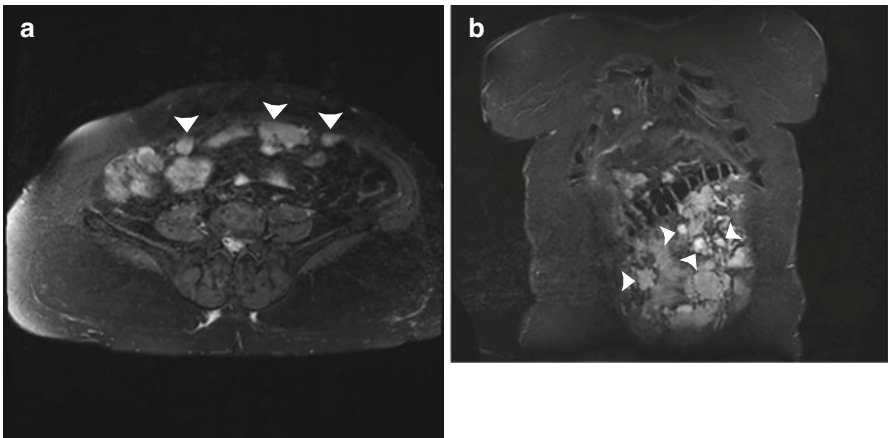


Fig. 8.36 Incidental peritoneal carcinomatosis with nodular peritoneal deposits (*arrows*) on (a) fat-saturated PD image and (b) coronal TIRM image. This 76-year-old woman had undiagnosed ovarian cancer

8.6.3 Peritoneum

Diseases of the abdominal organs or abdominal inflammation can irritate the peritoneum and give rise to free fluid. Peritoneal free fluid detected by imaging may be nonspecific, especially when the amount is small, or it may indicate pathology, primarily pancreatitis, cirrhosis, or tubo-ovarian disease. The peritoneum itself may be thickened. Nodular or diffuse peritoneal thickening is highly indicative of peritoneal carcinomatosis (Fig. 8.36). Circumscribed thickening may also represent a postoperative lesion. Occasionally, images may show isolated nodular or solid densities within the mesentery or at the mesenteric root. These are usually lymph nodes,

rarely residual blood (after surgery or trauma) or metastases. Mesenteric lymph nodes tend to calcify with age.

8.6.4 Stomach

Changes in the gastric wall associated with inflammation are difficult to depict with a cross-sectional imaging modality like MRI. The diagnosis of gastritis is typically suspected on the basis of a patient's history and epigastric symptoms. Occasionally, the diagnosis may be suggested by circumferential thickening of the antral wall or thickening along the greater curvature on MRI. Alternatively, abnormal wall thickening (which must not be confused with transient thickening during peristaltic contraction) may indicate an inflammatory ulcer. This should be considered along with clinical signs and symptoms as *Helicobacter pylori*, which is associated with type B gastritis, is widespread in western countries. Circumscribed thickening of more than 20 mm in the wall of the greater curvature, when accompanied by an irregular contour, may mimic gastric malignancy (Pickhardt and Asher 2003).

Early gastric cancer up to stage IIb or IIc is often missed with cross-sectional imaging (Lee and Ko 1998). MRI and CT, however, have a very important role in evaluating larger GI carcinomas but tend to overestimate T stage and underestimate N stage. A dedicated MRI protocol for gastric cancer evaluation must include a contrast-enhanced pulse sequence (Ziegler et al. 1993; Oi et al. 1997).

When a suspicious gastric mass is detected, imaging evaluation for nodal disease relies on identifying enlarged lymph nodes, with 9 mm as a widely used cutoff. This size criterion has a sensitivity of up to 75 % for detecting metastatic lymph nodes. As with identification of enlarged lymph nodes in other regions, it is important to estimate the transverse diameter and not the longitudinal diameter (Fukuya et al. 1995; Bollschweiler et al. 2001).

8.6.5 Small Intestine

Conditions associated with inflammatory bowel wall thickening, such as terminal enteritis or ulcerative colitis, cause recurrent intestinal problems of which the affected individuals are almost certainly aware. Localized inflammatory wall changes may point to duodenal ulcer but also occur in colitis or portal hypertension.

Occasionally, MRI may show mechanical bowel obstruction. In the routine diagnostic situation, obstruction is attributable to postoperative adhesions in up to 75 % of patients and to intraperitoneal inflammation (appendix, tubes, and ovaries) in 15 % of cases. Only 8 % of these patients have a hernia; in the remainder the cause is congenital or remains unknown (Bizer et al. 1981). When MR images show signs of intestinal obstruction, the radiologist should consider the patient's history and think of an underlying malignancy as a possible cause.

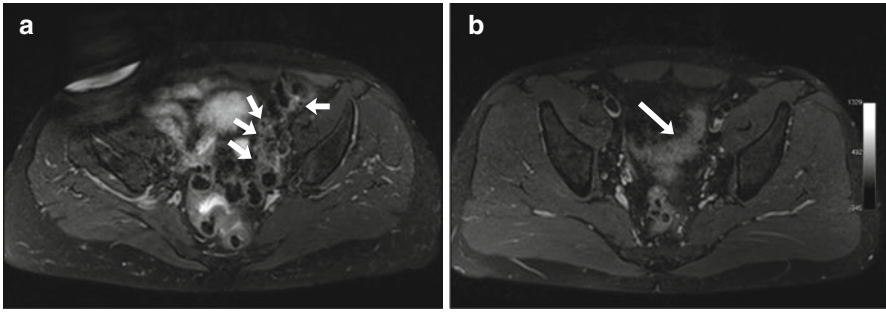


Fig. 8.37 Diverticular outpouchings of the sigmoid colon (*arrows in a*) are common incidental findings on pelvic images. Occasionally, inflammatory wall changes are seen, as illustrated in a second case. The subject has sigmoid diverticulitis (*arrow in b*)

Table 8.13 Diverticula

Incidence	30–50 % of all people over 50 have diverticulosis
Imaging findings	Outpouchings of the intestinal wall, primarily of the sigmoid colon
Complications	Inflammation with wall thickening and infiltration of mesocolic soft tissues or even perforation
Differential diagnosis	Colon cancer, radiation colitis, ischemic colitis
To do	Check history for infection and trauma

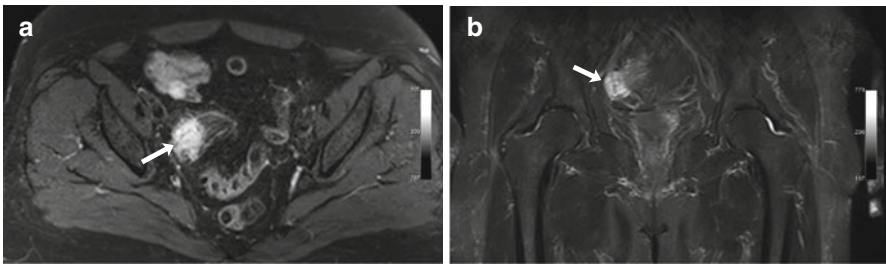


Fig. 8.38 Circumscribed wall abnormalities (*arrow*) involving only a short segment of the colon are highly suggestive of a malignant mass. (**a**) Fat-saturated axial PD image and (**b**) coronal TIRM image

8.6.6 Large Intestine

Colonic diverticula are the most common gastrointestinal abnormalities. They are pseudodiverticula with mucosal and submucosal protrusion through the muscle layers of the colon. Eighty percent of all diverticula will never cause symptoms (Fig. 8.37). About half of the western population over 70 have diverticula (Table 8.13). The condition can cause clinical problems when diverticula become inflamed. Diverticulitis is characterized by inflammatory infiltration of the fatty tissue, pericolonic edema, and involvement of a segment >10 cm. In contrast, an eccentric shouldered stricture of the intestine – the classic apple core appearance – is suspicious for cancer (Figs. 8.38 and 8.39) (Schreyer et al. 2004; Chintapalli et al. 1999) (Table 8.14).

Fig. 8.39 An occasional circumscribed wall thickening of the colon (*arrow*) is difficult to interpret. It may be due to peristaltic contraction or indicate inflammation or tumor

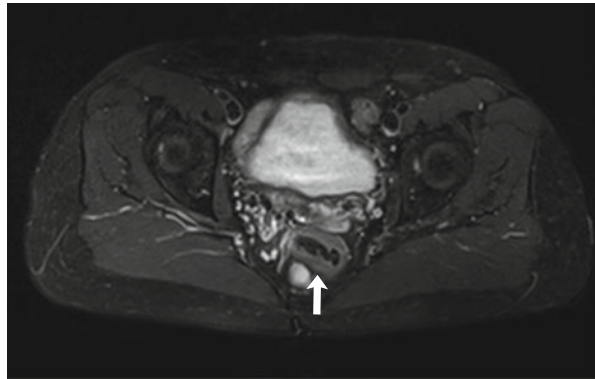


Table 8.14 Colorectal cancer

Incidence	Second most common cancer in men and women (3:2 ratio) in Germany
Imaging findings	Sigmoid > rectum > transverse colon; wall thickening of short segment, possibly with stricture; fat stranding, lymph nodes
Etiology	Adenocarcinoma, adenoma-carcinoma sequence
Differential diagnosis	Diverticulitis, ischemic colitis, infectious colitis
Prognosis	Depends on stage; mean 5-year survival rate of 50 %
To do	Estimate tumor size, search for suspicious lymph nodes and metastatic spread, look for second tumor (up to 10 %)

Clinical Management

Diverticulosis is asymptomatic in 80 % of cases and is noted incidentally.

Most instances of circumscribed thickening of a bowel wall segment on MRI are attributable to peristaltic contractions. The presence of clinical symptoms suggests an inflammatory process. An inflamed diverticulum may become encapsulated and obstruct the bowel.

If imaging demonstrates gastric wall thickening and the patient reports pertinent symptoms, a gastroscopy is warranted for workup because gastric ulcer is considered a precancerous stage of gastric carcinoma and MALT lymphoma.

Nodular mesenteric densities representing lymph nodes can indicate a non-specific, inflammatory process but can also be a sign of metastatic involvement. Proper interpretation of such findings requires that all information available be considered.

If MRI demonstrates mechanical obstruction of the colon, additional diagnostic tests are needed to rule out colon cancer (contrast-enhanced imaging, CT colonography, or an endoluminal diagnostic procedure).

References

- Aghdassi AA, Mayerle J, Kraft M, Sielenkaemper AW, Heidecke CD, Lerch MM (2006) Pancreatic pseudocysts -when and how to treat? *HPB (Oxford)* 8:432–441
- Angulo P (2002) Nonalcoholic fatty liver disease. *N Engl J Med* 346:1221–1231
- Assisi A, Papatzi R, Negri P, Bordoli M, Nardone A, Nespoli A (1998) Acute cholecystitis and gallbladder neoplasms: the experience of 2215 cases. *G Chir* 19:391–394
- Aubé C, Delorme B, Yzet T, Burtin P, Lebigot J, Pessaux P, Gondry-Jouet C, Boyer J, Caron C (2005) MR cholangiopancreatography versus endoscopic sonography in suspected common bile duct lithiasis: a prospective, comparative study. *AJR Am J Roentgenol* 184:55–62
- Balthazar EJ (2002) Acute pancreatitis: assessment of severity with clinical and CT evaluation. *Radiology* 223:603–613
- Banas B, Mussack T, Pfeifer KJ, Wörmlé M, Schmid H (2003) Große Nebennierenzysten: Zunehmende Inzidenz einer häufig malignen Erkrankung. *Dtsch Arztebl* 100:A-921
- Bizer LS, Liebling RW, Delany HM, Gliedmann ML (1981) Small bowel obstruction. *Surgery* 89:407–413
- Blum HE (1995) Variants of hepatitis B, C and D viruses: molecular biology and clinical significance. *Digestion* 56:85–95
- Bollschweiler E, Moenig S, Hoelscher AH (2001) Lymphknotenmetastasierung – Kann man sie vorhersagen? *Der Onkologe* 7:604–609
- Buetow PC, Pantongrag-Brown L, Buck JL, Ros PR, Goodman ZD (1996) Focal nodular hyperplasia of the liver: radiologic-pathologic correlation. *Radiographics* 16:369–388
- Cappellez O, Delhayé M, Deviere J, Le Moine O, Metens T, Nicaise N, Cremer M, Stryuven J, Matos C (2000) Chronic pancreatitis: evaluation of pancreatic exocrine function with MR pancreatography after secretin stimulation. *Radiology* 215:358–564
- Caremani M, Vincenti A, Benci A, Sassoli S, Tacconi D (1993) Ecographic epidemiology of non-parasitic hepatic cysts. *J Clin Ultrasound* 21:115–118
- Carrim ZI, Murchison JT (2003) The prevalence of simple renal and hepatic cysts detected by spiral computed tomography. *Clin Radiol* 58:626–629
- Cherqui D, Rahmouni A, Charlotte F, Boulahdour H, Métreau JM, Meignan M, Fagniez PL, Zafrani ES, Mathieu D, Dhumeaux D (1995) Management of focal nodular hyperplasia and hepatocellular adenoma in young women: a series of 41 patients with clinical, radiological and pathological correlations. *Hepatology* 22:1674–1681
- Chintapalli KN, Chopra S, Ghiatas AA, Esola CC, Fields SF, Dodd GD (1999) Diverticulitis versus colon cancer: differentiation with helical CT findings. *Radiology* 210:429–435
- Chuang WY, Chen TC, Hsu HL, Lee WC, Jeng LB, Huang SF (2002) Liver cell adenoma with concomitant hepatocellular carcinoma: report of two cases. *J Formos Med Assoc* 101:798–802
- de Porto AP, Lammers AJ, Bennink RJ, ten Berge IJ, Speelman P, Hoekstra JB (2010) Assessment of splenic function. *Eur J Clin Microbiol Infect Dis* 29:1465–1473
- de Wilt JH, de Man RA, Laméris JS, Zondervan PE, Tilanus HW, IJzermans JN (1998) Hepatocellular adenoma in 20 patients; recommendations for treatment. *Ned Tijdschr Geneesk* 142:2459–2463
- Dröge C, Löhlein D, Hausamen TU (1996) Acute intrahepatic bleeding in a male patient with focal nodular hyperplasia. *Dtsch Med Wochenschr* 121:902–905
- Dunnick NR, Korobkin M, Francis I (1996) Adrenal radiology: distinguishing benign from malignant adrenal masses. *AJR Am J Roentgenol* 167:861–867
- Eisenberg RL, Margulis AR (1991) Brief history of gastrointestinal radiology. *Radiographics* 11:121–132
- Escourrou J, Cordova JA, Lazorthes F, Frexinos J, Ribet A (1984) Early and late complications after endoscopic sphincterotomy for biliary lithiasis with and without the gallbladder in situ. *Gut* 25:598–602
- Fernandez-del Castillo C, Targarona J, Thayer SP, Rattner DW, Brugge WR, Warshaw AL (2003) Incidental pancreatic cysts: clinicopathologic characteristics and comparison with symptomatic patients. *Arch Surg* 138:427–434

- St Pierre, TG et al (2005) Noninvasive measurement and imaging of liver iron concentrations using proton magnetic resonance. *Blood* 105:855–861. Ferriscan, available under www.ferriscan.com
- Fukuya T, Honda H, Hayashi T, Kaneko K, Tatesho Y, Ro T, Maehara Y, Tanaka M, Tsuneyoshi M, Masuda K (1995) Lymph node metastases: efficacy for detection with helical CT in patients with gastric cancer. *Radiology* 197:705–711
- Gaines PA, Sampson MA (1989) The prevalence and characterization of simple hepatic cysts by ultrasound examination. *Br J Radiol* 62:335–337
- Gandon Y, Olivie D, Guyader D, Aubé C, Oberti F, Sebillé V, Deugnier Y (2004) Non-invasive assessment of hepatic iron stores by MRI. *Lancet* 363:357–362
- Glazer HS, Weyman PJ, Sagel SS, Levitt RG, McClennan BL (1982) Nonfunctioning adrenal masses: incidental discovery on computed tomography. *AJR Am J Roentgenol* 139:81–85
- Grebe P, Schild H, Kreitner KF, Ferber A (1994) The differentiation between benign and malignant liver lesions by unenhanced MRI. *Rofo* 161:412–416
- Hodges FV, Ellis FR (1958) Cystic lesions of the adrenal gland. *Arch Pathol* 66:53–58
- Holzapfel K, Eiber MJ, Fingerle AA, Bruegel M, Rummeny EJ, Gaa J (2012) Detection, classification, and characterization of focal liver lesions: Value of diffusion-weighted MR imaging, gadoteric acid-enhanced MR imaging and the combination of both methods. *37(1):74–82*, doi: [10.1007/s00261-011-9758-1](https://doi.org/10.1007/s00261-011-9758-1)
- Ito K, Mitchell DG, Honjo K, Fujita T, Uchisako H, Matsumoto T, Matsunaga N, Honma Y, Yamakawa K (1997) MR imaging of acquired abnormalities of the spleen. *AJR Am J Roentgenol* 168:697–702
- Kew MC (1998) Hepatitis viruses and hepatocellular carcinoma. *Res Virol* 149:257–262
- Kim HC, Park SJ, Park SI, Park SH, Kim HJ, Shin HC, Bae WK, Kim IY, Lee HK (2005) Multislice CT cholangiography using thin-slab minimum intensity projection and multiplanar reformation in the evaluation of patients with suspected biliary obstruction: preliminary experience. *Clin Imaging* 29:46–54
- Kojima S, Watanabe N, Numata M, Ogawa T, Matsuzaki S (2003) Increase in the prevalence of fatty liver in Japan over the past 12 years: analysis of clinical background. *J Gastroenterol* 38:954–961
- Kreft B, Sommer T, Vahlensieck M, Seewald S, Vetter H, Schild H (1995) Turbo-spin-echo (TSE) sequences with selective fat suppression (SPIR) compared with chemical shift sequences in MRI for differentiation of adrenal tumors. Spectral presaturation by inversion recovery. *Rofo* 162:311–318
- Labruzzo C, Haritopoulos KN, El Tayar AR, Hakim S (2002) Posttraumatic cyst of the spleen: a case report and review of the literature. *Int Surg* 87:152–156
- Lankisch PG, Struckmann K, Assmus C, Lehnick D, Maisonneuve P, Lowenfels AB (2001) Do we need a computed tomography examination in all patients with acute pancreatitis within 72 h after admission to hospital for the detection of pancreatic necrosis? *Scand J Gastroenterol* 36:432–436
- Lee DH, Ko YT (1998) The role of 3D spiral CT in early gastric carcinoma. *J Comput Assist Tomogr* 22:709–713
- Levy AD, Murakata LA, Jr Rohrmann CA (2001) Gallbladder carcinoma: radiologic-pathologic correlation. *Radiographics* 21:295–314
- Lieb JG, Draganov PV (2007) Early successes and late failures in the prevention of postendoscopic retrograde cholangiopancreatography pancreatitis. *World J Gastroenterol* 13:3567–3574
- Morgan DE, Logan K, Baron TH et al (1999) Pancreas divisum: implications for diagnostic and therapeutic pancreatography. *AJR Am J Roentgenol* 173:193–198
- Moulton JS (1988) CT of the adrenal glands. *Semin Roentgenol* 23:288–303
- Neubrand M, Sackmann M, Caspary W, Feussner H, Schild H, Lauchart W, Schildberg FW, Reiser M, Classen M, Paumgartner G, Sauerbruch T (2000) Guidelines by the German Society of Digestive and Metabolic Diseases for treatment of gallstones. German Society of Digestive and Metabolic Diseases. *Z Gastroenterol* 38:449–468
- NIH state-of-the-science statement on management of the clinically inapparent adrenal mass (“incidentaloma”) (2002). *NIH Consens State Sci Statements*. 4–6;19(2):1–25

- Nufer M, Stuckmann G, Decurtins M (1999) Benign liver tumors: diagnosis and therapy- a review. *Schweiz Med Wochenschr* 129:1257–1264
- Oi H, Matsushita M, Murakami T, Nakamura H (1997) Dynamic MR imaging for extraserosal invasion of advanced gastric cancer. *Abdom Imaging* 22:35–40
- Pickhardt PJ, Asher DB (2003) Wall thickening of the gastric antrum as a normal finding: multidetector CT with cadaveric comparison. *AJR Am J Roentgenol* 181:973–979
- Rabushka LS, Kawashima A, Fishman EK (1994) Imaging of the spleen. CT with supplemental MR examinations. *Radiographics* 14:307–332
- Robbins FG, Yellin AE, Lingua RW, Craig JR, Turrill F, Mikkelsen WP (1978) Splenic epidermoid cysts. *Ann Surg* 187:231–235
- Robertson F, Leander P, Ekberg O (2001) Radiology of the spleen. *Eur Radiol* 11:80–95
- Robson KJH, Merryweather-Clarke AT, Pointon JJ et al (2000) Diagnosis and management of haemochromatosis since the discovery of the HFE gene: a European experience. *Br J Haematol* 108:31–39
- Ros PR, Murphy BJ, Buck JL, Olmedilla G, Goodman Z (1990) Encapsulated hepatocellular carcinoma: radiologic findings and pathologic correlation. *Gastrointest Radiol* 15:233–237
- Rückert JC, Kenschake J, Kilian M. <http://www.charite.de/ch/chir/chir/leist/lebzyst.htm>
- Schneider G, Siveke JT, Eckel F, Schmid RM (2005) Pancreatic cancer: basic and clinical aspects. *Gastroenterology* 128:1606–1625
- Schreyer AG, Furst A, Agha A, Kikinis R, Scheibl K, Schölmerich J, Feuerbach S, Herfarth H, Seitz J (2004) Magnetic resonance imaging based colonography for diagnosis and assessment of diverticulosis and diverticulitis. *Int J Colorectal Dis* 19:474–480
- Semelka RC, Sofka CM (1997) Hepatic hemangiomas. *Magn Reson Imaging Clin N Am* 5:241–253
- Shaib Y, El-Serag HB (2004) The epidemiology of cholangiocarcinoma. *Semin Liver Dis* 24:115–125
- Sica GT, Reed MF (2000) Case 27: intrapancreatic accessory spleen. *Radiology* 217:134–137
- Soto JA, Barish MA, Alvarez O, Medina S (2000) Detection of choledocholithiasis with MR cholangiography: comparison of three-dimensional fast spin-echo and single and multi-section half-Fourier rapid acquisition with relaxation enhancement sequences. *Radiology* 215:737–745
- Stocker JT, Ishak KG (1981) Focal nodular hyperplasia of the liver: a study of 21 pediatric cases. *Cancer* 48:336–345
- Strobel D, Bernatik T (2006) Diagnostik bei fokalen Leberläsionen: Stellenwert der Kontrastmittelsonographie. *Dtsch Arztebl* 103:A789–A793
- Sun XJ, Quan XY, Huang FH, Xu YK (2005) Quantitative evaluation of diffusion-weighted magnetic resonance imaging of focal hepatic lesions. *World J Gastroenterol* 11:6535–6537
- Takagi H (1985) Diagnosis and management of cavernous hemangioma of the liver. *Semin Surg Oncol* 1:12–22
- Tanaka M, Ikeda S, Yoshimoto S, Matsumoto S (1987) The long-term fate of the gallbladder after endoscopic sphincterotomy. Complete follow-up study of 122 patients. *Am J Surg* 154:505–509, III
- Trastek VF, van Heerden JA, Sheedy PF 2nd, Adson MA (1983) Cavernous hemangiomas of the liver: resect or observe? *Am J Surg* 145:49–53
- Velázquez RF, Rodríguez M, Navascués CA, Linares A, Pérez R, Sotorriós NG, Martínez I, Rodrigo L (2003) Prospective analysis of risk factors for hepatocellular carcinoma in patients with liver cirrhosis. *Hepatology* 37:520–527
- Wahl HR (1951) Adrenal cysts. *Am J Pathol* 27:758
- Warshaw AL, Compton CC, Lewandrowski K, Cardenosa G, Mueller PR (1990) Cystic tumors of the pancreas. New clinical, radiologic, and pathologic observations in 67 patients. *Ann Surg* 212:432–443

-
- Wittenberg J, Stark DD, Forman BH, Hahn PF, Saini S, Weissleder R, Rummeny E, Ferrucci JT (1988) Differentiation of hepatic metastases from hepatic hemangiomas and cysts by using MR imaging. *AJR Am J Roentgenol* 151:79–84
- Yun EJ (2003) Gallbladder carcinoma and chronic cholecystitis: differentiation with two-phase spiral CT. *Abdom Imaging* 29:102–108
- Ziegler K, Sanft C, Zimmer T, Zeitz M, Felsenberg D, Stein H, Germer C, Deutschmann C, Riecken EO (1993) Comparison of computed tomography, endosonography, and intraoperative assessment in TN staging of gastric carcinoma. *Gut* 34:604–610

Michael Kirsch and Marcel Mohr

9.1 Stenosis

9.1.1 Intracranial Stenosis

Intracranial atherosclerosis is a major cause of stroke, especially in blacks, Asians, and Hispanics. In the Warfarin-Aspirin Symptomatic Intracranial Disease Trial, the 1-year ischemic stroke rate in the territory of a symptomatic intracranial stenosis (50–99 %) was 11 % in patients treated with warfarin and 12 % in patients treated with aspirin (WASID Trial Investigators 2005). Data on asymptomatic intracranial arterial stenosis are limited. Ischemic stroke rates for asymptomatic stenosis have only been reported for the middle cerebral artery, where the rate is 0–1.4 % per year (Kern et al. 2005). Intracranial atherosclerosis is thought to account for approx. 8–10 % of all ischemic strokes in whites (Arenillas et al. 2004). Nevertheless, its true importance in whites tends to be underestimated. A French autopsy study of 339 patients who died of ischemic or hemorrhagic stroke revealed a strikingly high prevalence of intracranial plaque and intracranial stenosis (Mazighi et al. 2008). It is probably safe to assume that intracranial stenosis represents merely the most advanced stage of intracranial atherosclerosis and that nonstenotic disease is far more common (Arenillas 2011).

Three-dimensional time-of-flight magnetic resonance angiography (TOF-MRA) allows good morphologic assessment of stenotic lesions in the proximal intracranial arteries (80–100 % sensitivity, 80–99 % specificity). One must be aware, however, that loss of signal due to turbulent flow or loss of laminar flow in the carotid bulb can simulate narrowing or lead to overestimation of stenosis.

M. Kirsch (✉) • M. Mohr
Institute of Diagnostic Radiology and Neuroradiology, University Medicine Greifswald,
Ferdinand-Sauerbruch-Straße, 17487 Greifswald, Germany
e-mail: kirschm@uni-greifswald.de; marcel.mohr@uni-greifswald.de

Table 9.1 Stenosis of extracranial cerebral arteries

Prevalence	Approx. 0.5 % below age 60, approx. 10 % over age 80; 28 % in patients with PAOD
Location	Extracranial carotid stenosis
Signs and symptoms	Approx. 2 % stroke rate per year when asymptomatic and detected incidentally

Clinical Management

All subjects with asymptomatic stenosis of the carotid artery, the vertebral arteries, or the intracranial circulation should see a neurologist to determine whether other risk factors for cerebrovascular events exist and whether drug therapy or interventional/surgical management is necessary.

9.1.2 Stenosis of Extracranial Cerebral Arteries

The prevalence of extracranial carotid stenosis is approx. 0.5 % in individuals under 60 and increases to approx. 10 % in those over 80. In patients with peripheral arterial occlusive disease, the prevalence may be as high as 28 % (Table 9.1). Risk factors for carotid stenosis include male sex, hypertension, hypercholesterolemia, and smoking. The risk of stroke in subjects with asymptomatic carotid stenosis is low (approx. 2 % per year) but correlates with the degree of stenosis and increases with stenosis progression (Hennerici et al. 1987). Patients with symptomatic internal carotid artery (ICA) stenosis have a markedly higher risk (Anonymous 1998).

Clinical Management

All subjects with asymptomatic stenosis of the carotid artery, the vertebral arteries, or the intracranial circulation should see a neurologist to determine whether other risk factors for cerebrovascular events exist and whether drug therapy or interventional/surgical management is necessary.

9.1.3 Stenosis of Lower Extremity Arteries

Peripheral arterial occlusive disease (PAOD) is an umbrella term for all forms of impaired arterial circulation caused by stenotic or obstructive vascular processes including lesions of the aorta and arteries supplying the extremities (Spengel et al. 2001). Chronic arterial occlusive disease, unlike acute disease, is characterized by slow development of single or multiple stenotic lesions, which in over 90 % of cases affect the arteries of the pelvic region and legs. Steno-occlusive disease of the leg arteries leads to intermittent claudication due to muscle ischemia and increasingly limits the pain-free walking distance. About 20 % of patients with poor circulation of the legs have PAOD (Alexander 1992).

Table 9.2 Stenosis of lower extremity arteries

Prevalence	Age related 2.5 % <60 years 18.8 % >70 years
Location	1. Aortoiliac PAOD 2. Femoropopliteal PAOD 3. Calf and foot (anterior tibial artery > posterior tibial artery > fibular artery)
Signs and symptoms	Asymptomatic incidental finding, reduced walking distance, rest pain, necrosis, gangrene

Three types of occlusive disease of the lower extremities can be distinguished by level of involvement: (1) aortoiliac disease with steno-occlusive lesions in the aorta and/or iliac arteries, (2) femoropopliteal PAOD, and (3) PAOD of more distal arteries (calf and foot). Only about one third of PAOD patients have ischemic symptoms (McDermott et al. 2002). Many patients limit their activities to reduce PAOD-related symptoms. Initially, they report feeling well but when questioned admit that they can only walk a short distance (Table 9.2).

The prevalence of stenotic and occlusive lesions of the distal leg varies with age and sex and also depends on the presence of risk factors (Kannel et al. 1970). The leading risk factors are smoking, diabetes mellitus, arterial hypertension, hyperlipoproteinemia, hypercholesterolemia, and hyperfibrinogenemia. The prevalence is 2.5 % before age 60 and as high as 18.8 % in those over 70 (Kannel 1996). Half of patients with lower leg occlusion have diabetes mellitus (Albers et al. 2005; Hirsch et al. 2005; Schneider et al. 1993).

PAOD patients have an increased risk of cerebrovascular and cardiovascular events (Criqui et al. 1997; Ness and Aronow 1999); the risk is the same regardless of whether they are symptomatic or asymptomatic (Hooi et al. 1998, 2001). Hence, the traditional concept of asymptomatic PAOD seems to downplay the risk. Patients with chronic PAOD have a mortality rate of over 20 % in the first year after diagnosis (Hirsch et al. 2005). Atherosclerotic occlusion most commonly affects the anterior tibial artery, followed by the posterior tibial artery and the fibular artery. Occlusion of a single calf artery with patency of the other branches is clinically silent. MR angiography with administration of gadolinium-based contrast medium is comparable to digital subtraction angiography (DSA) in terms of specificity and sensitivity for anatomic localization and grading of stenosis severity (Fig. 9.1).

Evaluation of vascular disease of the upper extremities was not part of the whole-body MRI protocol used.

Clinical Management

Multiple occlusions of lower leg arteries can be treated medically, interventional, or surgically. The best treatment should be determined by interdisciplinary consensus on the basis of clinical parameters.

When no symptoms are present or when the subject feels well, management focuses on identifying and reducing risk factors such as smoking, diabetes

mellitus, hypertension, and hyperlipoproteinemia. These risk factors should be screened for in a thorough history and brought to the subject's attention.

An inexpensive and simple test for evaluating arterial insufficiency is to determine the ratio of ankle systolic pressure to brachial systolic pressure, the ankle-brachial index (ABI). An ABI of 1.00–1.29 is considered normal, while values between 0.5 and 1.0 indicate moderate PAOD. Values below 0.4 suggest an increased risk of developing rest pain and ischemic necrosis (Hirsch et al. 2005). Another measure of disease severity is the distance an individual can walk without pain.

Treatment of Fontaine stage 2 disease is primarily physical and medical and aims at reducing or eliminating risk factors.

Chronic stage 3 and 4 occlusions require interventional or surgical revascularization but are unlikely to be encountered as incidental findings in the screening situation or in epidemiologic studies of healthy subjects.

Fig. 9.1 Stenosis (*arrow*) of the left superficial femoral artery on MIP image



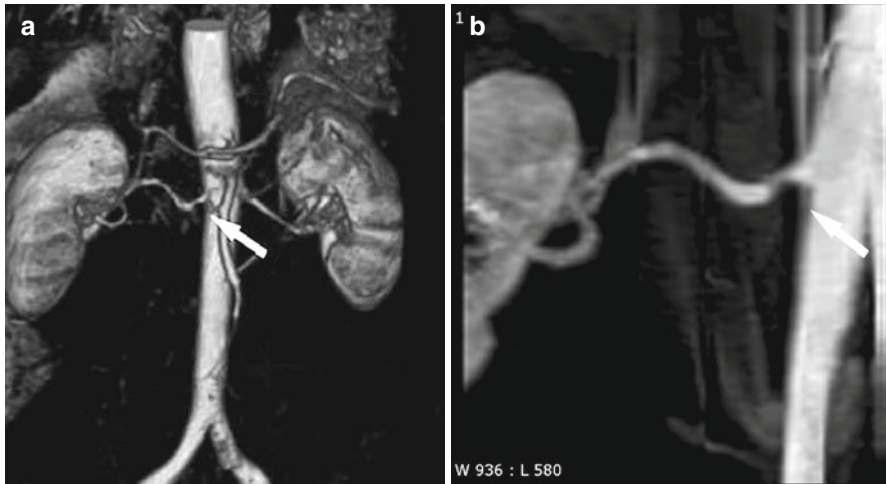


Fig. 9.2 Right-sided RAS (*arrow*) on VRT (a) and MIP (b) images

9.1.4 Renal Artery Stenosis

A prevalence of renal artery stenosis (RAS) of 6.8 % has been reported by Hansen et al. (2002), but in high-risk groups, it may be as high as 50–70 % (Schwartz and White 1964; Harding et al. 1992; Weber-Mzell et al. 2002; Jean et al. 1994). Roughly two thirds of renal artery stenoses are due to atherosclerotic plaques, and one third of these are bilateral. Fibromuscular dysplasia accounts for the other third. Uni- or bilateral RAS underlies the development of arterial hypertension in 1–5 % of cases. Fibromuscular dysplasia is the predominant cause of RAS in young patients, usually women aged 20–40, and tends to affect the distal renal arteries. New-onset hypertension or progression of known hypertension in older individuals is mostly attributable to atherosclerotic stenosis, which typically involves the proximal renal arteries (Fig. 9.2).

Clinically, RAS may be asymptomatic or may present with renovascular hypertension or renal dysfunction. Mixed forms are also possible (Balk et al. 2006; Safian and Textor 2001). RAS greater than 70 % is considered hemodynamically relevant.

Clinical Management

In the routine diagnostic setting, mild hypocalcemia, which indicates activation of the renin-angiotensin-aldosterone system, can alert the physician to the diagnosis of renal artery stenosis. Several tests are available to assess renin release. The sensitivity and specificity of plasma renin activity measurement can be improved by furosemide stimulation. When renin in renal vein blood is determined separately for each side, a ratio of renin levels ≥ 1.5 (stenotic versus non-stenotic side) is considered abnormal. An abnormal ratio and an absolute increase in plasma renin activity reliably predict RAS as the underlying cause of hypertension – a condition that is potentially curable by surgery or angioplasty.

9.1.5 Mesenteric Artery Stenosis

An acute ischemic event is not likely to be encountered in the classic screening situation. It is more likely to incidentally detect chronic mesenteric stenosis promoting or maintaining ischemia of upper abdominal organs and of the small and large intestines (abdominal angina).

The incidence of chronic occlusive disease of a mesenteric artery is approx. 5 % in patients presenting with abdominal pain of unknown cause. Because chronic occlusion progresses slowly and collaterals provide compensatory blood supply, the imaging appearance or autopsy findings do not tend to correlate with the clinical picture. Mesenteric stenosis is present in 80 % of individuals over 60 but rarely becomes clinically apparent. Symptoms do not develop unless there is appreciable ischemia in a target organ, which in turn requires a high-grade stenosis of at least 70 % (Luther 2001).

Clinical Management

There are four clinical stages of chronic mesenteric ischemia:

1. Asymptomatic stage
2. Intermittent abdominal complaints (abdominal angina, recurrent organ insufficiency)
3. Abdominal pain at rest
4. Ischemic organ lesion (infarct)

A typical manifestation is postprandial abdominal pain persisting for 3–4 h after eating. Chronic visceral artery occlusion is characterized by the classic triad of abdominal pain, weight loss, and paraumbilical murmur.

An asymptomatic individual (stage 1) needs no treatment. Stage 2 and 3 disease is an absolute indication for treatment, and stage 4 is an emergency.

9.2 Aneurysm

9.2.1 Intracranial Aneurysm

Time-of-flight MR angiography (TOF-MRA) of the intracranial arteries is a suitable screening tool for intracranial aneurysms (Raaymakers et al. 1999) (Fig. 9.3). The wide range of sensitivities (74–100 %) reported for aneurysm detection by MRA is in part attributable to the investigation of different patient populations (ruptured versus nonruptured aneurysm) and technical advances. The TOF-MRA technique used here offers better resolution than contrast-enhanced MRA (CE-MRA). Unlike CE-MRA, TOF-MRA is not limited by a narrow imaging window (which requires careful bolus timing) and thus avoids the problem of venous overlay in aneurysm imaging (Ozsarlak et al. 2004).

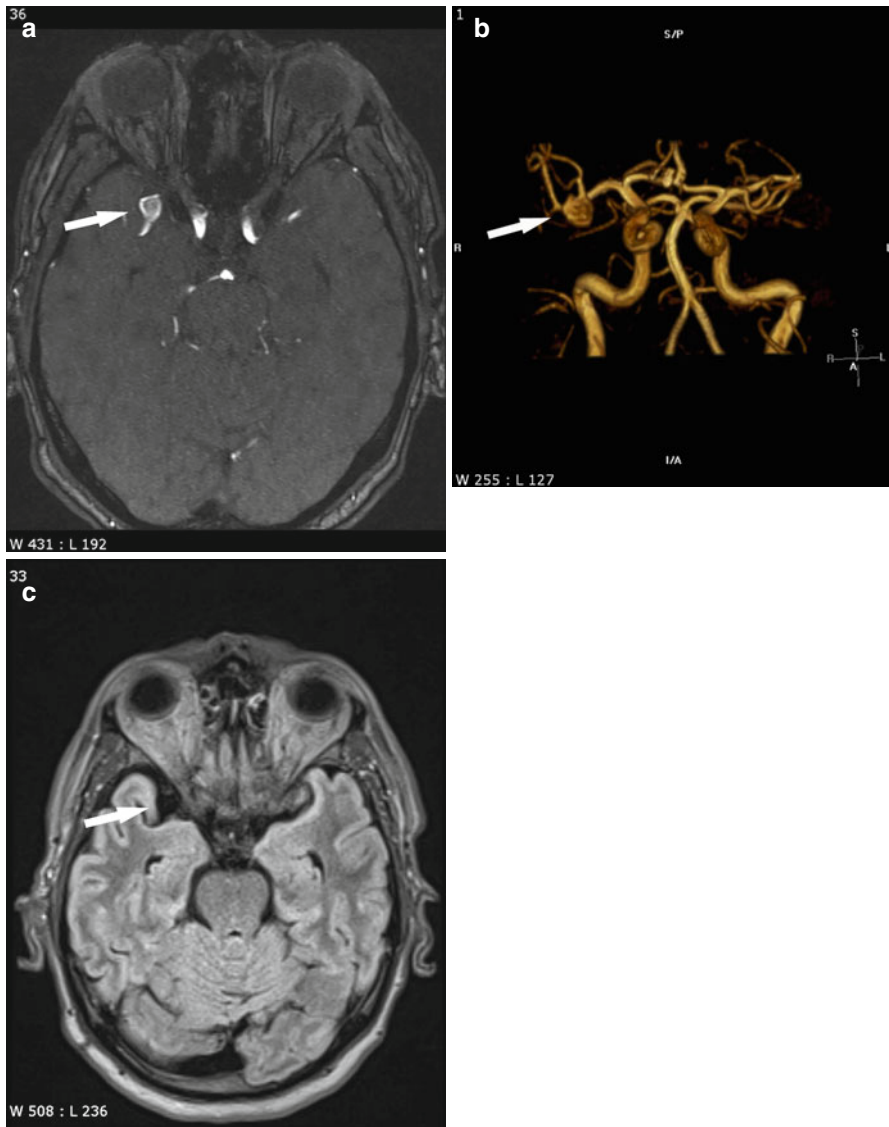


Fig. 9.3 Right-sided middle cerebral artery bifurcation aneurysm (*arrow*) on TOF (**a**) and VRT (**b**) images. The FLAIR image (**c**) shows normal flow void

Intracranial aneurysm is the most common cause of acute subarachnoid hemorrhage (SAH) and/or intracerebral bleeding, accounting for about 75 % of cases. Aneurysmal bleeding is estimated to occur in approx. 5–10 cases/100,000 population per year (Rinkel et al. 1998). The estimated prevalence of cerebral aneurysm is approx. 2.3 % in the adult population (Rinkel 2008). Most cerebral aneurysms are

Table 9.3 Intracranial aneurysm

Frequency	2.3 % An estimated 1.5–2 mill. Germans harbor aneurysms
Location	Carotid territory (85–95 %): anterior communicating and anterior cerebral arteries (approx. 40 %), posterior communicating and internal carotid arteries (approx. 30 %), middle cerebral artery (approx. 20 %) Vertebrobasilar territory (approx. 5–15 %): basilar artery (approx. 10 %), vertebral artery (approx. 5 %) Multiple aneurysms (approx. 20–30 %)
Signs and symptoms	Most common cause of subarachnoid hemorrhage (SAH) and/or intracerebral hemorrhage (75 %) Frequency of aneurysmal hemorrhage: 5–10/100,000 population/year

small and are located in the anterior circulation. In Germany, it is assumed that approx. 1.5–2 million individuals have aneurysms, among them 30 % with multiple aneurysms (Table 9.3).

Clinical Management

When imaging detects an incidental intracranial aneurysm, the possible complications of a preventive neurosurgical or endovascular intervention must be weighed against the risks of death or disability from future aneurysm rupture. Patient age is the most important factor in decision-making: the benefits of preventive treatment are high in young individuals, while the risks related to treatment are relatively low. With increasing age and decreasing life expectancy, however, the benefits of prophylactic intervention decrease, and the risk of complications increases (Rinkel 2008). Other factors to be considered in the decision include the presence of additional aneurysms and comorbidity.

9.2.2 Aortic Aneurysm

Contrast-enhanced whole-body MR angiography allows excellent evaluation, especially of the great arteries. An aneurysm is defined as a circumscribed fusiform or saccular dilation with a diameter of at least 3 cm in the abdominal aorta and at least 2 cm in the pelvic aorta (which corresponds to twice the normal width of these aortic segments). Accounting for over 60 % of all aneurysms, infrarenal aneurysm is the most common type involving the great vessels. The male-to-female ratio is 6:1. The prevalence of abdominal aortic aneurysm (AAA) is about 1 % after age 50 and can be as high as 10 % in hypertensive men over 65. The annual rupture rate in individuals harboring an aneurysm is 2.2 % (Brown and Powell 1999). The main risk factors are male sex, smoking, and age over 65 (Table 9.4).

Isolated pelvic artery aneurysms are rare, constituting only 1.3 % of all aneurysms. Over 50 % of pelvic artery aneurysms occur in individuals with a concomitant infrarenal aneurysm. Thoracic aortic aneurysms are less common than infrarenal aortic aneurysms. Their incidence is 6 per 100,000 population per year but is on the rise (Olsson et al. 2006).

Table 9.4 Aortic aneurysm	Frequency	Infrarenal aneurysms account for 60 % of all aneurysms
	Prevalence	Approx. 1 % over age 50 10 % over age 65
	Sex predilection	M:F ratio of 6:1

Table 9.5 Aneurysm of lower extremity arteries	Frequency	3–7 % of all patients with AAA
	Signs and symptoms	Thromboembolism and thrombosis

Clinical Management

The aim of treating an asymptomatic aneurysm is to prevent rupture or rare embolic events. The UK Small Aneurysm Trial has revealed that, for abdominal aortic aneurysms (AAA) <5.5 cm, early open surgery offers no survival advantage over regular sonographic follow-up (The UK Small Aneurysm Trial Participants 1998). Hence, current recommendations in Europe suggest elective treatment for AAA \geq 5.5 cm in transverse diameter (Hirsch et al. 2005). Definitive specific data on the best time for endovascular intervention are still lacking, which is why the recommendations are based on the existing indications for open surgery (Diehm 2009). Patients with untreated AAA are recommended to undergo regular sonographic monitoring. Morphologic risk factors for AAA rupture include diameter, shape, and growth rate. The rupture risk is approx. 3 % for aneurysms with diameters of 4.0–4.9 cm, 10 % for AAA diameters of 5.0–5.9 cm, and more than 60 % for diameters >7 cm. While fusiform aneurysms rarely rupture, the risk is much higher for saccular aneurysms and penetrating aortic ulcers.

9.2.3 Aneurysm of Lower Extremity Arteries

Concomitant aneurysms of femoral or popliteal arteries are present in 3–7 % of patients with AAA. Popliteal aneurysms, with an estimated incidence of 0.1–2.8 %, account for approx. 70 % of all lower extremity aneurysms. Unlike aortic aneurysms, which tend to grow and rupture, the natural history of popliteal aneurysms is associated with the risk of thromboembolism and thrombosis (Table 9.5).

Clinical Management

A popliteal aneurysm with a size of 2 cm or more should be operated on due to the risk of thromboembolic complications with possible limb loss. Subjects with asymptomatic dilation of the popliteal artery to twice its normal diameter are recommended to undergo an annual ultrasound examination. Individuals harboring a femoral or popliteal artery aneurysm benefit from antiplatelet therapy.

Table 9.6 Aneurysm of visceral and renal arteries

Frequency	60 % of visceral aneurysms occur in the splenic artery, 20 % in the hepatic artery; renal artery aneurysms are rare (incidence of 0.09 %)
Sex predilection	Most common in multiparous women
Signs and symptoms	Chronic development with upper abdominal pain, acute risk of rupture

9.2.4 Aneurysm of Visceral and Renal Arteries

Visceral and renal artery aneurysms are rare. They are most commonly found in multiparous women (Trastek et al. 1982; Cohen and Shamash 1987). Approx. 60 % of all visceral aneurysms occur in the splenic arteries, followed by aneurysms of the hepatic artery (20 %) (Table 9.6). Partial thrombosis is not uncommon and may obscure the aneurysm on MR angiograms; a thrombotic aneurysm may be easier to detect as an inhomogeneous mass related to an artery on T1-weighted and T2-weighted images (typically high T1 signal intensity and low T2 signal intensity).

Clinical Management

Approx. 20 % of patients with a splenic artery aneurysm either develop chronic upper abdominal pain or present with acute rupture. Open surgery or endovascular treatment of visceral aneurysms is probably indicated in women beyond reproductive age and in men when the diameter exceeds 2 cm. With definitive data still lacking, decisions on the treatment of visceral and renal artery aneurysms must be made on a case-by-case basis taking an interdisciplinary approach.

9.3 Cervical Artery Dissection

The incidence of carotid artery dissection is low with an estimated incidence of 2.6 per 100,000 inhabitants per year in a population-based study conducted in North America (Lee et al. 2006). A dissection may, however, go unnoticed when clinical symptoms are mild or absent, meaning that the true incidence is probably higher. Vertebral artery dissection is less common compared with other localizations (1/100,000/year). The typical imaging findings include long, tapering luminal narrowing, vascular occlusion, and pseudoaneurysm. Wall hematoma may be apparent on MR angiography due to high signal intensity resulting from T1 shortening. The typical appearance combines dilation of the dissected vessel with sickle-shaped wall hematoma and reduced residual lumen. The intimal flap is usually visualized when there is flow in both the true and false lumens.

Clinical Management

Asymptomatic carotid dissection is a very rare event, accounting for only approx. 6 % of all cases of carotid dissection (Lee et al. 2006). Hence, there are no definitive guidelines for the management of such lesions. In line with the recommendations for symptomatic cervical dissection, a limited course of antithrombotic therapy has been proposed to prevent ischemic events.

References

- Albers M, Romiti M, Brochado-Neto FC, Braganca Perira CA (2005) Meta-analysis of alternate autologous vein bypass to infrapopliteal arteries. *J Vasc Surg* 42:449–455
- Alexander K (1992) Krankheiten der Arterien. In: Siegenthaler W, Kaufmann W, Hornbostel H, Waller HD (eds) *Lehrbuch der inneren Medizin*, 3rd edn. Thieme, Stuttgart/New York
- Anonymous (1998) Randomised trial of endarterectomy for recently symptomatic carotid stenosis: final results of the MRC European Carotid Surgery Trial (ECST). *Lancet* 351:1379–1387
- Arenillas JF (2011) Intracranial atherosclerosis: current concepts. *Stroke* 42(1 Suppl):S20–S23
- Arenillas JF, Molina CA, Chacón P, Rovira A, Montaner J, Coscojuela P, Sanchez E, Quintana M, Alvarez-Sabín J (2004) High lipoprotein (a), diabetes, and the extent of symptomatic intracranial atherosclerosis. *Neurology* 63:27–32
- Balk E, Raman G, Chung M, Ip S, Tatsioni A, Alonso A, Chew P, Gilbert SJ, Lau J (2006) Effectiveness of management strategies for renal artery stenosis: a systematic review. *Ann Intern Med* 145:901–912
- Brown LC, Powell JT (1999) Risk factors for aneurysm rupture in patients kept under ultrasound surveillance. UK Small Aneurysm Trial Participants. *Ann Surg* 230:289–296, discussion 296–297
- Cohen JR, Shamash FS (1987) Ruptured renal artery aneurysms during pregnancy. *J Vasc Surg* 6:51–59
- Criqui MH, Denenberg JO, Langer RD et al (1997) The epidemiology of peripheral arterial disease: importance of identifying the population at risk. *Vasc Med* 2:221–226
- Diehm N (2009) Abdominal aortic aneurysm. *Internist (Berl)* 50:972–978
- Hansen KJ, Edwards MS, Craven TE et al (2002) Prevalence of renovascular disease in the elderly: a population-based study. *J Vasc Surg* 36:443–451
- Harding MB, Smith LR, Himmelstein SI et al (1992) Renal artery stenosis: prevalence and associated risk factors in patients undergoing routine cardiac catheterization. *J Am Soc Nephrol* 2:1608–1616
- Hennerici MG, Hülsbömer HB, Hefter H et al (1987) Natural history of asymptomatic extracranial arterial disease. Results of a long-term prospective study. *Brain* 110:777–791
- Hirsch AT, Haskal ZJ, Hertzner NR, Bakal CW, Craeger MA et al (2005) ACC/AHA 2005 practice guidelines for the management of patients with peripheral arterial disease. *Circulation* 113:e463–e654
- Hooi JD, Stoffers HE, Kester AD et al (1998) Risk factors and cardiovascular diseases associated with asymptomatic peripheral arterial occlusive disease. The Limburg PAOD Study. *Peripheral Arterial Occlusive Disease. Scand J Prim Health Care* 16:177–182
- Hooi JD, Kester AD, Stoffers HE et al (2001) Incidence of and risk factors for asymptomatic peripheral arterial occlusive disease: a longitudinal study. *Am J Epidemiol* 153:666–672
- Jean WJ, al-Bitar I, Zwicke DL et al (1994) High incidence of renal artery stenosis in patients with coronary artery disease. *Cathet Cardiovasc Diagn* 32:8–10

- Kannel WB (1996) The demographics of claudication and the aging of the American population. *Vasc Med* 1:60–64
- Kannel WB, Skinner JJ Jr, Schwartz MJ et al (1970) Intermittent claudication: incidence in the Framingham Study. *Circulation* 41:875–883
- Kern R, Steinke W, Daffertshofer M, Prager R, Hennerici M (2005) Stroke recurrences in patients with symptomatic vs asymptomatic middle cerebral artery disease. *Neurology* 65:859–864
- Lee VH, Brown RD, Mandrekar JN, Mokri B (2006) Incidence and outcome of cervical artery dissection: a population-based study. *Neurology* 67:1809–1812
- Luther BLP (2001) Intestinale Durchblutungsstörungen, Mesenterialinfarkt, Angina abdominalis. Therapieoptionen, Prognosen. Steinkopff, Darmstadt
- Mazighi M, Labreuche J, Gongora-Rivera F, Duyckaerts C, Hauw JJ, Amarenco P (2008) Autopsy prevalence of intracranial atherosclerosis in patients with fatal stroke. *Stroke* 39:1142–1147
- McDermott MM, Ferrucci L, Simonsick EM et al (2002) The ankle brachial index and change in lower extremity functioning over time: the Women's Health and Aging Study. *J Am Geriatr Soc* 50:238–246
- Ness J, Aronow WS (1999) Prevalence of coexistence of coronary artery disease, ischemic stroke, and peripheral arterial disease in older persons, mean age 80 years, in an academic hospital-based geriatrics practice. *J Am Geriatr Soc* 47:1255–1256
- Olsson C, Thelin S, Ståhle E et al (2006) Thoracic aortic aneurysm and dissection: increasing prevalence and improved outcomes reported in a nationwide population-based study of more than 14,000 cases from 1987 to 2002. *Circulation* 114:2611–2618
- Ozsarlak Ö, von Goethem JW, Maes M, Parizel PM (2004) MR angiography of the intracranial vessels: technical aspects and clinical applications. *Neuroradiology* 46:955–972
- Raaymakers TW, Buys PC, Jr Verbeeten B et al (1999) MR angiography as a screening tool for intracranial aneurysms: feasibility, test characteristics, and interobserver agreement. *AJR Am J Roentgenol* 173:1469–1475
- Rinkel GJ (2008) Natural history, epidemiology and screening of unruptured intracranial aneurysms. *J Neuroradiol* 35:99–103
- Rinkel GJ, Djibuti M, Algra A, van Gijn J (1998) Prevalence and risk of rupture of intracranial aneurysms: a systematic review. *Stroke* 29:251–256
- Safian RD, Textor SC (2001) Renal-artery stenosis. *N Engl J Med* 44:431–442
- Schneider JR, Walsh DB, McDaniel MD, Zwolak RM, Besso SR, Cronenwett JL (1993) Pedal bypass versus tibial bypass with autogenous vein: a comparison of outcome and hemodynamic results. *J Vasc Surg* 17:1029–1040
- Schwartz CJ, White TA (1964) Stenosis of renal artery: an unselected necropsy study. *Br Med J* 5422:1415–1421
- Spengel, FA, Diehm C, Heidrich H, Schulte KL, Theiss W (2001) Diagnostik und Therapie der arteriellen Verschlusskrankheit der Becken-Beinarterien. *VASA* 30(Suppl 57):1–20
- The UK Small Aneurysm Trial Participants (1998) Mortality results for randomised controlled trial of early elective surgery or ultrasonographic surveillance for small abdominal aortic aneurysms. *Lancet* 352:1649–1655
- Trastek VF, Pairolero PC, Joyce JW et al (1982) Splenic artery aneurysms. *Surgery* 91:694–699
- WASID Trial Investigators (2005) Comparison of warfarin and aspirin for symptomatic intracranial arterial stenosis. *N Engl J Med* 352:1305–1316
- Weber-Mzell D, Kotanko P, Schumacher M et al (2002) Coronary anatomy predicts presence or absence of renal artery stenosis: a prospective study in patients undergoing cardiac catheterization for suspected coronary artery disease. *Eur Heart J* 23:1684–1691

Katrin Hegenscheid and Martin Petrik

10.1 Introduction

Recent developments such as continuous table movement and the use of whole-body or phased-array coils in whole-body imaging have opened new horizons for MRI examinations of patients with suspected musculoskeletal disease.

MRI is well established for imaging individual anatomic regions, especially the joints and spine. Compared with other imaging modalities, MRI has the advantage of providing detailed images of bone structures and soft tissues, enabling highly sensitive and specific detection of abnormalities without radiation exposure.

A 1.5-Tesla whole-body MRI system equipped with 32 high-frequency channels allows simultaneous connection of 76 coil elements for complete high-resolution head-to-toe coverage in only 15 min using a fat-suppressed coronal short-tau inversion recovery (STIR) sequence. This survey scan can be used for orientation and for prescribing subsequent pulse sequences that target specific regions of the body according to the diagnostic question that needs to be answered. Musculoskeletal imaging should always be performed with a combination of T1- and T2-weighted pulse sequences in different planes. The spine is best imaged using sagittal T1-weighted spin echo (SE) and T2-weighted turbo spin echo (TSE) sequences. Coronal and axial fat-suppressed T1-weighted SE images acquired after IV administration of contrast medium are especially useful for detecting bone and soft tissue metastases but also for evaluating patients with inflammatory muscle and joint conditions. However, diagnostic evaluation of the small joints, such as the elbow, hand, and foot joints, is limited. Positioning for whole-body imaging often precludes visualization of these joints with enough detail. This is why additional pulse sequences are required for adequate evaluation of subjects with suspected rheumatic disease.

K. Hegenscheid (✉) • M. Petrik
Institute of Diagnostic Radiology and Neuroradiology,
University Medicine Greifswald, Ferdinand-Sauerbruch-Straße,
Greifswald 17487, Germany
e-mail: katrin.hegenscheid@uni-greifswald.de; martin.petrik@uni-greifswald.de

Musculoskeletal abnormalities are common incidental findings on screening MRI – in persons undergoing cardiovascular or cancer screening, for example. On the other hand, adequate evaluation and characterization of such findings may be limited because whole-body MRI is performed using protocols that have been optimized for the detection of extramusculoskeletal pathology. In individuals in whom MRI demonstrates degenerative changes in the joints and spine, there is often a striking discrepancy between the MRI appearance and the clinical presentation. In the screening situation, such incidental findings pose a challenge not only because they are difficult to interpret but even more so in terms of deciding about the need for further workup. This chapter provides an overview of the most common incidental findings of the musculoskeletal systems, discusses the possibilities and limitations of whole-body MRI, and makes recommendations on how to handle these findings (Vanel et al. 2009).

10.2 The Skeletal System

10.2.1 Bone Tumors and Tumorlike Lesions

Tumors and tumorlike lesions of bone are typically solitary and include primary tumors arising from bone tissue and secondary, metastatic bone tumors. Most primary bone tumors are benign (Subhas et al. 2009). In adults, primary bone tumors constitute only 1 % of all malignancies. Primary bone tumors tend to occur at typical sites and in certain age groups. Moreover, they tend to have a specific sex distribution and present with characteristic symptoms. Knowledge of these details helps the radiologist narrow the differential diagnosis. Primary bone tumors are differentiated from tumorlike lesions (Abdel Razek and Castillo 2010). According to their tissue of origin, bone tumors are classified as bone-forming, cartilage-forming, and fibrous tumors (Greenspan and Remagen 1998; Dorfman et al. 1998).

Coronal STIR sequences are used for the initial search in different screening scenarios (Delorme and Baur-Melnyk 2011; Schmidt et al. 2009). They have high sensitivity and diagnostic accuracy as well as excellent positive and negative predictive values for the detection of bone metastases (e.g., in patients with breast or prostate cancer) and for the diagnostic evaluation of patients with malignant bone marrow disorders such as malignant lymphoma or plasmacytoma (Delorme and Baur-Melnyk 2011; Kwee et al. 2011; Collins 2010; Abdel Razek and Castillo 2010; Schmidt et al. 2009; Mehta et al. 1995). STIR sequences are characterized by high spatial resolution, rapid acquisition, and high sensitivity for tissues with high fluid content (Schmidt et al. 2005; Ghanem et al. 2005). They are less sensitive for identifying sclerotic processes or fatty lesions. Therefore, for an adequate musculoskeletal evaluation, STIR imaging needs to be supplemented by T1-weighted pulse sequences to ensure highly sensitive and specific characterization of bone lesions. Signal intensities on STIR images allow a crude classification of the most common incidental skeletal findings (Fig. 10.1). Common incidental lesions that appear

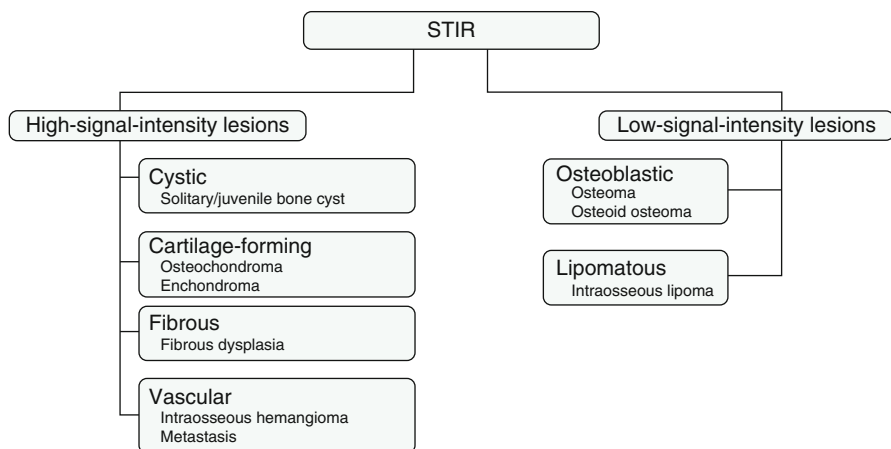


Fig. 10.1 Classification of common incidental bone lesions according to signal intensity on STIR images

Table 10.1 Juvenile/solitary bone cyst

Prevalence	3 % of all primary bone lesions
Age predilection	Occurs at any age, most commonly between 10 and 20 years
Sex predilection	M:F ratio of 2–3:1
Location	Typically metaphyseal, may extend to diaphysis 60–80 % humerus and femur 20–40 % calcaneus, talus, iliac bone
Type of lesion	Benign
Signs and symptoms	Asymptomatic incidental finding Pathologic fracture (66 %)
Differential diagnosis	Aneurysmal bone cyst, enchondroma, nonossifying fibroma

bright on STIR images include cystic lesions such as solitary bone cysts, cartilaginous lesions such as enchondroma or osteochondroma, fibrous conditions such as fibrous dysplasia, and highly cellular lesions such as hemangioma and metastasis. Common incidental abnormalities with low signal intensity are bone-forming lesions such as osteoma and osteoid osteoma and lipomatous lesions such as intraosseous lipoma (Abdel Razeq and Castillo 2010).

10.2.1.1 Tumorlike Bone Lesions

10.2.1.1.1 Juvenile/Solitary Bone Cyst

Juvenile or solitary bone cysts are tumorlike lesions of unclear etiology (Table 10.1). They are sharply demarcated and contain fluid, making them appear bright on T2-weighted images (Fig. 10.2). On T1-weighted images, these cysts

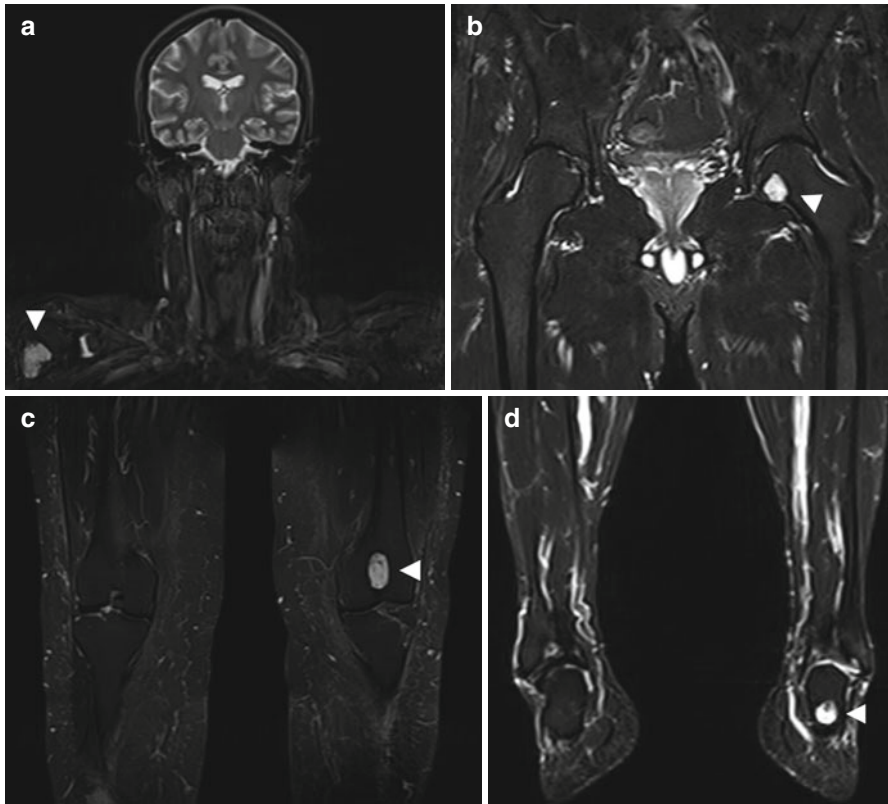


Fig. 10.2 Incidental screening findings (STIR). Solitary bone cysts (*arrowheads*) in different locations: in the right humeral head in a 46-year-old female subject (**a**), in the left femoral head in a 52-year-old male subject (**b**), in the left distal femoral metaphysis in a 43-year-old female subject (**c**), and in the left calcaneus in a 65-year-old male subject (**d**)

have intermediate to low signal intensity. Complications such as pathologic fracture or intralesional hemorrhage may result in an inhomogeneous appearance. Fluid levels or septa may also be present. Thinning of surrounding bone is common. A contrast-enhanced examination is only necessary in cases where a solid lesion cannot be ruled out with certainty. Simple bone cysts typically do not enhance (Lokiec and Wientroub 1998).

Clinical Management

Solitary bone cysts are benign lesions with no risk of malignancy. They usually stop growing with skeletal maturity and require no further diagnostic evaluation (Lokiec and Wientroub 1998).

Table 10.2 Intraosseous hemangioma/lipoma

	Hemangioma	Lipoma
Prevalence	10 %	0.1 %
Age predilection	Occurs at any age, with a peak at ages 20–60	5–75 years
Sex predilection	M:F ratio of 1:1.5–2	M:F ratio of 1:1
Location	Spine, 28 % Skull, 20 % Ribs, clavicle, mandible Long bones May be multifocal	Metaphysis of long bones, 60 % Calcaneus Ribs Pelvis Spine
Type of lesion	Benign	Benign
Signs and symptoms	Asymptomatic incidental finding Rarely pathologic fracture, spinal compression syndrome	Asymptomatic incidental finding Pain, swelling

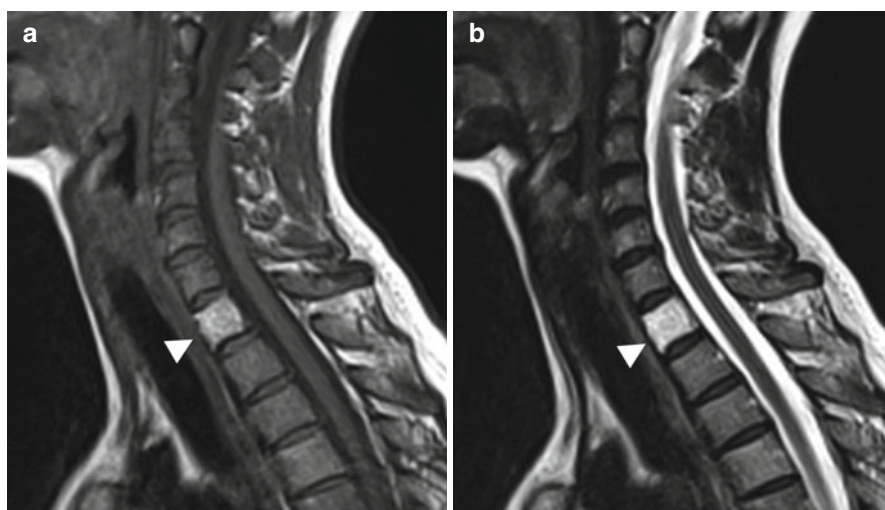


Fig. 10.3 Incidental screening finding. Vertebral hemangioma in a 45-year-old male subject. The hemangioma (*arrowhead*) involves the entire vertebral body, which has high signal intensity on sagittal T1w TSE image (a) and sagittal T2w TSE image (b)

10.2.1.1.2 Intraosseous Hemangioma/Lipoma

Hemangiomas are benign tumors composed of small blood vessels that are commonly found in the vertebral bodies (Table 10.2) but also occur in the appendicular skeleton (Rigopoulou and Saifuddin 2012). The vascular components have high T1 and T2 signal intensity, while thickened trabeculae have low signal intensity (Fig. 10.3). The thickened trabeculae are typically oriented vertically, resulting in a corduroy appearance on sagittal images and a polka dot pattern on axial images

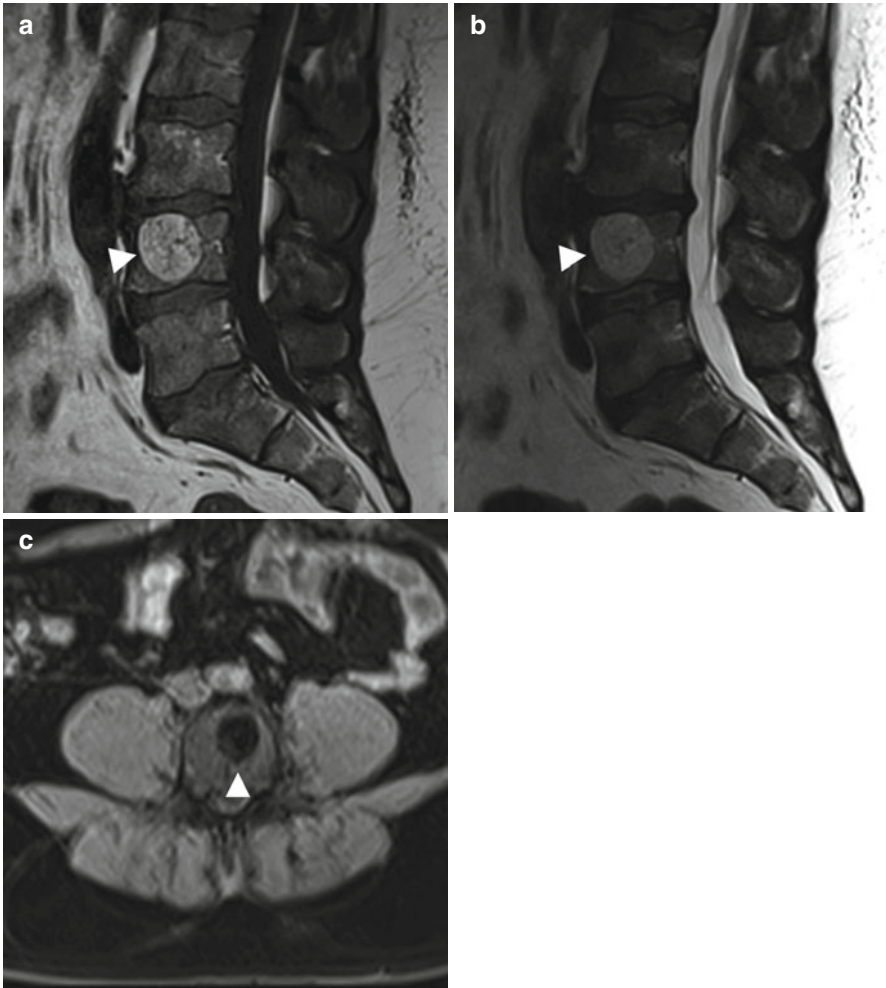


Fig. 10.4 Incidental screening finding. Intraosseous lipoma (*arrowhead*) in L4 in a 65-year-old subject. The lesion has the same signal intensity as fat on all pulse sequences, i.e., high signal intensity on T1w (**a**) and T2w (**b**) images (both sagittal TSE) and low signal intensity on fat-suppressed image (axial T1w TSE) (**c**)

(Friedman 1996). A fat-suppressed pulse sequence allows differentiation of intraosseous hemangioma from lipoma, which has the same signal intensity as subcutaneous fat (Fig. 10.4) (Williams et al. 1993; Blacksin et al. 1995). Following IV injection of contrast medium, the vascularized components of a hemangioma enhance strongly, while a lipoma does not enhance at all (Williams et al. 1993; Blacksin et al. 1995).

Clinical Management

When a small asymptomatic lipoma or hemangioma is detected, no diagnostic or therapeutic procedures are required. Malignant transformation has not been described for hemangioma and is extremely rare in lipoma. Lesions that are symptomatic or pose a risk of pathologic fracture can be treated by curettage and bone grafting.

Table 10.3 Osteochondroma (osteocartilaginous exostosis)

Prevalence	Most common benign tumor 12 % of all bone tumors 45 % of all benign bone tumors
Age predilection	10–35 years
Sex predilection	M:F ratio of 1.8–2:1
Location	Any bone that undergoes endochondral ossification Metaphysis of long bones Femur, tibia, humerus, hands and feet Rarely pelvis, scapula
Type of lesion	Benign; malignant transformation very rare Stops growing with skeletal maturity
Signs and symptoms	Often painless swelling Symptoms due to compression of nerves or vessels or limitation of joint motion
Differential diagnosis	Parosteal osteosarcoma, chondrosarcoma, juxtacortical myositis ossificans

10.2.1.2 Cartilage-Forming Bone Tumors**10.2.1.2.1 Osteochondroma (Osteocartilaginous Exostosis)**

Osteochondroma is a sessile or pedunculated bone tumor composed of normal cortical and medullary bone (Table 10.3). It is typically contiguous with the cortex and medullary cavity of the underlying parent bone (Fig. 10.5a, b), and its bony portions have the same signal intensity as the parent bone (Fig. 10.5c, d) (Greenspan 1989; Unni 2001). Osteochondromas have an overlying hyaline cartilage cap approx. 1 – 3 mm in thickness. The cap has the characteristic MR signal intensity of well-differentiated cartilage tumors, i.e., intermediate signal intensity on T1-weighted images and very high signal intensity on T2-weighted images (Fig. 10.5d). The cap is often surrounded by a delicate band of low signal intensity, which corresponds to perichondrium (Mehta et al. 1998).

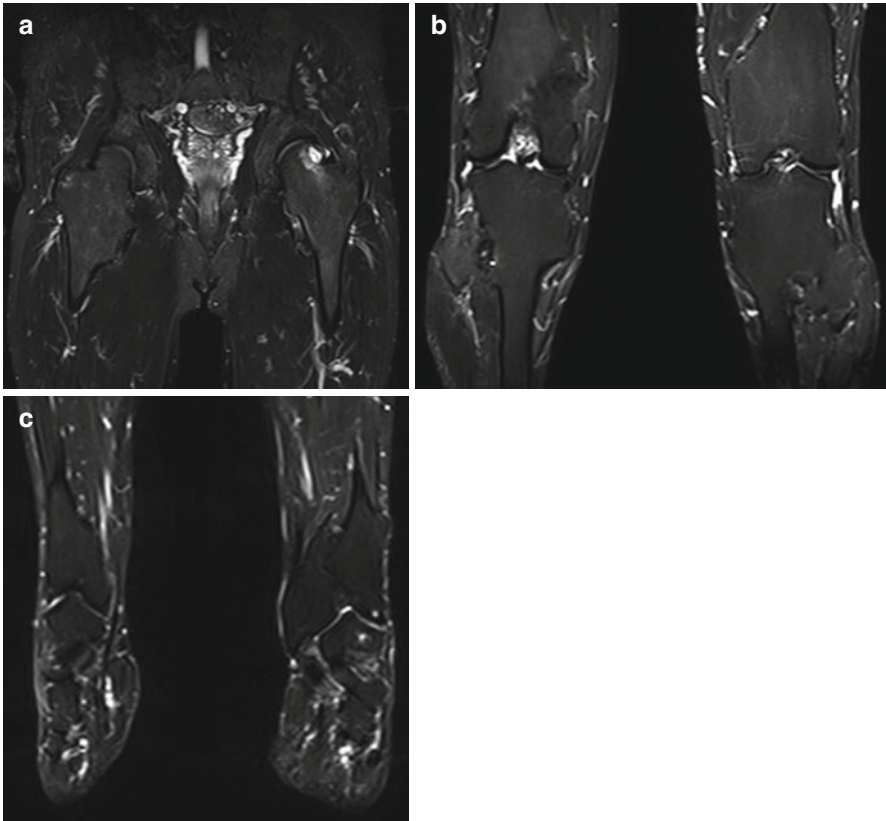


Fig. 10.5 Incidental screening finding (STIR). Thirty-nine-year-old male subject with multiple sessile and pedunculated osteochondromas in the proximal femoral metaphysis (a), the distal femoral metaphysis and proximal tibial metaphysis (b), and the distal tibial and fibular metaphysis (c) causing bone and joint deformities

Clinical Management

Most osteochondromas are asymptomatic incidental findings or present with a several-year history of painless swelling. Secondary chondrosarcoma arising in a solitary osteochondroma is very rare (1–2 %) (Ahmed et al. 2003). Therefore, further diagnostic tests need not be obtained unless the MRI findings are indeterminate. A cartilage cap thickness exceeding 2 cm on is considered an important marker of malignant transformation (Ahmed et al. 2003). In individuals with hereditary multiple osteochondroma, an autosomal dominant disorder associated with bone and joint deformities (Fig. 10.6), the risk of malignant transformation can be as high as 9 % (Altay et al. 2007). Surgical resection with wide margins is the best treatment option for patients with symptomatic osteochondroma (Ayerza et al. 2007).

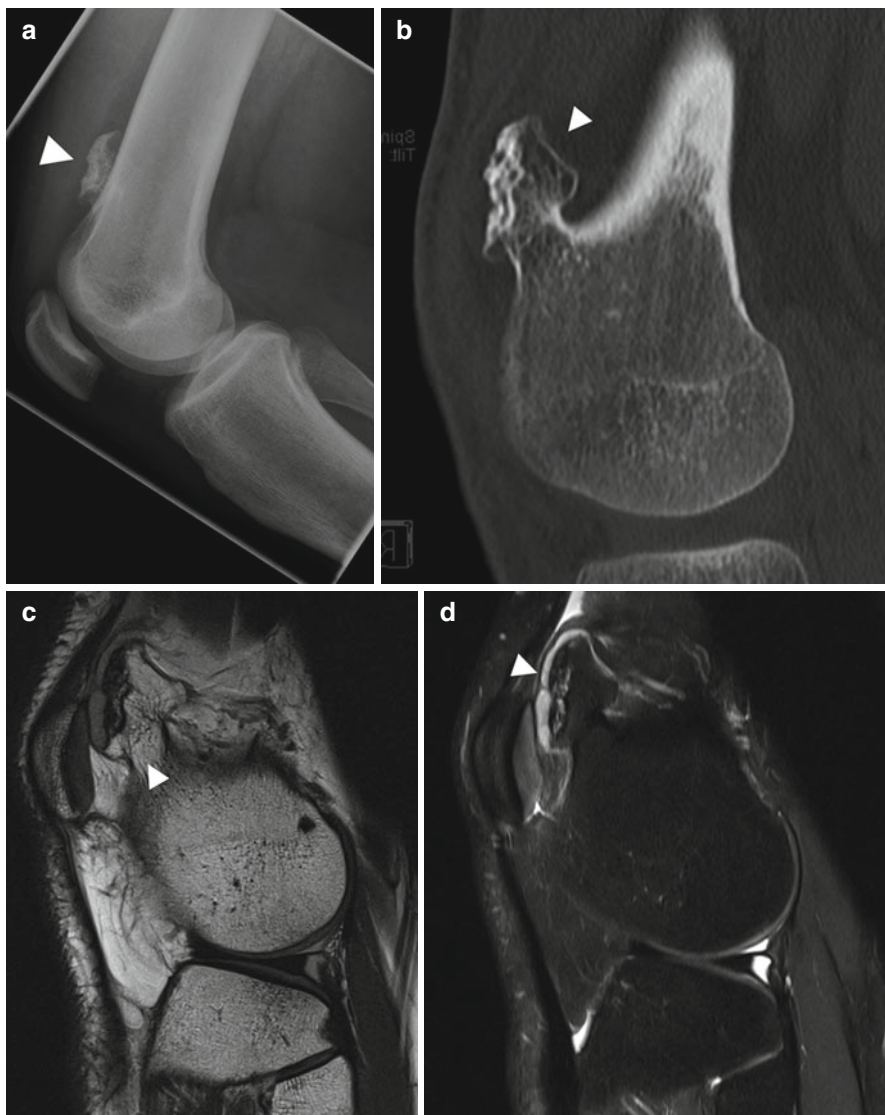


Fig. 10.6 Diagnostic workup. Same subject as Fig. 10.5. Conventional radiograph (a) shows a sessile osteochondroma (*arrowhead*) extending from the cortex of the distal femoral metaphysis. CT scan (b) demonstrates the cortical and medullary portions of the lesion to be continuous with the parent bone (*arrowhead*). On MRI, the thickness of the cartilage cap – an important criterion of malignancy – can be measured. The cap (*arrowhead*) has intermediate signal intensity on sagittal PD image (c) and high signal intensity on sagittal fat-suppressed T2w image (SPAIR) (d)

10.2.1.2.2 Chondroma/Enchondroma

Enchondroma is a well-defined osteolytic lesion with a chondroid matrix. It typically contains calcifications arranged in an arc-and-ring pattern, giving rise to the characteristic popcorn appearance on conventional radiographs (Greenspan 1989; Unni 2001) (Table 10.4). On MRI, an enchondroma appears as a sharply

demarcated, lobulated lesion of low to intermediate T1 and high T2 signal intensity (Fig. 10.7a). Calcifications within the matrix may appear as signal voids on all pulse sequences. On fat-suppressed T1-weighted images acquired after contrast medium administration, enhancement is predominantly peripheral and occurs in arcs or rings (Fig. 10.7d). This pattern may be obscured by the high signal intensity of hyaline cartilage on these images (Aoki et al. 1991; Geirnaerd et al. 1993).

Table 10.4 Chondroma/enchondroma

Chondroma/enchondroma	Arises in cortical bone Arises in the intramedullary cavity
Prevalence	Second most common benign tumor 2–20 % of all bone tumors 12–24 % of all benign bone tumors Multiple lesions in Ollier disease, Maffucci syndrome, and metachondromatosis
Age predilection	15–40 years
Sex predilection	M=F
Location	Metaphyseal and terminal diaphyseal regions Short tubular bones of hands and feet (60 %) Long bones (25–40 %), most commonly the femur and humerus
Type of lesion	Benign; malignant sarcomatous transformation in rare cases
Signs and symptoms	Asymptomatic incidental finding Pain, swelling, pathologic fracture
Differential diagnosis	Bone infarct, epidermoid, chondrosarcoma

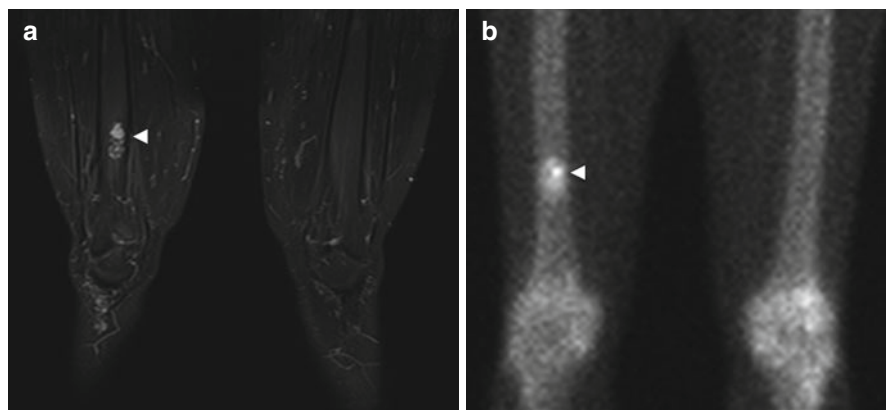


Fig. 10.7 Incidental screening finding (STIR) and diagnostic workup. Forty-five-year-old male subject with a sharply demarcated, lobulated lesion of high signal intensity (*arrowhead*) in the right distal femoral shaft (a). Diagnostic workup with scintigraphy and contrast-enhanced MRI. Tc-99m scan demonstrates high metabolic activity of the lesion (*arrowhead*) (b). On supplementary MRI, the lesion has the characteristic appearance of an enchondroma: hyperintense cartilage surrounded by a thin rim of hypointense perichondrium (*arrowhead*) (sagittal T2w TSE) (c) with a strong peripheral ring-and-arc pattern of enhancement (*arrowhead*) on axial contrast-enhanced image (T1w TSE) (d)

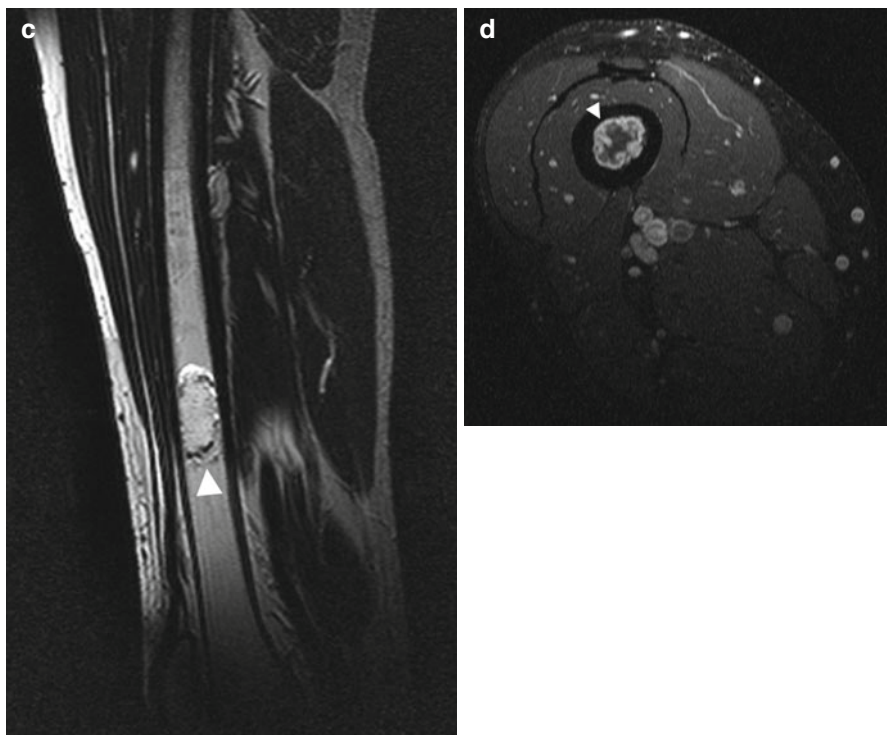


Fig. 10.7 (continued)

Clinical Management

Enchondroma is a common incidental finding (Hong et al. 2011), and if the diagnosis is clear, no further investigation or treatment is required. Symptomatic lesions can be treated by curettage and bone grafting. Although malignant transformation to chondrosarcoma is rare, regular radiologic follow-up is recommended (Müller et al. 2003). Vanel et al. (2013) have recently suggested that the presence of cartilaginous islands in the periphery of an unclear lesion has the potential to serve as a new MRI criterion for differentiating between enchondroma and chondrosarcoma. Detection of multiple enchondromas may suggest enchondromatosis (e.g., Ollier disease), which is associated with a 15–50 % risk of malignant transformation (Goodman et al. 1984).

10.2.1.3 Fibrous Bone Tumors

10.2.1.3.1 Fibrous Dysplasia (Jaffé-Lichtenstein Disease)

Fibrous dysplasia is a benign chronic disorder of bone development in which the normal medullary space is replaced by fibrous tissue, causing expansion and distortion of the bone. Monostotic fibrous dysplasia involves a single long bone and is far

Table 10.5 Fibrous dysplasia (Jaffé-Lichtenstein disease)

Prevalence	Most common skeletal anomaly in children and young adults but also occurs in adult life; occurs in patients with McCune-Albright syndrome and Mazabraud syndrome
Age predilection	5–50 years, with a peak at 10–20 years
Sex predilection	M=F
Location	Craniofacial bones Metaphysis of long bones (femur, tibia) Ribs
Type of lesion	Benign; malignant sarcomatous transformation extremely rare
Signs and symptoms	Monostotic form typically asymptomatic, pathologic fracture Polyostotic form often presents with symptoms in childhood (2/3 of cases)
Differential diagnosis	Neurofibromatosis, Paget disease, juvenile bone cyst

more common than the polyostotic form (85 vs. 15 %). The latter typically affects the skull and facial bones (Ippolito et al. 2003) (Table 10.5). On MRI, fibrous dysplasia is visualized as an expansive mass in the medullary space. The mass has homogeneous low signal intensity on T1-weighted images (Fig. 10.8b) and intermediate to high signal intensity on T2-weighted images (Fig. 10.8a). It is surrounded by a low-signal-intensity rim. Active portions show strong homogeneous enhancement after IV contrast medium administration (Jee et al. 1996).

Clinical Management

A skeletal survey with conventional radiographs is recommended to identify monostotic or polyostotic fibrous dysplasia. Computed tomography can be helpful in assessing skull involvement and identifying possible mass effects on intracranial and orbital structures (Chapurlat and Orcel 2008). Monostotic lesions usually stop growing during puberty, and in subjects with small asymptomatic lesions, further clinical evaluation is not necessary. Malignant sarcomatous transformation is extremely rare. In subjects with a risk of pathologic fracture from a large monostotic lesion, treatment is required. Lesions due to polyostotic fibrous dysplasia can continue to grow after puberty. The polyostotic form is often associated with endocrine disorders such as hyperthyroidism, hyperparathyroidism, or diabetes mellitus, which is why clinical workup is recommended (Chapurlat and Orcel 2008).

10.2.1.4 Bone-Forming Tumors

10.2.1.4.1 Osteoma

Osteomas are circumscribed sclerotic lesions that resemble mature cortical bone and arise juxtacortically (Table 10.6). The lesions have low signal intensity on T1- and T2-weighted images (Fig. 10.9a–c) and do not enhance after IV administration of contrast medium (Greenspan 1993).

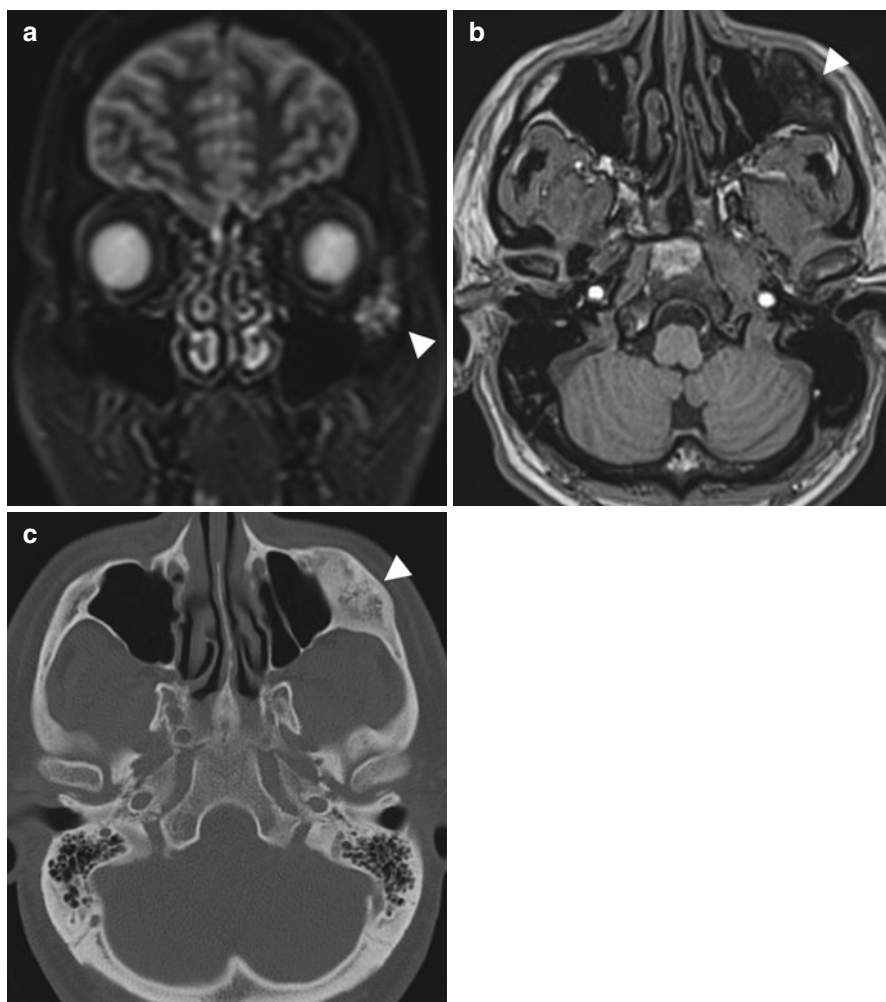


Fig. 10.8 Incidental screening finding (STIR) and diagnostic workup. Thirty-five-year-old male subject with an expansive mass of the left zygomatic arch (*arrowhead*). The mass has high signal intensity on STIR image (**a**) and low signal intensity on axial T1w TSE image (**b**). Diagnostic workup with CT demonstrates the characteristic appearance of fibrous dysplasia with incomplete mineralization of the fibrous matrix (**c**)

Clinical Management

Most osteomas are asymptomatic and can be left alone. For symptomatic osteomas, en bloc resection is currently recommended (Haddad et al. 1997).

Table 10.6 Osteoma

Prevalence	0.4 %
Age predilection	10–79 years, with a peak at 40–50 years
Sex predilection	M=F
Location	Paranasal sinuses (frontal, ethmoid) Skull, mandible Multiple osteoma in Gardner syndrome
Type of lesion	Benign
Signs and symptoms	Small lesions: typically asymptomatic and detected incidentally Expansion of bone, pain, sinusitis, mucocele, exophthalmos, double vision, visual disturbance
Differential diagnosis	Parosteal osteosarcoma, osteochondroma, enostoma

10.2.1.4.2 Osteoid Osteoma

An osteoid osteoma consists of a highly vascularized nidus, which is typically found in the cortex. Medullary or subperiosteal osteoid osteoma is less common. The nidus is less than 1.5 cm in size. A larger variant, known as osteoblastoma, commonly involves the spine. The lesion is rounded or spindle-shaped, and the nidus is surrounded by sclerotic bone (Greenspan 1993) (Table 10.7).

The nidus is isointense to muscle on T1-weighted images with intermediate to high signal intensity on T2-weighted images (Fig. 10.10a, b). It enhances strongly after IV contrast medium administration. The sclerotic rim is dark on all pulse sequences. Perifocal bone marrow and soft tissue edema may be present and is best seen on fat-suppressed T2-weighted or STIR images or on contrast-enhanced T1-weighted images (Assoun et al. 1994).

Clinical Management

Osteoid osteoma is often asymptomatic. Conventional radiographs are recommended for confirming the diagnosis and are necessary for treatment planning if surgery is contemplated (Fig. 10.10c). CT is the modality of choice for identification of the nidus (Frassica et al. 1996). In intra-articular osteoid osteoma, MRI can identify complications such as joint effusion and synovitis. Supplementary diagnostic information is obtained by bone scintigraphy and angiography. Initial treatment may be conservative: nonsteroidal anti-inflammatory drugs (NSAIDs) may be given, as many osteoid osteomas resolve spontaneously after 2–7 years (Winkelmann et al. 2003). Minimally invasive interventions include CT-guided radiofrequency ablation (Hoffmann et al. 2010) and CT-guided removal (Fenichel et al. 2006).

10.2.2 Bone Marrow Disorders

10.2.2.1 Conversion and Reconversion

Conversion of red-to-yellow marrow refers to the shift in bone marrow composition from highly cellular, hematopoietically active marrow (red) to inactive fatty marrow

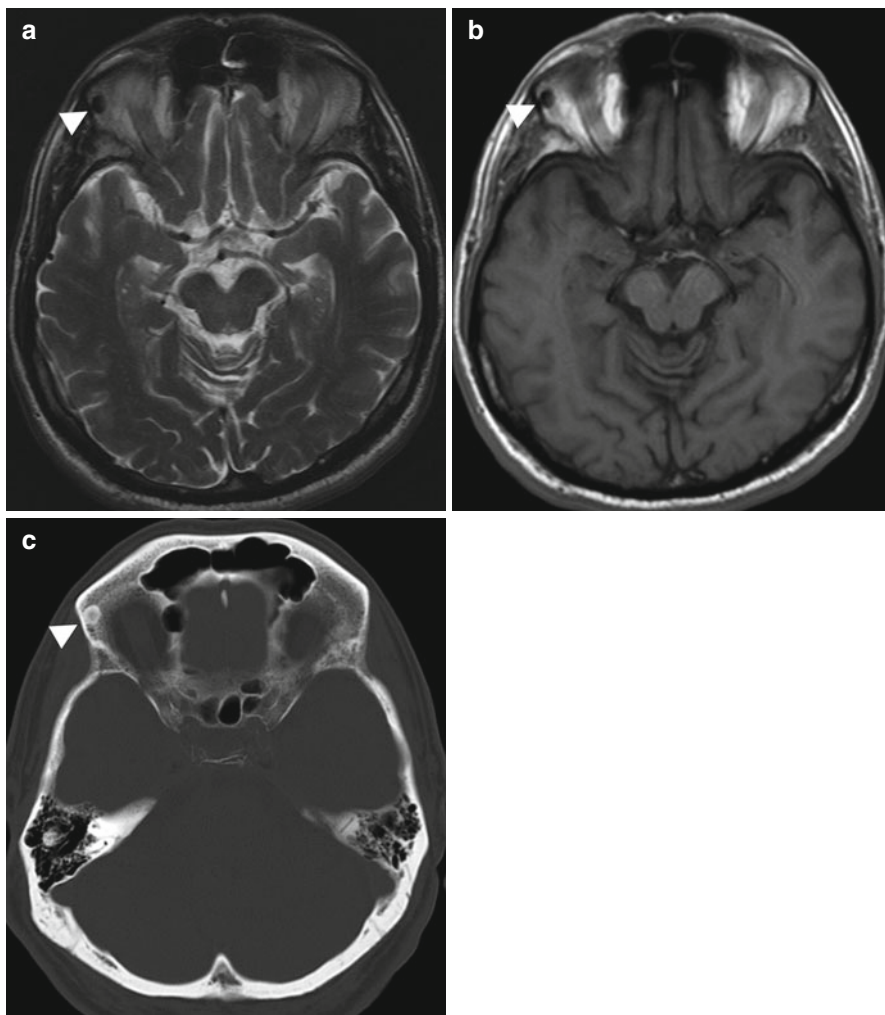


Fig. 10.9 Incidental screening finding and diagnostic workup. Sixty-five-year-old male subject with a sharply delineated, oval lesion (*arrowhead*) in the right orbital roof. The lesion has low signal intensity on axial T2w TSE image (**a**) and axial T1w SE image (**b**). Diagnostic workup with CT (**c**) demonstrates a homogeneously calcified lesion, consistent with an osteoma

(yellow). This conversion begins in the distal phalanges of the hands and feet and then progresses proximally. Conversion is best appreciated on unenhanced T1-weighted images. In the long bones, fatty degeneration starts in the apo- and epiphyses, progressing first to the diaphyses and then to the metaphyses. In the vertebral bodies, fatty degeneration begins near the central venous plexus and slowly progresses into the periphery. In adults, hematopoietic marrow is still present in the proximal metaphyses of the humerus and femur, the pelvis, the vertebrae, the ribs and sternum, the scapula, the calcaneus, and flat bones of the skull. With age, the

Table 10.7 Osteoid osteoma

Prevalence	4 % of all primary bone tumors 12 % of all benign bone tumors
Age predilection	10–35 years
Sex predilection	M:F ratio of 3:1
Location	Metaphysis, diaphysis Femur, tibia, phalanges, spine (posterior elements)
Type of lesion	Benign, no size increase
Signs and symptoms	Circumscribed pain, often most severe at night, readily controlled by nonsteroidal anti-inflammatory drugs (NSAIDs) (often within 30 min) Localized swelling, tenderness Spinal osteoid osteoma causes painful scoliosis
Differential diagnosis	Osteoblastoma, bone island, Brodie abscess

physiologic process of red-to-yellow marrow conversion slowly leads to a progressive increase in the proportion of fatty marrow. The adult pattern is characterized by a balanced distribution of red and yellow marrow but varies from person to person and is affected by a variety of factors (Vogler and Murphy 1988; Ricci et al. 1990).

Reconversion is the repopulation of yellow marrow by hematopoietic cells. This process follows the pattern of red-to-yellow marrow conversion in reverse, meaning that it progresses from the center toward the periphery. In the long bones, reconversion begins symmetrically, progressing from the metaphyses into the diaphyses. From here it may even continue into the epiphyses if the demand for red cells is strong enough. Bone marrow reconversion is triggered by conditions associated with an increased demand for red cells. This includes anemia or blood loss, competitive sports, time spent at high altitudes, heavy smoking, cyanotic heart disease, and chemotherapy. Reconverted bone marrow may have very high signal intensity on STIR images (Fig. 10.11a) and very low signal intensity on T1-weighted images (Fig. 10.11b), making it difficult to differentiate reconversion from diffuse infiltrative neoplastic conditions.

STIR sequences are very useful for detecting bone marrow pathology (Mehta et al. 1995; Mahnken et al. 2005; Schmidt et al. 2007). On STIR images, normal yellow marrow appears black, while hematopoietic marrow and lesions are of high signal intensity. STIR sequences have high sensitivity but poor specificity. Bone marrow pathology may be associated with decreased or increased cellularity (Fig. 10.12). When cellularity is decreased, yellow marrow predominates, making for a dark appearance on STIR images and a bright appearance on T1-weighted images. Conversely, pathology associated with increased cellularity is bright on STIR images and dark on T1-weighted images. A notable exception is storage disorders with excessive deposition of iron or calcium. These deposits produce a loss of signal intensity on both STIR and T1-weighted images. Two conditions associated with malignant cell infiltration of the bone marrow, metastasis and multiple myeloma, can commonly be detected incidentally on screening MRI (Delorme and Baur-Melnyk 2011; Kwee et al. 2011; Collins 2010). The other bone marrow pathologies listed in Fig. 10.12 are encountered less frequently.



Fig. 10.10 Incidental screening finding (STIR) and diagnostic workup. Twenty-three-year-old male subject with distention of the right proximal femoral shaft (*large arrowhead*) and extensive medullary cavity edema (*small arrowheads*) (**a**). Sagittal T1w TSE image (**b**) reveals a central nidus isointense to muscle (*large arrowhead*). The lesion is surrounded by a low-signal-intensity zone of sclerosis (*small arrowheads*). Workup using conventional radiography confirms marked reactive sclerosis (*arrowhead*) of the femoral shaft (**c**)

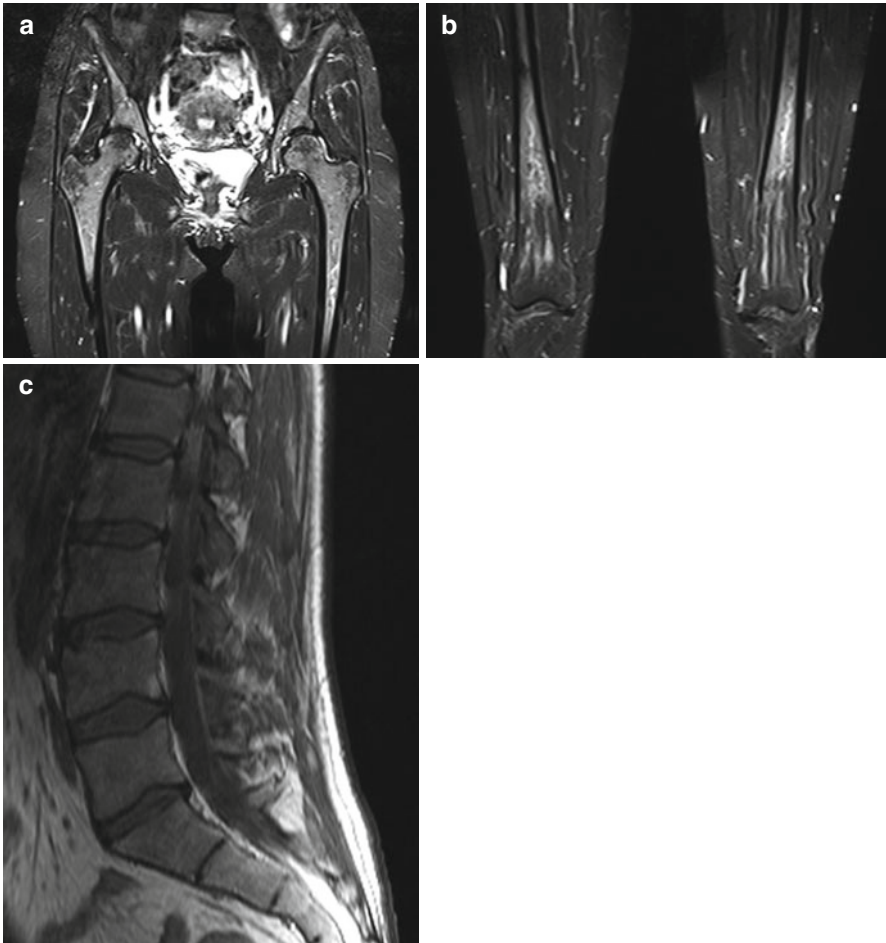


Fig. 10.11 Incidental screening finding (STIR). Forty-nine-year-old female subject with hematopoietically active bone marrow in the pelvic and thigh bones. The active marrow has high signal intensity on STIR images (a, b). T1w TSE image shows low signal intensity of spinal marrow (c). Diagnostic workup in this subject revealed chronic anemia due to hypermenorrhea

10.2.2.2 Bone Metastases

The bone marrow is the third most common site of metastatic disease. At autopsy, bone metastases have been found in 30–70 % of patients with a malignant tumor (Papac 1994). The skeleton may be affected by single or multiple osteolytic or osteoblastic metastases of variable size. Bone metastases are common in patients with breast, lung, prostate, thyroid, and renal cancer. Normally, malignant cells spread hematogenously to sites of residual hematopoietic bone marrow in the spine, ribs, pelvis, skull, humerus, and femur. Metastatic growth destroys the cortical layer, resulting in invasion of soft tissues. Vertebral metastases tend to destroy

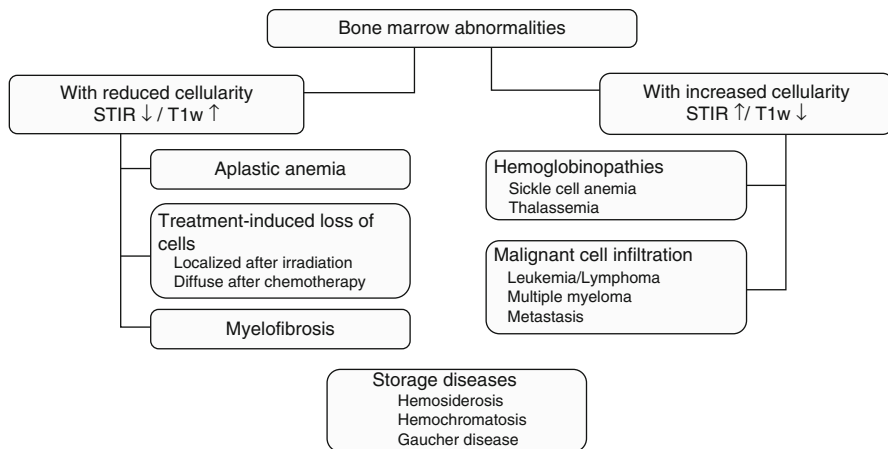


Fig. 10.12 Classification of bone marrow abnormalities by cellularity and MRI signal intensity

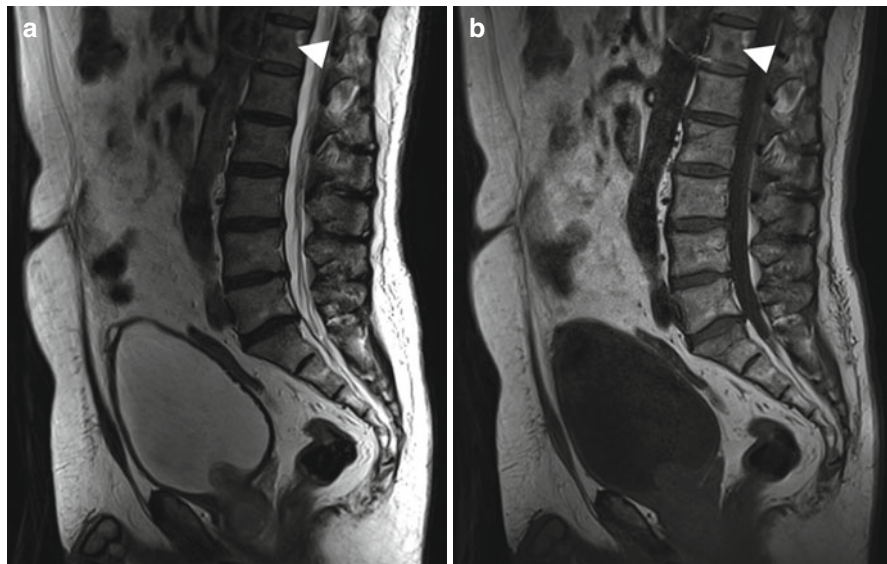


Fig. 10.13 Incidental screening finding. Sixty-six-year-old male subject with an inhomogeneous mass in the prostate. The mass extends through the bladder base into the bladder on sagittal T2w TSE image (a). In addition, this image and the corresponding T1w image show a low-signal-intensity round lesion (arrowhead) in the center of T12 (a, b). Workup yielded the diagnosis of osteoblastic metastasis from prostate cancer

the pedicles or endplates. Some primary malignancies, such as cancer of the prostate or urinary bladder (Fig. 10.13), produce factors that stimulate bone-forming cells. These give rise to osteoblastic metastases, which are characterized by the formation of new bone. Other tumors, including renal cell cancer or thyroid cancer,

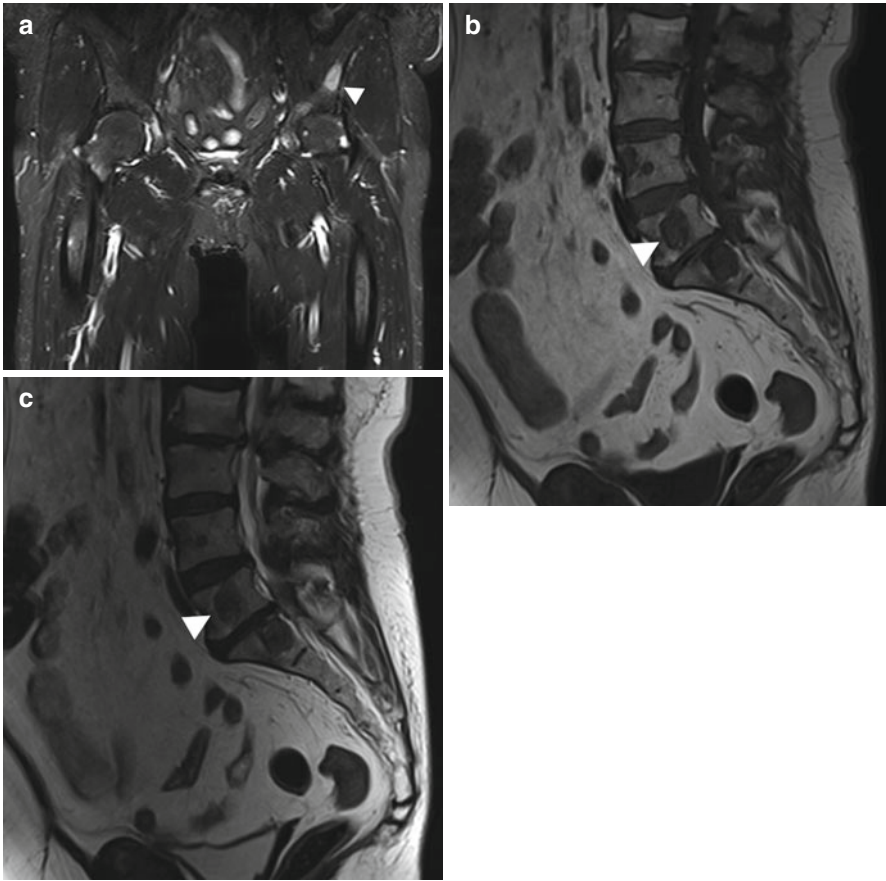


Fig. 10.14 Incidental screening finding. Sixty-four-year-old female subject with a high-signal-intensity lesion (*arrowhead*) in the left iliac bone (STIR) (**a**). In addition, there are multiple round lesions in L3 through L5 (*arrowhead* indicates L4 metastasis), which have low signal intensity on sagittal T1w TSE image (**b**) and sagittal T2w TSE image (**c**). Workup yielded the diagnosis of multiple osteolytic and osteoblastic metastases from breast cancer

secrete factors, such as TGF or PDGF, that stimulate osteoclast activity, which leads to osteolytic destruction of the bone matrix. In breast cancer, both osteolytic and osteoblastic bone metastases can occur (Fig. 10.14). The MR signal intensities of osteoblastic and osteolytic metastases on different pulse sequences are summarized in Table 10.8. With its high sensitivity and diagnostic accuracy, the coronal STIR sequence appears to become the first-line tool to search for bone metastases – preferred over other imaging modalities such as skeletal scintigraphy or PET-CT (Mehta et al. 1995; Mahnken et al. 2005; Schmidt et al. 2007; Papac 1994; Chiewvit et al. 2009).

Clinical Management

Incidentally detected bone metastases require prompt diagnostic workup to identify and treat possible complications and detect the primary tumor. Complications of vertebral metastases include pathologic fractures and neurologic problems. The search for the primary tumor is best undertaken using a whole-body screening modality such as CT or MRI (Schmidt et al. 2007; Papac 1994).

10.2.2.3 Multiple Myeloma/Plasmacytoma

Multiple myeloma, or plasmacytoma, is the most common primary malignant bone tumor, occurring predominantly in men between 40 and 80 years of age. It is a hematologic disorder characterized by an uncontrolled proliferation of abnormal plasma cells. The neoplastic plasma cells invade the bone marrow, and by secreting nonfunctional monoclonal immunoglobulins, they suppress benign polyclonal plasma cells. The simultaneous release of osteoclast-stimulating factors and inhibition of osteoblast activity result in osteolytic demineralization and destruction of normal bone. Bone involvement may be diffuse, or multiple sharply demarcated osteolytic lesions of variable size may be present. Multiple myeloma affects bones containing red marrow, most commonly the spine, ribs, pelvis, skull, humerus, and femur. Unlike vertebral metastases, myeloma lesions generally only involve the posterior elements of the vertebral bodies in advanced disease. On MRI, the osteolytic lesions have high signal intensity on STIR and T2-weighted images (Fig. 10.15b, c) and intermediate to low signal intensity on T1-weighted images (Fig. 10.15a) (Baur-Melnyk et al. 2005; Delorme and Baur-Melnyk 2011).

Clinical Management

A subject whose MRI findings point to plasmacytoma requires further diagnostic evaluation. The baseline workup includes comprehensive blood and urine tests and immunoelectrophoresis. The Durie-Salmon system classifies multiple myeloma into one of three stages based on the number of osteolytic bone lesions, hemoglobin and calcium blood levels, and immunoglobulin production. Whole-body MRI is very sensitive for evaluating bone marrow infiltration compared with traditional imaging modalities such as conventional radiographs (Baur-Melnyk et al. 2005; Delorme and Baur-Melnyk 2011). MRI protocols including coronal STIR sequences and T1- and T2-weighted sequences for spinal imaging have been established for the staging and monitoring of treatment in the clinical setting.

Table 10.8 Signal intensities of osteolytic and osteoblastic metastases on different pulse sequences

	Osteolytic	Osteoblastic
T1-weighted sequence	↓	↓
T2-weighted sequence	↑	↓
STIR	↑	↓
T1-weighted sequence after IV contrast medium	Variable enhancement	Variable enhancement

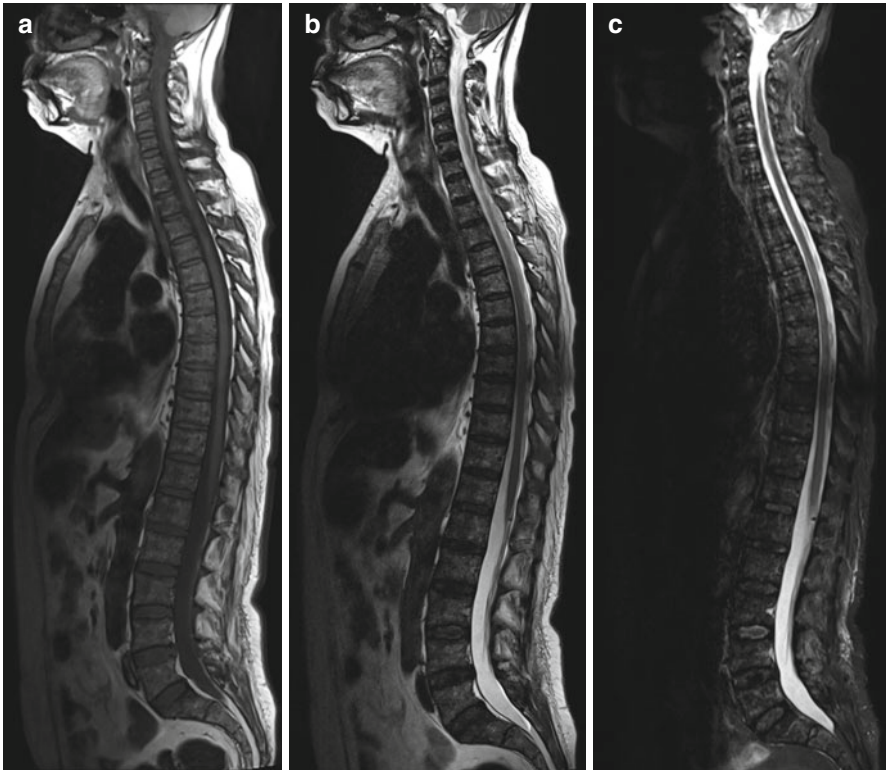


Fig. 10.15 Incidental finding at screening. Fifty-seven-year-old female subject with multiple focal lesions diffusely distributed within the bone marrow. The lesions are predominantly hypointense on T1w image (a) and hyperintense on T2w image (b) and on STIR image (c). This is the so-called salt-and-pepper pattern of diffuse plasmacytoma

10.2.3 The Joints

Though the body's major joints are typically depicted on MR images acquired with a whole-body protocol, whole-body MRI has several limitations. The elbows, for example, tend to be located outside the homogeneous magnetic field. A detailed evaluation of the internal joint structures is usually not possible with the pulse

Fig. 10.16 Bilateral medial gonarthrosis, more marked on the *right*. Image shows loss of height of the joint space, subchondral bone edema (*arrowheads*) of the medial tibial condyle, joint effusion, and mild varus deformity

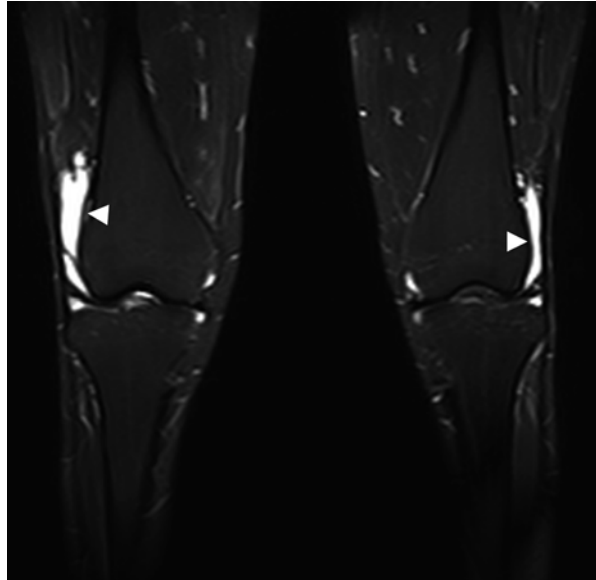


sequences included in whole-body MRI protocols. Furthermore, the protocol does not include the specific slice orientations for optimal evaluation of individual joints (e.g., shoulder: parasagittal, paracoronal; knee: aligned along long axis of cruciate ligament). Nevertheless, the coronal TIRM sequence in particular is an excellent screening sequence for detecting joint abnormalities. The most important morphologic imaging features of joint abnormalities include joint effusion and subchondral bone edema. They are conspicuous due to their high signal intensity (Fig. 10.16). The differential diagnosis of these findings includes acute arthritis (bacterial, rheumatoid) and aseptic bone necrosis. In both cases, clinical signs and symptoms will be present to assist in making a diagnosis, unless a subject has very early disease at the time of imaging. For this reason, only rarely are the findings truly incidental.

A variety of cystic lesions can affect the joints and are particularly common in and around the knee (Perdikakis and Skiadas 2013). These lesions should not be confused with dilated anatomic recesses caused by joint effusion. In a screening population with a large proportion of middle-aged and older individuals, joint effusion is a common incidental finding and often occurs bilaterally. When larger structural lesions are absent, joint effusion is most likely due to arthrosis – and a distinction must be made between inactive and activate disease. In active disease, there is concomitant synovitis, seen on imaging as a large effusion (Fig. 10.17).

Another common finding is bone marrow edema of variable degree, typically located in the metaphysis and/or epiphysis. The underlying cause is frequently not

Fig. 10.17 Extensive bilateral knee joint effusion (*arrowheads*) with otherwise only mild secondary signs of arthrosis



apparent in the initial screening. One possible cause is early aseptic bone necrosis such as transient osteoporosis of the proximal femur. More extensive edema may also point to bone necrosis or trauma such as contusion or even fracture (Fig. 10.18).

An occasional osteochondral lesion with or without displacement of an osteochondral fragment can be seen in younger, physically active individuals. These lesions are known as osteochondritis dissecans and typically involve the stress-bearing areas of the femoral or tibial condyle. Quatman et al. (2012) have shown that MRI is a useful noninvasive tool for the diagnosis and evaluation of osteochondritis dissecans. The terminal stage involves the formation of loose bodies, i.e., the complete detachment of an osteochondral fragment (Fig. 10.19).

10.3 The Spine

10.3.1 Introduction

Acute and chronic back pain is a major public health problem. Therefore, a whole-body MRI screening examination is likely to generate a multitude of spinal findings, such as vertebral hemangioma, Tarlov cyst, fibrolipoma, synovial cyst, and sacral meningocele (Park et al. 2011). Issues such as how to interpret and handle these findings and decide how and to what extent they should be communicated to the subject require careful consideration. Learning that a spinal abnormality is present on imaging might be harmful to some individuals because it could contribute to a chronification of harmless symptoms or encourage the person to seek early retirement. This is

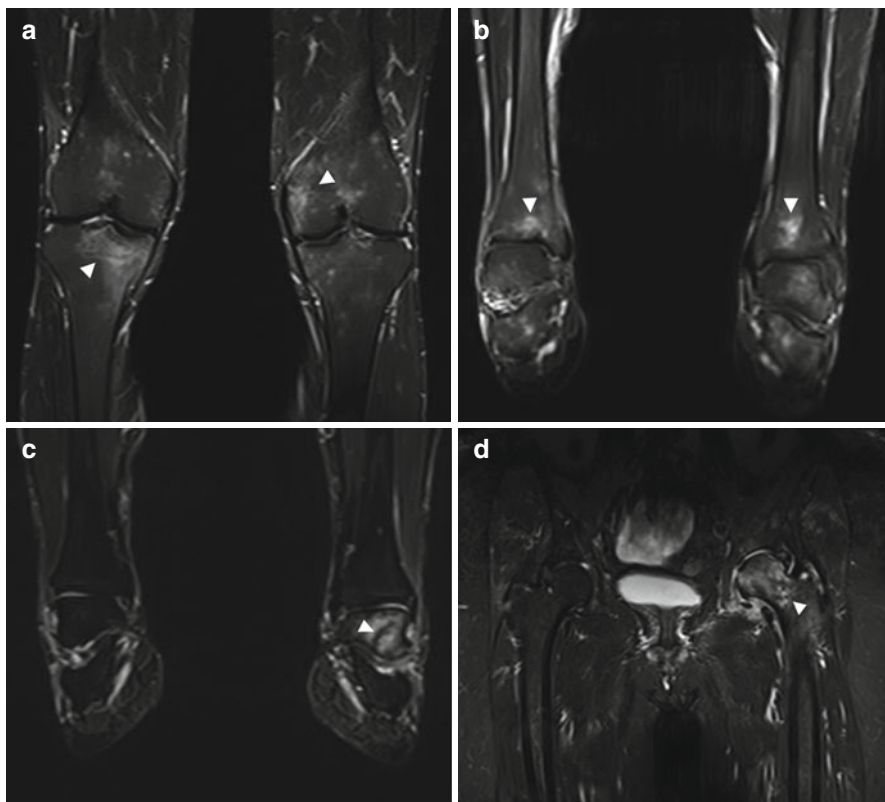
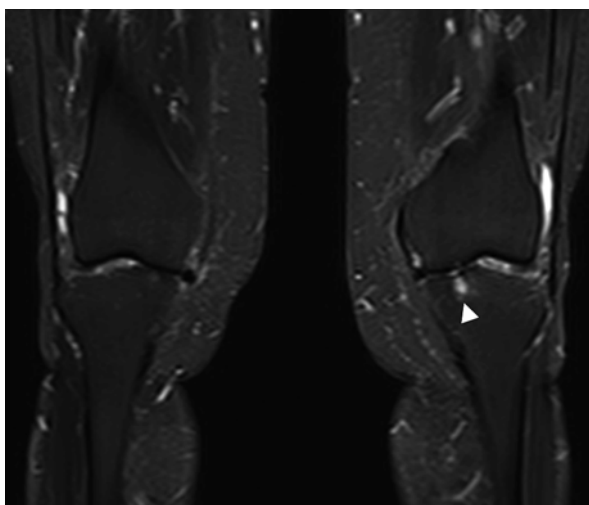


Fig. 10.18 Bone marrow edema (*arrowheads*) in different locations: in both knees (**a**), in both ankle joints (**b**), in the left ankle joint (**c**), and in the left femoral head and neck (**d**). The underlying causes are multifarious (e.g., overuse, arthrosis, trauma) and remain unclear in these cases

Fig. 10.19 Circumscribed focal osteochondral defect (*arrowhead*) in the tibial joint surface in a young man. The appearance is characteristic of stage 4 osteochondritis dissecans, while the osteochondral fragment (the mouse) is still in its bed, i.e., there is no intra-articular loose body



especially the case in a screening population mostly coming from lower socioeconomic rural regions like the population of SHIP. In Germany, one in five women and one in seven men suffer from chronic back pain. The data of the 1998 German Health Survey even indicate that back pain is the most common type of pain in all age groups, being far more common than headache and pain of the neck and shoulders. About half of affected women and 80 % of affected men described back pain to be the most severe pain they experienced in the week before the survey. Results of the 2008 Telephone Health Survey corroborate this situation, with 22 % of women and 15 % of men having reported chronic back pain persisting for at least 3 months and being noticeable daily or almost daily (Gesundheitsberichterstattung des Bundes 2008). Mental and social problems promote back pain. The majority of cases involve nonspecific back pain – pain that cannot be attributed to a specific cause. A series of typical risk constellations has been identified, which allow identification of groups prone to developing back pain. Back pain is more common in individuals with a lower socioeconomic status (based predominantly on education, profession, and income) than in those with a higher status. Whether there is also a corresponding correlation between social status and imaging findings is still open and may be investigated in the setting of screening studies. There is a reciprocal relationship between back pain and depressive symptoms or other indicators of mental health.

The socioeconomic burden of back pain is considerable. The total medical and socioeconomic costs of back pain are on a similar order as those for headache, cardiac disease, depression, or diabetes mellitus. Contrary to other diseases, the lion's share of costs that back pain incurs are indirect rather than direct costs for medical care. According to international estimates, approximately 85 % of the total costs are accounted for by a loss of productivity due to absenteeism from work, while only about 15 % are incurred by medical treatment itself. In 2002, the AOK (a large German public health insurance company) conducted a survey that provided data on the causes for absenteeism from work in Germany that year. They found that 33,785 days of missed work per 10,000 AOK members were accounted for by spine and back conditions (ICD-10: M40 to M54). This averages out to slightly over 3 days of work missed per member and constitutes nearly 18 % of all days of absenteeism from work.

This is the epidemiologic background underlining the radiologist's great responsibility in interpreting imaging findings of the spine. Given these considerations, great care is required in order to not give too much attention to normal anatomic variants and asymptomatic abnormalities. On the other hand, the radiologist must not overlook serious changes that require follow-up or even treatment. To ensure that the subjects receive adequate care, such situations require a comprehensive assessment with inclusion of history and clinical presentation, as well as prompt interdisciplinary discussion, ideally by referring such cases to a spine board.

10.3.2 MRI Technique for Spinal Imaging

Technical developments, such as advanced table movement techniques, allow imaging of the entire spine as part of a whole-body MRI protocol. The spinal protocol used in this setting is based on well-established imaging techniques used for

Table 10.9 MRI protocol for spinal imaging

Pulse sequence, plane	Slice thickness (mm)	Slice distance (mm)	Resolution	TR (ms)	TE (ms)	Fat suppression
T1w TSE, 2D, sagittal	4	4.4	448	676	12	No
T2w TSE, 2D, sagittal	4	4.4	448	3,760	106	No
T2w TIRM, 2D, coronal	5	6.0	320	4,891	67	Yes

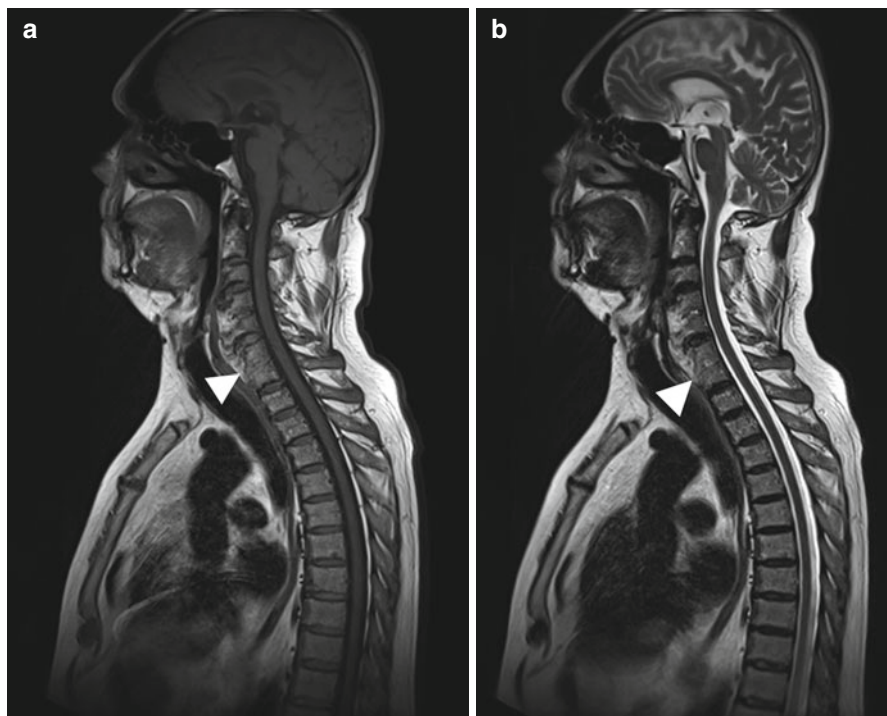


Fig. 10.20 Congenital squaring of C6/C7 (arrowhead) on sagittal T1w TSE image (a) and sagittal T2w TSE image (b). Note severe abnormalities of the two cervical segments above the squared vertebrae with massive loss of height of the C4/C5 intervertebral disc space. In addition, both segments exhibit extensive anterior spondylophytes/syndesmophytes (differential diagnosis: DISH). No involvement of the spinal canal

segmentwise spinal imaging (Table 10.9). The examination begins with acquisition of sagittal T1- and T2-weighted TSE sequences with 3–4 mm slice thickness and a maximum interslice gap of 10 %. It is important to acquire enough slices for complete visualization of the neuroforamina on both sides, especially when imaging subjects with scoliosis or spinal malposition. Coronal T2-weighted sequences with fat suppression supplement the protocol and can be particularly helpful in differentiating abnormalities. Contrast medium is not indicated in the primary screening protocol of the spine but may be helpful in further characterizing any abnormalities or differentiating scar tissue, inflammation, and tumor, which cannot be definitely evaluated on unenhanced images (Fig. 10.20).

10.3.3 Classification of Findings

Spinal pathology can be classified according to different criteria. Using the three-compartment model of the vertebra, pathology is classified according to the spinal structures involved. Another possible classification distinguishes between findings involving the locomotor system and those involving neural structures. Pathology of the spinal canal can be classified as extradural, intradural extramedullary, or intramedullary. In light of the complexity of spinal anatomy and in considering the specific requirements of the screening situation, we opted for the following classification:

Congenital and developmental anomalies

Inflammatory conditions

Degenerative conditions

Metabolic and other systemic disorders

Some overlap cannot be fully avoided and will be pointed out as we come across it in the following sections.

10.3.4 Congenital and Developmental Anomalies

10.3.4.1 Congenital Vertebral Fusion, Caudal Regression Syndrome, Incomplete Vertebral Arch Closure

Though fairly common, these anomalies are usually asymptomatic (Table 10.10). When there is overload of the spinal segments adjoining fused vertebrae, supplementary functional imaging may be helpful to rule out instability (Brossmann et al. 2001; Tortori-Donati et al. 1999, 2001; Rossi et al. 2004; Schijman 2003).

Clinical Management

Asymptomatic anomalies can be left alone. When a subject has pain, other causes must be ruled out. (Brossmann et al. 2001; Tortori-Donati et al. 1999, 2001; Rossi et al. 2004; Schijman 2003).

10.3.4.2 Scheuermann Disease

Scheuermann disease presents with varying degrees of common sequelae (Table 10.11) (Fig. 10.21). Adults participating in screening generally do not have any complaints from Scheuermann disease, and those with mild forms often cannot recall having had symptoms as teenagers (Schmorl 1929; Ali et al. 1999; Tribus 1998; Wenger and Fricks 1999).

Clinical Management

No treatment is needed in asymptomatic subjects. If pain is present, other causes must be ruled out. Symptomatic treatment may be indicated (Schmorl 1929; Ali et al. 1999; Tribus 1998; Wenger and Frick 1999).

Table 10.10 Congenital vertebral fusion, caudal regression syndrome, incomplete vertebral arch closure

Prevalence	2–4 % of the population
Age predilection	Congenital
Sex predilection	M = F
Location	Vertebral fusion: cervical > lumbar > thoracic Caudal regression syndrome: lumbar > thoracic Incomplete vertebral arch closure: lumbar > sacral bone
Type of lesion	Benign
Signs and symptoms	Typically asymptomatic at first A history of vertebral fusion may occasionally lead to degeneration of adjacent segments due to excessive loading
Differential diagnosis	Acquired vertebral fusion: secondary to trauma, infection, or inflammation (juvenile rheumatoid arthritis) Schmorl nodule: located anteriorly, other signs of Scheuermann disease Spina bifida, meningocele

Table 10.11 Scheuermann disease

Prevalence	10 % of the population
Age predilection	10–18 years
Sex predilection	M > F
Location	Predominantly involves the lower thoracic spine and thoracolumbar junction
Type of lesion	Benign
Signs and symptoms	Nonspecific back pain in juveniles Persistent hyperkyphosis
Differential diagnosis	Postural kyphosis Acquired kyphosis (vertebral compression fracture) Caudal regression syndrome: vertebral endplates tend to display flat indentations posteriorly Intradiscal disc herniation: typically in older individuals, no loss of vertebral height anteriorly

10.3.4.3 Deformities of the Axial Skeleton (Scoliosis/Hyperkyphosis/Flattening) and Vertebral Sliding

The Meyerding system, which distinguishes four grades of vertebral forward movement, is the most common grading system for spondylolisthesis (Fig. 10.22) (Table 10.12). The radiologist should estimate and report the severity by giving the Meyerding grade for serial evaluation (Coughlin and McMurdo 1989; Lee et al. 1999; Shipley and Beukes 1998; Cassar-Pullicino and Eisenstein 2002).

Clinical Management

Asymptomatic abnormalities need not be treated. If pain is present, other causes must be ruled out. Spondylolisthesis should be followed up. Surgery may be indicated if there is progression in subjects with scoliosis or spondylolisthesis (Coughlin and McMurdo 1989; Lee et al. 1999; Shipley and Beukes 1998; Cassar-Pullicino and Eisenstein 2002).

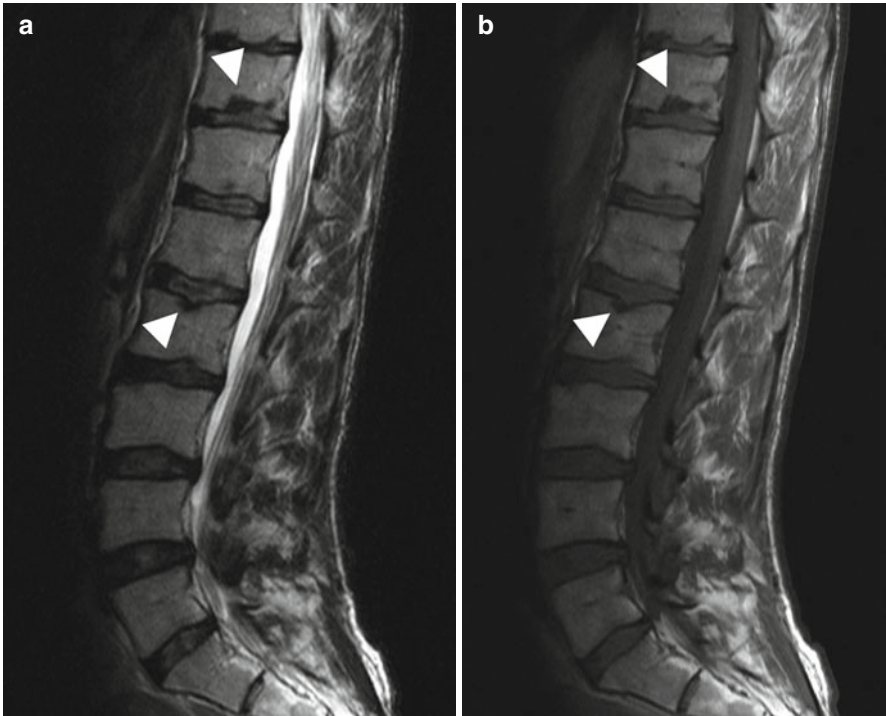


Fig. 10.21 Typical late sequelae of Scheuermann disease in a 50-year-old woman. Multiple Schmorl nodules (*arrowheads*), predominantly involving the lower thoracic and upper lumbar spine, and loss of lumbar lordosis due to decrease in anterior vertebral body height on sagittal T2w TSE image (**a**) and sagittal T1w TSE image (**b**). MRI shows no acute changes, and the woman had no complaints in this region

10.3.5 Inflammatory Conditions

A distinction must be made between acute and chronic inflammatory changes. Acute inflammatory conditions typically, though not always, present with acute or subacute onset of pain and general signs and symptoms of inflammation. We had no case of acute spondylodiscitis in our study population. Chronic inflammatory changes may persist after acute spondylodiscitis but are most commonly detected by MRI in subjects with rheumatoid arthritis or seronegative spondyloarthropathy.

10.3.5.1 Rheumatoid Arthritis

Detection of rheumatoid arthritis of the spine as a purely incidental finding is rare (Table 10.13). Subjects will typically have primary manifestations in the peripheral joints of the hands and feet and are usually aware of this. The diagnostic hallmark of spinal rheumatoid arthritis is soft tissue swelling around the dens axis (Fig. 10.23). In more advanced disease, subjects may develop atlantodental instability, which may result in dislocation (Arnett et al. 1988; Gabriel 2001; Resnick 1996a).

Clinical Management

When rheumatoid arthritis is first suspected, a subject should see a rheumatologist for further serologic and clinical diagnosis. In subjects with known rheumatoid arthritis, a cervical manifestation should be disclosed and follow-up recommended to monitor the response to medical treatment. Surgery may be indicated in case of marked atlantodental instability (Arnett et al. 1988; Gabriel 2001; Resnick 1996a, b).

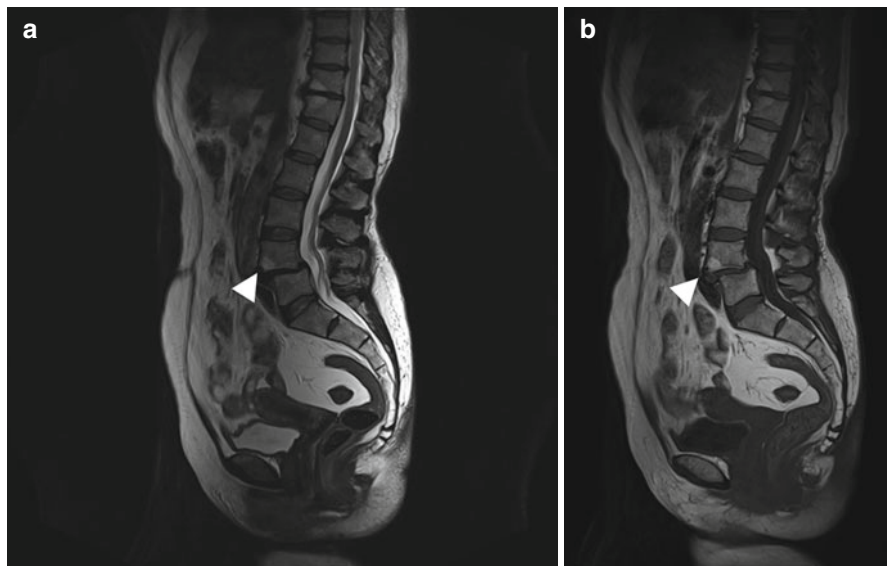


Fig. 10.22 Spondylolisthesis of L4/L5 (arrowhead), Meyerding grade 1. The defining feature is present, i.e., intervertebral disc degeneration with loss of height and reduced signal intensity on sagittal T2w TSE image (a). Mild Modic type 1 osteochondrosis. Anterior basal circumscribed fatty degeneration of L4, but also of T11/T12, with high signal intensity on T2w (a) and sagittal T1w TSE image (b) (corresponding to Modic type 2)

Table 10.12 Deformities of the axial skeleton (scoliosis/hyperkyphosis/flattening) and vertebral sliding

Prevalence	5–10 % of the population
Age predilection	Congenital; childhood
Sex predilection	F > M
Location	Predominantly thoracic and lumbar spine
Type of lesion	Benign
Signs and symptoms	Nonspecific back pain Spondylolisthesis may cause spinal claudication or neurologic deficits; severe lumbosacral pain
Differential diagnosis	Acquired vertebral fusion Postural anomalies (typically without a rotation component) Degenerative spondylolisthesis (or pseudospondylolisthesis) without spondylolysis, usually with marked facet joint arthrosis

Table 10.13 Rheumatoid arthritis

Prevalence	0.5–1.0 % of the population
Age predilection	Acquired; childhood
Sex distribution	F:M ratio of up to 3:1
Location	Peripheral joints, atlanto-occipital joints, upper cervical spine (facet joints), rarely sacroiliac joint
Type of lesion	Benign
Signs and symptoms	Peripheral: morning stiffness, joint swelling Central: neck or cervical spine pain, stiffness in some patients
Differential diagnosis	Seronegative spondyloarthropathy Degenerative spinal changes Infectious processes

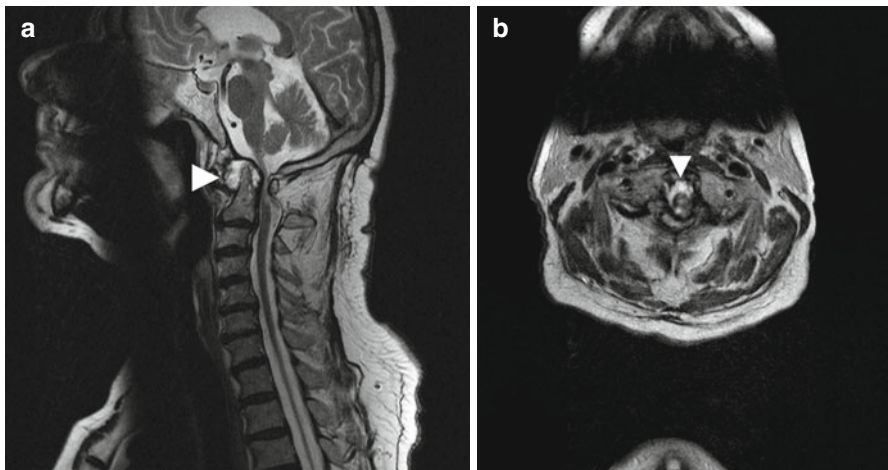


Fig. 10.23 Extensive pannus formation (*arrowhead*) around the tip of the dens in rheumatoid arthritis on sagittal T2w TSE image (**a**) and axial T2w TSE image (**b**). Large mass effect with atlantodental joint gap. There is high-grade myelopathy due to compression of the spinal cord. The subject only has mild ataxia, which is not consistent with the severity of these MRI abnormalities. The discrepancy suggests that the changes developed slowly

10.3.5.2 Seronegative Spondyloarthropathy

The seronegative spondyloarthropathies are a group of autoimmune disorders with similar morphologic changes on MRI (Table 10.14). The most important diseases subsumed under this label are psoriasis, Reiter syndrome, ankylosing spondylitis (Bechterew disease) (Maropaki 2007; Althoff et al. 2009), and gout.

It is not uncommon to find incidental signs of seronegative spondyloarthropathies in the axial skeleton. Here, the diagnostic hallmark is bone marrow edema in the area of the sacroiliac joint (Fig. 10.24) and entheses of the anterior longitudinal ligament (Romanus lesion). More advanced manifestations include syndesmophytes, parasyndesmophytes, and vertebral body squaring. The natural evolution of

ankylosing spondylitis in untreated individuals is characterized by ascending bony encasement of the intervertebral disc compartments and fusion of facet joints. Complete fusion of the vertebral column is known as bamboo spine (Freyschmidt 1997; Stern 1997; Dihlmann 1987; Hanson and Mirza 2000; Resnick 1996b).

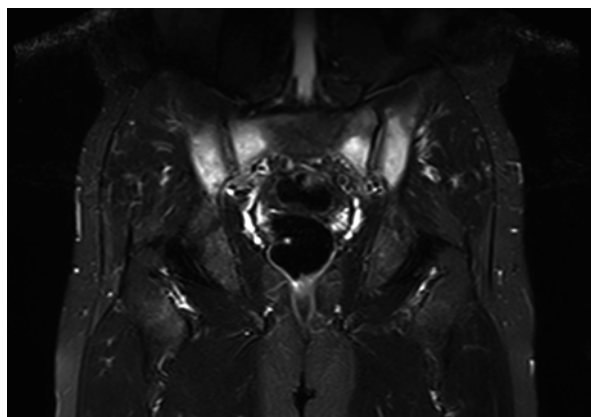
Clinical Management

A person first diagnosed with suspected seronegative spondyloarthropathy should see a rheumatologist for further serologic and clinical evaluation. If the disease has already been diagnosed, MRI findings should be disclosed to provide information on the current status, in conjunction with a recommendation for follow-up to monitor the effectiveness of medical treatment (Freyschmidt 1997; Stern 1997; Dihlmann 1987; Hanson and Mirza 2000; Resnick 1996a, b).

Table 10.14 Seronegative spondyloarthropathy

Prevalence	0.5–1.0 % of the population
Age predilection	20–40 years
Sex distribution	M:F ratio of up to 10:1
Location	Sacroiliac joints are often involved first Insidious progression from lumbar to thoracic and cervical Except for Bechterew disease, there is typically also involvement of peripheral joints; some patients have skin manifestations (psoriasis)
Type of lesion	Benign
Signs and symptoms	Axial skeletal involvement often first presents with low back pain (sacroiliitis) Increasing stiffness of lumbosacral junction, further course characterized by ascending stiffness
Differential diagnosis	Rheumatoid arthritis (typically involving cervical spine) Degenerative iliosacral joint or spinal changes Infectious changes DISH (Forestier disease)

Fig. 10.24 Sacroiliitis as an early sign of seronegative spondyloarthropathy. High-signal-intensity processes around both sacroiliac joints on sagittal T2w TSE image



10.3.6 Degenerative Conditions

Varying degrees of degenerative spinal changes (e.g., Rumboldt 2006) can be detected in virtually every adult. Early intervertebral disc degeneration is seen as a black disc on MR images, reflecting diminished water content. Gradual dehydration of the nucleus pulposus results in progressive disc space narrowing. Initial damage of the annulus fibrosus can promote disc protrusion and herniation. Individuals with advanced disc destruction often show the vacuum phenomenon after mobilization and fluid in the interspace after resting (D'Anastasi et al. 2011). Moreover, most individuals with severe disc degeneration have concomitant abnormalities of the vertebral endplates and adjacent bone marrow. We also consistently see signs of facet joint degeneration and ligamentum flavum hypertrophy. In addition, degenerative cysts may be encountered (Khalatbari and Ansari 2008). The mass effect from these abnormalities can narrow the bony spinal canal. Depending on the individual width of the bony spinal canal, such degenerative abnormalities can affect neural structures already at an early stage when they are still well localized. The effects on the spinal canal and cord can be appreciated on MR images. They range from simple external compression of the dural sac to manifest spinal canal stenosis with decreased subarachnoid and cisternal spaces. MRI also shows if a herniated disc causes nerve root compression in the lateral recess or in the neuroforamen. Surprisingly, there is no consistent direct correlation with clinical symptoms. The presence of any of these findings should thus be reported in very neutral terms. Intervertebral osteochondrosis is present in nearly all degenerative diseases of a spinal motion segment. If observed, the Modic stage must be given to assess acuteness, course, and prognosis of the disease.

10.3.6.1 Intervertebral Disc Herniation

Screening MRI will detect disc protrusion or prolapse in more than 50 % of subjects over 50 (Fig. 10.25) (Table 10.15). Most of these cases are asymptomatic and are a natural consequence of tissue aging due to axial loading of the spine resulting from upright gait. A herniated disc alone typically causes no pain. Complaints usually result from the involvement of neural structures and the presence of other degenerative processes of the affected motion segment such as spondyloarthritis and kissing spine (Baastrup disease). This is why the radiologist should always search for concomitant abnormalities and, if present, report them (Fardon et al. 2001; Milette 1997; Pardon and Milette 2001; Yasuma 1993; Zollner 2001).

Clinical Management

As a rule, the radiologist should be very cautious when making a clinical evaluation. Findings should be reported in a descriptive and neutral manner to avoid triggering a deterioration in an individual's subjective illness perception. A subject with neurologic deficits should be advised to see a neurologist/neurosurgeon/orthopedic surgeon (Fardon et al. 2001; Milette 1997; Pardon and Milette 2001; Yasuma 1993; Zollner 2001).

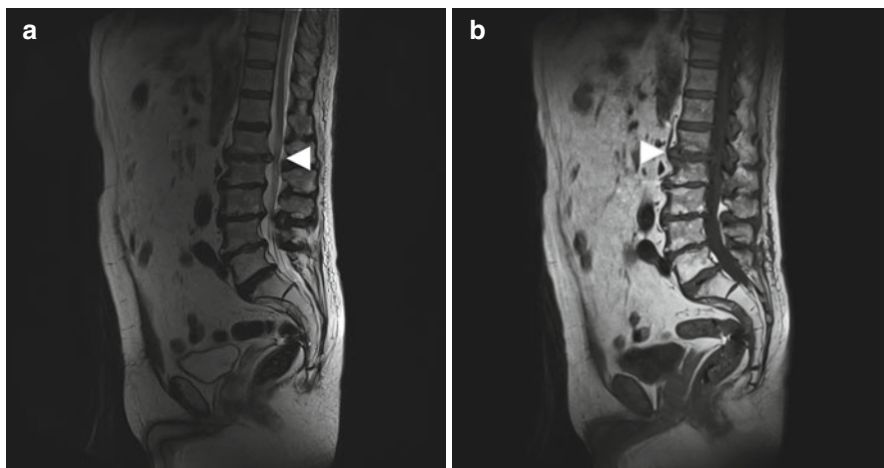


Fig. 10.25 Multisegmental changes in the lumbar spine. There is mediadorsal prolapse of the L1/L2 intervertebral disc (*arrowhead*) with the herniated material extending to the cauda equina but without signs of compression. All other lumbar levels display broad posterior protrusions and concomitant facet hypertrophy, with resultant relative spinal canal stenosis at the L3/L4 and L4/L5 levels. *Arrowhead* indicates posterior herniation of the L1/L2 disc on sagittal T2w TSE image (**a**) and anterior herniation on sagittal T1w TSE image (**b**)

Table 10.15 Intervertebral disc herniation

Prevalence	Common; no detailed data (highest incidence: 20–40 years)
Age predilection	20–40 years
Sex predilection	M=F; depends on general constitution and type of work
Location	L4/5 and L5/S1 > C5/6 and C6/7 > other lumbar and cervical segments; thoracic disc herniation moderately common and typically asymptomatic
Type of lesion	Benign
Signs and symptoms	Often unspecific pain as initial manifestation Root compression: corresponding segmental radicular symptoms with segmental sensory and/or motor loss in the most severe cases Lumbar disc herniation: can cause cauda equina syndrome or medullary cone syndrome, depending on level of involvement
Differential diagnosis	Spinal masses of other etiology: tumors, epidural hemorrhage or abscess, rarely spinal vascular malformation

10.3.6.2 Degenerative Spinal Stenosis

Degeneration of posterior spinal elements, such as hypertrophy of the facet joints or yellow ligaments, can occur in isolation but is commonly associated with degenerative disease of the anterior spine. Typically, individuals with facet joint arthrosis have concomitant yellow ligament hypertrophy, and the affected facets show the same changes as other joints: cartilage degeneration, incongruence of joint surfaces, effusion, increased subchondral sclerosis, and osteophytic outgrowths. However, there is one feature that is unique to facet joint degeneration: although cartilage attrition

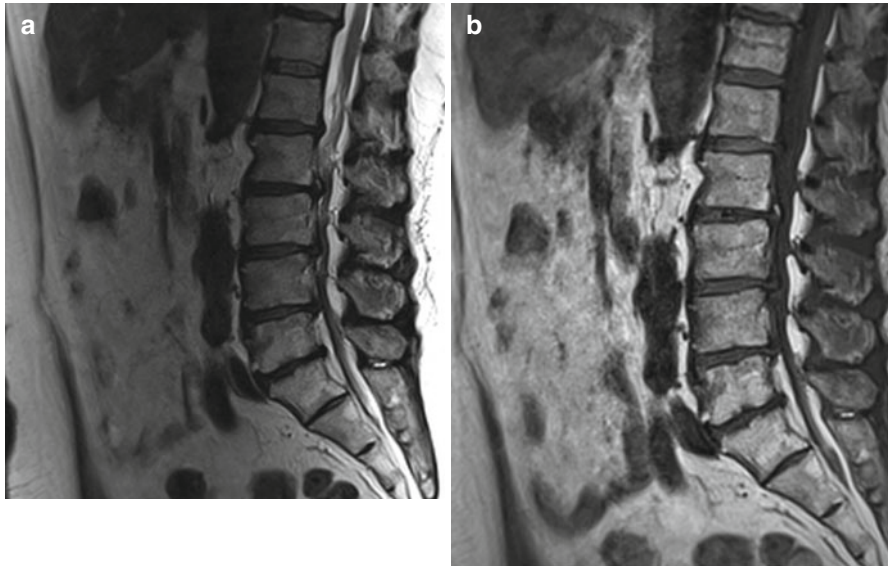


Fig. 10.26 Multisegmental absolute spinal canal stenosis of the lumbar spine with complete effacement of the CSF space and compression of the cauda equina at several levels. There is severe concomitant intervertebral osteochondrosis. Sagittal T2w TSE image (a) and sagittal T1w TSE image (b)

Table 10.16 Degenerative spinal stenosis

Prevalence	Common; no detailed data (highest incidence: 40–60 years)
Age predilection	40–60 years
Sex predilection	M=F; depends on general constitution and type of work
Location	L4/L5 and L5/S1 > C5/C6 and C6/C7 > other lumbar and cervical segments, rarely thoracic spine
Type of lesion	Benign
Signs and symptoms	Initially unspecific Occasionally lumbago (shooting pain) Spinal claudication Cervical myelopathy may occur
Differential diagnosis	Spinal masses of other etiology: tumors, epidural hemorrhage or abscess, rarely spinal vascular malformation

results in narrowing of the (radiologic) joint space, it is much more common to see a markedly widened (anatomic) joint space. This is attributable to a misalignment of the articulating surfaces, which is the result of an increased static load at the facets. There may be effusion in the widened joint space, but it is not uncommon to encounter a vacuum phenomenon, seen as a signal void (black) on T1- and T2-weighted MR images. In addition to bony outgrowths, we may encounter an occasional synovial cyst, which displaces adjacent structures when arising intraspinally.

Degenerative spinal stenosis occurs if the mass effect from abnormal posterior structures compromises the spinal canal (Fig. 10.26) (Table 10.16). The degree of

spinal stenosis should be estimated in relation to the congenital width of the bony spinal canal, which varies widely between individuals. In general, a distinction is made between relative stenosis, defined as a maximum anteroposterior spinal canal diameter of 10–15 mm, and absolute stenosis, which is assumed when the diameter is less than 10 mm. The radiologist's report must include an estimate of the width of the lateral recesses and state whether the cauda equina fiber configuration shows signs of compression. The radiologist must also evaluate the CSF spaces at the level of a spinal canal stenosis and identify possible additional mass effects from the intervertebral disc anteriorly and/or spondylophytes posteriorly. Higher-grade functional stenosis frequently obstructs outflow from the epidural venous plexus. Venous outflow obstruction aggravates clinical symptoms, and imaging will show multiple congested veins in the spinal canal, typically below the stenotic segment (de Graaf et al. 2006; Reith et al. 2006; Schulte et al. 2006; Modic 1999; Modic et al. 1988).

Clinical Management

A relative spinal canal stenosis or an absolute stenosis (<10 mm anteroposterior diameter) need not be reported as long as CSF spaces are sufficiently wide. Prompt communication of the findings to the subject is mandatory, however, if there are signs of imminent or manifest compression of the spinal cord or cauda equina. Urgent referral to a neurologist/neurosurgeon/orthopedic surgeon is especially important in subjects with neurologic deficits (de Graaf et al. 2006; Reith et al. 2006; Schulte et al. 2006; Modic 1999; Modic et al. 1988).

10.3.6.3 Intervertebral Osteochondrosis

Intervertebral disc pathology can lead to chronic irritation of adjacent bony structures, giving rise to a series of distinct reactive vertebral body changes. The first change seen is vertebral edema in the bone marrow adjacent to the endplates (Fig. 10.27). Edema formation results from chronic inflammatory irritation and in turn triggers progressive replacement of red marrow by yellow marrow. This degeneration of hematopoietic marrow is independent of the physiologic red-to-yellow marrow conversion related to aging. In the final stage of this process, the bone adjacent to the endplates becomes sclerotic and provides more stability (Fig. 10.28). Three types of vertebral changes with distinct MRI features are distinguished according to the classification of Modic (Table 10.17) (Modic 1999; Modic et al. 1988).

Intervertebral osteochondrosis is a disease of the elderly. The frequency of corresponding MRI findings (especially Modic type 1 and 2 lesions) varies with the age distribution of the screening population being investigated. A history of rapid clinical deterioration suggests erosive intervertebral osteochondrosis. This condition can be diagnosed by imaging, especially if earlier images are available for comparison. Clinically, it is important to differentiate intervertebral osteochondrosis from spondylodiscitis and vertebral fracture (Modic 1999; Modic et al. 1988).

Clinical Management

Management depends on the severity (Modic type), the number of motion segments involved, and the presence of concomitant degenerative processes. It will typically require a multimodal, multidisciplinary approach, especially in individuals with advanced disease. At our hospital, we have had excellent experience with presenting such cases to our spine board. Here, the individual's situation (family, job situation, mental health, exclusion of secondary gain from illness, prognosis) is comprehensively assessed, and a modular treatment approach including general pain management, physical therapy, CT-guided interventions, and surgical stabilization is used and tailored to the individual patient's situation (Modic 1999; Modic et al. 1988).

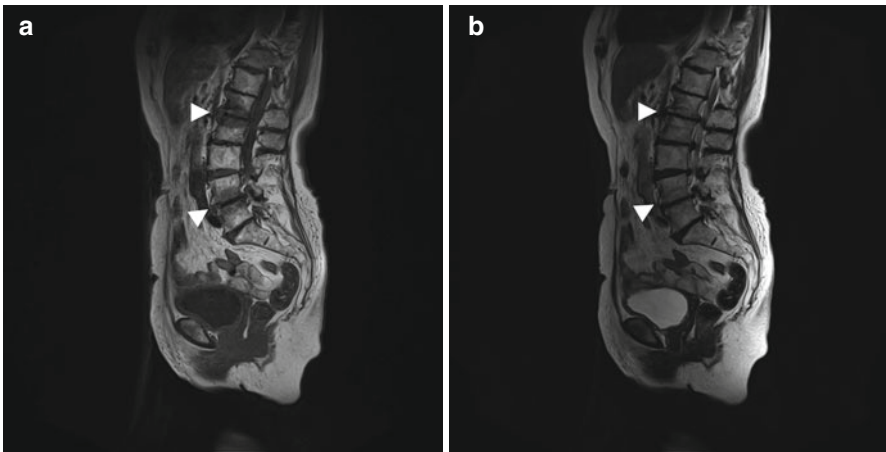


Fig. 10.27 Intervertebral osteochondrosis of the L1/L2 (*upper arrowhead*) and L4/L5 (*lower arrowhead*) segments. Bands of altered signal intensities along the involved endplates, predominantly low signal intensity on sagittal T1w TSE image (**a**) and predominantly high signal intensity on sagittal T2w TSE image (**b**) consistent with bone marrow edema (Modic type 1). Also note the peripheral low signal intensity of these band-like vertebral lesions on the T2w image, consistent with beginning marginal sclerosis. Concomitant disc protrusions/herniations

10.3.7 Metabolic and Other Systemic Disorders

The spine may be affected by a large variety of metabolic and hormonal disorders. The most common spinal manifestations of these disorders are changes in bone mineral density and changes in bone marrow composition. Osteoporotic abnormalities (Fig. 10.29) and fatty marrow conversion are relatively common incidental findings in the SHIP population. Quantitative MRI evaluation of manifest osteoporosis is still under investigation. Secondary changes, especially osteoporotic fractures, are regularly encountered (Baur et al. 2003; Bazzocchi et al. 2012).

Clinical Management

Signs and symptoms are often diverse and rarely specific in subjects with older vertebral compression fractures. Spinal canal stenosis and compression of neural structures must be described in the radiologist's report. Images must be evaluated for signs of fresh osteoporotic fractures, which is best accomplished by searching for vertebral edema on fat-saturated T2-weighted images. If a fracture is detected, stability of the vertebral body should be estimated. An unstable vertebra or fresh compression fracture must be disclosed to the subject. However, such findings are rare in the screening situation.

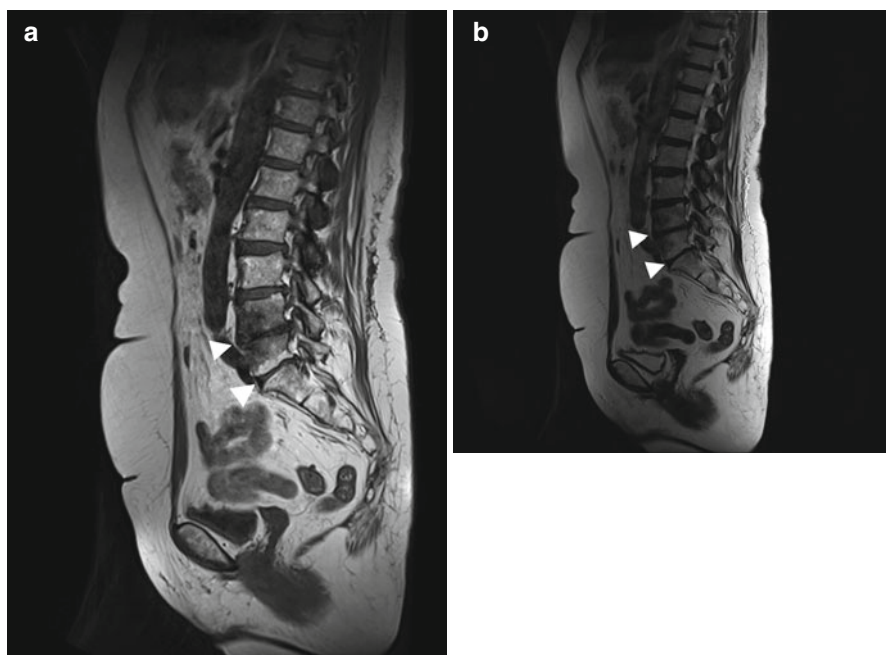


Fig. 10.28 Severe intervertebral osteochondrosis of L4/L5 (*upper arrowhead*) and L5/S1 (*lower arrowhead*): posterior portions of L4/L5 and bands along the endplates of L5/S1 display predominantly high-signal-intensity changes on sagittal T1w TSE image (**a**) and sagittal T2w TSE image (**b**), consistent with fatty degeneration (Modic type 2). Low T1 and T2 signal intensity of anterior portions of L4/L5 vertebral bodies indicating degenerative sclerosis (Modic type 3)

Table 10.17 Intervertebral osteochondrosis

Prevalence	Common; no detailed data (highest incidence: 20–40 years)
Age predilection	20–40 years
Sex predilection	M=F; depends on general constitution and type of work
Location	L4/L5 and L5/S1 > C5/C6 and C6/C7 > other lumbar and cervical segments, rarely thoracic spine
Type of lesion	Benign
Signs and symptoms	Unspecific local back pain of different intensity In patients with complete segmental instability, permanent pain may be so severe that they require opiate medication
Differential diagnosis	Bone marrow edema associated with vertebral fracture or compression Inflammatory edema, early spondylitis or spondylodiscitis Secondary hyperparathyroidism/renal osteodystrophy (ruger-jersey spine) Age-related fatty marrow conversion
MRI stages (Modic)	Stage 1 – edema: low T1, high T2 signal intensity Stage 2 – fat: high T1, high T2 signal intensity Stage 3 – sclerosis: low T1, low T2 signal intensity

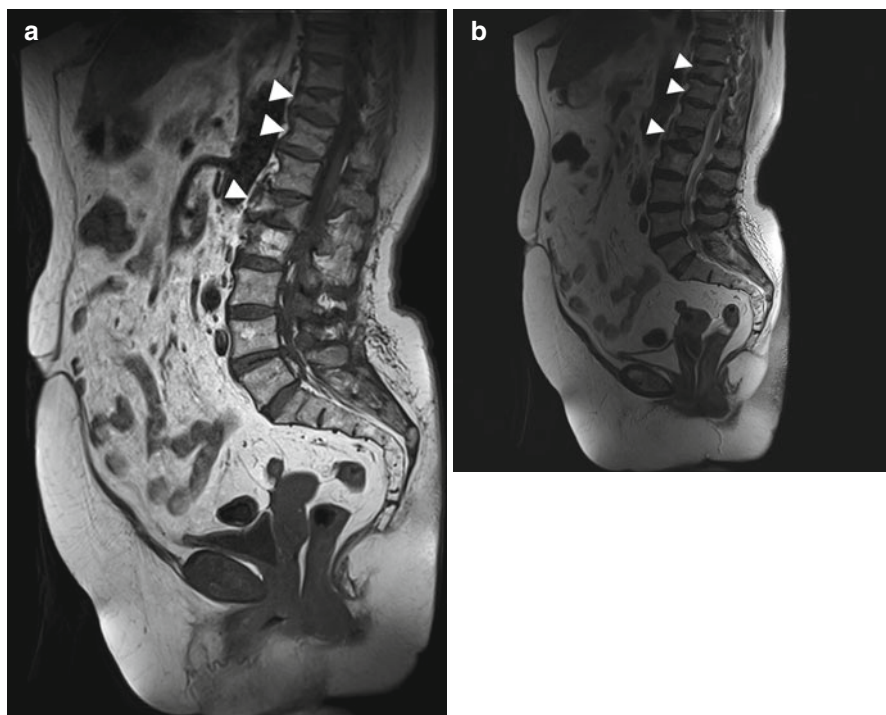


Fig. 10.29 Osteoporotic compression fractures of T10, T11, and L1 (*arrowheads*). No spinal canal narrowing or compression of neuronal structures. No signs of recent processes. Sagittal T1w (**a**) and T2w (**b**) TSE images. The subject reported chronic diffuse back pain but no circumscribed symptoms at the time of the examination. Additional findings: vertebral hemangiomas of L2 and L4; nearly complete fatty marrow degeneration

10.4 The Soft Tissues

10.4.1 Introduction

Highly sensitive STIR sequences are used to search for soft tissue abnormalities, especially in oncologic patients (Schmidt et al. 2009). On STIR images, metastases are easily detected as high-signal-intensity lesions within the low-signal-intensity muscle and fat (Fig. 10.30). Reliable data on the prevalence and incidence of soft tissue metastases are still lacking. Soft tissue metastases typically occur in advanced cancer. According to a recent study, metastases to skeletal muscles most commonly involve the widest muscles such as the gluteus, psoas, and erector spinae muscles (Arpaci et al. 2012). The STIR sequence is limited by poor specificity. There are other common soft tissue lesions that also have high signal intensity, including hemangioma and neurofibroma. In contrast, lipoma, the most common soft tissue tumor, has low signal intensity on STIR images. Additional pulse sequences are necessary for characterizing incidentally detected soft tissue lesions. The protocol should include a STIR sequence and T1-weighted sequences acquired before and after IV administration of contrast medium and, if lipoma is suspected, fat-suppressed pulse sequences.

10.4.2 Hemangioma

A hemangioma is a congenital benign tumor characterized by endothelial proliferation and secondary formation of vascular channels (Table 10.18). It is a sharply demarcated mass of high signal intensity on T2-weighted and STIR images (Fig. 10.31a, b). On T1-weighted images, a hemangioma may be difficult to detect because it is isointense to muscle (Fig. 10.31c). Areas of high T1 signal intensity may correspond to fat or slow-flowing blood. Phleboliths within a hemangioma cause signal voids on all pulse sequences. Following IV contrast medium administration, hemangiomas show strong enhancement, differentiating them from lipomas and hematomas (Fig. 10.31d) (Greenspan et al. 1992; Kransdorf 1995; Wild et al. 2000).

Clinical Management

Hemangiomas are benign and do not undergo malignant transformation. More than 90 % of capillary hemangiomas resolve by age 7. In contrast, cavernous hemangiomas rarely resolve, which is why they account for most of the hemangiomas detected at screening. Hemangiomas can become symptomatic when they compress adjacent structure and cause local destruction. If such complications are apparent on screening MR images, further diagnostic evaluation and possibly treatment are necessary (Wild et al. 2000; Canavese et al. 2008).



Fig. 10.30 Incidental screening finding (STIR): 54-year-old female subject with multiple metastatic lesions (*arrowheads*) in the left subcutaneous gluteal fatty tissue, paraspinally in the left chest, and in the left costodiaphragmatic angle. Diagnostic workup with ultrasound-guided biopsy revealed metastatic lipoblastoma

10.4.3 Lipoma

Lipoma is the most common mesenchymal tumor in humans (Table 10.19). It is an encapsulated homogeneous mass of fat cells and may occasionally be septated. Because of their composition, lipomas have the same signal intensity as fat on all pulse sequences, i.e., moderate to high signal intensity on T2-weighted images and high signal intensity on T1-weighted images (Fig. 10.33). Fat-suppressed imaging

Table 10.18 Hemangioma

Prevalence	7 % of all benign tumors Association with Kasabach-Merritt syndrome, Maffucci syndrome, Rendu-Osler-Weber syndrome, and Klippel-Trenaunay-Weber syndrome
Age predilection	1–36 years
Sex predilection	M=F
Location	Superficially in skin and subcutaneous fat (predominantly head and neck); deeper hemangioma in muscle tissue
Type of lesion	Benign
Signs and symptoms	Typically asymptomatic Light red to crimson vascular anomaly, often elevated above the skin level Movement-related pain
Differential diagnosis	Lipoma, hematoma

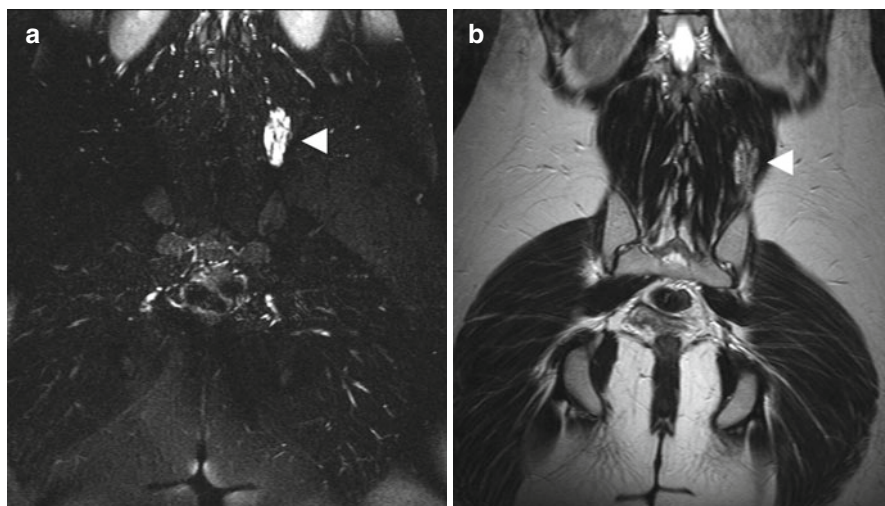


Fig. 10.31 Incidental screening finding (STIR) and diagnostic workup. Twenty-two-year-old female subject with a sharply demarcated lesion of high signal intensity (*arrowhead*) in the back muscles on the left (**a**). Diagnostic workup including an additional MRI examination with IV contrast medium administration confirmed the suspected asymptomatic intramuscular hemangioma. The lesion has high signal intensity on coronal T2w TSE image (**b**); is isointense to muscle on coronal T1w TSE image (**c**); and shows strong enhancement on fat-suppressed contrast-enhanced coronal T1w TSE image (**d**)



Fig. 10.31 (continued)

distinguishes lipomas from other soft tissue lesions. Because it has low signal intensity on STIR images, an intramuscular lipoma may be overlooked when this pulse sequence is used alone (Fig. 10.32). Following IV contrast medium administration, pure lipomas do not enhance, differentiating them from liposarcomas, which have a slightly inhomogeneous appearance on non-contrast-enhanced images (Fig. 10.33) (Murphey 2000; Einarsdottir et al. 1999). A systematic approach for interpreting MR images and differentiating between benign soft tissue lesions and sarcoma has been proposed by Chhabra and Soldatos (2012).

Clinical Management

Lipomas are benign and can be left alone if the MRI diagnosis is unequivocal. Only isolated cases of malignant transformation have been reported. If the margin is ill defined or the lesion enhances after IV contrast medium administration, a liposarcoma should be ruled out by diagnostic puncture (Einarsdottir et al. 1999). A symptomatic lipoma can be removed by en bloc excision or liposuction.

10.4.4 Neurofibroma and Schwannoma

Neurofibromas and schwannomas are benign tumors of neurogenic origin that arise in the soft tissues and skin along the neurovascular bundle (Table 10.20). They consist of neoplastic Schwann cells, fibroblasts, and perineurial cells. A schwannoma has a larger connective tissue component than a neurofibroma and has a true capsule

Table 10.19 Lipoma

Prevalence	1 % of the population Most common soft tissue tumor, accounts for 50 % of all soft tissue tumors More common in obese or diabetic individuals
Age predilection	5–75 years, with a peak at 40–60 years
Sex predilection	M=F
Location	Typically in the subcutaneous fat of the neck, back, and proximal extremities; deeper subcutaneous layers of the chest, retroperitoneum, at the hands and feet 5–8 % multifocal
Type of lesion	Benign Only a few cases of malignant transformation have been reported
Signs and symptoms	Typically asymptomatic Palpable, mobile mass characterized by slow growth Pain due to nerve compression
Differential diagnosis	Liposarcoma, hematoma

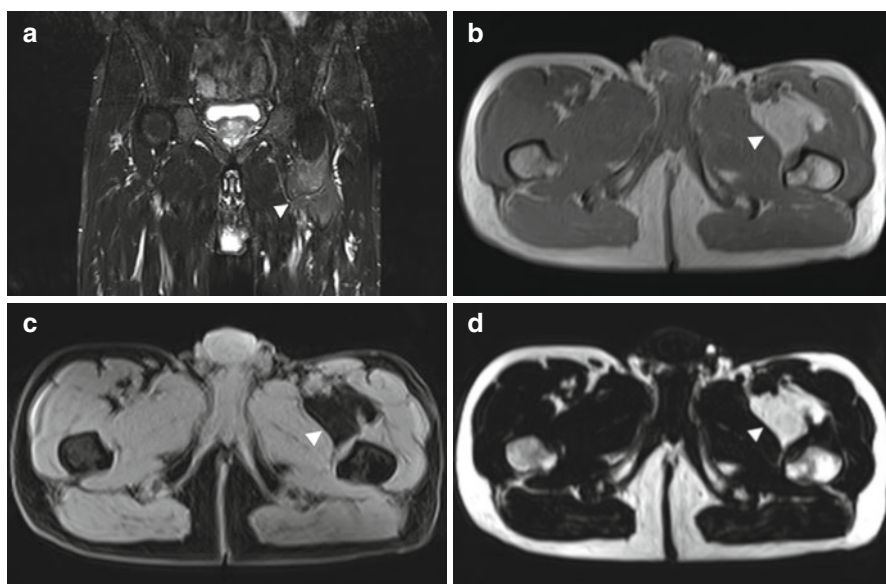


Fig. 10.32 Incidental screening finding (STIR). Sixty-nine-year-old male subject with a well-demarcated lesion (*arrowhead*), nearly isointense to muscle and fat, in the posterior thigh muscles of the left leg (**a**). On the axial T1w VIBE Dixon images, the signal intensity of the lesion is equivalent to that of fat: high on T1w image (**b**), low on corresponding fat-suppressed image (**c**), and high on water-suppressed image (**d**)

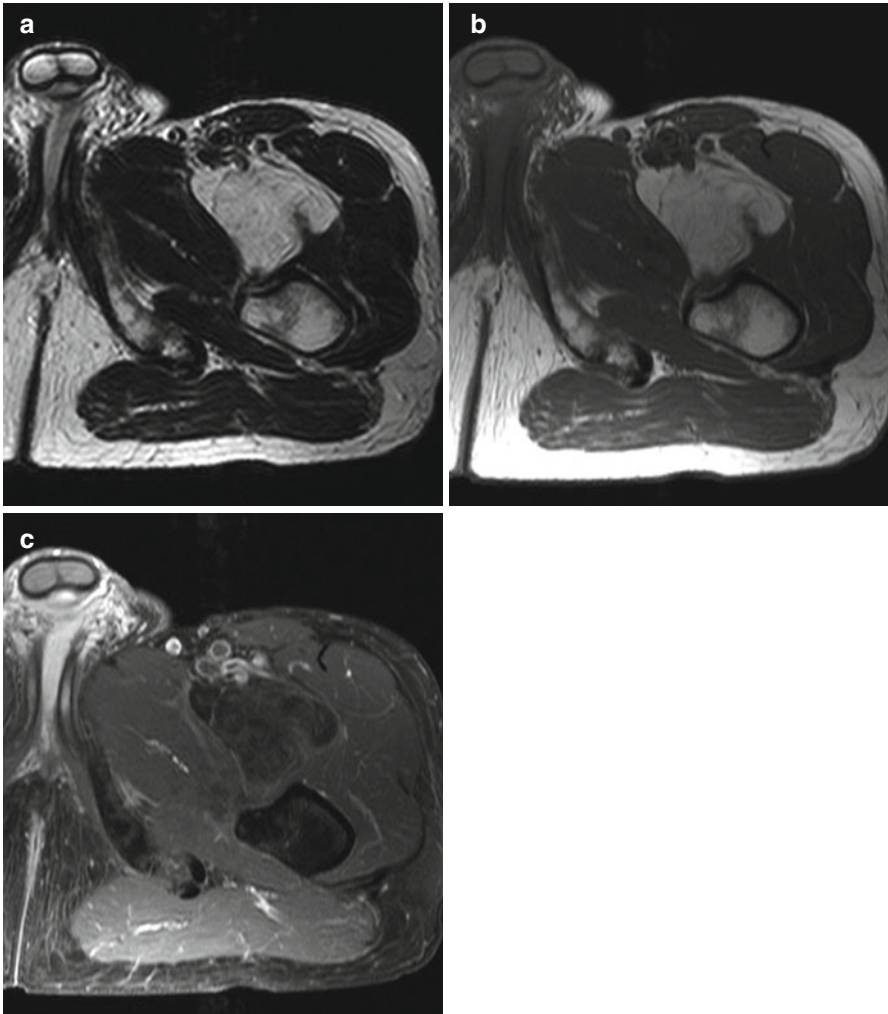


Fig. 10.33 Diagnostic workup (same subject as Fig. 10.32) with contrast-enhanced MRI allows differentiation of a simple lipoma from liposarcoma. Only a liposarcoma will enhance after IV contrast medium administration. Precontrast axial T1w TSE image (a) and axial T2w TSE image (b). The lesion does not enhance on postcontrast axial fat-suppressed T1w TSE image (c), confirming lipoma

Table 10.20 Neurofibroma and schwannoma

Prevalence	5 % of all benign soft tissue tumors 10 % of affected individuals have type 1 neurofibromatosis (von Recklinghausen disease)
Age predilection	20–30 years
Sex predilection	M=F
Location	Neurofibroma: nerve plexus, spinal nerves, peripheral nerves (often skin) Schwannoma: skin nerves of the head and neck, peroneal and ulnar nerves, posterior mediastinum, retroperitoneum
Type of lesion	Benign; malignant transformation is rare, but 4 % in type 1 neurofibromatosis
Signs and symptoms	Asymptomatic Slowly growing, painless mass Neurologic symptoms if major nerve is involved
Differential diagnosis	Malignant peripheral nerve sheath tumor, hematoma, liposarcoma

composed of epineurium. It is located eccentrically within the epineurium, displacing the affected nerve. In contrast, a neurofibroma is not encapsulated and arises centrally, causing spindle-shaped expansion of the parent nerve. On MRI, a neurofibroma is characterized by isointensity to skeletal muscle on T1-weighted images and hyperintensity on T2-weighted images (Fig. 10.34a, b). The center is of lower signal intensity (target sign). Following IV contrast medium administration, enhancement is highly variable and often confined to the periphery (Fig. 10.34c) (Kransdorf 1995; Suh et al. 1992).

Clinical Management

Schwannomas and neurofibromas are benign soft tissue tumors. Malignant transformation is very rare in schwannoma and solitary neurofibroma, but the risk is as high as 4 % in individuals with type 1 neurofibromatosis. Regular imaging follow-up is recommended for subjects with multiple neurofibromas. A sudden increase in size of an existing neurofibroma (>5 cm), typically along a large nerve, should alert the physician to the possibility of a neurofibrosarcoma. Surgical removal may become necessary in subjects with symptomatic tumors. While a schwannoma can be removed sparing the nerve, surgical resection of a neurofibroma typically requires sacrifice of a portion of the nerve (Gutmann et al. 1997).

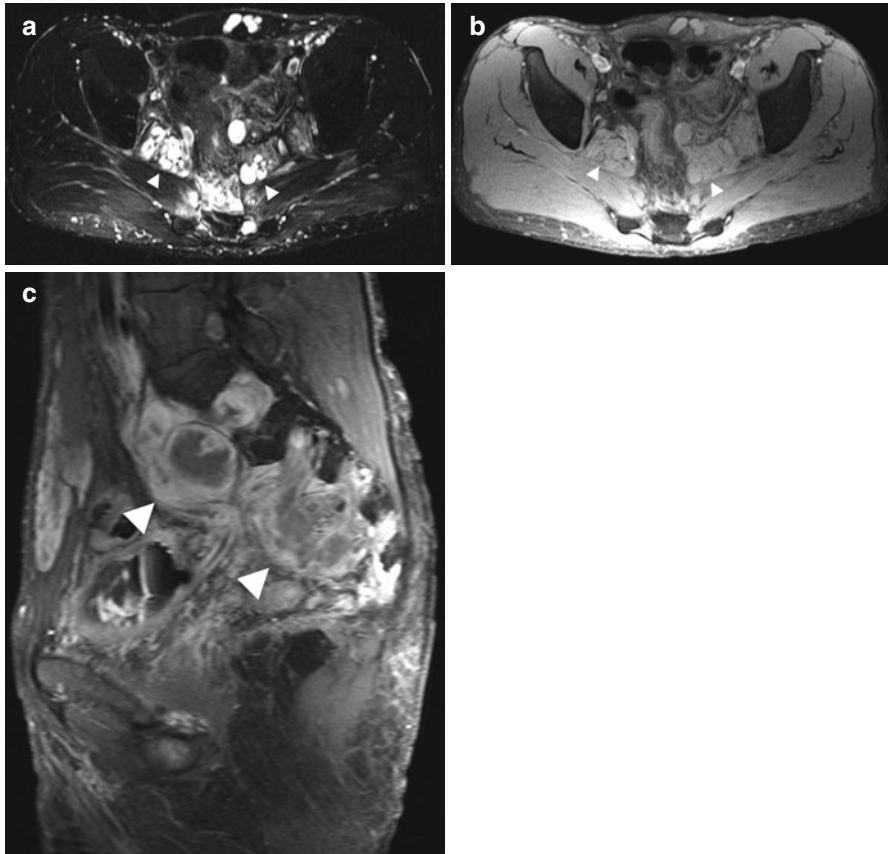


Fig. 10.34 Incidental screening finding and diagnostic workup. Twenty-five-year-old male subject with multiple spherical masses of high signal intensity (*arrowheads*) along the course of the lumbosacral plexus and within the abdominal muscles on axial T2w TSE image with fat suppression (**a**). Diagnostic workup with an additional MRI examination including IV administration of contrast medium reveals multiple neurofibromas of the lumbosacral plexus (*arrowheads*), which are isointense to muscle on fat-suppressed axial T1w TSE image (**b**) and exhibit peripheral enhancement on corresponding sagittal image acquired after IV contrast medium administration (**c**). Neurofibromas typically distend the neuroforamina

References

- Abdel Razeq AA, Castillo M (2010) Imaging appearance of primary bony tumors and pseudo-tumors of the spine. *J Neuroradiol* 37:37–50
- Ahmed AR, Tan TS, Unni KK, Collins MS, Wenger DE, Sim FH (2003) Secondary chondrosarcoma in osteochondroma: report of 107 patients. *Clin Orthop Relat Res* 411:193–206
- Ali RM, Green DW, Patel TC (1999) Scheuermann's kyphosis. *Curr Opin Pediatr* 11:70–75
- Altay M, Bayrakci K, Yildiz Y, Ereklis S, Saglik Y (2007) Secondary chondrosarcoma in cartilage bone tumors: report of 32 patients. *J Orthop Sci* 12:415–423

- Althoff CE, Feist E, Burova E, Eshed I, Bollow M, Hamm B, Hermann KG (2009) Magnetic resonance imaging of active sacroiliitis: do we really need gadolinium? *Eur J Radiol* 71:232–236
- Aoki J, Sone S, Fujioka F, Terayama K, Ishii K, Karakida O, Imai S, Sakai F, Imai Y (1991) MR of enchondroma and chondrosarcoma: rings and arcs of Gd-DTPA enhancement. *J Comput Assist Tomogr* 15:1011–1016
- Arnett FC, Edwotzhy SM, Bloch DA et al (1988) The American Rheumatism Association 1987 revised criteria for the classification of rheumatoid arthritis. *Arthritis Rheum* 31:315–324
- Arpaci T, Ugurluer G, Akbas T, Arpaci RB, Serin M (2012) Imaging of the skeletal muscle metastases. *Eur Rev Med Pharmacol Sci* 16:2057–2063
- Assoun J, Richardi G, Railhac JJ, Baunin C, Fajadet P, Giron J, Maquin P, Haddad J, Bonnevalle P (1994) Osteoid osteoma: MR imaging versus CT. *Radiology* 191:217–223
- Ayerza MA, Abalo E, Aponte-Tinao L, Muscolo DL (2007) Endoscopic resection of symptomatic osteochondroma of the distal femur. *Clin Orthop Relat Res* 459:150–153
- Baur A, Dietrich O, Reiser M (2003) Diffusion-weighted imaging of bone marrow: current status. *Eur Radiol* 13:1699–1708
- Baur-Melnyk A, Buhmann S, Dürr HR, Reiser M (2005) Role of MRI for the diagnosis and prognosis of multiple myeloma. *Eur J Radiol* 55:56–63
- Bazzocchi A, Spinnato P, Garzillo G, Ciccarese F, Albisinni U, Mignani S, Battista G, Rossi C (2012) Detection of incidental vertebral fractures in breast imaging: the potential role of MR localisers. *Eur Radiol* 22:2617–2623
- Blacksin MF, Ende N, Benevenia J (1995) Magnetic resonance imaging of intraosseous lipomas: a radiologic-pathologic correlation. *Skeletal Radiol* 24:37–41
- Brossmann J, Czerny C, Freyschmidt J (2001) Grenzen des Normalen und Anfänge des Pathologischen in der Radiologie des kindlichen und erwachsenen Skeletts. Thieme, Stuttgart
- Canavese F, Soo BC, Chia SK, Krajchich JI (2008) Surgical outcome in patients treated for hemangioma during infancy, childhood, and adolescence: a retrospective review of 44 consecutive patients. *J Pediatr Orthop* 28:381–386
- Cassar-Pullicino VN, Eisenstein SM (2002) Imaging in scoliosis: what, why and how? *Clin Radiol* 57:543–562
- Chapurlat RD, Orcel P (2008) Fibrous dysplasia of bone and McCune-Albright syndrome. *Best Pract Res Clin Rheumatol* 22:55–69
- Chhabra A, Soldatos T (2012) Soft-tissue lesions: when can we exclude sarcoma? *AJR Am J Roentgenol* 199:1345–1357
- Chiewvit P, Danchaivijitr N, Sirivitmaitrie K, Chiewvit S, Thephamongkhol K (2009) Does magnetic resonance imaging give value-added than bone scintigraphy in the detection of vertebral metastasis? *J Med Assoc Thai* 92:818–829
- Collins CD (2010) Multiple myeloma. *Cancer Imaging* 10:20–31
- Coughlin WF, McMurdo SK (1989) CT diagnosis of spondylolysis of the axis vertebra. *AJR Am J Roentgenol* 153:195
- D’Anastasi M, Birkenmaier C, Schmidt G, Wegener B, Reiser M, Baur-Melnyk A (2011) Correlation between vacuum phenomenon on CT and fluid on MRI in degenerative disks. *AJR Am J Roentgenol* 197:1182–1189
- de Graaf I et al (2006) Diagnosis of lumbar spinal stenosis: a systematic review of the accuracy of diagnostic tests. *Spine* 31:1168–1176
- Delorme S, Baur-Melnyk A (2011) Imaging in multiple myeloma. *Recent Results Cancer Res* 183:133–147
- Dihlmann W (1987) Spondylitis ankylosans. In: Dihlmann W (ed) *Gelenke – Wirbelverbindungen*. Thieme, Stuttgart, pp 591–605
- Dorfman HD et al (1998) *Bone tumors*, 1st edn. Mosby, St. Louis, pp 253–296
- Einarsdottir H, Söderlund V, Larson O, Jenner G, Bauer HC (1999) MR imaging of lipoma and liposarcoma. *Acta Radiol* 40:64–68
- Fardon DF et al (2001) Nomenclature and classification of lumbar disc pathology. Recommendations of the combined task force of the North American Spine Society, American Society of Spine Radiology, and American Society of Neuroradiology. *Spine* 26:E93–E113

- Fenichel I, Garniack A, Morag B, Palti R, Salai M (2006) Percutaneous CT-guided curettage of osteoid osteoma with histological confirmation: a retrospective study and review of the literature. *Int Orthop* 30:139–142
- Frassica FJ, Waltrip RL, Sponseller PD, Ma LD, McCarthy EF Jr (1996) Clinicopathologic features and treatment of osteoid osteoma and osteoblastoma in children and adolescents. *Orthop Clin North Am* 27:559–574
- Freyschmidt J (1997) Psoriasisarthritis. In: Freyschmidt J (ed) *Skeletterkrankungen. Klinisch-radiologische Diagnose und Differenzialdiagnose*. Springer, Berlin, pp 711–718
- Friedman DP (1996) Symptomatic vertebral hemangiomas: MR findings. *AJR Am J Roentgenol* 167:359–564
- Gabriel SE (2001) The epidemiology of rheumatoid arthritis. *Rheum Dis Clin North Am* 27:269–281
- Geirnaerdt MJ, Bloem JL, Eulderink F, Hogendoorn PC, Taminau AH (1993) Cartilaginous tumors: correlation of gadolinium-enhanced MR imaging and histopathologic findings. *Radiology* 186:813–817
- Gesundheitsberichterstattung des Bundes (Gesundheit, Statistik, GBE) (2008). http://www.gbe-bund.de/gbe10/trecherche.prc_them_rech?tk=200&tk2=210&p_uid=gast&p_aid=56308828&p_sprache=D&cnt_ut=1&ut=210
- Ghanem N, Uhl M, Brink I, Schäfer O, Kelly T, Moser E, Langer M (2005) Diagnostic value of MRI in comparison to scintigraphy, PET, MS-CT and PET/CT for the detection of metastases of bone. *Eur J Radiol* 55:41–55
- Goodman SB, Bell RS, Fornasier VL, De Demeter D, Bateman JE (1984) Ollier's disease with multiple sarcomatous transformations. *Hum Pathol* 15:91–93
- Greenspan A (1989) Tumors of cartilage origin. *Orthop Clin North Am* 20:347–366
- Greenspan A (1993) Benign bone-forming lesions: osteoma, osteoid osteoma, and osteoblastoma. Clinical, imaging, pathologic, and differential considerations. *Skeletal Radiol* 22:485–500
- Greenspan A, Remagen W (1998) Differential diagnosis of tumors and tumor-like lesions of bones and joints, 1st edn. Lippincott-Raven, Philadelphia, pp 125–146
- Greenspan A, McGahan JP, Vogelsang P, Szabo RM (1992) Imaging strategies in the evaluation of soft-tissue hemangiomas of the extremities: correlation of the findings of plain radiography, angiography, CT, MRI, and ultrasonography in 12 histologically proven cases. *Skeletal Radiol* 21:11–18
- Gutmann DH, Aylsworth A, Carey JC, Korf B, Marks J, Pyeritz RE, Rubenstein A, Viskochil D (1997) The diagnostic evaluation and multidisciplinary management of neurofibromatosis 1 and neurofibromatosis 2. *JAMA* 278:51–57
- Haddad FS, Haddad GF, Zaatar G (1997) Cranial osteomas: their classification and management. Report on a giant osteoma and review of the literature. *Surg Neurol* 48:143–147
- Hanson JA, Mirza S (2000) Predisposition for spinal fracture in ankylosing spondylitis. *AJR Am J Roentgenol* 174:150
- Hoffmann RT, Jakobs TF, Kubisch CH, Trumm CG, Weber C, Duerr HR, Helmberger TK, Reiser MF (2010) Radiofrequency ablation in the treatment of osteoid osteoma-5-year experience. *Eur J Radiol* 73:374–379
- Hong ED, Carrino JA, Weber KL, Fayad LM (2011) Prevalence of shoulder enchondromas on routine MR imaging. *Clin Imaging* 35:378–384
- Ippolito E, Bray EW, Corsi A, De Maio F, Exner UG, Robey PG, Grill F, Lala R, Massobrio M, Pinggera O, Riminucci M, Snella S, Zambakidis C, Bianco P, European Pediatric Orthopaedic Society (2003) Natural history and treatment of fibrous dysplasia of bone: a multicenter clinicopathologic study promoted by the European Pediatric Orthopaedic Society. *J Pediatr Orthop B* 12:155–177
- Jee WH, Choi KH, Choe BY, Park JM, Shinn KS (1996) Fibrous dysplasia: MR imaging characteristics with radiopathologic correlation. *AJR Am J Roentgenol* 167:1523–1527
- Khalatbari K, Ansari H (2008) MRI of degenerative cysts of the lumbar spine. *Clin Radiol* 63:322–328

- Kransdorf MJ (1995) Benign soft-tissue tumors in a large referral population: distribution of specific diagnoses by age, sex, and location. *AJR Am J Roentgenol* 164:395–402
- Kwee TC, de Klerk JM, Nievelstein RA (2011) Imaging of bone marrow involvement in lymphoma: state of the art and future directions. *Scientific World Journal* 11:391–402
- Lee J-H, Ehara S, Tamakawa Y et al (1999) Spondylolysis of the upper lumbar spine: radiological features. *Clin Imaging* 23:389
- Lokiec F, Wientroub S (1998) Simple bone cyst: etiology, classification, pathology, and treatment modalities. *J Pediatr Orthop B* 7:262–273
- Mahnken AH, Wildberger JE, Adam G, Stanzel S, Schmitz-Rode T, Günther RW, Buecker A (2005) Is there a need for contrast-enhanced T1-weighted MRI of the spine after inconspicuous short tau inversion recovery imaging? *Eur Radiol* 15:1387–1392
- Maropaki F (2007) Magnetresonanztomographische Befunde bei Morbus Bechterew unter besonderer Berücksichtigung von Veränderungen der Wirbelkörperabschlussplatte. Dissertation zum Erwerb des Doktorgrades der Medizin an der Medizinischen Fakultät der Ludwig-Maximilians-Universität zu München, pp 1–105
- Mehta RC, Marks MP, Hinks RS, Glover GH, Enzmann DR (1995) MR evaluation of vertebral metastases: T1-weighted, short-inversion-time inversion recovery, fast spin-echo, and inversion-recovery fast spin-echo sequences. *AJNR Am J Neuroradiol* 16:281–288
- Mehta M, White LM, Knapp T, Kandel RA, Wunder JS, Bell RS (1998) MR imaging of symptomatic osteochondromas with pathological correlation. *Skeletal Radiol* 27:427–433
- Milette PC (1997) The proper terminology for reporting lumbar intervertebral disorders. *AJNR Am J Neuroradiol* 18:10
- Modic MT (1999) Degenerative disc disease and back pain. *Magn Reson Imaging Clin N Am* 7:481
- Modic MT, Steinberg PM, Ross JS, Masaryk TJ, Carter JR (1988) Degenerative disc disease: assessment of changes in vertebral bone marrow with MR Imaging. *Radiology* 166:193
- Murphey MD, Choi JJ, Kransdorf MJ, Flemming DJ, Gannon FH (2000) Imaging of osteochondroma: variants and complications with radiologic-pathologic correlation. *Radiographics* 20(5):1407–1434
- Müller PE, Dürr HR, Wegener B, Pellengahr C, Maier M, Jansson V (2003) Solitary enchondromas: is radiographic follow-up sufficient in patients with asymptomatic lesions? *Acta Orthop Belg* 69:112–118
- Papac RJ (1994) Bone marrow metastases. A review. *Cancer* 74:2403–2413
- Pardon DF, Milette PC (2001) Nomenclature and classification of lumbar disc pathology. *Spine* 26:E93–E113
- Park HJ, Jeon YH, Rho MH, Lee EJ, Park NH, Park SI, Jo JH (2011) Incidental findings of the lumbar spine at MRI during herniated intervertebral disk disease evaluation. *AJR Am J Roentgenol* 196:1151–1155
- Perdikakis E, Skiadas V (2013) MRI characteristics of cysts and “cyst-like” lesions in and around the knee: what the radiologist needs to know. *Insights Imaging* 4:257–272
- Quatman CE, Quatman-Yates CC, Schmitt LC, Paterno MV (2012) The clinical utility and diagnostic performance of MRI for identification and classification of knee osteochondritis dissecans. *J Bone Joint Surg Am* 94:1036–1044
- Reith W, Nabhan A, Kelm J, Naumann N, Ahlhelm F (2006) Differentialdiagnose des Rückenschmerzes. *Radiologe* 46:443–453
- Resnick D (1996a) Rheumatoid arthritis. In: Resnick D (ed) *Bone and joint imaging*, 2nd edn. Saunders, Philadelphia, pp 211–234
- Resnick D (1996b) Ankylosing spondylitis. In: Resnick D (ed) *Bone and joint imaging*, 2nd edn. Saunders, Philadelphia, pp 246–264
- Ricci C, Cova M, Kang YS, Yang A, Rahmouni A, Scott WW, Zerhouni EA (1990) Normal age-related patterns of cellular and fatty bone marrow distribution in the axial skeleton: MR imaging study. *Radiology* 177:83–88
- Rigopoulou A, Saifuddin A (2012) Intraosseous hemangioma of the appendicular skeleton: imaging features of 15 cases, and a review of the literature. *Skeletal Radiol* 41:1525–1536

- Rossi A, Biancheri R, Cama A et al (2004) Imaging in spine and spinal cord malformations. *Eur J Radiol* 50:177–200
- Rumboldt Z (2006) Degenerative disorders of the spine. *Semin Roentgenol* 41:327–362
- Schijman E (2003) Split cord malformation: report of 22 cases and review of literature. *Childs Nerv Syst* 19:106–108
- Schmidt GP, Schoenberg SO, Reiser MF, Baur-Melnyk A (2005) Whole-body MR imaging of bone marrow. *Eur J Radiol* 55:33–40
- Schmidt GP, Schoenberg SO, Schmid R, Stahl R, Tiling R, Becker CR, Reiser MF, Baur-Melnyk A (2007) Screening for bone metastases: whole-body MRI using a 32-channel system versus dual-modality PET-CT. *Eur Radiol* 17:939–949
- Schmidt GP, Reiser MF, Baur-Melnyk A (2009) Whole-body MRI for the staging and follow-up of patients with metastasis. *Eur J Radiol* 70:393–400
- Schmorl G (1929) Über Knorpelknötchen an den Wirbelbandscheiben. *Fortschr Röntgenstr* 38:265
- Schulte TL et al (2006) Lumbale Spinalkanalstenose. *Orthopade* 35:675–694
- Shipley JA, Beukes CA (1998) The nature of the spondylytic defect: demonstration of a communicating synovial pseudarthrosis in the pars interarticularis. *J Bone Joint Surg Br* 80:662
- Stern RS (1997) Psoriasis. *Lancet* 350:349–353
- Subhas N, Bui KL, Sundaram M, Ilaslan H, Recht MP (2009) Incidental tumor and tumor-like lesions around the knee. *Semin Musculoskelet Radiol* 13:353–370
- Suh JS, Abenzoza P, Galloway HR, Everson LI, Griffiths HJ (1992) Peripheral (extracranial) nerve tumors: correlation of MR imaging and histologic findings. *Radiology* 183:341–346
- Tortori-Donati P, Fondelli MP, Rossi A, Raybaud CA, Cama A, Capra V (1999) Segmental spinal dysgenesis: neuroradiologic findings with clinical and embryologic correlation. *AJNR Am J Neuroradiol* 20:445–456
- Tortori-Donati P et al (2001) Magnetic resonance imaging of spinal dysraphism. *Top Magn Reson Imaging* 12:375–409
- Tribus CB (1998) Scheuermann's kyphosis in adolescents and adults: diagnosis and management. *J Am Acad Orthop Surg* 6:36–43
- Unni KK (2001) Cartilaginous lesions of bone. *J Orthop Sci* 6:457–472
- Vanel D, Ruggieri P, Ferrari S, Picci P, Gambarotti M, Staals E, Alberghini M (2009) The incidental skeletal lesion: ignore or explore? *Cancer Imaging* 9:38–43
- Vanel D, Kreshak J, Larousserie F, Alberghini M, Mirra J, De Paolis M, Picci P (2013) Enchondroma vs. chondrosarcoma: a simple, easy-to-use, new magnetic resonance sign. *Eur J Radiol* 82:2154–2160
- Vogler JB, Murphy WA (1988) Bone marrow imaging. *Radiology* 168:679–693
- Wenger DR, Frick SL (1999) Scheuermann kyphosis. *Spine* 4:2630–2639
- Wild AT, Raab P, Krauspe R (2000) Hemangioma of skeletal muscle. *Arch Orthop Trauma Surg* 120:139–143
- Williams CE, Close PJ, Meaney J, Ritchie D, Cogley D, Carty AT (1993) Intraosseous lipomas. *Clin Radiol* 47:348–350
- Winkelmann S, Hirsch W, Burdach S, Horneff G (2003) Therapy of osteoid osteomas – always surgically? *Klin Padiatr* 215:35–39
- Yasuma T (1993) The histology of lumbar intervertebral disc herniation. The significance of small blood vessels in the extruded tissue. *Spine* 18:1761–1765
- Zollner J (2001) Radiological assessment of loss of disk height in acute and chronic degenerative lumbar disk changes. *Rofo* 173:187–190

Saskia Ungerer

11.1 Introduction

Breast cancer is the most common malignancy in women in industrialized countries. In Germany, for instance, nearly 60,000 new cases are diagnosed each year. Early detection improves the chances of successful treatment.

Common imaging modalities used to examine the breasts include conventional X-ray mammography, ultrasonography, and magnetic resonance imaging (MRI) (Heywang-Köbrunner et al. 2013; Planche and Vinnicombe 2004). Mammography is the preferred modality in population-based screening programs (Prasad and Houserkova 2007; Schlossbauer et al. 2008). Breast MRI is still considered an adjunct to conventional mammography and ultrasound although it has been used clinically since 1988 (Heywang-Köbrunner et al. 2013; Fischer 2000; Heywang-Köbrunner 1994). However, its role in breast imaging is expanding (Schlossbauer et al. 2008; Seely 2012) because it is more sensitive than X-ray mammography alone or in conjunction with ultrasound (Le-Petross and Shetty 2011). Despite its low specificity, breast MRI can improve the detection of malignant lesions and is particularly helpful in identifying cancer in young women with dense breasts and in detecting early disease, such as carcinoma in situ, in high-risk women (DeMartini et al. 2008; Kuhl et al. 2007).

Breast MRI has therefore evolved into an additional screening tool for women at high risk due to a strong family history of breast cancer or a known BRCA1 or BRCA2 mutation (Dewey and Martus 2008; Lehman et al. 2005; Yu et al. 2008).

S. Ungerer
Institute of Diagnostic Radiology and Neuroradiology,
University Medicine Greifswald, Ferdinand-Sauerbruch-Straße,
Greifswald 17487, Germany
e-mail: sungerer@uni-greifswald.de

These are currently the main indications for breast MRI (Heywang-Köbrunner et al. 2013):

- To rule out multicentric disease or additional lesions in the contralateral breast before surgery in women diagnosed with breast cancer (Brasic et al. 2013)
- To distinguish postoperative scar after breast-sparing surgery from recurrent cancer
- To locate breast cancer of unknown primary (CUP) in women with histologic evidence of cancer
- To screen women with a high-risk profile (known gene mutation, family history) (Kuhl and Braun 2008; Lehman et al. 2005)

Unclear focal breast lesions detected by mammography or ultrasound can be promptly, inexpensively, and reliably characterized by percutaneous biopsy. In these cases, there is no need for an MRI examination, except when conventional diagnostic methods do not allow reliable cancer localization within the breast. Such exceptions include multifocal or multicentric disease and palpable lumps not detectable with mammography or ultrasound or visible in only one mammographic projection but not on ultrasound (DeMartini et al. 2008; Dewey and Martus 2008). A wider use of breast MRI is hampered by its high cost and a high rate of false positive results (Lehman et al. 2005). Another limiting factor is the restricted availability of MRI.

A comprehensive MRI examination of the breasts, including unenhanced and contrast-enhanced pulse sequences, provides important diagnostic information for characterizing and staging breast disease (Brasic et al. 2013) and may be helpful in planning surgery and monitoring neoadjuvant chemotherapy (Morrow et al. 2011; Monticciolo 2011). On the other hand, preoperative breast MRI has been linked to higher mastectomy rates and does not consistently reduce the need for re-excision. Overall, however, breast MRI detects many more occult contralateral cancers than conventional mammography or ultrasound (Miller et al. 2012).

The role of MRI in the initial diagnosis of suspicious breast lesions remains to be defined (Patani and Mokbel 2008). It is still a challenge for radiologists to correctly interpret the morphologic and kinetic features of a breast lesion seen on MRI and confidently categorize it as benign or malignant (Seely 2012).

11.1.1 Breast MRI Technique

Because of time constraints, an MRI examination of the breasts, when performed as part of a whole-body protocol, only includes axial pulse sequences, which limits evaluation of axillary lymph nodes. The protocol used here comprises a T2-weighted TIRM sequence, a T2-weighted TSE sequence without fat saturation, a fat-saturated diffusion-weighted SE sequence, and a dynamic T1-weighted 3D FLASH series consisting of an unenhanced acquisition and imaging at five time points after IV administration of gadobutrol (0.1 mL/kg body weight). Subtraction images are automatically generated to highlight enhancing structures. Maximum intensity projection (MIP) images created from the subtracted series allow rapid assessment of

the spatial distribution of enhancing tissue within the breast and enable good differentiation between small lesions and vessels seen in cross section.

The breasts are imaged with a series of thin slices following volumetric excitation. Acquisition of thin slices increases background noise compared with thicker slices.

Breast MRI is performed with the woman prone and the breasts suspended in the bilateral breast coil. Perfusion of the breast is subject to hormonal variation, which is why contrast medium accumulation varies through the menstrual cycle (Amarosa et al. 2013). Data from intraindividual comparison of premenopausal women suggest that confounding enhancement of normal glandular tissue is least pronounced in the second week of the menstrual cycle and most pronounced during the first and fourth weeks (Fischer 2000; Kuhl et al. 1995). For this reason, an attempt was made to schedule breast MRI during the second week of the cycle in premenopausal SHIP participants.

11.1.2 Lesion Classification and Management

The classification of incidental breast findings on screening MRI and the recommended clinical management were based on the ACR BI-RADS categories initially developed for mammography and later adapted for MRI (Table 11.1).

Outside the screening context, breast lesions categorized as BI-RADS 0 are very rarely encountered because breast MRI is typically performed after conventional mammography and ultrasound (Mendelson et al. 2003).

Criteria used to assess breast lesions on contrast-enhanced MR images include the shape and demarcation of enhancing lesions, the pattern of enhancement, and the time course of enhancement. Malignancy is suggested by an irregular, star-shaped appearance with ring enhancement or rapid initial enhancement with postinitial washout, while a sharply marginated, round, or oval lesion with slow and continuous contrast medium uptake tends to be benign (Fischer 2012; Macura et al. 2006) (Table 11.2).

The so-called Goettingen score has been developed and used as a standardized tool for the comprehensive multifactorial evaluation of breast abnormalities on MRI and is most useful for the characterization of hypervascularized mass lesions. The tool integrates a maximum of criteria that have shown promise in differentiating between malignant and benign breast lesions. The strongest malignancy criteria – ring enhancement, strong initial enhancement (>100 %), and postinitial washout – are each assigned a score of 2. Less suspicious features are assigned a score of 1 and include irregular shape, ill-defined margins, inhomogeneous enhancement, 50–100 % initial contrast enhancement, and postinitial plateau. A score of 0 is assigned to features suggesting a benign lesion; these include round or oval shape, sharp margin, homogeneous enhancement, moderate initial signal increase of <50 %, and continuous postinitial signal increase. A lesion can thus be assigned a total score of 0–8 points. Breast lesions with a total Goettingen score of 1 or 2 (corresponding to ACR BI-RADS categories 1 and 2) are more likely benign, while

Table 11.1 ACR BI-RADS (American College of Radiology *Breast Imaging Reporting and Data System*) assessment categories for the standardized description of breast findings. The categories are the same for mammography and breast MRI

Category (mammography and MRI)	Assessment	Probability of malignancy, description	Clinical management recommendation
BI-RADS 0	Incomplete diagnostic information	Category that is primarily assigned in screening situations	Needs additional diagnostic evaluation
BI-RADS 1	Negative	0 % probability of malignancy	Needs no diagnostic workup; normal interval follow-up
BI-RADS 2	Definitely benign	0 % probability of malignancy, e.g., cyst, fatty tissue necrosis, hamartoma (fibroadenolipoma), juvenile fibroadenoma	Needs no diagnostic workup; normal interval follow-up
BI-RADS 3	Probably benign	<2 % probability of malignancy, e.g., adult fibroadenoma	Short-interval follow-up (6 months)
BI-RADS 4	Suspicious abnormality	Lesion with a few features not typical of malignancy; probability of malignancy of 30 % (range, 2–90 %); subcategories: 4a: low suspicion (1–3 %) 4b: moderate suspicion (4–50 %) 4c: high suspicion (51–94 %)	Short-interval follow-up; biopsy should be considered
BI-RADS 5	Highly suggestive of malignancy	Typical imaging features of malignancy, e.g., irregular margin, spiculation, inhomogeneous appearance; >90 % probability of malignancy	Short-interval follow-up and initiation of appropriate treatment
BI-RADS 6	Histologically proven malignancy	Breast cancer confirmed by histology	Additional diagnostic workup before initiation of appropriate treatment

Modified from Mendelson et al. (2003)

lesions assigned a score of 4 or higher (corresponding to ACR BI-RADS categories 4 and 5) are more suspicious for malignancy (Fischer 2012).

Additional information for characterizing a breast lesion is provided by postprocessing tools that analyze contrast enhancement kinetics over time. This is done in a region of interest (ROI) placed in an area of contrast enhancement. In case of inhomogeneous lesion enhancement, the ROI is placed in the area showing the strongest enhancement. The ROI should include at least three pixels because misinterpretation of the enhancement pattern may result when the ROI is too small.

Table 11.2 Malignancy criteria of breast lesions on MRI

Criterion	Features suggesting malignancy	Nonspecific features
Lesion shape	Dendritic, star shaped	Round, oval
Lesion margin	Irregular margin, spiculated	Smooth margin
Enhancement pattern	Ring enhancement	Inhomogeneous
Enhancement kinetics	Strong initial signal increase; postinitial washout	Moderate initial signal increase; continuous postinitial signal increase, plateau phase
Water content on T2-weighted images	Low water content	High water content, septa

The signal increase after contrast medium administration can be expressed as a percentage relative to the baseline value on precontrast images or as a normalized value relative to the signal intensity of surrounding fat.

Strong initial enhancement with rapid washout is characteristic of a malignant breast lesion, while moderate initial enhancement with a slight further increase or plateau phase thereafter favors a benign lesion (Table 11.2).

Pitfalls in image interpretation arise from focal areas of enhancement within the glandular tissue in young premenopausal women (Amarosa et al. 2013) and in postmenopausal women on hormone replacement therapy (Pfleiderer et al. 2004). These foci may show the same rapid and strong initial enhancement as breast cancer. However, these foci are usually temporary and will no longer be detectable in a repeat examination (Kuhl et al. 1995; Liberman et al. 2002).

More recent studies suggest that fat-saturated diffusion-weighted SE images with generation of apparent diffusion coefficient (ADC) maps can help in characterizing breast lesions with inconclusive morphologic MRI features and dynamic kinetic patterns (Rahbar et al. 2011; Tsushima et al. 2009). High signal intensity of a suspicious lesion on diffusion-weighted images with low values in ADC maps suggests reduced perfusion and hypercellularity. Benign lesions or tumors that have responded to treatment usually have normal diffusion (De Bazelaire et al. 2010).

The following sections discuss the most important and most common incidental breast findings detected by MR mammography in the setting of whole-body MRI screening.

11.2 Benign Breast Lesions

11.2.1 Simple Breast Cysts

Breast cysts are round or oval fluid-filled structures that are highly variable in size (from microscopic to 5–6 cm). A larger cyst can often be palpated as a firm, elastic mass. Some breast cysts present with nipple discharge (Hines et al. 2010). Histologically, the fluid collection is surrounded by a double-layered wall – an inner epithelial and outer myoepithelial layer. Occasional thin septa may be present. Simple breast cysts are single or multiple (Fischer 2000) (Fig. 11.1 and Table 11.3).

Cysts are a typical feature of fibrocystic breast changes. There is no risk of malignant transformation. Cysts are best detected by a meticulous ultrasound examination of the breast (Bhate et al. 2007; Mendelson et al. 2003).

MRI Features

T2-weighted images:

- Very bright, fluid-filled, round or oval mass.
- High protein content results in lower signal intensity.
- Thin septa may be present within the cyst.

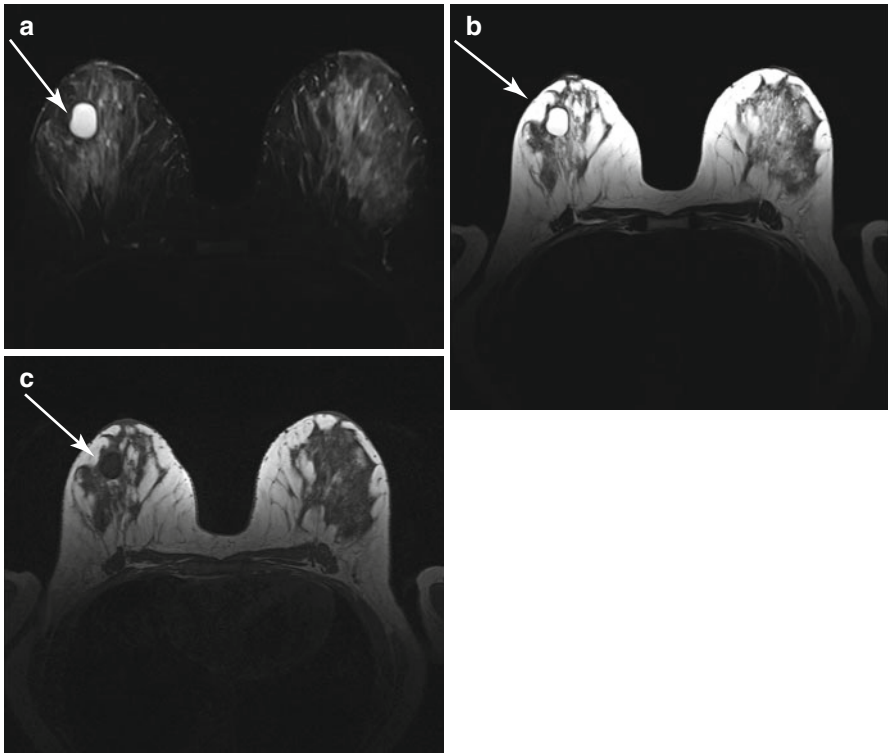


Fig. 11.1 Simple breast cyst (arrow) in a 48-year-old subject. (a) The cyst is depicted as a bright, sharply demarcated lesion on T2w TIRM image. (b) The cyst also has very high signal intensity on T2w TSE image. (c) Signal intensity is low on T1w image

Table 11.3 Simple breast cysts

Frequency	10 % of all women
Age predilection	Perimenopausal, typically between 30 and 50 years
Type of lesion	Benign
Signs and symptoms	Small breast cysts usually cause no symptoms; a large cyst is often palpable as a firm, elastic, freely movable mass

Non-contrast-enhanced T1-weighted images:

- Dark, fluid-filled, round or oval mass

Contrast-enhanced T1-weighted images:

- A simple breast cyst shows virtually no enhancement.
- Cystic lesions become more conspicuous due to enhancement of surrounding glandular tissue.
- Cyst content does not enhance (Uematsu and Kasami 2009b).

Differential Diagnosis

- *Complex breast cyst* (see next section; intralesional hemorrhage or higher protein content results in higher T1 and lower T2 signal intensity)
- *Postoperative seroma* (also high T2 and low T1 signal intensity; however, seroma is usually very large and sometimes painful; may appear heterogeneous and irregular and is typically located near the chest wall; and develops in the early postoperative phase) (Whipp and Halliwell 2008)
- *Other circumscribed lesions* (intramammary lymph node, abscess, metastasis, fatty tissue necrosis, papilloma)

11.2.2 Complex Breast Cysts

Complex or complicated breast cysts (Table 11.4) differ from simple cysts in that they have debris within the fluid-filled sac or in that the wall or fluid may show signs of inflammation, hemorrhage, or neoplasm (Bhate et al. 2007; Hines et al. 2010) (Fig. 11.2).

MRI Features

T2-weighted images:

- Bright, fluid-filled, round, or oval mass.
- High protein content results in lower signal intensity.
- Thin septa may be present.

Non-contrast-enhanced T1-weighted images:

- Sharply demarcated, dark lesion.
- High protein content or blood in the cyst fluid can lead to markedly higher signal intensity (Uematsu and Kasami 2009b).

Contrast-enhanced T1-weighted images:

- Thickening of portions of the cyst wall with contrast enhancement reflects inflammation (conspicuous rim enhancement) (Hines et al. 2010)
- Cyst content does not enhance

Table 11.4 Complex breast cysts

Frequency	10 % of all women
Age predilection	Perimenopausal, typically between 30 and 50 years
Type of lesion	Benign; neoplastic changes in rare cases (0.2 %)
Signs and symptoms	Small breast cysts usually cause no symptoms; a large cyst is often palpable as a firm, elastic, freely movable mass

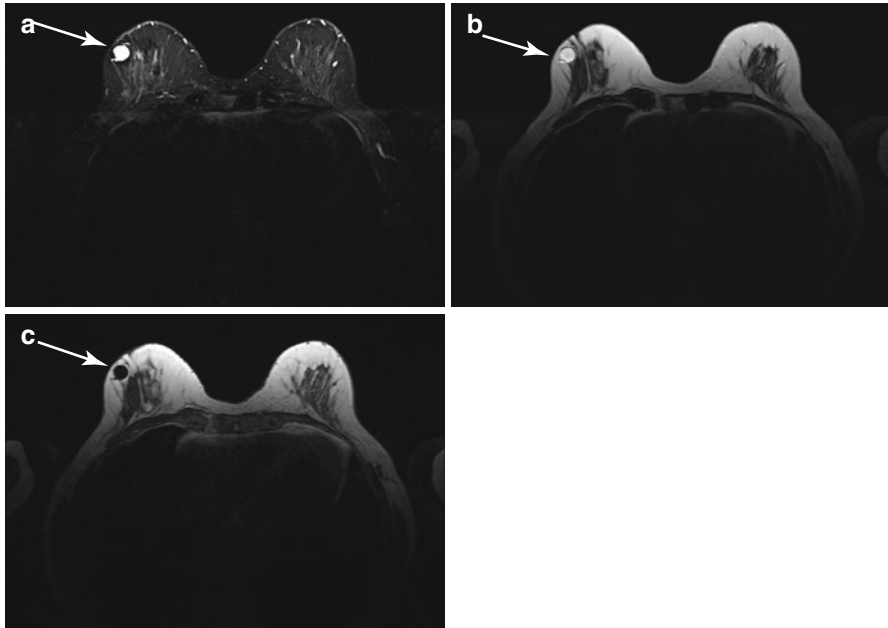


Fig. 11.2 Complex breast cyst (arrow) in a 66-year-old subject. (a) T2w TIRM image shows a smoothly demarcated lesion of predominantly high signal intensity. (b) On the T2w TSE image, the bright cyst fluid is surrounded by a hypointense rim. (c) On the T1w image, the cyst fluid has low signal intensity, and the rim appears bright

- Breast tissue surrounding a hemorrhagic cyst may enhance (inflammation)
- Solid portions may enhance (Uematsu and Kasami 2009a)

Differential Diagnosis

- *Simple cyst* (see preceding section; no enhancement of cyst content or wall; very bright on T2-weighted image and dark on T1-weighted image)
- *Abscess* (often accompanied by erythema, skin thickening, and edema; typically located close to the nipple; thickened wall)
- *Invasive ductal carcinoma* (see below; if there is central necrosis, invasive ductal carcinoma may be mistaken for a complex cyst; rim enhancement may be seen, typically when there is wall thickening (>2 mm))
- *Fibroadenoma* (see below; enhancement is strong in juvenile adenoma, while adult fibroadenoma is characterized by little initial enhancement and a continuous increase thereafter)

Clinical Management

Sharply demarcated cysts are classified as BI-RADS 2 and can be left alone. There is no risk of malignant transformation. Complex cysts are categorized as BI-RADS 3 and require further evaluation. Workup should include ultrasound-guided aspiration of cyst fluid for cytologic examination.

11.2.3 Intramammary Lymph Nodes

An intramammary lymph node is an oval mass with smooth borders in the breast parenchyma (Fig. 11.3). Histologically, it is identical to lymph nodes elsewhere in the body (Table 11.5). Intramammary lymph nodes can be found anywhere in the breast but are most common in the upper outer quadrant. As a rule, they are not palpable (Iglesias et al. 2007). As with other normal lymph nodes, they are characterized by the presence of a fatty hilum (Schmidt et al. 2001; Spillane et al. 1999).

MRI Features

T2-weighted images:

- Intermediate or high signal intensity, which, in some cases, may be confined to the margin.
- On fat-suppressed images, the fatty hilum shows loss of signal intensity.

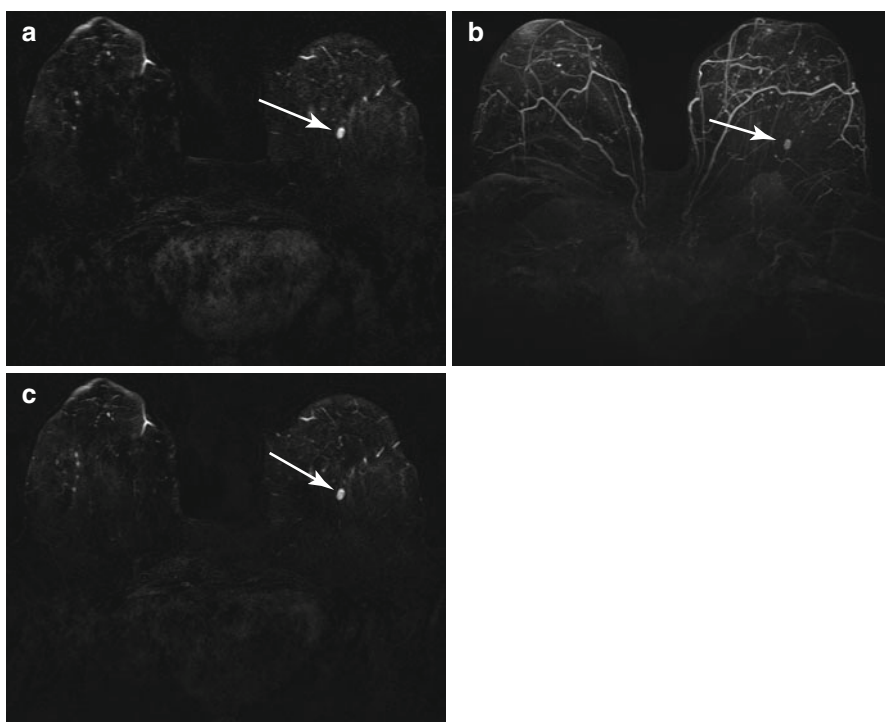


Fig. 11.3 Intramammary lymph node (*arrow*) in a 63-year-old subject. Contrast-enhanced T1w series. (a) Early postcontrast subtraction image. (b) Maximum intensity projection (MIP). (c) Late postcontrast subtraction image

Table 11.5 Intramammary lymph nodes

Frequency	47 % of all women
Age predilection	All ages
Type of lesion	Benign; harmless incidental finding
Signs and symptoms	No typical clinical presentation

Non-contrast-enhanced T1-weighted images:

- An intramammary lymph node within the parenchyma may be indistinct from the surrounding tissue.
- Outside the parenchyma, an intramammary lymph node is depicted as an oval, smooth mass of lower signal intensity.
- Hilar fat may appear bright.

Contrast-enhanced T1-weighted images:

- Typically no or very little contrast enhancement.
- In case of reactive inflammation, an intramammary lymph node may show rapid and strong enhancement, mimicking the enhancement kinetics of malignant breast lesions (Iglesias et al. 2007).
- Reactive inflammation of an intramammary lymph node may lead to rim enhancement sparing the fatty hilum

Differential Diagnosis

- Other well-circumscribed, encapsulated masses containing fat
- Examples include lipoma, fibroadenolipoma, galactocele, and clusters of cysts embedded in fat
- Other well-circumscribed, noncalcified masses
- Cysts, fibroadenoma, lymphoma, and metastasis (rare)

Clinical Management

An intramammary lymph node is assessed as BI-RADS 2, meaning that no further workup is needed. It is typically a harmless, incidental finding and has no malignant potential. Metastasis in an intramammary lymph node is extremely uncommon.

11.2.4 Fibroadenoma

Breast fibroadenoma is a mixed fibroepithelial tumor. The juvenile type of this benign tumor, occurring in younger women, has a large epithelial component (Fig. 11.4).

The fibrous component increases with age, undergoes progressive hyalinization and calcification, and becomes predominant in postmenopausal women (Fischer 2000; Kuusk 1988) (Fig. 11.5). Fibroadenomas account for 75 % of all breast lesions. They are multiple in approx. 25 % of cases (Table 11.6). Women with adult fibroadenoma have an increased risk of breast cancer (Dupont et al. 1994; McDivitt et al. 1992).

MRI Features

T2-weighted images:

- Juvenile fibroadenomas have high signal intensity, making them difficult to differentiate from cysts
- Adult fibroadenomas, containing a large amount of fibrous tissue, are usually isointense and occasionally hypointense to breast parenchyma

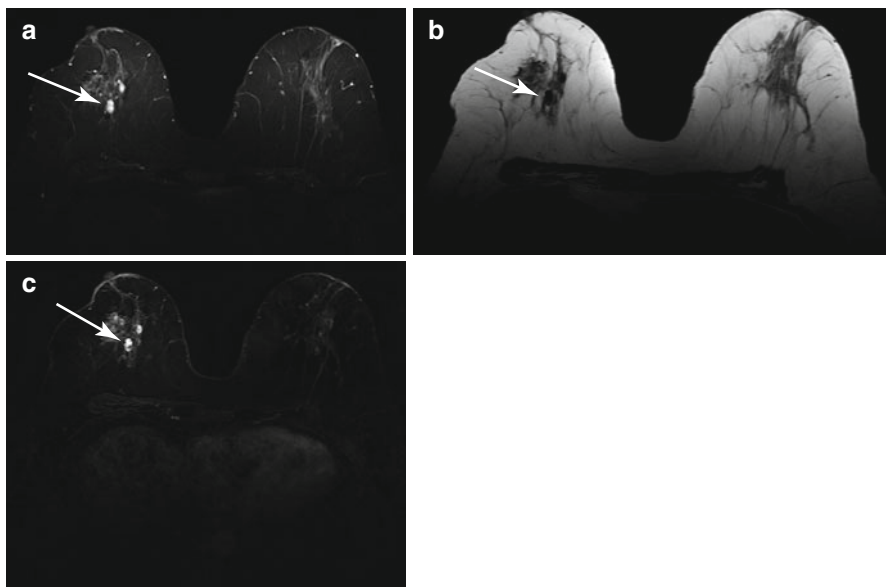


Fig. 11.4 Juvenile fibroadenomas (*arrow*) in a 33-year-old subject. (a) Conspicuous small foci of high signal intensity on T2w TIRM image. (b) The foci have low signal intensity on unenhanced T1w image. (c) Subtracted postcontrast T1w image shows strong enhancement of the lesions

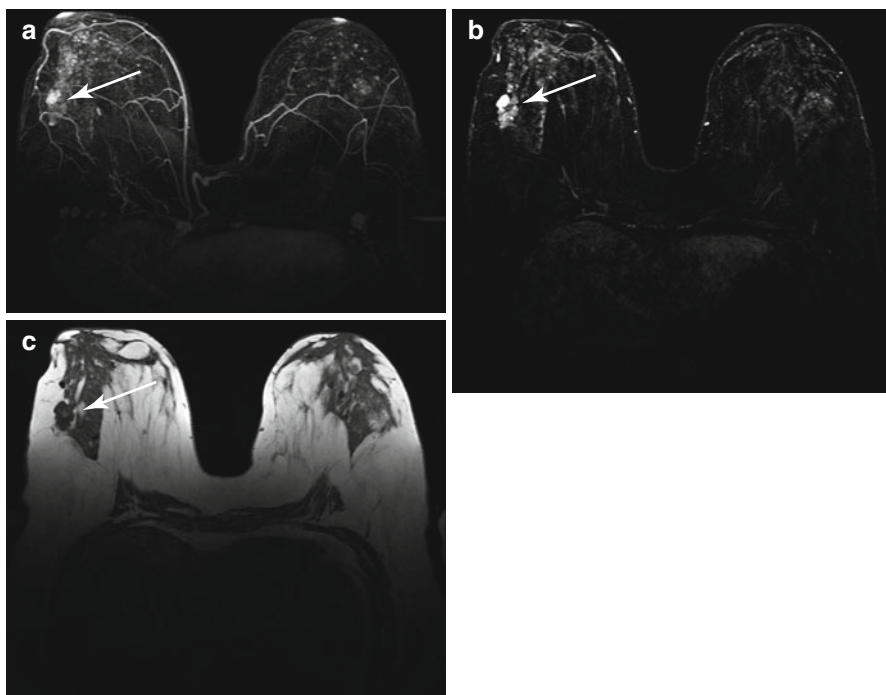


Fig. 11.5 Adult fibroadenoma in a 55-year-old subject. (a, b) Contrast-enhanced T1w imaging (MIP and subtracted image) shows inhomogeneous enhancement of the lesion with areas of strong and less strong contrast medium uptake (*arrow*). (c) Unenhanced T1w image depicts a lobulated focal lesion of predominantly low signal intensity (*arrow*)

Table 11.6 Fibroadenoma

Frequency	10 % of all women (most common benign breast tumor)
Age predilection	Occurs at any age, most common between 20 and 50 years
Type of lesion	Benign
Signs and symptoms	Small fibroadenoma is not palpable Larger fibroadenoma is palpable as a circumscribed, painless, movable lump

Non-contrast-enhanced T1-weighted images:

- Smooth round, oval, or lobulated mass of parenchymal signal intensity (adult type) or slightly lower signal intensity (juvenile type); hence, fibroadenoma is more difficult to identify on T1-weighted images unless it is surrounded by fatty tissue (Uematsu and Kasami 2009a)

Contrast-enhanced T1-weighted images:

- Enhancement is highly variable due to the inhomogeneous composition of fibroadenomas
- Strong and rapid enhancement of juvenile fibroadenomas as a result of the large epithelial component (Hirose et al. 2007)
- As the amount of fibrous tissue increases in older tumors, enhancement may be less strong and more inhomogeneous; internal septa do not take up contrast medium
- In adult fibroadenoma with a large fibrous component, there is little or no initial enhancement with a continuous increase thereafter; this curve distinguishes fibroadenoma from the enhancement kinetics typical of cancer (Jansen et al. 2011; Uematsu and Kasami 2009a)

Differential Diagnosis

- *Papilloma* (see below; similar contrast enhancement as juvenile fibroadenoma, i.e., strong enhancement, especially in the initial phase, and low T1 and high T2 signal intensity on unenhanced images)
- *Invasive papillary carcinoma* (1–2 % of all breast cancers, peak between 50 and 60 years; fingerlike projections, often with cystic component, can develop from benign papilloma; unenhanced T1-weighted images, oval, lobulated, or irregular focal lesion of low signal intensity, with unsharp borders, rarely smooth borders; contrast-enhanced images, typically moderate or strong initial enhancement with later plateau or washout, rarely rim enhancement; T2-weighted images, moderate signal intensity with cystic component, if present, appearing bright) (Brookes and Bourke 2008; Fischer 2000)
- *Complex cyst* (see above; inhomogeneous signal, low T1 signal intensity with hyperintensities indicating protein accumulation or hemorrhage)
- *Tubular adenoma* (benign; contrast enhancement similar to juvenile fibroadenoma, typically well-demarcated round or oval focal lesion) (Soo et al. 2000)
- *Medullary or mucinous breast cancer (rare)* (unenhanced T1-weighted images: star-shaped mass of low signal intensity; T2-weighted images: intermediate or slightly lower signal intensity than glandular parenchyma; contrast-enhanced images: strong initial enhancement, typically followed by postinitial plateau, rarely by washout) (Uematsu and Kasami 2009a)

Clinical Management

If the lesion is small and the MRI findings are consistent with fibroadenoma, it is classified as BI-RADS 2, and no diagnostic workup is necessary.

If the lesion is larger and the MRI findings are inconclusive, it is classified as BI-RADS 3, and further testing, including mammography and ultrasound, is recommended. A percutaneous biopsy should be obtained for confirmation.

11.3 Benign Breast Lesions with Increased Malignant Potential

11.3.1 Radial Scar

A radial scar consists of a fibroelastic (retracted) core surrounded by a stellate pattern of emanating ducts displaying variable epithelial hyperplasia and papillomatosis (Fig. 11.6 and Table 11.7). It has been attributed to chronic infection and reduced perfusion. Transition to tubular carcinoma is possible (Fischer 2000; Jacobs et al. 1999). Because of its malignant potential, surgical removal is recommended in most cases (Pediconi et al. 2005).

MRI Features

T2-weighted images:

- No characteristic features; often not apparent on fat-saturated T2-weighted images

Non-contrast-enhanced T1-weighted images:

- Star-shaped lesion with the same signal intensity as parenchyma
- Therefore difficult to identify when surrounded by parenchyma
- Easily seen when surrounded by fatty tissue

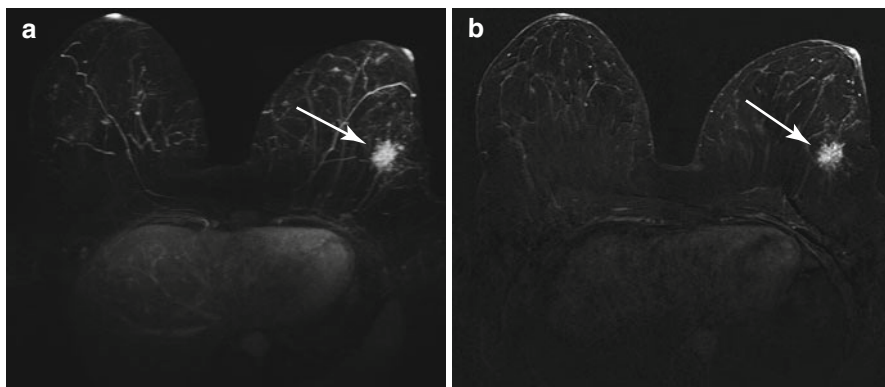


Fig. 11.6 Radial scar (*arrow*) in a 39-year-old subject on contrast-enhanced T1w images. (a) Maximum intensity projection (MIP). (b) Late postcontrast subtraction image shows an enhancing, spiculated mass in the left breast

Table 11.7 Radial scar

Frequency	Rare
Age predilection	All ages
Type of lesion	There is an association with malignancy, especially for radial scars >2 cm; transition to tubular carcinoma is possible
Signs and symptoms	Typically not palpable; often presents as an incidental finding on mammogram

Contrast-enhanced T1-weighted images:

- Typically little or moderate contrast uptake within the star-shaped lesion (Pediconi et al. 2005)
- An occasional radial scar may show rapid initial enhancement
- May be difficult to differentiate from breast cancer

Differential Diagnosis

- *Ductal carcinoma in situ (DCIS)* (see below; not apparent on T1- and T2-weighted images; on contrast-enhanced images, DCIS tends to lack the kinetic enhancement pattern of malignancy, but may occasionally show focal enhancement)
- *Invasive ductal carcinoma* (see below; T1-weighted images: irregularly shaped, spiculated mass; T2-weighted images: intermediate or low signal intensity; post-contrast images: strong initial enhancement with postinitial plateau or washout, irregular and often rim enhancement)
- *Tubular breast cancer (rare)* (can arise from radial scar; star-shaped lesion of low T1 signal intensity; T2-weighted images: intermediate or slightly lower signal intensity than glandular parenchyma, sometimes with hyperintense peritumoral edema; postcontrast images: spiculated focal lesion, often with strong initial enhancement followed by postinitial plateau, less often by washout, non-specific enhancement may also occur) (Fischer 2000)
- *Postoperative scar*

Clinical Management

A radial scar is classified as BI-RADS 4b because malignancy cannot be reliably excluded. This means that the finding should be communicated for prompt workup. Biopsy is recommended. If biopsy demonstrates atypia, the lesion should be excised.

11.3.2 Papilloma

Breast papillomas are intraductal tumors made up of benign epithelial cells (Fischer 2000). Central papillomas tend to be solitary and are often located behind the nipple. Bloody, milky, or clear nipple discharge is the presenting symptom in most women. Multiple papillomas are small and peripheral in location (Francis et al. 2002; Kramer et al. 2000) (Table 11.8).

Table 11.8 Papilloma

Frequency	Rare, 1–2 % of all benign tumors
Age predilection	40–50 years
Type of lesion	Benign; increased risk of transformation to DCIS or papillary breast carcinoma; the risk is 10–33 % if multiple papillomas are present
Signs and symptoms	Spontaneous or provoked nipple discharge, which may be bloody, milky, or clear

MRI Features

T2-weighted images:

- Signal intensity varies with lesion size: small papillomas tend to have intermediate or high signal intensity, while large papillomas typically have moderate and sometimes low signal intensity

Non-contrast-enhanced T1-weighted images:

- Focal lesion of low signal intensity, same as glandular parenchyma and therefore often difficult to identify

Contrast-enhanced T1-weighted images:

- Smooth tumor with homogeneous or inhomogeneous contrast enhancement.
- Typically stronger initial enhancement, followed by steady but less marked signal increase thereafter; an occasional papilloma may show a postinitial plateau.
- Washout is uncommon.
- In rare cases, malignant enhancement pattern has been observed (Tominaga et al. 2011).

Differential Diagnosis

- *Fibroadenoma* (see above)
- *Invasive papillary carcinoma* (1–2 % of all breast cancers, peak between 50 and 60 years; fingerlike projections, often with cystic component, can develop from benign papilloma; unenhanced T1-weighted images, oval, lobulated, or irregular focal lesion of low signal intensity, with unsharp borders, rarely smooth borders; postcontrast images, typically moderate or strong initial enhancement with later plateau or washout, rarely rim enhancement; T2-weighted images, moderate signal intensity with cystic component, if present, appearing bright) (Brookes and Bourke 2008; Fischer 2000)
- *Adenoma* (benign focal lesion, typically oval or round with smooth margins; T1-weighted images: same signal intensity as parenchyma, detectable as low-signal-intensity lesion when surrounded by fatty tissue; contrast-enhanced images: no or little enhancement, occasional adenoma may show strong initial and continuous postinitial enhancement; T2-weighted images: typically isointense, occasionally hyperintense) (Soo et al. 2000)

Clinical Management

Papillomas, like radial scars, are associated with an increased risk of malignancy. Therefore, the MRI diagnosis of papilloma requires histologic verification and should be communicated to the subject. Excision may be indicated.

11.4 Fibrocystic Breast Changes

Fibrocystic changes of the breast describe the proliferation of hormone-dependent mesenchymal or epithelial structures. The spectrum of breast changes includes microcysts and macrocysts, lobular hyperplasia, ductal and acinar hyperplasia, and glandular fibrosis. Hence, this condition has a wide range of morphologic and kinetic enhancement features on MRI (van den Bosch et al. 2005).

A classification into three groups has been proposed to assess the subsequent risk of breast cancer (Prechtel 1993) (Table 11.9).

MRI provides no information for classifying fibrocystic changes of the breast and identifying women at an increased risk for developing breast cancer (Chen et al. 2008a).

Fibrocystic changes constitute the most common incidental findings in the breast in whole-body screening MRI (Figs. 11.7, 11.8, 11.9, and 11.10 and Table 11.10).

Table 11.9 Classification system for fibrocystic breast changes (Prechtel 1993)

Group	Description	Risk for development of breast cancer
I (approx. 70 %)	Nonproliferative lesions (fibrocystic)	Not increased
II (approx. 20 %)	Proliferative lesions without atypia (epithelial proliferation)	Approx. 2-fold increased risk
III (approx. 10 %)	Proliferative lesions with atypia (ductal or lobular epithelial hyperplasia)	Approx. 4-/5-fold increased risk

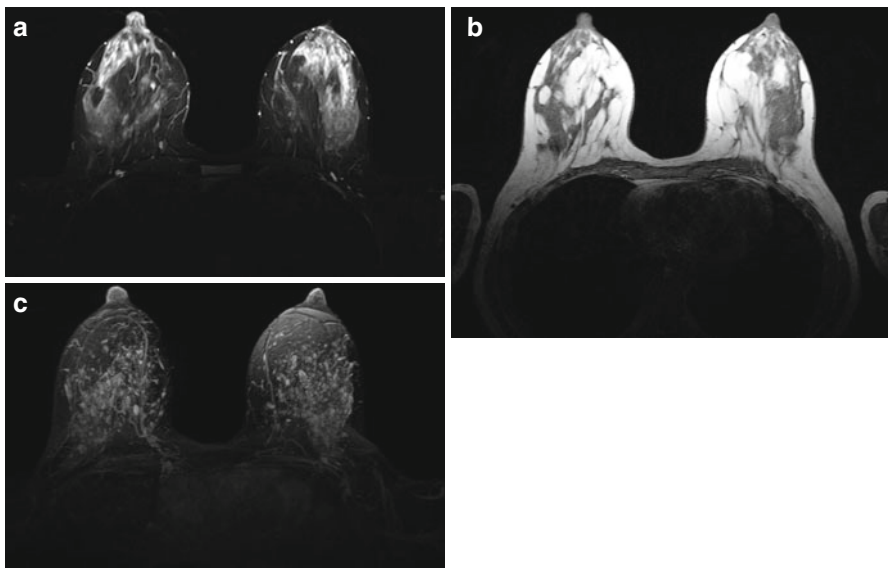


Fig. 11.7 Bilateral fibrocystic changes in a 40-year-old subject. (a) T2w TIRM image reveals tiny cystic lesions. (b) On unenhanced T1w image, the cystic lesions have low signal intensity. (c) Postcontrast image (MIP) shows symmetric bilateral patchy enhancement

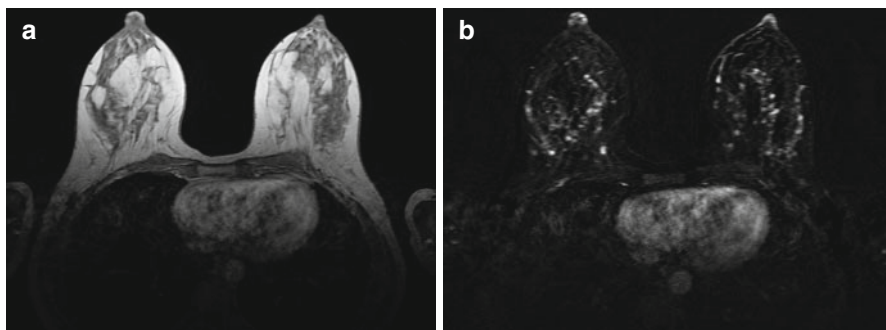


Fig. 11.8 Same subject as in Fig. 11.7. Fibrocystic changes during the initial phase of enhancement. (a) Postcontrast T1w image. (b) Corresponding subtraction image

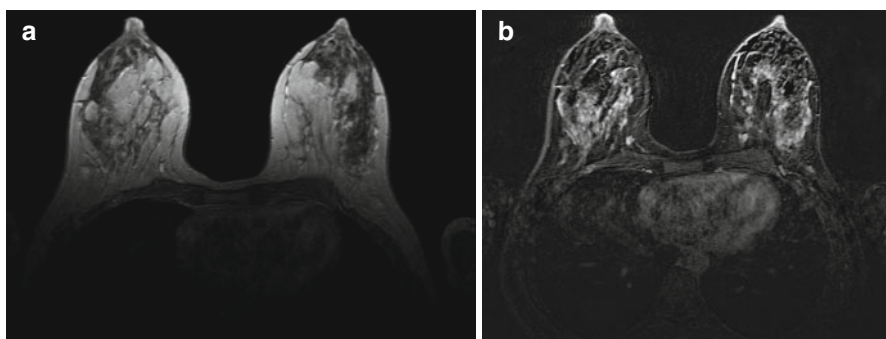


Fig. 11.9 Same subject as in Figs. 11.7 and 11.8. Fibrocystic changes during the late phase of enhancement. (a) Postcontrast T1w image. (b) Corresponding subtraction image. Involved tissue exhibits progressive enhancement

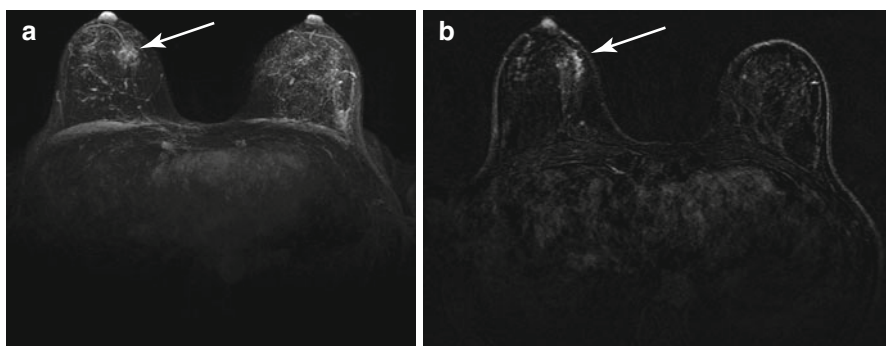


Fig. 11.10 Locoregional fibrocystic changes (*arrow*) in the right breast in a 50-year-old subject. (a) MIP of early postcontrast T1w data. (b) Corresponding subtraction image

Table 11.10 Fibrocystic breast changes

Frequency	Approx. 50 % of all women
Age predilection	All ages, predominantly women aged 40–60
Type of lesion	Risk of malignancy varies with histology
Signs and symptoms	Highly variable presentation, from clinically inapparent to tender nodularities with menstrual cycle-related breast pain Typically symmetric involvement

MRI Features

T2-weighted images:

- Some cases of fibrocystic breast changes exhibit diffusely increased signal intensity of involved breast tissue; if cysts are present, MRI will show variably sized lesions of high signal intensity with smooth borders (most conspicuous on fat-saturated/fat-suppressed sequences)

Non-contrast-enhanced T1-weighted images:

- Low-signal-intensity glandular tissue; if cysts are present, MRI will show variably sized lesions of low signal intensity with smooth borders

Contrast-enhanced T1-weighted images:

- Often symmetric parenchymal enhancement in both breasts with sparing of cystic component; the pattern may be patchy, patchy/regional, or regional; progressive enhancement is the most common kinetic type (Chen et al. 2008a)
- Focal fibrocystic changes may mimic breast cancer (rapid initial enhancement and subsequent washout) (Chen et al. 2008b)

Differential Diagnosis

Simple cyst (see above; no enhancement of cyst fluid or wall; very bright on T2-weighted image and dark on T1-weighted image)

Complex cyst (see above; intracystic hemorrhage or increased protein content results in higher T1 signal intensity and lower T2 signal intensity; enhancement may be seen if there is inflammatory wall thickening or if the cyst has solid components)

Clinical Management

Fibrocystic changes, which are subject to cyclic hormonal variation, constitute the most common incidental finding in the breast encountered in whole-body MRI. When the pattern of involvement is symmetric, the condition is classified as BI-RADS 2 and typically requires no further evaluation. When there is asymmetric enhancement in older women with still relatively dense glandular tissue, mammography and ultrasound should be performed for further evaluation.

11.5 Malignant Breast Lesions

This section focuses on the most relevant malignant breast tumors. A suspicious breast lesion detected by MRI always requires histologic evaluation to confirm or exclude malignancy and to establish a specific diagnosis.

11.5.1 Ductal Carcinoma in Situ

Ductal carcinoma in situ (DCIS) is the proliferation of malignant epithelial cells within mammary ducts (Fig. 11.11 and Table 11.11).

Neoplastic cells are confined to the ducts with no extension beyond the basement membrane (Orel et al. 1997). In recent years, research has confirmed that, of all imaging tools, MRI is most sensitive for detecting DCIS (Greenwood et al. 2013; Giess et al. 2013; Jansen 2011; Lehman 2010). Diffusion-weighted imaging (DWI) may help in defining the extent of DCIS. DCIS lesions have higher DWI signal intensity and lower ADC values than normal breast tissue (Giess et al. 2013; Rahbar et al. 2011).

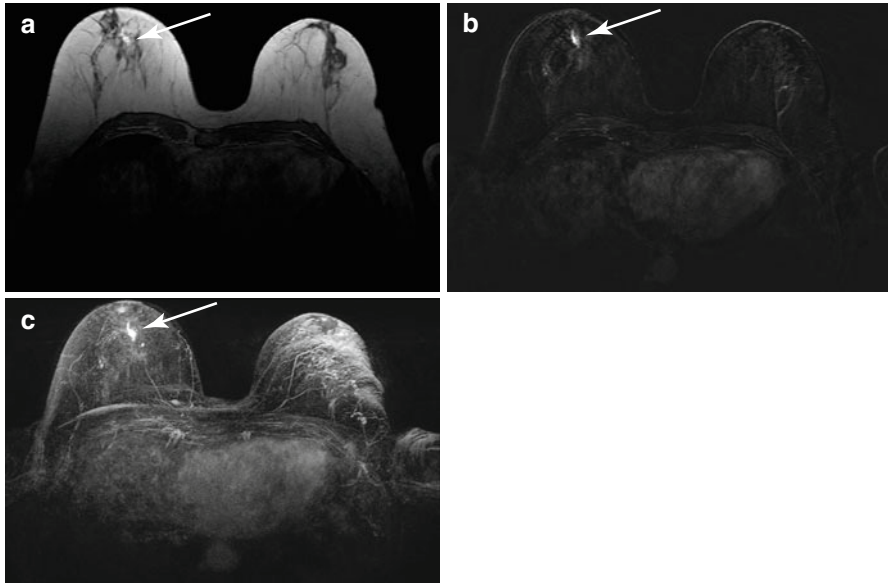


Fig. 11.11 Suspected ductal carcinoma in situ (DCIS) (*arrow*) in a 56-year-old subject. (a) Contrast-enhanced T1w image shows enhancement of the mammary duct system in the right breast. (b) Subtracted postcontrast T1w image. (c) Corresponding MIP

Table 11.11 Ductal carcinoma in situ

Frequency	20 % of women in screening populations
Predilection age	Age peak between 40 and 60 years
Type of lesion	Precancer; however, not all DCIS will progress to invasive disease
Signs and symptoms	Often not apparent, only approx. 10 % of DCIS lesions are palpable; abnormal nipple discharge or nipple changes in rare cases; 70 % of DCIS lesions show typical microcalcifications on mammograms

MRI Features

T2-weighted images:

- No specific changes, isointense to parenchyma.
- In some cases, DCIS is associated with a hyperintense fluid collection in the affected ductal system.

Non-contrast-enhanced T1-weighted images:

- No specific changes, isointense to parenchyma

Contrast-enhanced T1-weighted images:

- Enhancement reveals a lesion that is dendritic in shape, less commonly a star-shaped or rounded lesion.
- Enhancement is variable, ranging from no enhancement to malignant enhancement kinetics (rapid initial increase with postinitial plateau or washout); hence, a specific diagnosis based on enhancement at MRI is not possible (Greenwood et al. 2013; Kim et al. 2011).

Differential Diagnosis

- *Fibroadenoma* (juvenile fibroadenoma is characterized by strong contrast enhancement, while adult fibroadenoma tends to exhibit little initial enhancement and a continued rise thereafter)
- *Breast fat necrosis* (after injury, surgery, biopsy, or other trauma; typically isointense to parenchyma on unenhanced T1-weighted images; high T2 signal intensity, especially after recent trauma; intralesional fat has fat signal intensity with T1- and T2-weighted pulse sequences and becomes darker when fat suppression is used; contrast-enhanced sequences reveal fat necrosis (within the first 6 months of trauma) as a circumscribed, often sharply delineated area of moderate initial enhancement with a continuous increase or plateau postinitially; older lesions show no or only moderate enhancement) (Ganau et al. 2009)
- *Atypical ductal hyperplasia (ADH)* (is considered a precancerous condition; difficult to detect by MRI because T1 and T2 signal intensities and enhancement are nonspecific) (Strigel et al. 2010)

Clinical Management

Ductal carcinoma in situ (DCIS) is a heterogeneous group of precancerous conditions. Therefore, suspected DCIS requires further diagnostic procedures (mammography, ultrasound, biopsy). DCIS is usually categorized as BI-RADS 4b. However, not all DCIS will progress to invasive disease.

11.5.2 Invasive Ductal Carcinoma

Invasive ductal carcinoma (IDC) arises from the epithelium of the terminal lactiferous duct and involves the basement membrane. Lacking specific features of cellular differentiation, IDC is also known as not otherwise specified (NOS). It is the most common form of invasive breast cancer (65–75 %). Data suggest that IDC is multifocal in 15 % and bilateral in 5 % of cases (Figs. 11.12, 11.13, and 11.14).

IDC has the classic clinical findings of breast cancer: in most women, a hard lump with irregular borders is palpated. The mass is not very movable and causes no symptoms. External signs such as a change in skin texture (peau d'orange) over the site or nipple retraction may be present (Jacobs 2009; Jansen et al. 2008) (Table 11.12).

While IDC enhances more rapidly than invasive lobular carcinoma (see below), peak enhancement is similar for both cancers (Mann et al. 2011). Washout is more typical of IDC than invasive lobular carcinoma.

Perifocal edema tends to be more common in IDC (Dietzel et al. 2010). DWI may be helpful for grading. Lower ADC values have been shown to be associated with a higher grade of differentiation, a larger tumor mass, and axillary lymph node metastasis. ADC values therefore have the potential to identify aggressive IDC (Razek et al. 2010).

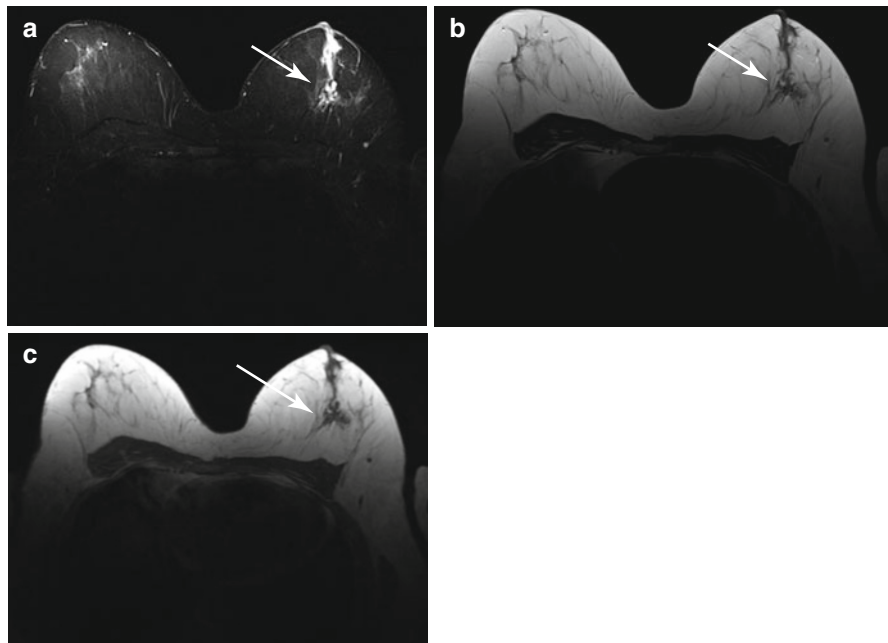


Fig. 11.12 Suspected invasive ductal carcinoma (IDC) (*arrow*) in a 76-year-old subject with a positive family history (sister died of breast cancer). (a) T2w TIRM image shows a right-left difference with diffuse hyperintensity in the left breast. (b) On T2w TSE image, the lesion is isointense to parenchyma with small areas of perifocal hyperintensity. (c) T1w image reveals low-signal-intensity stellate lesion with irregular margins

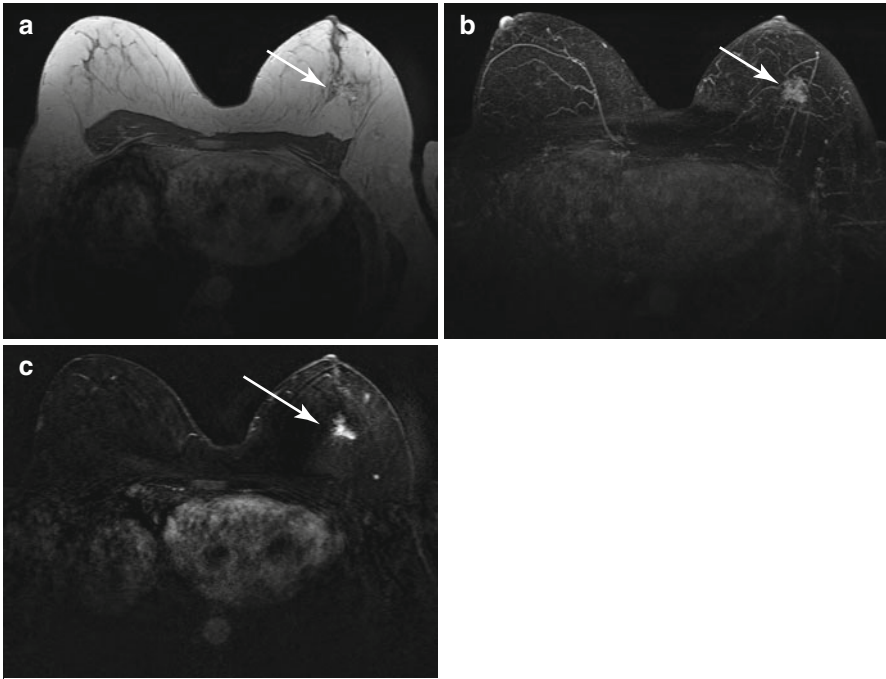


Fig. 11.13 Same subject as in Fig. 11.12. Early postcontrast images show rapid initial enhancement of the suspicious lesion (*arrow*). (a) T1w image from initial phase. (b) Corresponding MIP. (c) Corresponding subtraction image

MRI Features

T2-weighted images:

- Signal intensity is typically intermediate or slightly lower than that of glandular parenchyma; increased water content results in higher signal intensity.
- Peritumoral edema may be present, seen as a rim of high signal intensity around the lesion.

Non-contrast-enhanced T1-weighted images:

- Same signal intensity as parenchyma; therefore, some tumors may be difficult to detect.
- When surrounded by fat, an IDC is typically identified as an irregularly marginated, stellate mass of low signal intensity; an occasional IDC is oval, round, or lobulated.
- Microcalcifications are common, but are usually not seen on MRI.

Contrast-enhanced T1-weighted images:

- Contrast-enhanced images show a stellate (sometimes round or oval) lesion with irregular margins.
- Enhancement kinetics typical of breast malignancy with rapid, strong enhancement in approx. 60 % of lesions; moderate and mild initial enhancement in 35 and 5 % of cases, respectively.

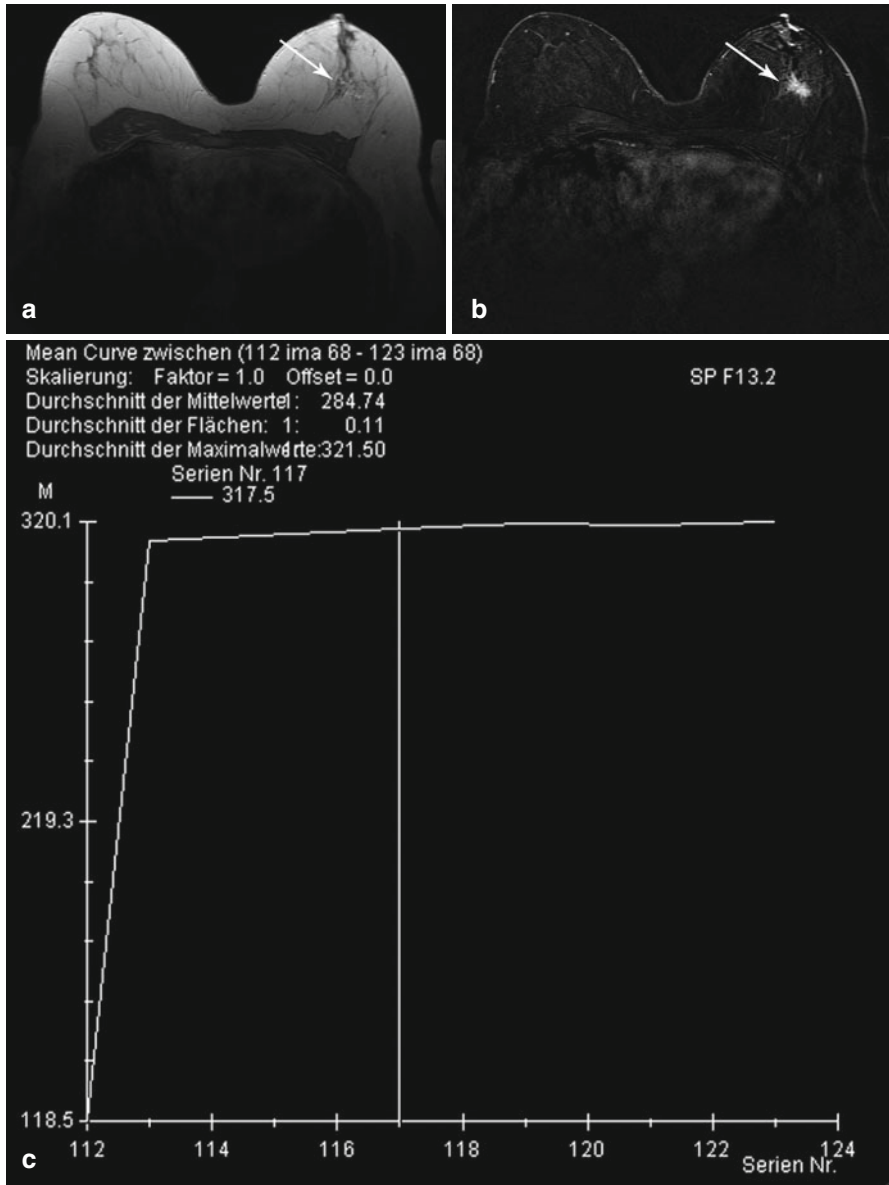


Fig. 11.14 Same subject as in Figs. 11.12 and 11.13. Late postcontrast phase and enhancement kinetics of the suspicious lesion (*arrow*). (a) T1w image from late phase shows postinitial plateau. (b) Corresponding subtraction image. (c) Enhancement curve with typical kinetic pattern of IDC, characterized by rapid initial enhancement and postinitial plateau

Table 11.12 Invasive ductal carcinoma

Frequency	65–75 % of all invasive breast cancers
Age predilection	All ages, predominantly women between the ages of 50 and 60
Type of lesion	Malignant
Signs and symptoms	Classic features of breast cancer: hard irregular mass, fixed in place, painless, peau d'orange, or nipple retraction 70 % of masses are first noted by the woman herself

- Postinitial plateau, rarely washout (Hirose et al. 2007).
- Rim enhancement occurs in approx. 50 % of IDC and usually indicates poor outcome.
- A definitive diagnosis cannot be made on the basis of MRI appearance alone, but requires a histopathologic examination (Mann et al. 2011).

Differential Diagnosis

- *Benign breast lesions* (fibroadenoma, fatty necrosis, radial scar, abscess, granuloma, or inflammatory lesions; however, benign breast lesions tend to exhibit different enhancement patterns and kinetics)
- *Other malignant breast lesions* (invasive lobular carcinoma (see below), rarely metastasis)

Clinical Management

A suspicion of breast cancer should be communicated immediately to ensure prompt referral for further examinations such as mammography and ultrasound. Suspicious lesions are classified as BI-RADS 4b–5, depending on imaging morphology. Lumpectomy is the first-line treatment option and is supplemented by adjuvant radiotherapy or chemotherapy as needed.

11.5.3 Invasive Lobular Carcinoma

Invasive lobular carcinoma (ILC), also known as infiltrating lobular carcinoma, is characterized by single rows of malignant cells that tend to grow around ducts and lobules (string of pearls or Indian file pattern) and from there extend into surrounding stroma.

ILC is a small cell carcinoma. Some ILC additionally contain signet ring cells (i.e., tumor cells with central mucoid globules) (Fischer 2000).

Growth may be diffuse or nodular (Giess et al. 2013; Jacobs 2009; Jansen et al. 2008) (Table 11.13).

Diffuse ILC is difficult to detect with any imaging modality (mammography, ultrasound, breast MRI).

Table 11.13 Invasive lobular carcinoma

Frequency	Second most common breast malignancy (10–15 % of all breast cancers)
Age predilection	All ages, predominantly women between the ages of 40 and 60
Type of lesion	Malignant
Signs and symptoms	Diagnosis is usually late because there are typically no clinical symptoms, and only some are palpable. Unusual metastatic pattern (abdominal, pelvic)

Moreover, mammography and ultrasound tend to underestimate the size of ILC (Mann 2010). MRI is helpful in determining the true extent of ILC and can rule out multifocal or multicentric lesions (Brasic et al. 2013; Giess et al. 2013).

Compared with invasive ductal carcinoma, ILC enhances more slowly, but peak enhancement is nearly the same (Mann et al. 2011). Washout, however, is less common than a postinitial plateau. Nevertheless, ILC and IDC are difficult to distinguish on the basis enhancement patterns and kinetics (Giess et al. 2013; Dietzel et al. 2010).

MRI Features

T2-weighted images:

- Signal intensity is typically intermediate or slightly lower than that of glandular parenchyma
- Occasionally, peritumoral edema is present, indicated by high signal intensity around the lesion

Non-contrast-enhanced T1-weighted images:

- ILC is isointense to surrounding tissue; therefore, especially the diffuse type may be difficult to detect
- Nodular type may be seen as a rounded, at times irregular, lesion within lipomatous tissue
- Architectural distortion

Contrast-enhanced T1-weighted images:

- Rounded, irregular, or stellate lesion (Hirose et al. 2007)
- While most cases show malignant-type enhancement kinetics with rapid initial enhancement, a postinitial plateau is more common than washout
- Nodular ILC shows rim enhancement in approx. 50 % of cases
- Diffuse ILC often shows unspecific enhancement (Mann et al. 2011)

Differential Diagnosis

- *Benign breast lesions* (scar; also causes architectural distortion, but typically does not enhance, especially if more than 18 months have elapsed since surgery) (fibrosis; no architectural distortion)
- *Radial scar* (see above; association with malignancy; stellate lesion with T1 isointensity to parenchyma; often not visible on T2-weighted images; mild to

moderate contrast enhancement; an occasional radial scar shows fast initial enhancement, mimicking malignancy)

- *Other malignant breast lesions* (DCIS, invasive ductal carcinoma, rarely metastasis)

Clinical Management

Suspicious lesions are classified as BI-RADS 4b to 5, depending on morphology. Prompt workup with mammography and ultrasound is warranted. Metastasis should be ruled out.

Proven ILC is removed by wide local excision or, in case of more extensive disease, mastectomy. Axillary lymph nodes should be removed and examined for the presence of cancer cells (sentinel node). The stage determines whether ipsilateral radiotherapy and neoadjuvant or adjuvant chemotherapy are indicated.

11.5.4 Paget Disease

Paget disease is an intraepidermal carcinoma in situ containing large round or oval tumor cells.

It is characterized by an eczematous lesion of the nipple and areola causing flattening or thickening of the nipple. There may be abnormal contrast enhancement of the nipple (Frei et al. 2005).

Ulceration is present in advanced disease (Table 11.14).

Sixty percent of women with Paget disease have DCIS in the same breast (Figs. 11.15 and 11.16). In approx. 30 % of cases, there is concomitant invasive ductal carcinoma (Dalberg et al. 2008; Fischer 2000).

MRI Features

T2-weighted images:

- Normal signal intensity or, if the nipple is thickened or inflamed, increased signal intensity

Non-contrast-enhanced T1-weighted images:

- Also inconspicuous; flattening of the nipple and/or thickening of the nipple region may be observed

Contrast-enhanced T1-weighted images:

- Variable findings from absence of contrast enhancement to malignant enhancement kinetics with rapid initial increase and subsequent plateau or washout

Table 11.14 Paget disease

Frequency	2 % of all breast cancers
Age predilection	All ages, predominantly women between the ages of 40 and 60
Type of lesion	Malignant
Signs and symptoms	Nonitchy rash in the nipple area, sometimes accompanied by oozing or scaling

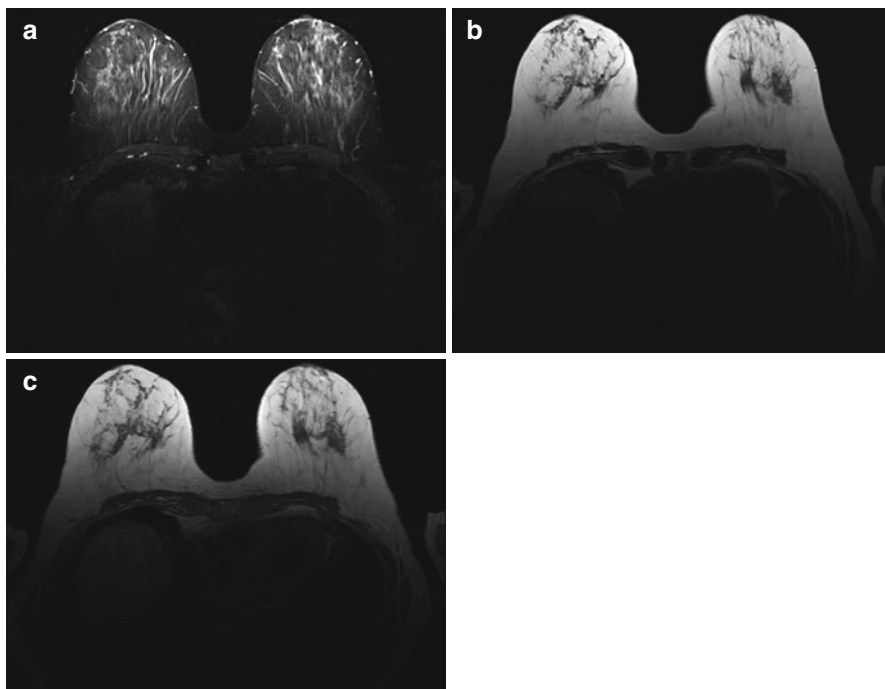


Fig. 11.15 Suspected Paget disease of the nipple in an 81-year-old subject before contrast medium administration. No abnormalities are apparent on T2w TIRM image (a), T2w TSE image (b), and T1w image (c)

- In most women with Paget disease, there is circumscribed abnormal enhancement of the nipple-areolar complex
- Additional abnormal retroareolar enhancement is common; extension of enhancement into ductal structures suggests DCIS (Frei et al. 2005)

Differential Diagnosis

- *Ductal carcinoma in situ (DCIS)* (see above)
- *Invasive ductal carcinoma* (see above)
- *Skin diseases*, e.g., seborrheic dermatitis, dermatomycosis, contact eczema (caused by nipple cream, for instance), malignant melanoma, atypical squamous cell carcinoma, or ectopic retroareolar papilloma (Lloyd and Flanagan 2000)

Clinical Management

Suspected Paget disease of the nipple may point to underlying DCIS (60 %) or even invasive ductal carcinoma (30 %), especially when the area of contrast enhancement extends to ductal structures. Therefore, rapid communication to the subject is vital. The findings on contrast-enhanced breast MRI are classified as BI-RADS 4b when enhancement is confined to the retroareolar area and as BI-RADS 4c–5 when enhancement also involves ductal structures.

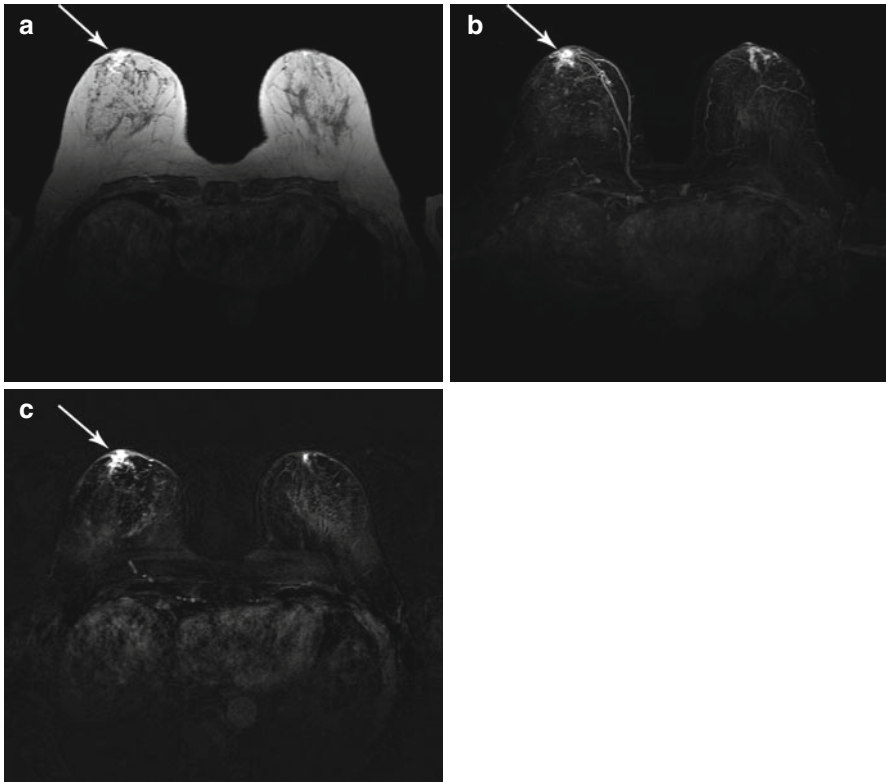


Fig. 11.16 Same subject as in Fig. 11.15. Images after contrast medium administration show strong enhancement of the nipple region and underlying ductal structures, predominantly in the right breast (*arrow*). (a) Postcontrast T1w image. (b) Corresponding MIP. (c) Corresponding subtraction image

11.6 Postoperative and Postinterventional Breast Changes

Breast changes due to surgery or other procedures are multifarious (Figs. 11.17 and 11.18) and are common in women with a history of breast cancer or mastitis. Scar tissue forming in the breast after iatrogenic injury (e.g., surgery, biopsy procedures) or trauma may show contrast enhancement and be indistinguishable from cancer. In such cases, additional diagnostic tests are required to differentiate between cancer and scar tissue (Table 11.15) (Fischer 2000).

MRI Features

T2-weighted images:

- Scars typically cause architectural distortion of low signal intensity; some scars appear as spiculated masses.

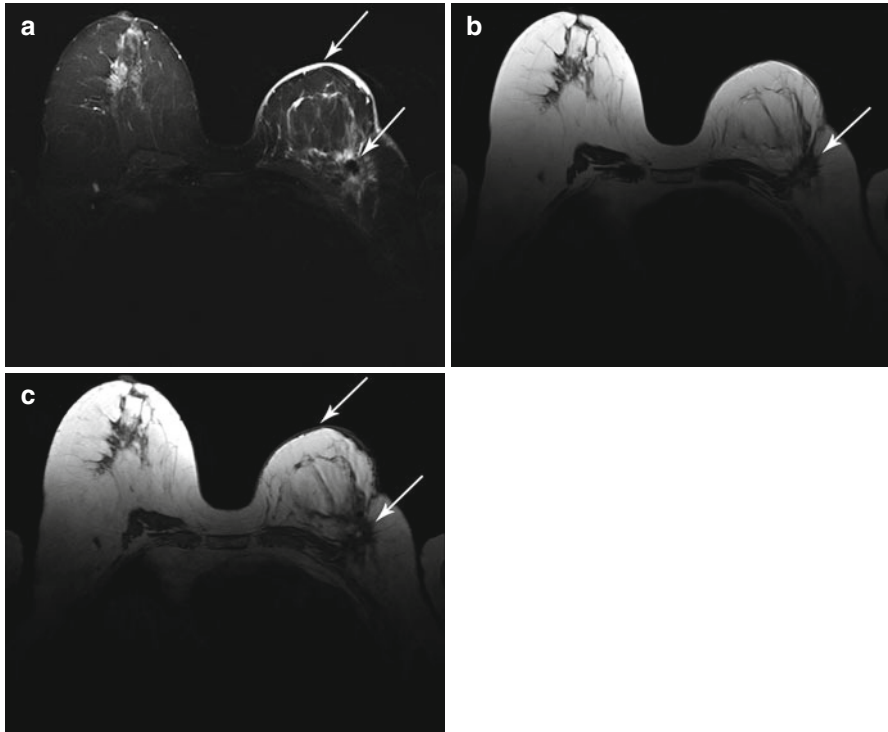


Fig. 11.17 Postoperative breast changes in a 68-year-old subject with invasive ductal carcinoma of the left breast 5 years earlier. (a) T2w TIRM image shows marked retraction of the left breast (*lower arrow*) and skin thickening (high signal intensity) (*upper arrow*). (b) T2w TSE image reveals an area of marked architectural distortion in the left breast with partially spiculated appearance (*arrow*). (c) Unenhanced T1w image confirms marked architectural distortion of the left breast with partially spiculated appearance (*lower arrow*). A contrast-enhanced series was not obtained in this subject due to contrast medium allergy; hence, there is no information on contrast enhancement in the scar region

- High-signal-intensity edema is common during the first postoperative months and is best appreciated on fat-saturated/fat-suppressed images.
- In women with a history of radiotherapy, postoperative edema may persist for several years.

Non-contrast-enhanced T1-weighted images:

- Typically low-signal-intensity architectural distortion; sometimes spiculated mass.
- Postoperative susceptibility artifact is common.

Contrast-enhanced T1-weighted images:

- Early postoperative scar may show strong enhancement.
- Enhancing scar tissue cannot be differentiated from recurrent or new cancer.

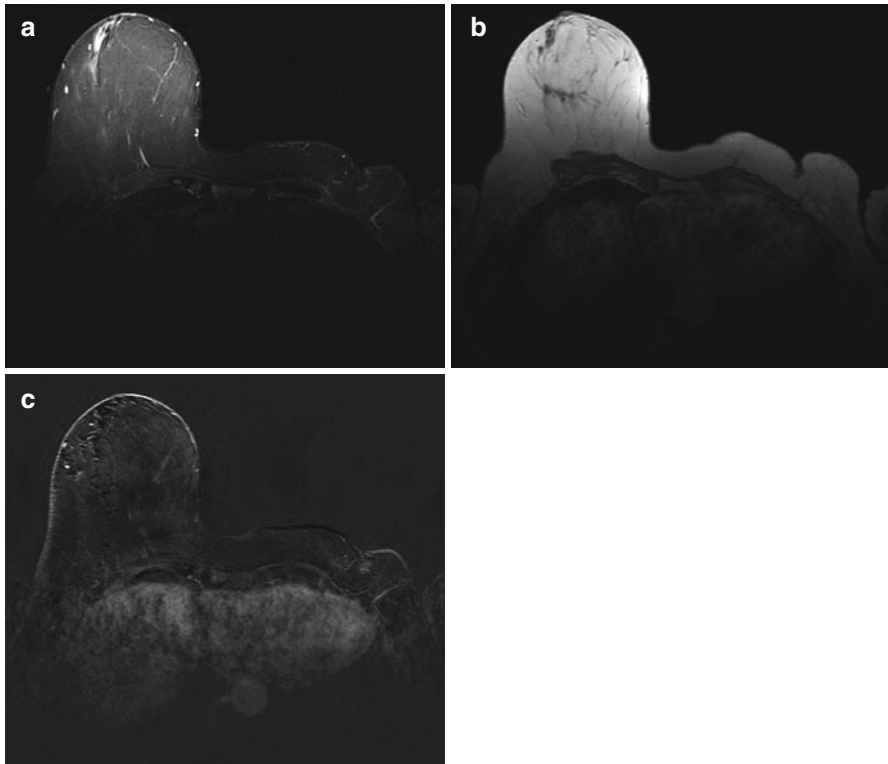


Fig. 11.18 Findings after left-sided mastectomy for breast cancer 15 years earlier in a 66-year-old subject. (a) T2w TIRM shows absence of left breast. (b) T1w image after contrast medium administration. (c) Subtracted T1w image after contrast medium administration. No contrast enhancement in the scar area. No evidence of focal lesion in the contralateral breast

Table 11.15 Postoperative and postinterventional breast changes

Frequency	Approx. 40 % of all women
Age predilection	All ages
Type of lesion	Benign; (recurrent/new) cancer may develop in scar tissue
Signs and symptoms	Presence of variable amounts of scar tissue at sites of surgical injury after open biopsy, lumpectomy, or mastectomy

- Over time, enhancement becomes less pronounced, and inactive scar tissue does not enhance.
- Absence of enhancement at the site of previous surgery rules out cancer with a high degree of confidence (Fischer 2000).

Differential Diagnosis

- *Breast cancer* of various etiologies (second cancer, recurrence)
- *Cancer in scar tissue*

Clinical Management

Absence of contrast enhancement in the scar area makes recurrence or scar carcinoma unlikely. When there is enhancement, MRI alone does not allow differentiation of postoperative scar from cancer. This is why further workup is required in such cases. The findings are classified as BI-RADS 3 or BI-RADS 4 and communicated to the subject.

References

- Amarosa AR, McKellop J, Klautau Leite AP et al (2013) Evaluation of the kinetic properties of background parenchymal enhancement throughout the phases of the menstrual cycle. *Radiology* 268:356–365
- Bhate RD, Chakravorty A, Ebbs SR (2007) Management of breast cysts revisited. *Int J Clin Pract* 61:195–199
- Brasic N, Wisner DJ, Joe BN (2013) Breast MR imaging for extent of disease assessment in patients with newly diagnosed breast cancer. *Magn Reson Imaging Clin N Am* 21:519–532
- Brookes MJ, Bourke AG (2008) Radiological appearances of papillary breast lesions. *Clin Radiol* 63:1265–1273
- Chen JH, Liu H, Baek HM et al (2008a) Magnetic resonance imaging features of fibrocystic change of the breast. *Magn Reson Imaging* 26:1207–1214
- Chen JH, Nalcioğlu O, Su MY (2008b) Fibrocystic change of the breast presenting as a focal lesion mimicking breast cancer in MR imaging. *J Magn Reson Imaging* 28:1499–1505
- Dalberg K, Hellborg H, Wärnberg F (2008) Paget's disease of the nipple in a population based cohort. *Breast Cancer Res Treat* 111:313–319
- De Bazelaire C, Pluvinage A, Chapelier M et al (2010) Diffusion-weighted MR imaging of the breast. *J Radiol* 91:394–404
- DeMartini W, Lehman C, Partridge S (2008) Breast MRI for cancer detection and characterization: a review of evidence-based clinical applications. *Acad Radiol* 15:408–416
- Dewey M, Martus P (2008) MRI breast screening. *Lancet* 371:1415–1416
- Dietzel M, Baltzer PA, Vag T et al (2010) Magnetic resonance mammography of invasive lobular versus ductal carcinoma: systematic comparison of 811 patients reveals high diagnostic accuracy irrespective of typing. *J Comput Assist Tomogr* 34:587–595
- Dupont WD, Page DL, Parl FF et al (1994) Long-term risk of breast cancer in women with fibroadenoma. *N Engl J Med* 331:10
- Fischer U (2000) *Lehratlas der MR-Mammographie*. Thieme, Stuttgart
- Fischer U (2012) *Practical MR mammography: high-resolution MRI of the breast*. Thieme, New York
- Francis A, England D, Rowlands D, Bradley S (2002) Breast papilloma: mammogram, ultrasound and MRI appearances. *Breast* 11:394–397
- Frei KA, Bonel HM, Pelte MF et al (2005) Paget disease of the breast: findings at magnetic resonance imaging and histopathologic correlation. *Invest Radiol* 40:363–367
- Ganau S, Tortajada L, Escribano F (2009) The great mimicker: fat necrosis of the breast – magnetic resonance mammography approach. *Curr Probl Diagn Radiol* 38:189–197
- Giess CS, Raza S, Birdwell RL (2013) Patterns of nonmasslike enhancement at screening breast MR imaging of high-risk premenopausal women. *Radiographics* 33:1343–1360
- Greenwood HI, Heller SL, Kim S, Sigmund EE, Shaylor SD, Moy L (2013) Ductal carcinoma in situ of the breasts: review of MR imaging features. *Radiographics* 33:1569–1588
- Heywang-Köbrunner SH (1994) Contrast-enhanced magnetic resonance imaging of the breast. *Invest Radiol* 29:94–104

- Heywang-Köbrunner SH, Hacker A, Sedlacek S (2013) Magnetic resonance imaging: the evolution of breast imaging. *Breast Suppl 2*:S77–S82
- Hines N, Slanetz PJ, Eisenberg RL (2010) Cystic masses of the breast. *Am J Roentgenol* 194:122–133
- Hirose M, Hashizume T, Seino N et al (2007) Atlas of breast magnetic resonance imaging. *Curr Probl Diagn Radiol* 36:51–65
- Iglesias A, Arias M, Santiago P et al (2007) Benign breast lesions that simulate malignancy: magnetic resonance imaging with radiologic-pathologic correlation. *Curr Probl Diagn Radiol* 36:66–82
- Jacobs MA (2009) Multiparametric magnetic resonance imaging of breast cancer. *J Am Coll Radiol* 6:523–526
- Jacobs TW, Byrne C, Colditz G, Connolly JL, Schnitt SJ (1999) Radial scars in benign breast-biopsy specimens and the risk of breast cancer. *N Engl J Med* 340:430–436
- Jansen SA (2011) Ductal carcinoma in situ: detection, diagnosis, and characterization with magnetic resonance imaging. *Semin Ultrasound CT MR* 32:306–318
- Jansen SA, Fan X, Karczmar GS et al (2008) Differentiation between benign and malignant breast lesions detected by bilateral dynamic contrast-enhanced MRI: a sensitivity and specificity study. *Magn Reson Med* 59:747–754
- Jansen SA, Shimauchi A, Zak L et al (2011) The diverse pathology and kinetics of mass, nonmass, and focus enhancement on MR imaging of the breast. *J Magn Reson Imaging* 33:1382–1389
- Kim JA, Son EJ, Youk JH et al (2011) MRI findings of pure ductal carcinoma in situ: kinetic characteristics compared according to lesion type and histopathologic factors. *Am J Roentgenol* 196:1450–1456
- Kramer SC, Rieber A, Gorich J et al (2000) Diagnosis of papillomas of the breast: value of magnetic resonance mammography in comparison with galactography. *Eur Radiol* 10:1733–1736
- Kuhl CK, Braun M (2008) Magnetic resonance imaging in preoperative staging for breast cancer: pros and contras. *Radiologe* 48:358–366
- Kuhl CK, Kreft BP, Hauswirth A et al (1995) Fokale und diffuse Läsionen in der dynamischen MR-Mammographie gesunder Probandinnen. *RÖFÖ* 163:219–224
- Kuhl CK, Schrading S, Bieling HB et al (2007) MRI for diagnosis of pure ductal carcinoma in situ: a prospective observational study. *Lancet* 370:485–492
- Kuusk U (1988) Multiple giant fibroadenomas in an adolescent female breast. *Can J Surg* 31:133
- Lehman CD (2010) Magnetic resonance imaging in the evaluation of ductal carcinoma in situ. *J Natl Cancer Inst Monogr* 2010:150–151
- Lehman CD, Blume JD, Weatherall P, International Breast MRI Consortium Working Group et al (2005) Screening women at high risk for breast cancer with mammography and magnetic resonance imaging. *Cancer* 103:1898–1905
- Le-Petross HT, Shetty MK (2011) Magnetic resonance imaging and breast ultrasonography as an adjunct to mammographic screening in high-risk patients. *Semin Ultrasound CT MR* 32:266–272
- Liberman L, Morris EA, Lee MJ et al (2002) Breast lesions detected on MR imaging: features and positive predictive value. *Am J Roentgenol* 179:171–178
- Lloyd J, Flanagan AM (2000) Mammary and extramammary Paget's disease. *J Clin Pathol* 53:742–749
- Macura KJ, Ouwerkerk R, Jacobs MA et al (2006) Patterns of enhancement on breast MR images: interpretation and imaging pitfalls. *Radiographics* 26:1719–1734
- Mann RM (2010) The effectiveness of MR imaging in the assessment of invasive lobular carcinoma of the breast. *Magn Reson Imaging Clin N Am* 18:259–276
- Mann RM, Veltman J, Huisman H et al (2011) Comparison of enhancement characteristics between invasive lobular carcinoma and invasive ductal carcinoma. *J Magn Reson Imaging* 34:293–300
- McDivitt RW, Stevens JA, Lee NC et al (1992) Histologic types of benign breast disease and the risk for breast cancer: The Cancer and Steroid Hormone Study Group. *Cancer* 69:1408–14014
- Mendelson EB, Baum JK, Berg WA, Merrit CR, Rubin E (2003) Breast imaging reporting and data system BI-RADS: ultrasound. American College of Radiology, Reston

- Miller BT, Abbott AM, Tuttle TM (2012) The influence of preoperative MRI on breast cancer treatment. *Ann Surg Oncol* 19:536–540
- Monticciolo DL (2011) Magnetic resonance imaging of the breast for cancer diagnosis and staging. *Semin Ultrasound CT MR* 32:319–330
- Morrow M, Waters J, Morris E (2011) MRI for breast cancer screening, diagnosis and treatment. *Lancet* 378(9805):1804–11
- Orel SG, Mendonca MH, Reynolds C et al (1997) MR imaging of ductal carcinoma in situ. *Radiology* 202:413–420
- Patani N, Mokbel K (2008) The utility of MRI for screening and staging of breast cancer. *Int J Clin Pract* 62:450–453
- Pediconi F, Occhiato R, Venditti F et al (2005) Radial scars of the breast: contrast-enhanced magnetic resonance mammography appearance. *Breast J* 11:23–28
- Pfleiderer SO, Sachse S, Sauner D et al. (2004) Changes in magnetic resonance mammography due to hormone replacement therapy. *Breast Cancer Res.* 6(3):R232–8
- Planche K, Vinnicombe S (2004) Breast imaging in the new era. *Cancer Imaging* 4:39–50
- Prasad SN, Houserkova D (2007) The role of various modalities in breast imaging. *Biomed Pap Med Fac Univ Palacky Olomouc Czech Repub* 151:209–218
- Prechtel K (1993) The pathology of mastopathy and breast cancer. *Radiologe* 33:236–242
- Rahbar H, Partridge SC, Eby PR et al (2011) Characterization of ductal carcinoma in situ on diffusion weighted breast MRI. *Eur Radiol* 21:2011–2019
- Razek AA, Gaballa G, Denewer A et al (2010) Invasive ductal carcinoma: correlation of apparent diffusion coefficient value with pathological prognostic factors. *NMR Biomed* 23:619–623
- Schlossbauer T, Hellerhoff K, Reiser M (2008) Value of breast MRI as supplement to mammography and sonography for high risk breast cancer patients. *Radiologe* 48:351–357
- Schmidt WA, Boudousquie AC, Vetto JT et al (2001) Lymph nodes in the human female breast: a review of their detection and significance. *Hum Pathol* 32:178–187
- Seely JM (2012) Management of breast magnetic resonance imaging-detected lesions. *Can Assoc Radiol J* 63:192–206
- Soo MS, Dash N, Bentley R et al (2000) Tubular adenomas of the breast: imaging findings with histologic correlation. *Am J Roentgenol* 174:757–761
- Spillane AJ, Donnellan M, Matthews AR (1999) Clinical significance of intramammary lymph nodes. *Breast* 8:143–146
- Strigel RM, Eby PR, Demartini WB et al (2010) Frequency, upgrade rates, and characteristics of high-risk lesions initially identified with breast MRI. *Am J Roentgenol* 195:792–798
- Tominaga J, Hama H, Kimura N et al (2011) Magnetic resonance imaging of intraductal papillomas of the breast. *J Comput Assist Tomogr* 35:153–157
- Tsushima Y, Takahashi-Taketomi A, Endo K (2009) Magnetic resonance (MR) differential diagnosis of breast tumors using apparent diffusion coefficient (ADC) on 1.5-T. *J Magn Reson Imaging* 30:249–255
- Uematsu T, Kasami M (2009a) MR imaging findings of benign and malignant circumscribed breast masses: part 1. Solid circumscribed masses. *Jpn J Radiol* 27:395–404
- Uematsu T, Kasami M (2009b) MR imaging findings of benign and malignant circumscribed breast masses: part 2. Cystic circumscribed masses. *Jpn J Radiol* 27:405–409
- Van den Bosch MA, Daniel BL, Mariano MN et al (2005) Magnetic resonance imaging characteristics of fibrocystic change of the breast. *Invest Radiol* 40:436–441
- Whipp EC, Halliwell M (2008) Magnetic resonance imaging appearance in the postoperative breast: the clinical target volume-tumor and its relationship to the chest wall. *Int J Radiat Oncol Biol Phys* 72:49–57
- Yu J, Park A, Morris E et al (2008) MRI screening in a clinic population with a family history of breast cancer. *Ann Surg Oncol* 15:452–461

Birger Mensel and Ralf Puls

12.1 The Female Genital Organs

12.1.1 Introduction

The external female genital organs include the labia majora and minora, the vestibule of vagina, and the clitoris, jointly referred to as the vulva. Since most women seek medical attention anyway when they notice abnormal changes in this area, whole-body screening by MRI is not expected to reveal any pathology here, and the external female genitalia will not be dealt with further in this chapter. The internal genital organs include the vagina (which, for the same reason, will not be discussed here), the cervix, the uterus, and the paired ovaries with the fallopian tubes.

The female reproductive organs pose a particular challenge in the setting of whole-body MRI screening in terms of how to deal with common benign lesions such as ovarian cysts and uterine fibroids.

In Germany, endometrial cancer is the fourth most common female tumor (11,700 newly diagnosed cases each year), ovarian cancer is fifth in frequency (9,660 cases), and cervical cancer is eleventh (6,190 cases) (Robert-Koch-Institut und die Gesellschaft der Epidemiologischen Krebsregister in Deutschland e.V. 2008). Until the 1970s, cervical cancer was the most common malignancy in women, but it has since declined markedly, thanks to the introduction of screening. Endometrial and ovarian cancer are more common in the postmenopausal period (45–50 years), which is why a screening program for these cancers in this age group would be

B. Mensel (✉)

Institute of Diagnostic Radiology and Neuroradiology, University Medicine Greifswald,
Ferdinand-Sauerbruch-Straße 1, Greifswald 17475, Germany
e-mail: birger.mensel@uni-greifswald.de

R. Puls

Institute of Diagnostic and Interventional Radiology and Neuroradiology,
HELIOS Klinikum Erfurt, Nordhäuser Straße 74, Erfurt, 99089, Germany
e-mail: ralf.puls@helios-kliniken.de

Table 12.1 Cervical cancer

Frequency	Incidence, <15/100,000 women/year
Age predilection	Mean age at presentation, 51 years
Risk factors	HPV infection, smoking
Type of lesion	Malignant
Signs and symptoms	Vaginal discharge, spotting, abnormal vaginal bleeding, painful defecation and/or bladder voiding
Differential diagnosis	Endometrial cancer, cervical sarcoma, uterine fibroid

desirable. Transvaginal ultrasound, which is highly sensitive and specific, should be used as a supplementary modality whenever suspicious findings are demonstrated by MRI. The CA-125 tumor marker test can also help in deciding between follow-up and surgical removal (Oyelese et al. 2002).

12.1.2 Cervix

Cervical cancer is the most relevant finding to be considered in interpreting screening MRI scans. Nabothian cysts are the most common incidentally detected benign lesions and will also be briefly discussed.

12.1.2.1 Cervical Cancer

In Germany, cervical cancer is newly diagnosed in 6,200 women each year, accounting for 1.7 % of all cancers in women (11th most common female cancer). The incidence is below 15/100,000 women. Cervical cancer has two age peaks, one between 35 and 54 years and another beginning around age 65. The mean age at presentation is 51 years. Infection with human papillomavirus (HPV) is the main risk factor (Table 12.1) (Robert-Koch-Institut und die Gesellschaft der Epidemiologischen Krebsregister in Deutschland e.V. 2008). Cervical cancer, including early disease, can be reliably detected by MRI, especially with use of T2-weighted images. On these images, cervical cancer has higher signal intensity than the surrounding cervical stroma (Fig. 12.1). Unenhanced T1-weighted images contribute no relevant information. Diffusion-weighted imaging (DWI) may also allow differentiation between normal and abnormal cervical tissue. Lower apparent diffusion coefficients (ADCs) have been found in cancer (Okamoto et al. 2003; Namimoto et al. 2009). The differential diagnosis includes cervical fibroids and polyps, nabothian cysts, advanced endometrial cancer, cervical sarcoma, and metastasis.

Clinical Management

Thickening of the cervical wall or localized lesions should be evaluated further, ideally using transvaginal ultrasound and contrast-enhanced MRI (Scheidler and Heuck 2002).

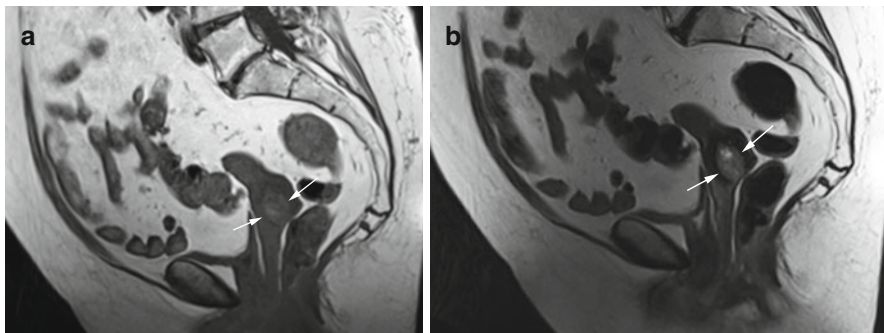


Fig. 12.1 (a) Sagittal T1w image shows distension of the cervix and an inhomogeneous mass of high signal intensity (*arrows*). (b) Sagittal T2w image confirms the high-signal-intensity cervical mass (*arrows*). The findings are suspicious for cervical cancer. Also seen is diverticulosis

Table 12.2 Nabothian cysts

Frequency	Very common
Age predilection	Before menopause
Location	Uterine cervix
Type of lesion	Benign
Signs and symptoms	Asymptomatic
Differential diagnosis	Cervical cancer (malignant adenoma)

12.1.2.2 Nabothian Cysts

Nabothian cysts are common, benign retention cysts that develop when one of the mucous glands of the cervix becomes obstructed. There is an association with chronic inflammatory conditions of the cervix and with multiparity (Table 12.2). Nabothian cysts range in size from a few millimeters to 4 cm. Women typically have multiple cysts located along the cervix. The cysts are very bright on T2-weighted images, while they are isointense or slightly hyperintense (protein content) on T1-weighted images. The most important differential diagnosis is malignant adenoma, a subtype of cervical cancer with an imaging appearance characterized by multiple cysts with a soft-tissue component. Unlike a nabothian cyst, malignant cervical adenoma enhances after administration of contrast medium (Okamoto et al. 2003; Togashi et al. 1987).

Clinical Management

Most nabothian cysts are asymptomatic and benign, and there is no need to report them (Okamoto et al. 2003).

Table 12.3 Uterine fibroids

Frequency	Incidence, approx. 80 %
Age predilection	>25 years, no growth after menopause
Type of lesion	Benign, <0.2 % risk of malignant transformation
Signs and symptoms	Present in only 25–50 % of cases; abnormal periods, pain, impaired fertility
Differential diagnosis	Adenomyosis, myometrial contraction, leiomyosarcoma

12.1.3 Uterus

The most common uterine findings are anomalies and tumors of different etiologies. They are discussed in this section along with endometriosis.

12.1.3.1 Anomalies

The normal uterus is a pear-shaped organ located between the urinary bladder and the rectum. The nonpregnant uterus is 7 cm long. A severe congenital anomaly such as absence of the uterus is usually known to the woman. In older women, an absent uterus is more likely due to hysterectomy. Relevant uterine anomalies that may be detected by screening MRI result from defective fusion or resorption and include bicornuate uterus (double uterus with or without a double cervix), duplex uterus (bicornuate uterus with two vaginas), and (sub-)septate uterus (persistent median septum, which completely or partially divides the cavity). The prevalence is approx. 1 % (Homer et al. 2000). MRI is highly sensitive and specific in demonstrating uterine anomalies, with a fat-suppressed T2-weighted pulse sequence being especially useful.

Clinical Management

Uterine anomalies may impair fertility and should therefore be communicated to younger women who wish to have children (Troiano and McCarthy 2004).

12.1.3.2 Tumors

This section discusses uterine fibroids or leiomyomas and endometrial cancer, which are, respectively, the most common benign and malignant tumors of the uterus.

12.1.3.2.1 Uterine Fibroids

Uterine fibroids are the most common gynecologic tumors in women of reproductive age (Table 12.3). In autopsy series, fibroids were found in up to 77 % of women with the incidence increasing with age, most markedly after age 40. This is because their development and growth is hormone dependent (Cramer and Patel 1990; Flake et al. 2003). Uterine fibroids are round to oval lesions consisting of smooth muscle cells, collagen, extracellular matrix, fat, and fibrin. Women usually have

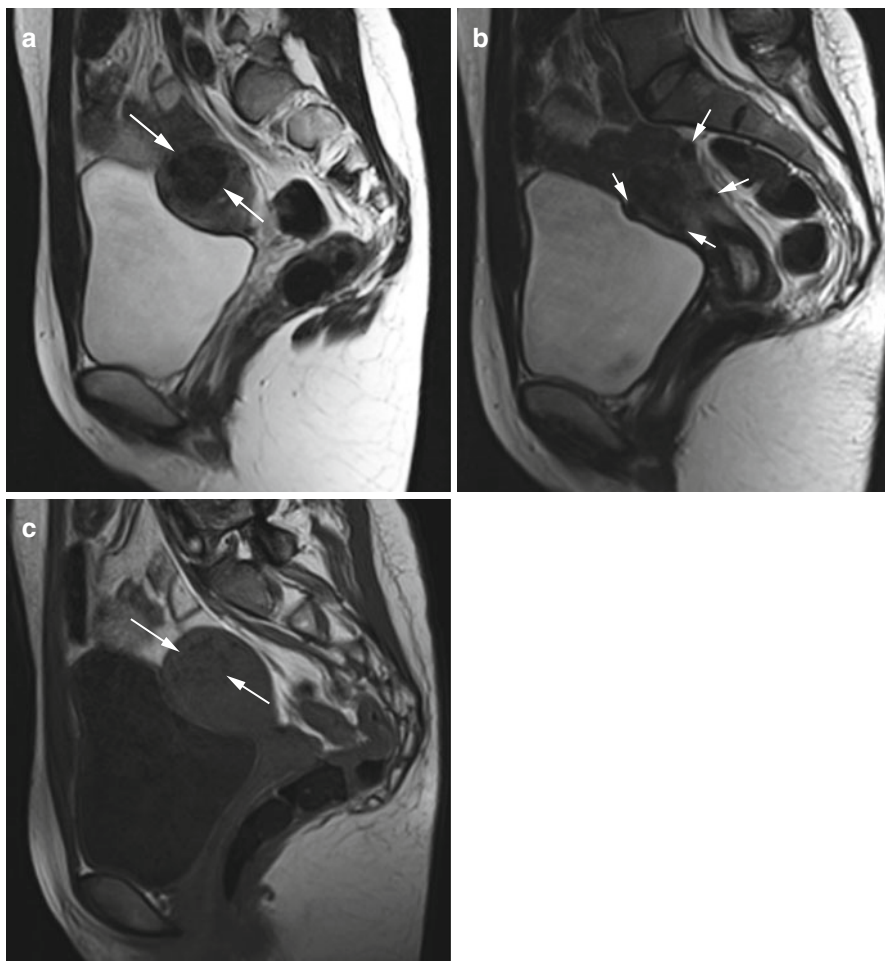


Fig. 12.2 (a) Sagittal T2w image reveals a well-defined, homogeneous mass of low signal intensity in the uterine myometrium (*arrows*) in a 27-year-old subject. (b) Sagittal T2w image demonstrates additional rounded masses, which are subserosal in location (*arrows*). (c) Sagittal T2w image again shows the large intramural mass, which is slightly hypointense (*arrows*). In summary, MRI shows a myomatous uterus with a large intramural fibroid and multiple subserosal fibroids

multiple fibroids. Fibroids are found within the endometrial cavity, in the uterine wall, or extending beyond the uterus. Diffuse presence of fibroids within the myometrium is referred to as myomatous uterus. MRI is considered the most suitable imaging modality for detecting and characterizing uterine fibroids. On T2-weighted images, fibroids are usually conspicuous as smooth and sharply demarcated homogeneous masses of low signal intensity compared with the surrounding myometrium (Fig. 12.2). On T1-weighted pulse sequences, they have the same signal intensity as the myometrium. Intralesional calcifications appear dark and are quite common.

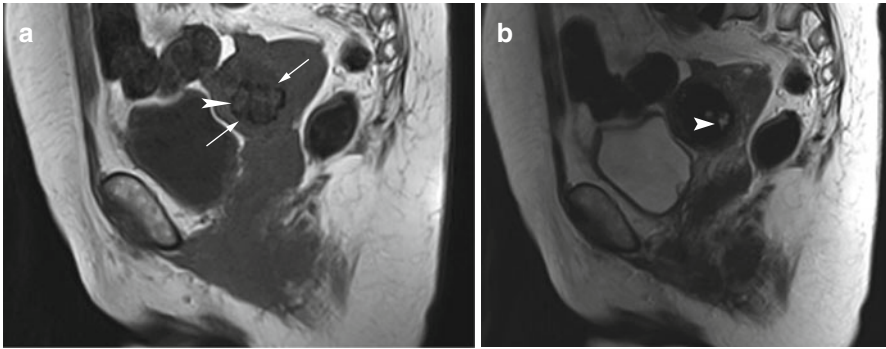


Fig. 12.3 (a) Sagittal T1w image reveals a rounded low-signal-intensity mass with slightly irregular borders in the uterine wall (*arrows*) in a 54-year-old woman. In addition, the image shows patchy hyperintensities (*arrowhead*). (b) Sagittal T2w image shows the hyperintense areas more clearly (*arrowhead*). In summary, the appearance is consistent with an intramural fibroid with hemorrhagic degeneration

Degeneration of fibroids is also common and is associated with the presence of intralesional hemorrhage (high T1 signal intensity, variable T2 signal intensity), cystic portions (high T2 signal intensity), or mucinous degeneration (very high T2 signal intensity) (Fig. 12.3). Fibroids can exhibit homogeneous contrast enhancement (Murase et al. 1999). Uterine fibroids must be distinguished from adenomyosis (a form of endometriosis formerly known as internal endometriosis). Adenomyosis is the presence of ectopic endometrial glands in the myometrium. It is usually diffuse but may also be focal. Diffuse adenomyosis is suggested by widening of the junctional zone (>12 mm) and is best evaluated on T2-weighted images. The junctional zone has low T2 signal intensity, delineating it from the endometrium (high signal intensity) and the myometrium (intermediate signal intensity). Areas of adenomyosis are characterized by low T2 signal intensity interspersed with bright foci. Focal forms of adenomyosis appear as poorly marginated areas of low signal intensity that are less well defined than fibroids (Murase et al. 1999). Other differential diagnoses are focal myometrial contraction (which can be ruled out by serial imaging) and leiomyosarcoma.

Clinical Management

Uterine fibroids can cause abdominal pain and heavy menstrual bleeding. Some forms compromise fertility and/or increase the risk of miscarriage, which is why younger women should be informed when uterine fibroids are detected by MRI screening (Murase et al. 1999). This is different in postmenopausal women, who need only be informed when very large fibroids are found or when there is diffuse involvement with a clear mass effect on adjacent organs (urinary bladder, rectum).

Table 12.4 Endometrial cancer

Frequency	Incidence, 20–30/100,000 women
Age predilection	Mean age at presentation, 68 years
Risk factors	Endogenous and exogenous estrogen, obesity
Type of lesion	Malignant
Signs and symptoms	Irregular bleeding, pain
Differential diagnosis	Endometrial hyperplasia, polyps, fibroids, endometrial sarcoma

12.1.3.2 Endometrial Cancer

Endometrial cancer is diagnosed in 11,700 women in Germany each year. The annual incidence is 20–30 new diagnoses per 100,000 women and is on the rise. It is the fourth most common cancer in women, accounting for 5.7 % of all cancers in women, and the most common cancer of the female reproductive organs. Most uterine cancers arise in the endometrium with over 90 % being adenocarcinomas. The mean age at presentation is 68 years (Table 12.4) (Robert-Koch-Institut und die Gesellschaft der Epidemiologischen Krebsregister in Deutschland e.V. 2008). MRI has limitations in detecting early endometrial cancer (especially when imaging protocols without contrast medium administration are used). Depending on the stage of endometrial cancer, the appearance on MR images may range from minimal changes to massive enlargement of the uterus. On T1-weighted images, endometrial cancer is isointense or hypointense relative to the endometrium or myometrium. On T2-weighted images, the cancer is isointense or hypointense to endometrium and usually slightly hyperintense relative to myometrium. The higher cellularity of endometrial carcinomas results in high signal intensity on diffusion-weighted images with lower ADC values. Following administration of contrast medium, endometrial cancer enhances earlier than normal endometrium and is hypointense to the myometrium (Namimoto et al. 2009; Sala et al. 2007). Several entities have to be considered in the differential diagnosis: endometrial hyperplasia or polyps (difficult to differentiate; DWI is helpful), fibroids, adenomyosis, and uterine sarcoma (2–6 % of malignant uterine tumors, typically larger and more heterogeneous).

Clinical Management

A suspected malignant tumor of the endometrium/uterus must be disclosed, and the woman should undergo further diagnostic workup with endosonography or contrast-enhanced MRI (Nalaboff et al. 2001).

12.1.4 Endometriosis

Endometriosis is the ectopic occurrence of functional endometrial tissue including glands outside the uterine cavity. The severity is variable, ranging from microscopic ectopic cysts to so-called endometriomas, which are circumscribed endometriotic

Table 12.5 Endometriosis

Frequency	Prevalence, 5–10 %
Age predilection	Mean age at presentation, 28 years
Risk factors	Environmental toxins may promote endometriosis
Type of lesion	Benign, <1 % risk of malignant transformation
Signs and symptoms	Cyclic cramping pain, dyspareunia, impaired fertility
Differential diagnosis	Dermoid, ovarian cancer

or chocolate cysts several centimeters in size. Endometriosis is typically seen during the reproductive years with a mean age at presentation of 25–29 years (Dmowski et al. 1997). The prevalence is 5–10 %, and up to 25 % of women suffering from endometriosis have lower abdominal pain (Table 12.5) (Eskenazi and Warner 1997; Olive and Schwartz 1993). It is assumed that endometrial tissue enters the peritoneal cavity through the fallopian tubes, a process known as retrograde menstruation. This assumption is supported by the anatomic distribution of endometriotic lesions, which are most commonly found on the ovaries (see next section) and along the uterine appendages and the uterus. Theoretically, ectopic endometriotic tissue may be found anywhere within the abdominal cavity. For correct interpretation of MR images, the examiner must be aware that ectopic endometrial tissue is subject to the same cyclic variation as within the uterine cavity. Ectopic endometrial tissue has a cystic appearance and is characterized by very high signal intensity on T1-weighted images (due to high protein and blood content). The appearance on T2-weighted images ranges from hyperintense to hypointense, depending on the amount and age of blood present (high iron content lowers T2 signal intensity). Following administration of contrast medium, the cyst walls show nonspecific enhancement (Sugimura et al. 1993; Siegelman and Outwater 1999). Malignant transformation of endometriotic tissue may occur but is very rare (<1 %). Endometriotic lesions must be differentiated from cystic tumors such as dermoids (which, unlike endometrial tissue, will show a drop in signal intensity on fat-suppressed images) and cystic ovarian cancer.

Clinical Management

Younger women, who are assumed to wish to have children, should be informed when endometriosis is detected, as 30–50 % of women with endometriosis are infertile (Eskenazi and Warner 1997).

12.1.5 Ovaries

Anomalies such as agenesis or multiple-anomaly syndromes, which either have no relevance or are so severe that affected women are aware of their condition, are not discussed here. Instead, we will focus on the more common ovarian lesions that

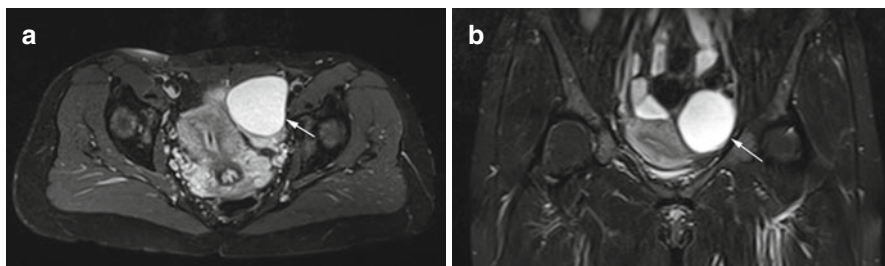


Fig. 12.4 Axial PD image (a) and coronal TIRM image (b) obtained in a 38-year-old woman show a smoothly marginated, homogeneous cyst of high signal intensity (*arrow*). The cyst has a size of up to 6.6 cm, and the appearance is consistent with a typical functional cyst

Table 12.6 Unilocular ovarian cysts

Frequency	Prevalence, 3–15 %
Age predilection	Premenopausal
Type of lesion	Benign
Signs and symptoms	Usually asymptomatic
Differential diagnosis	Serous cystadenoma, cystic ovarian cancer

may be detected by MRI including unilocular and multilocular ovarian cysts as well as solid or complex masses with variable cystic components.

Several morphologic MR features have been shown to be useful for characterizing ovarian lesions (Gore et al. 2010; Imaoka et al. 2006). The features include the site of the lesion and single versus multiple occurrences as well as the ratio of cystic to solid components (purely cystic, cystic with solid components, and predominantly solid).

Contrast enhancement is another important criterion for differentiating between benign and malignant ovarian lesions but is not available in screening MRI, which is typically performed without contrast medium. A number of features suggesting malignancy can be evaluated on unenhanced T1-weighted and T2-weighted images including a solid or predominantly solid appearance and, in the case of a cystic lesion, thickened cyst walls and multiple septa. Other criteria that may contribute to the differentiation include growth beyond the ovary, presence of ascites, and locoregional lymphadenopathy. When these criteria are applied in conjunction with contrast medium administration, MRI has over 90 % sensitivity and specificity in characterizing an ovarian mass (Hricak et al. 2000).

12.1.5.1 Unilocular Ovarian Cysts

The most common incidental findings are functional or retention cysts (Gore et al. 2010) (Fig. 12.4). They are frequently seen in premenopausal women but also occur during menopause (prevalence of 3.3–14.8 %) (Table 12.6). Functional ovarian cysts are fluid-filled cavities resulting from failure of the dominant follicle to ovulate (follicular cyst) or failure to regress (corpus luteum cyst).

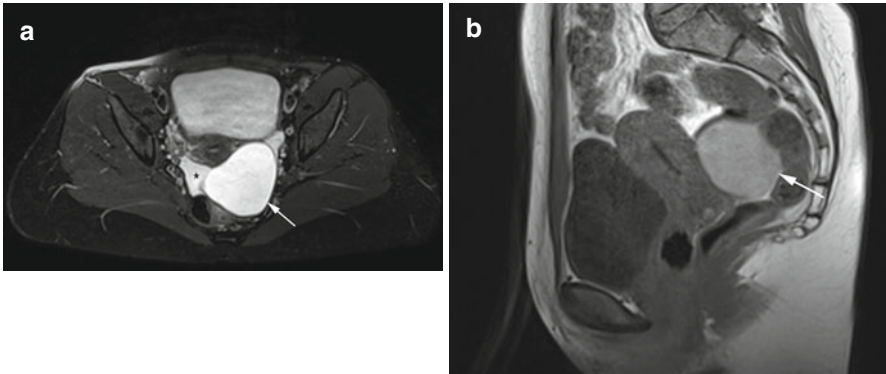


Fig. 12.5 Axial PD image (a) and sagittal T1w image (b) reveal a large, smoothly margined cyst (arrow) in a 45-year-old woman partially surrounded by free fluid (asterisk). The cyst has high signal intensity, and there is a small, physiologic amount of free fluid in the rectouterine pouch. There is good demarcation of both ovaries. The appearance is consistent with a hemorrhagic paraovarian cyst

These cysts are usually unilocular simple cysts with a smooth margin and range in size from 1 to 8 cm. Corpus luteum cysts are often larger and may contain blood. Paraovarian cysts are rare simple cystic tumors (Fig. 12.5) arising from the mesothelium or embryonic ducts (Müllerian and Wolffian ducts). These cysts must be differentiated from the normal ovaries. A hydrosalpinx developing on the basis of salpingitis or endometriosis can also mimic an ovarian cyst. Serous cystadenoma (cystoma) is not easily differentiated from a functional cyst based on morphologic imaging features when it is unilocular and no solid portions are seen. Serial examinations are necessary to make the distinction.

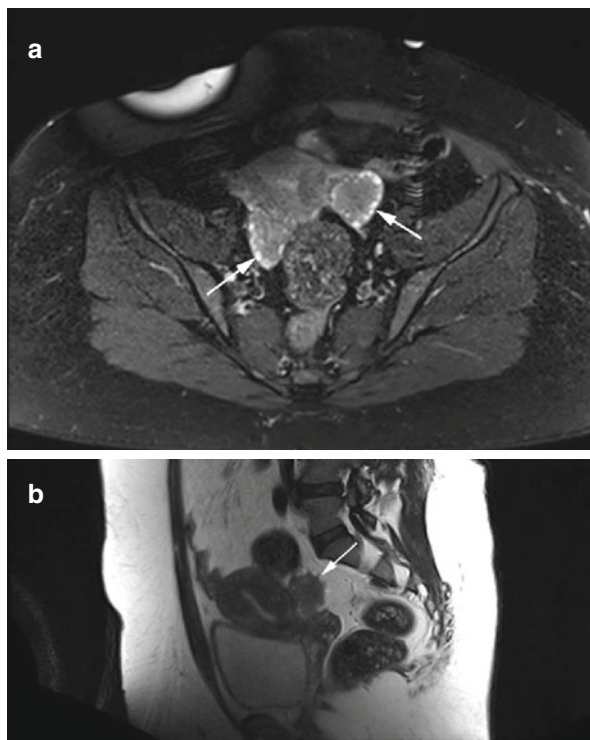
Clinical Management

Most ovarian cysts recede within 2 months in premenopausal women (up to age 45). Since there is a risk of rupture and since it is important to differentiate a cyst from serous cystadenoma, ovarian cysts larger than 2 cm should be reported and followed up. As no cyclic regulation occurs in postmenopausal women, the primary aim should be to initiate further diagnostic workup with transvaginal ultrasound and CA-125 tumor marker test (Oyelese et al. 2002; Dikensoy et al. 2007; McDonald and Modesitt 2006). Paraovarian cysts should be followed up by imaging.

12.1.5.2 Multilocular Ovarian Cysts

Polycystic ovaries can be encountered in healthy premenopausal women (Balen et al. 1995). Endocrine dysfunction presenting in the second or third decade of life may point to polycystic ovary syndrome (formerly known as Stein-Leventhal syndrome).

Fig. 12.6 Axial PD image (a) and sagittal T2w image (b) obtained in a 34-year-old obese woman. There are prominent ovaries with lower signal intensity in the center and follicular cysts arranged around the periphery of both ovaries, producing the string-of-pearls sign (arrows). The diagnosis is polycystic ovary syndrome

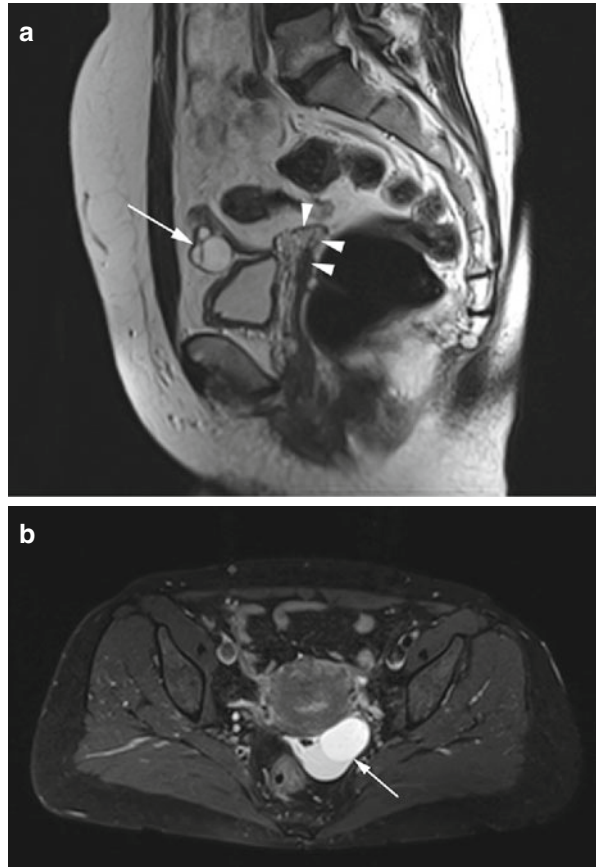


This syndrome is characterized by the classic triad of obesity, hirsutism, and infertility (Fig. 12.6). In affected women, MRI demonstrates enlarged ovaries containing follicular cysts (<1 cm). The cysts typically occur in the periphery of the ovaries, giving the appearance of a string of pearls. Other multilocular cystic tumors are serous and mucinous cystadenomas (Fig. 12.7), which account for about 25 % of benign ovarian neoplasms. They are bilateral in 20 % of cases and tend to be more common after menopause (Dorum et al. 2005). Cystadenomas frequently contain septa and calcifications. Half of the women with endometriosis have ectopic endometriotic tissue on the ovaries. MR imaging demonstrates multiple endometriomas containing old blood (Fig. 12.8). The lesions are known as chocolate cysts and characteristically have high signal intensity on T1-weighted images and low signal intensity on T2-weighted images, a pattern known as T2 shading.

Clinical Management

Multilocular ovarian cysts have the potential for malignant transformation, which is why they should be monitored or characterized further (transvaginal ultrasound and CA-125 test) (Dikensoy et al. 2007; McDonald and Modesitt 2006).

Fig. 12.7 (a) Sagittal T2w image of a 62-year-old woman with a history of hysterectomy (*arrowheads*) reveals a cystic ovary with multiple septa (*arrow*). The diagnosis is cystadenoma. (b) Axial PD image of a 45-year-old woman shows a septated cyst of mixed signal intensity (*arrow*)



12.1.5.3 Mixed Cystic and Solid Ovarian Tumors

Primary ovarian cancer and metastases to the ovary (Figs. 12.9 and 12.10) are mainly solid but frequently have cystic spaces (Table 12.7). Ovarian cancer is most common in the fourth to seventh decade of life, and 90 % of ovarian cancers arise from the epithelium (Imaoka et al. 2006). The most common histologic types, in order of frequency, are serous and mucinous carcinoma, cystadenocarcinoma, endometrioid carcinoma, and undifferentiated carcinoma. Malignant germ cell tumors are very rare. Metastases usually involve both ovaries with gastric cancer being the most common primary tumor (e.g., Krukenberg tumor).

Dermoid or mature teratoma is a benign tumor usually occurring before the second decade of life, which is why this tumor is unlikely to be encountered at screening (Gore et al. 2010).

Fig. 12.8 (a) Axial PD image of a 50-year-old woman shows multiple ovarian cysts (*arrows*) of variable signal intensity in both ovaries. (b) Sagittal T2w image demonstrates a hydrosalpinx with a tortuous course of the tube (*arrow*)

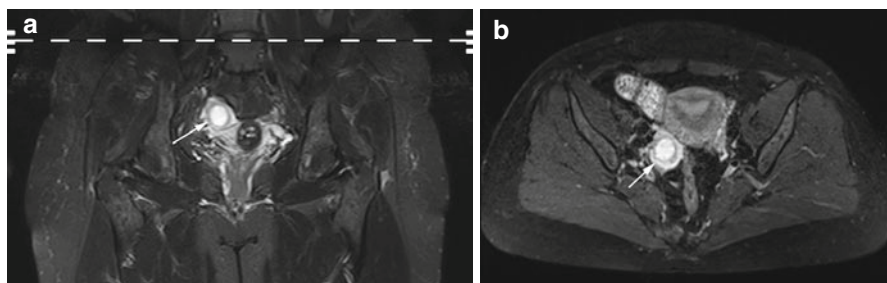
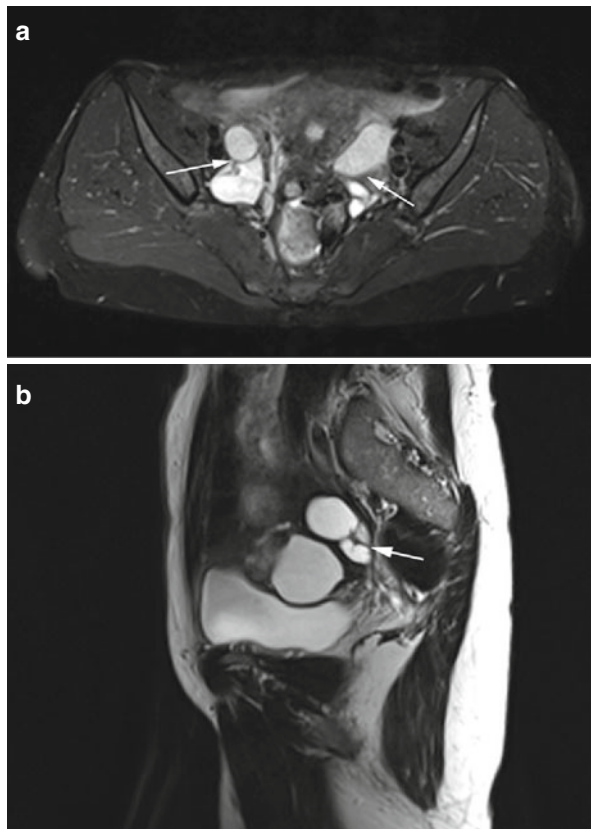


Fig. 12.9 Coronal TIRM image (a) and axial PD image (b) obtained in a 45-year-old woman with a partially cystic (*center*) and partially solid mass (*periphery*) in the right ovary (*arrow*). The diagnosis is cystadenocarcinoma

Clinical Management

Mixed cystic and solid ovarian masses require further diagnostic workup (transvaginal ultrasound and CA-125 test) because they are more likely to be malignant (Dikensoy et al. 2007; McDonald and Modesitt 2006).

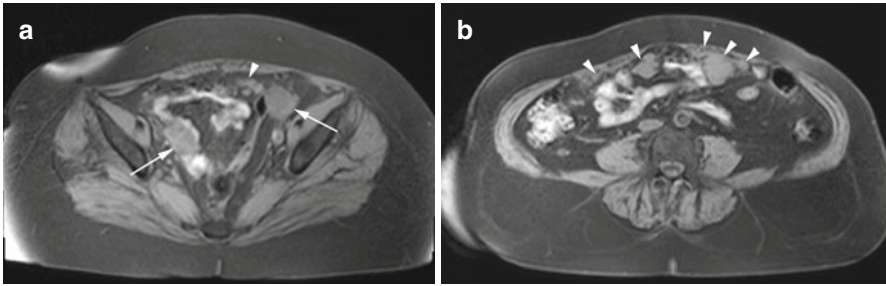


Fig. 12.10 T1w 3D FLASH images obtained in a 76-year-old woman demonstrate solid masses (*arrows*) in both ovaries (**a**) and multiple metastatic implants (*arrowheads*) in the peritoneal cavity (**b**). The findings are consistent with metastatic ovarian cancer

Table 12.7 Mixed cystic and solid ovarian tumors

Frequency	Incidence, 14/100,000 women/year
Age predilection	58–65 years
Risk factors	Risk increases with the duration of the reproductive phase, genetic predisposition, childlessness
Type of lesion	Malignant
Signs and symptoms	Nonspecific, genital hemorrhage
Differential diagnosis	Benign ovarian cyst, cystadenoma, dermoid

12.2 The Male Genital Organs

12.2.1 Introduction

The penis and the scrotum constitute the external male genital organs, while the internal reproductive organs include the testicles with the epididymis and spermatic cords, the prostate, the seminal vesicles, and other accessory gonads.

Relevant abnormalities of the penis and scrotum are not expected to be seen in the setting of screening MRI as such changes would most likely have already been discovered by the affected man and led him to see a doctor.

12.2.2 Testicles

The most important testicular imaging findings are hydrocele, aberrations in number, abnormal size, cryptorchidism, and mass lesions.

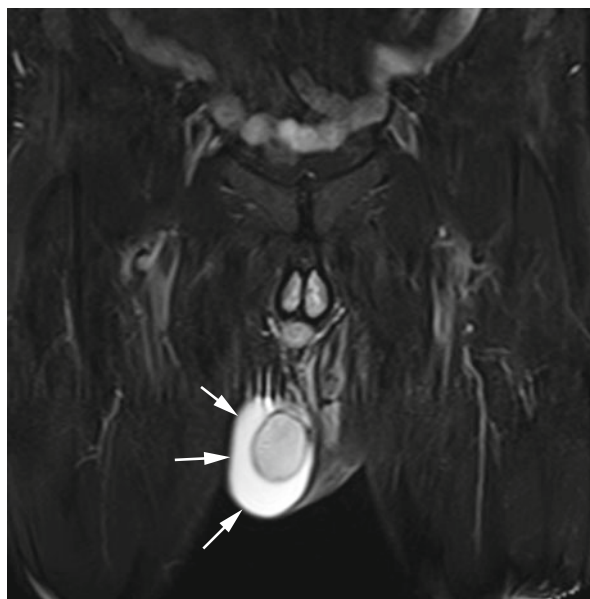
12.2.2.1 Hydrocele

A hydrocele is a congenital or acquired collection of serous fluid in the space of the tunica vaginalis testis (Table 12.8). Detection of acquired hydroceles is relevant in

Table 12.8 Hydrocele

Frequency	Incidence, >15 %
Age predilection	Acquired hydrocele, >40 years
Type of lesion	Benign
Signs and symptoms	Unusually asymptomatic; painless testicular swelling
Differential diagnosis	Hematocele, pyocele

Fig. 12.11 Coronal *TIRM* image demonstrates a crescent-shaped area of homogenous high signal intensity surrounding the right testis (*arrows*). This appearance indicates serous fluid in the tunica vaginalis testis and is typical of a hydrocele. The tunica albuginea is clearly delineated as a low-signal-intensity line around the testis

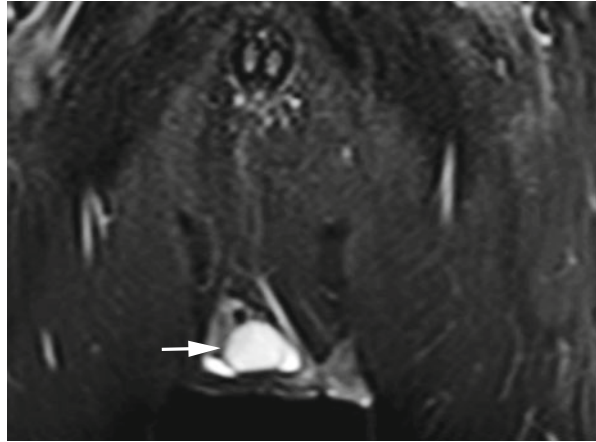


the screening situation (Akin et al. 2004). They tend to occur in middle-aged or older men on one or both sides. A definitive pathomechanism has not been established (Woodward et al. 2003). A thin layer of fluid around the testis is normal and has been demonstrated in 86 % of men in an ultrasound study (Leung et al. 1984). Acquired hydroceles are usually idiopathic in origin and predominantly affect men after age 40. Less commonly, acquired hydroceles are associated with tumors, inflammation, or infection. Hydrocele is bilateral in 7–10 % of cases (Leung et al. 1984). It is depicted with very high contrast on fat-saturated T2-weighted images; usually there is no compression of the underlying testis (Fig. 12.11). In the differential diagnosis, hematocele and pyocele must be ruled out (Woodward et al. 2003).

Clinical Management

There is no need to report an idiopathic hydrocele; treatment is necessary only when swelling and pain lead to problems, for which an affected man seeks treatment on his own (Gyapong et al. 2000).

Fig. 12.12 Coronal TIRM image shows a slightly smaller testicle on the right (*arrow*) and a small hydrocele



12.2.2.2 Aberration in Number

Aberrations in number are easily identified and are usually known to a man. Polyorchidism is very rare, with about 100 cases reported in the literature worldwide. The most common form is the presence of three testicles within the scrotum. However, supernumerary testicles may also be located inguinally or intra-abdominally. It is still under debate whether surgical exploration or a conservative approach with serial imaging is the best management option in these cases (Sheah et al. 2004; Yeniyol et al. 2004; Chung and Yao 2002). On MR images, an accessory testicle has the same signal intensity as orthotopic intrascrotal testicles. A testicular tumor must be ruled out in the differential diagnosis.

The absence of one or both testicles from the scrotum is nearly always due to surgical removal, because of testicular cancer or testicular torsion, for instance. Nevertheless, a careful search for a cryptorchid testis should always be done in such cases.

Clinical Management

Polyorchidism should be reported and at least followed up by imaging (Bhogal et al. 2007). The absence of one or both testicles is usually known and requires no further workup.

12.2.2.3 Abnormal Size

A normal adult testis is 3–5 cm long, 2–4 cm wide, and about 3 cm in anteroposterior extension with marked interindividual variation in dimensions (Kim et al. 2007). An exact size threshold for diagnosing testicular atrophy does not exist. This is why both testicles are measured and atrophy is assumed when there is a significant difference (>50 %) in one or more dimensions between the two testicles (Fig. 12.12). When bilateral testicular atrophy is present, the size of both testicles is

Table 12.9 Cryptorchidism

Frequency	Prevalence in adults, approx. 1 %
Age predilection	Congenital
Type of lesion	Benign (fivefold higher risk of testicular cancer)
Signs and symptoms	Asymptomatic, impaired fertility
Differential diagnosis	Retractile testis, monorchism

well below the normal range. Often, there is concomitant atrophy of the epididymis and vascular structures. Testicular atrophy may be due to cryptorchidism, postinflammatory changes, or trauma.

Significant enlargement of one testicle should prompt further diagnostic workup to rule out a testicular tumor.

Clinical Management

Marked unilateral testicular atrophy should be reported, one reason being that it may be associated with an increased risk of testicular cancer. Imaging follow-up may be indicated, depending on the individual's age. When imaging demonstrates unilateral testicular enlargement and malignancy cannot be ruled out with certainty, this should prompt further diagnostic evaluation.

12.2.2.4 Cryptorchidism

Cryptorchidism is the failure of one or both testes to descend into the scrotum (Table 12.9). An undescended testis may be found anywhere along its normal pathway of descent (abdominal, inguinal). Incomplete or absent testicular descent is the most common congenital anomaly in boys (2–8 %). The unilateral form is four times more common than bilateral cryptorchidism. Congenital cryptorchidism usually disappears within the first year of life (due to endogenous testosterone production), resulting in a prevalence of 1–2 % at the age of 3–12 months (Virtanen et al. 2007). An infant diagnosed with cryptorchidism should undergo orchidopexy. An undescended testicle compromises fertility and has a five times higher risk of testicular cancer (Dieckmann and Pichlmeier 2004). A retractile testis is an intermediate form with the testis tending to retract from its normal position in the scrotum.

When MRI fails to demonstrate one or both testicles in the scrotum, this should prompt an evaluation for cryptorchidism. A coronal T2-weighted pulse sequence with fat saturation is well suited for this purpose, as it increases the contrast between the high-signal-intensity testicle and surrounding tissue (Fig. 12.13). An atrophic undescended testis may be more difficult to detect. A careful search along the course of the spermatic cord may help the radiologist in identifying a missing testis (Nguyen et al. 1999).

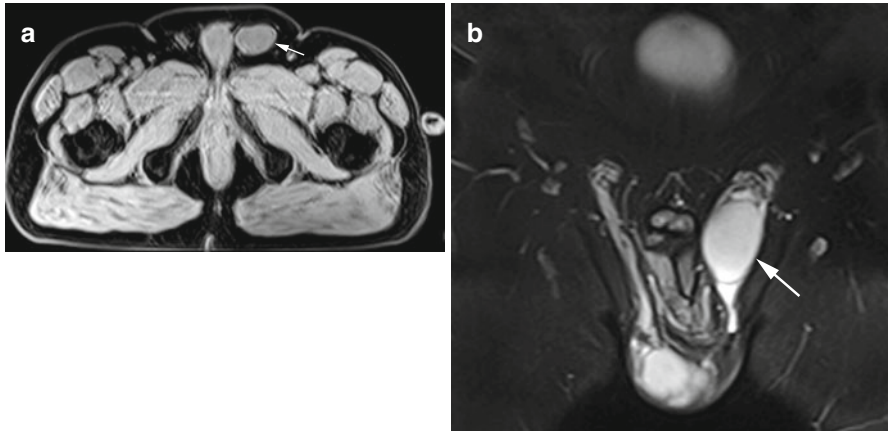


Fig. 12.13 (a) Axial T1w VIBE image reveals a mass of soft-tissue signal intensity in the left inguinal canal (*arrow*). (b) Coronal TIRM image with better visualization of the undescended testis in the left inguinal canal (*arrow*). There is fluid in the inguinal canal. Also clearly seen is the tortuous course of the spermatic cord above the testis

Clinical Management

Cryptorchidism must be communicated in all cases (although the condition is probably known). Orchiectomy is indicated in men up to 50 if no contraindications are present. In men over 50 and men at significant anesthetic risk, follow-up to rule out testicular cancer should be recommended (Wood and Elder 2009).

12.2.3 Epididymis

Disease of the epididymis is very rare (except for epididymitis). The most common lesions are cysts such as true epididymal cysts, dermoids, and spermatoceles. The most common solid epididymal masses are lipomas and adenomatoid tumors. Rarities include granuloma in men with sarcoidosis and malignant neoplasms (Woodward et al. 2003).

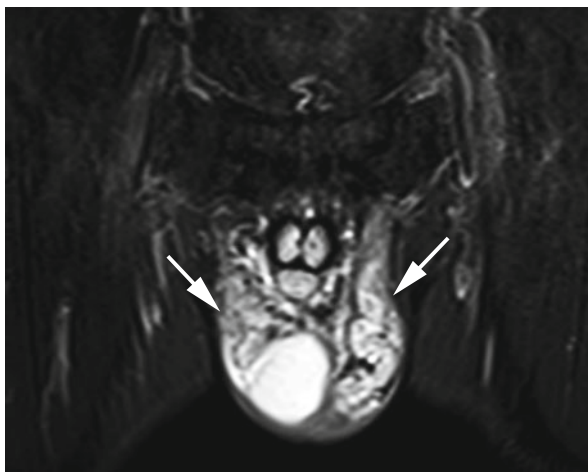
Clinical Management

Epididymal tumors, especially malignant ones, are very rare. Nevertheless, further diagnostic workup is indicated if MRI demonstrates solid tumor components or marked epididymal enlargement.

Table 12.10 Varicocele

Frequency	Prevalence, approx. 15 %
Age predilection	Becomes more common with age
Type of lesion	Benign
Signs and symptoms	Usually asymptomatic, tenderness at times, impaired fertility
Differential diagnosis	Spermatic cord tumor

Fig. 12.14 Coronal TIRM image reveals markedly dilated and elongated pampiniform plexus veins bilaterally (*arrows*). Part of the right testis is also depicted in the image



12.2.4 Spermatic Cord

The most common disease of the spermatic cord is a varicocele. Tumors of the spermatic cord are rare.

12.2.4.1 Varicocele

A varicocele is the dilatation of the veins of the pampiniform plexus, which may be secondary or idiopathic. A secondary varicocele results from compromised venous drainage, e.g., when a tumor is present. The more common idiopathic form has been attributed to incompetent testicular vein valves. Varicoceles are found in about 15 % of all men and in 40 % of infertile men (Table 12.10). A varicocele is considered to be present if pampiniform plexus veins are dilated to diameters of 2–3 mm (Kim and Lipshultz 1996). The markedly dilated and tortuous veins are clearly depicted on coronal T2-weighted images with fat saturation (Fig. 12.14). The veins have intermediate signal intensity on T1-weighted images and are markedly hyperintense on T2-weighted images with the signal intensity generally being determined by the flow rate. The varicose veins enhance after contrast medium administration.

A spermatic cord tumor must be ruled out in the differential diagnosis (Mattrey 1991; Cramer et al. 1991).

Table 12.11 Prostate cancer

Frequency	Incidence, approx. 100/100,000 men
Age predilection	Mean age at presentation, 69 years
Risk factors	Androgen dependency, obesity, smoking, genetic predisposition
Type of lesion	Malignant
Signs and symptoms	Disturbed bladder voiding, back pain
Differential diagnosis	Benign prostatic hyperplasia

Clinical Management

Younger men who can be assumed to wish to have children should be informed so that treatment can be contemplated to improve fertility (Kim and Lipshultz 1996). Disclosure is not necessary in older men.

12.2.4.2 Tumors

Spermatic cord tumors are very rare. Lipomas account for half of all masses of the spermatic cord and, as elsewhere in the body, have characteristic MRI features (Beccia et al. 1976). Other benign spermatic cord tumors include leiomyoma, dermoid cysts, and lymphangioma. Once a lipoma has been ruled out on the basis of its MRI appearance, the likelihood of a malignant tumor increases to over 50 % (Beccia et al. 1976). The most common malignant tumors are sarcomas (rhabdo- and leiomyosarcoma, liposarcoma).

Clinical Management

Spermatic cord tumors are very rare, and about half of them are accounted for by lipomas. Once a lipoma has been ruled out, the likelihood of a malignant tumor is markedly higher. This situation needs to be reported for further diagnostic workup (Beccia et al. 1976).

12.2.5 Prostate

Prostate changes are very common, especially in older men. The most common finding is enlargement of the prostate, which may be due to benign prostatic hyperplasia or prostate cancer. These two entities are discussed below.

12.2.5.1 Prostate Cancer

Prostate cancer is the most common cancer in men, accounting for 25 % of all male malignancies (Table 12.11). In Germany, 58,000 men are diagnosed with prostate cancer each year. It is the third most common cause of death from cancer. The mean age at diagnosis is 69 years. However, it is assumed that over 50 % of all prostate cancers diagnosed with the PSA test would not have become apparent through

symptoms during a man's lifetime (Robert-Koch-Institut und die Gesellschaft der Epidemiologischen Krebsregister in Deutschland e.V. 2008). Ninety-five percent of all prostate cancers are adenocarcinomas.

The zonal anatomy of the prostate is helpful for interpreting and reporting MRI findings.

Four zones are distinguished:

- The peripheral zone, which accounts for 70 % of the total prostate volume and is the most common site of prostate cancer (70 %)
- The central zone, which accounts for 25 % of the prostate and harbors 5 % of prostate cancers
- The transitional zone, where 20 % of cancers are found
- The periurethral zone (anterior fibromuscular stroma), making up the smallest portion of the prostate (McNeal 1988; Seitz et al. 2009)

The normal prostate gland has homogeneous intermediate signal intensity on T1-weighted images, which do not depict the zonal anatomy and provide poor soft-tissue contrast for identification of pathology. T2-weighted images are more useful, allowing differentiation of the zonal anatomy. The peripheral zone has high signal intensity and is surrounded by a black line, which corresponds to the prostate capsule. The central and transitional zones are of inhomogeneous low signal intensity due to the high proportion of stroma. Prostate cancer usually has low T2 signal intensity (and may be multifocal), which is why it is easier to detect in the hyperintense peripheral zone than in the remaining prostate (Fuchsjager et al. 2008; Turkbey et al. 2009). DWI may show restricted diffusion with an increased signal intensity and low ADC values (Issa 2002). Common accessory findings include infiltration of the bladder base, invasion of surrounding fatty tissue, locoregional lymph node metastases, and (osteoblastic) bone metastases.

The differential diagnosis includes benign prostatic hyperplasia (typically developing in the transitional zone), hemorrhage, prostatitis, and bladder cancer extending into the prostate (Fuchsjager et al. 2008; Chang et al. 2008). It is likely that, with the protocol used for a whole-body screening examination, many prostate cancers are overlooked (thick slices, surface coils).

Clinical Management

Suspected prostate cancer should be disclosed, regardless of the man's age, and further diagnostic workup recommended (PSA test). Inconclusive findings, which are not uncommon, should also be reported as a variety of specific diagnostic options are available (Fuchsjager et al. 2008).

12.2.5.2 Benign Prostatic Hyperplasia

Benign prostatic hyperplasia (BPH) is nonmalignant enlargement of the prostate gland resulting from a nodular increase in volume of the transitional zone due to cellular hyperplasia. The prevalence increases with age (Table 12.12). An autopsy

Table 12.12 Benign prostatic hyperplasia

Frequency	Prevalence in 60-year-old men, 70 %
Age predilection	BPH becomes more common with age
Risk factors	Androgen dependency, age
Type of lesion	Benign
Signs and symptoms	Difficult bladder voiding
Differential diagnosis	Prostate cancer

study showed a prevalence of 40 % at age 50 and of 70 % at age 60 with 90 % of men in the ninth decade of life having signs of BPH (Berry et al. 1984). The predominant symptoms are due to obstruction and irritation. One method of diagnosing BPH is measurement of prostate volume. However, changes in prostate volume over time are subject to wide interindividual variation. While hyperplasia is common, a considerable proportion of aging men have a stable or decreasing prostate size (Loeb et al. 2009). The only feature seen on T1-weighted images is enlargement, while T2-weighted pulse sequences also show that the enlarged transitional zone is very heterogeneous and of low signal intensity. Often, the enlarged gland will elevate the bladder base. In advanced BPH, MRI depicts signs of urinary obstruction with a large bladder volume or evidence of a trabeculated bladder. Ultimately, however, BPH cannot be confidently differentiated from prostate cancer in the screening situation (Fig. 12.15) (Fuchsjager et al. 2008).

Clinical Management

We recommend performing volumetry with measurement of all three diameters for calculating the prostate volume according to the following formula: $V = 1/6 \Pi abc$. Prostate enlargement should be reported when the calculated volume is greater than 45 cm³ or when signs of urinary obstruction are present.

12.2.6 Seminal Vesicles

The seminal vesicles are paired glands located posterior to the urinary bladder and distal to the ureters. They are approx. 3 cm long and 1.5 cm wide, and their size first increases with age to then decrease again in very old age. Differences in size between the two seminal vesicles are not uncommon (Aboul-Azm 1979). There may be congenital unilateral or bilateral agenesis of the seminal vesicles or cystic degeneration (Arora et al. 2007). The latter is frequently associated with other congenital anomalies of the urogenital tract (Chen et al. 2006). Tumors of the seminal vesicles are very rare. Primary malignancies are less common than seminal vesicle metastases, predominantly from cancer of the prostate, urinary bladder, or rectum (King et al. 1989).

The normal seminal vesicle is a fluid-containing ovoid, septated structure of low T1 signal intensity and high T2 signal intensity. Seminal vesicle tumors are seen as masses of soft-tissue signal intensity on T1-weighted images and have reduced T2 signal intensity (Fig. 12.16).

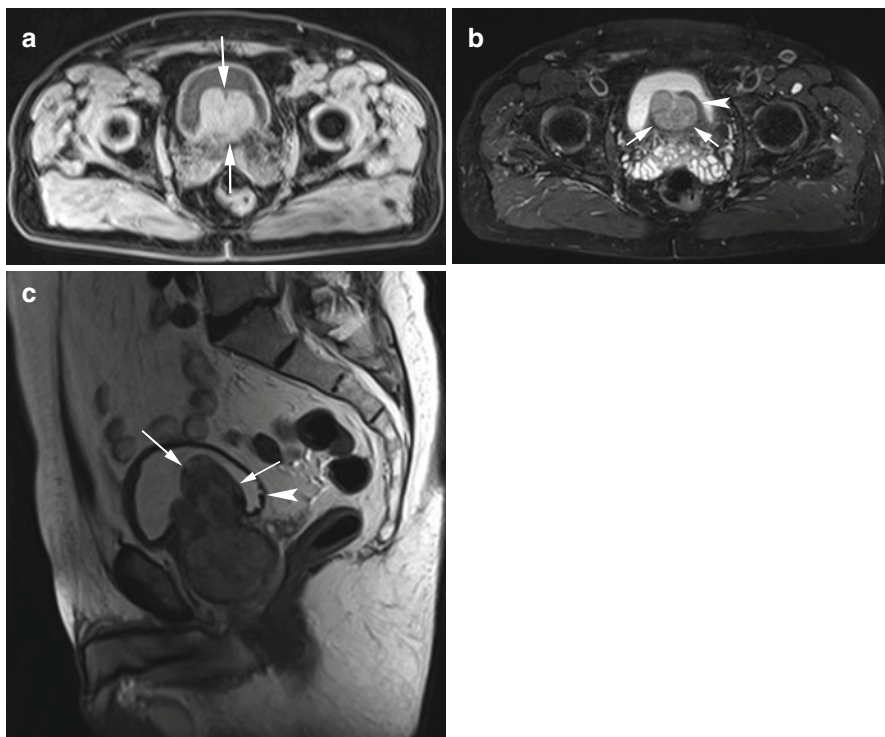
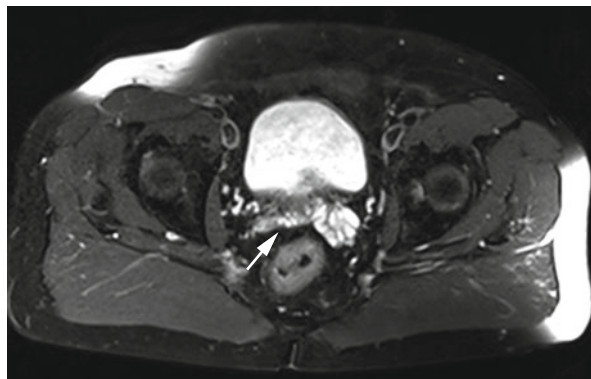


Fig. 12.15 (a) Axial T1w VIBE image reveals a polypous mass in the urinary bladder (*arrows*). The mass appears homogeneous and isointense to soft tissue. (b) PD image also demonstrates the slightly inhomogeneous and smoothly margined mass (*arrows*). Portions of the bladder wall are intact (*arrowhead*), suggesting that the mass arises outside the bladder. Both seminal vesicles are somewhat enlarged. (c) Sagittal T2w image confirms a polypous mass of the prostate with massive extension into the bladder lumen (*arrows*). The mass is predominantly hypointense with a zone of inhomogeneous signal intensity and has a volume of about 100 cm³. There is evidence of urinary obstruction, and early signs of trabeculation are apparent in the posterior wall (*arrowhead*)

Fig. 12.16 PD image clearly reveals a decrease in size of the right seminal vesicle (*arrow*) compared with its counterpart. There is good demarcation of the bright seminal vesicles from the dark surrounding fat



Clinical Management

Younger men should be informed about seminal vesicle agenesis, as it affects fertility. Solid tumors must be reported to initiate further workup (Kim et al. 2009a, b).

12.3 The Kidneys and Urinary Tract

12.3.1 Introduction

Screening MRI has an important role in detecting and evaluating morphologic changes in the kidneys and urinary tract. In appraising the data, the radiologist's task is to properly classify harmless incidental findings and anatomic variants that require no further measures and to differentiate them from abnormal conditions that require diagnostic workup or treatment.

12.3.2 Kidneys

12.3.2.1 Introduction

Evaluation of the kidneys is crucial in interpreting screening MRI. The large number of incidental findings (renal cysts in particular) and the wide range of potential pathologies that may be encountered place high demands on the radiologist interpreting the images.

In this section, we discuss renal anomalies, cystic and solid masses, and inflammatory and vascular conditions.

12.3.2.2 Renal Anomalies

Screening MRI allows good evaluation of congenital renal anomalies. The most important anomalies include agenesis (complete absence of one or both kidneys), aplasia (presence of a rudimentary kidney), hypoplasia (kidney with a reduced number of pyramids and hypoplastic calyces), supernumerary kidney, duplex kidney (kidney with two pyelocaliceal systems) (Fig. 12.17), ectopia (malposition of one or both kidneys) (Fig. 12.18), crossed ectopia (both kidneys on one side), malrotation, and horseshoe kidney (midline fusion of the lower kidney poles). Subjects with fusion, malrotation, and positional anomalies may be susceptible to urinary obstruction with dilatation of the collecting system.

Clinical Management

The above-described renal anomalies do not generally require reporting or further evaluation. However, additional diagnostic tests should be contemplated when signs of urinary obstruction are present.

Fig. 12.17 Coronal 3D FLASH image of duplex kidney on the right

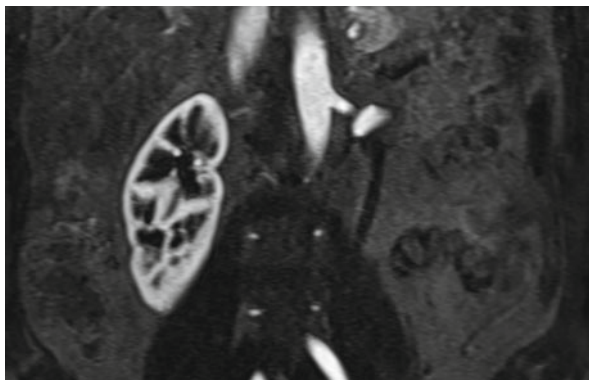


Fig. 12.18 Coronal TIRM image shows a slightly deformed kidney in a lower position to the left of the midline. The kidney extends to the level of the pelvic inlet (arrows)

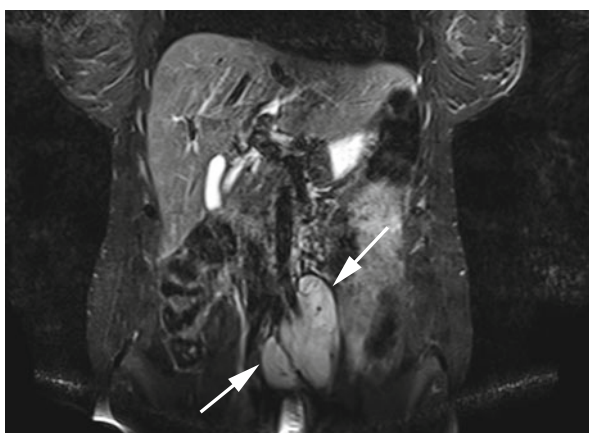


Table 12.13 Cystic renal masses

Frequency	Prevalence, >60 %
Age predilection	Become more common with age
Sex predilection	M:F ratio of 2:1
Type of lesion	Usually benign, 10 % complex cysts
Signs and symptoms	Asymptomatic
Differential diagnosis	Cystic renal cell cancer

12.3.2.3 Cystic Renal Masses

Cystic lesions of the kidneys are among the most common incidental findings in screening MRI (Table 12.13). Cystic renal lesion is a descriptive term that refers to any cystic mass of the kidney regardless of its etiology. Cystic renal lesions can have many different causes: postinflammatory, postischemic, or posttraumatic parenchymal changes, phacomatosis (tuberous sclerosis, von Hippel-Lindau disease), genetic disorders (polycystic kidney disease), tumors (cystic renal carcinoma, cystic nephroma), vascular lesions (arteriovenous malformation), and unclear etiologies.

The heterogeneity of renal cystic disorders explains the challenge faced by the radiologist when characterizing these lesions.

12.3.2.3.1 MRI Diagnosis of Cystic Renal Lesions

MRI is highly sensitive in demonstrating cystic renal lesions and is superior to ultrasound and CT in detecting small cysts (≤ 1 cm) (Nascimento et al. 2001). However, in a screening setting, it is just as important to reliably distinguish between benign and malignant cystic lesions.

The Bosniak classification of renal cysts (published in 1986) is a useful tool for assessing the likelihood of malignancy of these lesions and was also used by us (Bosniak 1986; Siegel et al. 1997; Curry et al. 2000). This classification system defines five categories of cystic renal lesions based on imaging features that help the radiologist in distinguishing between benign and malignant lesions (Bosniak 1986; Israel and Bosniak 2003a, b; Bradley et al. 2011). The criteria were originally proposed for CT scans but can be applied to the interpretation of MR images as well (Israel et al. 2004). MRI is inferior to CT in detecting and characterizing intralésional calcification, which is used as a differential criterion in the original classification proposed by Bosniak. This drawback of MRI is, however, very small as recent studies suggest that the presence of calcification has only a negligible predictive value in classifying a cystic renal lesion as benign or malignant (Israel and Bosniak 2003a, b).

The Bosniak classification modified for the interpretation of MR images is presented in more detail below.

12.3.2.3.2 Bosniak Classification of Cystic Renal Lesions on MRI

Category 1: These are simple cysts with a smooth and sharp margin and a hairline-thin, homogeneous wall. They do not contain septa. No calcifications are apparent within the cyst or in the periphery. The cyst content appears homogeneous and has fluid signal intensity. On T1-weighted images, the signal intensity of the cyst fluid ranges from homogeneously hypointense (low protein content) to slightly hyperintense (high protein content). On T2-weighted images, cysts are very bright (Bradley et al. 2011). There is no enhancement after intravascular administration of gadolinium-based contrast medium. Renal lesions with these features are definitely benign, and no follow-up is required.

Category 2: These cysts also have a smooth and sharp margin with a predominantly hairline-thin wall. Small portions of the wall may show minimal thickening, and the cysts may contain a few hairline-thin septa (≤ 1 mm). Fine calcification might be present along the septa or wall. There is no soft-tissue component. The signal intensity is the same as that of category 1 cysts (low T1 and high T2 signal intensity), unless blood is present in the cyst fluid. In a hemorrhagic cyst, the MR signal intensity is variable, depending on the concentration and age of blood breakdown products (which shorten relaxation time) and on protein content. T1 signal intensities range from slightly hyperintense (little blood and/or protein in cyst fluid) to markedly hyperintense (proteinaceous and/or hemorrhagic fluid). T2-weighted images typically show a high-signal-intensity lesion. An occasional category 2 cyst may have low T2 signal intensity. The cysts do not enhance after administration of gadolinium-based contrast medium. However, some moderate enhancement in the nonthickened wall or septa (if there are any) does not exclude a cyst from this

category. Category 2 renal cysts are benign, and no additional diagnostic measures need to be taken.

Category 2F: Category 2 lesions are assigned to this category when they contain multiple hairline-thin septa and/or when portions of the wall show minimal thickening. These cysts may contain calcification that is possibly nodular and thick. Again, contrast medium enhancement in the area of thin walls or septa does not exclude a cystic lesion from this category. Category 2F cysts require follow-up (F for follow-up) or a biopsy for definitive classification.

Category 3: These lesions are cystic masses with at least partially blurred margins. The wall and any septa may be blurred with focal or longer segments of the wall showing marked thickening or containing thick and heterogeneous calcification. The signal intensity on T1-weighted images is variable; the appearance on T2-weighted images is hyper- to hypointense. Thickened portions of the wall and/or septa exhibit measurable enhancement after administration of gadolinium-based contrast medium. Category 3 includes benign lesions (hemorrhagic or chronically infected cysts, cystic nephroma) and malignant lesions (cystic renal cell carcinoma). This means that, unless there are contraindications, surgical removal and histologic workup are indicated as about 60 % of category 3 lesions are accounted for by cystic renal cell carcinoma (Harisinghani et al. 2003).

Category 4: The cystic masses assigned to this category are frankly malignant. The main features of malignancy are solid tumor components in the center or periphery of the mass. Peripheral solid portions are difficult or impossible to differentiate from normal renal parenchyma. The wall and any septa are at least partially thickened and may be indistinguishable from the noncystic components. T2-weighted pulse sequences are especially helpful in identifying inhomogeneous walls of mixed high and low signal intensity, which are clearly distinct from central cystic areas (necrosis). The solid portions enhance. Renal lesions exhibiting these features are definitely malignant (renal cell carcinoma, sarcoma) and require surgical removal or local ablation treatment.

As MRI screening does not usually involve the administration of contrast medium, contrast enhancement patterns are not available for making the crucial diagnostic distinction between category 2 or 2F lesions (no further diagnostic measures or follow-up) and category 3 lesions (surgery). However, this limitation can be compensated for by assessment of diffusion-weighted sequences, which also provide useful information for differentiating between benign and malignant renal cysts (Zhang et al. 2008; Kim et al. 2009a, b).

12.3.2.3.3 Category 1 and 2 Cystic Lesions

Simple cysts of the kidney are among the most common incidental findings in general, with an incidence of up to 63 % according to one MRI study (Nascimento et al. 2001). Isolated cysts may occur, but multiple cysts are more common. More men than women have renal cysts. Sixty percent of renal cysts are ≤ 1 cm in diameter. Renal cysts increase in size and number with age. They are attributed to degeneration of the basal membrane and the distal tubules (Nascimento et al. 2001; Baert and Steg 1977). Renal cysts may be cortical, intrarenal, or parapelvic. A cyst that is not

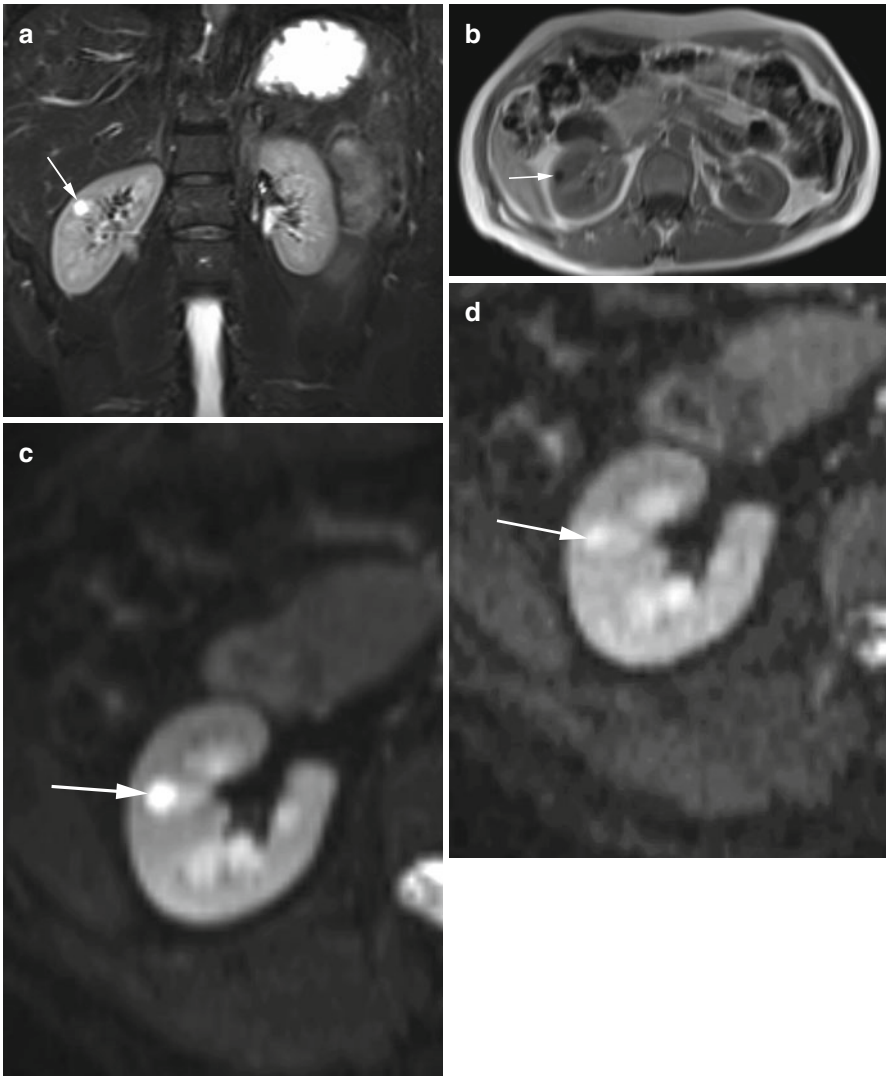


Fig. 12.19 (a) Coronal TIRM image shows a smoothly margined, uniform cyst of high signal intensity at the corticomedullary junction in the right kidney (*arrow*). (b) On axial T1w image, the cyst has low signal intensity (*arrow*) and appears smaller than on the TIRM image. (c–e) Axial diffusion-weighted images acquired with b values of 50, 400, and 800 mm^2/s . There is a clear signal-intensity drop with increasing b values (*arrow*), suggesting freely diffusing water and absence of cellular components. This is a Bosniak category 2 cyst

completely embedded in the parenchyma may cause a focal bulge in the renal contour. On non-contrast-enhanced images, simple cysts in parapelvic location cannot always be distinguished from the diverticula of the renal pelvis or calyces. The MRI appearance is the same as that of a Bosniak category 1 cyst (Fig. 12.19).

A T2-weighted pulse sequence, in the axial or coronal plane, is most suitable for identifying cystic renal lesions, as it provides the best contrast between these lesions

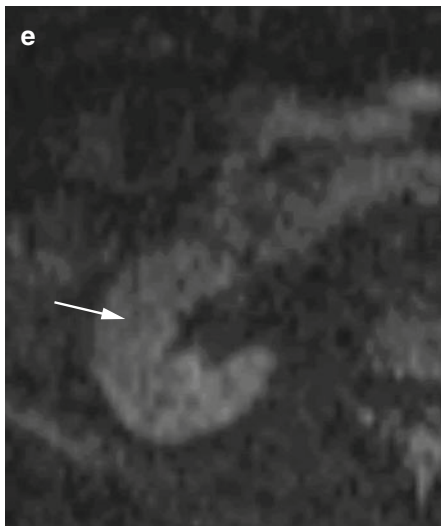


Fig. 12.19 (continued)

and the renal parenchyma (Bradley et al. 2011). Once a cystic lesion has been detected, T1-weighted images are helpful for further characterization, especially for assessing the nature of the cyst fluid and delineation of the lesion from the renal parenchyma. It is important to analyze sequences acquired without and with fat saturation. Fat-saturated images are useful for evaluating an extrarenal cyst wall and the interface between the lesion and surrounding parenchyma (Fig. 12.20).

The incidence of complex renal cysts (septa, calcification, content altering MR signal intensity, contrast enhancement) is assumed to be over 10 % (Nascimento et al. 2001). The presence of septa is an important diagnostic feature and can be reliably evaluated using MRI. As already mentioned above, MRI is limited in detecting calcification. More recently, however, it has been proposed that the presence and appearance of calcifications in a cystic renal mass is less important for diagnosis than the presence of enhancing soft-tissue elements (Israel and Bosniak 2003a, b).

MRI enables excellent evaluation of cyst fluid and its composition (water, protein content, blood breakdown products, calcium). The presence of protein in a cyst shortens T1 and T2 relaxation times. Fat-suppressed T1-weighted images improve the conspicuity of proteinaceous cyst fluid by eliminating signal from surrounding fat (Fig. 12.21).

As with cysts that contain water alone, diffusion-weighted images show progressive signal loss with increasing b values. The signal loss is, however, somewhat less pronounced, with a slightly hyperintense signal still persisting for b values of >800–1,000 mm²/s, as free diffusion is minimally restricted by protein molecules.

A *renal milk of calcium cyst* (i.e., a cyst with high calcium content) is characterized by a fluid level in the dependent portion (posteriorly when the patient is imaged in the supine position) on both T1-weighted and T2-weighted images.

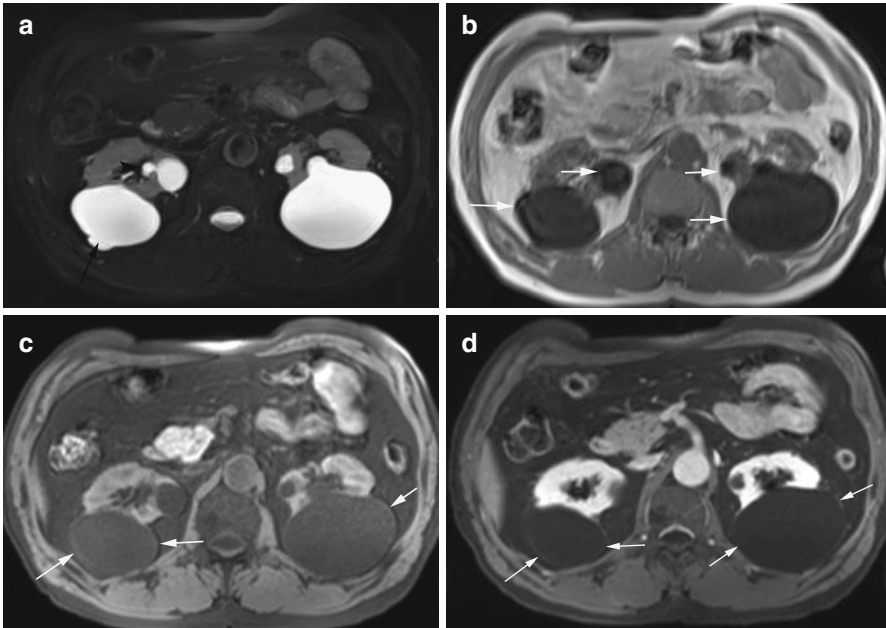


Fig. 12.20 (a) Axial T2w BLADE image reveals two large, sharply margined renal cysts, one in each kidney. The cysts arise from the posterior parenchyma with the largest portions lying outside the kidneys. A thin septum is seen in the posterior aspect of the cyst in the right kidney (*arrow*). Each kidney contains one additional cyst in the medial parenchyma, and the right kidney harbors a third cyst in parapelvic location (*arrowhead*). (b) Axial T1w VIBE image depicts homogeneous cysts of low signal intensity (*arrows*) in both kidneys. The extrarenal cyst walls are not visualized. (c) Axial 2D FLASH image with fat saturation clearly delineates the thin cyst wall (*arrows*) from the pararenal fat, whose signal has been eliminated. The septa in the cyst on the right side are seen as well. (d) Fat-saturated axial 2D FLASH image after contrast medium administration shows minimal enhancement of the cyst walls on both sides (*arrows*) – another feature consistent with category 2 cysts

A *hemorrhagic cyst* appears more inhomogeneous with signal intensities varying depending on the degree of iron oxidation (which in turn is determined by the age of the hemorrhage), the protein concentration, hematocrit, and clot formation. MR signal intensity is predominantly altered by the heme molecule and its iron-containing degradation products (deoxyhemoglobin, methemoglobin, and hemosiderin) and to a minor extent by the globulin protein family as well (Janick et al. 1991; Gomori and Grossman 1988; Bradley 1993). Basically, both components shorten relaxation time, thus increasing the T1 signal and, to a variable extent, reducing the T2 signal.

Physiologic oxyhemoglobin is diamagnetic and therefore does not affect the MR signal. Deoxyhemoglobin and methemoglobin are paramagnetic, and hemosiderin is superparamagnetic (Gomori and Grossman 1988; Saini et al. 1988). Moreover, the effect of hemoglobin on MR signal intensity also depends crucially on whether hemoglobin is intracellular or extracellular (Table 12.14). Intracellular deoxy- or methemoglobin produces a strong inhomogeneous magnetic field that influences diffusing water molecules, causing a drop in MR signal intensity by shortening T2.

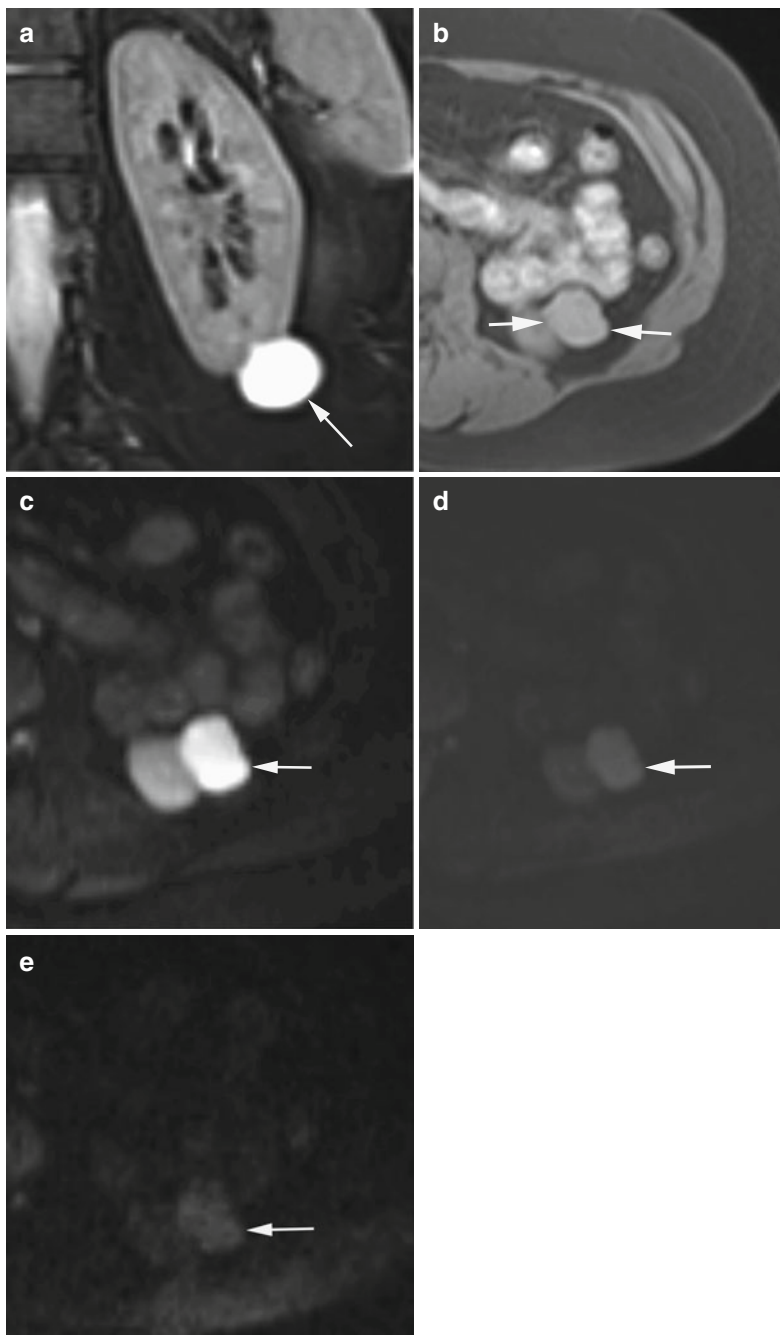
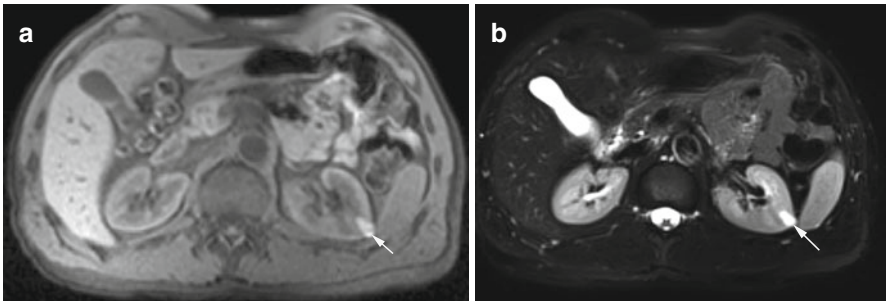


Fig. 12.21 (a) Coronal T2w image shows a homogeneous high-signal-intensity cyst arising in the cortex of the lower pole of the left kidney (*arrow*). (b) On this axial 2D FLASH image with fat suppression, the cyst has intermediate signal intensity (*arrows*). (c–e) Axial diffusion-weighted images acquired with b values of 0, 400, and 800 mm^2/s show a drop in signal intensity with increasing b values (*arrow*), consistent with a proteinaceous cyst. A cyst with low protein content would have produced a greater decrease in signal intensity

Table 12.14 Sequence of oxidation stages of hemoglobin and its breakdown products, magnetic properties, and resulting effects on MRI signal intensity

Hemoglobin/breakdown product	Magnetic property	Effect on MRI signal intensity
Oxyhemoglobin	Diamagnetic	None
Deoxyhemoglobin	Paramagnetic	T2 ↓, within red blood cells
Methemoglobin	Strongly paramagnetic	T2 ↓, within red blood cells T1 ↑↑
Hemosiderin	Superparamagnetic	T2 ↓↓ T1 ↑

**Fig. 12.22** (a) Axial 2D FLASH image with fat suppression shows a relatively uniform lesion of very high signal intensity in the cortex of the left kidney (*arrow*). (b) Axial T2w image with fat suppression also shows markedly hyperintense lesion (*arrow*). The findings suggest extracellular methemoglobin in a hemorrhagic cyst

Lysis of red blood cells leads to dispersion of the breakdown products with homogenization of the magnetic field and cancellation of the T2 effect (Janick et al. 1991; Gomori and Grossman 1988).

As red blood cells in a hemorrhagic cyst typically undergo lysis, most cysts appear bright on both T1-weighted and T2-weighted images (Fig. 12.22). However, it is possible for all stages of hemoglobin breakdown products and both intact and lysed red blood cells to be present side by side, which results in cysts with mixed signal patterns.

A hemorrhagic cystic lesion must be differentiated from cystic or solid renal cell cancer, which may also contain hemorrhage but will appear much more heterogeneous on T1-weighted and T2-weighted images.

A reliable feature indicating a benign hemorrhagic cystic lesion is the so-called hematocrit effect (Fig. 12.23) resulting from sedimentation of red blood cells (and the breakdown products they contain). These sediments typically produce a sickle-shaped area of high T1 and low T2 signal intensity layering in the dependent portion of the cyst. This intratumoral fluid-iron level has not been yet been observed in renal cell carcinoma containing hemorrhage (Hilpert et al. 1986).

Category 1 and 2 renal cysts cannot be differentiated on unenhanced MR images when no septa, calcifications, or signal-altering components (blood) are present.

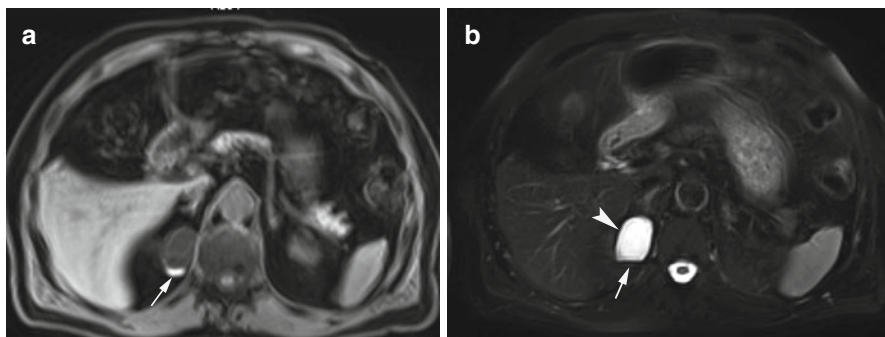


Fig. 12.23 (a) Axial T1w VIBE image nicely depicts a cystic lesion with a sickle-shaped posterior area of increased signal intensity in the upper kidney pole (*arrow*). (b) Axial T2w image with fat saturation shows a fluid level in the cyst with the dependent portion appearing black (*arrow*) and the overlying fluid appearing bright (*arrowhead*). This is an example of the hematocrit effect, produced by sedimentation of red blood cells

In this situation, contrast-enhanced images quite often lead to an upgrade from category 1 to category 2 (enhancement of hairline-thin wall). As both categories are benign, though, in the screening setting, no further differentiation is necessary.

Clinical Management

Category 1 and 2 renal cysts are benign and need not be reported or evaluated further (Israel and Bosniak 2005; Silverman et al. 2008; Bradley et al. 2011).

12.3.2.3.4 Category 2F and 3 Cystic Lesions

Indeterminate lesions, which cannot be reliably classified as either benign or malignant, require special attention in screening examinations, and further diagnostic evaluation may be needed to make the distinction.

The radiologist should carefully analyze images obtained with at least two different weightings, searching for wall irregularities, inhomogeneity of the cyst fluid, and poor delineation from the normal renal parenchyma. When the radiologist cannot confidently assign a cystic renal lesion to category 1 or 2, it should be classified as category 2F. Differentiation from category 3 lesions can also be challenging or downright impossible when no contrast-enhanced series is available (Fig. 12.24). Again, evaluation of the cyst wall and of any septa is crucial for correct classification (Fig. 12.25). Nodularity is highly suspicious and should classify a lesion as category 3. Hemorrhagic cysts <1 cm also belong in this category if there is doubt that they are purely cystic in nature and a small hemorrhagic renal cell cancer cannot be definitely ruled out.

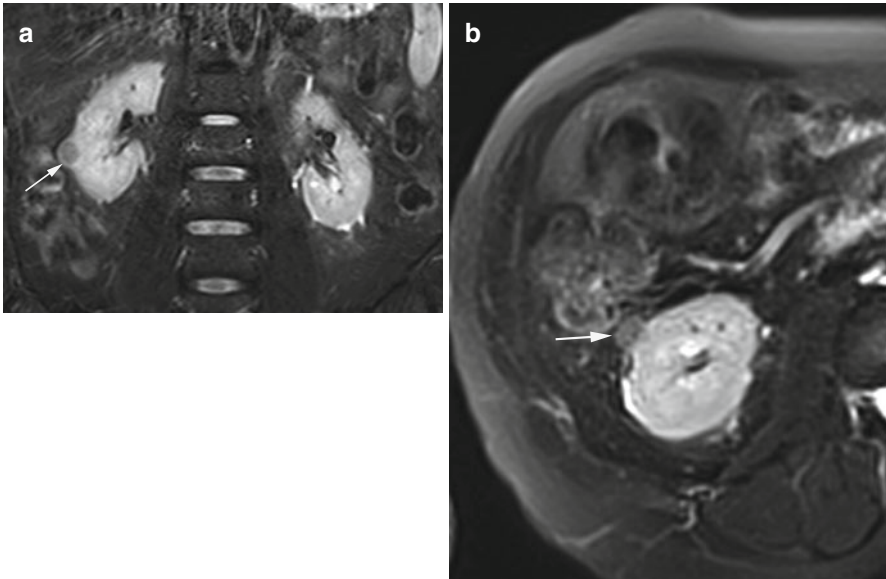


Fig. 12.24 (a) Coronal TIRM image reveals a cystic lesion in the cortex of the right kidney. The wall is thick and the cyst fluid has low signal intensity. The interface with the parenchyma cannot be clearly evaluated (*arrow*). (b) Axial T2w BLADE image also does not allow evaluation of the interface with the parenchyma (*arrow*). Hence, this hemorrhagic cyst with a thickened wall is classified as a category 2F lesion

Clinical Management

Category 2F lesions require follow-up (contrast-enhanced CT or MRI) at intervals of 3, 6, and 12 months for definitive classification. If serial imaging studies remain unclear, a biopsy may be contemplated.

Category 3 cysts are excised and examined histologically (Israel and Bosniak 2005; Silverman et al. 2008).

12.3.2.3.5 Category 4 Cystic Lesions

These lesions are definitely malignant (renal cell carcinoma), containing cystic components of variable size, which typically correspond to liquefied tumor tissue. DWI is helpful for differentiation, as malignant (highly cellular) cystic tumors tend to show no or a very moderate signal drop compared with benign cystic lesions (Fig. 12.25). Solid portions adjacent to a cystic area are always suspicious for malignancy. The radiologist should also pay attention to secondary signs of renal cell cancer such as lymphadenopathy, invasion of the renal vein or inferior vena cava, and distant metastasis (bone, brain). Administration of contrast medium will help in identifying soft-tissue components but is not mandatory.

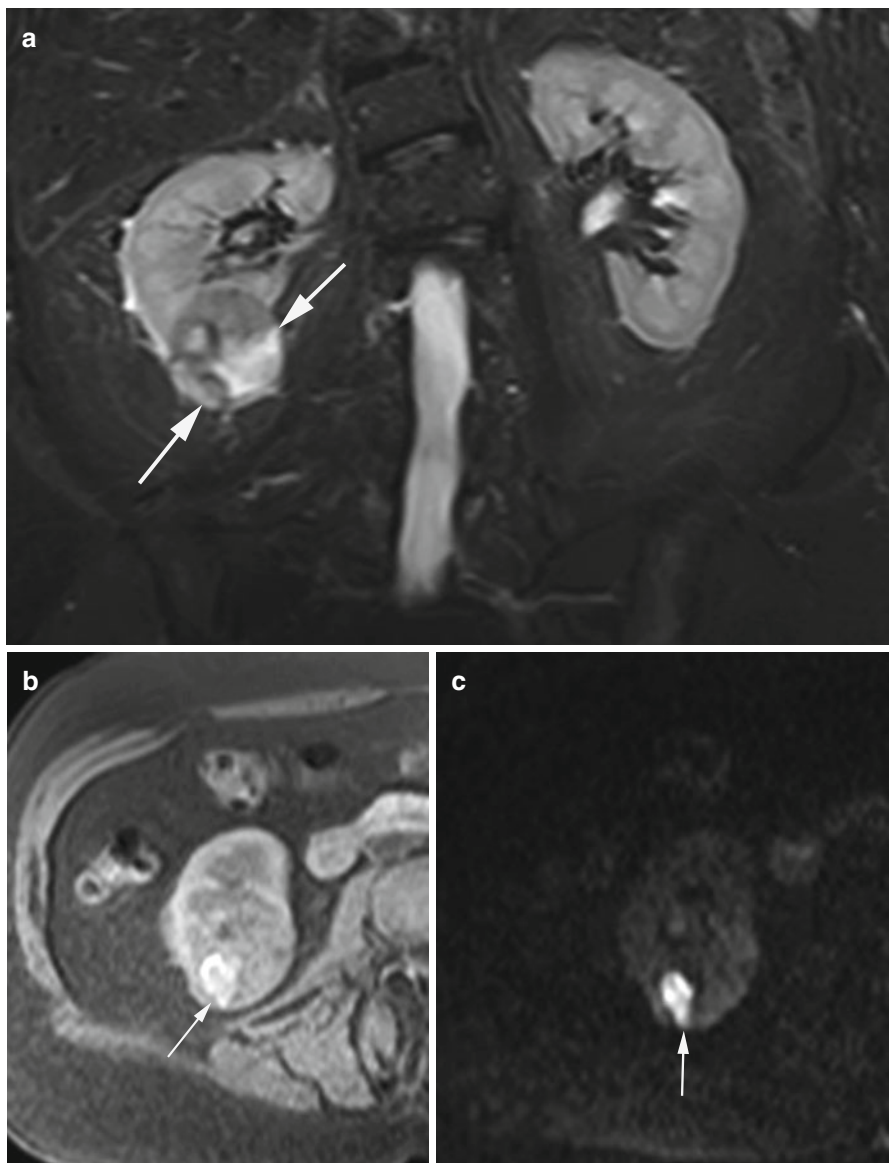


Fig. 12.25 (a) Coronal TIRM image shows a predominantly solid cystic mass of heterogeneous signal intensity (*arrows*) in the lower pole of the right kidney. (b) Axial 2D FLASH image with fat saturation clearly delineates hyperintense cystic components (*arrow*). (c) Axial diffusion-weighted image acquired with $b = 800 \text{ mm}^2/\text{s}$; the high signal intensity (*arrow*) suggests the presence of cellular components. There has probably also been an episode of bleeding. The diagnosis is partially necrotic renal cell cancer

Clinical Management

Category 4 renal cysts are definitely malignant and therefore should be examined by an additional imaging modality for comprehensive evaluation and staging (Israel and Bosniak 2005; Silverman et al. 2008).

12.3.2.4 Specific Types of Cystic Renal Masses**12.3.2.4.1 Polycystic Kidney Disease**

Polycystic kidney disease (PKD) refers to a heterogeneous group of disorders of different etiologies and clinical and functional significance. Virtually all cases of PKD are hereditary or congenital. The disease is characterized by the presence of multiple cysts (Bosniak category 1 or 2) of different sizes and MR signal intensities as well as hemorrhage of different ages in both kidneys (Hilpert et al. 1986). PKD plays only a minor role in adult screening programs as the disease is either known (due to the functional impairment it causes) or requires no treatment.

12.3.2.4.2 Cystic Nephroma and Cystic Partially Differentiated Nephroblastoma

These two are rare, nonmalignant cystic renal masses with two age peaks: one in infancy (3–24 months; male-to-female ratio of 2:1) and another in adults over 30 years, with a female predominance (Eble and Bonsib 1998). Both entities are characterized by the presence of a capsule enclosing noncommunicating cysts of different sizes that are usually separated by very thin septa. No other soft-tissue components are present in these tumors. The cyst fluid is of variable signal intensity. The mass can protrude into the collecting system and cause urinary obstruction (Madewell et al. 1983).

12.3.2.5 Solid Renal Masses

Improved imaging modalities have led to an increasing detection of solid renal masses in recent years. The primary aim of MRI screening is to identify those that are malignant.

12.3.2.5.1 Renal Cell Cancer

In Germany, renal cell cancer (hypernephroma) accounts for 4.7 % of all cancers in men (approx. 10,000 new diagnoses/year) and for 3.2 % in women (approx. 6,000 new diagnoses/year). It is among the most common causes of cancer death (11th most common in women, sixth most common in men). The mean age at diagnosis is about 67 years in men and nearly 71 years in women. Renal cell cancer constitutes 85 % of all renal malignancies in adults (Robert-Koch-Institut und die Gesellschaft der Epidemiologischen Krebsregister in Deutschland e.V. 2008) (Table 12.15). With its high intrinsic soft-tissue contrast, MRI is a very sensitive imaging modality for visualizing solid renal cell carcinoma. The MRI appearance varies with the histologic

Table 12.15 Renal cell cancer

Frequency	Incidence, 13–19/100,000 population/year, on the rise
Age predilection	5th–6th decade
Sex predilection	M:F ratio of 3:2
Risk factors	Smoking, obesity, environmental toxins, genetic predisposition
Type of lesion	Malignant
Signs and symptoms	Hematuria, flank pain
Differential diagnosis	Angiomyolipoma, oncocytoma, lymphoma, metastasis

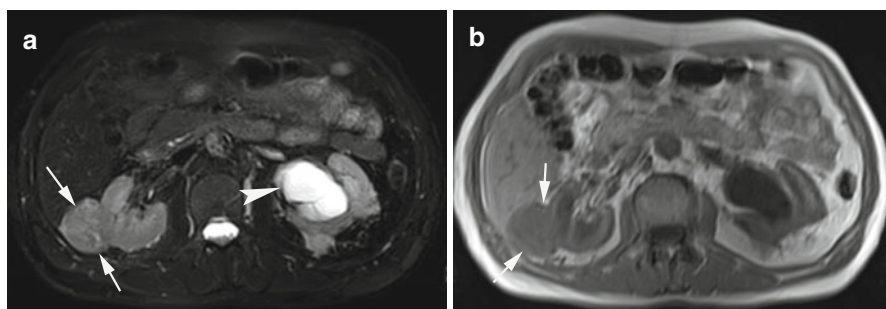


Fig. 12.26 (a) Axial T2w BLADE image reveals a rounded solid mass in the right kidney. The mass markedly extends beyond the normal renal contour (*arrows*). Also seen are parapelvic cysts in the left kidney (*arrowhead*). (b) Axial T1w image also shows a mass isointense to soft tissue in the right kidney (*arrows*). Chemical shift imaging (*not shown*) revealed no fatty components. This is a solid renal cell carcinoma

subtype and the presence of necrosis, hemorrhage, and fat (Shinmoto et al. 1998). The typical renal cell carcinoma is isointense to renal parenchyma on T1-weighted images and has inhomogeneous high signal intensity on T2-weighted images, but both T1 and T2 signal intensity may be hyperintense, isointense, or hypointense (Fig. 12.26). A renal cell carcinoma may be surrounded by a pseudocapsule, seen as a low-intensity rim on T1-weighted and T2-weighted sequences (Outwater et al. 1997). When intracellular fat is present, with a signal drop on fat-saturated or opposed-phase images, renal cell cancer may be mistaken for angiomyolipoma (see below).

Necrosis is common in solid tumor portions. If contrast-enhanced images are available and show enhancement of solid tumor portions, this is highly suggestive of malignancy and should prompt further diagnostic evaluation. Special attention must also be paid to any additional findings that might corroborate the diagnosis of renal cell cancer such as locoregional lymph node enlargement, vascular invasion (renal vein, inferior vena cava), and distant metastasis (para-aortic lymphoma, bone and brain metastases).

The differential diagnosis includes renal metastasis, lymphoma (uniform appearance), benign masses such as angiomyolipoma or oncocytoma, and renal abscess (see below).

Table 12.16
Angiomyolipoma

Frequency	Incidence, 0.3 %
Age predilection	40–60 years
Sex predilection	M:F ratio of 1:4
Type of lesion	Benign, risk of rupture
Signs and symptoms	80 % asymptomatic
Differential diagnosis	Renal cell cancer

Clinical Management

A solid renal mass of any size that cannot be confidently classified as benign requires further imaging evaluation.

12.3.2.5.2 Angiomyolipoma

An angiomyolipoma is a benign mesenchymal tumor composed of variable amounts of fat, smooth muscle tissue, and abnormal blood vessels. The incidence in autopsy series is about 0.3 %, and it is more common in women than in men (4:1). Angiomyolipoma is the most common benign renal tumor (Table 12.16) (Prasad et al. 2008).

The MR signal characteristics of angiomyolipoma are crucially determined by the relative proportions and architecture of the three main tumor components. A large fatty component within the mass is considered definitive evidence of an angiomyolipoma and can be identified by comparing T1-weighted images without and with fat suppression or/and by chemical shift imaging (Fig. 12.27) (Bradley et al. 2011). A large amount of fat is suggested by a marked drop in signal intensity on opposed-phase images compared with in-phase images (Logue et al. 2003; Prasad et al. 2008). When little fat is present, the signal loss is much less pronounced. An angiomyolipoma with a very large smooth muscle component is isointense to soft tissue and difficult to distinguish from renal cell cancer. The demonstration of calcification within a mass is highly indicative of renal cell cancer. An angiomyolipoma may rupture (aneurysm of intralésional blood vessels); the risk is about 10 % for a tumor size of >4 cm (Steiner et al. 1993). There is no risk of malignant transformation.

Clinical Management

Because of the risk of rupture, patients with an angiomyolipoma >4 cm should be informed and surgical removal should be discussed. Smaller angiomyolipoma should also be reported to initiate long-term follow-up for identifying any increase in size (Steiner et al. 1993; Prasad et al. 2008).

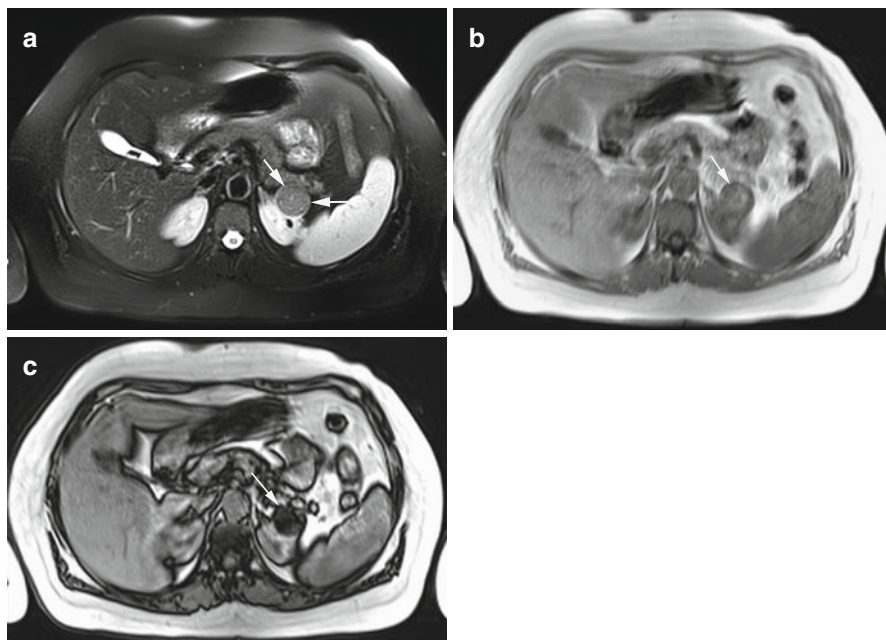


Fig. 12.27 (a) Axial T2w BLADE image depicts a well-defined rounded mass of low signal intensity in the lower pole of the left kidney. The mass is surrounded by a thin high-signal-intensity line (*arrows*). The mass has the same signal intensity as extra-abdominal fat. The image also shows stones in the gallbladder. (b, c) Axial T1w in-phase and opposed-phase images demonstrate a marked and homogeneous signal drop (*arrow* in c) of the mass on the opposed-phase image. The signal drop confirms fat within the mass and is diagnostic of an angiomyolipoma

12.3.2.5.3 Oncocytoma

Oncocytoma is a benign epithelial tumor accounting for 5 % of all solid renal masses (Schatz and Lieber 2003; Prasad et al. 2008). It is depicted as a solid spherical nodule with smooth margins and is most commonly found in the renal cortex. The MRI appearance is unspecific. Most oncocytomas have low signal intensity relative to renal parenchyma on T1-weighted images and high T2 signal intensity. More than half of all oncocytomas have a central scar with absent or delayed enhancement on postcontrast images. A capsule or pseudocapsule is also quite common (Harmon et al. 1996). Oncocytoma must be differentiated from renal cell cancer, which is not possible with high enough confidence in MRI screening.

Clinical Management

The unspecific MRI features of oncocytoma and the problems in differentiating it from renal cell cancer mean that, if oncocytoma is suspected, the subject should receive prompt further evaluation, initially using contrast-enhanced MRI (Pedrosa et al. 2008; Bradley et al. 2011).

12.3.2.6 Inflammatory Renal Conditions

12.3.2.6.1 Acute Inflammation

Acute pyelonephritis is the most common acute inflammatory condition and is typically caused by ascending infection through the collecting system. It is twice as common in women as in men. Inflammatory changes may be circumscribed or diffuse, resulting in focal or generalized enlargement of the kidney with loss of the corticomedullary differentiation. Parenchymal edema causes a decrease in T1 signal intensity and appears bright on T2-weighted images. Areas of acute pyelonephritis have restricted perfusion, depicted as bright areas on diffusion-weighted images and as dark areas on ADC maps (Verswijvel et al. 2002). Following administration of contrast medium, an inflammatory area (which may be segmental or wedge-shaped) will show reduced enhancement. Other imaging features include a thickened Gerota fascia, increased enhancement of the collecting system, and fluid in the perirenal space (Goldman and Fishman 1991). The diagnostic significance of perirenal fluid alone without other findings is unclear.

The differential diagnosis of pyelonephritis includes renal masses, postinflammatory scars, and renal infarction.

12.3.2.6.2 Renal Abscess

Intrarenal or perirenal abscess may develop as a complication of acute inflammation of the renal parenchyma. It has no age preference and affects men and women equally. A renal abscess is depicted as a rounded to oval cystic lesion. The lesion has inhomogeneous low signal intensity on T1-weighted images and high signal intensity on T2-weighted images, depending on the protein and fluid content and the amount of cell debris present within the abscess. Fluid levels and air inclusions (low signal intensity) are common findings (Goldman and Fishman 1991). DWI shows diffusion restriction. Contrast administration produces a characteristic rim sign with enhancement of the periphery but no enhancement of the central cystic portion. The differential diagnosis includes solid masses (renal cell cancer) and cystic lesions (categories 2 and 3).

12.3.2.6.3 Chronic Inflammation

Residual changes often persist in the kidney following inflammation that has run its course or an acute inflammation that has become chronic. These include contraction of the cortex due to scarring or marked atrophy of the kidney – the most severe form of which is shrunken kidney. Other changes include ectasia and strictures of the renal calyces, thickening of the Gerota fascia, and scars within the perirenal fat (Fig. 12.28). Such areas may occasionally fail to enhance after administration of contrast medium.

12.3.2.6.4 Perirenal Fluid

Perirenal fluid is a very common finding after age 50 but may also be noted in younger persons.

Perirenal fluid collections may be irregular but of similar configuration on both sides; they may also take the form of a thin fluid stripe outlining the kidneys.

Fig. 12.28 Axial TIRM image shows a much smaller left kidney compared with the right kidney. There is marked thinning of the medulla and cortex. In addition, the renal contour is irregular with scars, and there are fat deposits around the renal pelvis (*arrows*)

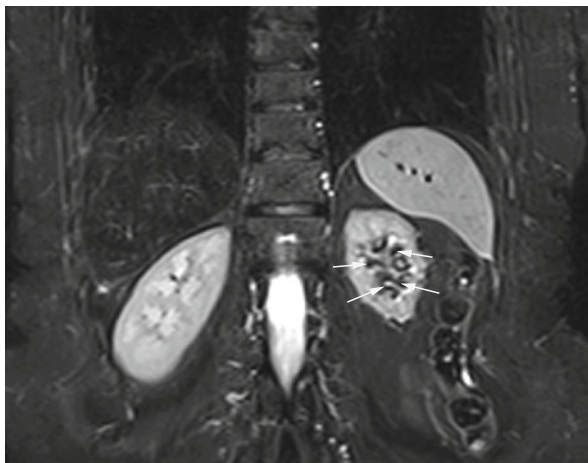
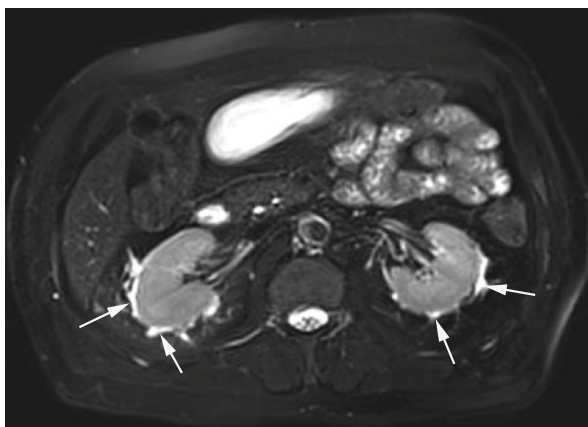


Fig. 12.29 Axial T2w BLADE image obtained in a 62-year-old subject. A considerable amount of high-signal-intensity perirenal fluid (*arrows*) is present on both sides without signs of renal atrophy or contraction due to scars



The fluid has high signal intensity on T2-weighted images and is hypo- to isointense to renal parenchyma on T1-weighted images (Fig. 12.29).

It is not clear at all whether perirenal fluid is a sign of acute or chronic/postinflammatory changes or simply occurs with normal aging.

Clinical Management

Acute inflammatory renal changes are virtually always symptomatic and need to be reported and treated. Chronic inflammatory changes, if they are severe (e.g., shrunken kidney) and not already known, should be reported in order to test renal function and initiate treatment as required. Perirenal fluid alone without any concomitant findings need not be reported.

12.3.2.7 Vascular Renal Conditions

12.3.2.7.1 Renal Infarction

Renal infarction is characterized by focal or global ischemic necrosis of the renal parenchyma due to embolic or thrombotic occlusion.

In most individuals, renal infarction occurs secondary to complete or segmental renal artery occlusion.

As most occlusions are caused by embolism, screening MR images should be scrutinized for left ventricular thrombus.

Renal swelling may be seen in acute infarction, while the chronic stage is characterized by atrophy of the infarcted area.

In segmental infarction, the affected area is typically wedge-shaped with the widest part at the cortex. An infarcted area has low T1 and T2 signal intensity. Acute renal infarction has increased signal intensity on DWI. After contrast medium administration, infarcted renal areas fail to enhance, while the outer renal cortex, which is perfused by capsular branches, will enhance in the subacute phase (cortical rim sign) (Haaga and Morrison 1980). Renal infarction must be differentiated from renal inflammatory conditions and abscess.

Clinical Management

Acute renal infarction should be communicated to elucidate the underlying etiology and prevent future ischemic events.

12.3.3 Urinary Tract

12.3.3.1 Collecting System and Ureters

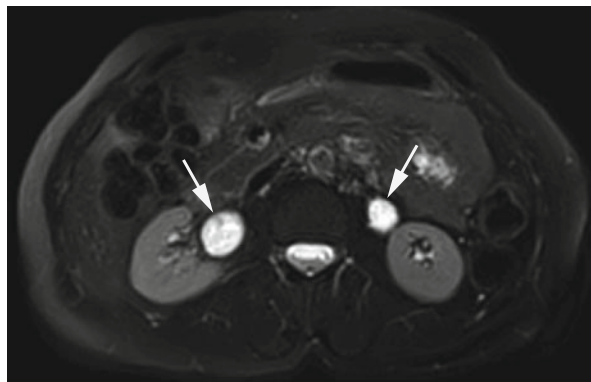
The urinary tract includes the renal collecting systems and ureters, the urinary bladder, and the urethra.

The most relevant urinary tract pathologies that play a role in the screening situation include anomalies, urinary obstruction, urinary calculi, and masses.

12.3.3.1.1 Anomalies

Various anomalies involving the collecting system exist, including extrarenal calyces, calyceal diverticula, incomplete renal duplication, megacalycosis (nonobstructive dilatation of the renal calyces), and extrarenal pelvis (Fig. 12.30). An important variant that is occasionally observed is an ampullary renal pelvis, which is a large pelvis with strong calyceal necks. In contrast, a normal-sized collecting system has long, slender calyceal necks and a delicate renal pelvis. This variant is at times difficult to differentiate from parapelvic cysts or urinary obstruction (see below). If obstruction is suspected, evaluation of the renal parenchyma may be helpful (Turkvatan et al. 2009).

Fig. 12.30 Axial T2w BLADE image reveals hyperintense cyst-like masses anterior to the kidneys (*arrows*). The masses are consistent with extrarenal pelves. The proximal ureters and collecting systems appeared normal (*not shown*)



The most important ureteral anomalies are double and bifid ureters. A bifid ureter is the incomplete duplication of the ureter with two collecting systems but a single ureter terminating in the urinary bladder. In contrast, a double ureter refers to complete doubling with two separate ureters, each with its own collecting system and ureteral orifice. A ureterocele is the protrusion of a dilated distal ureter (typically due to congenital stricture of the intramural segment) into the bladder lumen (cobra head or spring onion appearance).

Anatomic variants can predispose an individual to urinary obstruction and development of calculi.

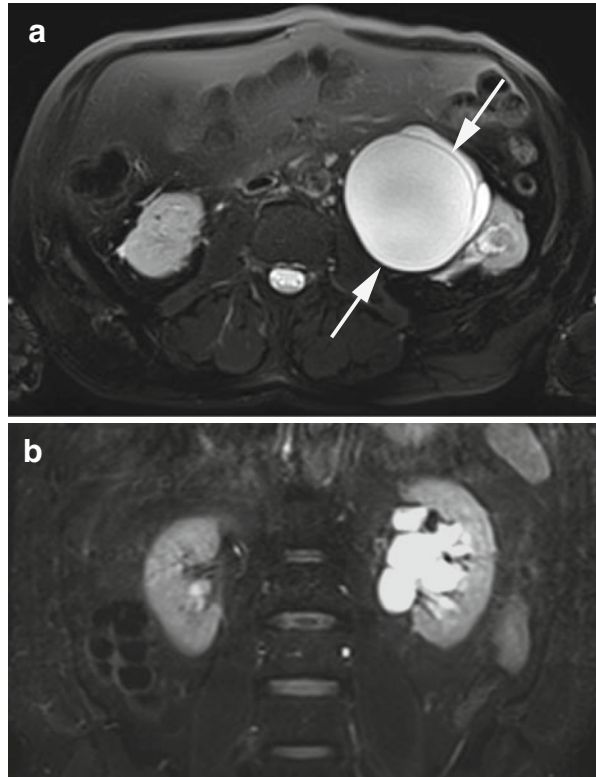
Clinical Management

Asymptomatic anomalies or variants without obstruction need not be reported as they do not require further evaluation or treatment.

12.3.3.1.2 Urinary Obstruction

Urinary obstruction encompasses any impediment to the flow of urine including morphologic changes of the urinary tract. Obstructions can develop at any level of the urinary tract, from the kidneys to the ureter to the bladder to the urethra. The most common causes in adults are calculi, benign prostatic hyperplasia/prostate cancer in men, and pelvic or retroperitoneal masses (Dhar and Denstedt 2009; Passerotti et al. 2009). The appearance is characterized by normal caliber of the urinary tract distal to the obstacle and variable dilatation proximally, depending on the level and duration of acute obstruction (Fig. 12.31). T2-weighted sequences are most suitable for evaluating these changes. Chronic urinary obstruction is associated with shrinkage of the renal parenchyma, allowing it to be differentiated from acute forms. As with renal inflammation, acute obstruction is associated with loss of the corticomedullary differentiation and the presence of perirenal fluid. Differentiation

Fig. 12.31 (a) Axial T2w BLADE image reveals a cystic mass with a thin anterolateral septum in the left kidney (*arrows*). (b) Coronal TIRM image shows marked dilatation and separation of the renal calyces in the left kidney. These findings are consistent with urinary obstruction secondary to a parapelvic cyst with mass effect



from cystic lesions of other etiology such as an ampullary renal pelvis or parapelvic cysts may be difficult at times. Here, use of a contrast agent that highlights the collecting system is helpful. At the same time, evaluation of the shape of the calyces is helpful in establishing the differential diagnosis: dilated calyces corroborate the diagnosis of urinary obstruction.

Clinical Management

Acute or chronic urinary obstruction should be reported so that testing for the underlying cause can be initiated.

12.3.3.1.3 Urinary Calculi

In Germany, the lifetime prevalence of renal calculi is nearly 5 % and is on the rise. Calculi are slightly more common in men than women. The vast majority of calculi, 97 %, are found in the renal collecting system and ureter, with only 3 % being located in the urinary bladder or urethra (Table 12.17). As no free protons are present in calculi, they have low signal intensity on all pulse sequences. When a stone

Table 12.17 Urinary calculi

Frequency	Lifetime prevalence, 5 %; on the rise; 60 % recurrence
Age predilection	3rd–5th decade
Sex predilection	Slightly more common in men
Type of lesion	Benign; may cause urinary obstruction
Signs and symptoms	Colic, hematuria
Differential diagnosis	Renal cell cancer, inflammatory conditions

Table 12.18 Tumors of the collecting system and ureters

Frequency	Incidence, 20/100,000 population/year
Age predilection	6th decade
Sex predilection	M:F ratio of 3:1
Risk factors	Smoking, environmental toxins
Type of lesion	Malignant
Signs and symptoms	Painless hematuria
Differential diagnosis	Blood clot, renal cell cancer, inflammatory conditions

has been detected, the examiner must search for signs of concomitant urinary obstruction (Passerotti et al. 2009). However, the majority of urinary calculi will probably be missed at screening. In very rare cases, for instance, when additional perifocal hemorrhage is present, a stone can be difficult to differentiate from a small transitional cell carcinoma.

Clinical Management

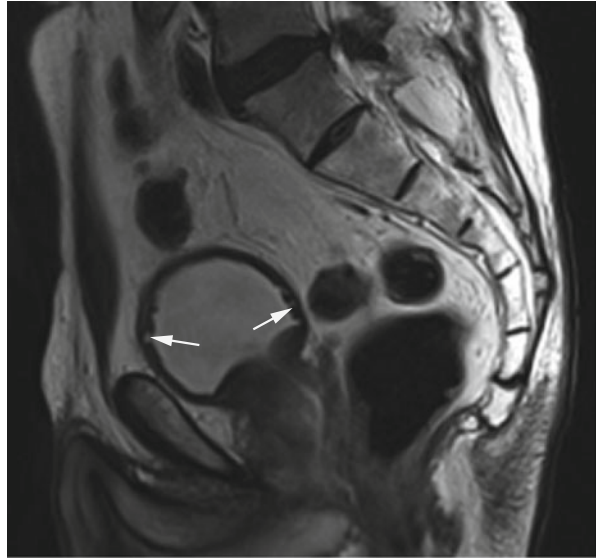
Calculi may be reported, but in most cases do not require treatment.

12.3.3.1.4 Tumors

Transitional cell cancer is the most common malignancy of the renal collecting system and ureter. This cancer arises in the epithelium of the urinary tract. The age peak is in the sixth decade with a male-to-female ratio of 3:1. The annual rate of transitional cell cancers newly diagnosed in Germany is 20/100,000 population (Table 12.18). MRI depicts transitional cell cancer as an intraluminal polypous mass that is isointense or slightly hypointense on T1-weighted images and isointense to slightly hyperintense on T2-weighted images. However, it is clearly demarcated as a hypointense lesion from the fluid in the urinary tract (Browne et al. 2005). The cancers show high signal intensity on DWI (Takeuchi et al. 2008). Transitional cell cancer is poorly vascularized with mild enhancement on postcontrast images. Imaging may demonstrate signs of urinary obstruction proximal to the site of cancer.

The differential diagnosis of tumors located in the renal pelvis includes renal cell cancer, stones, clotted blood, and inflammatory conditions (tuberculosis).

Fig. 12.32 Sagittal T2w image reveals an enlarged prostate with irregular, nodular thickening of the anterior and posterior bladder wall on the luminal side (arrows)



Clinical Management

Masses in the collecting system and urinary tract that are isointense to soft tissue require further imaging evaluation; contrast-enhanced CT or MRI with urography have proven to be useful (Browne et al. 2005).

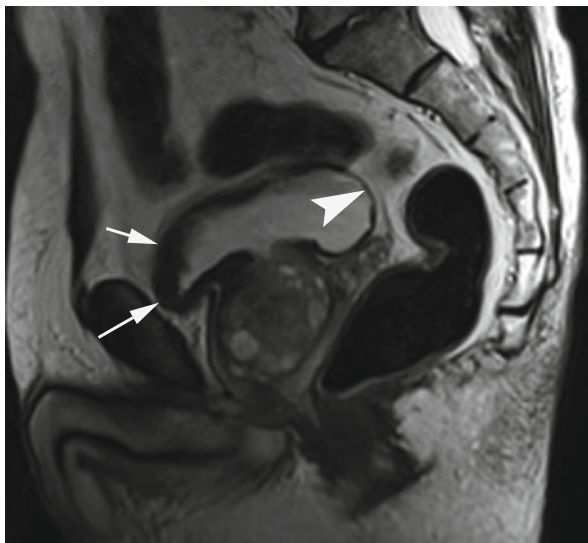
12.3.3.2 Urinary Bladder and Urethra

In the screening situation, evaluation of the urinary bladder and urethra focuses on bladder wall thickening, diverticula and pseudodiverticula, calculi, and tumors.

12.3.3.2.1 Bladder Wall Thickening

Diffuse bladder wall thickening occurs in a heterogeneous group of conditions including bacterial and viral infections, cystitis of different etiology, neurologic disorders, neoplasm, and bladder outlet obstruction (Wong-You-Cheong et al. 2006). The MRI appearance is characterized by single or multiple foci of thickened bladder wall or by diffuse thickening with isointensity to the muscular coat on T1-weighted and T2-weighted images. Invasion of the surrounding fat suggests a malignant tumor. Diffuse wall thickening associated with a trabeculated bladder is most commonly seen in middle-aged or elderly men (>50 years) with benign prostatic hyperplasia. A trabeculated bladder is characterized by the occurrence of prominent trabeculae in the bladder wall and develops after initial diffuse thickening of the muscular coat and subsequent muscle degeneration (Figs. 12.32 and 12.33).

Fig. 12.33 Sagittal T2w image obtained in another case of enlarged prostate with cystic degeneration. The urinary bladder wall is moderately thickened anteriorly due to muscular hypertrophy (*arrows*) secondary to outflow obstruction, and there is rarefaction of the posterior bladder wall (*arrowhead*) with a slightly irregular contour



Clinical Management

The typical appearance of a trabeculated bladder in men with known benign prostatic hyperplasia need not be reported, whereas focal or diffuse thickening without an apparent cause should be reported and further evaluated (Wong-You-Cheong et al. 2006).

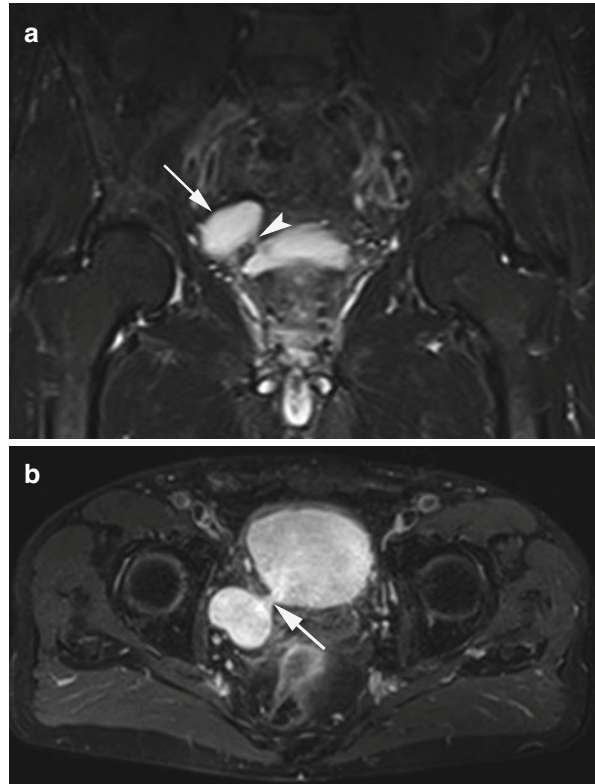
When evaluating bladder wall thickness, the radiologist must take bladder filling into account, as a nondistended bladder with only little urine in it may mimic wall thickening.

12.3.3.2 Diverticula/Pseudodiverticula

Diverticula are focal outpouchings of the urinary bladder wall which include all three wall layers and are usually congenital. Pseudodiverticula are more common and develop secondary to bladder outlet obstruction (prostatic hyperplasia). They do not involve all wall layers (Fig. 12.34) and are nearly ten times more common in men. The pouches can be seen on both T1-weighted and T2-weighted images, but T2-weighted images provide better contrast due to the high signal intensity of urine. The neck is of variable thickness and may not be visualized when it is very thin. As the detrusor muscle is not involved in the outpouching, pseudodiverticula have a thinner wall. Bladder diverticula may harbor neoplasms, which the examiner must rule out when a bladder diverticulum has been demonstrated (Mallampati and Siegelman 2004). Diverticula and pseudodiverticula can obstruct bladder outflow, leading to secondary inflammatory changes. The differential diagnosis includes ureteroceles and cystic masses of the true pelvis (e.g., arising from the ovaries).

Diverticula of the urethra occur mostly in women.

Fig. 12.34 (a) Coronal TIRM image reveals a cystic mass posterior to the bladder on the right (*arrow*). There is a communication with the bladder, seen as a flow void due to accelerated urine flow (*arrowhead*). This appearance is consistent with a pseudodiverticulum. (b) PD image shows that the wall of the cystic lesion is much thinner than that of the bladder, which is also more in keeping with a pseudodiverticulum than with a diverticulum. The connection to the bladder is also clearly seen (*arrow*)



Clinical Management

The mere presence of urinary bladder diverticula need not be reported; however, pseudodiverticula with signs of bladder outlet obstruction should be reported so that further workup can be initiated.

12.3.3.2.3 Urinary Calculi

Calculi in the urinary bladder have the same signal characteristics as elsewhere in the urinary tract (see above). When a calculus is detected in the bladder, the examiner should look for adjacent masses (transitional cell cancer) and signs of bladder outlet obstruction.

Clinical Management

Urinary bladder calculi need not be reported.

Table 12.19 Bladder cancer

Frequency	Incidence, 15/100,000 population/year
Age predilection	65–70 years
Sex predilection	M:F ratio of 2:1
Risk factors	Smoking, environmental toxins
Type of lesion	Malignant
Signs and symptoms	Painless hematuria
Differential diagnosis	Blood clot, inflammatory conditions, invasive cancer of adjacent organs

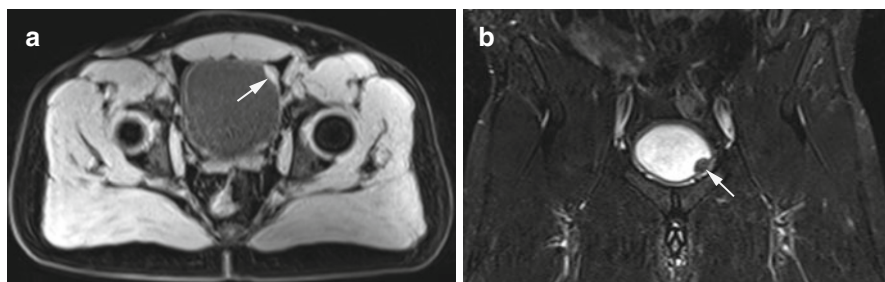


Fig. 12.35 (a) Axial T1w VIBE image reveals a localized mass of slightly higher signal intensity at the anteroinferior bladder wall (*arrow*). (b) Coronal TIRM image clearly delineates the low-signal-intensity mass (*arrow*) from the bright urine. The largest portion of the mass is intraluminal in location but there is infiltration of the bladder wall

12.3.3.2.4 Bladder Cancer

Almost 29,000 new cases of bladder cancer are diagnosed in Germany each year. Nearly all bladder cancers are of the transitional cell type. Men are nearly three times as likely as women to be diagnosed with bladder cancer. The mean age at diagnosis is 71 in men and 74 in women (Table 12.19). A distinction is made between flat and papillary cancers (Robert-Koch-Institut und die Gesellschaft der Epidemiologischen Krebsregister in Deutschland e.V. 2008). On T1-weighted images, bladder cancer is slightly hyperintense or isointense to urine. On T2-weighted images, the signal intensity is intermediate, meaning that it is higher than that of the bladder wall and lower than that of urine (Fig. 12.35). On contrast-enhanced images, bladder cancer displays early, minimal enhancement. Multifocal bladder cancer is not uncommon. Depending on the stage at diagnosis, locoregional lymph nodes may be enlarged, or the cancer may have invaded nearby organs such as the rectum, the uterus, or the seminal vesicles (Fisher et al. 1985).

Bladder cancer must be differentiated from blood clot within the bladder (lower signal intensity), inflammation of the bladder with an inflammatory pseudotumor, trabeculated bladder, and tumors of adjacent organs (including endometriosis) (Wong-You-Cheong et al. 2006).

Clinical Management

All intraluminal bladder masses that are isointense to soft tissue must be reported for initiation of diagnostic workup as malignancy is common in these cases (Wong-You-Cheong et al. 2006; Fisher et al. 1985).

References

- Aboul-Azm TE (1979) Anatomy of the human seminal vesicles and ejaculatory ducts. *Arch Androl* 3:287–292
- Akin EA, Khati NJ, Hill MC (2004) Ultrasound of the scrotum. *Ultrasound Q* 20:181–200
- Arora SS, Breiman RS, Webb EM, Westphalen AC, Yeh BM, Coakley FV (2007) CT and MRI of congenital anomalies of the seminal vesicles. *AJR Am J Roentgenol* 189:130–135
- Baert L, Steg A (1977) On the pathogenesis of simple renal cysts in the adult. A microdissection study. *Urol Res* 5:103–108
- Balen AH, Conway GS, Kaltsas G, Techatrasak K, Manning PJ, West C et al (1995) Polycystic ovary syndrome: the spectrum of the disorder in 1741 patients. *Hum Reprod* 10:2107–2111
- Beccia DJ, Krane RJ, Olsson CA (1976) Clinical management of non-testicular intrascrotal tumors. *J Urol* 116:476–479
- Berry SJ, Coffey DS, Walsh PC, Ewing LL (1984) The development of human benign prostatic hyperplasia with age. *J Urol* 132:474–479
- Bhogal RH, Palit A, Prasad KK (2007) Conservative management of polyorchidism in a young man: a case report and review of literature. *Pediatr Surg Int* 23:689–691
- Bosniak MA (1986) The current radiological approach to renal cysts. *Radiology* 158:1–10
- Bradley WG Jr (1993) MR appearance of hemorrhage in the brain. *Radiology* 189:15–26
- Bradley AJ, Lim YY, Singh FM (2011) Imaging features, follow-up, and management of incidentally detected renal lesions. *Clin Radiol* 66:1129–1139
- Browne RF, Meehan CP, Colville J, Power R, Torreggiani WC (2005) Transitional cell carcinoma of the upper urinary tract: spectrum of imaging findings. *Radiographics* 25:1609–1627
- Chang JM, Lee HJ, Lee SE, Byun SS, Choe GY, Kim SH et al (2008) Pictorial review: unusual tumours involving the prostate: radiological-pathological findings. *Br J Radiol* 81:907–915
- Chen HW, Huang SC, Li YW, Chen SJ, Sheih CP (2006) Magnetic resonance imaging of seminal vesicle cyst associated with ipsilateral urinary anomalies. *J Formos Med Assoc* 105:125–131
- Chung TJ, Yao WJ (2002) Sonographic features of polyorchidism. *J Clin Ultrasound* 30:106–108
- Cramer SF, Patel A (1990) The frequency of uterine leiomyomas. *Am J Clin Pathol* 94:435–438
- Cramer BM, Schlegel EA, Thueroff JW (1991) MR imaging in the differential diagnosis of scrotal and testicular disease. *Radiographics* 11:9–21
- Curry NS, Cochran ST, Bissada NK (2000) Cystic renal masses: accurate Bosniak classification requires adequate renal CT. *AJR Am J Roentgenol* 175:339–342
- Dhar M, Denstedt JD (2009) Imaging in diagnosis, treatment, and follow-up of stone patients. *Adv Chronic Kidney Dis* 16:39–47
- Dieckmann KP, Pichlmeier U (2004) Clinical epidemiology of testicular germ cell tumors. *World J Urol* 22:2–14
- Dikensoy E, Balat O, Ugur MG, Ozkur A, Erkilic S (2007) Serum CA-125 is a good predictor of benign disease in patients with postmenopausal ovarian cysts. *Eur J Gynaecol Oncol* 28:45–47
- Dmowski WP, Lesniewicz R, Rana N, Pepping P, Noursalehi M (1997) Changing trends in the diagnosis of endometriosis: a comparative study of women with pelvic endometriosis presenting with chronic pelvic pain or infertility. *Fertil Steril* 67:238–243

- Dorum A, Blom GP, Ekerhovd E, Granberg S (2005) Prevalence and histologic diagnosis of adnexal cysts in postmenopausal women: an autopsy study. *Am J Obstet Gynecol* 192:48–54
- Eble JN, Bonsib SM (1998) Extensively cystic renal neoplasms: cystic nephroma, cystic partially differentiated nephroblastoma, multilocular cystic renal cell carcinoma, and cystic hamartoma of renal pelvis. *Semin Diagn Pathol* 15:2–20
- Eskenazi B, Warner ML (1997) Epidemiology of endometriosis. *Obstet Gynecol Clin North Am* 24:235–258
- Fisher MR, Hricak H, Tanagho EA (1985) Urinary bladder MR imaging. Part II. Neoplasm. *Radiology* 157:471–477
- Flake GP, Andersen J, Dixon D (2003) Etiology and pathogenesis of uterine leiomyomas: a review. *Environ Health Perspect* 111:1037–1054
- Fuchsjäger M, Shukla-Dave A, Akin O, Barentsz J, Hricak H (2008) Prostate cancer imaging. *Acta Radiol* 49:107–120
- Goldman SM, Fishman EK (1991) Upper urinary tract infection: the current role of CT, ultrasound, and MRI. *Semin Ultrasound CT MR* 12:335–360
- Gomori JM, Grossman RI (1988) Mechanisms responsible for the MR appearance and evolution of intracranial hemorrhage. *Radiographics* 8:427–440
- Gore RM, Newmark GM, Thakrar KH, Mehta UK, Berlin JW (2010) Pelvic incidentalomas. *Cancer Imaging* 10:15–26
- Gyapong M, Gyapong J, Weiss M, Tanner M (2000) The burden of hydrocele on men in Northern Ghana. *Acta Trop* 77:287–294
- Haaga JR, Morrison SC (1980) CT appearance of renal infarct. *J Comput Assist Tomogr* 4:246–247
- Harisinghani MG, Maher MM, Gervais DA, McGovern F, Hahn P, Jhaveri K et al (2003) Incidence of malignancy in complex cystic renal masses (Bosniak category III): should imaging-guided biopsy precede surgery? *AJR Am J Roentgenol* 180:755–758
- Harmon WJ, King BF, Lieber MM (1996) Renal oncocytoma: magnetic resonance imaging characteristics. *J Urol* 155:863–867
- Hilpert PL, Friedman AC, Radecki PD, Caroline DF, Fishman EK, Meziane MA et al (1986) MRI of hemorrhagic renal cysts in polycystic kidney disease. *AJR Am J Roentgenol* 146:1167–1172
- Homer HA, Li TC, Cooke ID (2000) The septate uterus: a review of management and reproductive outcome. *Fertil Steril* 73:1–14
- Hricak H, Chen M, Coakley FV, Kinkel K, Yu KK, Sica G et al (2000) Complex adnexal masses: detection and characterization with MR imaging—multivariate analysis. *Radiology* 214:39–46
- Imaoka I, Wada A, Kaji Y, Hayashi T, Hayashi M, Matsuo M et al (2006) Developing an MR imaging strategy for diagnosis of ovarian masses. *Radiographics* 26:1431–1448
- Israel GM, Bosniak MA (2003a) Calcification in cystic renal masses: is it important in diagnosis? *Radiology* 226:47–52
- Israel GM, Bosniak MA (2003b) Follow-up CT of moderately complex cystic lesions of the kidney (Bosniak category IIF). *AJR Am J Roentgenol* 181:627–633
- Israel GM, Bosniak MA (2005) An update of the Bosniak renal cyst classification system. *Urology* 66:484–488
- Israel GM, Hindman N, Bosniak MA (2004) Evaluation of cystic renal masses: comparison of CT and MR imaging by using the Bosniak classification system. *Radiology* 231:365–371
- Issa B (2002) In vivo measurement of the apparent diffusion coefficient in normal and malignant prostatic tissues using echo-planar imaging. *J Magn Reson Imaging* 16:196–200
- Janick PA, Hackney DB, Grossman RI, Asakura T (1991) MR imaging of various oxidation states of intracellular and extracellular hemoglobin. *AJNR Am J Neuroradiol* 12:891–897
- Kim ED, Lipshultz LI (1996) Role of ultrasound in the assessment of male infertility. *J Clin Ultrasound* 24:437–453
- Kim W, Rosen MA, Langer JE, Banner MP, Siegelman ES, Ramchandani P (2007) US MR imaging correlation in pathologic conditions of the scrotum. *Radiographics* 27:1239–1253
- Kim S, Jain M, Harris AB, Lee VS, Babb JS, Sigmund EE et al (2009a) T1 hyperintense renal lesions: characterization with diffusion-weighted MR imaging versus contrast-enhanced MR imaging. *Radiology* 251:796–807

- Kim B, Kawashima A, Ryu JA, Takahashi N, Hartman RP, King BF Jr (2009b) Imaging of the seminal vesicle and vas deferens. *Radiographics* 29:1105–1121
- King BF, Hattery RR, Lieber MM, Williamson B Jr, Hartman GW, Berquist TH (1989) Seminal vesicle imaging. *Radiographics* 9:653–676
- Leung ML, Gooding GA, Williams RD (1984) High-resolution sonography of scrotal contents in asymptomatic subjects. *AJR Am J Roentgenol* 143:161–164
- Loeb S, Kettermann A, Carter HB, Ferrucci L, Metter EJ, Walsh PC (2009) Prostate volume changes over time: results from the Baltimore Longitudinal Study of Aging. *J Urol* 182:1458–1462
- Logue LG, Acker RE, Sienko AE (2003) Best cases from the AFIP: angiomyolipomas in tuberous sclerosis. *Radiographics* 23:241–246
- Madewell JE, Goldman SM, Davis CJ Jr, Hartman DS, Feigin DS, Lichtenstein JE (1983) Multilocular cystic nephroma: a radiographic-pathologic correlation of 58 patients. *Radiology* 146:309–321
- Mallampati GK, Siegelman ES (2004) MR imaging of the bladder. *Magn Reson Imaging Clin N Am* 12:545–555
- Mattrey RF (1991) Magnetic resonance imaging of the scrotum. *Semin Ultrasound CT MR* 12:95–108
- McDonald JM, Modesitt SC (2006) The incidental postmenopausal adnexal mass. *Clin Obstet Gynecol* 49:506–516
- McNeal JE (1988) Normal histology of the prostate. *Am J Surg Pathol* 12:619–633
- Murase E, Siegelman ES, Outwater EK, Perez-Jaffe LA, Tureck RW (1999) Uterine leiomyomas: histopathologic features, MR imaging findings, differential diagnosis, and treatment. *Radiographics* 19:1179–1197
- Nalaboff KM, Pellerito JS, Ben-Levi E (2001) Imaging the endometrium: disease and normal variants. *Radiographics* 21:1409–1424
- Namimoto T, Awai K, Nakaura T, Yanaga Y, Hirai T, Yamashita Y (2009) Role of diffusion-weighted imaging in the diagnosis of gynecological diseases. *Eur Radiol* 19:745–760
- Nascimento AB, Mitchell DG, Zhang XM, Kamishima T, Parker L, Holland GA (2001) Rapid MR imaging detection of renal cysts: age-based standards. *Radiology* 221:628–632
- Nguyen HT, Coakley F, Hricak H (1999) Cryptorchidism: strategies in detection. *Eur Radiol* 9:336–343
- Okamoto Y, Tanaka YO, Nishida M, Tsunoda H, Yoshikawa H, Itai Y (2003) MR imaging of the uterine cervix: imaging-pathologic correlation. *Radiographics* 23:425–445, quiz 534–535
- Olive DL, Schwartz LB (1993) Endometriosis. *N Engl J Med* 328:1759–1769
- Outwater EK, Bhatia M, Siegelman ES, Burke MA, Mitchell DG (1997) Lipid in renal clear cell carcinoma: detection on opposed-phase gradient-echo MR images. *Radiology* 205:103–107
- Oyelese Y, Kueck AS, Barter JF, Zalud I (2002) Asymptomatic postmenopausal simple ovarian cyst. *Obstet Gynecol Surv* 57:803–809
- Passerotti C, Chow JS, Silva A, Schoettler CL, Rosoklija I, Perez-Rossello J et al (2009) Ultrasound versus computerized tomography for evaluating urolithiasis. *J Urol* 182:1829–1834
- Pedrosa I, Sun MR, Spencer M, Genega EM, Olumi AF, Dewolf WC et al (2008) MR imaging of renal masses: correlation with findings at surgery and pathologic analysis. *Radiographics* 28:985–1003
- Prasad SR, Surabhi VR, Menias CO, Raut AA, Chintapalli KN (2008) Benign renal neoplasms in adults: cross-sectional imaging findings. *AJR Am J Roentgenol* 190:158–164
- Robert Koch-Institut und die Gesellschaft der epidemiologischen Krebsregister in Deutschland e.V. (2008) *Krebs in Deutschland 2003–2004. Häufigkeiten und Trends. 6. überarbeitete Auflage.* Berlin
- Saini S, Frankel RB, Stark DD, Ferrucci JT Jr (1988) Magnetism: a primer and review. *AJR Am J Roentgenol* 150:735–743
- Sala E, Wakely S, Senior E, Lomas D (2007) MRI of malignant neoplasms of the uterine corpus and cervix. *AJR Am J Roentgenol* 188:1577–1587
- Schatz SM, Lieber MM (2003) Update on oncocytoma. *Curr Urol Rep* 4:30–35

- Scheidler J, Heuck AF (2002) Imaging of cancer of the cervix. *Radiol Clin North Am* 40:577–90, vii
- Seitz M, Shukla-Dave A, Bjartell A, Touijer K, Sciarra A, Bastian PJ et al (2009) Functional magnetic resonance imaging in prostate cancer. *Eur Urol* 55:801–814
- Sheah K, Teh HS, Peh OH (2004) Supernumerary testicle in a case of polyorchidism. *Ann Acad Med Singapore* 33:368–370
- Shinmoto H, Yuasa Y, Tanimoto A, Narimatsu Y, Jinzaki M, Hiramatsu K et al (1998) Small renal cell carcinoma: MRI with pathologic correlation. *J Magn Reson Imaging* 8:690–694
- Siegel CL, McFarland EG, Brink JA, Fisher AJ, Humphrey P, Heiken JP (1997) CT of cystic renal masses: analysis of diagnostic performance and interobserver variation. *AJR Am J Roentgenol* 169:813–818
- Siegelman ES, Outwater EK (1999) Tissue characterization in the female pelvis by means of MR imaging. *Radiology* 212:5–18
- Silverman SG, Israel GM, Herts BR, Richie JP (2008) Management of the incidental renal mass. *Radiology* 249:16–31
- Steiner MS, Goldman SM, Fishman EK, Marshall FF (1993) The natural history of renal angio-myolipoma. *J Urol* 150:1782–1786
- Sugimura K, Okizuka H, Imaoka I, Kaji Y, Takahashi K, Kitao M et al (1993) Pelvic endometriosis: detection and diagnosis with chemical shift MR imaging. *Radiology* 188:435–438
- Takeuchi M, Matsuzaki K, Kubo H, Nishitani H (2008) Diffusion-weighted magnetic resonance imaging of urinary epithelial cancer with upper urinary tract obstruction: preliminary results. *Acta Radiol* 49:1195–1199
- Togashi K, Noma S, Ozasa H (1987) CT and MR demonstration of nabothian cysts mimicking a cystic adnexal mass. *J Comput Assist Tomogr* 11:1091–1092
- Troiano RN, McCarthy SM (2004) Mullerian duct anomalies: imaging and clinical issues. *Radiology* 233:19–34
- Turkbey B, Albert PS, Kurdziel K, Choyke PL (2009) Imaging localized prostate cancer: current approaches and new developments. *AJR Am J Roentgenol* 192:1471–1480
- Turkvatan A, Olcer T, Cumhur T (2009) Multidetector CT urography of renal fusion anomalies. *Diagn Interv Radiol* 15:127–134
- Verswijvel G, Vandecaveye V, Gelin G, Vandevenne J, Grieten M, Horvath M et al (2002) Diffusion-weighted MR imaging in the evaluation of renal infection: preliminary results. *JBR-BTR* 85:100–103
- Virtanen HE, Bjerknes R, Cortes D, Jorgensen N, Rajpert-De Meyts E, Thorsson AV et al (2007) Cryptorchidism: classification, prevalence and long-term consequences. *Acta Paediatr* 96:611–616
- Wong-You-Cheong JJ, Woodward PJ, Manning MA, Davis CJ (2006) From the archives of the AFIP: Inflammatory and nonneoplastic bladder masses: radiologic-pathologic correlation. *Radiographics* 26:1847–1868
- Wood HM, Elder JS (2009) Cryptorchidism and testicular cancer: separating fact from fiction. *J Urol* 181:452–461
- Woodward PJ, Schwab CM, Sesterhenn IA (2003) From the archives of the AFIP: extratesticular scrotal masses: radiologic-pathologic correlation. *Radiographics* 23:215–240
- Yeniol CO, Nergiz N, Tuna A (2004) Abdominal polyorchidism: a case report and review of the literature. *Int Urol Nephrol* 36:407–408
- Zhang J, Tehrani YM, Wang L, Ishill NM, Schwartz LH, Hricak H (2008) Renal masses: characterization with diffusion-weighted MR imaging—a preliminary experience. *Radiology* 247:458–464

Index

A

AAA. *See* Abdominal aortic aneurysm (AAA)

Abdomen

- adrenal glands, 198–202
- bile ducts, 186–190
- GI, 202–207
- liver (*see* Liver)
- pancreas, 190–194
- spleen, 194–198

Abdominal aortic aneurysm (AAA), 55, 220, 221

Acute and chronic myocarditis

- delayed enhancement, 159
- echocardiography, 159
- fat-saturated T2-weighted images, 157, 159
- focal/diffuse involvement, 157, 159
- ischemic cardiomyopathy, 159
- nonischemic dilated cardiomyopathy, 159
- pericardial effusion, 159
- systolic dysfunction, 157

Acute pyelonephritis, 350

ADC. *See* Apparent diffusion coefficient (ADC)

Adrenal glands

- adrenal tumors (*see* Adrenal tumors)
- lesions, 198, 199

Adrenal tumors, 199–202

American College of Radiology Breast Imaging Reporting and Data System (ACR BI-RADS), 279, 280

Ampullary renal pelvis, 352, 354

Aneurysm

- aortic, 220–221
- intracranial, 23, 218–220
- lower extremity arteries, 221–222

myocardial, 141

visceral and renal arteries, 222

Angiographic System for Unlimited

- Rolling Field-of-views (*AngioSURF*), 33, 34, 49

Angiomyolipoma, 348–349

AngioSURF. *See* Angiographic System for Unlimited Rolling Field-of-views (*AngioSURF*)

Aortic aneurysm, 220–221

Apparent diffusion coefficient (ADC), 81, 172, 281, 295, 297, 312, 317, 331, 350

Arachnoid cysts, 58–60, 70, 71

Arrhythmogenic right ventricular cardiomyopathy (ARVC), 145, 152–153

ARVC. *See* Arrhythmogenic right ventricular cardiomyopathy (ARVC)

Astrocytomas, 67, 68

Atelectasis, 121, 126

Axillary lymphadenopathy, 124–125

B

Benign adrenal tumors

- adenoma, 199–200
- cysts, 200–201

Benign breast lesions

- complex cysts, 283–284
- fibroadenoma, 286–289
- IDC, 300
- ILC, 301
- intramammary lymph node, 285–286
- papilloma, 290–291
- radial scar, 289–290
- simple cysts, 281–283

- Benign prostatic hyperplasia (BPH), 331–332
- Benign solid liver lesions
- FNH, 176, 177
 - hepatocellular adenoma, 176–178
- Bilateral hilar lymphadenopathy, 122–123
- Bile ducts
- biliary system, 186–187
 - cholecystitis, 188–189
 - cholecystolithiasis, 187–188
 - choledocholithiasis, 188
 - intra- and extrahepatic, 189, 190
 - MRCP, 187
- Bladder cancer, 331, 359–360
- Blood-brain barrier (BBB) disruption, 67
- Bone marrow disorders
- conversion and reconversion, 238–242
 - metastases, 242–245
 - multiple myeloma/plasmacytoma, 245–246
- Bone metastasis, 52, 344
- Bone tumors
- cartilage-forming, 231–235
 - classification, 226
 - fibrous, 235–236
 - primary, 226, 245
- BPH. *See* Benign prostatic hyperplasia (BPH)
- Brain tumors
- classification, 67
 - extra-axial tumors, 70–71
 - intra-axial tumors, 67–69
 - radiotherapy, 82
 - vascular conditions, 80–89
- Breast cancer
- adrenal tumors, 201
 - adult fibroadenoma, 286
 - axillary lymph nodes, 125
 - benign lesions (*see* Benign breast lesions)
 - clinical management, 300, 307
 - differential diagnosis, 306
 - fibrocystic changes, 292–294
 - focal fibrocystic changes, 294
 - hormone replacement therapy, 281
 - IDC, 297
 - imaging modalities, 277
 - invasive ductal carcinoma, 304, 305
 - left-sided mastectomy, 304, 306
 - lesion classification and management, 279–281
 - malignant lesions (*see* Malignant breast lesions)
 - medullary/mucinous, 288
 - MRI, 278–279, 304–306
 - oncologic protocol, 53
 - osteolytic and osteoblastic bone metastases, 244
 - papillary carcinoma, 288
 - postoperative and postinterventional changes, 306
 - supraclavicular lymph nodes, 124
 - tubular, 290
- Broken heart syndrome, 154
- Bullous emphysema, 127, 129
- C**
- CAA. *See* Cerebral amyloid angiopathy (CAA)
- CAD. *See* Computer-aided diagnosis (CAD)
- Carcinoma of unknown primary (CUP), 53, 116, 278
- Cardiac imaging
- cine sequences, 136, 137
 - electrocardiogram (ECG), 154
 - endocardium, 163
 - flow-sensitive imaging technique, 136
 - long-axis/short-axis, 134
 - MRI protocol, 140
 - pericardium, 159
 - standard functional parameters, 134
- Cardiomyopathy
- ARVC, 152–153
 - DCM, 146–149
 - HCM/HOCM, 150–151
 - mechanical and electrical dysfunction, 145
 - MRI features, 145, 156
 - myocardial morphology and function, 146
 - NCCM, 155
 - primary and secondary, 146
 - RCM, 151–152
 - Takotsubo, 154
 - types, 145
 - WHO classification, 145, 146
- Cardiovascular protocol, 48–49
- Cartilage-forming bone tumors
- chondroma/enchondroma, 233–235
 - osteochondroma, 231–233
- Cavernomas, 82–85
- Cerebral amyloid angiopathy (CAA), 84–86
- Cerebral ischemia, 80–82
- Cerebral microbleeds, 84–87
- Cerebrospinal fluid (CSF) system
- arachnoid cysts, 58
 - chronic intermittent obstruction, 60
 - clinical management, 61
 - incidental screening, 62
 - meningioma, 76
 - normal pressure hydrocephalus, 78–80
 - pineal cysts, 70
 - pseudotumor cerebri, 76–78

- pulse sequences, 63
 - spinal canal stenosis, 261
 - Cervical artery dissection, 222–223
 - Cervical cancer
 - age peaks, 312
 - clinical management, 312
 - DWI, 312
 - signal intensity, 312, 313
 - Cervix, 312–313
 - Chest
 - abnormal lymph nodes, 104
 - focal pulmonary lesions, 115–121
 - lymphadenopathy, 122–125
 - mediastinal masses, 129–130
 - myocardial ischemic injury, 137
 - pneumonia, effusion, and atelectasis, 126–129
 - postoperative seroma, 283
 - Takotsubo cardiomyopathy, 154
 - thoracic stomach, 203
 - Cholangiocellular carcinoma (CCC), 182–183
 - Cholecystitis, 188–189
 - Cholecystolithiasis, 187–188
 - Choledocholithiasis, 188
 - Chondroma/enchondroma, 233–235
 - Chordal regression syndrome, 252, 253
 - Choroid plexus cysts, 61–62
 - Ciliary dyskinesia, primary, 93
 - Cirrhosis, 183–184
 - Colloid cysts, 60–61
 - Colorectal cancer, 53, 116, 179, 207
 - Computer-aided diagnosis (CAD), 41
 - Congenital and developmental anomalies
 - axial skeleton deformities, 253, 255
 - chordal regression syndrome, 252, 253
 - Scheuermann disease, 252–254
 - vertebral fusion, 252, 253
 - Congenital vertebral fusion, 252, 253
 - Continuous table advancement
 - contrast-enhanced peripheral MRA, 39, 40
 - gradient nonlinearities, 37
 - imaging data acquisition, 38
 - musculoskeletal disease, 225
 - whole-body MRI, 39
 - Contrast agent administration
 - cancer staging, 45
 - liver-specific, 54–55
 - MRI, 46–47
 - pulse sequence protocols, 48–54
 - Craniopharyngioma, 72
 - CUP. *See* Carcinoma of unknown primary (CUP)
 - Cystic liver lesions
 - abscess, 175
 - fibrosis, 172
 - hemangioma, 173–175
 - hepatic, 172–173
 - signal intensity, 171
 - Cystic renal masses
 - Bosniak classification, 336–337
 - category 1 and 2 lesions, 337
 - category 2F and 3 lesions, 343–344
 - category 4 lesions, 344–346
 - MRI diagnosis, 336
 - nephroma, 346
 - partially differentiated nephroblastoma, 346
 - PKD, 346
 - Cysts, breast
 - complex, 283–284
 - simple, 281–283
- D**
- DCIS. *See* Ductal carcinoma in situ (DCIS)
 - DCM. *See* Dilated cardiomyopathy (DCM)
 - Degenerative conditions, spine
 - disc herniation, 258, 259
 - intervertebral osteochondrosis, 261–264
 - spinal stenosis, 259–261
 - Developmental venous anomaly (DVA), 82, 83
 - Diffusion-weighted imaging (DWI)
 - abnormalities detection, 58
 - ADC, 81
 - cervical cancer, 312
 - diffusion restriction, 62, 331, 350
 - ischemic lesions, 81
 - perifocal edema, 297
 - respiratory-triggered, 171
 - Dilated cardiomyopathy (DCM)
 - heart failure, 147
 - hypertrophic/hypertrophic obstructive, 149
 - ischemic heart disease, 148
 - myocardial damage, 147
 - PSIR, 147, 149
 - pump function, 149
 - restrictive cardiomyopathy, 149
 - systolic dysfunction, 146, 148
 - valvular diseases, 149
 - ventricular dilation, 147
 - Disc herniation, intervertebral, 258–259
 - Diverticula/pseudodiverticula, 206, 357–358
 - Ductal carcinoma in situ (DCIS)
 - clinical management, 296
 - differential diagnosis, 296
 - MRI features, 296

- Ductal carcinoma in situ (DCIS) (*cont.*)
 neoplastic cells, 295
 Paget disease, 303
 radial scar, 290
- DVA. *See* Developmental venous anomaly (DVA)
- DWI. *See* Diffusion-weighted imaging (DWI)
- E**
- Edema
 coronary artery territories, 138
 inflammatory processes and scar tissue, 137
 myocarditis/cardiomyopathy, 137
- Empirical feasibility, population-based research, 12
- Enchondroma, 233–235
- Endocardium, 163–164
- Endometrial cancer, 311, 312, 314, 317
- Endometriosis, 316–318, 320, 321
- Endoscopic retrograde
 cholangiopancreatography (ERCP), 194
- ERCP. *See* Endoscopic retrograde cholangiopancreatography (ERCP)
- Ethical legitimation, 12
- Extra-axial tumors, 67, 70–71
- Extracranial carotid stenosis, 214
- F**
- Female genital organs
 cervix, 312–313
 endometriosis, 317–318
 external, 311
 internal, 311
 ovaries, 318–324
 uterus, 314–317
- Fibroadenoma
 adult, 286, 287
 clinical management, 289
 complex breast cysts, 284
 DCIS, 296
 differential diagnosis, 288
 juvenile, 286, 287
 MRI features, 286, 288
- Fibrocystic breast changes
 bilateral, 292
 classification system, 292
 clinical management, 294
 differential diagnosis, 294
 initial phase, enhancement, 293
 late phase, enhancement, 293
- locoregional, 293
 MRI features, 294
- Fibrous bone tumors, 235–236
- Fibrous dysplasia, 235–236
- Financial incentives, study participation, 6, 11, 13–14
- Focal liver lesions
 diagnostic and therapeutic management, 171
 non-contrast-enhanced images, 170–171
 standardized protocol, 170
 T2 signal intensity, 170
 T1-weighted pulse sequences, 171
 whole-body, 169–170
- Focal nodular hyperplasia (FNH), 176, 177
- Focal organizing pneumonia (FOP), 121
- Focal pulmonary lesions, 115–121, 126
- FOP. *See* Focal organizing pneumonia (FOP)
- G**
- Gastrointestinal tract (GI)
 hernias, 202–204
 large intestine, 206–207
 normal peristaltic contraction, 202, 203
 peritoneum, 204–205
 small intestine, 205
 stomach, 205
- Gd-EOB-DTPA, 46, 54
- Generalized lymphadenopathy, 122, 125
- GI. *See* Gastrointestinal tract (GI)
- Glioblastoma multiforme, 67
- Goettingen score, breast MRI, 279
- Goiter, thyroid enlargement., 103–105, 129
- H**
- HCM/HOCM. *See* Hypertrophic and hypertrophic obstructive cardiomyopathy (HCM/HOCM)
- Head
 anomalies and tumor-like lesions, 58–67
 brain tumors, 67–80
 left femoral, 249
 magnetic resonance imaging, 57
 neuroradiologic evaluation, 57
 to toe, 35–36
 vascular conditions, 80–89
- Heart
 cardiac imaging, 133–137, 140
 edema, 137–138
 endocardial disease, 140
 endocardium, 163–164
 ischemic myocardial injury, 138–139

- MRI, 133
 - myocardial perfusion, 139
 - pericardium, 159–163
 - Hemangioma
 - clinical management, 265
 - description, 265, 267
 - liver, 173–175
 - phleboliths, 265
 - Hepatic cysts, 172–173
 - Hepatic steatosis, 185
 - Hepatocellular adenoma, 176–178
 - Hepatocellular carcinoma (HCC), 180–182
 - Hernias, 202–204
 - Hilar/mediastinal lymphadenopathy, 123
 - Hypertensive encephalopathy, 86–87
 - Hypertrophic and hypertrophic obstructive cardiomyopathy (HCM/HOCM), 150–151
- I**
- ICP. *See* Intracranial pressure (ICP)
 - IDC. *See* Invasive ductal carcinoma (IDC)
 - IHD. *See* Ischemic heart disease (IHD)
 - ILC. *See* Invasive lobular carcinoma (ILC)
 - Incomplete vertebral arch closure, 252, 253
 - Infiltrating lobular carcinoma. *See* Invasive lobular carcinoma (ILC)
 - Inflammatory renal conditions
 - acute, 350
 - chronic, 350
 - perirenal fluid, 350–351
 - renal abscess, 350
 - Intervertebral osteochondrosis
 - clinical management, 262
 - diagnosis, 261
 - edema formation, 261
 - MRI features, 264
 - severe, 260, 263
 - Intra-axial cystic lesions, 62–64, 67–69
 - Intracranial pressure (ICP), 76
 - Intracranial stenosis, 213–214
 - Intralesional fat, 121, 296
 - Intramammary lymph node
 - clinical management, 286
 - description, 285
 - differential diagnosis, 286
 - MRI features, 285–286
 - Intraosseous hemangioma/lipoma, 229–231
 - Invasive ductal carcinoma (IDC)
 - breast cysts, 284
 - clinical management, 300
 - differential diagnosis, 300
 - diffuse hyperintensity, 297
 - initial enhancement, lesion, 297, 298
 - low-signal-intensity stellate lesion, 297
 - MRI features, 298, 300
 - perifocal edema, 297
 - postcontrast phase and enhancement kinetics, lesion, 299
 - postoperative breast changes, 305
 - radial scar, 290
 - Invasive lobular carcinoma (ILC)
 - clinical management, 302
 - description, 300
 - differential diagnosis, 301–302
 - MRI features, 301
 - peak enhancement, 297
 - Ischemic heart disease (IHD)
 - acute myocardial infarction, 142
 - akinesia, hypokinesia and dyskinesia, 141
 - atherosclerosis, 140, 141
 - balanced circulation, 142
 - coronary artery, 142–144
 - Frank–Starling mechanism, 142
 - mitral regurgitation, 144
 - myocardial ischemia, 141
 - nonischemic cardiomyopathy, 142
 - pseudoaneurysm, 144
 - pump function, 144
 - subendocardial enhancement, 141, 142
 - Ischemic myocardial injury
 - gadolinium-based contrast medium, 138
 - microvascular obstruction, 139
 - myocardium, 138
 - phase-sensitive reconstruction, 138
 - single-shot inversion recovery sequences, 139
- J**
- Jaffé–Lichtenstein disease. *See* Fibrous dysplasia
 - Joints
 - bilateral knee effusion, 247, 248
 - bone marrow edema, 247–249, 256
 - deformities, 232, 233
 - effusion and subchondral bone edema., 247
 - elbows, 246
 - facet arthrosis, 259
 - focal osteochondral defect, 249
 - medial gonarthrosis, 247
 - osteochondritis dissecans, 248
 - sacroiliac, 256, 257
 - Juvenile/solitary bone cyst, 227–229

K**Kidneys**

- cystic renal masses (*see* Cystic renal masses)
- inflammatory renal conditions, 350–351
- renal anomalies, 334–335
- solid renal masses, 346–349
- vascular renal conditions, 352

L

- Large intestine, 206–207
- Left ventricular ejection fraction (LVEF), 134, 147, 152, 155, 156
- Left ventricular end-diastolic volume (LVEDV), 134
- Left ventricular mass (LVM), 22, 134
- Leukoaraiosis, 87
- Life-threatening abnormalities, 15
- Lipoma(s)
 - angiomyolipoma, 347–349
 - asymptomatic, 231
 - clinical management, 67, 231, 268
 - description, 267, 269
 - differential diagnosis, 286
 - epididymis, 328
 - imaging features, 107
 - intralesional fat, 121
 - intramuscular, 268
 - intraosseous, 229, 230
 - liposarcomas, 268
 - mesenchymal tumor, 267
 - signal intensity, STIR images, 265
 - soft tissue tumor, 265
 - solid lesions, 107
 - spermatic cord, 330
 - tumor-like lesions, 66–67
- Literary Digest* disaster, 8
- Liver
 - cirrhosis, 183–184
 - cystic, 171–175
 - focal liver lesions, 169–171
 - hepatic steatosis, 185
 - hepatocellular contrast agent, 49
 - rectal cancer, 45
 - solid, 175–183
- Liver metastasis, 178–180
- Lung cancer, 45, 53, 115, 118, 122, 201
- LVEDV. *See* Left ventricular end-diastolic volume (LVEDV)
- LVEF. *See* Left ventricular ejection fraction (LVEF)
- LVM. *See* Left ventricular mass (LVM)

- Lymphadenopathy, 96, 105, 122–125, 319, 344
- Lymph node metastasis, 52–53, 98, 297

M

- Magnetic resonance cholangiopancreatography (MRCP), 187, 188, 190, 192
- Magnetic resonance imaging (MRI) system
 - back pain, 248
 - brain scans, 15
 - breast technique, 278–279, 281
 - cardiac function, 133
 - coil systems, 90
 - contrast agents, 46–47
 - cystic lesions, 70
 - diagnosis, 60
 - disc protrusion, 258
 - emphysema-related changes, 127, 129
 - gradient system, 30–31
 - hydrocephalus, 78
 - intranodular fat, 119
 - ischemia imaging, 138
 - liver, 186
 - multichannel imaging, 90
 - musculoskeletal abnormalities, 226
 - nasal secretions, 93
 - oxidation stages, hemoglobin, 340, 342
 - pancreas, 190
 - radiofrequency (RF) system, 31–32
 - splenic malignancy, 205
 - STIR, 225
 - supraclavicular lymphadenopathy, 124
 - virtual colonoscopy, 53
 - whole-body coil systems, 57
- Male genital organs
 - epididymis, 328
 - penis and scrotum, 324
 - prostate, 330–332
 - seminal vesicles, 332–334
 - spermatic cord, 329–330
 - testicles, 324–328
- Malignant breast lesions
 - DCIS, 295–296
 - IDC, 297–300
 - ILC, 300–302
 - initial enhancement, rapid washout, 281
 - Paget disease, 302–304
- Mediastinal lymphadenopathy, 122–123
- Meningiomas, 70, 74–76
- Mesenteric artery stenosis, 218
- Meyerding system, spondylolisthesis grading system, 253, 255

- Microvascular leukoencephalopathy, 88, 89
- Mononuclear phagocytic system, 46
- Monro–Kellie doctrine, 76, 78
- MRCP. *See* Magnetic resonance cholangiopancreatography (MRCP)
- MRI contrast agents
- dynamic imaging studies, 47
 - extracellular gadolinium chelates, 46
 - hepatocyte-specific agent, 46
 - linear ionic and nonionic complexes, 46
 - macrocyclic complexes, 46
 - NSF, 46
 - spasmolytic medication, 47
- Multiple myeloma/plasmacytoma, 240, 245–246
- Multiple pulmonary nodules, 119–120
- Multistation imaging techniques, 29, 33, 35–40, 48
- Musculoskeletal system. *See* Skeletal system
- Myocardium
- acute and chronic myocarditis, 157–159
 - cardiomyopathy (*see* Cardiomyopathy)
 - delayed enhancement, 140
 - IHD, 140–144
- N**
- Nabothian cysts, 312, 313
- Nasal mucosal abnormalities, 91
- NCCM. *See* Noncompaction cardiomyopathy (NCCM)
- Neck
- ampullary renal pelvis, 342
 - bone marrow edema, 248, 249
 - lymph node enlargement, 96–99
 - paranasal sinuses, 90–96
 - pharynx and larynx, 105–109
 - salivary glands, 99–101
 - thyroid, 102–105
- Neck lymph node enlargement
- clinical management, 99
 - reactive inflammatory enlargement, 96
 - supraglottic cancer, 107
 - swollen nodes, 96, 97
 - Virchow node, 98
- Neoplastic disease, 54, 55
- Nephrogenic systemic fibrosis (NSF), 46
- Neuroepithelial/neuroglial cysts, 62–64
- Neurofibromas and schwannomas, 268, 271, 272
- Noncompaction cardiomyopathy (NCCM), 155, 158
- Nondisclosure, 11
- Noninterventional epidemiologic study, 6, 11
- Normal pressure hydrocephalus (NPH), 78–80
- NPH. *See* Normal pressure hydrocephalus (NPH)
- O**
- Oncocytoma, 347, 349
- Oncologic protocol
- bone metastasis, 52
 - colorectal and prostate cancer, 53
 - CUP, 53
 - imaging patients, 49, 52
 - lung and breast cancer, 53
 - lymph node metastasis, 52–53
 - organ metastasis, 52
 - pulse sequences, 49–51
- Organ systems, 22, 23, 45, 53, 89
- Osteocartilaginous exostosis. *See* Osteochondroma
- Osteochondroma, 227, 231–233
- Osteoid osteoma, 227, 238, 240
- Osteoma, 236–238
- Ovaries
- mixed cystic and solid ovarian tumors, 322–324
 - multilocular ovarian cysts, 320–322
 - unilocular ovarian cysts, 319–320
- P**
- Paget disease, 236, 302–304
- Pancreas
- chronic pancreatitis, 190, 191
 - cystic duct, 190
 - pancreatic pseudocysts, 192
 - secretin-enhanced MRCP, 190, 191
 - secretin stimulation, 191, 193
 - solid masses, 192–194
- Pancreatic pseudocysts, 192
- PAOD. *See* Peripheral arterial occlusive disease (PAOD)
- Papillomas
- clinical management, 291
 - description, 290
 - differential diagnosis, 291
 - MRI features, 291
 - multiple, 290
- Paranasal sinuses
- mucocoele, 94–96
 - sinonasal polyposis, 93–94
 - sinusitis, 90–93
 - suprahyoid neck, 105

- Patient generations, 8–10, 15, 16
- Pericardial effusion, 160
- Pericarditis, 161–162
- Pericardium
 - constrictive pericarditis, 162–163
 - effusion, 160
 - inflammatory processes, 159
 - pericarditis, 161–162
- Peripheral arterial occlusive disease (PAOD), 214–216
- Peritoneum, 204–205
- Pharynx and larynx
 - cystic lesions, 105–107
 - parapharyngeal space, 105
 - solid lesions, 107–109
- Phased-array surface coil technology, 34
- Phase-sensitive inversion recovery (PSIR), 138, 140, 147, 149
- Pineal cysts, 70, 71
- Pituitary adenoma
 - classification, 72
 - incidental screening findings, 72, 73
 - intracranial tumors, 72
 - microadenoma, 72
- Plasmacytoma, 226, 245–246
- Pleomorphic adenomas, 99–100, 106
- Pleural calcinosis, 121
- Pleural effusion and fibrosis, 127, 128, 144
- Pneumonia, 118, 126–129
- Population-based research
 - diagnosis, clinical disease, 21–22
 - human subjects research, 4–6
 - incidental findings, 6–12
 - management, incidental findings, 9
 - methodological implications, 6
 - nondisclosure, 11
 - whole-body MR imaging, 23–27
- Primary brain tumors, 67–69, 74
- Primary lung cancer, 115, 116
- PRIND. *See* Prolonged reversible ischemic neurologic deficit (PRIND)
- Prolonged reversible ischemic neurologic deficit (PRIND), 80
- Prostate cancer
 - benign hyperplasia, 330, 332
 - BPH, 331–332
 - clinical management, 331
 - coronal STIR sequences, 226
 - cystic degeneration, 356
 - oncologic, 53
- Pseudotumor cerebri, 76–78
- PSIR. *See* Phase-sensitive inversion recovery (PSIR)
- Pulmonary artery embolism, 127, 128
- Pulmonary nodules
 - benign and malignant, 115
 - CT screening populations, 117
 - definition, 116
 - multiple, 119–120
 - solitary, 116–119
- R**
- Radial scar
 - clinical management, 290
 - differential diagnosis, 290
 - MRI features, 289–290
 - spiculated mass, 289
- Randomization procedure, 10
- RAS. *See* Renal artery stenosis (RAS)
- RCM. *See* Restrictive cardiomyopathy (RCM)
- Renal artery stenosis (RAS), 217
- Renal cell cancer, 53, 337, 342, 344, 346–349, 355
- Restrictive cardiomyopathy (RCM), 151–152
- Retrograde menstruation, 318
- RF coils from head to toe, 35–36
- Rheumatoid arthritis, 254–257
- S**
- SAE. *See* Subcortical atherosclerotic encephalopathy (SAE)
- Salivary glands, 99–101
- Scheuermann disease, 252–254
- Sellar lesions, 71–76
- Sella turcica, 71
- Seminal vesicles, 332–334
- Septum pellucidum, 64–65
- Seronegative spondyloarthropathy, 254, 256–257
- Sinonasal polyposis, 93–94
- Sinusitis
 - acute/chronic, 91
 - bone destruction, 91
 - classification, 90
 - fungal infection, 91
 - osteomyelitis, frontal bone, 91, 92
 - squamous cell carcinoma and lymphoma., 91
 - viral/bacterial, 90
 - Wegener granulomatosis, 91
- Skeletal system
 - bone lesions classification, 226, 227
 - bone marrow disorders, 238–246
 - bone tumors (*see* Bone tumors)
 - joints, 246–248
 - spine (*see* Spine)

- STIR imaging, 226
 tumorlike bone lesions (*see* Tumorlike bone lesions)
- Small intestine, 205
- Solid liver lesions
 benign, 176–178
 malignancy assessment, 175, 176
 malignant, 178–183
- Solid renal masses
 angiomyolipoma, 348–349
 oncocytoma, 349
 renal cell cancer, 346–348
- Solitary pulmonary nodules, 115, 117–119
- Spasmolytic medication, 47
- Spermatic cord
 tumors, 330
 varicocele, 329
- Spine
 back pain, 248, 250
 congenital and developmental anomalies, 252–254
 degenerative conditions, 258–262
 inflammatory conditions, 254–257
 metabolic and systemic disorders, 262–264
 MRI technique, imaging, 250, 251
 pathology classification, 252
 soft tissue, 265–272
- Spleen
 cysts, 196–197
 embryonic development, 195
 hematopoiesis, 194
 lesions, 197–198
 liver parenchyma, 194, 195
 parenchymal, 196
 solid splenic lesions, 197–198
- Stenosis
 aortic, 150
 cerebral artery, 80
 extracranial cerebral arteries, 214
 intracranial, 213–214
 lower extremity arteries, 214–216
 mesenteric artery stenosis, 218
 quantitative estimation, 136
 RAS, 217
 valvular, 163
- Stepping kinematic imaging platform (SKIP), 33
- Stomach, 205
- Stress-induced cardiomyopathy, 154
- Subcortical atherosclerotic encephalopathy (SAE), 81
- Subendocardial/transmural myocardial infarction, 144
- Supraclavicular lymphadenopathy, 124
- Susceptibility-weighted imaging (SWI), 58, 60, 82–85, 87, 88
- Suspicious adrenal tumors, 201–202
- SWI. *See* Susceptibility-weighted imaging (SWI)
- T**
- Takotsubo cardiomyopathy, 145, 146, 154
- Testicles
 aberrations, number, 326
 abnormal size, 326–327
 cryptorchidism, 327–328
 hydrocele, 324–325
- Thoracic stomach, 129, 130, 203, 204
- Thyroid
 bone metastases, 242
 goiter, 103–105
 nodules, 102–103
 primary tumors, 201
 size, 22
- TIA. *See* Transient ischemic attack (TIA)
- Time-of-flight magnetic resonance angiography (TOF-MRA), 48, 58, 76, 84, 213, 218
- TOF-MRA. *See* Time-of-flight magnetic resonance angiography (TOF-MRA)
- Tornwaldt cysts, 105, 106
- Total imaging matrix (Tim), 35, 49
- Transient ischemic attack (TIA), 80, 82
- Tumorlike bone lesions
 intraosseous hemangioma/lipoma, 229–231
 juvenile/solitary bone cyst, 227–229
- U**
- Urinary bladder and urethra
 bladder cancer, 359–360
 calculi, 358
 diverticula/pseudodiverticula, 357–358
 wall thickening, 356–357
- Urinary calculi, 352, 354–355, 358
- Urinary obstruction, 332–334, 346, 353–354
- Urinary tract
 bladder and urethra, 356–360
 collecting systems and ureters, 352–355
- Urogenital system
 female genital organs (*see* Female genital organs)
 kidneys (*see* Kidneys)
 male genital organs (*see* Male genital organs)
 urinary tract, 352–360

Uterine fibroids
 adenomyosis, 316
 clinical management, 316
 description, 314
 intralesional calcifications, 315
 MRI, 315
 myomatous uterus, 315

Uterus
 anomalies, 314
 endometrial cancer, 317
 uterine fibroids, 314–316

V

Valvular disease, 163–164

Vascular system

 aneurysm, 218–222
 cervical artery dissection, 222–223
 stenosis, 213–218

W

White matter lesions, 23, 57,
 87–89, 105